Vol. 165, December 1, 1984
Complete in one issue
ISSN 0003-2670

ANALYTICA CHIMICA ACTA

International journal devoted to all branches of analytical chemistry

ELSEVIER

ANALYTICA CHIMICA ACTA

International journal devoted to all branches of analytical chemistry
Revue internationale consacrée à tous les domaines de la chimie analytique
Internationale Zeitschrift für alle Gebiete der analytischen Chemie

PUBLICATION SCHEDULE FOR 1984

	J	F	M	A	M	J	J	A	S	O	N	D
Analytica Chimica Acta	156	157/1	157/2	158/1 158/2	159	160	161	162	163	164	165	166

Scope. *Analytica Chimica Acta* publishes original papers, short communications, and reviews dealing with ev aspect of modern chemical analysis, both fundamental and applied.

Submission of Papers. Manuscripts (three copies) should be submitted as designated below for rapid and efficie handling:

Papers from the Americas to: Professor Harry L. Pardue, Department of Chemistry, Purdue University, West Lafayet IN 47907, U.S.A.

Papers from all other countries to: Dr. A. M. G. Macdonald, Department of Chemistry, The University, P.O. Box 3(Birmingham B15 2TT, England. Papers dealing particularly with computer techniques to: Professor J. T. Cle Universität Bern, Pharmazeutisches Institut, Baltzerstrasse 5, CH-3012 Bern, Switzerland.

Submission of an article is understood to imply that the article is original and unpublished and is not being consider for publication elsewhere. Upon acceptance of an article by the journal, authors will be asked to transfer the copyrig of the article to the publisher. This transfer will ensure the widest possible dissemination of information.

Information for Authors. Papers in English, French and German are published. There are no page charg Manuscripts should conform in layout and style to the papers published in this Volume. Authors should cons Vol. 160 for detailed information. Reprints of this information are available from the Editors or from: Elsevier Editor Services Ltd., Mayfield House, 256 Banbury Road, Oxford OX2 7DH (Great Britain).

Reprints. Fifty reprints will be supplied free of charge. Additional reprints (minimum 100) can be ordered. An or form containing price quotations will be sent to the authors together with the proofs of their article.

Advertisements. Advertisement rates are available from the publisher.

Subscriptions. Subscriptions should be sent to: Elsevier Science Publishers B.V., Journals Department, P.O. B 211, 1000 AE Amsterdam, The Netherlands. Tel: 5803 911, Telex: 18582.

Publication. *Analytica Chimica Acta* appears in 11 volumes in 1984. The subscription for 1984 (Vols. 156–166) Dfl. 2145.00 plus Dfl. 231.00 (p.p.h.) (total approx. US $914.00). All earlier volumes (Vols. 1–155) except Vols. and 28 are available at Dfl. 215.00 (US $82.70), plus Dfl. 15.00 (US $6.00) p.p.h., per volume.

Our p.p.h. (postage, packing and handling) charge includes surface delivery of all issues, except to subscribers Australia, Brazil, Canada, China, Hong Kong, India, Israel, Japan, Malaysia, New Zealand, Pakistan, Singapore, So Africa, South Korea, Taiwan and the U.S.A. who receive all issues by air delivery (S.A.L. — Surface Air Lifted) at extra cost. For the rest of the world, airmail and S.A.L. charges are available upon request.

Claims for issues not received should be made within three months of publication of the issues. If not they canno honoured free of charge.

For further information, or a free sample copy of this or any other Elsevier Science Publishers journal, readers in U.S.A. and Canada can contact the following address: Elsevier Science Publishing Co., Inc., Journal Informat Center, 52 Vanderbilt Avenue, New York, NY 10017, U.S.A., Tel: (212) 916-1250.

ANALYTICA CHIMICA ACTA
VOL. 166 (1984)

ANALYTICA CHIMICA ACTA

International journal devoted to all branches of analytical chemistry

ELSEVIER Amsterdam–Oxford–New York–Tokyo

Printed in The Netherlands

Analytica Chimica Acta, 166 (1984) 1—26
Elsevier Science Publishers B.V., Amsterdam — Printed in The Netherlands

CHARACTERIZATION OF INTERNAL SALTS BY LASER MASS SPECTROMETRY

K. BALASANMUGAM and DAVID M. HERCULES*
Department of Chemistry, University of Pittsburgh, Pittsburgh, PA 15260 (U.S.A.)
(Received 9th July 1984)

SUMMARY

An intermolecular alkyl transfer reaction (ATR) leading to ion-pair formation has been observed for internal salts by using laser mass spectrometry (l.m.s.). Positive- and negative-ion spectra both show evidence for alkyl transfer. Both the LAMMA-500 (transmission) and LAMMA-1000 (reflection) laser mass spectrometers were used. The positive-ion laser mass spectra obtained by these two instruments show some significant differences; no significant differences were observed in the negative-ion spectra. Results obtained for quaternary ammoniohexanoates as a function of laser power indicate that the extent of ATR is greater at high laser power. Addition of a small amount of *p*-toluenesulfonic acid to the ammoniohexanoates reduces fragmentation and enhances the intensity of the quasimolecular ion $(M + H)^+$ relative to ATR. Results from deuterated sultaines were used to confirm intermolecular alkyl transfer and to elucidate some fragmentation processes. Field-desorption (f.d.) mass spectra of internal salts show similarities and differences from l.m.s.; not all internal salts showed the alkyl transfer reaction in f.d. Cluster ion formation was observed in f.d.m.s. but not in l.m.s.

The low volatility and thermally labile nature of internal salts (i.e., zwitterions) limits the use of conventional mass spectrometry for such compounds. However, characterization of zwitterionic compounds has been reported by using secondary-ion mass spectrometry (s.i.m.s.) [1], field-desorption (f.d.) [2, 3], pyrolysis [4] and laser mass spectrometry (l.m.s.) [5]. There are two potential advantages for using laser mass spectrometry (l.m.s.) for internal salt characterization over other mass spectrometric techniques. First, negative-ion spectra can be obtained readily, which is difficult with some other methods. Second, identification of zwitterionic compounds in biological materials [6] can be done with thin sections directly by l.m.s. Thus, it is important to understand the fragmentation behavior, ion-molecule reactions, and related phenomena for this class of compounds.

Quaternary ammoniocarboxylates have been studied by f.d.m.s. by Keough and co-workers [7, 8], who postulated an intermolecular alkyl transfer reaction

0003-2670/84/$03.00

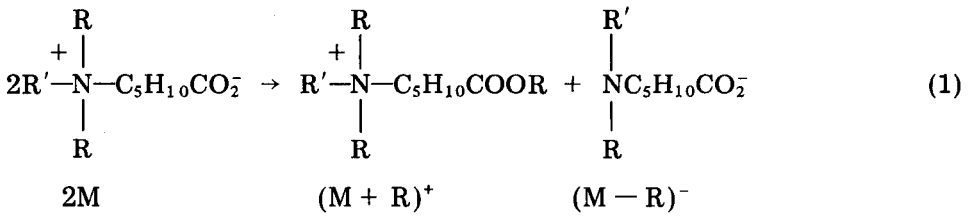

$$2R'\text{—}N^{+}(R)\text{—}C_5H_{10}CO_2^- \rightarrow R'\text{—}N^{+}(R)\text{—}C_5H_{10}COOR + NC_5H_{10}CO_2^- \quad (1)$$

2M $\quad (M + R)^+ \quad (M - R)^-$

The positive-ion f.d. spectrum showed strong evidence for this reaction. However, negative-ion spectra were not reported. Ion-pair production has been observed for a variety of compounds in l.m.s. [9]. Therefore, l.m.s. was used to document the reaction of Eqn. 1. Preliminary results have been reported [5].

Here, a detailed study of a series of internal salts of different structural classes is reported. The specific compounds studied are listed in Table 1. In the quaternary ammoniohexanoates (**1a—1d**), the $-(CH_3)_2N-C_5H_{10}CO_2^-$ moiety is kept constant and the length of one alkyl chain is varied. Hydroxyammonioalkanoates (**2a**, **2b**) are similar to **1a**, except for a hydroxyl group on the alkyl chain between the quaternary nitrogen and the carboxyl group. Sultaines (**3a—3e**) are structurally similar to ammoniohexanoates, but have a sulfonic acid group substituted for the carboxyl group; here again only one alkyl chain is varied. The chain between the sulfonate and quaternary nitrogen groups contains only three methylene groups, i.e., $-(CH_3)_2N-C_3H_6SO_3^-$, compared to five in the ammoniohexanoates.

TABLE 1

Compounds studied	Compounds studied
(1) Quaternary ammoniohexanoates	(3) Sultaines
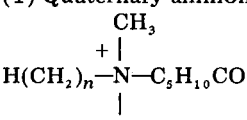	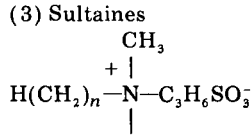
n = 1 8 12 24	n = 1 6 8 10 12
Compound = **1a** **1b** **1c** **1d**	Compound = **3a** **3b** **3c** **3d** **3e**
(2) Hydroxyammonioalkanoates	(4) Deuterated Sultaines
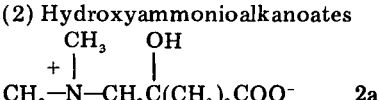 **2a**	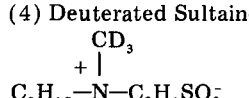 **4**
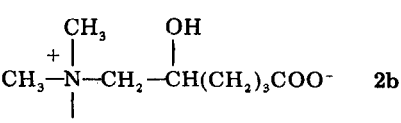 **2b**	

Positive-ion laser mass spectra show ions corresponding to alkyl transfer, such as $(M + R)^+$ and $(M + CH_3)^+$; the corresponding anions $(M-R)^-$ and $(M-CH_3)^-$ are observed in the negative-ion laser mass spectra. Although the LAMMA-1000 and 500 instruments give essentially the same information, there are some significant differences observed between the two with respect to the alkyl transfer reaction.

EXPERIMENTAL

Samples and synthesis of deuterated compounds

Quaternary ammoniohexanoates and hydroxyammonioalkanoates [7] were provided by Dr. T. Keough, Proctor and Gamble Company and were used without further purification. Sultaines were obtained from Professor S. Weber, University of Pittsburgh and run without further purification. Deuterated compounds were synthesized as described below.

Preparation of CD_3I. Red phosphorus (2.5 g) and 10 g of deuterated methanol (CD_3OH) were placed in a 250-ml round-bottom flask and 25.5 g of iodine was added gradually into this mixture. The flask was swirled and cooled with ice-water during addition. The mixture was stirred for 4 h and then refluxed for 2 h. Water (15 ml) was added to the cooled reaction mixture and the mixture was distilled into 100 ml of ice-water. The organic phase was separated and washed with 100 ml of 10% sodium hydroxide followed by water. The product was dried over calcium chloride and distilled.

Preparation of $C_8H_{17}N(CD_3)_2$. Octylamine (12.9 g) was placed in a 25-ml round-bottom flask and 10 g of glycerol was added, followed by 0.2 mol of CD_3I. Anhydrous sodium hydrogencarbonate (0.2 mol) was added and the mixture was refluxed for 48 h. The mixture was then poured into 50 ml of water and the product was extracted with three 10-ml aliquots of ether. The ether phase was dried over sodium hydroxide pellets and distilled under reduced pressure. Water (30 ml) was added to the distillate followed by 0.05 mol of sodium acetate and 0.5 mol of benzoyl chloride to destroy any primary and secondary amines. Then 50 ml of 2 M sodium hydroxide was added to the mixture and the product was extracted with three 10-ml aliquots of ether. The ether phase was dried over sodium hydroxide pellets; the product was verified by n.m.r. Because the deuterated methanol used was not isotopically pure, the electron impact (e.i.) mass spectrum of $(CD_3)_2NC_8H_{17}$ showed the following intensity ratios between the major isotopic peaks: $C_2D_6:C_2D_5H:C_2D_4H_2$ = 13:9:6. This isotopic peak distribution was found to be approximately equal to that obtained by l.m.s. for $C_8H_{17}\overset{+}{N}(CD_3)_2C_3H_6SO_3^-$ (14:9:6).

Preparation of $C_8H_{17}\overset{+}{N}(CD_3)_2C_3H_6SO_3^-$. The $C_8H_{17}N(CD_3)_2$ and 1,3-propane sulfone ($\overline{SO_2CH_2CH_2CH_2O}$) (1:1 mole ratio) were refluxed in toluene for 4 h. The precipitated product was filtered and recrystallized several times from 1:1 acetone/methanol mixture. The crystalline product was dried over calcium chloride. Purity was checked by 300-MHz n.m.r. which showed that

$C_8H_{17}\overset{+}{N}(CD_3)_2C_3H_6SO_3^-$ was 78.3% isotopically pure. The value calculated from l.m.s. is 83.5%; these values agree within experimental error.

Laser mass spectrometry

Laser mass spectra were obtained using both the LAMMA-500 and LAMMA-1000 laser microprobe mass spectrometers (Leybold-Heraeus); both have been described elsewhere [10, 11]. In the case of the LAMMA-500, a frequency quadrupled Q-switched Nd-YAG laser (265 nm, 15-nm pulse width) is focused onto the sample using one of three microscope objectives: 10X, 32X, 100X. In most cases, the 32X objective was used. Ions were accelerated (3 keV) into the drift tube of a time-of-flight mass spectrometer. The output from a 17-stage electron multiplier coupled with a transient recorder functioned as a storage buffer for selected portions of the mass spectrum. The timing sequence was triggered by the laser pulse and in all cases mass spectra were displayed on an oscilloscope; hard-copy was obtained via a strip-chart recorder. Mass assignments were determined by hand measurement of the chart paper. Mass spectra were linear in time giving a mass scale proportional to $(m/z)^{1/2}$. The proportionality constant for these calculations was estimated from sodium and potassium ions. Masses in higher ranges were calculated approximately by using this constant. These approximate masses were used to calculate the exact proportionality constant for the higher mass range, from which the accurate masses were calculated. This procedure was iterated until all masses were assigned with self-consistent values.

In the case of the LAMMA-1000, the ion acceleration voltage was 4 keV and the laser was focused to a spot size about 5 μm in diameter (spot size was approximately 2 μm in the case of the LAMMA-500). Other variables were the same as the LAMMA-500. Ions are extracted at an angle of 180° to the incident beam in the LAMMA-500 (transmission mode) and in the case of the LAMMA-1000, they are extracted at 45° to the incident beam (reflection mode).

To obtain laser mass spectra with the LAMMA-500, samples were dissolved in methanol and evaporated onto a Formvar-filmed copper grid. Methanol solutions of samples were deposited either on a glass slide or on a zinc foil for the LAMMA-1000. Spectra obtained from these two matrices showed no significant differences. The Formvar (polyvinyl formal) films used (LAMMA-500) to support the samples were sufficiently thin that they did not contribute significant peaks to the mass spectra.

RESULTS

Quaternary ammoniohexanoates

Positive-ion spectra. The positive-ion laser mass spectra of quaternary ammoniohexanoates are given in Table 2. Typical spectra have been published previously [5]. As shown by Eqn. 1, the alkyl transfer reaction is evident by the peaks corresponding to $(M + CH_3)^+$ and $(M + R)^+$ (R = long alkyl chain)

TABLE 2

Relative peak intensities of the positive-ion spectra of ammoniohexanoates obtained by the LAMMA-1000 and LAMMA-500

Compound	Instrument	Relative ion intensities[a]						
		$(M + R)^+$[b]	$(M + CH_3)^+$	$(M + H)^+$	$(M + CH_3—CO_2)^+$	$(M + H—CO_2)^+$	$(M + H—C_5H_{11}COOH)^+$	$(M + H—H(CH_2)_nH)^+$
1a	L-1000	—[c]	100(188)	60(174)	7(144)	40(130)	100(58)	00
	L-500	—[c]	94	39	7	46	100	00
1b	L-1000	29(384)	100(286)	26(272)	8(242)	70(228)	14(156)	14(158)
	L-500	00	16	63	16	100	63	11
1c	L-1000	41(496)	100(342)	49(328)	41(298)	100(284)	—[d]	—[d]
	L-500	00	45	74	16	100	16(212)	1.8(158)
1d	L-1000	10(832)	58(510)	58(496)	28(466)	100(452)	—[d]	—[d]
	L-500	00	13	41	4	100	6(380)	49(158)

[a]Masses are given in parentheses; base peak = 100. [b]R = long alkyl chain. [c]Equivalent to $(M + CH_3)$ for compound 1a. [d]Spectra were not obtained in these ranges.

in the positive ion l.m.s. of all ammoniohexanoates. Ions corresponding to $(M + CH_3)^+$ dominate the higher mass range and are more abundant than $(M + H)^+$. The ions which arise from long alkyl chain transfer $(M + R)^+$, are not as intense as $(M + CH_3)^+$.

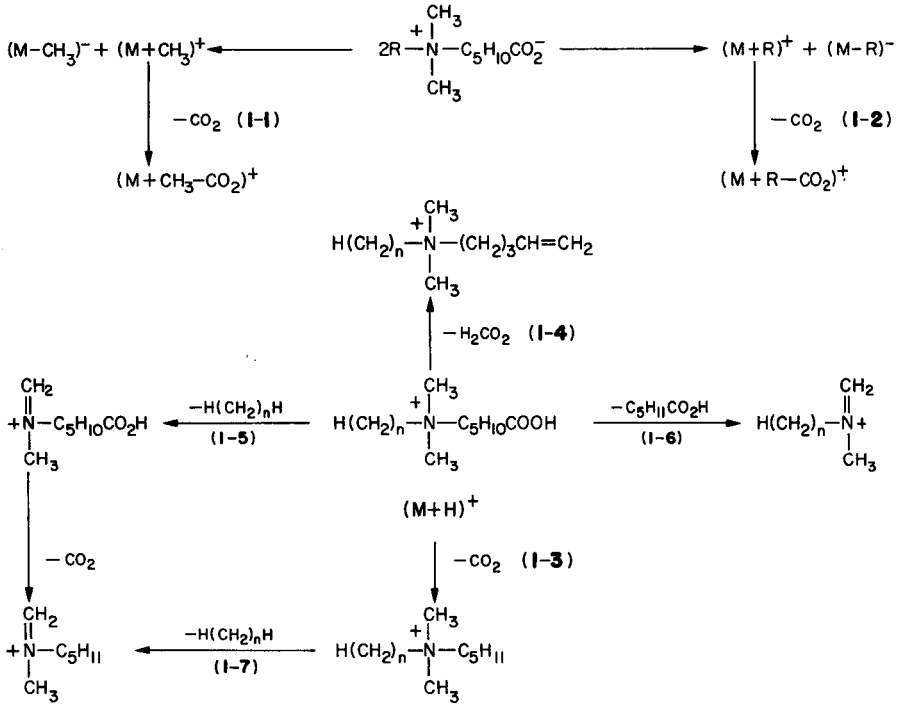

Scheme 1.

Scheme 1 shows the general fragmentation pattern for the ammoniohexanoates. Common fragments in the positive-ion spectra correspond to loss of CO_2 and H_2CO_2 from $(M + H)^+$ and loss of CO_2 from both $(M + CH_3)^+$ and $(M + R)^+$ (**1—1**, **1—4**). The peak at $m/z = 114$ found in all compounds can be rationalized as $+N(CH_2)—C_5H_{11}$, arising from loss of RH from $(M + H—CO_2)^+$ (**1—7**). Ions corresponding to loss of CH_4 from $(M + H—CO_2)^+$ are also seen for some examples. Loss of $C_5H_{10}COOH$ from $(M + H)^+$ produces $+N(CH_2)—R$ ions for all ammoniohexanoates (**1—6**). Loss of the long alkyl chain RH from $(M + H)^+$ leads to $+N(CH_2)—C_5H_{10}COOH$ for all ammoniohexanoates (**1—5**). The

peak at m/z = 553 in the positive-ion spectrum of compound **1c** can be rationalized as $(2M + H—C_4H_9COOH)^+$. No other compound showed this kind of fragmentation at any laser power. Lower mass ranges of the positive-ion laser mass spectra are very simple; only sodium (m/z = 23) and potassium (m/z = 39) from impurities are observed.

Negative-ion spectra. Figure 1 shows the negative ion spectra of the ammoniohexanoates; fragmentation is detailed in Scheme 2. The highest mass peak detected in the negative-ion l.m.s. of any example studied corresponds to $(M—CH_3)^-$ as seen in Fig. 1. The $(M—R)^-$ ion which corresponds to $N(CH_3)_2C_5H_{10}CO_2^-$ (m/z = 158) (**2—1**) was detected in all cases. These results along with the positive-ion spectra provide strong evidence for an intramolecular alkyl transfer reaction as shown in Eqn. 1. The lower mass ranges of the negative-ion spectra ($m/z < 158$) of the ammoniohexanoates are nearly identical because most ions correspond to fragments of m/z = 158 (Scheme 2).

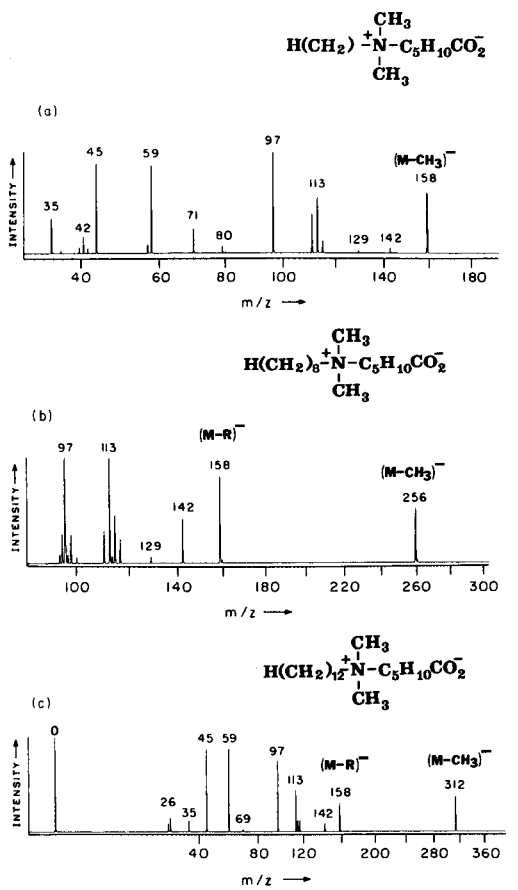

Fig. 1. Negative-ion l.m.s. of $H(CH_2)_n—\overset{+}{N}(CH_3)_2C_5H_{10}CO_2^-$: (a) n = 1; (b) n = 8; (c) n = 12. Laser power density $\approx 5 \times 10^8$ W cm^{-2}.

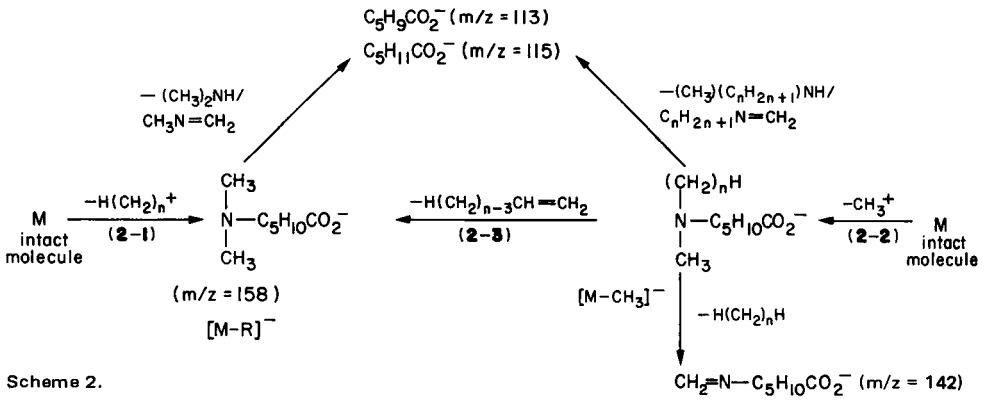

Scheme 2.

Lower mass ranges of the negative-ion spectra show CN^- (m/z = 26) and OCN^- (m/z = 42) which are commonly found in l.m.s. of compounds containing nitrogen and oxygen; other peaks correspond to $CH_3CH_2^-$ (m/z = 59) and $CH_2{=}CHCO_2^-$ (m/z = 71).

Contrast of the two instruments. Table 2 shows the positive l.m.s. peaks and their relative intensities obtained from the LAMMA-500 and LAMMA-1000 instruments. No ions corresponding to long-chain alkyl transfer were observed at any laser power with the LAMMA-500. However, all of the other ions detected with the LAMMA-1000 were detected by the LAMMA-500. Generally, the higher mass range in the LAMMA-500 is dominated by ions corresponding to $(M + H{-}CO_2)^+$, which are more abundant than $(M + H)^+$; the latter are more intense than $(M + CH_3)^+$. In contrast, spectra obtained by the LAMMA-1000 are dominated by ions corresponding to $(M + CH_3)^+$ which are generally more abundant than ions such as $(M + R)^+$, $(M + H{-}CO_2)^+$ and $(M + H)^+$. Here again, ions corresponding to $(M + H{-}CO_2)^+$ are more intense than the quasimolecular ions $(M + H)^+$. Thus the major difference between the results obtained by the two instruments is the extent of the alkyl transfer reaction. In contrast, no significant differences were observed in the negative-ion spectra obtained by the two instruments.

Effect of laser power. Figure 2 shows the positive-ion l.m.s. of compound **1c** as a function of laser power obtained with the LAMMA-1000 and Fig. 3 shows the intensity variation of some ions as a function of laser power. At threshold energy (0.03 μJ) only fragment ions such as $CH_2{=}\overset{\overset{CH_3}{|}}{\underset{\underset{CH_3}{|}}{N^+}}$ (D) and $C_{12}H_{25}{-}\overset{\overset{CH_2}{||}}{\underset{\underset{CH_3}{|}}{N^+}}$ (E) are observed (Fig. 2a). At slightly higher laser powers (0.08—0.09 μJ) (Fig. 2c), the quasimolecular ion $(M + H)^+$ (G) appears. As the laser power is increased (0.14 μJ; Fig. 2d), a peak corresponding to

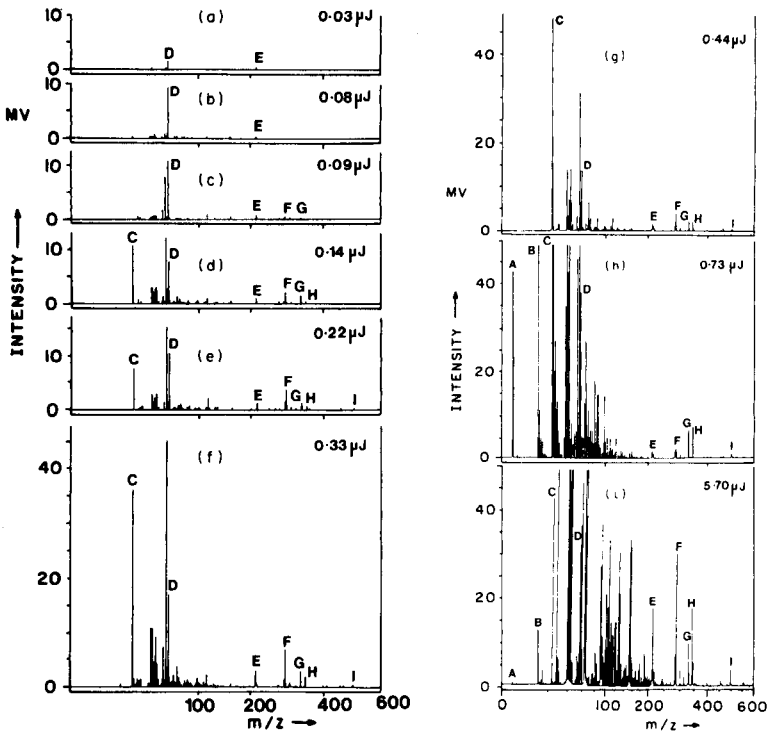

Fig. 2. Positive-ion l.m.s. of $C_{12}H_{25}N(CH_3)_2C_5H_{10}CO_2^-$ as a function of laser power (W cm^{-2}): (a) 7.5 × 10^6; (b) 2.0 × 10^7; (c) 2.3 × 10^7; (d) 3.5 × 10^7; (e) 5.5 × 10^7; (f) 8.3 × 10^7; (g) 1.1 × 10^8; (h) 1.8 × 10^8; (i) 1.4 × 10^9. Peaks: (A) H^+; (B) C^+; (C) Na^+; (D) $CH_2{=}\overset{+}{N}(CH_3)_2$; (E) $CH_2{=}\overset{+}{N}(CH_3)C_{12}H_{25}$; (F) $(M + H{-}CO_2)^+$; (G) $(M + H)^+$; (H) $(H + CH_3)^+$; (I) $(M + R)^+$.

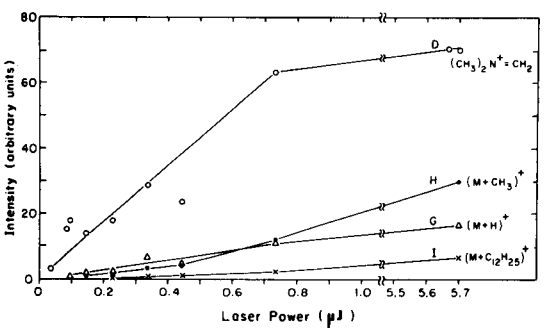

Fig. 3. Intensity variation of ions from $C_{12}H_{25}\overset{+}{N}(CH_3)_2C_5H_{10}CO_2^-$ as a function of laser power (W cm^{-2}): (○) $CH_2{=}\overset{+}{N}(CH_3)_2$; (●) $(M + CH_3)^+$; (△) $(M + H)^+$; (×) $(M + C_{12}H_{25})^+$.

methyl group transfer $(M + CH_3)^+$ (H) is observed. At 0.14 μJ, Na^+ ions (C) are detected; these were detected at all higher powers but were absent at all lower powers. Thus, the threshold energy for sodium ions is 0.14 μJ under the conditions of this experiment. Ions corresponding to long alkyl chain transfer $(M + C_{12}H_{25})^+$ (I) are detected with further increases in laser power (0.22 μJ, Fig. 2e). The intensities of all peaks increase with increasing laser power. Up to a power level of 0.33 μJ, $(M + H)^+$ (G) is more intense than $(M + CH_3)^+$ (H) or $(M + C_{12}H_{25})^+$ (I). The intensity of $(M + H)^+$ (G) becomes nearly equal to $(M + CH_3)^+$ (H) around a laser power 0.44 μJ (Fig. 2g). At higher laser powers (Figs. 2h, 2i) the $(M + CH_3)^+$ ion dominates the higher mass range and the intensity of $(M + C_{12}H_{25})^+$ increases. Intense peaks are observed for protons (m/z = 1) (A) and carbon ions (m/z = 12) (B) at higher laser powers, in addition to the other fragment ions.

Figure 4 shows the positive-ion l.m.s. of compound 1c (LAMMA-1000) mixed with a small amount of *p*-toluenesulfonic acid (*p*-TSA), run as a function of laser power. The striking observation here is the nearly complete absence of most fragment ions at $m/z > 100$. Only the quasimolecular ion $(M + H)^+$ (G) is detected at relatively high laser powers.

This result should be compared with the spectrum of Fig. 2 at comparable laser powers with which one can clearly observe the alkyl transfer reaction. As the laser power is increased (1.22, 2.84 μJ), ions corresponding to methyl

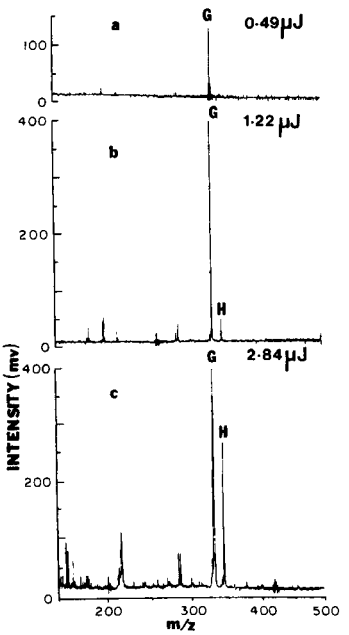

Fig. 4. Positive-ion l.m.s. of a $C_{12}H_{25}N^+(CH_3)_2C_5H_{10}CO_2^-$ and *p*-toluenesulfonic acid (1:1) mixture as a function of laser power (W cm^{-2}): (a) 1.2×10^8; (b) 3.0×10^8; (c) 7.1×10^8.

group transfer $(M + CH_3)^+$ appear (H). However, the quasimolecular ion $(M + H)^+$ is still much more intense than $(M + CH_3)^+$ and fragmentation is still minimal (particularly given the high laser power used). Thus, addition of a small amount of *p*-TSA changes the chemical environment by protonating the intact molecule. Mixtures of the salt and *p*-TSA were studied several times and the results were found to be the same as described above in all cases.

Hydroxyammoniohexanoates

The positive- and negative-ion l.m.s. spectra of one hydroxyammoniohexanoate are shown in Fig. 5. Hydroxyammonioalkanoates behave similarly to the ammoniohexanoates. However, in all spectra, the quasimolecular ion $(M + H)^+$ is more intense than $(M + CH_3)^+$. Loss of CO_2 and H_2CO_2 from the quasimolecular ion $(M + H)^+$ and loss of CO_2 from $(M + CH_3)^+$ are also seen for the hydroxy compounds. Ions corresponding to m/z = 102, 84, 74, 72 and 58 are detected for both compounds (**2a, 2b**) and can be rationalized as

$(CH_3)_3\overset{+}{N}CH{=}CH(OH)$, $(CH_3)_3N^+C{\equiv}CH$, $(CH_3)_4N^+$, $(CH_3)_2\overset{+}{N}(H)-CH{=}CH_2$ and $(CH_3)_2\overset{+}{N}{=}CH_2$, respectively. Sodium ($m/z$ = 23), potassium (m/z = 39) and $CH_2{=}\overset{+}{N}{=}CH_2$ (m/z = 42) are the only ions detected in the lower mass range.

The negative-ion laser mass spectra of an hydroxyammonioalkanoate is shown in Fig. 5(b). Alkyl transfer is confirmed by the $(M{-}CH_3)^-$ ions in the negative-ion spectra. Ions corresponding to loss of $(CH_3)_3N$ from $(M{-}CH_3)^-$

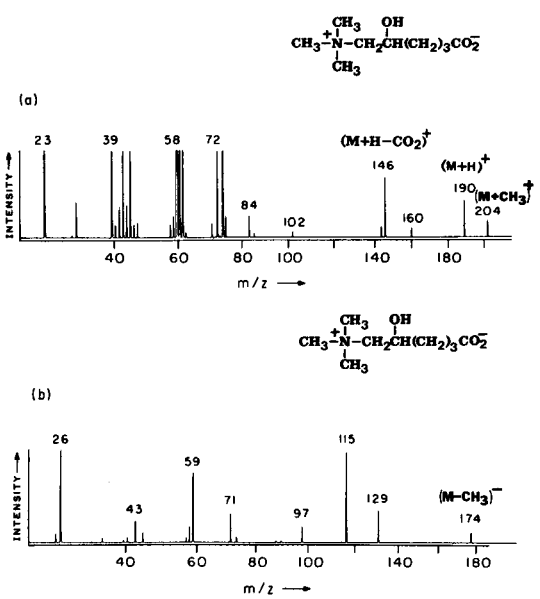

Fig. 5. L.m.s. of $(CH_3)_3\overset{+}{N}CH_2CH(OH)(CH_2)_3CO_2^-$: (a) positive-ion spectrum; (b) negative-ion spectrum. Laser power density $\approx 5 \times 10^8$ W cm^{-2}.

dominate the negative-ion spectra of both hydroxy compounds (**2a, 2b**) (m/z = 115 in Fig. 5b). Fragmentation patterns are very similar to those described in Scheme 2. Ions at $m/z < 129$ arise from the long alkyl chain containing the carboxyl groups. Thus, the ions at m/z = 129, 115, and 97 can be rationalized as $CH_2{=}C(OH)(CH_2)_3CO_2^-$, $CH(OH){=}CH(CH_2)_2CO_2^-$ and $CH{\equiv}C(CH_2)_2CO_2^-$. Other ions generally observed in the lower mass range correspond to $CH_2{=}CHCO_2^-$ (m/z = 71), $CH_3CO_2^-$ (m/z = 59) and HCO_2^- (m/z = 45).

Sultaines

Positive-ion spectra. The alkyl transfer reaction has been observed for a series of zwitterionic compounds known as sultaines (see Table 1 for structures). The positive-ion laser mass spectra of the sultaines are summarized in Table 3; some positive-ion spectra were published earlier [5]. Alkyl transfer is evidenced by ions corresponding to $(M + CH_3)^+$ and $(M + R)^+$. The spectra are dominated by the quasimolecular ion $(M + H)^+$ in the higher mass range. Thus, quasimolecular ions are more intense than ions such as $(M + CH_3)^+$, $(M + R)^+$ and $(M + H{-}SO_3)^+$. Neutral losses correspond to the loss of SO_3 and H_2SO_3 from $(M + H)^+$ and SO_3 from $(M + CH_3)^+$, similar to the loss of CO_2 and H_2CO_2 from the ammoniohexanoates. In addition, an ion corresponding to $(M + H{-}SO_2)^+$ was detected for all compounds. Intense peaks are observed for ions corresponding to 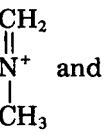 and 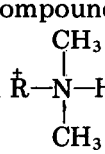 , resulting from loss of $C_3H_7SO_3H$ and $C_3H_5SO_3H$, respectively, from $(M + H)^+$. Loss of RH and (R—H) from $(M + H)^+$ leads to ions such as 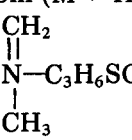 (m/z = 166) and 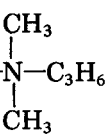 (m/z = 168). Thus, the positive-ion l.m.s. fragmentation patterns of the sultaines are very similar to those described for the carboxylate analogs in Scheme 1.

Negative-ion spectra. The negative ion laser mass spectra of some sultaines are shown in Fig. 6. Ions corresponding to $(M{-}CH_3)^-$ and $(M{-}R)^-$ are observed in all spectra; these along with positive ion spectra provide evidence for bimolecular reaction. The fragmentation patterns of the negative-ion l.m.s. of sultaines are very similar to the ammoniohexanoates (Scheme 2). Ions in the lower mass ranges ($m/z < 166$) are nearly identical and can be interpreted as fragments of $(CH_3)_2N{-}C_3H_6SO_3^-$ (m/z = 166) which is $(M - R)^-$. Thus, the peak at m/z = 150 can be rationalized as $CH_2{=}N{-}C_3H_6SO_3^-$ which arises by loss of CH_4 from $(M{-}R)^-$. Other common ions found in the lower mass ranges

TABLE 3

Relative peak intensities of the positive-ion spectra of sultaines

Compound	Instrument	Relative ion intensities[a]						
		$(M + R)^{+}$[b]	$(M + CH_3)^{+}$	$(M + H)^{+}$	$(M + CH_3{-}SO_3)^{+}$	$(M + H{-}SO_3)^{+}$	$(M + H{-}C_3H_7SO_3H)^{+}$	$(M + H{-}H(CH_2)_nH)^{+}$
2a	L-1000	—[c]	41(196)	75(182)	53(116)	102(100)	—[d]	4(166)
	L-500	—[e]	—	—	—		—	—
2b	L-1000	5(336)	72(266)	100(252)	23(186)	50(172)	—[d]	—[d]
	L-500	00	24	100	44	88	—[d]	—[d]
2c	L-1000	2(392)	44(294)	100(280)	15(214)	37(200)	—[d]	—[d]
	L-500	00	36	99	15	38	100(156)	13(166)
2d	L-1000	5(448)	55(322)	91(308)	9(242)	19(228)	100(184)	—[d]
	L-500	00	18	100	13	38	86	19(166)
2e	L-1000	5(504)	47(350)	100(336)	10(270)	38(256)	61(212)	—[d]
	L-500	00	6	100	23	46	58	50(166)

[a]Masses are given in parentheses; base peak = 100. [b]R = long alkyl chain. [c]$(M + R)^{+}$ is equivalent to $(M + CH_3)^{+}$. [d]Spectra were not obtained in these ranges. [e]No good spectrum was obtained with the LAMMA-500 instrument.

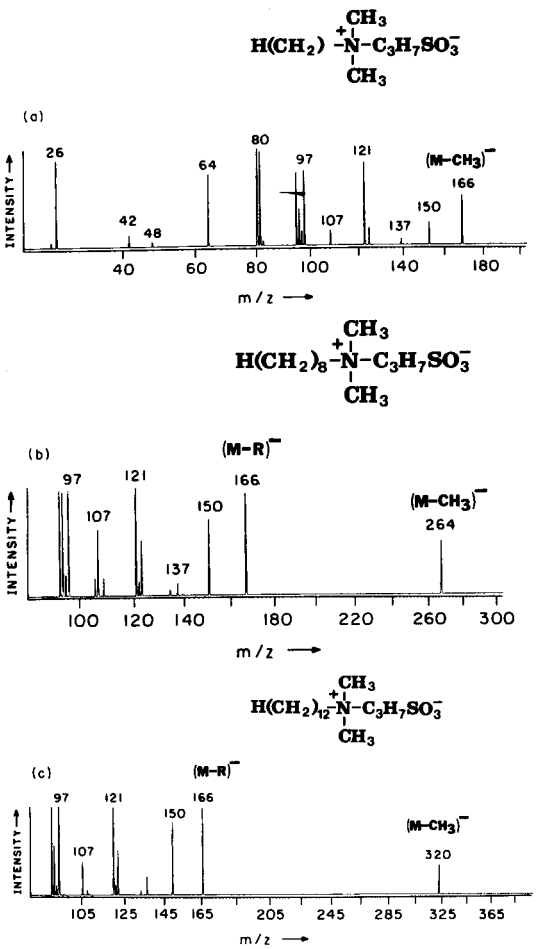

Fig. 6. Negative-ion l.m.s. of $H(CH_2)_n\overset{+}{N}(CH_3)_2C_3H_6SO_3^-$: (a) $n = 1$; (b) $n = 8$; (c) $n = 12$. Laser power density $\approx 5 \times 10^8$ W cm^{-2}.

can be rationalized as $C_3H_7SO_3^-$ (m/z = 123), $C_3H_5SO_3^-$ (m/z = 121), $CH_2{=}CHSO_3^-$ (m/z = 107) and $CH_3SO_3^-$ (m/z = 95).

Contrast of the two instruments. Table 3 also shows the positive-ion laser mass spectra of the sultaines observed with the LAMMA-500. No long alkyl chain transfer was observed and the extent of methyl group transfer is less than that observed with the LAMMA-1000. The LAMMA-500 spectra are dominated by the quasimolecular ions $(M + H)^+$, as in the case of the LAMMA-1000. No significant differences were observed for the other fragmentation processes in the positive-ion spectra. Negative-ion laser mass spectra of sultaines obtained by both the LAMMA-500 and LAMMA-1000 are nearly the same with little variation in intensities.

Deuterated sultaines. Figure 7 shows the laser mass spectra of the deuterated compound, 4 (Table 1). Fragment ions along with the quasimolecular ion $(M + H)^+$ and the ion corresponding to methyl group transfer $(M + CD_3)^+$ are centered at the clusters of peaks. Clusters are observed because the deuterated methanol used to prepare compound 4 was not isotopically pure as discussed in the experimental section. The isotopic distribution calculated from Fig. 7 agrees with that measured for the deuterated methanol used. Thus, the possibility of hydrogen scrambling in these experiments can be excluded. The peak at $m/z = 303$ in the positive-ion spectrum corresponds to $(M + CD_3)^+$; peaks at $m/z = 206$ and 204 can be rationalized as $[(M + H)-SO_3]^+$ and $[M + H-H_2SO_3]^+$. The ion centered at $m/z = 161$ arises from loss of the alkyl chain $D(CH_2)_3SO_3H$ from $(M + H)^+$. Loss of SO_2 and SO_3 from $(M + H)^+$ and $(M + CD_3)^+$, respectively, also are detected ($m/z = 222$ and 223).

The highest mass ion detected in the negative-ion spectrum corresponds to $(M-CD_3)^-$ ($m/z = 267$). Loss of the long alkyl chain leads to the ion $(CD_3)_2N-C_3H_6SO_3^-$ ($m/z = 172$). The peak centered at $m/z = 152$ can be rationalized as $[M-C_8H_{17}-CD_4]^-$, which corresponds to $CD_2=N-C_3H_6SO_3^-$. Ions

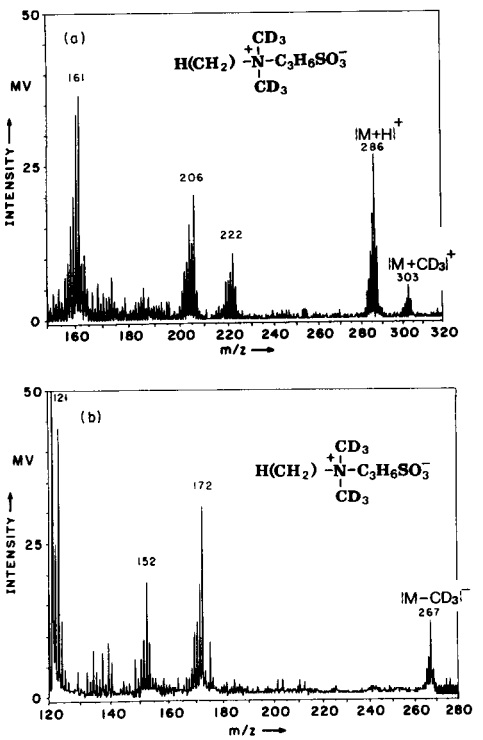

Fig. 7. L.m.s. of $C_8H_{17}\overset{+}{N}(CD_3)_2C_3H_6SO_3^-$ (compound 4): (a) positive-ion spectrum; (b) negative-ion spectrum.

corresponding to $CH_2{=}CH{-}CH_2SO_3^-$ (m/z = 121), $CH_2{=}CHSO_3^-$ (m/z = 107) and HSO_4^- (m/z = 97) also are detected.

Field-desorption spectra. The important ions found in the positive-ion f.d. spectra of some sultaines are presented in Table 4. Cluster ions $(nM + H)^+$ (n = 1, 2, 3) are evident in these spectra. Neutral losses such as SO_3 and H_2SO_3 from $(nM + H)^+$ (where n = 1, 2, 3) are observed. Intense peaks are also observed for ions corresponding to loss of $CH_2{=}CHSO_3H$ or $CH_3CH_2SO_3H$, from $(nM + H)^+$. Peaks corresponding to the loss of long alkyl chains from $(M + H)^+$ are very weak or absent in the f.d. spectra.

DISCUSSION

Intermolecular alkyl transfer reaction

All of the internal salts studied show ions corresponding to $(M + CH_3)^+$ and $(M + R)^+$ in positive-ion l.m.s. and $(M{-}CH_3)^-$ and $(M{-}R)^-$ in negative-ion l.m.s. Thus, both positive- and negative-ion spectra provide conclusive evidence for alkyl transfer in the l.m.s. of internal salts. Ions corresponding to methyl group transfer appear at m/z = 303 for $C_8H_{17}\overset{+}{N}(CD_3)_2C_3H_6SO_3^-$ (compound 4), which corresponds to $(M + CD_3)^+$. If the methyl group involved in this reaction came from other than a $-CD_3$ group, an intense peak would appear at m/z = 300 corresponding to $(M + CH_3)^+$. Such a peak is not observed. The negative-ion l.m.s. of compound 4 shows that the highest mass ion detected corresponds to $(M{-}CD_3)^-$. These results provide conclusive evidence that intermolecular methyl transfer involves only the methyl groups attached to nitrogen and not the alkyl chain.

Although both positive- and negative-ion l.m.s. give complementary information and conclusive evidence for the alkyl transfer reaction, the mechanism of alkyl transfer is not obvious. One possibility, referred to as "pair-production" by analogy with proton transfer reactions in amino acids [9] is

$$2MA \xrightarrow{h\nu} (MA + A)^+ + M^- \qquad (2)$$

TABLE 4

Field-desorption mass spectra of sultaines

$C_{12}H_{25}{-}\overset{+}{N}(CH_3)_2{-}C_3H_6SO_3^-$ (30-mA emitter current)

$C_8H_{17}{-}\overset{+}{N}(CH_3)_2{-}C_3H_6SO_3^-$ (25 mA emitter current)

Fragments	Relative intensities			Fragments	Relative intensities		
	n = 1	2	3		n = 1	2	3
$[nM + H]^-$	100	41	31	$[nM + H]^-$	88	17	26
$[(nM + H){-}SO_3]^+$	25	46	13	$[(nM + H){-}SO_3]^+$	87	100	21
$[(nM + H){-}H_2SO_3]^+$	41	46	17	$[(nM + H){-}H_2SO_3]^+$	100	100	28
$[(nM + H){-}CH_2{=}CHSO_3H]^+$	74	100	42	$[(nM + H){-}CH_2{=}CHSO_3H]^+$	100	100	100
$CH_2{=}CHCH_2SO_3H_2^+$	78	—	—	$CH_2{=}CHCH_2SO_3H_2^+$	15	—	—

where MA is the intact zwitterion. This corresponds to methyl (or alkyl) transfer from one molecule to another giving rise to $(M + CH_3)^+$ and $(M—CH_3)^-$ ions directly in one step. However, production of CH_3^+ and subsequent attack on an internal salt molecule cannot be ruled out on the basis of these experiments. For example

$$MA \xrightarrow{h\nu} M^-(g) + A^+(g) \xrightarrow{MA(g)} MA_2^+ + M^- \qquad (3)$$

where MA = intact molecule.

The fact that there is a threshold for formation of $(M + CH_3)^+$ and $(M—CH_3)^-$ ions is consistent with either mechanism. The decrease in $(M + CH_3)^+$ formation by addition of *p*-toluenesulfonic acid tends to support pair production (Eqn. 2) as will be discussed below.

The dissociation energy for the $\geqslant N^+—C$ bond is higher when C is a methyl group than when it is a long alkyl chain [12, 13]. This is consistent with the results for both positive- and negative-ion l.m.s. of internal salts. No ions corresponding to $(M + H—CH_4)^+$ and $(M—CH_3—CH_4)^-$ were observed in the positive- and negative-ion l.m.s. respectively; in contrast, ions corresponding to $(M + H—RH)^+$ and $(M—CH_3—RH)^-$ were observed. Further, ions corresponding to $(M + H—C_3H_7SO_3H)^+$ or $(M + H—C_5H_{11}COOH)^+$ are more intense than $(M + H—RH)^+$ in the positive-ion spectra of both sultaines and ammoniohexanoates (Tables 2 and 3). Thus, the bond dissociation energies for the C—N bond in these compounds decrease in the order $\geqslant N^+—CH_3 > \geqslant N^+—R > \geqslant N^+—C_3H_6SO_3H$, where R is a long alkyl chain.

Equation 3 represents a two-step reaction; the first step involves dissociation of the $\geqslant N^+—R_1$ bond where $R_1 = CH_3$ or R. Given that $\geqslant N^+—R$ cleavage is easier than $\geqslant N^+—CH_3$, a fairly intense peak would be expected for $(M + R)^+$ ions, if process 3 is operative. However, the intensity of $(M + R)^+$ ions is smaller than $(M + CH_3)^+$ in the l.m.s. for all zwitterions (Table 1). Thus, process 3 is an unlikely mechanism for alkyl transfer. This is further supported by the absence of peaks corresponding to CH_3^+ and R^+ in the l.m.s. of zwitterions.

Further, if alkyl transfer takes place as described by Eqn. 3, one would expect long alkyl chain transfer to occur at laser powers lower than methyl group transfer since the $\geqslant N^+—R$ bond dissociation energy is less than that of $\geqslant N^+—CH_3$. However, the results from the effect of laser power (Fig. 3) show that methyl group transfer takes place at lower laser powers (0.14 μJ, Fig. 2d) than long alkyl transfer (0.22 μJ, Fig. 2e). Similar results were obtained for the *p*-TSA/sample mixture, where only methyl group transfer is observed Fig. 4). Thus, the above results indicate the methyl group transfer is favored over long alkyl chain transfer, again suggesting that process 3 is not operative. Thus, the negative evidence for process 3 tends to support mechanism 2.

If process 2 is operative, proper orientation of the molecules will be important for alkyl transfer. Because $(CH_3)_3\overset{+}{N}C_5H_{10}CO_2^-$ compound (**1a**) and $(CH_3)_3\overset{+}{N}C_3H_6SO_3^-$ compound (**3a**) are symmetrical with respect to orientation

of methyl groups around nitrogen, the second molecule can approach for methyl group transfer from any direction. The alkyl transfer would be expected to be greater for compounds **1a** and **3a**. In fact, very strong peaks corresponding to $(M + CH_3)^+$ are observed for both of these compounds. Thus, the extent of methyl group transfer is higher for compounds **1a** and **3a**, than when a longer alkyl group is attached to the nitrogen atom.

The probability for methyl group transfer is also higher than for transfer of the long alkyl group when both groups are present in one molecule. Each compound other than **1a** and **3a** has two methyl groups and one longer alkyl chain. Based only on the number of alkyl groups, the statistical ratio of $(M + CH_3)^+:(M + R)^+$ expected would be 2:1. Ratios calculated from the spectra are always found to be higher than 2:1; measured values are in the range 2.3—4.2, meaning that methyl group transfer is preferred.

Preference for methyl group transfer may be due to one of the following reasons. Consider the details of process 2 as shown in Scheme 3. The transition state [P] may lead either to alkyl transfer (path a) or to decomposition (path b). Thus, there will be competition between alkyl transfer and fragmentation from the transition state. It has been shown already that the $\geqslant N^+—R$ bond breaks more readily than $\geqslant N^+—CH_3$. In the transition state [P], the $\geqslant N^+—R$ bond is even weaker, leading to decomposition by path (b). This decomposition may take place to a greater extent in the case of $\geqslant N^+—R$, compared to $\geqslant N^+—CH_3$, for two reasons. First, the bond dissociation energy of $\geqslant N^+—R$ is less than that of $\geqslant N^+—CH_3$. Second, long alkyl chains are much bulkier than methyl group (steric hindrance) and thus the transfer reaction will be slower. The above will be the deciding factor in determining the $(M + CH_3)^+/(M + R)^+$ ratio and hence the preferential methyl transfer reaction.

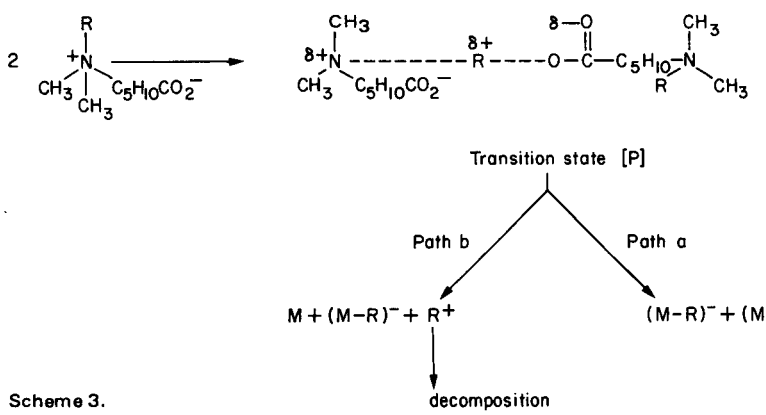

Scheme 3.

In contrast to the above observation $[(M + CH_3)^+/(M + R)^+ > 2]$, the intensity of ions corresponding to $(M—R)^-$ was always found to be higher than that of $(M—CH_3)^-$. This indicates that some $(M—R)^-$ ions are produced

by a process other than alkyl transfer. In fact, $(M-R)^-$ ions can be produced by several processes as outlined in Scheme 2: alkyl transfer, direct loss of R^+ or from $(M-CH_3)^-$. According to Scheme 3, more $(M-R)^-$ ions should be produced than $(M + R)^+$ ions, because some of the molecules in the transition state P, undergo decomposition leading to $(M-R)^-$ ions (path b). Because the bond dissociation energy is higher for $\geqslant N^+-CH_3$ than for $\geqslant N^+-R$, the intensity of $(M-R)^-$ (Scheme 2—1) ions produced by loss of R^+ will be higher than from $(M-CH_3)^-$ (Scheme 2—2). Some $(M-CH_3)^-$ ions may decompose to produce $(M-R)^-$ ions as shown in Scheme 4A. Evidence for this type of fragmentation is obtained from the positive ion spectra, where the presence of ions such as $C_{12}H_{25}-\overset{\overset{CH_2}{\|}}{\underset{\underset{CH_3}{|}}{N^+}}$(E) and $(CH_3)_2\dot{N}=CH_2$(D) at threshold energy, is

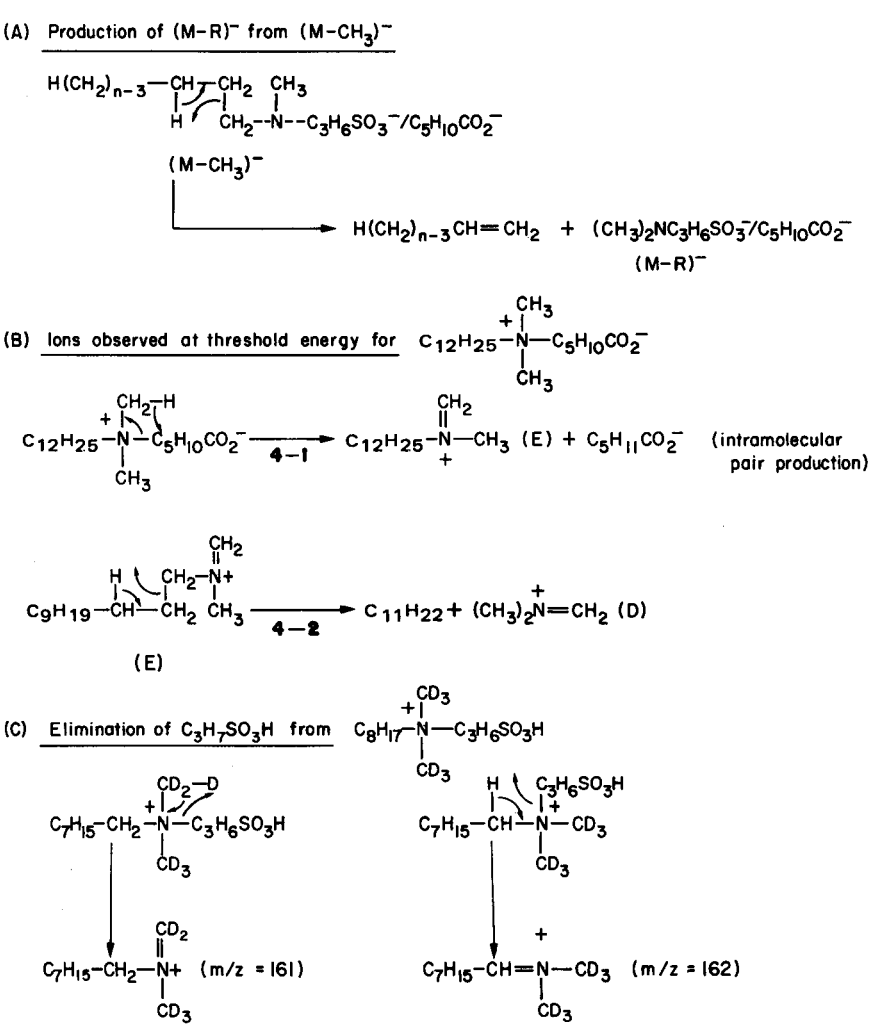

Scheme 4.

explained by a similar type of fragmentation (Scheme 4B). The above discussion indicates that the intensity of $(M-R)^-$ should be higher than that of $(M-CH_3)^-$, in agreement with the observed results.

The results obtained for hydroxyammonioalkanoates (compounds **2a** and **2b**) are different with respect to the alkyl transfer reaction. Though the hydroxyammonioalkanoates **2a** and **2b** are symmetrical with respect to orientation of methyl groups around nitrogen, the methyl transfer reaction takes place only to a small extent. The most probable explanation involves intramolecular hydrogen bonding (**5**) between the hydroxy and carboxylate groups. The reactivity of the carboxylate group will be reduced by the diffuse character of its negative charge caused by hydrogen bonding. Thus, the carboxyl basicity will be effectively reduced.

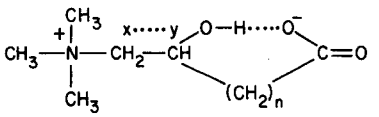

Also, there is an inductive effect on the bond marked x····y in **5**, because this bond is influenced both by the quaternary nitrogen and the hydroxyl group. Thus, cleavage of the x—y bond should be easier in the hydroxy compounds. The negative-ion spectra of both hydroxy compounds are dominated by an ion which corresponds to cleavage of the x—y bond as shown in process 4

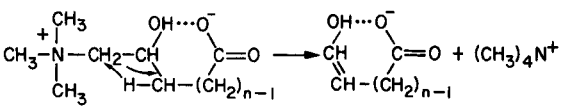

(4)

The positive-ion spectra of the hydroxy compounds also show a strong peak from $(CH_3)_4N^+$ ions ($m/z = 74$) which also arise from x—y bond cleavage. The absence of an ion corresponding to $(CH_3)_4N^+$ at $m/z = 74$ for $(CH_3)_4N^+ \cdot C_5H_{10}CO_2^-$ strongly supports this idea that the ion-pair produced by process 4 is characteristic of hydroxy compounds. Process 4 corresponds to an interesting mechanism, intramolecular pair-production. This is the first known example of this type of process in l.m.s.

Effect of laser power

At very low laser powers, neither the quasimolecular ions $(M + H)^+$ nor ions corresponding to methyl group transfer are observed (Fig. 2). However, the fragment ions $C_{12}H_{25}-\overset{\overset{CH_2}{\|}}{\underset{\underset{CH_3}{|}}{N}} + (E)$ and $(CH_3)_2\overset{+}{N}=CH_2(D)$ are seen. Figure 3 shows intensity variations of some ions as a function of laser power. Ions corresponding to $CH_2=\overset{+}{N}(CH_3)_2$ (Fig. 3) are detected at threshold energy and their intensity increases with laser power relative to $(M + H)^+$. The quasi-

molecular ions $(M + H)^+$ appear at laser powers higher than threshold energy (Fig. 3). Ions corresponding to the alkyl transfer reaction are observed at relatively higher laser powers (Fig. 3). The intensity of $(M + CH_3)^+$ is less than that of $(M + H)^+$ at low laser powers and, in contrast, the intensity of $(M + CH_3)^+$ becomes higher than that of $(M + H)^+$ at high laser powers (Fig. 3). This clearly indicates that the production and relative intensity of ions depends on laser power. Ions observed at threshold energy such as $(CH_3)_2\overset{+}{N}=CH_2$(D) and $C_{12}H_{25}-\underset{\displaystyle CH_3}{\overset{\displaystyle CH_2}{\overset{\|}{\underset{|}{N}}}}^+$ (E) arise from internal hydrogen transfer as shown in Scheme 4B. Detection of $C_5H_{11}CO_2^-$ (m/z = 115) and $C_5H_9CO_2^-$ (m/z = 113) at threshold energy in the negative-ion l.m.s. supports the above mechanism. The overall energy involved in step 1 of Scheme 4B will depend on the bond dissociation energy for the C—N σ-bond and the formation energy for the C—N π-bond. The second step involves dissociation of a C—C σ-bond and formation of C—C π-bond. These reactions are favored at low laser powers because the overall energy requirements are low (C—N $\approx$ 79.0 kcal mol^{-1}, C=N $\approx$ 154 kcal mol^{-1}, C—C $\approx$ 82.6 kcal mol^{-1}, C=C $\approx$ 145.8 kcal mol^{-1}). The approximate energy involved in step 4—1 in Scheme 4B is about 4 kcal mol^{-1} (0.17 eV) and in step 4—2 is about 19 kcal mol^{-1} (0.82 eV).

Quasimolecular ions, $(M + H)^+$, are not observed at threshold energy. Protonation probably takes place as follows:

$$RCH\ (\text{intact molecule}) + RCOO^-\ (\text{intact molecule}) \rightarrow RC^- + RCOOH \qquad (5)$$

where RCH and $RCOO^-$ represent the alkyl and carboxyl parts of the molecule respectively. Process 5 can be considered formally by the following sequence

$RCH \rightarrow RC\cdot + H\cdot$	D(C—H) = bond dissociation energy for C—H
$RC\cdot + e^- \rightarrow RC^-$	EA(RC·) = electron affinity of the alkyl radical RC·
$H\cdot \rightarrow e^- + H^+$	IP(H) = ionization potential of the hydrogen atom
$RCOO^- + H^+ \rightarrow RCOOH$	E($RCOO^-$, H^+) = energy associated with the formation O—H bond

Thus the overall energy ΔE involved in process 5 will be

$$\Delta E = D(\text{C—H})^{13} + EA(\text{RC}\cdot)^{14} + IP(\text{H})^{15} + E^{16}(RCOO^-, H^+)$$

$$\simeq 4.80\ \text{eV} - 0.08\ \text{eV} + 13.60\ \text{eV} - 16.25\ \text{eV} \simeq +2.07\ \text{eV}$$

Process 5 requires $\approx$2.07 eV, which is significantly higher than that required for either process 4—1 or 4—2 in Scheme 4B. Thus, production of quasimolecular ions $(M + H)^+$, will be unlikely at low laser powers, for which the "effective temperature" is low. The energy at low laser powers is not enough to produce either quasimolecular ions or to initiate an alkyl transfer reaction.

Production of protons to initiate the protonation reaction in the gas phase is unlikely, because it involves high-energy processes, illustrated as follows

$$\geqslant C{-}H \rightarrow \geqslant C\cdot + H\cdot \quad (+4.8\ eV)$$

$$H\cdot \rightarrow H^+ + e^- \quad (+13.6\ eV)$$

The overall process can be written as

$$\geqslant C{-}H \rightarrow \geqslant C\cdot + H^+ + e^- \quad (+18.4\ eV)$$

Thus, the probability for gas-phase protonation is rather low. However, a concerted type of reaction leading to protonation of the intact molecule as described in process 5 is quite likely in the condensed phase. By analogy, a corrected mechanism for methyl group transfer (Eqn. 2) will be a lower-energy process than will be a mechanism involving direct ion products initially (Eqn. 3). Thus, these results support direct methyl transfer as a mechanism for producing $(M + CH_3)^+$ and $(M{-}CH_3)^-$.

The above discussion indicates that protonation in the gas phase is unlikely. This is supported by the absence of H^+ ions at laser powers at which quasimolecular ions $(M + H)^+$ are detected (see Figs. 2c–g). Further, we have shown for the deuterated isomer (compound 4) that the calculated value for $(M + H)^+/(M + D)^+$ agrees with the experimental value within experimental error, assuming that all protons in compound 4 are available for protonation (see discussion on structural information). No ions corresponding to either D^+ or H^+ were observed in the positive-ion spectrum of compound 4. Thus, it can be concluded that in l.m.s. of internal salts, the quasimolecular ions are produced by direct protonation from intact molecules.

The lowest laser power at which $(M + H{-}CO_2)^+$ (F) ions were detected is the same as that at which the $(M + H)^+$ (G) ion appears, initially (0.09 μJ, Fig. 2c). The intensity of $(M + H{-}CO_2)^+$ ions increases in parallel with the intensity of $(M + H)^+$ ions (Fig. 2). This suggests strongly that $(M + H{-}CO_2)^+$ ions arise from $(M + H)^+$ ions by unimolecular decomposition.

Addition of a small amount of *p*-toluenesulfonic acid (*p*-TSA) changes the chemical environment by protonating the intact molecules; under these conditions, the spectra are dominated by $(M + H)^+$ ions. Methyl group transfer reactions take place to a much smaller extent and no ions corresponding to alkyl transfer $(M + R)^+$ are observed. The fragmentation observed is minimal; $(M + H{-}CO_2)^+$ ions which normally dominate the positive-ion spectra are weak in the presence of *p*-TSA. This observation can be explained if the process involved in the presence of *p*-TSA is to desorb the quasimolecular ions $(M + H)^+$ already present in the sample. Such an effect has been observed in f.d. of similar compounds [16]. Protonated molecular ions already formed should desorb with low energy and fragmentation should be minimal.

The observation of quasimolecular ions $(M + H)^+$ of high intensity with minimum fragmentation and ions corresponding to methyl transfer

$(M + CH_3)^+$ indicates that two processes may take place in the presence of *p*-TSA

$$(CH_3)_2R\overset{+}{N}C_5H_{10}CO_2^- \underset{p\text{-TSA}}{\rightleftharpoons} R(CH_3)_2\overset{+}{N}C_5H_{10}CO_2H \xrightarrow{h\nu} (M + H)^+ \qquad (6A)$$

$$2(CH_3)_2R\overset{+}{N}C_5H_{10}CO_2^- \xrightarrow{h\nu} (M + CH_3)^+ + (M{-}CH_3)^- \qquad (6B)$$

As mentioned earlier, the process involved in 6A is to desorb the quasimolecular ions $(M + H)^+$ already present. Under these conditions, the quasimolecular ion $(M + H)^+$ appears at higher threshold energy (0.49 μJ) than when *p*-TSA is absent. The higher threshold energy in the presence of *p*-TSA is probably caused by the energy needed to separate the ion pair produced by protonation. Though the lattice energy for this type of ion-pair has not been reported, data [14] for quaternary ammonium salts suggest that 5—7 eV for the lattice energy would be reasonable. Thus, the energy involved in process 6A is higher than that of process 5 ($\approx$2.0 eV).

Process 6B above (methyl group transfer) probably occurs in an area of relatively high temperature (probably at the center of the laser pulse). However, ions corresponding to long alkyl chain transfer $(M + R)^+$ are not observed even at very high laser powers. Very high laser powers at the highest instrumental sensitivity were used in an effort to detect $(M + R)^+$ ions (if they are produced in very small quantity). Though most of the peaks went off scale, no ions corresponding to $(M + R)^+$ were observed. Thus, it can be concluded that ions corresponding to $(M + R)^+$ are not produced in the presence of *p*-TSA.

Structural information on sultaines and ammonioalkanoates

Positive-ion laser mass spectra of the ammoniohexanoates and sultaines can be used for both molecular-weight and structure determinations. The molecular weight can be obtained from the quasimolecular ion $(M + H)^+$. Ions such as $(M + CH_3)^+$, $(M{-}CH_3)^-$, $(M + R)^+$ and $(M{-}R)^-$ can be used as supporting evidence for molecular weight determination.

The presence of a carboxyl group can be deduced from ions such as $(M + H{-}CO_2)^+$ and $(M + CH_3{-}CO_2)^+$, i.e., loss of 44 mass units from the quasimolecular ions. Neutral losses detected for sultaines correspond to loss of SO_3 and H_2SO_3 from $(M + H)^+$ and SO_3 from $(M + CH_3)^+$ similar to the loss of CO_2 and H_2CO_2 for ammoniohexanoates. Thus, information about the sulfonic acid group can be deduced from the loss of 80 mass units from quasimolecular ions. Ions corresponding to $(M + H{-}SO_3)^+$ are weaker than $(M + H)^+$ and $(M + CH_3)^+$; this contrasts with the ammoniohexanoates in which $(M + H{-}CO_2)^+$ ions dominate the spectra.

Fragment ions such as $[M + H{-}RH]^+$ and $[M + H{-}C_5H_{11}COOH]^+$ provide information about the nature of the alkyl chains for the ammoniohexanoates. Similarly, ions corresponding to $[M + H{-}C_3H_7SO_3H]^+$ and $[M + H{-}RH]^+$ are observed for sultaines. However, the relative intensity of $[M + H{-}RH]^+$

for the sultaines is greater than for the ammoniohexanoates; this stands in contrast to $(M + H{-}SO_3)^+$ and $(M + H{-}CO_2)^+$. Thus, comparison of the intensities of ions corresponding to $[M + H{-}SO_3]^+$ and $[M + H{-}RH]^+$ from sultaines with those of $(M + H{-}CO_2)^+$ and $[M + H{-}RH]^+$ from ammoniohexanoates indicates that the fragmentation pattern varies considerably when carboxylate groups (ammoniohexanoates) are replaced by sulfanoates (sultaines).

The negative-ion l.m.s. of sultaines and ammoniohexanoates complement the positive-ion l.m.s. The nature of the alkyl chain attached to nitrogen can be deduced from ions such as $(M{-}CH_3)^-$, $(M{-}CH_3{-}RH)^-$ and $(M{-}R)^-$. Ions in the lower mass range ($m/z \leqslant 158$) are characteristic of the alkyl chain containing the carboxyl group in the case of ammoniohexanoates, e.g., $CH_2{=}NC_5H_{10}CO_2^-$ (m/z = 142) and $C_5H_9CO_2^-$ (m/z = 113). These ions are useful for confirming the length of the chain between the nitrogen and the carboxyl group. Similarly, ions in the lower mass ranges ($m/z \leqslant 166$) are identical for all sultaines and correspond to fragments of $(CH_3)_2NC_3H_6SO_3^-$ (m/z = 166); these ions provide information about the alkyl chain containing the sulfonic acid group.

Results for the isotopically labelled sultaine $C_8H_{17}\overset{+}{N}(CD_3)_2C_3H_6SO_3^-$ (compound 4) give support for some of the fragmentation mechanisms proposed above. Loss of $D(CH_2)_3SO_3H$ from $(M + H)^+$ in compound 4 leads to ions corresponding to $C_8H_{17}{-}\overset{+}{N}(CD_2){=}CD_3$ (m/z = 161, Fig. 7a). This four-centered elimination reaction can occur by two different pathways as shown in Scheme 4C. However, the one which leads to $C_7H_{15}CH{=}\overset{+}{N}(CD_3){-}CD_3$ (m/z = 162) can be excluded, because the intensity of the peak at m/z = 162 is very small. Thus the four-centered elimination leading to loss of $-(CH_2)_3SO_3H$ group from $(M + H)^+$ involves only the methyl groups attached to nitrogen. The origin of peaks such as $(M + H{-}SO_3)^+$ and $(M + CD_3{-}SO_3)^+$ can be confirmed by compound 4, because these ion masses are shifted by the appropriate mass increment for the deuterium atoms present.

Similar information can be obtained from the negative-ion spectrum of compound 4. Peaks at $m/z > 123$, such as $(M{-}CD_3)^-$, $(M{-}R)^-$ and $(M{-}CD_3{-}RD)^-$, are shifted by the appropriate number of mass units compared to the proton isomer. Elimination of RD from $(M{-}CD_3)^-$ indicates that a deuterium in the CD_3 group is involved in this elimination, rather than a hydrogen from the $C_3H_7SO_3^-$ group. This is confirmed by the ion corresponding to $CD_2{=}NC_3H_6SO_3^-$ at m/z = 152 (Fig. 7b). The peak at m/z = 169 is more intense than a peak considered to be the hydrogen isomer contribution of $(CD_3)_2NC_3H_6SO_3^-$ (CD_3 groups are only 80% isotopically pure). Thus, the peak at m/z = 169 $[(CH_3)N(CD_3)C_3H_6SO_3^-]$ is produced from $(M{-}CD_3)^-$, which confirms the fragmentation shown in Scheme 4A. Ions at $m/z \leqslant 123$

for $C_8H_{17}\overset{+}{N}(CD_3)_2C_3H_6SO_3^-$ are identical with those found for other sultaines, because production of these ions involves only fragmentation of $C_3H_7SO_3^-$ [e.g., $C_3H_7SO_3^-$ ($m/z = 123$), $C_3H_5SO_3^-$ ($m/z = 121$) and $C_2H_3SO_3^-$ ($m/z = 107$)].

In addition to the protonated molecular ion $(M + H)^+$ ($m/z = 286$), a considerable amount of deuterated molecular ion $(M + D)^+$ [45% of $(M + H)^+$] is observed in the positive-ion spectrum of compound 4 (see Fig. 7a). This indicates that part of the protons involved in the protonation reaction come from the CD_3 groups. If one assumes that all protons in compound 4 (80% isotopically pure) are available for protonation, a statistical value of 5:1 would be expected for the $(M + H)^+/(M + D)^+$ ratio. The ratio calculated from the intensities of the $(M + H)^+$ molecular-ion cluster gives a value of 4.5:1. These values agree within the experimental error of intensity measurements in l.m.s. (±15—20%).

Comparison of f.d.m.s. with l.m.s.

Comparison of positive-ion f.d. spectra of quaternary ammonioalkanoates [7, 8] with laser mass spectra reveals some similarities and differences. One striking difference between f.d.m.s. and l.m.s. is the appearance of cluster ions $(nM + H)^+$ in f.d.m.s. ($n = 1$—3) at low emitter currents; intensities of the cluster ions decrease as the emitter current is increased. No cluster ions were observed in l.m.s. at any laser power.

In addition to cluster-ion formation, other significant differences are observed, especially for hydroxyammonioalkanoates. No ions corresponding to methyl group transfer were observed for hydroxy compounds **2a** and **2b** (Table 1) in f.d.m.s.; methyl group transfer occurs to a small extent for these compounds in l.m.s. The other important difference between f.d.m.s. and l.m.s. of hydroxy compounds is the presence of an ion corresponding to $(M + H—ROH)^+$ (R = alkyl group) in f.d.m.s. but not in l.m.s. Formation of $(M + H—ROH)^+$ ions in f.d.m.s. has been explained by lactone formation involving the hydroxyl group [8]. Such a mechanism may be possible in f.d.m.s., because of the slow (i.e., thermal) processes involved in the f.d. desolvation mechanism, which also is responsible for cluster-ion formation [17]. By contrast, l.m.s. involves a process whereby the sample is rapidly converted into a dense plume, because a high energy pulse is absorbed in a short time by a small volume. Thus, the formation of $(M + H—ROH)^+$, and cluster ions is unlikely in l.m.s. This implies strongly that thermal reactions are not important in the l.m.s. of internal salts.

Sultaines have been studied by various mass spectrometric techniques and a detailed comparison of the results will be published separately.

Conclusions

Zwitterionic compounds (internal salts) give readily interpretable laser mass spectra. The LAMMA-1000 gives more informative spectra for internal salts than the LAMMA-500. All internal salts studied show alkyl transfer reactions during laser irradiation. The complementary nature of positive- and

negative-ion spectra gives evidence for pair-production through intermolecular alkyl transfer reactions. Results obtained for hydroxyammonioalkanoates at threshold energy indicate that an ion-pair can be produced by simple cleavage of the neutral molecule. Here, this process is referred to as "intramolecular pair-production". The positive ion spectra of ammoniohexanoates are dominated by $(M + CH_3)^+$ in the higher mass range. Addition of a small amount of *p*-toluenesulfonic acid reduces fragmentation to a minimum; the spectra are dominated by $(M + H)^+$ in the higher mass range. In the case of the sultaines, alkyl transfer takes place to a smaller extent than for the ammoniohexanoates; positive-ion spectra are dominated by $(M + H)^+$ in the higher mass ranges. Results from deuterium-labeling studies provide information about the alkyl groups involved in the alkyl transfer reaction. Information about the proton source and fragmentation mechanism are also obtained from deuterated compounds. Both similarities and differences between results from l.m.s. and f.d.m.s. were observed.

We are grateful to Dr. T. Keough for providing the quaternary ammoniohexanoates and for running the f.d. spectra of the sultaines. We thank Drs. S. Weber and W. Tramposch for providing the sultaines, and Drs. R. J. Day, N. G. Rondan and K. N. Houk for their valuable assistance. Support of this work by the Office of Naval Research is gratefully acknowledged.

REFERENCES

1 K. L. Busch, S. E. Unger, A. Vincze, R. G. Cooks and T. Keough, J. Am. Chem. Soc., 104 (1982) 1507.
2 G. W. Wood, P.-Y. Lau, G. Morrow, G. N. S. Rao, D. E. Schmidt, Jr. and J. Tuebnuer, Chem. Phys. Lipids, 18 (1977) 316.
3 G. W. Wood and R. J. Collacott, Org. Mass Spectrom., 18 (1983) 42.
4 K. Ohya, Y. Yotsui, K. Yamazaki and M. Sano, Org. Mass Spectrom., 18 (1983) 27.
5 K. Balasanmugam and D. M. Hercules, Spectrosc. Lett., 16 (1983) 1.
6 S. Konosu, M. Murakami, T. Hayashi and S. Fuke, Bull. Jpn. Soc. Sci. Fish., 39 (1973) 645.
7 R. A. Sanders, A. J. Destefano and T. Keough, Org. Mass Spectrom., 15 (1980) 348.
8 T. Keough, A. J. Destefano and R. A. Sanders, Org. Mass Spectrom., 15 (1980) 351.
9 R. J. Day, A. L. Forbes and D. M. Hercules, Spectrosc. Lett., 14 (1981) 703.
10 R. Kaufman, R. Hillenkamp and R. Wechsung, Med. Prog. Technol., 6 (1979) 109.
11 H. J. Heinen, S. Meier and H. Vogt, in A. Benninghoven (Ed.), Spring. Ser. Chem. Phys. (Ion Formation from Organic Solids), Vol. 25, Springer-Verlag, Berlin, 1983, p. 229.
12 V. I. Vedeneyev, L. V. Guruvich, V. N. Kondrat'yev, V. A. Medvedev and Ye. L. Frankevich, Bond Energies, Ionization Potentials and Electron Affinities, Butler and Tanner, Frome and London, 1966, p. 54.
13 R. C. Weast, CRC Handbook of Chemistry and Physics, CRC Press, FL, 1979—1980.
14 G. B. Ellison, P. C. Engelking and W. C. Lineberger, J. Am. Chem. Soc., 100 (1978) 2556.
15 R. D. Levin and S. G. Lias, Ionization Potential and Appearance Potential Measurements, U.S. Department of Commerce, National Bureau of Standards, Washington, 1971.
16 J. Pople, Carnegie-Mellon Quantum Chemistry Archive.
17 F. W. Röllgen, in A. Benninghoven (Ed.), Spring. Ser. Chem. Phys. (Ion Formation from Organic Solids) Vol. 25, Springer-Verlag, Berlin, 1983, p. 2.

Analytica Chimica Acta, 166 (1984) 27—38
Elsevier Science Publishers B.V., Amsterdam — Printed in The Netherlands

AN ATMOSPHERIC-PRESSURE, ARGON-AFTERGLOW DETECTOR FOR GAS CHROMATOGRAPHY

G. W. RICE[a], A. P. D'SILVA and V. A. FASSEL*
Ames Laboratory, Iowa State University, Ames, Iowa 50011 (U.S.A.)
(Received 14th May 1984)

SUMMARY

The development of an atmospheric-pressure argon-afterglow, produced from an ozonizer-type discharge tube, for element-selective, multielement detection in gas chromatography is described. Characteristic atomic emission is observed from chlorine, bromine, iodine, carbon, sulfur and phosphorus in organic compounds, with limits of detection ranging from 0.02 ng for phosphorus to 20 ng for bromine. Element-selective detection for several pesticides is demonstrated.

Earlier reports have described techniques for producing active nitrogen afterglows at atmospheric pressure (APAN) and their utilization for a variety of quantitative applications [1—4]. The characteristic atomic and molecular emission generated in the APAN afterglow on the introduction of a variety of analyte species is a result of dissociation and excitation produced by energy transfer from long-lived excited states of atomic and molecular nitrogen present in the afterglow. It has been postulated that the N_2 ($^5\Sigma_g^+$) metastable state, formed by recombination of N(^{4}S) ground-state atoms and having an excitation energy of 9.5 eV, may represent the highest energy transferable in the APAN afterglow. The APAN afterglow may therefore not be readily applicable for processes requiring greater excitation energies.

This limitation became apparent when chlorine- and bromine-containing compounds were injected into the afterglow. Only emission from NCl, NBr, and Br_2 was observed [5]. The absence of the near-infrared Cl and Br atomic emission lines, requiring 10.62 and 9.72 eV to populate the relevant excited states, suggested the absence of sufficiently energetic species in the afterglow.

There is abundant documentation that relatively long-lived, metastable atomic and molecular argon species possessing the requisite energy can be formed in static or flowing, low-pressure discharges [6—9], in the conventional argon-ionization detector for gas chromatography (g.c.) [10, 11], and in inductively-coupled plasmas and microwave-induced plasmas at atmospheric pressure [12, 13]. None of these studies involved the utilization of

[a]Present address: Department of Chemistry, The College of William and Mary, Williamsburg, VA 23185, U.S.A.

0003-2670/84/$03.00

the energetic argon afterglows that can be formed under appropriate experimental conditions. This paper describes the generation of such an argon afterglow at atmospheric pressure and its quantitative applications. Because the afterglow is formed at atmospheric pressure, sample introduction is greatly simplified in comparison to low-pressure operation.

EXPERIMENTAL

Apparatus

A schematic diagram of the ozonizer-type discharge tube utilized for producing the argon afterglows is shown in Fig. 1. The 0.025-mm thick platinum sheet wrapped inside the 2-mm o.d. quartz tube was connected to the a.c. power supply. The outer platinum sheet was wrapped around the outside of the 6-mm o.d. quartz tube and grounded. This primary discharge and afterglow tube is significantly smaller and requires far less power for stable operation than those utilized in previous studies on nitrogen afterglows [1, 4]. With the exception of a new discharge tube power supply, all spectrometric, gas chromatographic (g.c.), and interfacing instrumentation has previously been described [1, 4]. The new discharge tube power supply is a variable frequency (10—100 kHz) a.c. power amplifier coupled to an impedance-matched 10-kV transformer (Model EGR 800, ENI Power Systems, Rochester, NY).

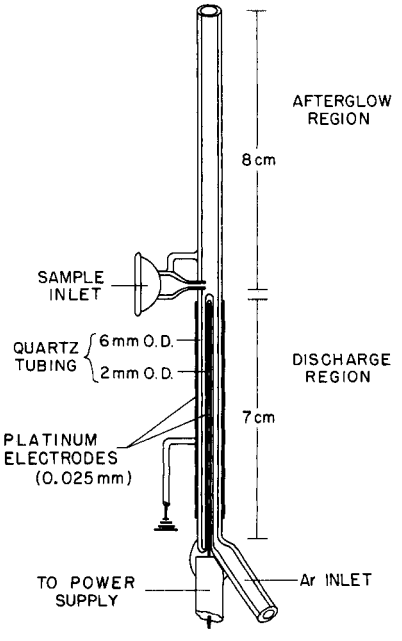

Fig. 1. Schematic diagram of the ozonizer-type discharge tube for generation of the argon afterglow.

Procedures

The operating conditions for the discharge, spectrometric, and chromatographic systems are summarized in Table 1. The frequency of the power supply was tuned to minimum reflected power signal. The argon flow rate (5 l min^{-1}) required to sustain the afterglow was significantly lower than those required in the APAN studies (15—30 l min^{-1}).

To obtain characteristic atomic and/or molecular emission profiles from analyte species, compounds of interest were introduced into the afterglow region by vapor purge techniques. In the latter, an auxiliary flow of argon at approximately 0.1 l min^{-1} served to transport and inject relatively constant amounts of volatile compounds into the afterglow. Trichloroethylene, dibromoethane, iodomethane, thiophene, and trimethylphosphite were used to examine emission from Cl, Br, I, S, and P, respectively.

Reference mixtures containing known concentrations of the aforementioned elements were prepared from selected g.c. reference compounds (Chem Services, West Chester, PA) for the g.c. studies. All mixtures were prepared in anhydrous diethyl ether.

RESULTS AND DISCUSSION

Spectral characteristics of the argon afterglow

The argon afterglow is bluish-white in color. Contact of the afterglow with the atmosphere results in an intense violet color characteristic of the N_2 ($C^3\Pi_\mu \rightarrow B^3\Pi_g$) second positive system emission spectrum. An unusual feature of the afterglow was its filamentary shape and confinement to the center of the afterglow tube. Grounding of the afterglow by insertion of a stainless steel rod into the afterglow tube significantly intensified the emission of

TABLE 1

Operating conditions of the discharge, spectrometric, and chromatographic systems

(A) Discharge system	
Ar flow rate	5 l min^{-1}
Incident power	80 Watts
Frequency	75 kHz
(B) Spectrometric system	
Monochromator	0.3 m (McPherson)
Bandpass (FWHM)	0.2 nm
PMT/180—300 nm	EMI solar blind (1850V)
300—500 nm	EMI 6256 (1150V)
500—900 nm	Centronic extended S-20 (750V)
(C) Chromatographic system	
Gas chromatograph	Hewlett-Packard Model 5710A capillary gas chromatograph
Carrier gas	Argon
Column	Durabond 5 (J&W); 30 m
Injection volumes	1 μl
Interface temperature	300—350° C

both the emitting argon and analyte species. The grounded configuration was used for all subsequent studies.

Background spectra obtained from conventional tank argon and the boil-off from a liquid argon tank are compared in Fig. 2. In the 190—400-nm spectral region, emission was observed primarily from the OH ($A^2\Sigma_i \rightarrow X^3\Pi_i$), N_2 ($C^3\Pi_\mu \rightarrow B^3\Pi_g$), and NH ($A^3\Pi_i \rightarrow X^3\Sigma_{\bar{\mu}}$) systems, as well as C (*I*) atomic emission. A substantial difference in emission intensity was observed from impurities present in the two different argon sources utilized, as indicated by the relative attenuation factors required. The liquid argon boil-off was observed to give significantly less emission because of lower levels of impurities in the gas phase, with the exception of carbon-containing species. Thus, all subsequent studies were made with liquid argon boil-off, in the expectation that competing reactions with analyte species would be minimized.

Spectra of the argon afterglow in the visible and near infrared regions are shown in Figs. 3 and 4, respectively. Because emission in these regions was observed to be very similar for both argon sources, only the background spectra for the liquid argon boil-off are shown. Characteristic atomic emission from argon was observed as well as O (*I*) emission from oxygen impurities in the gas stream. The emissions observed from impurities in the liquid argon boil-off are summarized in Table 2.

Continuous introduction of analyte species into the afterglow resulted in the generation of characteristic atomic emission from compounds containing Cl, Br, I, C, P or S. Typical spectra obtained from the introduction of trichloroethane and trimethylphosphite are shown in Figs. 5 and 6, respectively.

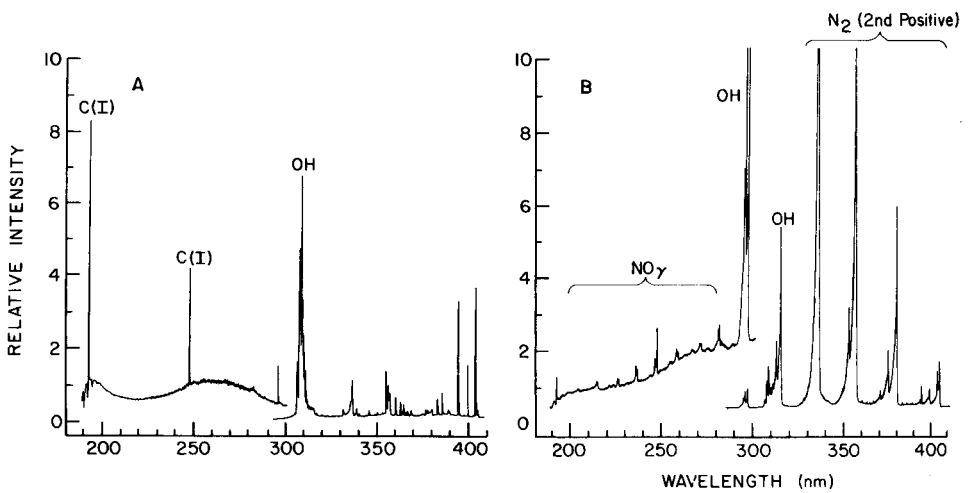

Fig. 2. Background emission observed in the 190—400-nm region of the argon afterglow from the boil-off of (A) liquid argon and (B) tank argon. Amplifier gains: (A) 200—300 nm, 3×10^{-10} A; 300—400 nm, 3×10^{-9} A; (B) 200—300 nm, 1×10^{-9} A; 300—400 nm, 3×10^{-8} A.

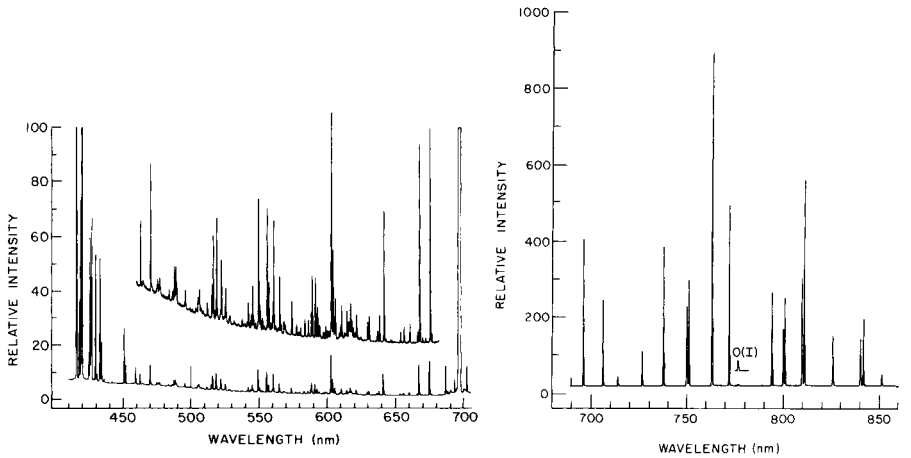

Fig. 3. Background emission observed in the 400—700-nm region from the argon afterglow. Bottom scan is attenuated by a factor of five.

Fig. 4. Background Ar (*I*) emission observed in the 700—850-nm region from the argon afterglow. Emission from O (*I*) is labeled.

TABLE 2

Atomic and molecular emission observed from impurities in the argon afterglow

Species	Transition	Wavelength region (nm)
N_2	$C^3\Pi_\mu \rightarrow B^3\Pi_g$	310—430
NH	$A^3\Pi_i \rightarrow X^3\Sigma^-_\mu$	336.0, 337.0
NO	$A^2\Sigma^+_\mu \rightarrow X^2\Pi_r$	210—290
OH	$A^2\Sigma^+_\mu \rightarrow X^2\Pi_i$	300—310
O	O (*I*)	777.2, 844.6
C	C (*I*)	193.1, 247.9

Hexane, thiophene, dibromomethane, and iodomethane were used for obtaining the spectra of C, S, Br, and I, respectively. No attempt was made to quantify the mass flow of the above compounds into the afterglow. The most intense wavelengths observed for each element are listed in Table 3. Observations in the 180—200 nm region were achieved by flushing the optical path and monochromator with nitrogen.

No ion emission was observed from any analyte species. Intense molecular C_2 emission was observed from carbon, with maximum emission at 516.5 nm. Weak CS and S_2 emission was also detected from sulfur-containing compounds.

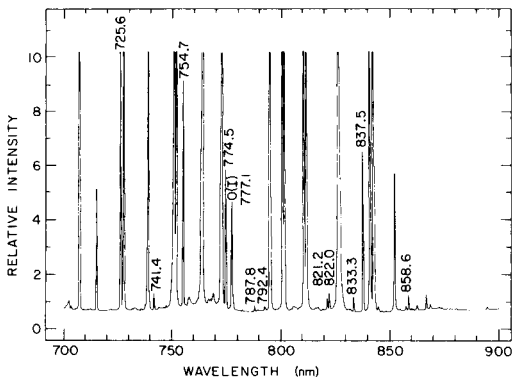

Fig. 5. Atomic emission observed from chlorine introduced as dichloroethylene in the argon afterglow. All identified lines, unless otherwise labeled, are Cl (*I*) emission lines.

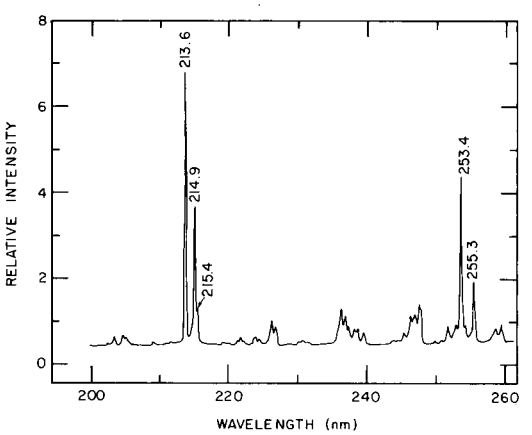

Fig. 6. Atomic emission observed from phosphorus introduced as trimethylphosphite in the argon afterglow. All identified lines are P (*I*) emission lines. Background emission bands are part of the NO_γ system.

Analytical studies

The analytical utility of the argon afterglow was evaluated by connecting the sample inlet at the base of the afterglow to a heated interface from the g.c. oven, as previously described [4]. The capillary column from the g.c. was inserted directly into the afterglow with no dead volume or gas mixing required. The most intense atom lines were selected from the tabulated spectral data previously discussed.

Typical chromatograms for the separation of reference mixtures containing several chlorine- and bromine-containing compounds are shown in Figs. 7 and 8, respectively. The concentration of each compound was adjusted so that the total amount of halogen per compound injected was 10 ng and 100 ng, respectively. The relatively high background at these concentrations

TABLE 3

Prominent emission lines observed from Cl, Br, I, S, P, and C in the argon afterglow

Element	Wavelength (nm)[a]	Element	Wavelength (nm)[a]	Element	Wavelength (nm)[a]
Cl	725.6	I	183.0	P	213.6
	754.7		206.2		253.4
	837.6	C	193.1		214.9
	774.4		247.6		255.3
Br	734.9		516.5[b]	S	182.0
	700.5				182.6
	635.1				180.7
	663.1				190.0
	780.3				191.4
	655.9				

[a]Wavelengths listed in order of decreasing intensity. [b] C_2 molecular emission.

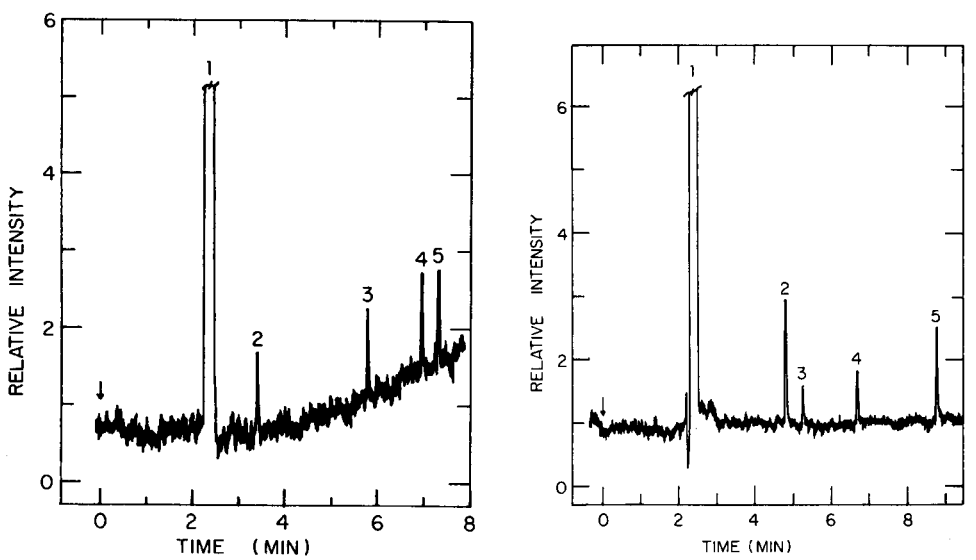

Fig. 7. Chromatogram obtained from a mixture of chlorine-containing compounds: (1) solvent, (2) trichloroethylene, (3) chlorobenzene, (4) 1,2,3-trichloropropane, (5) hexachloroethane. Conditions: 10 ng μl^{-1} Cl; 725.6 nm; temperature program, 50° C (2 min)—32° C min^{-1}—300° C; amplifier gain, 1 × 10^{-8}.

Fig. 8. Chromatogram obtained from a mixture of bromine-containing compounds: (1) solvent, (2) 1,2-dibromoethane, (3) 3,4-dibromobutane, (4) bromobenzene, (5) 1,6-dibromo-2-naphthol. Conditions: 100 ng μl^{-1} Br; 734.8 nm; temperature program, 45° C (2 min)—16° C min^{-1}—300° C; amplifier gain, 1 × 10^{-8}.

appears to result from far scatter of the argon lines associated with the near i.r. region. The intensities of the near i.r. lines of argon can be estimated by comparing the internally consistent relative intensities of the argon spectrum shown in Fig. 4 with the background level shown in Figs. 7 and 8. The significant solvent peak from diethyl ether appears in both cases to arise from far scattering of molecular band emission from CN, which may be formed from solvent carbon and nitrogen impurities in the afterglow. For the chromatogram of bromine-containing compounds shown in Fig. 8, the momentary background signal decrease that precedes the appearance of main solvent peak emission is the result of a temporary quenching of the total argon emission background as the solvent "plug" enters the afterglow region. It is not only the argon far scatter radiation at 734.8 nm that is quenched, but also the wing contribution from a relatively intense nearby argon line at 735.2 nm. The combined quenching of these background contributions causes the short-term background signal depression. The cause of the baseline shift in the chromatogram of chlorine-containing compounds is not known at this time.

The low background scatter associated with the u.v. spectral region of the afterglow allowed for significant improvements in the detection of compounds containing I, C, P, and S. A typical chromatogram from the separation of a mixture of phosphorus-containing compounds, each at a level of 1 ng of phosphorus per compound, is shown in Fig. 9. The fairly intense solvent peak probably results from spectral overlap with molecular bands from C_2 formed in the afterglow from the presence of carbon in the solvent.

Chromatograms from the separation of a mixture of seven pesticides are shown in Fig. 10 for element-selective detection of C (193.1 nm), P (213.6 nm), and S (182.0 nm). The amount of each pesticide injected was approximately 20 ng. As expected, all seven pesticides were separated and detected at the carbon wavelength, but only the phosphorus- and sulfur-containing pesticides were detected at their respective analytical wavelengths. The ability fully to resolve malathion and parathion, which have very similar retention times, clearly demonstrates that the afterglow detector did not degrade the chromatographic resolution significantly.

Table 4 shows a comparison of limits of detection (in nanograms) reported for several element-selective emission techniques that have been utilized for the detection of Cl, Br, I, C, P, and S. These limits of detection are based on measurements of the concentrations of analyte species required to produce peak height signals that were three times greater than the background scatter. As shown in Table 4, the limits of detection for the argon afterglow detector were found to be superior to values given for the argon inductively-coupled plasma (i.c.p.) and were comparable to the helium microwave-induced plasma (m.i.p.) values for phosphorus and sulfur. However, the m.i.p. literature values for C, Cl, Br, and I were generally one to two orders of magnitude superior to those obtained with the argon afterglow.

Because of band-broadening effects occasioned by g.c. column overloading at higher concentrations, peak height measurements did not provide accurate

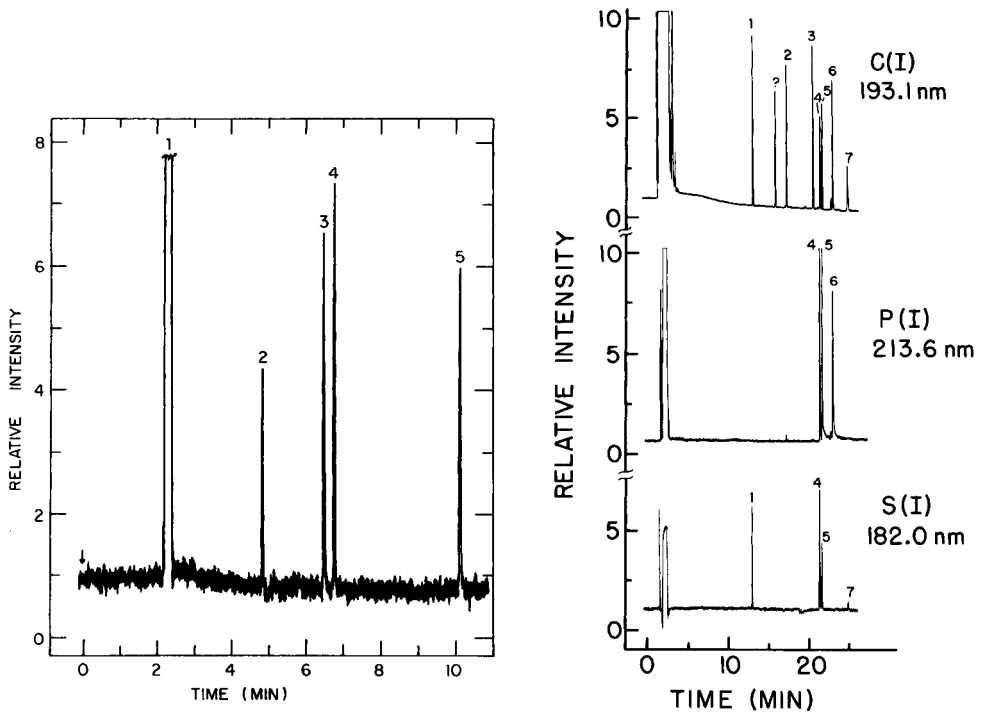

Fig. 9. Chromatogram obtained from a mixture of phosphorus-containing compounds: (1) solvent, (2) triethylphosphate, diethylethylphosphonate, (4) triethylphosphate, (5) tributylphosphate. Conditions: 1 ng μl^{-1} P; 213.6 nm; temperature program, 60° C (2 min)—32° C min^{-1}—310° C; amplifier gain, 3 × 10^{-9}.

Fig. 10. Element-selective detection of C, P, and S in a pesticide mixture separated by g.c.: (1) butylate, (2) trifluralin, (3) alachlor, (4) malathion, (5) parathion, (6) crotoxyphos, (7) endosulfan. Conditions: 20 ng of each compound injected (20 $\mu g\ ml^{-1}$); temperature program, 60° C (2 min)—8° C min^{-1}—260° C.

linear response evaluations for the entire g.c. afterglow detector system. To accommodate the band-broadening effects at the higher concentrations, peak area measurements were used. In general, all of the compounds studied gave a linear signal response to concentrations up to approximately 1000 mg l^{-1} of the element in the 1 μl of solution injected into the g.c. Selectivity was based on the ratio of a non-analyte compound (naphthalene) reference concentration to an analyte reference concentration which gave equivalent signals when measured at the analyte wavelength. In all cases, the selectivity was observed to be over three orders in magnitude, confirming the element-selective detection capabilities of the argon afterglow detection system.

No quenching or extinction of the afterglow has ever occurred during the chromatographic elution of microliter volumes of the sample solvent, a factor which primarily results from the afterglow being continuously regenerated

TABLE 4

Comparison of detection limits for several element-selective spectrometric g.c. detectors

Element	Wavelength (nm)[a]	Excitation energy (eV)	Detection limits (ng)		
			Present	M.i.p.[b]	I.c.p.[c]
Cl	725.6	10.62	2	0.31	50[d]
Br	734.9	9.72	10	0.21	50[d]
I	183.0	6.74	0.5	0.05	4
C	193.1	7.65	0.1	0.012	12
P	213.6	7.18	0.04	0.056	0.6
S	182.0	6.83	0.1	0.140	6[e]

[a]Present work. [b]Helium microwave-induced plasma [14]. [c]Argon inductively-coupled plasma [15]. [d]Gas sampling loop injection of analytes into i.c.p. [16]. [e]Gas sampling loop [17].

from the primary discharge. No detectable deposits were observed on the walls of the afterglow tube after approximately 200 h of operation.

Energy carrier considerations

The dissociation of analyte compounds and subsequent atomic emission in the argon afterglow is primarily determined by those argon species which have sufficient excitation energies and lifetimes to populate the afterglow region substantially. The most likely long-lived energy carriers in the argon afterglow are listed in Table 5, together with their respective energies, lifetimes if known, evidence for existence, and possible formation processes. Unfortunately, most of the information on the long-lived argon states has been obtained under low pressure (<10 torr), flowing or static conditions. The role that each of these states plays at atmospheric pressure in the analyte dissociation and excitation processes through collisional transfer of energy is difficult to assess because of uncertainties in lifetimes, number density in the afterglow, and collisional cross-section considerations. Moreover, an understanding of the various pathways involved in fragmenting large organic molecules into free atoms followed by excitation of the latter, all via energy transfer from the energetic species in the afterglow, requires the collection of a data base far more extensive than is now available. Any speculation on the degree to which the energy carriers listed in Table 5 participate in the degradation-excitation processes must therefore be deferred. Based solely on the energy requirements for analyte excitation, which range from 6.7 eV for iodine to 10.6 eV for chlorine (see Table 4), it is clear that all of the energy carriers listed in Table 5 are energetically positioned to play an important role.

The Ames Laboratory is operated for the U.S. Department of Energy by Iowa State University under Contract No. W-7405-Eng-82. This research was

TABLE 5

Known or presumed long-lived argon states

Species	State or configuration	Potential energy (eV)	Lifetime (s)	Evidence for existence	Formation: experimental evidence or speculation
Ar	$^3P_2$	11.55	>1.3	Unusual high intensity of emission from N_2 ($C^3\Pi_\mu \rightarrow B^3\Pi_\mu$) second positive emission as a result of energy transfer from Ar (^3P) metastable states [8, 18]. Resonance emission at 104.8 and 106.7 nm [6]	Direct electron excitation in primary discharge. Ion–electron recombination of Ar_2^+ ions via $Ar_2^+ + e^- \rightarrow Ar + Ar(^3P)$ [6]. Population may be sustained by radiation trapping [6]
	$^3P_0$	11.73	>1.3		
Ar^+	^2P	16.0	>1	Mass spectrometry [19]	Ionization in primary discharge. Ionization from metastable states via $Ar(^3P) + e^- \rightarrow Ar^+ + 2e^-$ [6]. Collision of two metastable atoms via $Ar(^3P) + Ar(^3P) \rightarrow Ar^+ + Ar + e^-$ [9]
Ar_2	$^3\Sigma_\mu^+$	10.2	?	U.v.-visible continuum assigned to Ar_2 emission [20, 21]	Three-body collision of metastable Ar (^3P) with neutral Ar atoms via $Ar(^3P) + Ar + Ar \rightarrow Ar_2 + Ar$ [20]
Ar_2^+	$^1\Sigma_\mu^+$	14.0	?	Mass spectrometry [19, 22]	Three-body collisions via $Ar^+ + Ar + Ar \rightarrow Ar_2^+ + Ar$ [22]

supported by the Division of Chemical Sciences, Budget Code KC-03-02-02, Office of Energy Research. The authors thank Thomas Gibbons for his active participation in the development of this research project.

REFERENCES

1 A. P. D'Silva, G. W. Rice and V. A. Fassel, Appl. Spectrosc., 34 (1980) 578.
2 G. W. Rice, J. J. Richard, A. P. D'Silva and V. A. Fassel, Anal. Chem., 53 (1981) 1519.
3 G. W. Rice, J. J. Richard, A. P. D'Silva and V. A. Fassel, J. Assoc. Off. Anal. Chem., 65 (1982) 14.
4 G. W. Rice, J. J. Richard, A. P. D'Silva and V. A. Fassel, Anal. Chim. Acta, 142 (1982) 47.
5 G. W. Rice, A. P. D'Silva and V. A. Fassel, Appl. Spectrosc., 38 (1984) 149.
6 J. Delcroix, C. M. Ferreira and A. Ricard, in G. Bekefi (Ed.), Principles of Laser Plasmas, Ch. 5, Wiley, New York, 1976, and references therein.
7 J. H. Kolts and D. W. Setser, in D. W. Setser (Ed.), Reaction Intermediates in the Gas Phase, Ch. 3, Academic Press, New York, 1979, and references therein.
8 J. F. Prince, C. B. Collins and W. W. Robertson, J. Chem. Phys., 40 (1963) 2619.
9 J. A. Strauss, N. P. Ferreira and H. G. C. Human, Spectrochim. Acta, Part B, 37 (1982) 947.
10 J. E. Lovelock, Anal. Chem., 33 (1961) 163.
11 W. A. Ave, V. Paramagigasami and J. H. Kim, Can. J. Chem., 59 (1981) 1439.
12 H. V. Eckert, High Temp. Sci., 6 (1974) 99.
13 A. T. Zander and G. M. Hieftje, Appl. Spectrosc., 35 (1981) 357.
14 P. C. Uden, Specific Elemental Detection in Chromatography by Plasma Emission Spectroscopy, in F. E. Brinkman and R. H. Fish (Eds.), Environmental Speciation and Monitoring Needs for Trace Metal Containing Substances from Energy-Related Processes, NBS Spec. Publ. 618, U.S. Government Printing Office, Washington, DC, 1981.
15 D. L. Windsor and M. Bonner Denton, Appl. Spectrosc., 32 (1978) 366.
16 S. K. Hughes and R. C. Fry, Anal. Chem., 53 (1981) 1111.
17 S. K. Hughes and R. C. Fry, Appl. Spectrosc., 35 (1981) 493.
18 D. W. Setser, D. H. Stedman and J. A. Coxon, J. Chem. Phys., 53 (1970) 1004.
19 R. S. Houk, V. A. Fassel, G. D. Flesch, H. J. Svec, A. L. Gray and C. E. Taylor, Anal. Chem., 52 (1980) 2283.
20 J. F. Prince and W. W. Robertson, J. Chem. Phys., 45 (1966) 2577.
21 T. D. Strickler and E. T. Arakawa, J. Chem. Phys., 41 (1964) 1783.
22 M. Grossi, M. Langenwalter, H. Helm and T. D. Mark, J. Chem. Phys., 74 (1981) 1728.

Analytica Chimica Acta, 166 (1984) 39—49
Elsevier Science Publishers B.V., Amsterdam — Printed in The Netherlands

DIRECT ANALYSIS OF SOLIDS FOR TRACE ELEMENTS BY COMBINED ELECTROTHERMAL FURNACE/QUARTZ T-TUBE/FLAME ATOMIC ABSORPTION SPECTROMETRY

R. KANIPAYOR, D. A. NARANJIT, B. H. RADZIUK and J. C. VAN LOON*

Department of Geology and Chemistry and the Institute for Environmental Studies, University of Toronto, Toronto, Ontario M5S 1A1 (Canada)

Y. THOMASSEN

Institute of Occupational Health, Gydas vei 8, Oslo 1 (Norway)

(Recieved 11th April 1984)

SUMMARY

The analysis of solid samples by a combined graphite-furnace/air-acetylene flame technique based on generally available atomic absorption instrumentation is described. Samples are injected into the furnace and atomized via a slotted T-tube in the flame. Non-specific absorption is greatly reduced compared to that obtained in graphite-furnace atomic absorption spectrometry (a.a.s.). Sensitivity is reduced by 10—200 times compared to the direct graphite-furnace method, so that large sample sizes (up to 0.2 g) can be used; this minimizes problems caused by sample inhomogeneity. The elements considered are cadmium, lead, copper, arsenic, cobalt, mercury, antimony and selenium. Volatile elements such as mercury and arsenic can be determined without the need for a char step. Simple calibration procedures are possible in some cases and the precision is usually better than 10%. Background reduction capabilities are compared with those of conventional graphite-furnace a.a.s., the isothermal-furnace and the hollow graphite T-tube techniques. Analytical capabilities and results are presented for the direct determination of trace elements in numerous biological and some geological samples.

The direct determination of trace elements in solid samples is highly desirable. Wet chemical treatments including separations and concentration steps are omitted, and samples can be analyzed quickly with minimal risk of loss or contamination. The direct analysis of samples is far from simple. It introduces a very high level of matrix into the system, which produces a large background (non-specific) absorption in atomic absorption spectrometry. The conventional methods of background correction are capable of compensating only limited levels of non-specific absorption, hence, a suitable procedure for solid samples should include the reduction of such large background absorbances to values that can be easily and accurately corrected by using conventional background correctors.

Many methods for direct analysis of solid samples have been proposed for use with atomic absorption (a.a.s.), emission (a.e.s.) and fluorescence (a.f.s.) spectrometry [1]. However, with the exception of arc and spark a.e.s., no

0003-2670/84/$03.00

approach to direct analysis of solid samples by these techniques has gained widespread acceptance. In addition, most of the proposed methods, including arc and spark a.e.s., are plagued by poor precision and difficulties with standardization.

Direct analyses of solid samples for trace metals by a.a.s. have been reviewed [1—3]. In direct graphite-furnace a.a.s., the solid sample is placed in the atomizer and is volatilized and atomized in the optical path. There are several disadvantages inherent in this method. The typical sample weight used to obtain reasonable absorption signals is 1 mg; with such small weights, sample inhomogeneity and inaccuracies in weighing and transfer contribute to errors. Additionally, the aerosol within the optical path may lead to a high background absorbance for which most of the commercially available background correction techniques are inadequate. This problem is particularly severe for elements with resonance lines below 250 nm. In order to reduce this problem, two main approaches have been used: (1) samples are diluted with an inert substance such as powdered graphite [4], which can cause problems of contamination and sample inhomogeneity; (2) time-resolved selective volatilization [5, 6] is used to remove the sample matrix and thus reduce the level of background absorption. The results appear promising for certain elements [7, 8], but volatile elements like As, Hg, Sb, Se and Cd may be lost during the charring step. Sample pretreatment, e.g., "analyte modification" [9, 10], has been found useful in reducing interferences without loss of analyte in certain cases [7, 8]. Another problem with the use of electrothermal atomizers is that solid organic and biological samples often produce a carbon skeleton during the charring and atomization steps; in direct graphite-furnace a.a.s., this will affect reproducibility and may even severely attenuate the light beam.

Methods in which volatilization of the sample is done elsewhere than in the optical path, appear to address these problems much better than direct graphite-furnace a.a.s. For example, the capsule-in-flame [3], isothermal furnace [11], and hollow graphite T-atomizer [12] methods reduce non-specific absorption to a great extent. In this paper, it is shown that a conventional atomic-absorption graphite furnace coupled to an air-acetylene flame atomizer can be used for the analysis of solid samples. This system largely eliminates the above-described problems. The basic construction and operation of the system, the background reduction capabilities and the analytical capabilities are described. A prototype of the system has been described for the determination of lead in rocks and sea water [13].

EXPERIMENTAL

Instrumentation

A Perkin-Elmer 603 atomic absorption spectrometer equipped with a deuterium arc for background correction, a three-slot burner head, and a Perkin-Elmer model 56 recorder were used. An electrothermal atomizer

(Perkin-Elmer HGA-2000) was used for dry sample aerosol production. Both end windows of the furnace were removed. At one end of the furnace an adaptor for the gas inlet tube was inserted and a continuous stream of argon was passed through the furnace; at the other end a graphite support for the quartz T-tube was inserted. The support was precisely machined to fit within the graphite cone and around the quartz T-tube. A schematic diagram of this modification for the HGA-2000 is shown in Fig. 1. The T-tube used was constructed of 2.0-mm thick quartz; the stem of the "T" was 20 cm long (8 mm o.d.) and the top was 8 cm long (16 mm o.d.). A slot (8 × 2 mm) was cut along the top bar of the "T" so that the flame gases could enter.

The volatilized sample from the furnace was swept into the quartz tube by the argon carrier gas. The quartz tube was positioned in such a way that the optical beam passed through the top tube of the "T". This section of the quartz tube was heated by an air-acetylene flame supported on a three-slot burner head; a portion of the flame gases enters the bar of the quartz T-tube through the slot. The active chemical environment in the tube improves dissociation of the analyte and matrix species during the atomization step.

Standards

The standard solid samples examined included: National Bureau of Standards Bovine Liver (SRM 1577), Orchard Leaves (SRM 1571), Tomato Leaves (SRM 1573), Spinach Leaves (SRM 1570), Oyster Tissue (SRM 1566), Phosphate Rock (Florida) (SRM 120b), Coal Fly Ash (SRM 1633a), River Sediment (SRM 1645) and Pine Needles (SRM 1575); Scandinavian standard ASK-3 sulfide ore; National Research Council marine biological standards (NRC 494 and 833); and an International Council for the Exploration of the Sea sample (ICES 35).

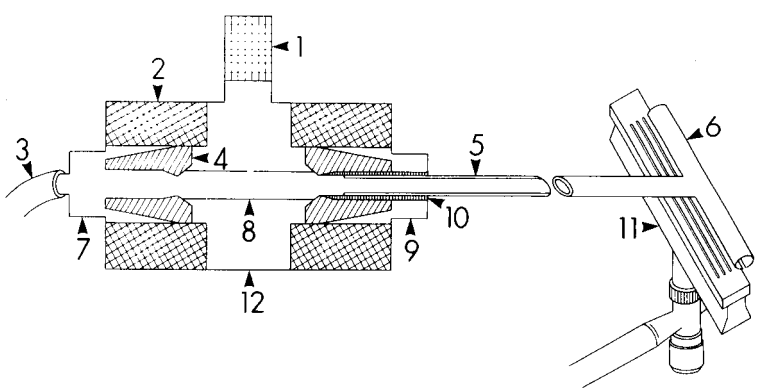

Fig. 1. Perkin-Elmer HGA-2000 graphite furnace (modified) with a quartz T-tube/flame arrangement for solid sampling. (1) Sample injection and observation tube; (2) atomizer body with assembled cooling chamber; (3) carrier gas inlet tube; (4) graphite cone; (5) quartz tube, stem of the "T"; (6) quartz tube, top of the "T"; (7) aluminum holder for gas inlet tube; (8) graphite tube; (9) aluminum support for quartz T-tube; (10) graphite support for quartz T-tube; (11) three-slot burner; (12) HGA-2000 housing.

A primary 1000 μg ml^{-1} standard of mixed metals (Cd, Hg, Cu, Cr, Pb, Co and Se) was prepared by separately dissolving the pure metals in a minimum amount of nitric acid, combining these solutions and diluting to volume with distilled water. The final nitric acid content was about 1%. A primary standard solution of arsenic(III) (1000 μg ml^{-1}) was prepared by dissolving arsenic trioxide in a minimum amount of 1 M sodium hydroxide. A 1000 μg ml^{-1} antimony(V) solution was prepared by dissolving antimony potassium tartrate hemihydrate in distilled water. Secondary standards were prepared daily by appropriate dilution of the stock solutions.

Procedure

An aluminum sample transfer tool was designed for the purpose of transferring samples (1—200 mg) quickly into the center of the graphite tube. The tool was weighed before and after the transfer. Solid biological samples were weighed and placed in the graphite tube with the sampling tool. For solid geological samples, "L'vov type" graphite platforms (which can handle up to 50 mg of sample) were placed in the furnace to prevent fusion of the residue to the tube. The samples were weighed together with the platforms and inserted into the graphite tube. Standard solutions (when used) were injected directly into the tube through the sample port or on to the platform placed inside the tube. In all cases, the drying temperature used was 100° C. The deuterium arc background corrector used in this work could correct background absorbances up to about 0.8. Analyte modification for cadmium was obtained by injecting 100 μl of a saturated ammonium sulfate solution on to the samples prior to drying. The standard addition method was applied as outlined in ref. 7. All results were obtained by measuring the height of the analyte peak absorbance on the strip-chart recorder.

RESULT AND DISCUSSION

Effect of carrier gas flow rate

The transient analyte absorbance signal recorded when the volatilized sample was swept into the flame depended on the particular analyte element, the carrier gas flow rate, and the sample matrix. For all elements studied, there was a carrier gas flow rate at which maximum peak-height sensitivity was obtained. Relatively broad analyte signals were obtained at low flow rates. At flow rates above the optimum value, the analyte signal continued to narrow, but the peak height of the signal decreased. The optimum ranges of gas flow rate for Cd, Hg, Sb and Se in bovine liver are given in Table 1.

Sensitivity

The proposed method of analysis is 10—200 times less sensitive than earlier graphite-furnace techniques (Table 2). The lower sensitivity makes it possible to take larger sample weights than those normally used in direct graphite-furnace a.a.s. The actual sample weight that can be used depends on

TABLE 1

Optimum ranges of carrier gas (argon) flow rate for NBS bovine liver (recorded without a char step)

Element	Optimum range (l min^{-1})	Element	Optimum range (l min^{-1})
Cadmium	0.07—0.13	Antimony	0.36—0.46
Mercury	0.60—0.74	Selenium	0.07—0.12

TABLE 2

Sensitivity (in pg/0.0044 absorbance) for aqueous standard solutions obtained with conventional graphite-furnace a.a.s., the proposed method and the graphite-T atomizer method [12]

Element	λ (nm)	HGA-2100 method[a]	Proposed method[b]	Graphite-T atomizer [12]
Cadmium	228.8	2	70	0.08
Mercury	253.4	11 000	27 200	600
Arsenic	193.4	60	2500	100
Selenium	196.0	350	1400	400
Lead	283.4	50	2550	0.2
Copper	324.7	50	650	100
Chromium	357.9	25	4400	800

[a]As given by Perkin-Elmer (1975). [b]Without a char step.

three features: (i) the concentration of the analyte in the matrix; (ii) the type of the matrix; and (iii) whether or not a char step can be used without loss of the analyte. Sensitivity data for several elements in different solid matrices are presented in Table 3.

Non-specific (background) absorption

The non-specific absorption produced during the direct analysis of solid samples results from the molecular absorptions of both inorganic and organic species produced from the sample matrix. Some of the commonest interfering inorganic species in conventional graphite-furnace a.a.s. are salts of the halides [14, 15]. The non-specific absorptions from such species were found to be much lower in the proposed system than those reported for conventional graphite-furnace a.a.s. and the isothermal furnace method [11], by about three (Table 4) and two orders of magnitude, respectively. A similar study of organic solvents showed that the non-specific absorptions generated by the proposed method were 1—2 orders of magnitude lower than those reported by Robinson and Wolcott [12] for their hollow graphite-T atomizer (Table 5).

The proposed method was used to investigate three NBS samples (bovine liver, orchard leaves and oyster tissue) in order to evaluate the contribution of inorganic and organic species to the non-specific absorptions. Figure 2

TABLE 3

Sensitivity for solid samples with the proposed method

Element	λ (nm)	NBS SRM	Char temp. (°C)	Sensitivity[a]
Cadmium	228.8	Bovine Liver	Nil	57
		Orchard Leaves	Nil	7
		Tomato Leaves	Nil	47
		Oyster Tissue	Nil	60
		Phosphate Rock	Nil	1320
Mercury	253.4	Bovine Liver	Nil	4
		Orchard Leaves	Nil	21
		Oyster Tissue	Nil	10
		ASK-3 Sulfide Ore	Nil	1340
Antimony	217.4	Bovine Liver	Nil	0.4
Selenium	196.0	Bovine Liver	Nil	180
Arsenic	193.7	Bovine Liver	Nil	1.7
		Tomato Leaves	Nil	13
		Oyster Tissue	200	1840
Copper	324.7	Orchard Leaves	Nil	88
		Tomato Leaves	Nil	118
		Spinach Leaves	Nil	96
Cobalt	240.7	Bovine Liver	1000	792
		Tomato Leaves	1000	660
		Oyster Tissue	1000	1354

[a]pg/0.0044 absorbance.

TABLE 4

Background absorbance of inorganic species in direct graphite-furnace a.a.s. [14] and the proposed methods

Compound	λ (nm)	Absorbance/μg	
		Graphite-furnace a.a.s.	Proposed method
NaF	220	0.05	0.00007
NaCl	230	0.12	0.00012
NaI	220	0.20	0.00017
Na_2HPO_4	220	—	0.00003

summarizes the background absorptions recorded with and without a char step for these samples. The results show that when no char step was used, by far the greater contributions to the non-specific background absorption were from the organic species (volatiles). The levels of non-specific absorption produced by the proposed system were sufficiently low to allow the use of about 10 mg of samples without a char step and about 100 mg of samples when a char step was employed.

TABLE 5

Background absorbance of organic compounds in the hollow graphite T-tube atomizer [12] and the proposed method

Compound	λ (nm)	Absorbance/μl	
		Graphite T-tube	Proposed
Benzene	200	0.295	0.023
Hexane	210	—	0.007
Heptane	210	0.400	—
Methanol	200	0.03	ND[a]

[a]No signals were detected for 100 μl of the solvent in the range 190—350 nm.

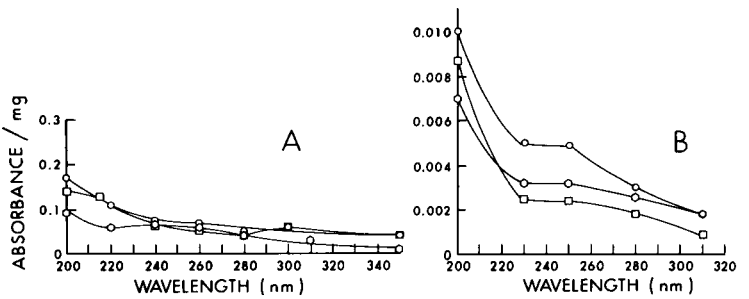

Fig. 2. Variation of background absorbance with wavelength recorded (A) without a char step and (B) with a char step at 600°C (120 s): (○) NBS oyster tissue; (□) NBS bovine liver; (○) NBS orchard leaves.

In order to compare the various methods for analysis of solid samples, the background absorbances from bovine liver, orchard leaves and oyster tissue were recorded at the cadmium 228.8-nm line (Table 6). The results show that approximately 10 times the sample weight (without a char step) and 100 times the sample weight (with a char step) could be used with the proposed method compared to the direct graphite-furnace a.a.s. method.

Analyte absorption

Calibration curves were prepared for cadmium, mercury and arsenic in a number of different matrices (Figs. 3—5). All these curves were recorded without a char step except for arsenic in oyster tissue which was charred at 200°C (at this temperature, no loss of arsenic was observed). In all cases, except for cadmium in oyster tissue and spinach leaves (where the concentration of cadmium exceeded 1 mg kg^{-1}) and arsenic in bovine liver (where the curve had a positive deviation), it was possible to use up to about 10 mg of samples. For elements in lower concentrations (<1 mg kg^{-1}), it was possible to use up to 10 mg of sample for oyster tissue and spinach leaves.

TABLE 6

Background absorbance at 228.8 nm from various standard reference materials

NBS SRM	Sample weight (mg)	Char step		Background absorbance
		Temp. (°C)	Time (s)	
Direct graphite-furnace a.a.s.[a]				
Bovine Liver	0.5	Nil	50	>2.50
	0.5	650	50	0.30
Oyster Tissue	1.0	300	50	1.30
	1.0	650	50	0.25
Proposed method				
Bovine Liver	8.0	Nil	60	0.77
	50.0	400	120	1.00
	100.0	800	200	0.19
Orchard Leaves	10.0	Nil	60	0.68
	100.0	700	200	0.14
Oyster Tissue	10.0	Nil	60	0.78
	100.0	600	200	0.30
Isothermal furnace[b]				
Unknown liver[c]	50.0	337	1500	1.80
Orchard Leaves	33.0	337	1500	0.50

[a]From Chakrabarti et al. [7, 8]. [b]From Nichols et al. [11]. [c]Not NBS standard.

The use of "analyte modification" and a proper char step extended the linearities of the calibration curves in all cases. For example, a char step at 400°C extended the linearity of the calibration curve for cadmium in bovine liver to about 30 mg of sample without the background absorption being too high for adequate correction; at temperatures higher than 400°C, loss of cadmium was observed. When ammonium sulfate was used as an analyte modifier to stabilize cadmium in bovine liver at char temperatures above 400°C (as recommended by Chakrabarti et al. [7]) the linearity of the curve was extended to 100 mg of sample with the proposed system. Similarly, a satisfactory linear calibration curve up to 300 mg of sample was obtained for cadmium in orchard leaves by using a char step of 600°C and ammonium sulfate as modifier (Fig. 6).

Method of calibration and results

Calibration with aqueous standards is the simplest approach in the analysis of solid samples. In the proposed method, this is possible in some but not all cases (e.g., aqueous standard solutions were used to determine cadmium in orchard leaves but could not be used for bovine liver). An alternative is to apply the standard addition technique (adding aqueous standards to the solid samples). This method was useful in certain cases (e.g., for the determination of cadmium in bovine liver). The best general approach to calibration is to

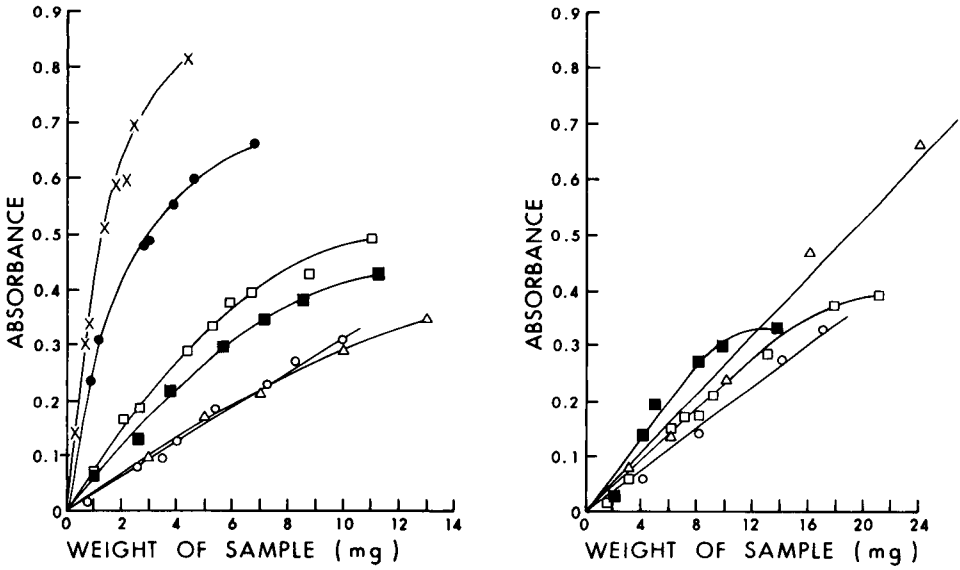

Fig. 3. Calibration curves for cadmium without a char step: (○) bovine liver; (■) orchard leaves; (X) oyster tissue; (●) spinach leaves; (□) phosphate rock (all values recorded at 228.8 nm); (△) ASK-3 sulfide ore (recorded at 326.1 nm).

Fig. 4. Calibration curves for mercury without a char step (recorded at 253.4 nm): (○) bovine liver; (■) orchard leaves; (□) oyster tissue; (△) ASK-3 sulfide ore.

use solid standards with matrices similar to those of the samples to be analyzed. However, it is possible to use standards with different matrices for some analyses (e.g., cadmium in oyster tissue and cobalt in bovine liver were determined by using tomato leaves as the standard). Sometimes this can be done even without a char step (e.g., cadmium in oyster tissue based on tomato leaves). More work will be needed in order to establish calibration procedures for other types of samples. Results are given in Table 7.

Precision

Precision of replicate analyses of solids by the proposed method depends on the matrix of the sample, gas flow rate and whether or not a char step is used. The precision is generally better than 10% r.s.d. (for 10 or more replicate measurements) when peak heights are measured. Precision values and typical detection limits (S/N = 3) for Cd, Hg, Sb and Se in bovine liver are given in Table 8.

In summary, the results indicate that the proposed method has advantages over the direct graphite-furnace a.a.s. method, the isothermal-furnace method [11] and the hollow graphite T-tube method [12] for the analysis of solid samples. It is a simple straightforward method which uses commercially available instrumentation with only slight modifications. Thus the proposed

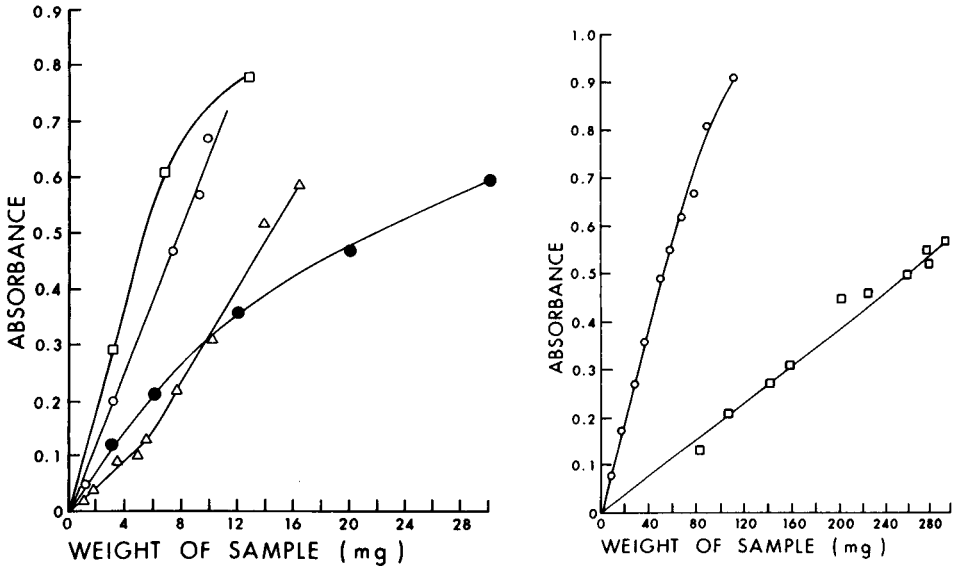

Fig. 5. Calibration curves for arsenic (at 196.0 nm): (△) bovine liver; (□) spinach leaves; (○) tomato leaves (all values recorded without a char step); (●) oyster tissue (recorded with a char step at 200° C for 60 s).

Fig. 6. Calibration curves for cadmium (at 228.8 nm): (○) bovine liver; (□) orchard leaves. All values obtained with a char step at 600° C and saturated ammonium sulfate as the analyte modifier.

TABLE 7

Results of analysis by the proposed method (values based on peak-height measurement)

Element	λ (nm)	Sample	Sample weight (mg)	Char temp. (°C)	Concentration ± s.d. (μg g^{-1})		Calibration method
					Found	Certified[a]	
Cd	228.8	NBS Orchard Leaves	10—30	400	0.12 ± 0.04	0.11 ± 0.02	Aqueous standard solution
		NBS Bovine Liver	4—7	400	0.28	0.27 ± 0.04	Standard addition
		NBS Oyster Tissue	1—5	Nil	3.5 ± 0.5	3.5 ± 0.4	NBS Tomato Leaves[b]
		NBS Orchard Leaves	1—5	Nil	0.26 ± 0.07	0.11 ± 0.02	NBS Tomato Leaves[b]
		NBS Spinach Leaves	1—5	Nil	1.5 ± 0.3	(1.5)	NBS Tomato Leaves[b]
Pb	283.4	NBS Bovine Liver	40—60	800	0.35	0.34 ± 0.08	Standard addition method
		NBS Tomato Leaves	2—10	Nil	5.2 ± 0.8	6.3 ± 0.3	NBS Orchard Leaves[b]
		NBS Spinach Leaves	2—10	Nil	3.4 ± 0.6	1.2 ± 0.2	NBS Orchard Leaves[b]
		NBS Pine Needles	2—10	Nil	10.7 ± 2.0	10.8	NBS Orchard Leaves[b]
Cu	324.7	NBS River Sediment	5—12	1000	90.9 ± 11.2	109 ± 19	Aqueous standard solution
		NBS Coal Fly Ash	5—10	1000	96.6 ± 10.7	118 ± 3	Aqueous standard solution
		NBS Orchard Leaves	1—2	Nil	13.0 ± 1.7	12 ± 1	NBS Spinach Leaves[b]
		NBS Tomato Leaves	1—2	Nil	8.7 ± 1.9	11 ± 1	NBS Spinach Leaves[b]
		NBS Pine Needles	1—2	1000	3.2 ± 0.4	3.3	NBS Spinach Leaves[b]
As	193.7	NRC MB 833[c]	5—11	250	25.3 ± 1.7	24.0 ± 1.8[d]	NBS Oyster Tissue[b]
		NRC MB 494[c]	3—14	250	21.6 ± 1.5	24.2 ± 2[d]	NBS Oyster Tissue[b]
		ICES 35	2—5	200	28.0 ± 1.8	27.8 ± 1.5[d]	NBS Oyster Tissue[b]
Co	240.7	NBS Bovine Liver	100—200	1000	0.19 ± 0.02	(0.18)	NBS Tomato Leaves[b]

[a]NBS values (values in parentheses are not certified). [b]Taken as a solid sample. [c]NRC Marine Biological Samples. [d]Value obtained with ARL ICP 34.000 emission spectrometer.

TABLE 8

Precision (r.s.d.) and detection limits (S/N = 3) for elements in NBS Bovine Liver (without a char step and based on peak-height measurements)

Element	λ (nm)	R.s.d. (%)	Detection limit (pg)
Cadmium	228.8	6.5	106
Mercury	253.4	13.3	30
Antimony	217.4	9.8	4
Selenium	196.0	8.7	1240

method can be readily used in any laboratory having routine atomic absorption instruments.

The authors gratefully acknowledge the financial support of the Ontario Geological Survey.

REFERENCES

1 J. C. Van Loon, Anal. Chem., 52 (1980) 955A.
2 F. J. Langmyhr, Analyst (London), 104 (1979) 993.
3 B. V. L'vov, Talanta, 23 (1976) 109.
4 F. J. Langmyhr, J. R. Stubergh, Y. Thomassen, J. E. Hanssen and J. Dolezal, Anal. Chim. Acta, 71 (1974) 35.
5 D. A. Segar and J. G. Gonzalez, Anal. Chim. Acta, 58 (1972) 7.
6 T. Nakahara and C. L. Chakrabarti, Anal. Chim. Acta, 104 (1979) 99.
7 C. L. Chakrabarti, C. C. Wan and W. C. Li, Spectrochim. Acta, Part B, 35 (1980) 93.
8 C. L. Chakrabarti, C. C. Wan and W. C. Li, Spectrochim. Acta, Part B, 35 (1980) 547.
9 R. D. Ediger, At. Absorpt. Newsl., 14 (1975) 127.
10 R. D. Ediger, G. E. Peterson and J. D. Kerber, At. Absorpt. Newsl., 13 (1974) 61.
11 J. A. Nichols, R. D. Jones and R. Woodriff, Anal. Chem., 50 (1978) 2071.
12 J. W. Robinson and D. K. Wolcott, Anal. Chim. Acta, 74 (1975) 43.
13 D. J. Koop, M. D. Silvester and J. C. Van Loon, Pittsburgh Conference on Analytical Chemistry and Applied Spectroscopy, Cleveland, OH, March, 1979.
14 B. R. Culver and T. Surles, Anal. Chem., 47 (1975) 920.
15 M. J. Adams, G. F. Kirkbright and P. R. Rienvatana, At. Absorpt. Newsl., 14 (1975) 105.

Analytica Chimica Acta, 166 (1984) 51—60
Elsevier Science Publishers B.V., Amsterdam — Printed in The Netherlands

APPLICATION OF INDUCTIVELY-COUPLED PLASMA ATOMIC EMISSION SPECTROMETRY WITH AN INTERNAL REFERENCE TO THE DETERMINATION OF SULFATE AND CALCIUM IN WATERS AND BRINES

I. B. BRENNER*, H. ELDAD, S. ERLICH and N. DALMAN

Geochemistry Division, Geological Survey of Israel, 30 Malkhe Israel Street, Jerusalem, 95501 (Israel)

(Received 27th September 1983)

SUMMARY

A method is described for the determination of sulfate and calcium in waters and brines; an inductively-coupled plasma is used with a multichannel vacuum spectrometer. Study of the behavior of the line-to-background intensity ratios for the S I 180.734, Ca II 317.933, Sc I 402.04 and Sc II 361.384-nm lines as functions of the observation height, aerosol carrier gas, power, and concentration of an easily ionized element shows that Sc II 361.384 nm can be used as an internal reference for sulfur and calcium. In the presence of high salt concentrations, the efficiency and quality of nebulization are degraded and at high aerosol gas flows in the presence of sodium, the line-to-background ratios for the ion lines are depressed and those of the atom lines are enhanced. However, under compromise conditions, the S I 180.734-nm and Ca II 317.933-nm lines exhibit significant freedom from interference caused by an easily ionized element. With the Sc II 361.384-nm line used as the internal reference, short-term precision is improved by a factor of 1.5—4, and long-term precision is improved by a factor of 2, producing data for sulfate and calcium that compare favorably with those obtained by gravimetry, titrimetry, and atomic absorption spectrometry. A detection limit of 70 $\mu g\ l^{-1}$ and a linear dynamic range of 1 $g\ l^{-1}$ were obtained for sulfate.

Sulfate in water is usually determined by precipitation with an excess of barium ions followed by measurement of turbidity of the suspended precipitate, gravimetry [1], or indirect flame atomic absorption or flame emission spectrometry [2—5]. Several disadvantages are associated with these techniques. The chemical methods, although reliable, are tedious. The indirect flame procedures are not well suited for sulfate determination in highly saline matrices because of interferences observed in the flame, even in the presence of ionization suppressors.

Several investigators have studied the ground-state atomic spectral lines of sulfur in the short-wavelength ultraviolet (u.v.) region with d.c. plasmas [6, 7] and inductively-coupled plasmas (i.c.p.) [8, 9]. Spectral line interferences with the S I 180.734-nm line were reported. A calcium line, Ca II 180.734 nm, was identified by Lee and Pritchard [10]. Applications of the i.c.p. have recently been described for routine testing of water and for

0003-2670/84/$03.00

hydrogeochemical reconnaissance programs [11, 12]. Calcium, Mg, Na and K were among the major cations determined, but sulfate was not included.

There are several difficulties in the determination of sulfate in water and brines by inductively coupled plasma-atomic emission spectroscopy (i.c.p./a.e.s.). First, vacuum or purged spectrometers and optical trains are necessary. Secondly, water samples having both high and variable salt contents result in irregularities in nebulization and aerosol transport which affect the precision and accuracy of measurements. Thirdly, the presence of an easily ionizable element such as sodium has been reported to cause enhancements and depressions of spectral line intensities [11]. One approach that takes these factors into account is matrix matching. In order to overcome the necessity of matrix matching, which is impracticable because of sample diversity, a study was made of the capability of the internal reference method to compensate these variations and to improve precision and accuracy. This procedure is capable of correcting nonrandom fluctuations in atomic emission spectrometry [13]; analyte and internal reference intensities fluctuate similarly in response to fluctuations in excitation conditions. Dahlquist and Knoll [14] concluded that ratioing to an internal reference is generally not helpful in improving i.c.p. precision, and can degrade precision if the internal reference and analyte atomic emission transitions are not similar. However, Belchamber and Horlick [15] and Myers and Tracy [16] evaluated the full potential of the internal reference method and demonstrated that the technique can compensate short-term drift, variations in sample uptake, and signal variations caused by inefficient aerosol production from solutions with high salt contents. Myers and Tracy [16] indicated that very good correlation and closely similar noise proportionality can be observed for elements with widely differing excitation and ionization energies for compromise conditions for i.c.p./a.e.s. operation even for a single choice of internal reference.

In the present investigation, the behaviors of the S I 180.734-nm and Ca II 317.933-nm lines and ion and atom lines of scandium (Sc II 361.384 and Sc I 402.04 nm) are examined as a function of some of the i.c.p. operating conditions and the sodium ion concentration in the samples. The accuracy of results obtained by the proposed i.c.p. procedure is evaluated by comparison with results for sulfate and calcium in surface and subsurface waters and brines obtained by the conventional gravimetry, titrimetry and flame atomic absorption spectrometry.

EXPERIMENTAL

Instrumentation

The instrumentation, described previously [17], consisted of a Jobin-Yvon JY48 spectrometer under continuous vacuum to prevent u.v. absorption by oxygen. The optical path between the plasma and the entrance optics of the vacuum spectrometer was purged with argon, using a quartz

tube attached to the entrance slit of the spectrometer and extending to the i.c.p. The outer coolant tube extended 27 mm beyond the end of the plasma tube to the bottom of the observation zone. This modification reduced air entrainment into the plasma, thus reducing the intensity of N emission. In order to avoid memory effects caused by salt deposition on the inner wall of the alumina injector, a Trassy sheathing system [18] was added at the exit of the spray chamber.

Evaluation of scandium as an internal reference

Because radiofrequency power, aerosol flow rate, observation zone, and the concentration of an easily ionizable element are important parameters affecting the line/background ratio [19], a suitable internal reference would be one which responds in a similar way to the elements to be quantified when these parameters vary. In order to evaluate the suitability of scandium as an internal reference for the determination of sulfur and calcium, the background-corrected intensity and net line-to-background intensity ratios of the Sc II 361.384-nm and Sc I 402.04-nm lines were studied as functions of these i.c.p. operating conditions and sodium ion concentration. The observation zone was varied from 0 to 16 mm above the initial radiation zone; the power was varied from 1 to 1.5 kW; the aerosol flow rate was varied from 0.4 to 0.8 l min^{-1} (at 30 psi) and the sheathing gas was varied from 0 to 0.5 l min^{-1}. In order to evaluate the effect of an easily ionizable element on the intensity and intensity ratios, known concentrations of calcium, sulfate and scandium ions (250, 50 and 50 mg l^{-1}, respectively) were added to pure aqueous solutions and to solutions containing sodium chloride varying from 0.01 to 5% (w/v) sodium. For each experimental condition, the background intensity at each line of interest was first measured by aspirating a blank sodium chloride solution, followed by nebulization of the same solution and the pure aqueous solutions containing the analytes. Two different types of nebulizers were used, they were the Jobin-Yvon Pt-teflon concentric nebulizer and the high-salt Meinhard glass concentric nebulizer (TR-C-30).

Calibration and quantitation

All standards were prepared from ultrapure acids (Merck Suprapur) and spectrographically pure reagents. Calcium carbonate, magnesium metal, sodium chloride, standardized sulfuric acid and scandium oxide were used to prepare stock solutions (10 g l^{-1}) for each species of interest. Multi-element standards containing Ca, Mg, Na and sulfate were prepared by diluting aliquots of these stock solutions. Scandium, used as an internal reference, was added to all samples and standard solutions to give a concentration of 50 mg l^{-1}.

Two calibration ranges were used to quantify sulfate in a wide range of water types varying in total salt concentration. One range was used for water having low salt concentrations and another for high salt concentrations.

The former range had 10—500 mg l^{-1} calcium, 10—300 mg l^{-1} magnesium, 50—500 mg l^{-1} sodium and 5—500 mg l^{-1} sulfate. In brines, the concentrations were 50—500 mg l^{-1} calcium and magnesium, 100—1500 mg l^{-1} sodium and 100—500 mg l^{-1} sulfate. Two-point calibrations were obtained by measuring the net or gross intensity ratios (depending on the concentration level of sulfate) by using the Ca II 317.933-nm, S I 180.734-nm and Sc II 361.384-nm lines.

Spectral line interference

Because brines contain high concentrations of sodium, calcium and magnesium ions, the nature of the spectral structure around the S I 180.734-nm line in the presence of very high concentrations of these concomitants was studied. This was achieved by moving the entrance slit under computer control 0.08 nm on both sides of the S I 180.734-nm line while aqueous solutions of Ca, Mg and Na (1000 mg l^{-1} each) and sulfate (100 mg l^{-1}) were continuously aspirated. The interference of the Ca II 180.734-nm line on the S I 180.734-nm line was taken into account by calculating an additive interference coefficient from the relationship

$$C_{TR} = C_{OB} - kC_{IN}$$

where C_{TR} is the true concentration of sulfate, C_{OB} is the observed concentration of sulfate, C_{IN} is the concentration of interfering species, and k is the correction coefficient for the interference. This coefficient was determined by using concentrations of 50—1000 mg l^{-1} calcium in the presence and absence of 3 mg l^{-1} sulfate.

Long-term variation and accuracy

The long-term variation for compromise conditions was determined by aspirating a solution containing 500 mg l^{-1} sodium, 100 mg l^{-1} calcium, 50 mg l^{-1} sulfate and 50 mg l^{-1} scandium 20 times at approximately 5-min intervals during a routine sequence. The accuracy of the procedure was evaluated by replicate runs on several natural and synthetic standard water samples. These samples varied considerably in total dissolved salts from low-salt waters to highly saline brines from the Dead Sea. The latter contained 30% total dissolved solids and were diluted 50—100-fold in order to bring them into the quantitative range. Sulfate was quantified in all natural samples by using standard gravimetric, titrimetric, and a.a.s. procedures.

RESULTS AND DISCUSSION

Compensation for variations in the observation zone height and in power

Figure 1 shows that the maximum net line-to-background intensity ratios for the ion lines of calcium and scandium occur low in the plasma, whereas for the S I 180.734-nm line, the maximum ratio is located higher in the plasma. Heights of observation are measured above the tip of the

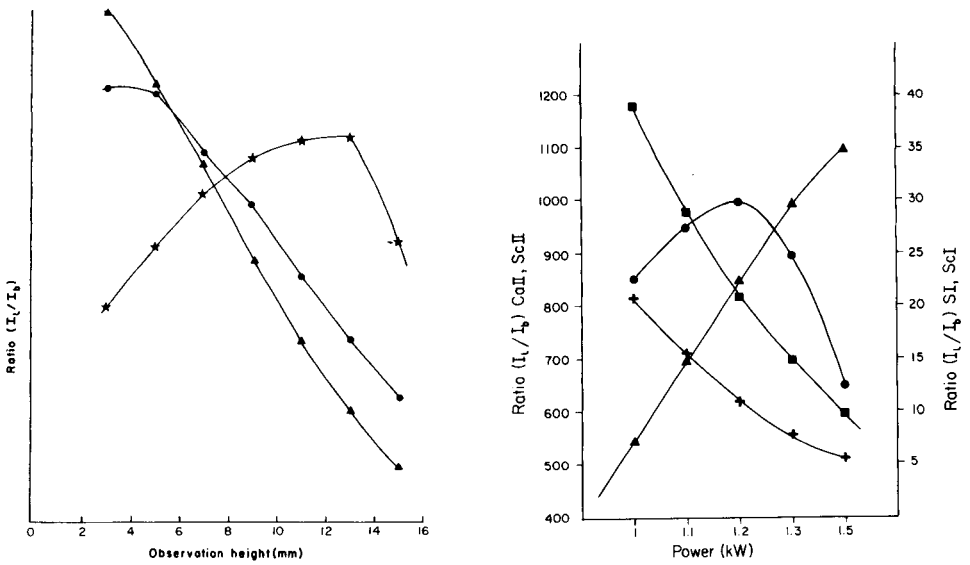

Fig. 1. Variation of the net line-to-background intensity ratio (I_l/I_b) as a function of the observation height above the top of the initial radiation zone: (★) S I 180.734 nm; (●) Sc II 361.384 nm; (▲) Ca II 317.933 nm. Conditions: Meinhard concentric glass nebulizer (TR-C-30); 1.25 kW power; Ar cooling gas, 12 l min^{-1}; Ar sheathing gas, 0.2 l min^{-1}; aerosol carrier gas, 0.4 l min^{-1} (30 psi); solution delivery rate, 2 ml min^{-1}; 250 mg l^{-1} calcium, 50 mg l^{-1} sulfate; 50 mg l^{-1} calcium; 500 mg l^{-1} sodium.

Fig. 2. The effect of power on the net line-to-background intensity ratios (I_l/I_b): (■) S I 180.734 nm; (▲) Ca II 317.933 nm; (●) Sc II 361.384 nm; (+) Sc I 402.04 nm. Jobin-Yvon Pt-teflon nebulizer; 9-mm height above initial radiation zone; other conditions as in Fig. 1.

initial radiation zone. Therefore, the scandium ion line will not compensate for variations in the observation height. This might have been predicted from the findings of Blades and Horlick [19].

The effect of power on the line-to-background intensity ratios for the S I 180.734-nm, Ca II 317.933-nm, Sc I 402.04-nm and Sc II 361.384-nm lines is shown in Fig. 2. At low power, the line-to-background intensity ratios of the atom lines are maximal and decrease with increasing power, whereas, for the ion lines, the ratios increase. Although an increase of the radiofrequency power results in intensification of the background for all wavelengths, the rate of increase is less for calcium, so that the net line intensity for calcium increases with increased power.

For all the lines investigated, the net line-to-background ratios increase with sodium concentration up to about 1000 mg l^{-1} and only for concentrations of 1% Na is a small decrease observed. The results in this figure indicate that the Sc I 402.04-nm and Sc II 361.384-nm lines are candidates as internal references for the S I 180.734-nm and Ca II 317.933-nm lines (up to 1.2 kW), respectively.

Compensation for variations in aerosol and sheathing gas flow rates

Figure 3 shows that the line-to-background intensity ratios for the Ca II 317.933-nm and Sc II 361.384-nm lines decrease with increasing flow rates, whereas the net line-to-background intensity ratio for the Sc I 402.04-nm line increases. The net intensity for the S I 180.734-nm line decreases slightly up to 0.6 l min^{-1} and then remains relatively constant. Thus, the Sc II 361.384-nm line might be a suitable internal reference for the Ca II 317.933-nm line but will not significantly compensate for variations of the S I 180.734-nm line caused by changes of the aerosol flow rate.

Figure 4 shows that there is almost a colinear increase of the net line-to-background intensity ratios for the S I 180.734-nm and Sc I 402.04-nm lines and for the Ca II 317.933-nm and Sc II 361.384-nm lines, and that the Sc II 361.384-nm line can be used as an internal reference up to a sheathing gas flow rate of 0.3 l min^{-1}.

Compensation for variation in sodium ion concentration

The effect of sodium on the analyte-to-scandium intensity ratios is illustrated in Fig. 5. Normalized net signal-to-background intensity ratios as a function of aerosol carrier flow rate for solutions containing up to 2% (w/v) sodium are presented in Fig. 6. As indicated by other investigators [16],

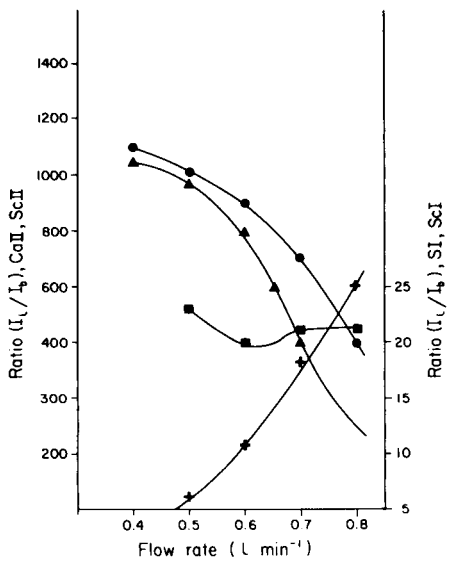

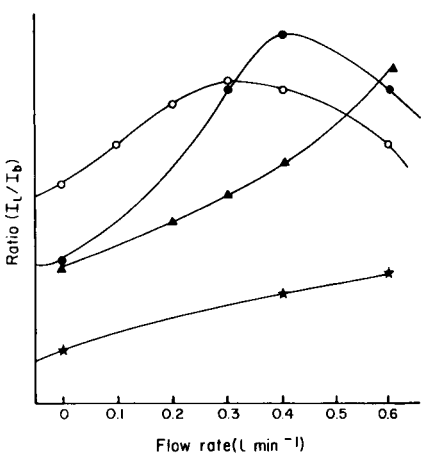

Fig. 3. Variation of the net line-to-background intensity ratios as a function of the aerosol flow rate. Conditions and symbols as in Fig. 2. Power, 1.25 kW.

Fig. 4. Variation of the net line-to-background intensity ratios as a function of the sheathing gas flow rate: Conditions as in Figs. 1 and 2. (▲) S I 180.734 nm; (●) SC II 361.384 nm; (★) SC I 402.04 nm; (○) Ca II 317.933 nm.

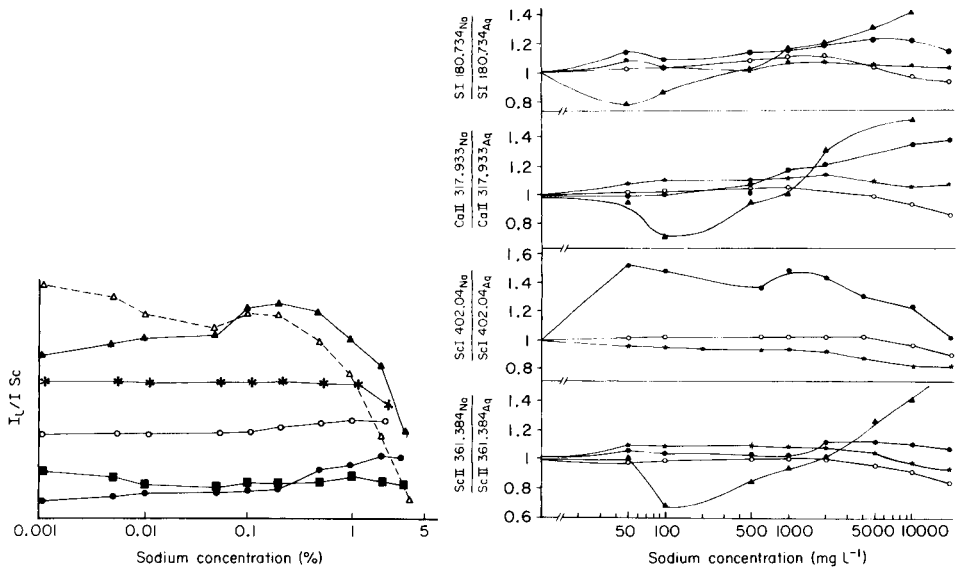

Fig. 5. Analyte-to-Sc II 361.384 line intensity ratios (I_I/I_{Sc}) as a function of the sodium ion concentration in solution: (▲) S I 180.734/Sc I 402.04 nm, Pt-teflon nebulizer; (△) Ca II 317.933/Sc I 402.04 nm, Pt-teflon nebulizer; (●) S I 180.734/Sc II 361.384 nm, Pt-teflon nebulizer; (○) S I 180.734/Sc II 361.384 nm, high-salt Meinhard nebulizer; (★) Ca II 317.933/Sc II 361.384 nm, Pt-teflon nebulizer; (■) Ca II 317.933/Sc II 361.384 nm, high-salt Meinhard nebulizer. Power, 1.25 kW; sheathing gas, 0.2 l min^{-1}; aerosol carrier gas, 0.4 l min^{-1} for Meinhard nebulizer and 0.5 l min^{-1} (30 psi) for Pt-teflon nebulizer.

Fig. 6. Normalized net signal-to-background intensity ratios as a function of the sodium ion concentration in solution. Analyte solutions contain 250 mg l^{-1} Ca, 50 mg l^{-1} Mg and 50 mg l^{-1} Sc. Jobin-Yvon Pt-teflon nebulizer. Aerosol gas flow rates (30 psi): (▲) 0.8 l min^{-1}; (●) 0.7 l min^{-1}; (★) 0.6 l min^{-1}; (○) 0.5 l min^{-1}. Other plasma operating conditions as listed in Figs. 1 and 2.

the net and gross intensities for both the neutral and the ion lines decline with increasing salt concentrations, owing to the reduction in the efficiency of analyte delivery to the plasma. With the Jobin-Yvon concentric Pt-teflon nebulizer, this happens regardless of the composition of the solution. However, preliminary data indicate that the Meinhard concentric nebulizer is capable of continuously nebulizing solutions containing more than 0.5% (w/v) sodium ion. The background also increases with increasing sodium concentration; with background compensation, this variation is reduced. Figure 5 shows that the Sc II 361.384-nm line as internal reference compensates for irregularities in nebulization and aerosol transport, whereas the Sc I 402.04-nm line does not. Figure 6 demonstrates that at aerosol flow rates exceeding 0.6 l min^{-1}, the addition of sodium ion generally causes enhancements of the S I 180.734-nm, Ca II 317.933-nm, Sc II 361.384-nm and Sc I 402.04-nm lines and that this effect is minimized for low aerosol flow rates.

Spectral line interferences

A wavelength profile shows that the S I 180.734-nm line is affected by the adjacent Ca II 180.734-nm line, but that background enhancement caused by 1000 mg l^{-1} each of Ca, Mg and Na is insignificant and needs to be considered only when the sulfate concentration approaches the limit of detection.

The interference correction constant, K, is, in fact, the slope of the graph relating the apparent analyte concentration (interference equivalent concentrations) to the concentration of the interferent in the solutions. Figure 7 shows that the variation of these factors is small (0.0234 ± 0.0004) with increasing calcium content. Consequently, it can be concluded that there is a linear relationship between interference equivalent concentrations and calcium content for the plasma operating conditions. For very low sulfate concentrations, the correction coefficient should be evaluated and applied after a suitable background correction. The interference correction is made by simultaneously quantifying sulfate from the S I 180.734-nm line and the interfering calcium from the Ca II 317.933-nm line followed by subtraction of the interference-equivalent sulfate concentration from the total apparent concentration.

Limit of detection

The limit of detection for the S I 180.734-nm line is defined as that concentration of analyte which gives a response equal to three times the standard deviation of a blank value, determined using a solution containing 10 mg l^{-1} sulfate and an acid blank containing 3% (v/v) nitric acid. Ten measurements were made and limit of detection of 70 μg l^{-1} sulfate was obtained.

Accuracy and precision

The experimental data indicate that the S I 180.734-nm, SC I 402.04-nm and Sc II 361.384-nm lines behave differently under some plasma operating conditions. Nevertheless, the use of the Sc II 364.384-nm line as a single internal reference results in an overall improvement in short- and long-term precision of the determinations of sulfate and calcium in the presence of variable, and large quantities of salt.

It is evident from Table 1 that the accuracy and precision of the calcium and sulfate data produced by the proposed scheme are similar to those obtained by the more time-consuming gravimetric, titrimetric, and a.a.s. procedures. The values obtained for these diverse groups of waters, based on two-point interpolations, for the S I 180.734-nm and Ca II 317.933-nm lines indicate that the calibration plots are generally linear over the entire range of three orders of magnitude.

The short-term measurement imprecision (average of five 10-s integrations) with and without the scandium internal reference is listed in Table 2. The imprecisions of gross analyte and scandium intensities are relatively high (RSD

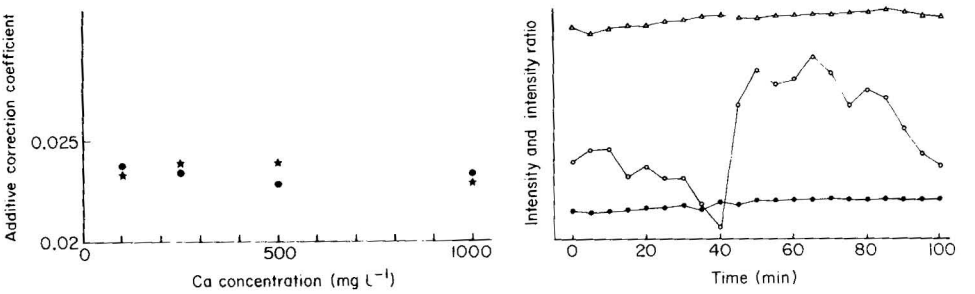

Fig. 7. Relationship between correction coefficient for calcium interference on sulfate and calcium concentration: (•) Ca in aqueous solution; (⋆) Ca in aqueous solution containing 3 mg l^{-1} sulfate.

Fig. 8. Short-term variation for compromise conditions of quantitation. (○) Sc II 361.384 nm (RSD = 1.2%); (△) Ca II 317.933/Sc II 361.384 nm (RSD = 0.5%); (•) S I 180.734/Sc II 361.384 nm (RSD = 0.5%).

TABLE 1

Least-squares statistics for comparison of concentrations quantified with i.c.p./a.e.s., gravimetry (sulfate) and titrimetry (calcium)

Sample	Species	Slope ± s	Intercept ± s	Standard error	Correlation coefficient	No. of samples
Ground waters[a]	SO_4^{2-}[a]	1.03 ± 0.09	−0.002 ± 0.03	0.025	0.98	6
	Ca[b]	1.01 ± 0.04	0.0006 ± 0.001	0.002	0.997	6
Dead Sea brine[a]	SO_4^{2-}[c]	0.979 ± 0.005	0.027 ± 0.005	0.006	0.9997	5
	Ca[d]	1.00 ± 0.05	0.19 ± 0.8	0.3	0.997	5
Synthetic solutions[g]	SO_4^{2-}[e]	1.000 ± 0.002	−0.001 ± 0.001	0.003	0.99998	12
	Ca[f]	1.01 ± 0.01	−0.003 ± 0.009	0.009	0.999	12

[a–f]Relative standard deviations (%) by i.c.p.: [a]0.5—0.7, [b]0.7—1.5, [c]2.0—2.8, [d]1.06—1.1, [e]0.22—0.92, [f]0.11—1.5. [g]All synthetic solutions also contained 10—300 mg l^{-1} Mg and 200—500 mg l^{-1} Na.

TABLE 2

Short-term imprecision

Time (min)	Sc (intensity)	RSD (%)	S/Sc	RSD (%)	Ca/Sc	RSD (%)
0	110 690	0.43	1.598	0.074	0.3203	0.26
45	108 860	0.32	1.596	0.083	0.3161	0.103
60	106 830	0.45	1.598	0.15	0.3211	0.20
75	110 530	0.40	1.609	0.10	0.3217	0.30
90	108 510	0.48	1.616	0.18	0.3218	0.25

for Sc = 1.21%). However, a marked improvement in precision results when the Sc internal reference method is used; the RSD is 0.5% for the Ca II 317.933-nm line and 0.51% for the S I 180.734-nm line (Fig. 8).

In conclusion, the principal advantage of the technique described is that it circumvents the necessity of tedious matrix matching of the calibration standards when sulfate is determined by indirect flame techniques and avoids time-consuming sample handling when the samples are processed by the gravimetric method. Consequently, it offers an attractive and convenient alternative to chemical and other indirect procedures, producing similar, if not superior, results.

REFERENCES

1 Standard Methods for the Examination of Water and Wastewater, 15th edn., American Public Health Association, Washington, DC, 1981.
2 R. Dunk, R. A. Mostyn and H. C. Hoare, At. Absorpt. Newsl., 8 (1979) 79.
3 M. I. Couto and A. J. Curtius, Appl. Spectrosc., 34 (1980) 228.
4 D. D. Siemer, R. Woodriff and J. Robinson, Appl. Spectrosc., 31 (1977) 168.
5 G. H. Wagner and K. F. Steele, Int. Lab., Sept. 12 (1982).
6 P. C. Uden, R. M. Barnes and F. P. Dishonzo, Anal. Chem., 50 (1978) 852.
7 S. R. Ellebracht, P. D. Swaim and D. S. Treybig, in R. M. Barnes (Ed.), Developments in Atomic Plasma Spectrochemical Analysis, Heyden, London, 1981, p. 351.
8 G. F. Kirkbright and M. Marshall, Anal. Chem., 44 (1972) 1228.
9 G. F. Kirkbright, A. F. Ward and T. S. West, Anal. Chim. Acta, 62 (1972) 241.
10 J. Lee and M. W. Pritchard, Spectrochim. Acta, Part B, 36 (1981) 594.
11 H. E. Taylor, in R. M. Barnes (Ed.), Developments in Atomic Plasma Spectrochemical Analysis, Heyden, London, 1981, p. 575.
12 G. F. Larson, R. T. Goodpasture and R. W. Morrow, in R. M. Barnes (Ed.), Developments in Atomic Spectrochemical Analysis, Heyden, London, 1981, p. 611.
13 W. B. Barnett, V. A. Fassel and R. N. Kniseley, Spectrochim. Acta, Part B, 23 (1968) 643; 25 (1970) 139.
14 R. L. Dahlquist and J. W. Knoll, Appl. Spectrosc., 32 (1978).
15 R. M. Belchamber and G. Horlick, Spectrochim. Acta, Part B, 37 (1982) 1037.
16 S. A. Myers and D. H. Tracy, Spectrochim. Acta, Part B, 38 (1983) 1227.
17 Z. Goldbart and I. B. Brenner, ICP Inf. Newsl., 8 (1983) 566.
18 C. Trassy, Instruments SA, Inc., French Patent 7915575 (1979).
19 M. W. Blades and G. Horlick, Spectrochim. Acta, Part B, 36 (1981) 861, 881.

Analytica Chimica Acta, 166 (1984) 61—69
Elsevier Science Publishers B.V., Amsterdam — Printed in The Netherlands

ANALYSIS OF MINERAL SUSPENSIONS BY D.C. PLASMA EMISSION SPECTROMETRY

R. DERIE

Department of Ore Dressing, Université Libre de Bruxelles, 50 avenue F. D. Roosevelt, B-1050 Brussels (Belgium)

(Received 4th January 1984)

SUMMARY

Dilute aqueous suspensions of sub-sieve fractions of various minerals are analyzed for their major constituents by d.c. plasma emission spectrometry. In favourable cases (e.g., determination of zinc in sphalerite or smithsonite powders below 5 μm), the suspensions may be analyzed quantitatively simply by comparison with standard solutions, and with a relative error less than 10%. In other cases (e.g., determination of beryllium in beryl powders), the required element is so poorly atomized that the analysis is impossible, even when very fine-grained suspensions are used. As expected, the atomization efficiency for a particular element decreases with increasing particle size, and with increasing free energy of formation of its oxide at high temperatures. The region extending along the vertical branch of the plasma is a convenient excitation zone for suspensions containing elements that are difficult to atomize but the high background in this region limits the analytical possibilities.

As has been pointed out by numerous authors during the last decade, there is a need, especially in mineral and geochemical exploration, for atomic absorption or emission spectrometric techniques of analysis that do not require prior dissolution of the sample. Comprehensive reviews on the subject have been prepared by Willis [1] and Van Loon [2]. Most of the proposed solid-sampling systems are discontinuous by nature. The simplest technique, i.e., nebulization of a slurry of suspended solids, is said to give erratic results; indeed, the efficiency of nebulization for the suspended solid decreases rapidly with particle size, and there is also a risk of gradual obstruction of the nebulizer by the largest particles. Saba et al. [3] have tested the efficiency of various nebulizers and spray chambers for suspensions of iron powders in 1:1 mixtures of kerosene and lubricating oil. In this particular case, the best system was claimed to be a combination of a ceramic nebulizer and a glass cylindrical spray chamber. The upper size limit for quantitative analysis of the iron particles was about 15 μm.

In the present work, aqueous suspensions of definite size fractions of various minerals were analyzed by means of a d.c. plasma spectrometer, fitted with a ceramic nebulizer and a plastic "diamond" spray chamber. The results are surprisingly good in the case of finely divided substances for which plasma atomization is not too difficult.

0003-2670/84/$03.00

EXPERIMENTAL

Minerals

For this exploratory study, a few minerals were selected that differ both in their refractoriness and their density (Table 1). All of them, except silicon carbide, are of natural origin. Beryl, cassiterite, sphalerite and smithsonite were hand-picked mineralogical specimens; ferberite and columbotantalite were industrial concentrates from a magnetic separation stage. Silicon carbide was an industrial-grade abrasive powder.

Preparation of size fractions and chemical analysis

The minerals were ground in an electric agate mortar for 2 h; the fractions passing a 44-μm sieve (more than 90% in all cases) were classified into subsieve fractions by means of a centrifugal air classifier (Bahco, Sweden). As certain impurities could concentrate in definite size fractions, 100 mg of each was dissolved and analyzed conventionally (by means of the d.c. plasma spectrometer).

The following dissolution techniques were used. For ferberite and columbotantalite, fusion with 2 g of sodium hydroxide, digestion with 50 ml of hot water, and addition of 5 ml of concentrated hydrochloric acid and 1 ml of concentrated hydrofluoric acid, was followed by dilution to 200 ml. For cassiterite, fusion with 2 g of sodium hydroxide with addition of 0.1 g of sodium cyanide during the fusion, digestion with 50 ml of hot water, and addition of 6 ml of concentrated hydrochloric acid was completed by dilution to 200 ml. For beryl, fusion with 0.5 g of sodium carbonate for 30 min at 900°C, digestion with concentrated hydrochloric acid, dehydration and

TABLE 1

Density and thermal properties of the minerals investigated

Name	Formula	Density ($g\ cm^{-3}$)	Thermal properties [4]
Cassiterite	SnO_2	7.0	b.p. ≈ 2000° C (dec.).
Ferberite	$Fe\ WO_4$	7.5	not determined; WO_3 sublimes at an appreciable rate above 1100°C; b.p. WO_2 ≈ 1850° C.
Columbo-tantalite	$(Nb,Ta)_2\ (Fe,Mn)_2O_6$	≈7	not determined; b.p. FeO ≈ 2430°C; b.p. Nb_2O_5 ≈ 2950°C; Ta_2O_5 decomposes on melting (1870°C).
Sphalerite	ZnS	4.1	sublimes above 1350°C (m.p. ≈ 1600°C).
Smithsonite	$ZnCO_3$	4.4	loses CO_2 at 300°C; ZnO sublimes at appreciable rate above 1400°C (m.p. ≈ 1970°C).
Beryl	$Be_3Al_2Si_6O_{18}$	2.6	m.p. 1650°C; b.p. BeO ≈ 3900°C; b.p. Al_2O_3 ≈ 3000°C.
Silicon carbide	SiC	3.2	sublimes (dec.) ≈ 2700° C.

separation of silica, was followed by dilution to 200 ml. Detailed procedures were given by Owens and Yoe [5]. For smithsonite, dissolution in a few ml of concentrated hydrochloric acid and dilution to 200 ml sufficed; for sphalerite, dissolution in a few ml of aqua regia, and dilution to 200 ml. For silicon carbide, fusion with 2 g of sodium hydroxide and 2 g of sodium peroxide, digestion with 100 ml of 2 M hydrochloric acid, and dilution to 200 ml was satisfactory; a detailed procedure was given by Kato [6]. A little hydrofluoric acid was added in order to prevent precipitation of silica.

Apparatus

The measurements were done on a Spectraspan IV d.c. plasma emission spectrometer (Spectrametrics), fitted with the original ceramic nebulizer and plastic spray chamber. The peristaltic pump was used only for the drain of the spray chamber, the samples (solutions or suspensions) being nebulized directly by means of thin polyethylene tubing (30 cm length, 0.38 mm i.d., 1.09 mm o.d.) connected to the inlet of the ceramic nebulizer. The nebulization pressure was 1.5 bar (22 psi) and the argon flow rate was 5.5 l min^{-1}; this ensured a liquid uptake rate of 0.80 ml min^{-1}. From this, 18% (about 0.15 ml min^{-1}) was effectively nebulized, the rest being collected on the walls of the chamber and removed through the drain. The solids (50 mg in 100 ml) were maintained in suspension by means of a magnetic stirrer; the intake capillary tubing was held near the side of a beaker. The length of the magnetic agitator was 1—2 mm less than the inner diameter of the bottom of the beaker. The suspending medium was water with 0.05% surfactant in the case of sphalerite and smithsonite powders; in the other cases, the correct amount of sodium chloride was added so that the suspensions and the solutions of the same mineral had the same sodium concentration.

Procedure

All the analyses were done with the 100 × 500-μm input slit and the 50 × 500-μm output slit. The following wavelengths (nm) were used: Be, 332.1; Al, 396.2; Si, 288.2; Fe, 372.0; Zn, 213.9; Nb, 309.4; Sn, 284.0; Ta, 240.1; W, 400.9. The solutions and suspensions of the minerals were analyzed by comparison with solutions of known concentration, prepared from commercial 1000 mg l^{-1} standards, and containing the same sodium concentration as the unknowns.

When a d.c. plasma spectrometer is used, the plasma must be positioned so that the entrance slit views an area within the bend of the inverted Y-shaped plasma. The possibilities of adjustment are quite limited; in the present case, the distance between the centre of the slit and the image of the inner border of the plasma was judged (by visual estimation) to be 1 mm. In this immediate locality in the plasma, the best conditions were obtained for the excitation of refractory elements such as tantalum or tungsten, while the background emission remained low enough to ensure a high signal-to-background ratio.

RESULTS AND DISCUSSION

Influence of suspension concentration

Preliminary analyses for zinc were made with aqueous suspensions of 4—7-μm sphalerite particles, an aqueous zinc solution (1000 mg l^{-1}) being used as the standard. The results are shown in Table 2. At least up to 0.3% (w/w) suspended solids, the zinc emission intensity was a linear function of the concentration of the suspension, and the zinc contents of sphalerite calculated from the experimental values were in reasonable agreement with the 64.4% (w/w) determined conventionally (see also Table 7).

Determination of relative atomization efficiencies

On the basis of the previous results, the concentration of the suspensions was fixed at 0.05% (w/w) in all experiments (i.e., 50 mg/100 ml), and the various mineral suspensions were analyzed. The results are summarized in Tables 3—8.

TABLE 2

Analysis of sphalerite suspensions (4—7 μm)

Concentration of suspension (mg ZnS/100 ml)	9.6	23	96	307
Zn found (mg l^{-1})	64.3	146	665	2010
Calculated Zn content (wt. %)	66.9	63.5	69.3	65.4

TABLE 3

Analysis of ferberite

Mean size (μm)	Tungsten (%)		ϵ_W[a]	Iron (%)		ϵ_{Fe}[a]
	soln.	susp.		soln.	susp.	
1.0	57.6	58.1	1.01	19.6	21.6	1.10
2.7	54.6	58.9	1.08	18.6	19.4	1.04
6.5	60.5	50.9	0.84	19.6	11.9	0.61
15.3	56.5	5.4	0.10	20.2	2.2	0.11

[a]Relative atomization efficiency (see text).

TABLE 4

Analysis of columbotantalite concentrate

Mean size (μm)	Niobium (%)		ϵ_{Nb}	Tantalum (%)		ϵ_{Ta}	Iron (%)		ϵ_{Fe}
	soln.	susp.		soln.	susp.		soln.	susp.	
0.5	11.6	8.4	0.72	13.0	7.9	0.61	6.5	5.7	0.88
1.6	11.4	8.1	0.71	12.0	7.2	0.60	6.0	6.2	1.03
7.4	12.3	6.1	0.50	11.6	2.9	0.25	5.4	4.9	0.91
14.7	13.0	0.4	0.03	12.2	0.2	0.02	5.5	0.4	0.08

TABLE 5

Analysis of cassiterite

Mean size (μm)	Tin (%)		ϵ_{Sn}
	soln.	susp.	
0.5	58.1	53.8	0.93
1.6	66.1	64.7	0.98
4.4	65.4	70.7	1.08
7.6	66.4	15.7	0.24

TABLE 6

Analysis of beryl

Mean size (μm)	Beryllium (%)		ϵ_{Be}	Aluminium (%)		ϵ_{Al}
	soln.	susp.		soln.	susp.	
0.8	2.70	0.42	0.16	12.4	1.17	0.09
3.4	2.95	0.20	0.07	13.1	0.44	0.03
10.5	3.55	0.04	0.01	14.6	0.15	0.01
21.5	3.40	n.d.		13.3	0.05	

TABLE 7

Analysis of sphalerite and smithsonite

Mean size (μm)	Zinc (%)		ϵ_{Zn}
	soln.	susp.	
Sphalerite			
2.3	63.4	65.7	1.04
5.6	64.4	66.3	1.03
9.8	63.3	52.2	0.82
16.7	64.6	38.8	0.60
Smithsonite			
1.3	47.8	51.8	1.08
4.8	48.1	45.6	0.95
13.5	51.7	29.2	0.56
24.0	45.4	19.7	0.43

The relative atomization efficiency, ϵ_{rel}, as defined by Willis [1], is the ratio of the concentration of free atoms of the analyte in the emission zone when a suspension of particles is sprayed, to that concentration obtained when an identical amount of analyte is sprayed as a solution. It is thus the ratio of the characteristic line intensities, and also of the apparent concentrations of an element, as calculated from the data given by the spectrometer. On the basis of the present results, the following comments can be made. As expected, within experimental error, the relative atomization

TABLE 8

Analysis of silicon carbide

Mean size (μm)	Silicon (%)		ϵ_{Si}
	soln.	susp.	
2.5	68.2	14.8	0.22
6.5	70.5	8.1	0.11
10.9	70.6	6.9	0.10
18.5	62.7	0.7	0.01

efficiency decreases markedly with increasing particle size. Four of the seven minerals studied (ferberite, cassiterite, sphalerite and smithsonite), if ground below 5 μm, may be analyzed by the suspension technique with a relative error of less than 10%. Columbotantalite, even when very finely ground, gives low results, but they may be satisfactory for prospecting work. The substances giving the worst results, beryl and silicon carbide, are also those having the lowest densities. This property, therefore, does not seem to be critical in the present experimental conditions, at least for the smallest particles.

The efficiency of the sampler/nebulizer system was tested by collecting the particles effectively nebulized over a given period of time; this was done with sphalerite particles of various mean sizes, in the same way as described by Saba et al. [3]. The collected particles were dissolved, and the zinc content was determined in the usual way. The results may be expressed as the ratio, r, of the amount of zinc effectively collected to the amount that may be expected from the concentration of the suspension, the liquid uptake rate and the fraction of liquid being nebulized, i.e., 18%. These results are shown in Table 9.

It may seem surprising that particles as large as 16-μm diameter, and having a density of 4.1 g cm^{-3}, are transported through the nebulizer and spray chamber, and effectively reach the vicinity of the plasma. The values of r obtained, however, are still less than those found by Saba et al. [3], using a ceramic nebulizer and a cylindrical glass spray chamber. For instance, r was 0.69 for 14—28-μm iron particles (density 7.9 g cm^{-3}). The same authors showed that the ceramic nebulizer was 2.5 times more efficient for transporting particles than a conventional glass concentric one.

TABLE 9

Sampler/nebulizer efficiency

Diam. sphalerite particles (μm)	2.3	5.6	9.8	16.7
r[a]	0.85	0.83	0.76	0.54

[a] See text.

The values of ϵ_{Zn} (Table 7) for the smallest sphalerite particles (2.3 and 5.6 μm) are close to unity; the corresponding r values are 0.85 and 0.83. In this particular case, the fine-sized suspensions apparently give a stronger emission than solutions containing the same amount of zinc.

For a given mineral (e.g., columbotantalite), the values of ϵ may differ from one element to another. As in this particular case, ϵ increases with the ability of the corresponding oxide to be dissociated, therefore an attempt was made to correlate the free energies of formation of the oxides (expressed in kJ mol^{-1} O_2 and calculated from the data of Barin et al. [7]) with the values of ϵ for 2.5-μm particles (obtained by interpolation of the experimental values). These data are given in Table 10. The linear regression coefficient between the ΔG_{2300} and ϵ values is 0.91 (highly significant); this coefficient is 0.90 when the ΔG_{3000} values (more appropriate in this case) are used, but fewer data are available. This should mean that the most important factor controlling the atomization efficiency, at least in this particular case, is the chemical affinity for oxygen at high temperatures. In other words, the thermal effect of the plasma radiation, in the usual excitation region, should be sufficient to dissociate the finest particles into their constituting oxides, but only partially to dissociate these oxides into metal and oxygen.

The temperature in the excitation region, just below the bend of the plasma, has been estimated by the manufacturer to be 6000—7000 K, while the temperature in the plasma itself approaches 10 000 K. After a short stay in this excitation region, which is highly turbulent, the sample flows along the vertical branch of the plasma, towards the cathode; this external argon stream contributes to the stability of the discharge. This constitutes potentially a "warmer" excitation region, in which, however, it is not recommended to work, because the entrance slit directly views the plasma, and the background emission (plasma continuum) is very high, although quite stable.

The Spectraspan IV spectrometer is not designed to permit measurements

TABLE 10

Free energies of formation of the oxides (expressed as kJ mol^{-1} O_2) and corresponding atomization efficiencies ϵ

Oxidation reaction	ΔG at 2300 K (kJ)	ΔG at 3000 K (kJ)	ϵ
$2Be + O_2 \rightarrow 2BeO$	—745	—564	0.10
$4/3Al + O_2 \rightarrow 2/3Al_2O_3$	—623	—465	0.05
$Si + O_2 \rightarrow SiO_2$	—494	—363	0.22
$2Fe + O_2 \rightarrow 2FeO$	—265	—190	1.01, 1.05
$2Zn + O_2 \rightarrow 2ZnO$	—20	—	1.04, 1.04
$Sn + O_2 \rightarrow SnO_2$	—130	—	1.01
$4/5Nb + O_2 \rightarrow 2/5Nb_2O_5$	—390	—	0.68
$4/5Ta + O_2 \rightarrow 2/5Ta_2O_5$	—560	—356	0.55
$2/3W + O_2 \rightarrow 2/3WO_3$	—205	—	1.07

of the background near an emission line. It is possible, however, by carefully rotating the wavelength selector thumbwheel on both sides of the position of the maximum emission signal, to measure the background level with acceptable precision. For ease of manipulation, it is advantageous to connect a recorder (10-V full scale) to the analog output of the spectrometer. In such a way, it was possible to measure the intensity of an emission line as a function of the vertical distance along the axis of the plasma. This was done with 2.3-μm sphalerite and 0.8-μm beryl suspensions (300 mg/100 ml), and with solutions containing the same amounts of zinc and beryllium, respectively. The entrance slit was 300 X 50 μm; the other experimental conditions were as previously described.

The results are presented in Fig. 1. The two emission curves for zinc are similar, except that the solution begins to emit at a greater distance below the plasma. In particular, the maxima are situated in the same place (about 0.5 mm below the bend), and their intensities are nearly equal, as might be expected from the results already given. The situation is strikingly different for beryllium. The emission maximum of the suspension is found about 0.5 mm inside the plasma, while the most intense emission of the solution takes place close to the bend, but below the plasma. The two emission curves intersect at about 2 mm above the bend, the emission of the suspension then being higher than that of the solution above this position. This shows that the d.c. plasma itself may be considered as a convenient source of excitation for sub-sieve solid suspensions, but that, under the usual working conditions the residence time in the vicinity of the plasma is

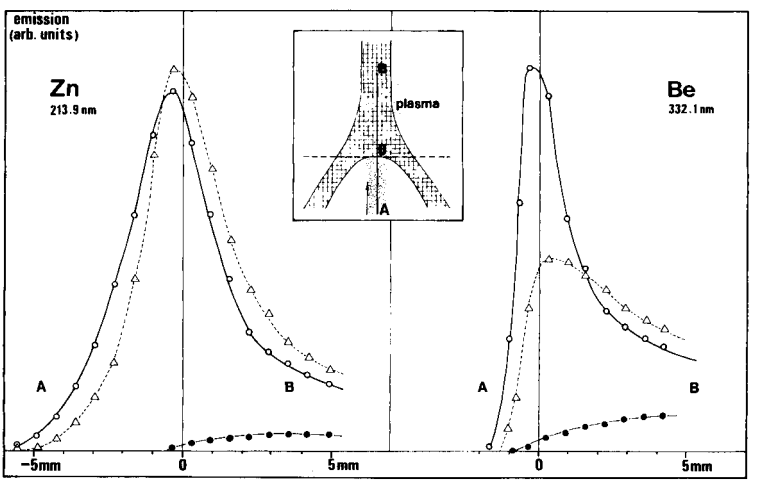

Fig. 1. Emission profiles of nebulized solutions (○) and suspensions (△) having the same concentrations of zinc (3000 mg l^{-1} ZnS, 2.3 μm and 2000 mg l^{-1} Zn^{2+}, respectively) and (3000 mg l^{-1} beryl, 0.8 μm, and 80 mg l^{-1} Be^{2+}). (●) Background emission around 214.0 nm for zinc and around 332.2 nm for beryllium. The emission is expressed in arbitrary units; the background has been deducted.

too short to allow complete dissociation of many molecules to their elements. In addition, when the entrance slit directly views the plasma, the background increases considerably. This decreases greatly the analytical possibilities, but the similarity of the emission profiles within this part of the plasma may at least be useful for the determination of the major components of powder suspensions.

Conclusions

The work described above is concerned with the chemical analysis of ores and concentrates. The number of substances analyzed was limited so that general conclusions should not be. However, the following conclusions may be drawn. Dilute suspensions of finely powdered solids (under ≈ 10 μm diameter) may be reproducibly and nearly quantitatively introduced into the excitation region by the nebulization system of the d.c. plasma spectrometer. When the measurements are made in the usual excitation region (below the bend in the plasma), the most important factors controlling the atomization efficiency are the dimensions of the particles and the chemical affinity of the element being determined for oxygen at high temperatures. The atomization efficiencies are higher in the region extending along the vertical branch of the plasma, but the high background level then limits the analytical possibilities.

We thank Prof. Dr. Georges Panou, Director of the Department, for fruitful discussions, Mr. Claude Van Bogaert for helpful technical assistance, and the Fonds National de la Recherche Scientifique (Belgium) for financial support.

REFERENCES

1 J. Willis, Anal. Chem., 47 (1975) 1752.
2 J. Van Loon, Anal. Chem., 52 (1980) 955A.
3 C. Saba, W. Rhine and K. Eisentraut, Anal. Chem., 53 (1981) 1099.
4 G. V. Samsonov, The Oxide Handbook, I.F.I./Plenum, New York, 1973.
5 E. Owens and J. Yoe, Anal. Chem., 32 (1960) 1345.
6 K. Kato, At. Absorpt. Newsl., 15 (1976) 4.
7 I. Barin, O. Knacke and O. Kubaschewski, Thermochemical Properties of Inorganic Substances, Springer, Berlin, 1973; suppl., 1977.

Analytica Chimica Acta, 166 (1984) 71—78
Elsevier Science Publishers B.V., Amsterdam — Printed in The Netherlands

REACTIONS BETWEEN TECHNETIUM(VII) AND SOME HYDRAZONES AND THE SPECTROFLUORIMETRIC DETERMINATION OF TECHNETIUM(VII) WITH 2,2′-DIPYRIDYLKETONE HYDRAZONE

F. GRASES* and J. G. MARCH

Department of Analytical Chemistry, Faculty of Sciences, University of Palma de Mallorca (Spain)

F. MATA and A. PEÑAFIEL

Nuclear Medicine Section, Residencia Sanitaria "Virgen de Lluch", Palma de Mallorca (Spain)

(Received 24th April 1984)

SUMMARY

The reactions between pertechnetate and five hydrazones are described. Of these, the technetium(VII)/2,2′-dipyridylketone hydrazone system was found to be most sensitive, and is studied in detail. Spectrofluorimetric procedures for the determination of technetium(VII) over the range 0.01—12 mg l^{-1} are reported. The reaction proceeds most favourably under acidic conditions (1.4 M hydrochloric acid). For 1 mg l^{-1} technetium(VII), 100 mg l^{-1} levels of U(VI), Re(VII), Mo(VI) or W(VI) do not interfere when the reaction proceeds at room temperature. Sensitivity improves at higher temperatures.

Manganese, technetium and rhenium constitute group VII of the Periodic classification of the elements, technetium being by far the least common; for a long time, the quantities available were very small. Attention has been drawn to the lack of information on the chemistry of technetium [1, 2]. The recent production of appreciable quantities of technetium in radiochemical processing plants has aroused interest in the development of methods of analysis that could be used to supplement the radiochemical procedures commonly used. Also, the unfavourable counting characteristics of the low-energy β-activity of technetium-99 have created added interest in alternative sensitive quantitative methods. Few methods have been described so far for technetium determinations by non-radiochemical processes; the most important ones are shown in Table 1. None is based on a fluorimetric measurement. For spectrophotometry, the reagents used are usually thiocyanate, hexacyanoferrate(II), sulphosalicylic acid, 2-picolinic acid, thioglycolic acid, 1,5-diphenylcarbohydrazide and toluene-3,4-dithiol.

In this paper, the interaction between technetium and various hydrazones is studied, in order to increase knowledge of the chemical behaviour of this element. As a result, new methods for its determination have been developed. The study of the interaction between 2,2′-dipyridylketone hydrazone and

0003-2670/84/$03.00

TABLE 1

Analytical methods for the determination of technetium

Method	Detection limit (g)	Ref.
Atomic absorption spectrometry	4.5×10^{-6}	3
Polarography	5×10^{-8}	4—6
Spectrophotometry	10^{-6}—10^{-8}	6—16
Atomic emission spectrometry	1×10^{-7}	17, 18
Infrared spectrometry	5×10^{-6}	19
Gravimetry	2×10^{-6}	6, 18, 20
X-ray fluorescence spectrometry	1.8×10^{-5}	21

technetium(VII) led to the development of a catalytic-fluorimetric method. The reagents investigated are shown below.

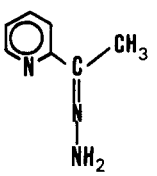

MPKH

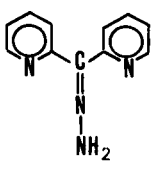

DPKH

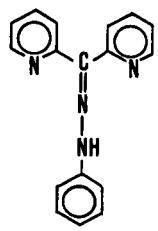

DPKFH

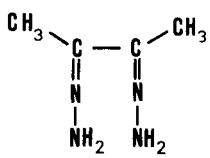

DMDKH

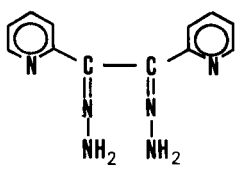

DPDKH

EXPERIMENTAL

Reagents, solutions and apparatus

The hydrazones were synthesized as described previously [22, 23] in a single-step process by mixing the appropriate ketone with hydrazine or phenylhydrazine. Stock solutions included an aqueous 1 g l^{-1} solution of DPKH and ethanolic 1 g l^{-1} solutions of MPKH, DPKFH, DMDKH and DPDKH.

Technetium-99, in solution as ammonium pertechnetate (116 μg Tc ml^{-1}) was supplied by Amersham/Searle Corporation (Arlington Heights, IL).

A Perkin-Elmer LS-5 spectrofluorimeter and a Perkin-Elmer 552 spectrophotometer, with 1.0-cm cells, were used.

Procedure for technetium determination

In a 1.5 × 16-cm test tube, place 1 ml of an aqueous 5×10^{-4} M DPKH solution, an aliquot containing an appropriate amount of pertechnetate and

7 ml of 2 M hydrochloric acid. Make up to 10 ml with deionized water, and measure the fluorescence intensity (λ_{ex} = 360 nm, λ_{em} = 430 nm) after 4 h at room temperature for 0.5—12 μg Tc ml^{-1}, 2 h in a steam bath for 0.05—6 μg Tc ml^{-1}, and 5 h in a steam bath for 0.01—1 μg Tc ml^{-1}.

RESULTS AND DISCUSSION

Reactions of technetium(VII) with some hydrazones

Possible reactions between technetium(VII) and methyl-2-pyridylketone hydrazone (MPKH), 2,2′-dipyridylketone hydrazone (DPKH), 2,2′-dipyridylketone phenylhydrazone (DPKFH), dimethyldiketone dihydrazone (DMDKH) and dipyridylglyoxal hydrazone (DPDKH) were investigated by mixing pertechnetate and one of the reagents, in the presence or absence of a reducing agent (tin(II) chloride) and at different pH values. In each case, changes of colour, fluorescence or turbidity were observed. In the absence of tin(II) chloride, only DPKH gave an observable reaction, the formation of an intensive fluorescence as a result of reagent oxidation. This reaction is studied in detail later. The products that result from oxidation of the other hydrazones had no colour or fluorescence in acidic media. In the presence of tin(II) chloride, all five reagents gave coloured reaction products with technetium(VII) in acidic media. DMDKH initially gave yellow or reddish-yellow solutions, depending on the concentration of the reagent. When the solutions were warmed in a steam bath, different colours were obtained, varying from yellow to mauve-red, depending on the reagent:technetium ratio (Fig. 1). For DPDKH, a greenish-yellow solution was obtained initially; on warming in a steam bath, the colour varied from bright yellowish green to dark brown, depending on the reagent:technetium ratio (Fig. 2). For MPKH, a yellowish-brown solution was obtained initially; for certain reagent:technetium ratios, on warming in a steam bath, the colour changed to intense violet (Fig. 3). For DPKH, a yellowish colour was first obtained; it became more intense on standing and on warming in a steam bath (Fig. 4). Finally, for DPKFH, no reaction was detected initially, but on warming, the solution became dark brown (Fig. 5). From these results, it can be deduced that DMDKH reacts most rapidly with technetium, followed by DPDKH, MPKH and DPKH; DPKFH reacts least readily, possibly because of steric hindrance by the phenyl group attached to the amino nitrogen.

The order of addition of the reagents was always very important; maximum colour intensity was obtained when tin(II) chloride was added last. This occurs because if tin(II) chloride is added to pertechnetate, a colloidal precipitate of technetium(IV) oxide is obtained, and its redissolution to allow formation of soluble coloured complexes is probably slow.

The formation of soluble coloured species only in acidic media can be explained on the basis that reduction of technetium(VII) is more favoured in such media, and not because the coloured species are unstable in basic media; this was shown by adding alkali to the coloured species obtained in

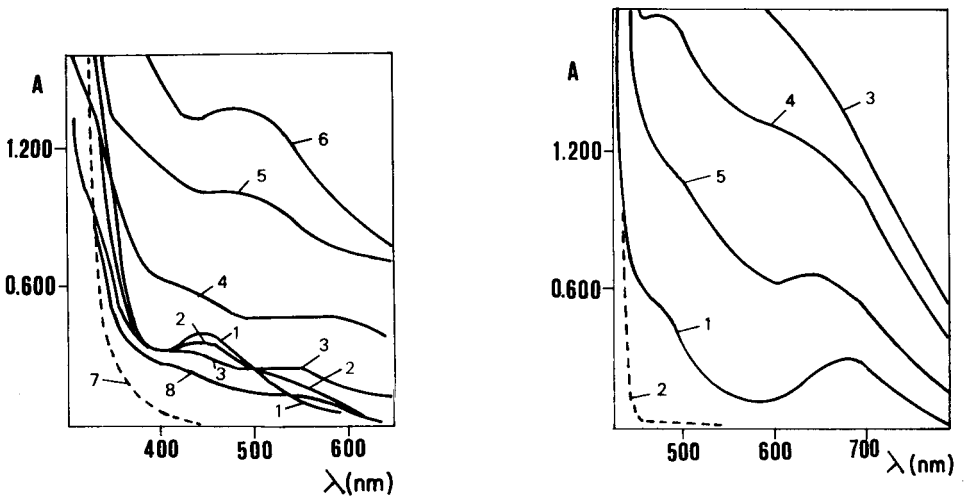

Fig. 1. Absorption spectra for the Tc—DMDKH system. [DMDKH]: (1) 9×10^{-5} M; (2) 1.7×10^{-4} M; (3) 4.4×10^{-4} M; (4) 8.9×10^{-4} M; (5) 1.8×10^{-3} M; (6) 4.4×10^{-3} M warming; (7) reagent blank (all with 45-min warming); (8) as (3) without warming. (50% ethanol, 46 μg Tc ml^{-1}, 0.2 M HCl, 0.01 M $SnCl_2$.)

Fig. 2. Absorption spectra for the Tc—DPDKH system. [DPDKH]: (1) 2.1×10^{-3} M (without warming); (2) reagent blank; (3) 2.1×10^{-3} M; (4) 1.2×10^{-3} M; (5) 4.2×10^{-4} M. (All with 1-h warming, conditions otherwise as in Fig. 1.)

acidic solutions. The appearance of different final colours depending on the reagent:technetium ratio probably results from the presence of different oxidation states of technetium (III, IV or V).

The DPKH/technetium(VII) system

From the data above, it can be deduced that technetium(VII) reacts in acidic medium with DPKH to form a product that shows an intense blue fluorescence. This compound, which has maximum fluorescence in acidic solution, is the same as the substance which results from DPKH oxidation, and was extensively studied in previous papers [22, 23]. Technetium in lower oxidation states also reacts with the reagent to produce non-fluorescent yellow compounds, as shown above. Figure 6 shows the fluorescence/time curves for the DPKH/technetium(VII) system at room temperature and on heating. An increase in temperature notably accelerates the reaction.

It is interesting to compare the fluorescence/time curves for the technetium(VII) and manganese(VII) systems shown in Fig. 6. For technetium(VII), there is a clear induction period which shows the participation of a reduced technetium species (probably as a complex) in the acceleration process. This effect is not present in the manganese(VII) system. This can be explained if one considers that the stable reduced species formed is Mn^{2+},

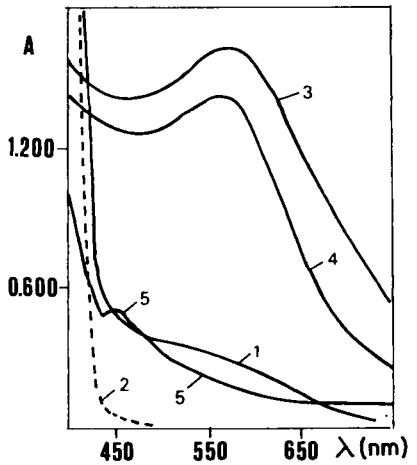

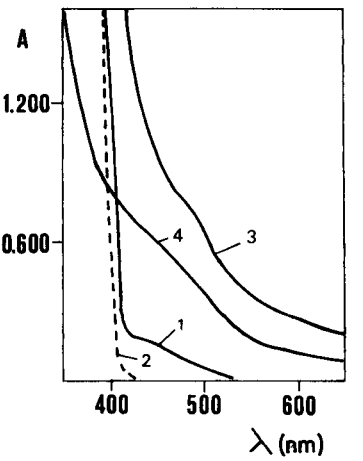

Fig. 3. Absorption spectra for the Tc—MPKH system. [MPKH]: (1) 3.7×10^{-3} M, without warming; (2) reagent blank; (3) 3.7×10^{-3} M; (4) 4.9×10^{-4} M; (5) 1.5×10^{-4} M. (2—5 with 1-h warming, conditions otherwise as in Fig. 1.)

Fig. 4. Absorption spectra for the Tc—DPKH system [DPKH]: (1) 2.5×10^{-3} M, without warming; (2) reagent blank; (3) 2.5×10^{-3} M, 1-h warming; (4) 7.5×10^{-4} M, 1-h warming. (No ethanol, conditions otherwise as in Fig. 1.)

a cation which, in acidic solution, has no effect on the reaction. The effect of atmospheric oxygen was also studied by conducting the reaction in anaerobic conditions. Prior deoxygenation of the solutions with nitrogen had practically no effect on the technetium reaction.

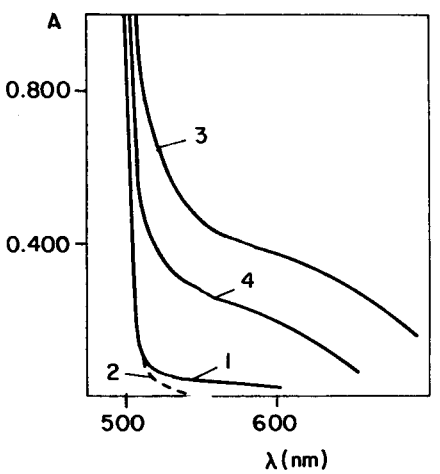

Fig. 5. Absorption spectra for the Tc—DPKFH system. [DPKFH]: (1) 1.8×10^{-3} M, without warming; (2) reagent blank; (3) 1.8×10^{-3} M, 1-h warming; (4) 5.4×10^{-4} M, 1-h warming. (Conditions otherwise as in Fig. 1.)

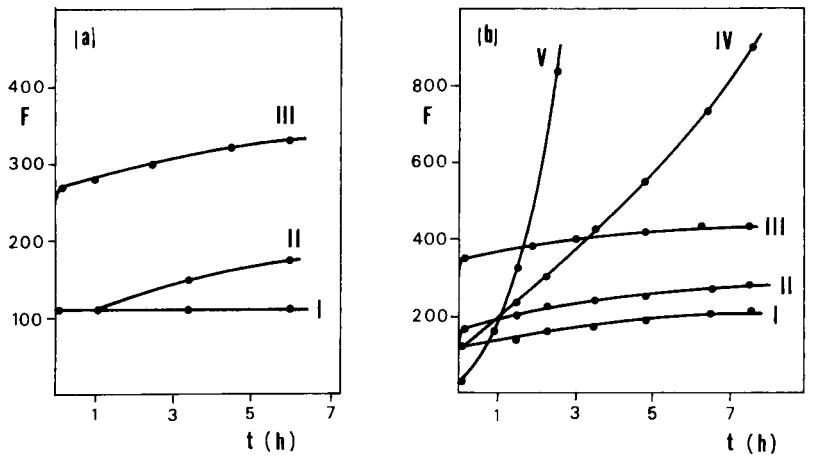

Fig. 6. Effect of time (t) on the fluorescence of the Tc(VII)—DPKH and Mn(VII)—DPKH systems with 5×10^{-5} M DPKH and 1.4 M HCl: (a) without warming; (b) warming on a steam bath. Curves in (a): (I) reagent blank; (II) 1.2 μg Tc(VII) ml^{-1}; (III) 0.05 μg Mn(VII) ml^{-1}. Curves in (b): (I) reagent blank; (II) 0.01 μg Mn(VII) ml^{-1}; (III) 0.05 μg Mn(VII) ml^{-1}; (IV) 1.2 μg Tc(VII) ml^{-1}; (V) 50 μg Tc(VII) ml^{-1}.

The effect of acidity on the fluorescence obtained for the DPKH—technetium(VII) system was studied. The results are shown in Fig. 7; maximum fluorescence was obtained in 1.4 M hydrochloric acid. This results from the increasing oxidizing power of technetium(VII) and the decreasing fluorescence of the product with increasing acidity. The influence of DPKH concentration on the fluorescence intensity is very small (Fig. 8).

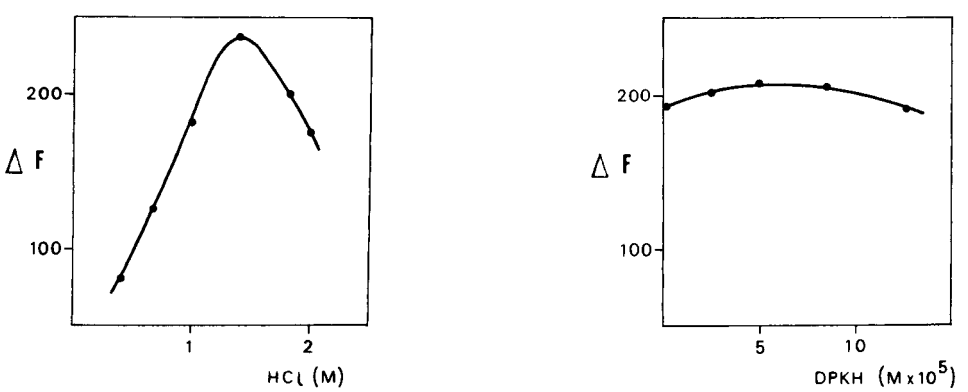

Fig. 7. Effect of hydrochloric acid concentration on the fluorescence of the Tc(VII)—DPKH system. (1×10^{-4} M DPKH; 6.1 μg Tc(VII) ml^{-1}, 2-h warming on steam bath.)

Fig. 8. Effect of reagent concentration on the fluorescence of the Tc(VII)—DPKH system. (2.4 μg Tc(VII) ml^{-1}, 1.4 M HCl, 2-h warming on steam bath.)

Interferences

The very slow aerial oxidation of DPKH occurs more readily when the medium is more alkaline, and is catalyzed very effectively in slightly alkaline or neutral media by Cu(II), Co(II), Hg(II), Mn(II) and Cr(III) [22, 23]. However, this catalysis remains very much inhibited in acidic media. Thus, for the determination of 1 mg l^{-1} technetium at room temperature, the presence of 100 mg l^{-1} Co(II), Hg(II), Mn(II) or Cr(III) does not cause any interference. For copper(II), which is a much stronger catalyst, the presence of only 0.1 mg l^{-1} can be tolerated. When heating is used, 100 mg l^{-1} Mn(II), 10 mg l^{-1} Co(II) and 1 mg l^{-1} Hg(II) or Cr(III) do not interfere. It was not considered necessary to study the effects of other cations because the separation of technetium as pertechnetate from most other cations can readily be accomplished by precipitation in alkaline media, by ion-exchange chromatography, or by liquid—liquid extraction [6, 18]. The most important interferences in technetium determinations are normally those caused by U(VI), Re(VII), Mo(VI) and W(VI), elements that frequently accompany technetium. It was shown that, in the determination of 1 mg l^{-1} technetium at room temperature, the presence of 100 mg l^{-1} U(VI), Re(VII), Mo(VI) or W(VI) did not cause interference. When the reaction was conducted with warming, the presence of 100 mg l^{-1} W(VI) did not interfere, but 100 mg l^{-1} U(VI) or Re(VII) produced a slight positive interference and only <1 mg l^{-1} Mo(VI) could be tolerated.

In conclusion, the differences in the behaviour of permanganate, pertechnetate and perrhenate with DPKH are of interest. Although the sensitivity of the procedure with heating of solutions is far better, the selectivity obtained at room temperature is better, especially with respect to molybdenum(VI), a species that can cause serious interference in most non-radiochemical determinations of technetium.

REFERENCES

1 A. G. Jones and A. Davison, Int. J. Appl. Radiat. Isot., 33 (1982) 867.
2 A. Davison and A. G. Jones, Int. J. Appl. Radiat. Isot., 33 (1982) 875.
3 W. A. Hareland, E. R. Ebersole and T. P. Ramachandran, Anal. Chem., 44 (1972) 520.
4 J. Grassi, N. Karisa, M. G. Perez-Caballero and J. Devynck, Analusis, 7 (1979) 294.
5 L. Astheimer and K. Schwoachare, J. Electroanal. Chem., 15 (1967) 61.
6 A. K. Lavrukhina and A. A. Pozdnyakov, Analytical Chemistry of Technetium Promethium, Astatine and Francium, Humphrey Science, Ann Arbor, MI, 1970.
7 R. Villareal, M. S. Thesis, University of Idaho, Moscow, ID, 1967.
8 C. Crouthamel, Anal. Chem., 29 (1957) 1756.
9 O. Howard and C. Weber, Anal. Chem., 34 (1962) 530.
10 F. Miller and H. Zittel, Anal. Chem., 35 (1963) 299.
11 F. J. Miller and P. F. Thomason, Anal. Chem., 32 (1960) 1429.
12 F. J. Miller and P. F. Thomason, Anal. Chem., 33 (1961) 404.
13 R. Colton, U.K. At. Energy Auth. Rep., AERER 3746, 1961.
14 M. Al-Kayssi, R. J. Magee and C. L. Wilson, Talanta, 9 (1962) 125.
15 F. Jasim, R. J. Magee and C. L. Wilson, Talanta, 2 (1959) 93.

16 F. Jasim, R. J. Magee and C. L. Wilson, Talanta, 4 (1960) 17.
17 W. Meggers, Spectrochim. Acta, 4 (1951) 317.
18 J. W. Cobble, in Treatise on Analytical Chemistry Part II, Sect. A, Vol. 6, Interscience, New York (1964).
19 R. J. Magee and M. Al-Kayssi, Anal. Chim. Acta, 27 (1962) 469.
20 F. Jasim, R. J. Magee and C. L. Wilson, Microchim. Acta, 5—6 (1960) 721.
21 S. G. Metcalf, Anal. Chim. Acta, 93 (1977) 297.
22 F. Grases, F. Garcia-Sanchez and M. Valcarcel, Anal. Chim. Acta, 119 (1980) 359.
23 F. Grases, F. Garcia-Sanchez and M. Valcarcel, Anal. Chim. Acta, 125 (1981) 21.

Analytica Chimica Acta, 166 (1984) 79—92
Elsevier Science Publishers B.V., Amsterdam — Printed in The Netherlands

A METHOD OF DETERMINING AND REMOVING SULPHIDE TO ALLOW THE DETERMINATIONS OF SULPHATE, PHOSPHATE, NITRITE AND AMMONIA BY CONVENTIONAL METHODS IN SMALL VOLUMES OF ANOXIC WATERS

D. AIREY*,[a], G. DAL PONT and G. SANDARS[b]

Division of Oceanography, CSIRO Marine Laboratories, G.P.O. Box 1538, Hobart, Tasmania 7001 (Australia)

(Received 30th May 1984)

SUMMARY

Mercury(II) chloride is used to precipitate free sulphide from <10-ml samples of anoxic water. The sulphide-free supernatant solution can be used for estimation of sulphide by measuring the concentration of unreacted mercury(II) ion and for determinations of sulphate, inorganic phosphate, ammonia and nitrite by spectrophotometric methods which normally cannot be used because of sulphide interference. Concentrations that can be determined lie within the ranges: sulphide 0.5—180 000 μg S l^{-1}, sulphate 0.024—2.77 g S l^{-1}, ammonia 1—70 000 μg N l^{-1}, nitrite 1—3000 μg N l^{-1}, inorganic phosphate 1—4000 μg P l^{-1}. Interstitial waters from estuarine sediments, tidal flats, mangrove swamps, and an anoxic estuarine basin were examined.

When sedimentary organic matter decomposes, oxidized components in interstitial water accept electrons and are reduced in the sequence oxygen > nitrate > sulphate [1]. Some of the resulting chemical constituents in the aqueous phase are essential nutrients for food webs but they coexist with toxic concentrations of sulphide formed by bacterial reduction of sulphate. After aeration, such water is highly nutritious and non-toxic.

To proceed with a study of the formation, diffusion and effects of hydrogen sulphide on other chemical species at dredge sites and below dredge dump sites, and in a periodically anoxic basin, it was first necessary to devise techniques that would overcome the following analytical problems. A major problem is the small volume of interstitial water extractable from sediments. Multiple element interactions are difficult to study when only small volumes of interstitial water are available. Extraction techniques [1—4] are time-consuming and the volumes of water extracted are small (5—40 ml). The volume available for analysis is even less when a sediment core is sectioned to study chemical changes over small increments of depth. Another problem is

Present addresses: [a]ECO Logic, 98 Grays Point Rd., Grays Point, NSW 2232 (Australia). [b]CSIRO Division Energy Chemistry, Lucas Hts. Research Laboratories, Private Bag Sutherland, NSW 2232 (Australia).

0003-2670/84/$03.00

the alteration of chemical species by oxidation. To prevent oxidation, which would alter the redox-controlled concentrations of many chemical species in anoxic waters or sediment pore-water samples, cumbersome equipment, such as nitrogen-filled glove boxes, is commonly used during water extraction and some determinations [3, 5]. Finally, various difficulties are caused by sulphide interference. Even in an antimony/molybdophosphate blue method [6], modified to determine phosphate in sulphide-contaminated waters [7], interference occurs at sulphide concentrations greater than 200 μM (6 mg l^{-1}). Sulphide (2 mg l^{-1}) also interferes with ammonia determinations [8]. In sulphate determinations, sulphide may be oxidized and measured as additional sulphate [9]. In nitrite determinations, the sulphide destroys the azo dye [10]. In order to remove sulphide interference, samples are usually acidified and purged with nitrogen [7—9, 11]. Such treatment changes the chemical speciation of some components that are pH-controlled and the sample is spoiled for further analysis [12].

The aim of this work was to develop techniques to overcome these problems. Previously reported techniques to determine sulphide and many of the other constituents of both interstitial and the overlying water did not meet the requirements. For instance, the iodimetric method [13] requires large sample volumes, and is affected by nitrite interference [10]. It was found here that nitrite and sulphide often coexist at high concentrations in pore waters. The method based on N,N-dimethyl-*p*-phenylenediamine sulphate [14] requires a 50-ml sample and a pH change to 0.35. The non-routine speciation method in which pore waters are titrated with mercury(II) chloride with a Ag/Ag_2S electrode as sulphide sensor [3] requires the sample pH to be adjusted to 13 and the use of glove boxes for manipulations. The method in which the pore waters are titrated with lead nitrate in 1 M sodium hydroxide containing ascorbic acid and hydrazine reductants [15] is suitable only for traces of sulphide (2—150 μg l^{-1}) and presents two problems: first, some sulphide is absorbed on the lead sulphide as it precipitates, and secondly, pH is increased.

To develop the techniques reported here, interstitial water samples from accessible sediments in experimental tanks were used. The method was then tested on interstitial waters from estuarine sediments, tidal flats and mangrove swamps, from experimental tanks containing muds of different composition, and from an anoxic estuarine basin. Sulphide in these samples was quantified without changing the pH. In aliquots of the same sample, sulphate, ammonia, nitrite and phosphate were determined sequentially by procedures that, because of sulphide interference, cannot normally be used for anoxic waters. For low sulphide levels, the minimum volume of water required to determine all analytes is 5.0 ml; less is required for waters with high sulphide concentrations.

In this study, interstitial water samples are classified into ranges A, B, C and D, based on their estimated sulphide content.

EXPERIMENTAL

Reagents

Analytical reagents used were A.R. grade chemicals free from detectable concentrations of mercury. Distilled water deionized in a Millipore Milli-Q purification system was used, unless otherwise specified (pure water).

Ammonia and phosphate-free sea water (APFSW). Collect open-ocean sea water in polyethylene containers that have been equilibrated with sea water for several months. Store the waters outdoors and shake often to ensure that the plankton removes ammonia and phosphate from solution. Remove any remaining phosphate by passing the water through a zirconium hydroxide column [16]. Filter the treated sea water through a Millipore HAWP142-50 filter in an all-glass Millipore filtration vessel and store in 2-l polyethylene containers at room temperature. Use this water to prepare blanks and standards and as a diluent. Degas fractions in an ultrasonic bath as required.

Mercury(II) chloride precipitating solution (11.0 g Hg^{2+} l^{-1}). Dissolve 15.0 g of $HgCl_2$ in pure water and make up to 1 l. Store this solution in 10-ml aliquots in sealed ampoules. This procedure will ensure consistent mercury concentrations. This solution can be used to precipitate sulphide in range A (interstitial waters) and as stock solution for preparing the diluted mercury(II) chloride precipitating solution for ranges B, C and D. For the diluted precipitating solution, dilute the concentrated solution (11.0 g Hg^{2+} l^{-1}) from the ampoules with pure water by factors of 10, 100 and 1000 for ranges B, C and D, respectively.

Stock sulphide solution (69.6 mg S^{2-} l^{-1}). Dissolve 130 mg of $Na_2S \cdot 9H_2O$ in 10 ml of pure water which has been degassed in an ultrasonic bath, and make up to 250 ml with degassed APFSW. Do not prepare this solution until required, to avoid losses of volatile sulphide. The stock solution and dilutions of this stock, used to construct calibration graphs (ranges A—D), are standardized by an iodimetric method [13].

Supernatant acid diluting solution. Prepare 0.05% (w/v) potassium dichromate solution in diluted (1 + 19) nitric acid.

Acidic saline solution. Prepare 0.5% sodium chloride in diluted (1 + 9) sulphuric acid.

Commercial mercury standard solution (1 mg Hg^{2+} ml^{-1} in 1 M nitric acid). This standard solution cannot be used directly as the stock for the precipitating solutions because of the presence of preserving acid. It is used to standardize the precipitating solution.

Reducing solution. Dissolve 0.5 g sodium chloride, 1.0 g hydroxylammonium sulphate, and 2.0 g tin(II) chloride or sulphate in 100 ml diluted (1 + 9) sulphuric acid.

EDTA solution. Dissolve 30 g disodium ethylenediaminetetraacetate in 2 l of APFSW.

Equipment

Experimental tanks were set up with permanently immersed sample ports as shown in Fig. 1. Glass syringes (20 or 50 ml) were used for sample collection. A Gilmont burette (2 ml) and an Eppendorf multipette 4780 with 12.5-ml disposable combitips served for solution transference. A filter unit (Millex-PF 0.45 μm; Millipore model SLA-A-025LS) was placed on-line between the glass sample syringe and Eppendorf multipette to filter turbid samples without exposure to air.

Other equipment included pyrex centrifuge tubes (15 ml), pyrex tubes (50 ml) with teflon-lined screw caps and a laboratory centrifuge.

General procedure

Sulphide dissolved in de-aerated sea water and interstitial water from experimental tanks was determined. The interstitial water samples (5—30 ml) were withdrawn by syringe to prevent oxidation of sulphide by contact with air. Sampling from the permanently immersed sample ports of the experimental tanks (Fig. 1) allowed pore waters that had accumulated in the tubes between sampling to be withdrawn without strong suction which would disturb the sediments. By sampling different depths, there was a readily available supply of pore-water samples which differed in chemical properties, especially in the concentrations of interfering substances.

As samples were collected, they were immediately injected through a 0.45-μm Millipore filter into the multipette, from which they were injected into the bottom of a centrifuge tube containing a known quantity of mercury(II) chloride solution. The tubes were sealed without delay, and shaken well. At this stage, samples can be stored at room temperature. They were centrifuged to precipitate the sulphide. The supernatant solution was treated as follows: (a) 100 μl was diluted in acidic solution for determination of excess of Hg^{2+} by cold-vapour atomic absorption spectrometry (a.a.s.), the difference between the concentration of Hg^{2+} added and the unreacted portion being used to calculate the amount of sulphide precipitated by the

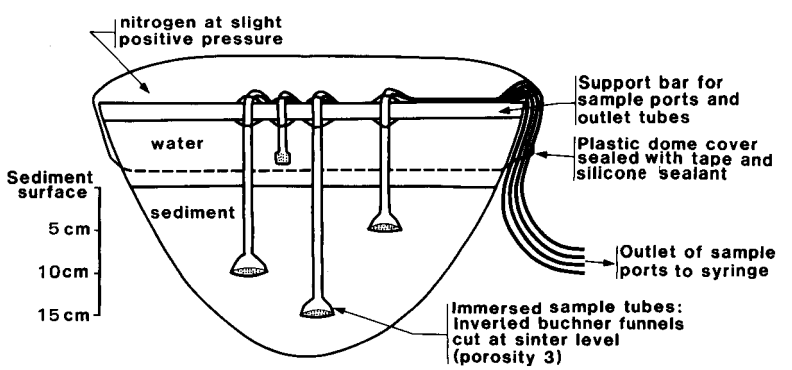

Fig. 1. Laboratory sediment tanks showing immersed sample ports.

mercury; (b) 1 ml was used for sulphate determination; (c) the remainder of the solution served directly, or after dilution with APFSW, for determinations of ammonia, nitrite and inorganic phosphate by manual or automatic methods.

Sulphide standards and calibration graphs

The sulphide concentration in test samples ranged from 0.5 $\mu g\ l^{-1}$ in deoxygenated bottom waters to 180 000 $\mu g\ l^{-1}$ in pore waters. In order to maximize the sensitivity of the method, less mercury was used in the precipitating solution for samples expected to have lower sulphide concentrations. Table 1 shows the required dilutions of the mercury precipitating solution used in the four ranges (A—D). Also shown are the upper and lower limits of sulphide concentrations within each range. At the upper limits all of the mercury is precipitated and thus there is no detectable excess of mercury. Above this limit the method is invalid as some sulphide would not be precipitated. The lower limits are established by a decrease in the mercury/sulphide ratio in the precipitate caused by too great an excess of mercury. The reasons for this are discussed later.

For an unknown sample, an estimate of sulphide concentration (range A—D) is made to allow assessment of the mercury level required for the precipitating solution (Fig. 2 and Table 1). Test samples from a batch of unknown samples are injected into four tubes containing the concentration

TABLE 1

Experimental parameters used or evaluated for each range of sulphide concentrations

Range	A	B	C	D
Dilution of Hg precipitating soln.	None	1/10	1/100	1/1000
Sulphide conc. ($mg\ l^{-1}$)	5.0—50[a]	0.5—5.0	0.05—0.5	0.004[b]—0.05
Hg:S ratio in precipitate[c]	8.0—8.8	7.6—7.7	7.1—7.2	5.6—5.7
Precision for sulphide (%)[d]	9.8	7.9	4.3	12.4
Regression data[e]				
Intercept (a)	−1710.6	−387.7	−25.5	−1.59
Slope (b)	0.126	0.146	0.149	0.167
S.e. of slope	0.0035	0.0036	0.0019	0.0054
r^2	0.995	0.996	0.999	0.990

[a] > 50 with less sample. [b] Detection limit. [c] Varies with batches of reagents. [d] Calculated for $n = 8$ for slopes A—D in Fig. 4 on 95% confidence band. [e] For sulphide (Y ng) on mercury (X ng) in the precipitate (cf. Fig. 4) with $n = 8$.

of precipitating solution required for each range as shown in Table 1. The excess of mercury is determined as described later and the range of standards required to test the samples can be determined from Fig. 2. For pore waters, range A solution is always suitable. However, samples with sulphide concentrations above 55 000 $\mu g\ l^{-1}$ have to be diluted as described below. Standard curves must be redrawn if sampling procedures are varied, if new batches of reagents are used, or if samples lie outside the range previously selected.

To construct calibration graphs for a selected range, 500 μl of the mercury-(II) chloride precipitating solution appropriate for that range is dispensed into eleven centrifuge tubes followed by 0, 1, . . . 10 ml of APFWS from the Eppendorf multipette. Stock sulphide solution (10, 9, . . . 0 ml) is immediately dispensed below the surface of the precipitating solution to make a final volume of 10.5 ml. (This dilution must be taken into account in calculating the levels of excess of mercury.) The tubes are sealed immediately with parafilm and shaken and the precipitate is allowed to settle for 15 min. The sample is centrifuged at 2000 rpm for 10—15 min. The clear supernatant solution is used for the determination of excess of mercury as described below.

Samples

Anoxic water samples were collected by using syringes, water bottles or low pressure pumps operated by divers. Pore waters from mangrove swamps and estuarine sediments were collected by using immersed syringes as shown in Fig. 1. Samples were collected without contact with air as described above to prevent oxidation. Other methods of collection are described in the literature [1, 3, 4].

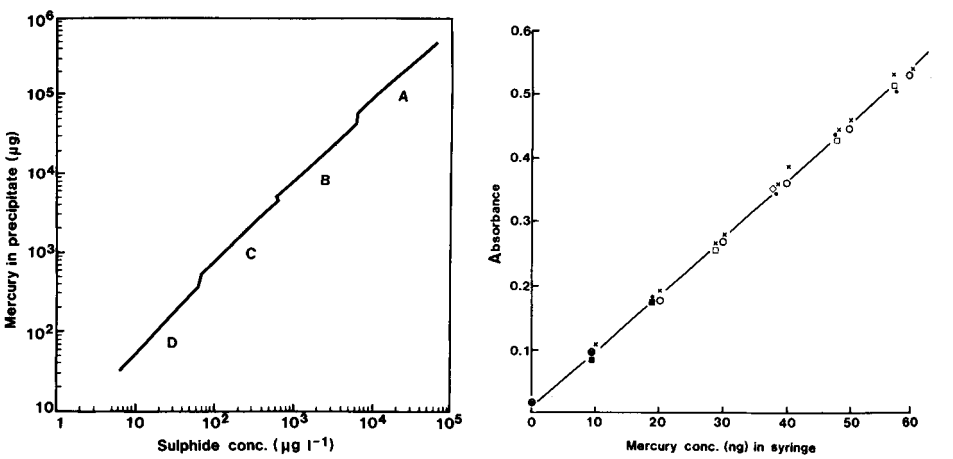

Fig. 2. Plot (log scale) of mercury precipitated (μg) vs. sulphide concentration ($\mu g\ l^{-1}$) to determine the ranges (A—D) of sulphide standards required.

Fig. 3. Calibration graph of excess of mercury(II) ion (ng) vs. absorbance (a.a.s.): (×) A; (○) B; (□) C; (●) D.

Pore water. A preliminary check of the pore-water sulphide content was made to ensure that the capacity of the precipitating solution was not exceeded (approximately 65 mg S^{2-} l^{-1}). To do this, a few drops of each sample was discharged so that the hydrogen sulphide present could be smelt. 10 ml of the sample with apparently the highest concentration of hydrogen sulphide was mixed with 500 μl of the concentrated precipitating solution, and the tube was sealed with parafilm and shaken. If the precipitate was yellow-brown, this sample and all those above it in the sample core were within the range of the method and could be treated similarly. However, if the precipitate was black, the sample was out of range and such samples had to be diluted by a method which prevented sulphide loss by volatilization or by oxidation by the diluent.

The volume of pore water to be diluted (1—9 ml; with experience this amount can be judged easily by the smell) was estimated, and then the volume of APFSW required for a total volume of 10 ml was calculated. The APFSW, and then the sample, were added to a centrifuge tube which already contained 500 μl of the concentrated precipitating solution. The tube was sealed with parafilm, shaken and centrifuged as described above. Again the supernatant solution was used in further analysis.

Determination of excess of mercury(II) by cold-vapour a.a.s.

Range A. In step (a), dilutions were made by mixing 100 μl of supernatant solution with 10 ml of oxidant (potassium dichromate diluting solution) in pyrex tubes. In step (b), 100 μl of this was mixed with 20 ml of the acidic saline solution in another pyrex tube. In step (c), 2 ml of the resulting solution was taken into a syringe followed by 2 ml of tin(II) chloride reductant and 16 ml of air. The syringe was shaken to reduce the Hg(II) and release mercury vapour, which was then measured by syringe injection and cold-vapour a.a.s. [17, 18].

Range B. In step (a), 1 ml of supernatant solution was added to 9 ml of the oxidant; steps (b) and (c) were then completed as above.

Range C. In step (a), 100 μl of supernatant solution was mixed with 20 ml of acidic saline solution. (Oxidant was not used, as it suppressed the reduction at low mercury levels.) Step (c) was the same as for range A.

Range D. In step (a), 1 ml of supernatant solution was mixed with 19 ml of acidic saline solution and step (c) was completed as above.

The linearity of the a.a.s. response was checked as follows. The stock mercury solution (0, 100, . . . 600 μl) was dispensed into 15-ml centrifuge tubes and made up to 10.5 ml with APFSW. Dilutions and measurements were made as described for range A.

The above procedure for determining excess of mercury(II) ions was used for standards, samples and blanks. The blank sample contained only precipitating solution and APFSW. Figure 3 shows the blank-corrected absorbance for increasing excesses of mercury in a series of standards, or in samples from the experimental tanks.

Calculation of sulphide

Figure 4 shows plots of the sulphide concentrations in the standards determined iodimetrically against the mercury precipitated by the sulphide. Figure 3 shows the amount of mercury(II) (ng) available for reduction by tin(II) chloride in the final stage of the a.a.s. determination. From this, the excess of mercury(II) (mg) in the undiluted supernatant solution was calculated after taking into account the dilutions used for ranges A—D. The mercury precipitated was calculated from the difference between the concentration in the precipitating solution and the excess of mercury(II) in the supernatant solution.

Sulphide concentrations in unknown samples were determined by using the linear portion of the calibration graphs (solid lines in Fig. 4). The extremes

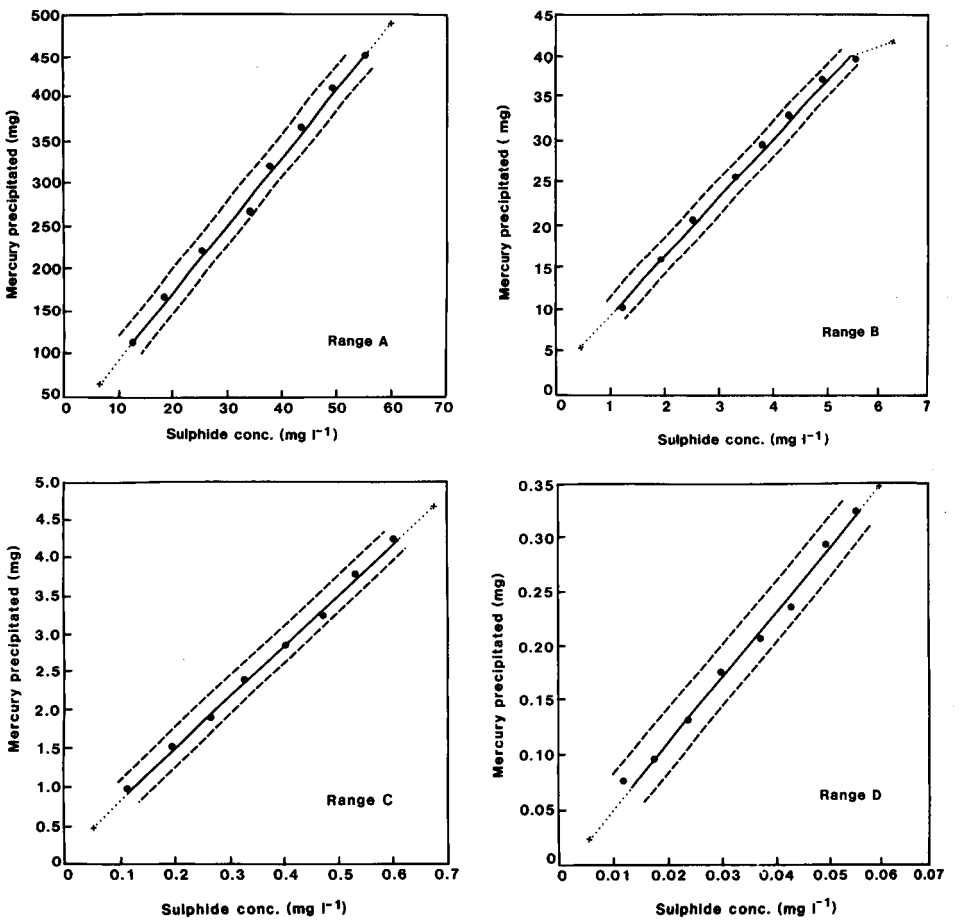

Fig. 4. Calibration graphs: mercury(II) ion precipitated by sulphide (mg) vs. sulphide standard (mg l^{-1}) for pore waters and natural waters (ranges A—D). Dashed lines are the 95% confidence bands for sulphide using data in the working range, denoted by solid line.

of the curves (dotted lines) must not be used (see below). Samples with concentrations greater than those in the linear section of range A were diluted while samples with concentrations greater than the linear sections of ranges B—D were re-analysed with a precipitating solution containing a higher concentration of mercury. Samples with concentrations less than those in the linear section were re-analysed with a precipitating solution containing less mercury. Interstitial water with sulphide concentrations greater than those in range A is rare. However, such high levels may be found in highly anoxic waste waters, in anoxic waters at sediment/water interfaces, or in waters trapped in basins, fjords or enclosed seas.

Determinations of sulphate, ammonia, phosphate and nitrite

The procedures described below cannot normally be used for sulphidic waters. However, aliquots of the sulphide-free supernatant solutions can be analysed successfully with the modifications described below.

Titrimetric determination of sulphate. Sulphide-free samples are important for fresh or brackish waters where the oxidation of sulphide during determinations of sulphate will cause significant errors. In sea water, the problem is less important because of the large amounts of sulphate present compared to sulphide.

Sulphate was determined in a 1-ml aliquot of the supernatant solution, to which was added 2 ml of EDTA solution. This was boiled to complex metals including the excess of mercury. On cooling, sulphate was precipitated as barium sulphate. The precipitate was filtered off and dissolved in EDTA at pH 10, and the excess of EDTA was titrated with 0.025 M magnesium chloride from a Gilmont burette [9]. The concentrations that were determined lay in the range 0.024—2.77 g l^{-1}.

Manual determination of ammonia. Errors in the determination of ammonia usually occur because of interferences or during dilution. These can be avoided by using a Conway diffusion cell, and then the standard spectrophotometric method [19]. Up to 2 ml of sample was placed in the outer chamber of the diffusion cell with 0.5 ml of saturated potassium carbonate solution (110 g in 100 ml of pure water, boiled to remove ammonia). (Smaller volumes of sample should be made up to 2 ml with APFSW.) Then 1 ml of 0.01 M hydrochloric acid was pipetted into the inner chamber and ammonia was allowed to diffuse overnight in the covered cell. The acid was then pipetted from the centre chamber into a 50-ml conical flask, the central chamber was rinsed several times with pure water, and the combined acid washings were made up to 25 ml. Ammonia was quantified as described elsewhere [19]. The detection limit was 50 μg l^{-1} and the concentrations found lay in the range 1—70 000 μg l^{-1}.

Manual determinations of inorganic phosphate. As the concentrations of inorganic phosphate in anoxic waters are high (up to 4 mg l^{-1}), a determination for lipid phosphorus [20] was modified. Thus 1 ml of the sulphide-free supernatant solution was injected into 3 ml of APFSW or pure water in

a 15-ml test tube, followed by 4 ml of a molybdate reagent (a fresh solution containing equal volumes of 3 M sulphuric acid, 2.5% (w/v) ammonium molybdate, and 10% (w/v) ascorbic acid solutions, diluted with a double volume of pure water). This was incubated at 37° C for 2 h, and the absorption was measured at 820 nm in a 1-cm cell. (If the absorbances are off-scale at 820 nm, 620 nm will give 1/3 of the sensitivity.) The procedure was standardized by using 1—4 μg of phosphate-phosphorus per 4 ml of APFSW or pure water (same as used for the sample). The detection limit was 25 $\mu g\ l^{-1}$ and up to 4000 $\mu g\ l^{-1}$ phosphate-phosphorus can be determined.

Manual determination of nitrite. The standard azo-dye method was used [10]. Concentrations of 1—3000 $\mu g\ l^{-1}$ can be determined.

Determination of ammonia, nitrite and inorganic phosphate by automatic spectrophotometry. These methods were used for determinations of nutrients in a water column and in limited volumes of interstitial water samples.

After the aliquot had been taken for the determination of excess of mercury(II), 10 ml of the remaining supernatant solution was treated as follows. The aliquot was thoroughly mixed with 0.5 ml of EDTA solution to mask the excess of mercury(II) so that the resulting sample solution was suitable for standard Technicon AutoAnalyzer determinations of inorganic phosphate, nitrite and ammonia [21]. For concentrations of ammonia up to 500 $\mu g\ l^{-1}$ and inorganic phosphate up to 4 $\mu g\ l^{-1}$, this solution was used directly with on-line dilutions of (1 + 10) for ammonia and (1 + 3) for phosphate. However, for higher concentrations, the samples were diluted by using a Hamilton digital diluter: 500 μl of supernatant solution was diluted with 1.5% EDTA solution to give a final volume of 100 ml and 10 ml of this was transferred to a polypropylene tube for automatic processing as above.

RESULTS AND DISCUSSION

Table 2 shows the concentrations of the sulphide, sulphate, nitrite, ammonia and inorganic phosphate in several pore waters, in anoxic waters from an estuarine basin and in experimental tanks. Some dissolved organic carbon values are also given. These results indicate the variability that must be expected and that can be tackled by using this technique. For example, in the mangrove swamp sediments, taken when the tide was out, the sulphide concentrations were less than half those determined when the tide was in. This is probably caused by oxygen diffusion into the exposed sediments and consequent oxidation of the sulphidic pore waters. In the bottom waters of the estuarine basin during an anoxic period, repeated sampling over a 30-min period indicated sulphide concentrations ranging from 2.9 to 4.0 mg l^{-1}. A profile of the water column above this sediment/water interface during an aerobic period showed that sulphide released from the sediments is rapidly oxidized but phosphate diffuses into the water column in high concentrations.

TABLE 2

Concentrations of sulphide, phosphate, ammonia, nitrite, DOC and sulphate in anoxic waters

Sample	No.	Description	Distance from sediment surface (cm)	Range Hg^{2+} ppt. soln.	Sulphide ($mg\ l^{-1}$)	Phosphate ($\mu g\ l^{-1}$)	Ammonia ($\mu g\ l^{-1}$)	Nitrite ($\mu g\ l^{-1}$)	Other parameters
Sediment pore water									
Mangrove	ma	Tide in	−8	A	8.4	550	1500	0	
swamp	ma	Tide out	−8	A	10.6	215	1500	0	
	mb	Tide out	−12	A	3.5	35	1100	0	
	mb	Tide out	−12	B	3.5	ND	1100	0	
Intertidal	ea	Silty	−5	D	ND[a]	14	ND	0	
sediment	eb	Shelly	−5	C	0.3	10	ND	0	
(tide out)	ec	Sandy	−5	D	0.003	3	ND	0	
Water									
Estuarine	00	Time	+4	B	3.5	133	ND	0	
Basin	05	series	+4	B	3.8	146	ND	0	
Bottom	10	in	+4	B	3.5	119	ND	0	
water	15	minutes	+4	B	3.8	163	ND	0	
	20		+4	B	4.0	169	ND	0	
	25		+4	B	3.5	136	ND	0	
	30		+4	B	2.9	117	ND	0	
Profile			+5	D	0.02	170	ND	0	
of			+45	D	0.0	73	ND	0	
water			+145	D	0.0	33	ND	0	
column			+245	D	0.0	25	ND	0	
Laboratory experiment									Dissolved organic carbon
Tank X (mud-		After	water +4	C	0.3	1600	600	290	6.2
high anaerobic		one	−5	A	>100.0	2600	25000	1240	10.6 } mg l^{-1}
bacterial		month	−10	A	>100.0	3150	50000	3460	12.6
activity)		in tank	−15	A	98.0	4000	74000	1260	15.8
Tank Y (mud-		After	water +4	D	0.0	200	0	0	ND
low anaerobic		four	−5	B	5.7	2900	400	0	7.2
bacterial		months	−10	B	3.7	2650	3700	0	8.6 } mg l^{-1}
activity)		in tank	−15	A	10.0	3400	6300	60	11.0
									Sulphate
Tank Z (mud-		Fresh	−5	A	22.0	ND	ND	ND	2.18
highly			−10	A	41.0	ND	ND	ND	1.65 } g l^{-1}
organic)			−15	A	37.0	ND	ND	ND	1.99
			−20	A	57.0	ND	ND	ND	1.72
		Two	−5	A	0.0	ND	ND	0	2.1
		months	−10	A	1.15	ND	ND	0	2.03 } g l^{-1}
		later	−15		ND	ND	ND	ND	ND
			−20	A	0.55	ND	ND	0	1.99

[a]Not done.

Determinations of nitrite and ammonia

In the laboratory tanks, during periods of high anaerobic bacterial activity when organic carbon levels were high, sulphide levels were >100 mg l^{-1} and nitrite and ammonia levels were also high. There has been a suggestion [10] that ammonia and nitrite cannot co-exist in anoxic pore waters and that nitrite comes from ammonia oxidized during sampling procedures. Table 3

TABLE 3

Nitrite concentrations (mg l^{-1}) in pore waters containing high concentrations of sulphide and ammonia, before and after storage in air

Depth of sample	Nitrite conc. found (mg l^{-1})		
	Treatment (a)[a]	Treatment (b)[a]	Treatment (c)[a]
Surface water	0.00	0.00	0.00
5 cm	0.78	0.77	0.76
10 cm	0.69	0.68	0.68
15 cm	1.40	1.33	1.44

[a]See text for detail.

shows the nitrite concentrations found in samples taken from three depths in the experimental tanks and treated differently: (a) the sample was treated immediately with mercury(II) ion; (b) the sample was treated immediately with mercury(II) ion and more sample was added to make up to a volume that eliminated air from the centrifuge tube; (c) the sample was left exposed to air overnight and then treated with mercury(II) ion. The results are similar for three treatments, showing that nitrite is not oxidized to ammonia and that these two substances do co-exist in the presence of sulphide. Ammonia concentrations in these samples were 29, 48 and 62 mg l^{-1} and sulphide concentrations were >100 mg l^{-1}.

Precipitation and estimation of sulphide

Many heavy-metal ions have been used in the determination of sulphide, e.g., lead [15, 22—24], silver [25, 26], cadmium [27], zinc [13] and mercury [3]. Usually, these are titrimetric methods in alkaline media to avoid loss of sulphide as hydrogen sulphide, and with anti-oxidants to prevent atmospheric oxidation. Addition of the reagents mentioned above increases the chance of contamination and changes the pH of the sample. During development of the method, mercury and zinc ions were tested as the precipitating agent. Mercury was favoured over zinc because it is very difficult to control zinc contamination of samples and reagents even in a Class 100 clean-room [28, 29], because mercury can be quantified quickly and more precisely than zinc by a.a.s. or anodic stripping voltammetry, and because excess of zinc in the supernatant solution interferes with phosphate determinations.

However, zinc sulphide is easily dissolved in acid to release sulphide. Also zinc ions precipitate only sulphide, whereas mercury(II) ions precipitate thiosulphate as well as sulphide from sea water spiked with both. These properties were used to establish whether thiosulphate was present in the interstitial water in sufficient amount to cause error in the mercury precipitation method. Zinc and mercury were used to precipitate the sulphide. After centrifugation, the supernatant solution was removed from the zinc sulphide

which was then dissolved in acid; the diluted suspension was quantitatively dissolved in a known amount of acidic iodate-iodide solution and the excess of iodine was back-titrated with thiosulphate [10]. The concentration of sulphide found was similar to that calculated from the mercury precipitation method described above. No thiosulphate was found in any natural samples tested. Hence, mercury precipitation can be related accurately to the sulphide levels.

Composition of the precipitate

When a solution containing sulphide is added to a solution of mercury(II) chloride, the composition of the mercury sulphide formed can vary. When mercury(II) is in excess, a white precipitate of mercury(II) chlorosulphide ($Hg_3S_3Cl_2$, weight ratio Hg:S = 9.3) is formed (e.g., the dotted section at the low sulphide values of the curves in Fig. 4), whereas in the presence of excess of sulphide, a black precipitate of mercury(II) sulphide is formed (weight ratio Hg:S = 6.4) [30]. Intermediate proportions of mercury and sulphide produced a yellow-orange or brown precipitate which is a mixture of the two compounds.

In order to find conditions for a constant stoichiometric ratio in the yellow-orange precipitate, a range of natural sulphide concentrations was tested. In experiments to optimize the conditions for range A, sea water spiked with varying amounts of sulphide was added to 5.5 mg of Hg^{2+} (i.e., 500 μl of 11.0 g l^{-1} Hg^{2+}). If 25—85% of the mercury(II) remained in excess after the precipitation (i.e., after 16—54 mg S^{2-} l^{-1} had reacted) then the weight ratio was constant (e.g., Hg:S = 8.4 ± 0.2). In each range, this ratio can vary slightly but remains constant for any one batch. Table 1 shows the range of ratios observed in this work.

Once it had been established that the method worked in range A, it was considered best, and simplest, for lower sulphide concentrations to decrease the amount of mercury(II) ion used for each subsequent range by a factor of ten, instead of calculating the amount of mercury required to get the same ratio as in range A. Table 1 shows that the Hg:S ratio decreased in the samples as the concentration of sulphide standard decreased. This did not affect the accuracy of the technique, because each range was standardized by the iodimetric method and the non-linearity at the ends of the curves (Fig. 4) indicated when a new curve had to be constructed.

Conclusion

The limited amount of sample that can be extracted from pore waters has made multi-element interactions difficult to study. Interference from sulphide in many determinations also increases the difficulty associated with such studies. This paper describes a technique in which the sulphide is precipitated with mercury. Sulphide, sulphate, nitrite, ammonia and phosphate can be determined in a single, small sample of anoxic pore water, waste water or natural water without interferences. The method is simple enough for routine

work. Samples are fixed prior to analysis or storage without changing the sample pH, which would alter chemical speciation.

We thank D. Reid (CSIRO Division of Mathematics and Statistics, Sydney); M. Sandstrom (AIMS, Townsville), E. Kiss (ANU, Canberra); F. Deprez (Antarctic Division, Hobart); and J. Ivey (AGAL, Hobart) for helpful comments about the manuscript.

REFERENCES

1 J. W. Murray, V. Grundmanis and W. M. Smethie, Geochim. Cosmochim. Acta, 42 (1978) 1011.
2 G. E. Batley and M. S. Giles, Water Res., 13 (1979) 879.
3 J. Boulegue, J. P. Ciabrini, C. Fouillac, G. Michard and G. Ouzounian, Chem. Geol., 25 (1979) 19.
4 M. B. Goldhaber, R. Allen, J. K. Cochran, J. K. Rosenfield, C. S. Martens and R. A. Berner, Am. J. Sci., 277 (1977) 193.
5 J. Boulegue, C. J. Lord and T. M. Church, Geochim. Cosmochim. Acta, 46 (1982) 453.
6 J. Murphy and J. P. Riley, Anal. Chim. Acta, 27 (1962) 31.
7 V. N. De Jonge and L. A. Villerius, Mar. Chem., 9 (1980) 191.
8 L. Solorzono, Limnol. Oceanogr., 14 (1969) 799.
9 W. Howarth, Limnol. Oceanogr., 23 (1978) 1066.
10 K. Grasshoff (Ed.), Methods of Seawater Analysis, Verlag Chemie, New York, 1976.
11 T. Almgren and T. Johansson, Medd. Havsfiskelab. Lysekil Rep., 125 (1972) 1.
12 W. Stumm and J. J. Morgan, Aquatic Chemistry, 2nd edn., Wiley, New York, 1981.
13 S. Fonselius, in K. Grasshoff (Ed.), Methods of Seawater Analysis, Verlag Chemie, New York, 1976, pp. 76—77.
14 J. D. Cline, Limnol. Oceanogr., 14 (1969) 454.
15 T. M. Florence and Y. J. Farrar, Anal. Chim. Acta, 116 (1980) 1975.
16 A. A. Novosolev, A. I. Sheremet'yeva and A. F. Danilenko, Oceanology, 16 (1977) 358.
17 D. Gardner and G. Dal Pont, Anal. Chim. Acta, 108 (1979) 13.
18 D. Gardner, Anal. Chim. Acta, 119 (1980) 167.
19 G. A. Major, G. Dal Pont, J. Kyle and B. Newell, CSIRO (Aust.) Div. Fish. Oceanogr. Rep., 51 (1976).
20 P. S. Chen, T. Y. Toriba and H. Warner, Anal. Chem., 28 (1956) 1756.
21 D. Airey and G. Sanders, CSIRO (Aust.) Mar. Lab. Rep., 166 (1985).
22 H. Clysters and F. Adams, Anal. Chim. Acta, 92 (1977) 251.
23 J. Slanina, J. Agterdenbos and B. Griepink, Mikrochim. Acta, (1970) 1225.
24 R. Naumann and C. H. Weber, Fresenius Z. Anal. Chem., 253 (1971) 111.
25 T. M. Hseu and G. A. Rechnitz, Anal. Chem., 40 (1968) 1054.
26 J. Barica, J. Fish. Res. Board Canada, 30 (1973) 1589.
27 E. J. Green and D. Schnitker, Mar. Chem., 2 (1974) 111.
28 D. Gardner, Lab. Pract., 28 (1979) 1071.
29 G. E. Batley and D. Gardner, Water Res., 11 (1977) 745.
30 F. A. Cotton and G. Wilkinson, Advanced Inorganic Chemistry, 2nd edn., Interscience, 1966, pp. 529—530.

Analytica Chimica Acta, 166 (1984) 93—101
Elsevier Science Publishers B.V., Amsterdam — Printed in The Netherlands

PREDICTION OF THE DYNAMIC RESPONSE OF THE POTENTIOMETRIC CARBON DIOXIDE ELECTRODE

BART VAN DER SCHOOT* and PIET BERGVELD

Department of Electrical Engineering, Twente University of Technology, P.O. Box 217, 7500 AE Enschede (The Netherlands)

(Received 30th May 1984)

SUMMARY

The dynamic behaviour of the potentiometric carbon dioxide electrode is predicted by means of a digital simulation that considers both diffusion and reaction kinetics. The method allows for complete description of the electrode response without requiring the assumption that one of these processes can be neglected. The validity of the simulation was tested experimentally by using a commercial pCO_2 electrode provided with various silicone rubber and teflon membranes. The measured values are in good agreement with those of the simulation.

The dynamic response of potentiometric gas-sensing electrodes is governed by diffusion processes and the reaction kinetics of the species involved. Although several papers have been published (see, e.g. [1—4]), there is no unanimity about the rate-determining step in the response of these devices. Because of the complexity of the system, only approximate equations have been given for computation of the response time, based on assumptions that differ from one author to another.

In an attempt to solve this problem, digital simulation is examined in this paper. The model takes into account all the time-dependent processes involved; the various dynamic processes that occur simultaneously can be separated and their influence on the overall response can be studied. The validity of the simulation was checked by measuring the responses of a commercially available CO_2 electrode fitted with the membranes supplied originally as well as with other teflon membranes. This investigation formed part of a project to construct a miniature carbon dioxide electrode based on an ISFET. Eventual mass production of such devices requires that all techniques and materials involved are reasonably compatible with common integrated circuit technology. In order to make a proper choice of materials and to estimate the best dimensions, the digital simulation can be used to predict the dynamic behaviour of the devices.

THEORY

The potentiometric gas-sensing electrode was introduced by Severinghaus and Bradley [5] for the measurement of carbon dioxide in blood. It consists of a pH glass electrode in contact with a thin electrolyte layer which is held in position with a gas-permeable membrane. Carbon dioxide diffuses through the membrane until equilibrium is established between the internal electrolyte layer and the external sample solution or gas stream. At this equilibrium state, the pH of the internal electrolyte is given by the Henderson—Hasselbalch buffer equation

$$pH = pK_1 - \log [CO_2]/[HCO_3^-] \qquad (K_1 = 4.45 \times 10^{-7}) \tag{1}$$

This equation describes the result of a process that actually consists of two steps [6]. The first step is the hydration of CO_2 and the dehydration of carbonic acid: $CO_2 + H_2O \rightleftharpoons H_2CO_3$. The forward reaction is slow and might affect the dynamic response of the sensor; the rate law is pseudo-first-order

$$-d[CO_2]/dt = k_{CO_2}[CO_2] \qquad (k_{CO_2} = 0.03\ s^{-1}) \tag{2}$$

The reverse (dehydration) reaction is governed by

$$-d[H_2CO_3]/dt = k_{H_2CO_3}[H_2CO_3] \qquad (k_{H_2CO_3} = 20\ s^{-1}) \tag{3}$$

Equilibrium is reached when both reactions proceed at the same rate, i.e., $k_{CO_2}[CO_2] = k_{H_2CO_3}[H_2CO_3]$ with the equilibrium constant

$$K = [CO_2]/[H_2CO_3] = k_{H_2CO_3}/k_{CO_2} = 6.7 \times 10^2. \tag{4}$$

The second step is the dissociation of carbonic acid, $H_2CO_3 \rightleftharpoons H^+ + HCO_3^-$. This reaction is believed to occur instantaneously. The actual acidity constant K_a is thus much greater than the apparent constant K_1 in Eqn. 1 for carbonic acid: $K_a = [H^+][HCO_3^-]/[H_2CO_3] = 2.5 \times 10^{-4}$, whereas $K_1 = [H^+][HCO_3^-]/([CO_2] + [H_2CO_3]) = 4.45 \times 10^{-7}$. From the above expressions for K, K_a and K_1, it follows that the relationship between the various constants can be written as

$$K_a = K_1(1 + K). \tag{5}$$

It must be noted that these equations describe the situation only when the internal electrolyte layer is at $pH < 8$. Above this pH, other reactions such as $CO_2 + OH^- \rightleftharpoons HCO_3^-$ can occur. The operation of the electrode at such high pH values of the internal electrolyte layer is not recommended, because the response time and linearity are unfavourably affected by the formation of carbonate ions [1]. In the concentration range investigated here, these effects can be neglected.

If the sample solution is perfectly mixed, the dynamic response is governed by the seven processes shown in Fig. 1. The first is diffusion of CO_2 through the membrane; the rate is determined by the diffusion coefficient D and the distribution of CO_2 between the membrane and the solution, with distribu-

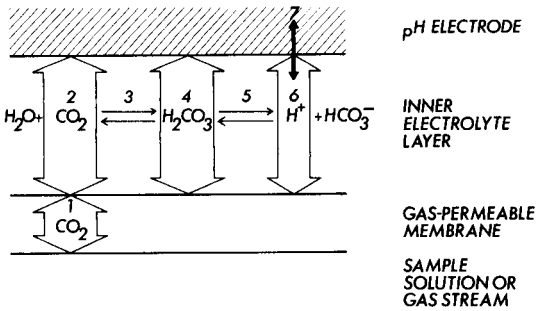

Fig. 1. The response time of the CO_2 electrode is governed by: (1) diffusion through the membrane; (2, 4, 6) diffusion in the electrolyte layer; (3, 5) reaction kinetics; and (7) the response of the pH electrode.

tion constant K_d. This results in an apparent diffusion coefficient $D_m = K_d D$. The second process is diffusion of CO_2 in the internal electrolyte layer with a diffusion coefficient D_1. The third involves hydration and dehydration of CO_2 in the electrolyte layer with rate constants k_{CO_2} and $k_{H_2CO_3}$. The fourth is diffusion of carbonic acid in the internal electrolyte layer, the diffusion coefficient being of the same order of magnitude as that for CO_2. Steps 1, 2 and 4 are determined by the dimensions of the sensor, i.e., the thickness of the membrane and of the electrolyte layer. The speed of the third step may be increased by addition of carbonic acid anhydrase [2].

Figure 1 also shows a number of processes that are not taken into account in the simulation. Thus, step 5 is the dissociation of carbonic acid, which is instantaneous and does not affect the response time. Step 6 is diffusion of hydrogen ion in the internal electrolyte layer. Because of the speed of step 5 and because $[H_2CO_3] \gg [H^+]$, the pH at any point in the solution is governed completely by the ratio $[H_2CO_3]/[HCO_3^-]$, and diffusion of hydrogen ion can be neglected. Finally, there is the response time of the glass electrode. At the usual dimensions of CO_2 electrodes, the response of the pH glass electrode is fast enough not to be a limiting factor. When the dimensions of the sensor are decreased, the total response time will decrease and the response time of a glass electrode may then become important. However, with miniaturization of CO_2 electrodes, probably other pH sensors will be used, such as metal/metal oxide electrodes [7] or ISFETs, with an inherently shorter response time. The response time of the pH electrode was therefore not included in the simulations.

DIGITAL SIMULATION

The digital simulation actually consists of discretization in space and time of the system under investigation, as first described by Feldberg [8]. The method has been treated more extensively by Britz [9].

If it is assumed that the diameter of the electrode is much greater than the thickness of the membrane and electrolyte layer, the problem can be limited to one dimension perpendicular to the electrode surface. Changes in concentrations as a function of time can then be separated into the various processes involved. In the membrane, there are no chemical reactions and only the diffusion of CO_2 is of importance. There will also be a small amount of undissociated carbonic acid diffusing through the membrane but with the ratio between CO_2 and carbonic acid concentrations as shown in Eqn. 4 this can be neglected. In the internal electrolyte layer, chemical reactions do occur. The concentration of CO_2, for instance, may change because of diffusion but simultaneously it will decrease by formation of carbonic acid and increase by dehydration of the latter. Thus:

$$d[CO_2]/dt = \text{diffusion} - \text{hydration} + \text{dehydration} \tag{6}$$

When a number of points in the one-dimensional space is considered, at any point i the concentration c_i will change over a time interval dt to a new concentration c_i'. The concentration change caused by diffusion can be derived easily from the Fick's second diffusion equation, which leads [9] to

$$c_i' = c_i + (D dt/h^2)(c_{i-1} - 2c_i + c_{i+1}) \tag{7}$$

in which D is the diffusion coefficient and h is the distance between two adjacent points in the space. This equation enables concentration changes in the membrane to be calculated. To describe the situation in the electrolyte layer, the equation has to be expanded. Equations 2 and 3 give the changes in CO_2 concentration caused by hydration and dehydration, so that a new concentration c_i' of CO_2 in point i is given, in accordance with Eqns. 6 and 7, by

$$c_i' = c_i + (D dt/h^2)([CO_2]_{i-1} - 2[CO_2]_i + [CO_2]_{i+1}) - k_{CO_2}[CO_2]_i dt + k_{H_2CO_3}[H_2CO_3]_i dt \tag{8}$$

So far, the procedure is quite straightforward, but the processes that take place at the various interfaces of the electrode need closer examination. First, at the surface of the pH electrode, diffusion takes place in only one direction. One extra point is therefore defined; this point is virtually in the pH electrode and follows the concentration of the surface point at all times so that no diffusion takes place between these points. Secondly, the diffusion coefficient in the polymeric membrane material (D_m) may differ from that in the solution (D_1). The equation used at the point defined at the interface between the electrolyte layer and the polymeric membrane has to be separated in two parts:

$$dc_i/dt = (D_1 dt/h^2)(c_{i-1} - c_i) + (D_m dt/h^2)(c_{i+1} - c_i) \tag{9}$$

At the outside of the membrane, it is assumed that the sample solution is ideally mixed. The point located there can thus be the last point considered in the simulation and its concentration can be changed at will.

The method outlined above serves to describe the new situation of the system after a time interval dt. From this point, the whole procedure can be repeated for any desired number of time intervals and thus the behaviour of the system with time can be investigated. The accuracy of the simulation depends, of course, on the number of time steps and the size of the space increments. The relationship between space and time intervals is given in the expression $\lambda = Ddt/h^2$ as shown in Eqn. 7. Its value must not exceed $\lambda = 0.5$ if a stable simulation result is to be obtained [9]. If both the electrolyte layer and the membrane are divided in ten space intervals, the 90% response will be reached within some thousands of time steps. This task can be completed within an acceptable computation time.

RESULTS

Results of simulation

The parameters that are varied in the simulation are the direction of the change in CO_2 concentration, the dimensions of the sensor and the diffusion coefficient in the membrane material. The inner electrolyte contains 0.005 M hydrogen carbonate in all cases. The time scale in the following figures is in seconds while the dimensions are as indicated. As is obvious from Eqn. 7, the time increments dt are proportional to the square of the space increments, thus if the dimensions of the sensor are increased by a factor of ten, then the time scale will expand hundredfold, if only diffusion is considered.

Figure 2 shows the pH change at the surface of the glass electrode as a result of a stepwise increase or decrease of the CO_2 concentration in the sample solution. It can be seen that the response time depends on the direction of the change in pCO_2. This phenomenon is well known for common membrane electrodes as described by Morf et al. [10] and it is independent of absolute activity levels.

There is no unanimity in the literature whether or not the hydration of CO_2 plays a role in the response time of the electrode. With the present

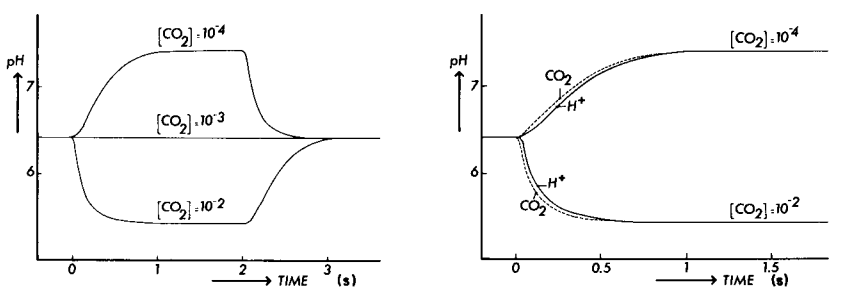

Fig. 2. The direction of the change in CO_2 concentration governs the speed of response. Stepwise changes occur at $t = 0$ and $t = 2$ s.

Fig. 3. Difference between the change in CO_2 concentration (dashed lines) and pH (solid lines) at the surface of the glass electrode.

simulation, it is possible not only to predict the pH response but also to follow the concentration of CO_2 in the sensor. In Fig. 3, the dashed line represents the CO_2 change at the glass electrode surface while the solid line gives the change in pH. It must be noted that the time scale in this figure is absolute because the hydration of CO_2 is independent of the dimensions of the sensor.

It is obvious that the thinnest membrane with the highest diffusion coefficient will yield the fastest sensor. There are, however, some limitations in the choice of the membrane, such as the mechanical strength. Figure 4 shows the response of a stepwise change in pCO_2 for different membranes. A diffusion coefficient $D = 10^{-5}$ cm^2 s^{-1} is typical for silicone rubber, whereas $D = 10^{-7}$ cm^2 s^{-1} is relevant to certain homogeneous teflon membranes. Decreasing the membrane thickness will cause the response time to drop, as can be seen in Fig. 5 for a membrane giving a low diffusion coefficient.

Experimental verification

To test the validity of the simulation, a Radiometer E5036 pCO_2 electrode was used. The electrode was mounted in a flow-through assembly as shown in Fig. 6. The inlet is fitted with a stainless steel tube (0.25 mm i.d.) providing a high fluid speed at the electrode surface. Stepwise changes in pCO_2 of the sample solution were obtained with a four-way rotary valve which selected one of two streams of different concentration. A similar set-up was used previously to test the time response of ISFETs [11].

The dynamic response of the electrode was studied for stepwise changes in CO_2 concentration between 10% and 100% partial pressure or approximately 2×10^{-3} and 2×10^{-2} mol l^{-1}. The concentration of hydrogen carbonate in the internal electrolyte layer was 0.005 mol l^{-1} and the pH changes recorded were between 6.4 and 5.4, approximately. At these concentrations, the change in hydrogen carbonate concentration caused by the dissociation of carbonic acid can be neglected.

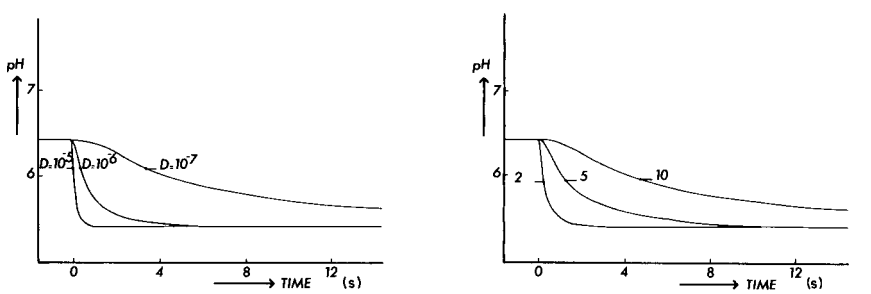

Fig. 4. Influence of the diffusion coefficient in the membrane on the response time. In all cases, the membrane is 10 μm thick.

Fig. 5. The response time of the CO_2 electrode as a function of the membrane thickness in the case of a teflon membrane. The numbers on the curves indicate membrane thickness in μm.

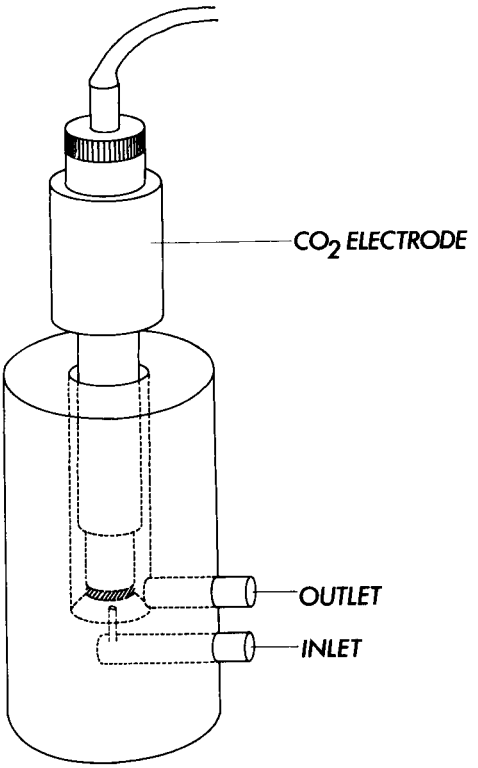

Fig. 6. Flow-through assembly used for the experimental verification of the simulation results.

The membranes tested were Radiometer silicone film (25 μm), Radiometer teflon (12 μm) and other PTFE membranes with a thickness of 1.5 μm or 3 μm. Mechanically, the PTFE membranes were rather fragile and tended to stretch under the weight of the electrolyte inside the electrode. To avoid any increase in the thickness of the electrolyte layer between membrane and pH electrode, and so in the response time, the membrane was supported externally with a nylon net. In the construction of a miniature pCO_2 electrode, this fragility is of no importance because the membrane area is only a fraction of that in a conventional electrode.

In the simulation, it was assumed that the sample solution is perfectly stirred so that there is no stagnant layer at the outside of the electrode. In practice, this situation is not achieved. Accordingly, the behaviour of the system was tested with interchange between two solutions as well as between two humidified gas streams of different concentration. The response times in the latter case were somewhat smaller and those results are summarized in Table 1, which gives the time required to reach 90% of the total response.

TABLE 1

Results of the simulation and experimental verification of the 90% response times of the CO_2 electrode for a stepwise increase or decrease in CO_2 concentration in a humidified gas stream

Membrane	Thickness (μm)	D ($cm^2\ s^{-1}$)	Conc. change[a]	90% response time (s)	
				Simulation	Exper.
Radiometer silicone	25	10^{-5}	Up	3.0	3.5
			Down	6.5	12
Radiometer teflon	12	10^{-7}	Up	39	35
			Down	89	85
PTFE	3	2.5×10^{-8}	Up	10	8.0
			Down	23	22
PTFE	1.5	2.5×10^{-8}	Up	4.0	4.6
			Down	8.7	12

[a]Concentration change between ca. 2×10^{-3} and 2×10^{-2} mol l^{-1} and vice-versa, indicated by up and down.

DISCUSSION

From Fig. 3 it can be seen that, with the indicated dimensions, the delay in response arising from hydration of CO_2 is rather small. As conventional CO_2 sensors are provided with thicker membranes and electrolyte layers, this effect will be relatively even less important. Thus it can be concluded that under these circumstances the slow hydration of CO_2 plays no role in the response of the electrode and therefore the addition of carbonic acid anhydrase [2] is of no use.

The diffusion coefficient ($D = 1.1 \times 10^{-5}$ $cm^2\ s^{-1}$) and distribution coefficient ($K_d = 2.6$) for silicone rubber are well known [1]. Comparison of the experimental values with the simulations in Table 1 shows that they are in fair agreement.

For teflon membranes, the literature values are more scanty, varying from 2×10^{-7} to 2×10^{-8} with $K_d = 1.1$ [10]. Two types of teflon (the Radiometer membranes and some other PTFE membranes) were tested and the simulations were used to estimate the diffusion coefficients which are indicated in Table 1.

It is obvious that the experimental set-up used provides optimal conditions for fast response. In more practical circumstances, such as blood gas analysis equipment or in-vivo applications, the response will be influenced by the fluid dynamics of the sample solution and will thus be somewhat slower than the values indicated. For in-vitro use, however, the development of miniature sensors offers the opportunity to improve on these fluid dynamics without enlarging the sample volume.

In conclusion, it can be said that digital simulation offers a useful means of studying the behaviour of the chemical species involved in the response of

the CO_2 electrode. The mathematics are quite straightforward and simple to use. The properties of new sensors under development can be predicted very well. Teflon was used here as a membrane for technological reasons; the electrode response is almost totally governed by the thickness of this membrane, limiting the 90% response times to ca. 2 and 5 s, respectively for an increase and a decrease in CO_2 concentration. If silicone rubber could be used at thicknesses of a few micrometres, then diffusion would no longer be the limiting factor. Under those circumstances, the response would be governed by the reaction kinetics of CO_2 and would be limited to a few tenths of a second.

The authors thank Mr. A. J. Verloop for the construction of the flow cell and Prof. Dr. W. E. van der Linden and Dr. M. Bos for their interest in this work.

REFERENCES

1 J. W. Ross, J. H. Riseman and J. A. Krueger, in G. Moody (Ed.), International Symposium on Selective Ion-sensitive Electrodes, Butterworths, London, 1973, p. 473.
2 T. L. Donaldson and H. J. Palmer, AIChE J., 25 (1979) 143.
3 J. Buffle and M. Spoerri, J. Electroanal. Chem., 129 (1981) 67.
4 M. A. Jensen and G. A. Rechnitz, Anal. Chem., 51 (1979) 1972.
5 J. W. Severinghaus and A. F. Bradley, J. Appl. Physiol., 13 (1955) 515.
6 D. M. Kern, J. Chem. Educ., 37 (1960) 14.
7 M. Markdahl-Bjarme and G. Edwall, Med. Biol. Eng. Comput., 19 (1981) 447.
8 S. W. Feldberg, in A. J. Bard (Ed.), Electroanalytical Chemistry, Vol. 3, Dekker, New York, 1969, p. 199.
9 D. Britz, Digital Simulation in Electrochemistry, Springer Verlag, Berlin, 1981.
10 W. E. Morf, E. Lindner and W. Simon, Anal. Chem., 47 (1975) 1596.
11 B. H. van der Schoot, P. Bergveld, M. Bos and L. J. Bousse, Sensors Actuators, 4 (1983) 267.

Analytica Chimica Acta, 166 (1984) 103—109
Elsevier Science Publishers B.V., Amsterdam — Printed in The Netherlands

RELATIVE MOBILITIES OF IONS IN ION-SELECTIVE ELECTRODES WITH POLY(VINYL CHLORIDE) MEMBRANES

R. D. ARMSTRONG*, A. K. COVINGTON and G. P. EVANS

Electrochemistry Research Laboratories, School of Chemistry, Bedson Building, University of Newcastle upon Tyne, Newcastle upon Tyne, NE1 7RU (Great Britain)

(Received 23rd May 1984)

SUMMARY

A.c. impedance measurements are used to calculate relative mobilities for ionic species in PVC-matrix neutral-carrier ion-selective electrode membranes. It is deduced that the membrane must include anionic sites to achieve Nernstian response, and that the selectivity of the membrane occurs as a result of a high equilibrium concentration of the primary ion within the membrane, relative to the concentration of interfering ions.

In an earlier communication [1], it was shown how impedance measurements can be used to determine both the bulk and interfacial charge-transfer resistances of valinomycin-based, PVC-matrix potassium-selective membranes in contact with aqueous solutions. It was apparent from that study that many of these membranes undergo ion exchange with the aqueous contacting solutions so that their composition, in terms of charged species, was time-dependent and a function of the particular contacting solution. This was particularly true of membranes that were prepared without any potassium-ion containing salt initially present.

The present study is concerned with measurements on ion-containing membranes, where the initial salt levels in the membranes are such as to swamp the effects of any ionic impurities. The possibility of ion exchange with the initial solutions was also much reduced by contacting membranes containing K^+, with only potassium chloride solutions, and those containing Na^+ with only sodium chloride solutions. When these methods were used, it became possible to avoid a number of the problems which arose in the interpretation of the earlier results. In particular, we believe that the ionic composition of the membranes studied here is essentially unchanged during the course of the experiments.

Several theories have been proposed to explain the origin of cation selectivity in neutral-carrier membranes, and these fall into essentially three groups. The first group requires significant deviations from electroneutrality within the bulk of the membrane, as it is assumed that the cation-carrier complex is the only charged species present in the membrane interior. This theory was first put forward by Ciani et al. [2] for thin liquid membranes,

0003-2670/84/$03.00

and was later extended to thicker membranes by Buck [3]. It is unlikely to apply to the membranes used in the present study. The second suggestion is that the selectivity arises out of slow interfacial kinetics for the anions relative to the cations [4]. The third view is that the membrane is electroneutral, but the anions present in the membrane bulk are immobile relative to the cations. The immobility of the anions could be a result of chemical bonding to the membrane support [5], poor water solubility [6], or merely a very low anion-transport number [7, 8]. This third view is currently the most favoured.

EXPERIMENTAL

The impedance measurements on the membrane were made in the same PTFE cell as described earlier [1]. The measuring system was upgraded by using a Solartron 1174 frequency-response analyser coupled to a Solartron 1186 electrochemical interface. This system allows four-electrode measurements to be made on the membranes with two current-carrying electrodes and two reference electrodes. The frequency-response analyser is controlled via an Apple II microcomputer using software developed in these laboratories. The membrane impedance can thus be measured repeatedly with preset time delays, permitting the time-dependence of the membrane impedance to be followed continuously until a steady state is achieved. The system is shown schematically in Fig. 1.

For both impedance and potential difference measurements, a cell of the form

$$\mathrm{Ag|AgCl|}m_1\mathrm{|Membrane|}m_2\mathrm{|AgCl|Ag}$$

was used. For membranes containing potassium tetraphenylborate ($KBPh_4$), impedance measurements were made with $m_1 = m_2 = 0.1$ mol dm^{-3} KCl (aqueous); for membranes containing sodium tetraphenylborate ($NaBPh_4$), $m_1 = m_2 = 0.1$ mol dm^{-3} NaCl (aqueous), as shown in Table 1. The impedance of the membrane containing no salt and no valinomycin was also measured by using stainless steel electrodes, contacting directly onto the membrane.

Measurements of potential difference were made on the membranes after all impedance measurements had been completed (after ca. 48 h). The same cell was used as for the impedance measurements, with a ten-fold ionic concentration difference across the membrane (i.e., $m_1 = m_2/10$). Selectivities were measured by using the mixed solution method [9] after all other measurements had been completed.

All measurements were made at 25.0 ± 0.5° C.

All solutions were prepared with AnalaR chemicals (BDH Chemicals).

RESULTS

The impedance spectra of the membranes were found to be time-dependent. In most cases, it was possible to identify from the spectra a distorted

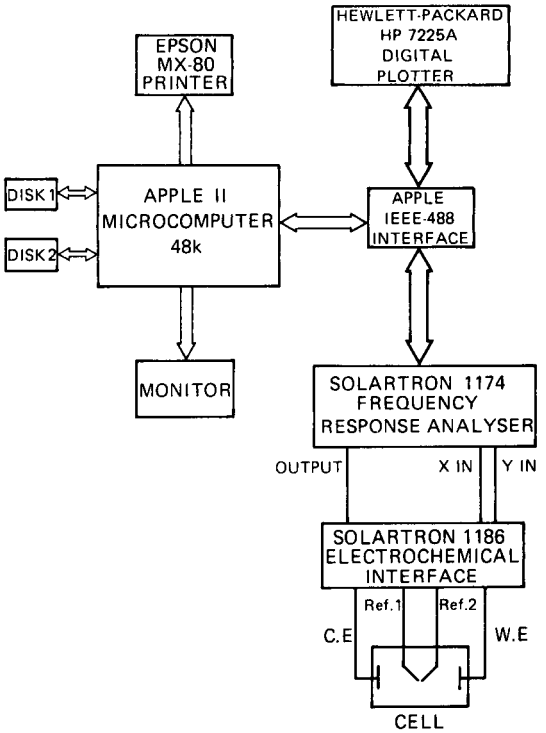

Fig. 1. Schematic diagram of the computer-controlled impedance measuring system.

TABLE 1

Bulk membrane resistance values (normalised to 1 cm^2 membrane area)

$KBPh_4$ (mg)	$NaBPh_4$ (mg)	Ligand (mg)	Contacts	R_b initial (Ω cm^2)	R_b final[a] (Ω cm^2)
0	0	0	Stainless steel	2.34×10^6	2.34×10^6
0	0	0	0.1 mol dm^{-3} KCl	1.64×10^6	1.95×10^6
0.05	0	0	0.1 mol dm^{-3} KCl	2.3×10^5	5.69×10^5
0.50	0	0	0.1 mol dm^{-3} KCl	4.45×10^4	1.17×10^5
0	0.05	0	0.1 mol dm^{-3} NaCl	1.64×10^5	4.84×10^5
0.05	0	4.4	0.1 mol dm^{-3} KCl	4.29×10^5	5.07×10^5
0	0.05	4.4	0.1 mol dm^{-3} NaCl	7.8×10^5	1.17×10^6

[a]Values reached after three days.

semicircle, which could be attributed to the bulk of the membrane, and a second semicircle at lower frequency, which could be associated with the transfer of ions between the membrane and the aqueous contacting solutions. The initial values of these quantities and the final, time-independent values (measured after three days) are shown in Tables 1 and 2.

The potential differences produced by the membranes (with a ten-fold difference in concentration in the two contacting solutions) are shown in Table 3.

The selectivities of the various membranes for potassium over sodium were measured as described above. For all membranes containing no valinomycin, no selectivity was apparent (though all membranes produced Nernstian calibration curves with the relevant primary ion, either Na^+ or K^+). For membranes containing valinomycin, the selectivity for potassium over sodium was greater than 10^3:1.

DISCUSSION

Throughout this discussion, it is assumed that the bulk of the membrane is electrically neutral [10].

The potential differences (Table 3) measured for the membranes containing potassium tetraphenylborate are close to those which would be expected theoretically for membranes in which the anion is immobile with respect to

TABLE 2

Charge-transfer resistances (normalised to 1 cm^2 membrane area)

$KBPh_4$ (mg)	$NaBPh_4$ (mg)	Valinomycin (mg)	Contacts	R_{ct} initial (Ω cm^2)	R_{ct} final[a] (Ω cm^2)
0	0	0	0.1 mol dm^{-3} KCl	3.12×10^6	7.8×10^5
0.05	0	0	0.1 mol dm^{-3} KCl	3.90×10^4	3.90×10^4
0	0.05	0	0.1 mol dm^{-3} NaCl	6.24×10^4	3.90×10^5
0.05	0	4.4	0.1 mol dm^{-3} KCl	3.90×10^4	3.90×10^4
0	0.05	4.4	0.1 mol dm^{-3} NaCl	3.9×10^5[b]	3.9×10^5[b]

[a]Values reached after three days. [b]These values are estimates only, as potassium impurity in NaCl solutions produces an unsteady state.

TABLE 3

Measured potential differences for ten-fold concentration difference across membrane[a]

$KBPh_4$ (mg)	$NaBPh_4$ (mg)	Valinomycin (mg)	Contacts	P.d. (mV)	Theoretical[b]
0.05	0	0	KCl	109.2	110.16
0	0.05	0	NaCl	103.8	110.61
0.05	0	4.4	KCl	108.9	110.16
0	0.05	4.4	NaCl	—	110.61

[a]All values take account of any asymmetry potential found for the membranes with equal concentrations of the ion (Na^+ or K^+) on either side, and were measured after 1 h. [b]$E = RTF^{-1} \ln (m_1 \gamma_{\pm(1)} / m_2 \gamma_{\pm(2)})$.

the cation. The theoretical values are shown in Table 3, and were calculated by using the mean activity coefficient, $\gamma_{\pm}$ for either potassium chloride or sodium chloride.

The membranes containing sodium tetraphenylborate produced slightly lower potential difference values than the membranes containing potassium tetraphenylborate, indicating that the relative mobility of the anions is greater in the sodium tetraphenylborate membranes. This may be due to penetration of the membranes by chloride ions. The cation transport number in both cases, however, is close to unity.

Table 1 shows that addition of salts to the membrane results in a bulk resistance appreciably lower than in the absence of the additive. The inherent conductance arising in the absence of additives is probably due to ionic impurities in the PVC and/or plasticizer. From Table 1, it can be seen that a ten-fold change in additive concentration does not produce a ten-fold change in the bulk resistance of the membrane. The bulk resistance is decreased by a factor of about six, which would seem to indicate that at higher tetraphenylborate concentrations, there is association between the anions and cations in the membrane.

By using the values in Table 1, and by assuming that the membrane conductivity arises almost exclusively from cation conduction, it is possible to construct a table of relative ionic mobilities (Table 4). From this Table, it is apparent that Na^+ and K^+, in the absence of valinomycin, have comparable mobilities and that the presence of valinomycin causes a greater reduction in Na^+ mobility than K^+ mobility. Because it seems likely that the valinomycin molecules are immobilised in the membrane and that very little free K^+ is present when there is an excess of valinomycin, it may be concluded that K^+ ions can exchange rapidly between valinomycin molecules.

The values of the charge-transfer resistances (Table 2) show that there is a fast equilibrium between potassium ion in the aqueous phase and in the membrane, both in the presence and absence of valinomycin. In the absence of valinomycin there is also a fast equilibration between sodium ions in aqueous solution and in the membrane phase. When valinomycin was included

TABLE 4

Relative mobilities

Ion	Initial	After equilibration with water
K^+	1.00	1.00
Na^+	1.7 ± 0.3	1.2 ± 0.2
K^{+a}	0.6 ± 0.1	1.1 ± 0.2
Na^{+a}	0.3 ± 0.1	—[b]
$B(Ph)_4^-$	0.01	0.02

[a]With valinomycin present. [b]This value was uncertain because of K^+ uptake from impurities in the NaCl solutions.

in the sodium tetraphenylborate membranes, the charge-transfer part of the impedance spectra was poorly defined, except for the initial runs, most probably because of the uptake of potassium from the sodium solutions, which although of high purity, still contain levels of potassium which complex with the valinomycin to a significant extent.

Finally, some conclusions can be drawn with respect to the operation of the membranes as ion-selective electrode membranes. First, the membranes must depend on the presence of relatively immobile anions if a Nernstian response to potassium ion is to be expected. (With no added salt or valinomycin in the membrane and a ten-fold difference in K^+ concentration, a potential difference of only 92.8 mV is produced, indicating a considerable degree of chloride penetration. In the absence of added potassium tetraphenylborate, it is by no means certain that adventitious immobile anions will be present in the membrane, although it seems likely that some will be incorporated as impurities into a membrane from its components or otherwise, when it is fabricated.

Secondly, the selectivity of the membranes in the presence of valinomycin does not arise from a change in the relative mobility of K^+ over Na^+, because this change is very much less than the measured selectivity. (Approximately 2:1 compared to a selectivity of greater than 1000:1). Rather, it seems probable that the selectivity arises because the equilibrium concentration of sodium ions in the membrane in equilibrium with a sodium chloride solution is extremely small, because of the large increase in the electrostatic potential in the bulk of the membrane brought about by the presence of valinomycin (Fig. 2). Thus, with no valinomycin in the membrane, sodium ions in a contacting aqueous solution will readily exchange with potassium ions in the membrane until the sodium and potassium ions are both in equilibrium across the interface, whereas with valinomycin present, there will be very little tendency for sodium ions in aqueous solution to exchange with potassium ions in the membrane unless the activity ratio of Na^+/K^+ in the aqueous phase is $>10^3$.

The time dependence exhibited by the membranes is considered to be due primarily to the uptake of water by the membranes, causing a change of local environment for the mobile ions, together with a swelling effect.

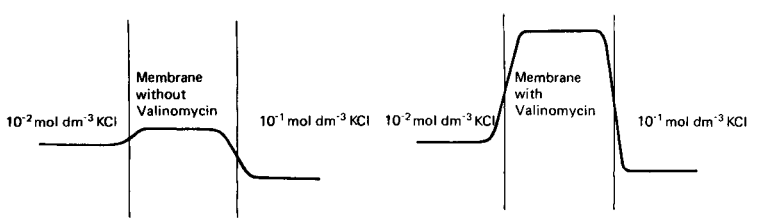

Fig. 2. Electrostatic potential profiles for: (a) a membrane containing no valinomycin; (b) a membrane with ligand incorporated.

REFERENCES

1 R. D. Armstrong, A. K. Covington and G. P. Evans, J. Electroanal. Chem., 159 (1983) 33.
2 S. M. Ciani, G. Eisenman and G. Szabo, J. Membr. Biol., 1 (1969) 1.
3 R. P. Buck, Anal. Chem., 46 (1974) 28R.
4 R. P. Buck, Anal. Chem., 48 (1976) 23R.
5 P. Läuger, Science, 178 (1972) 24.
6 W. E. Morf, G. Kahr and W. Simon, Anal. Lett., 7 (1974) 9.
7 W. E. Morf, P. Wuhrman and W. Simon, Anal. Chem., 48 (1976) 1031.
8 A. P. Thoma, A. Viviani-Nauer, S. Arvanitis, W. E. Morf and W. Simon, Anal. Chem., 49 (1977) 1567.
9 A. K. Covington, in A. K. Covington (Ed.), Ion-selective Electrode Methodology, Vol. 1, CRC Press, Boca Raton, Florida, 1979, p. 16.
10 O. Kedem, M. Perry and R. Block, IUPAC International Conference on Selective, Ion-Sensitive Electrodes, Paper 44, Cardiff, 1973.

Analytica Chimica Acta, 166 (1984) 111—118
Elsevier Science Publishers B.V., Amsterdam — Printed in The Netherlands

DETERMINATION OF GLUCOSE IN BLOOD BY FLOW INJECTION ANALYSIS AND AN IMMOBILIZED GLUCOSE OXIDASE COLUMN

M. MASOOM and ALAN TOWNSHEND*
Chemistry Department, University of Hull, Hull HU6 7RX (Great Britain)
(Received 10th May 1984)

SUMMARY

A flow-injection system for glucose determination is described. Glucose oxidase is immobilized on controlled porosity glass (CPG) and used in a glass column (2.5 mm diameter × 2.5 cm). The hydrogen peroxide produced by the enzymatic reaction ($\geq 1 \times 10^{-6}$ M) is detected by the current produced in a flow-through cell, with two platinum electrodes having a potential difference of 0.6 V. Glucose (0—20 mmol l^{-1}) can be determined in blood plasma either with a dialyser in the system or, better, by incorporating a column of copper(II) diethyldithiocarbamate on CPG before the enzyme column. The results compared well with those obtained by a conventional analyser system. The glucose oxidase column showed little change in activity over a 10-month period.

Glucose is routinely determined in clinical laboratories for the identification and control of diabetes. The use of enzymes as highly selective and efficient catalytic reagents in analysis has been given considerable attention in the past two decades. The advent of effective procedures for the immobilization of enzymes by chemical bonding to various carriers has presented new opportunities for their practical application. The uses of immobilized enzymes include their incorporation into enzyme electrodes and in enzyme reactors, of the packed-bed and open tubular types.

Since Updike and Hicks [1] introduced the term "enzyme electrode" and constructed the first working model for the determination of glucose on the basis of immobilized glucose oxidase and the Clark oxygen electrode, several papers on the development or application of enzyme electrodes for D-glucose measurement have been published [2—4]. Nevertheless, enzyme electrodes have not yet found general application in the clinical laboratory. They provide poor reproducibility in clinical situations, and suffer from the added disadvantages of long response and recovery times. Enzyme reactors have been used with sample injection techniques for determination of glucose [5, 6], and the feasibility of flow injection analysis (f.i.a.) for routine applications in a clinical laboratory has been reviewed recently [7].

The combination of f.i.a. with an immobilized enzyme reactor column would seem to have many advantages. This paper describes the determination of glucose by f.i.a., using glucose oxidase chemically immobilized on

0003-2670/84/$03.00

controlled porosity glass (CPG), and an amperometric flow-through detector. The method is very rapid, and has been applied to blood samples.

EXPERIMENTAL

Reagents

Glucose oxidase (Glucose:oxygen oxidoreductase EC.1.1.3.4. (ex. *Aspergillus niger*, 250 U mg^{-1}) was obtained from Sigma Chemicals. Controlled porosity glass (CPG-240, 120/200 mesh, 22.6-nm mean pore diameter) was obtained from BDH Chemicals. Glucose (BDH AnalaR) standards were prepared in saturated benzoic acid, at least 24 h before use to ensure attainment of mutarotation equilibrium. 3-Aminopropyltriethoxysilane (Sigma) was stored, protected from moisture, at 4°C. Control serum [Commercial Horse Serum A (L711302) and B (11F9834)] was a gift from Doncaster Royal Infirmary. The pre-analysed blood plasma samples from patients were obtained fresh from the same hospital. All other chemicals used were of analytical grade.

Preparation of packings for reactors

Enzyme immobilization. A 10-g amount of CPG-240 was boiled in 100 ml of 5% nitric acid for 30 min. The CPG-240 was filtered on a glass filter, washed with deionized water and dried in an oven at 95°C. Aqueous aminoalkylating agent was prepared by adding 5 ml of 3-aminopropyltriethoxysilane to 45 ml of water and the pH was carefully adjusted to 3.45 with 5 M hydrochloric acid. The dried glass was added, the pH was checked and the mixture was kept at 75°C on a water bath for 150 min, the flask being swirled every 15 min. The alkylaminated glass was filtered through a porosity G3 sintered glass filter, and washed and dried as before. The alkylamination process was repeated to ensure complete activation of the glass. The dried alkylamino glass was stored in an air-tight bottle and kept in this condition until batches were needed.

The cross-linking agent, glutaraldehyde (2.5%), was prepared by adding 2.5 ml of 50% glutaraldehyde (BDH Chemicals) to phosphate buffer (0.1 M, pH 7.0), and diluting to 50 ml with the buffer. Alkylamino glass (1.0 g) was added to 5 ml of the glutaraldehyde/buffer solution in a well-stoppered vessel, through which nitrogen had been bubbled to remove oxygen. The reaction was allowed to proceed for 1 h at room temperature with brief nitrogen deoxygenation every 10 min for the first 30 min. The activated glass was washed well with distilled water.

Glucose oxidase (6.0 mg, 1500 U) was dissolved in 3.0 ml of cold (4°C) phosphate buffer (0.1 M, pH 6.0) and added to the activated glass. Nitrogen was bubbled through the solution as before. The solution was kept at 4°C for 2.5 h. The immobilized enzyme derivative was washed first with cold phosphate buffer and then with cold water to ensure the removal of any unlinked enzyme. The immobilized enzyme was stored moist at 4°C in a well-stoppered tube. No bacterial growth in the stock immobilized enzyme was noticed even after 10 months storage.

Copper dithiocarbamate-treated CPG. Copper diethyldithiocarbamate was adsorbed on CPG as follows. Copper(II) sulphate pentahydrate (0.0393 g) was dissolved in water and the solution was diluted to exactly 1 l; 10 ml of this solution (containing about 100 μg of Cu) was pipetted into a beaker, and 5.0 ml of 25% (w/v) citric acid was added. The solution was made slightly alkaline with dilute ammonia and the excess of ammonia was boiled off. The pH was adjusted to 8.5 (pH meter), and 15 ml of 4% (w/v) EDTA solution was added. The cooled solution was transferred to a separating funnel, shaken for 45 s with 10 ml of aqueous 0.2% (w/v) sodium diethyldithiocarbamate solution, and then shaken with 20 ml of n-butyl acetate for 30 s. After cooling, the funnel was shaken for 15 s and the phases were allowed to separate. The aqueous layer was removed and the organic phase was shaken with 20 ml of (1 + 19) sulphuric acid for 15 s and then removed. A portion (5 ml) of this copper diethyldithiocarbamate solution was shaken well with 1 g of CPG and left at room temperature for 1 h. The CPG was then filtered off, washed well with distilled water and packed into a glass column (2.5 cm × 2.5 mm).

Construction of flow-through electrochemical detector

The detector was a flow-through glass cell (4.9 mm diameter × 30 mm) containing two rectangular platinum electrodes (6 × 3 mm). Figure 1 shows the cell and its electrical circuitry. A potential of 0.6 V was applied across the electrodes. The hydrogen peroxide formed was determined by reduction at one of the platinum electrodes. The current produced was proportional to the hydrogen peroxide concentration.

Flow system and procedure for the determination of hydrogen peroxide or glucose

The simple manifold used for hydrogen peroxide determination is shown in Fig. 2. Phosphate buffer (0.1 M, pH 4.5, unless otherwise stated) was used as the carrier stream, and was pumped at 2.0 ml min^{-1}, by using a peristaltic

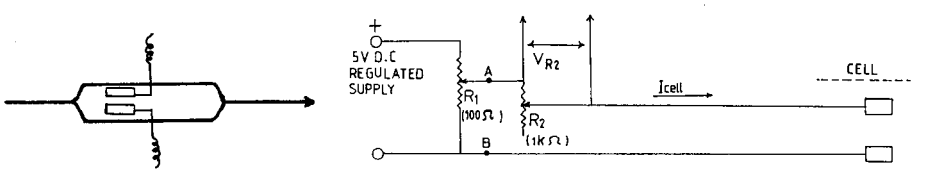

Fig. 1. Schematic representation of the flow-through electrochemical cell and its electrical circuitry.

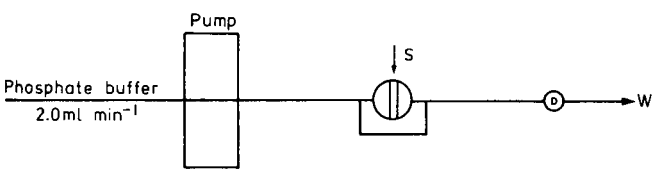

Fig. 2. Manifold used for the determination of hydrogen peroxide.

pump (Ismatec Mini-S-820). Polyethylene tubing (0.3 mm i.d.) was used to connect the injection valve to the detector. Samples were injected into the buffer carrier stream by means of a rotary valve, which delivered a fixed sample volume of ca. 20 μl. The output current signal was fed to a strip-chart recorder. The peak-height current was measured.

For glucose determination, an immobilized enzyme column (2.5 mm diameter × 2.5 cm) was inserted into the manifold shown in Fig. 2, just after the injection valve. Glucose in blood plasma was determined with and without a dialysis unit in the system. The manifold with the dialysis unit is shown in Fig. 3. The dialysis unit consisted of two perspex blocks with a triple-pass channel machined out of each. The total length of the channel was 240 mm with a width of 2.0 mm and a depth of 0.3 mm. A pre-conditioned Cuprophan dialysis membrane (Elkay 170-0406-020) was clamped between the two blocks.

RESULTS AND DISCUSSION

Optimization of experimental conditions

Experiments were conducted to establish the optimum pH and flow rate for the determination of glucose. The effect of pH on the activity of the immobilized glucose oxidase was investigated by using 0.1 M phosphate buffer of various pH values as the carrier stream. The greatest response was obtained at pH 4.5, as is shown in Fig. 4, whereas the pH optimum for the soluble enzyme is 5.5. Such shifts of optimum pH after immobilization are common, the extent depending on the method of immobilization. Therefore, pH 4.5 was generally used for glucose determination, except for plasma samples, for which pH 7.0 phosphate buffer was used. The latter, although giving only 50% of the sensitivity at pH 4.5, gave better reproducibility for plasma samples.

Increasing the flow rate from 1.0 to 2.0 ml min^{-1} gave a 17% increase in peak height, but higher flow rates gave a continuously decreasing peak height sensitivity. Thus 2.0 ml min^{-1} is recommended for achieving good sensitivity and a reasonable sample throughput. As sampling rates exceeding 150 h^{-1} are rarely required, too much emphasis should not be placed on sampling frequency. However, a short residence time of the sample in the system is highly desirable as it makes the analytical readout quickly available. In the case of blood glucose determinations, the flow rate was increased to 3.0 ml min^{-1} to have the readout quickly available and to demonstrate the fast possible sample thoughput (300 h^{-1}) that can be achieved.

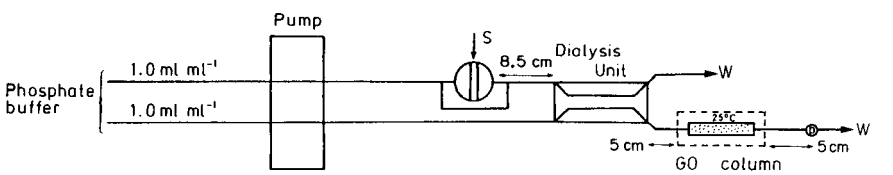

Fig. 3. Manifold with dialysis unit for determination of glucose in plasma.

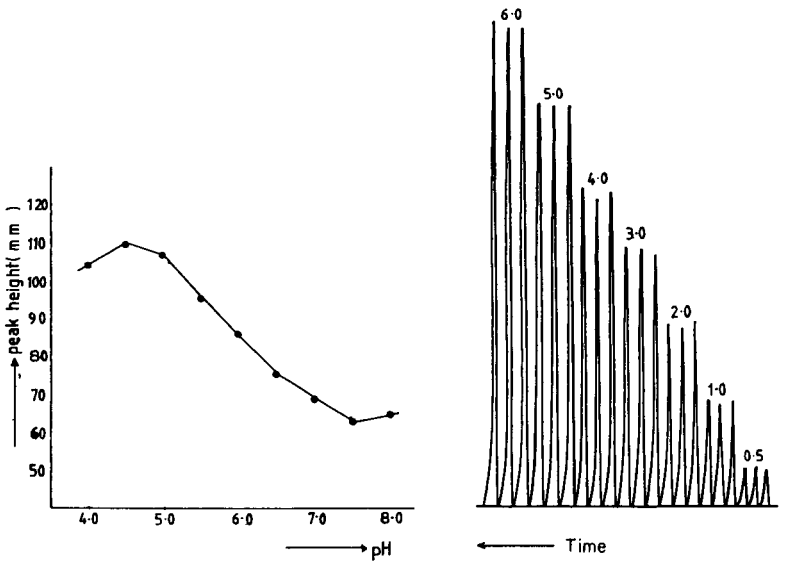

Fig. 4. Effect of pH on the activity of glucose oxidase immobilized on CPG (1×10^{-4} M glucose).

Fig. 5. Typical recorder peaks for triplicate injections of $0.5—6.0 \times 10^{-3}$ M hydrogen peroxide.

Determinations of hydrogen peroxide and glucose

Hydrogen peroxide could be detected by injection into the phosphate buffer carrier, and passage directly to the detector, without incorporating the enzyme column. Reproducible responses were obtained down to 1×10^{-6} M hydrogen peroxide. Figure 5 shows some typical responses. The peak shapes are smooth and show only slight tailing.

Insertion of the enzyme into the manifold slightly decreased the flow rate, for example, from 2.0 to 1.9 ml min^{-1}. However, the peak shape and width obtained after injections of glucose samples were almost the same as those obtained from hydrogen peroxide samples in the absence of the column. Thus the enzyme column had little effect on the dispersion of the sample zone. This enabled the concentration of hydrogen peroxide produced by the enzyme-catalysed reaction to be calculated from the hydrogen peroxide calibration graph obtained above. The results (Table 1) show that the % glucose conversion increased as the glucose concentration decreased, reaching a maximum (30%) at 5×10^{-5} M glucose. The log—log calibration graph for glucose extended from 1×10^{-6} to 1×10^{-2} M, and was linear up to ca. 1×10^{-3} M (Fig. 6).

Glucose determination in blood plasma

Use of a dialysis unit. A dialysis unit was incorporated into the manifold before the enzyme column to separate glucose from interfering macro-

TABLE 1

Hydrogen peroxide produced from glucose

Glucose (M)	H_2O_2 produced (M)	(%)
5×10^{-2}	1.4×10^{-3}	3
5×10^{-3}	1.0×10^{-3}	18
5×10^{-4}	1.4×10^{-4}	28
5×10^{-5}	1.5×10^{-5}	30
5×10^{-6}	1.0×10^{-6}	18

molecules. Each side of the membrane had a surface area of 4.9 cm^2 and the device had a hold-up volume of 150 μl. The flow rates of both streams were kept the same (1.0 ml min^{-1}) in the same direction, to minimize dispersion within the dialysis unit. By injecting aqueous glucose standards into the manifold with and without the dialysis unit, transfer was found to be 13%. Table 2 shows calibration data for aqueous standards ($5—20 \times 10^{-3}$ M). Two control sera were each analysed 6 times by this procedure. The results obtained were 10.4 and 5.1 mM, compared with the expected value of 10.6 and 5.1 mM, with relative standard deviations of 2.3% and 3.1%, respectively.

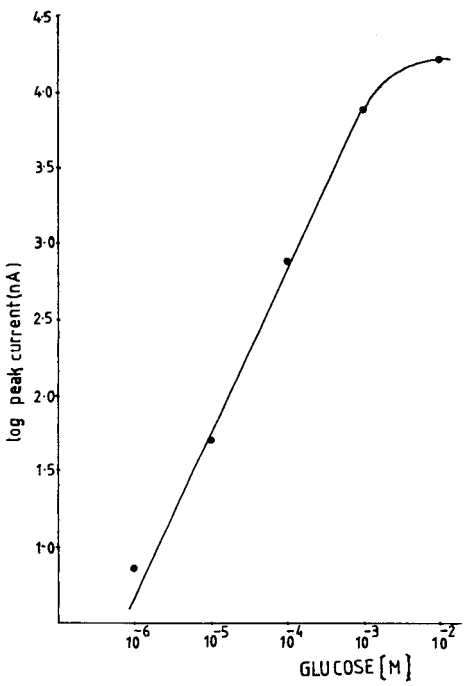

Fig. 6. Log—log calibration curve for glucose.

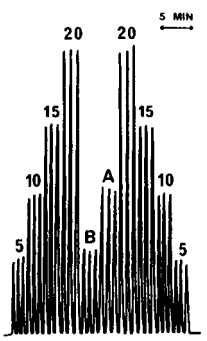

Fig. 7. Typical recorder peaks for triplicate injections of standard glucose solutions ($5—20 \times 10^{-3}$ M) and (A, B) two control sera.

TABLE 2

Calibration results for standard glucose solutions

Glucose conc. ($\times 10^{-3}$ M)	5	10	15	20
With dialysis				
Mean peak height (nA)[a]	45.5	75.4	116.1	150.8
S.d. (nA)	2.4	1.6	1.7	2.3
R.s.d. (%)	3.1	2.1	1.4	1.5
Without dialysis				
Mean peak height (nA)[a]	500	931	1391	1934
S.d. (nA)	10	10	26	13
R.s.d. (%)	2.00	1.07	1.86	0.67

[a]For 6 results.

The flow rates were kept low to give a reasonable residence time in the dialyzer, and therefore sufficient glucose transfer. The readout was available after 45 s. The sampling rate was a relatively low 70 h^{-1}.

Use of a copper diethyldithiocarbamate column. Yao et al. [8] have recommended the use of a column of copper diethyldithiocarbamate adsorbed on silica gel to remove interferences when glucose is determined in blood. Therefore, in this investigation, a column of copper diethyldithiocarbamate adsorbed on CPG was inserted in the manifold before the enzyme column. Ten plasma samples were analysed for glucose using this system, and the results were compared with those obtained by using commercial immobilized enzyme tubes in a Beckman II analyser, a procedure routinely used in clinical laboratories. The results were in excellent agreement, with a regression equation of $y = 1.0077x \pm 0.123$, with a correlation coefficient of 0.992 (y = present method result, x = Beckman result). In the present method, the readout was available in 12 s. The possible sample throughput was 300 h^{-1}. The use of this column is to be preferred to a dialysis system.

It should be mentioned that successful analyses of the control sera were possible without including any separation stage in the manifold. Figure 7 shows a typical recorder output for a series of glucose standards, and two control sera, obtained with a manifold having no dialysis unit or copper diethyldithiocarbamate column. The calibration data obtained from these results are summarized in Table 2. The concentration range (0—20 mM) covers the normal range for plasma glucose (4.2—6.7 mM) as well as the hypo- and hyper-glycaemic levels that result from metabolic disorders [9]. When the two control sera were each analysed 6 times by this procedure, the results were 10.5 and 5.6 mM glucose, compared with the expected values of 10.6 and 5.1 mM, with relative standard deviations of 1.5 and 1.9%, respectively.

The immobilized enzyme was found to be extremely stable. The same column has been used continuously for 10 months at room temperature, without significant deterioration of its performance.

Conclusions

This paper demonstrates the effectiveness of using a column of an enzyme immobilized on CPG in a flow-injection system. Dispersion is little affected, rapid analyses and sample throughput are achieved, and there is no pronounced deterioration of the enzyme. This should make it extremely suitable for use in a clinical laboratory.

The principle described here will be extended in subsequent papers to provide techniques for the simultaneous determination of carbohydrate mixtures, as well as other oxidase substrates.

The authors thank Mr. G. E. Palin for the design of the electrical circuitry for the detector, Dr. P. J. Worsfold for valuable discussions, and John Leverton, Doncaster Royal Infirmary, for the provision of control sera and analysed blood samples. One of us (M. M.) thanks the Ministry of Education, Government of Pakistan, for a research grant and the University of Baluchistan, Quetta, for study leave.

REFERENCES

1 S. J. Updike and G. P. Hicks, Nature, 214 (1967) 986.
2 G. G. Guilbault and G. J. Lubrano, Anal. Chim. Acta, 64 (1973) 439.
3 S. J. Updike, M. C. Shults and M. Busby, J. Lab. Chim. Med., 93 (1979) 518.
4 D. R. Thevenot, R. Sternberg, P. R. Coulet, J. Laurent and D. C. Gautheron, Anal. Chem., 51 (1979) 96.
5 L. Gorton and L. Ögren, Anal. Chim. Acta, 130 (1981) 45.
6 P. J. Worsfold, Anal. Chim. Acta, 145 (1983) 117.
7 B. Rocks and C. Riley, Clin. Chem., 28 (1982) 409; C. Riley, B. F. Rocks and R. A. Sherwood, Talanta, 31 (1984) 879.
8 T. Yao, M. Akino and S. Musha, Bunseki Kagaku, 30 (1981) 740; 31 (1982) 409.
9 J. F. Zilva and P. R. Pannall, Clinical chemistry in diagnosis and treatment, Lloyd-Luke, London, 1981, pp. 174—211.

Analytica Chimica Acta, 166 (1984) 119—127
Elsevier Science Publishers B.V., Amsterdam — Printed in The Netherlands

DIFFERENTIAL PULSE VOLTAMMETRY WITH FAST PULSE REPETITION TIMES IN A FLOW-INJECTION SYSTEM WITH A COPPER-AMALGAM ELECTRODE

PETER W. ALEXANDER* and UMAPORN AKAPONGKUL

Department of Analytical Chemistry, University of New South Wales, P.O. Box 1, Kensington, 2033 N.S.W. (Australia)

(Received 28th February 1984)

SUMMARY

The reductive determination of cadmium and zinc is used to illustrate the effects of pulse repetition time in differential pulse voltammetry at solid electrodes. With 100-ms repetition times, signal-to-background ratio is shown to improve in flow-injection response studies at a copper-amalgam working electrode for both voltage scanning and amperometric operation, allowing scan rates up to 100 mV s^{-1}, and detection limits of 0.07—0.15 ng for cadmium and zinc after deaeration of sample solutions. Peak widths at baseline in the range 12—30 s, depending on flow rate, are obtained in the flow-injection system for cadmium and zinc at working potentials of —0.77 and —1.27 V, respectively. Interferences occur when cadmium is in large excess over zinc, although the voltammetric peaks do not overlap.

The application of differential pulse voltammetry (d.p.v.) at solid electrodes for reductive determinations has possible advantages of selectivity and sensitivity over d.c. amperometric detection in continuous flow analysis or flow injection analysis (f.i.a.). Many reports have appeared on d.p.v. detection in high-performance liquid chromatography (l.c.). For example, Swartzfarger [1] and MacCrehan and Durst [2, 3] have reported d.p.v./l.c. at carbon paste and gold amalgam electrodes, respectively, indicating improved selectivity over d.c. amperometric methods. The disadvantages of d.p.v. for detection in liquid chromatography, however, have been discussed by Kissinger [4] and Ivaska and Smyth [5]; the problems are poor sensitivity and the more complex instrumentation required.

Other pulse methods reported for l.c. detection include normal pulse [6], and reverse pulse [7], while for continuous flow analysis, d.p. amperometry at the dropping mercury electrode has been used [8—10]. For solid electrodes, however, problems associated with d.p.v. for reductive determinations include high and variable background currents, slow response, and slow scan rates.

Considerable work has been reported on d.p.v. in static solution, aimed at improving sensitivity and scan rates for a variety of applications. Modifying the current-measuring sequence [11, 12] or pulse waveform [13, 14]

0003-2670/84/$03.00

enables better sensitivity to be obtained. Modifications of d.p.v. for fast scanning have been described [14—19]. Bond and Grabaric [17] demonstrated that analytically useful results at a single-drop mercury electrode could be obtained under conditions where the pulse time was comparable with the gap between pulses. Ashley and Levine [19] also reported that short pulse repetition times were applicable for rapid scanning with pulse techniques.

This study reports on d.p.v. measurements at a copper-amalgam wire electrode in a flow-through cell described previously [20]. The aim was to establish the response characteristics of d.p.v. with short pulse repetition times at a solid electrode for reductive determinations in flow analysis.

EXPERIMENTAL

Flow systems and reagents

The flow system, the equipment, and the electrodes used in this study have been described [20]. Briefly, a buffer was pumped at a constant flow rate of 2.8 ml min^{-1} to a flow cell containing a copper-amalgam wire as the working electrode, a platinum wire as the auxiliary electrode, and a saturated calomel reference electrode (SCE). Samples were injected into the buffer stream through a liquid chromatographic septum injector with a hypodermic syringe. In the continuous flow method, samples were pumped continuously from a sample reservoir through the flow cell. The polarographic analyzer used was the Princeton Applied Research (PAR) Model 174A.

The same buffer and sample solutions were used as described previously [20]. Ammonia buffer (1 M) served as the carrier stream; copper nitrate and zinc nitrate solutions (1.0×10^{-2} M) prepared in 1 M ammonia buffer were used as sample solutions. The buffer and sample solutions also contained sodium hydrogen sulphite (8.0×10^{-3} M) to remove oxygen.

Instrumental modifications. In order to obtain short delay times between pulses during d.p.v. operation of the PAR 174A, the time clock resistors were altered. Two resistors numbered R63 and R64 in the circuit diagram in Fig. IX-9 of the operating manual were altered from 1 M and 402 K to 20 K and 40 K, respectively. This had the effect of changing the 5-s and 2-s times on the front panel of the instrument to 0.1 s and 0.2 s, respectively. Differential pulse operation was then possible with the following parameters: scan rates 2—200 mV s^{-1}, initial potential —0.6 V, voltage range 1.75 V, current sensitivity variable as required, low pass filter 0—3 s, time between pulses 0.1—1.0 s, pulse amplitude 5—100 mV.

Procedures

Voltage scan operation. Hydrodynamic voltammograms were recorded while test solutions of either the blank ammonia buffer or buffered metal ion solutions were pumped continuously through the flow cell. The solutions

were deaerated with nitrogen saturated with ammonia, and also contained 8.0×10^{-3} M sodium sulphite to remove dissolved oxygen. The scans were recorded in the d.p. operation mode in the voltage range (—0.6 to —1.6 V) with the instrument parameters varied within the ranges given above in order to investigate the effects of scan rate and delay time between pulses on the peak shape of the d.p. voltammograms.

Flow-injection system. Once the d.p. peak potentials for the metal ions tested (Cd and Zn) had been established, aliquots (100 μl) of each metal ion solution (1.0×10^{-2} M) were injected into the ammonia buffer stream, flowing at 2.8 ml min^{-1}. The d.p. current was monitored continuously at a fixed operating potential, i.e., d.p. amperometric operation. The operating potential (E_{op}) was set at a more positive potential than the peak potential (E_p) by choosing the value of E_{op} which gave optimum sensitivity and speed of response in the flow-injection system. This procedure ensured that the potential was stepped from E_{op} to near the value of E_p when each pulse was applied to the electrode.

The d.p. current was recorded continuously at E_{op} for injections of cadmium or zinc ions (1×10^{-2} M) with volumes of 1—5 μl and operating potentials of —0.77 V and —1.27 V, respectively. Mutual interference effects were then studied by injecting mixtures of cadmium and zinc ions at ratios varying from 1:100 to 100:1 and recording the peak heights at the two operating potentials.

RESULTS

Effect of short pulse repetition times on hydrodynamic voltammograms

The modified polarograph was used to record hydrodynamic d.p. voltammograms of cadmium and zinc solutions with pulse repetition times below those used in previous studies [15, 18, 21—23]. The range 0.1—1.0 s was available with this modified polarograph, compared to 0.5—5.0 s on the original instrument. Figure 1 shows the pulse waveforms for 0.1 and 0.5 s pulse repetition times. For the pulse width of 56.7 ms used in the PAR 174, the delay time between pulses was therefore 43.3 ms and 443.3 ms for the two cases shown in Fig. 1. The short delay time obviously provides a greater number of current samplings per unit time during a d.p. scan or for d.p. amperometric operation. The short delay has advantages over the longer times for d.p.v. at solid electrodes not only for scanning operation but also for sensitivity in flow injection analysis.

Figure 2 shows hydrodynamic voltammograms for a solution containing cadmium and zinc, both at a concentration of 5.0×10^{-4} M, recorded under flow conditions (2.8 ml min^{-1}) after deaeration. For a slow scan rate of 5 mV s^{-1}, there was some loss in sensitivity at the pulse repetition time of 0.1 s compared to that at 1.0 s, but the peaks remained well defined. When the scan rate was increased at the two different times between pulses, the results were as shown in Fig. 2. For the 1.0-s repetition time, the peaks for

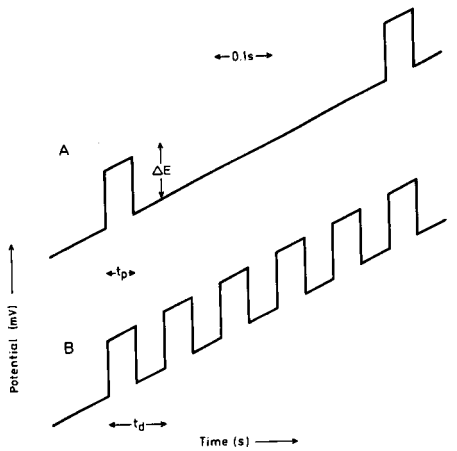

Fig. 1. Pulse waveforms operated with a fixed pulse width (t_p) and with different times between pulses (t_d): (A) 0.5 s, (B) 0.1 s.

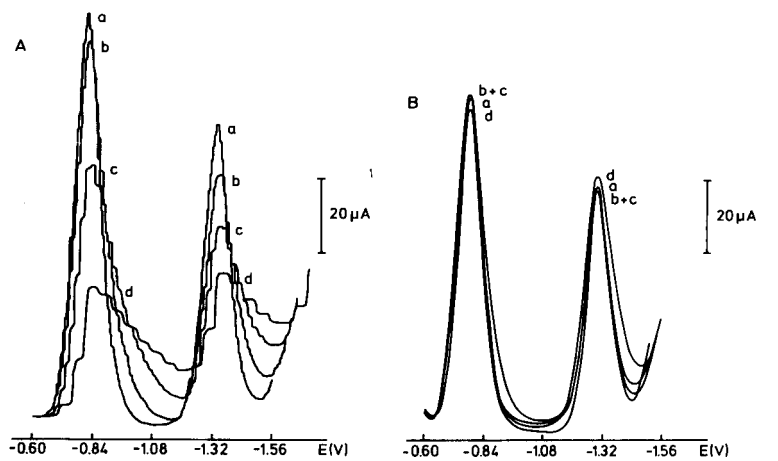

Fig. 2. Effect of scan rate on d.p.v. scans at different pulse repetition times (t_d): (A) 1.0 s; (B) 0.1 s. Scan rate: (a) 5; (b) 10; (c) 20; (d) 50 mV s^{-1}. Cadmium and zinc solution (each 5.0 × 10^{-4} M) in 1 M ammonia/ammonium chloride (pH 10.2) pumped continuously at 2.8 ml min^{-1}.

cadmium and zinc decreased in height and broadened at scan rates > 5 mV s^{-1}, as observed for the DME [24]. For the 0.1-s repetition time, little effect was observed up to a scan rate of 50 mV s^{-1}. However, with further increases to 200 mV s^{-1}, the peaks again decreased in height and became broader.

Table 1 summarizes the values observed for peak potentials, peak heights, and peak widths at half height ($w_{1/2}$) for both cadmium and zinc at various scan rates when the short t_d of 0.1 s was used. At scan rates above 100 mV s^{-1}, the peak distortion became unacceptably high, but operation was viable at 100 mV s^{-1}, about a 20-fold improvement over the 1.0-s repetition time.

TABLE 1

Differential pulse characteristics at fast scan rates[a] for 5×10^{-4} M cadmium and zinc in 1 M ammonia/ammonium chloride (pH 10.2)

Scan rate ($mV\ s^{-1}$)	$-E_p$ (V)		i_p (μA)		$w_{1/2}$ (V)	
	Cd	Zn	Cd	Zn	Cd	Zn
5	0.79	1.31	88	62	0.114	0.114
10	0.79	1.30	89	61	0.114	0.114
20	0.79	1.30	89	60	0.114	0.120
50	0.79	1.31	84	60	0.120	0.138
100	0.81	1.32	68	55	0.132	0.144
200	0.84	1.34	48	42	0.168	0.168

[a]For t_d = 0.1 s, amplitude 100 mV.

The relationship between d.p. peak heights and amplitude is known to be linear at the DME with conventional pulse-timing parameters [24—26]. This aspect was therefore tested for the short delay times. Figure 3 shows the d.p. scans for the cadmium and zinc solution at pulse amplitudes of 5—100 mV. The peak heights increased linearly with amplitude, despite the fact that $t_p > 1/2\ t_d$. The E_p and peak widths also changed as expected for increasing amplitude [24] (Fig. 3, Table 1).

Flow injection analysis with d.p.v. detection

The flow-injection system with d.p.-amperometric operation was then tested at potentials set at a fixed value near the peak potentials for cadmium and zinc. The operating potential was chosen as outlined under Experimental; E_{op} was set at a more positive potential than E_p, depending on amplitude, in such a way that the potential was stepped up to the E_p value during each

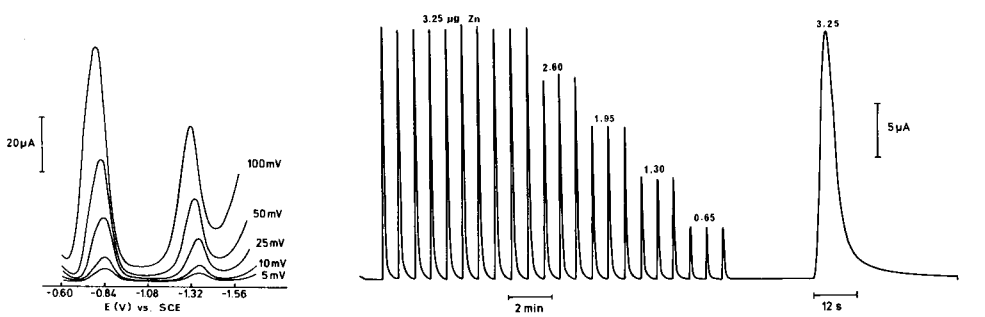

Fig. 3. Effect of pulse amplitude on d.p.v. scans with a short pulse repetition time (t_d = 0.1 s). Solution conditions as for Fig. 2.

Fig. 4. Flow-injection peaks for d.p. amperometric detection of microgram quantities of zinc (as shown) at −1.27 V with t_d = 0.1 s, using sample injection volumes of 1—5 μl.

pulse application. Figure 4 shows the flow-injection results for zinc at an operating potential of −1.27 V, and indicates the speed of electrode response with d.p. amperometric operation.

The sensitivity, detection limits, linear working ranges, and d.p. operating potentials for cadmium and zinc are shown in Table 2. The d.p. detection limits were about 10-fold lower than reported previously [20] for d.c. operation, provided that the short pulse repetition time was used for d.p. operation with an amplitude of 100 mV.

Effect of fast pulses. The high sensitivity observed above was largely due to the short pulse repetition time used. The electrode response to injected samples at various t_d values (0.1—1.0 s) is shown in Fig. 5 for fast chart recording speeds. There was a marked decrease in peak height at the higher t_d values, together with an increase in peak width. The background current also decreased slightly (Table 3), but not enough to offset the advantage of increased sensitivity at the t_d value of 0.1 s.

The increased sensitivity and faster response at the short delay times can be attributed to the greater number of current samplings while the injected

TABLE 2

Characteristic parameters for d.p. amperometric operation with 0.1-s pulse repetition time in the flow-injection system

Characteristics	Analyte	
	Cd	Zn
E_{op}(V)[a]	−0.77	−1.27
Baseline noise (nA)	4.8	10.0
Background current of the oxygenated buffer (μA)	3.7	5.1
Background current of the deoxygenated buffer (μA)	2.8	3.1
Linear range (μg)	3×10^{-3}—4.5	1×10^{-2}—3.3
Detection limit (ng)	0.07	0.19

[a] In 1 M ammonium chloride buffer pH 10.

TABLE 3

Signal-to-background ratio with varying pulse repetition times (t_d) at an operating potential of −0.77 V

t_d (s)	i_p[a] (μA)	i_b[b] (μA)	i_p/i_b
0.1	77.0	2.8	27.5
0.2	44.5	1.7	26.2
0.5	25.5	1.6	15.9
1.0	16.0	1.6	10.0

[a] For injection of 4.5 μg of cadmium in 1 M ammonium chloride buffer. [b] Background at E_p.

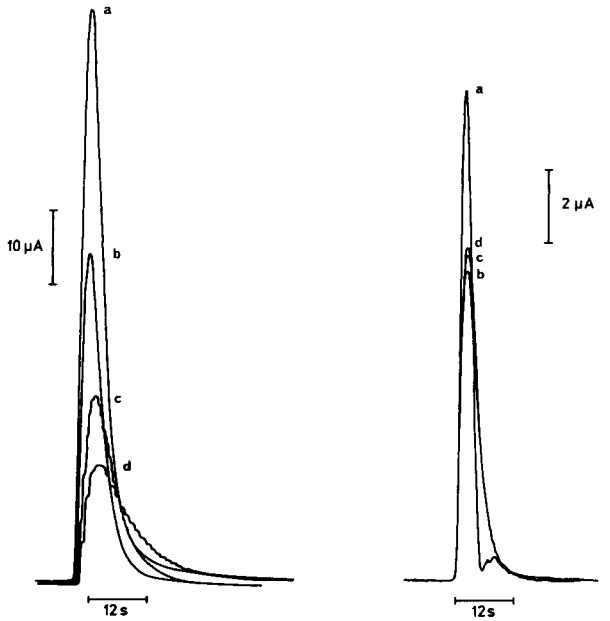

Fig. 5. Flow-injection peaks for injection of 4.5 μg of cadmium with d.p. amperometric detection at −0.77 V and the following pulse repetition times: (a) 0.1; (b) 0.2; (c) 0.5; (d) 1.0 s.

Fig. 6. Interference of cadmium on the flow-injection peak for zinc (1.3 μg) recorded with E_{op} = −1.27 V, t_d = 0.1 s with the following Zn:Cd ratios: (a) 1:100; (b) 1:10; (c) 1:1; (d) 1:0.

samples pass through the electrode flow cell. Furthermore, for differential pulse operation at the DME, the drop time is usually synchronized with the pulse time, giving a smaller surface area at short delay times. With a solid electrode, in contrast, the electrode area remains constant as the pulse time is changed, and a distinct advantage in sensitivity is therefore obtained for flow-injection analysis with d.p. operation.

Interference effects

The improved selectivity of d.p. amperometric operation at both the DME and solid electrodes has often been discussed [1−4, 9, 10]. In this work, it was also found that the selectivity for flow-injection determination of a single metal ion was significantly improved by use of d.p.v. rather than d.c. amperometric operation; interferences became apparent only when a large excess of the interfering metal ion was present.

As an example, the interference effects observed for cadmium and zinc peaks measured by f.i.a. with d.p. amperometric detection are shown in Table 4 and Fig. 6. At −0.77 V, there was little effect of excess of zinc on the cadmium peak height, with 10% reduction observed for a Cd:Zn molar

TABLE 4

Interference effects on 1×10^{-3} M analyte

Analyte:interference	i (μA)	
	Cd:Zn[a]	Zn:Cd[b]
1:0	5.9	9.0
1:1	5.5	8.8
1:10	5.5	8.4
1:100	5.3	13.2 (0.6)[c]
E_{op}(V)	−0.77	−1.27

[a] 3-μl injection volume. [b] 20-μl injection volume. [c] Split peak.

ratio of 1:100. Although zinc is not reduced at −0.77 V, the large concentration of zinc solution injected (0.1 M) affected the d.p. peak current, presumably because of a change in total electrolyte concentration in the injected zone in comparison to solutions of cadmium alone. A similar effect of supporting electrolyte concentration on d.p. peak currents has been reported by Parry et al. [25].

In the reverse situation, a large excess of cadmium over zinc would be expected to interfere seriously with the d.c. amperometric detection of zinc by f.i.a. at −1.27 V. The use of d.p. amperometry allowed determination of zinc with little interference up to a Cd:Zn ratio of 10:1, as shown in Fig. 6 and Table 4. This ratio would have caused at least a 10-fold increase in the zinc peak from f.i.a. with d.c. amperometric operation. At the 100:1 Cd:Zn ratio, however, the cadmium interference on the zinc peak became serious, causing about 50% positive error.

Interestingly, Fig. 6 shows the electrode response curve split into two peaks for 100:1 ratio of the Cd/Zn mixture recorded with d.p. amperometric operation at −1.27 V. The initial high peak (zinc) showed much faster response than for pure zinc solutions, but was followed by small peaks arising from the d.c. component of the pulse current for reduction of the large amount of cadmium.

It is clear therefore that for d.p. amperometric operation at the Cu/Hg electrode, matrix interference problems must be evaluated before complex samples can be analyzed accurately. Matrix matching and standard addition techniques would be necessary.

Conclusions

The sensitivity and selectivity of d.p. amperometric operation with short delay times between pulses were evaluated in this study of f.i.a. with a copper-amalgam electrode. By use of short t_d times, d.p. sensitivity at a solid electrode was improved by a factor of about 10 compared with d.c. operation [20], but with selectivity limited by overlapping peaks or co-

deposited metals. The analytical applications of this technique were shown to be suited to single, selective reductive determinations by f.i.a., or multiple element determinations by d.p. rapid scanning. Alternatively, d.p. operation may be useful as a detection method after h.p.l.c. separation when reduction peaks overlap.

Although the d.c. response times were about half the d.p. times [20], the use of short t_d values was shown to improve both the sensitivity and response times for f.i.a. compared to conventional d.p. timing parameters. In addition, scan rates were improved by a factor of at least 10 for voltage scan operation. The pulse waveform conforms fairly closely to the square-wave technique [27, 28], but with use of a commercial polarographic analyzer after simple modification.

REFERENCES

1 D. G. Swartzfager, Anal. Chem., 48 (1976) 2189.
2 W. A. MacCrehan and R. A. Durst, Anal. Chem., 50 (1978) 2108.
3 W. A. MacCrehan, Anal. Chem., 53 (1981) 74.
4 P. T. Kissinger, Anal. Chem., 49 (1977) 447A.
5 A. Ivaska and W. F. Smyth, Anal. Chim. Acta, 114 (1980) 283.
6 A. MacDonald and P. D. Duke, J. Chromatogr., 83 (1973) 331.
7 P. Maitoza and D. C. Johnson, Anal. Chim. Acta, 118 (1980) 233.
8 P. W. Alexander and S. H. Qureshi, J. Electroanal. Chem., 71 (1976) 235.
9 P. W. Alexander and M. H. Shah, Talanta, 26 (1979) 97.
10 P. W. Alexander and H. Marpaung, Talanta, 29 (1982) 213.
11 S. C. Rifkin and D. H. Evans, Anal. Chem., 48 (1976) 2174.
12 D. R. Canterford and R. W. Brown, J. Electroanal. Chem., 119 (1981) 355.
13 R. F. Lane and A. T. Hubbard, Anal. Chem., 48 (1976) 1287.
14 K. F. Drake and R. P. van Duyne, J. Electroanal. Chem., 89 (1978) 231.
15 H. E. Keller and R. A. Osteryoung, Anal. Chem., 43 (1971) 342.
16 H. Blutstein and A. M. Bond, Anal. Chem., 48 (1976) 248.
17 A. M. Bond and B. S. Grabaric, Anal. Chem., 51 (1979) 126.
18 V. Gajda and K. Horak, Anal. Chim. Acta, 134 (1982) 219.
19 L. A. Ashley and S. L. Levine, Talanta, 30 (1983) 515.
20 P. W. Alexander and U. Akapongkul, Anal. Chim. Acta, 148 (1983) 103.
21 G. D. Christian, J. Electroanal. Chem., 22 (1969) 333.
22 T. P. DeAngelis, R. E. Bond, E. E. Brooks and W. R. Heineman, Anal. Chem., 49 (1977) 1792.
23 A. M. Bond and B. S. Grabaric, Anal. Chim. Acta, 88 (1977) 227.
24 J. H. Christie, J. Osteryoung and R. A. Osteryoung, Anal. Chem., 45 (1973) 210.
25 E. P. Parry and R. A. Osteryoung, Anal. Chem., 37 (1965) 1634.
26 S. K. Vohra and G. W. Harrington, J. Chromatogr. Sci., 18 (1980) 379.
27 G. C. Barker and I. L. Jenkins, Analyst (London), 77 (1952) 685.
28 G. C. Barker, in G. Charlot (Ed.), Modern Electroanalytical Methods, Elsevier, Amsterdam, 1958, 118.

Analytica Chimica Acta, 166 (1984) 129—140
Elsevier Science Publishers B.V., Amsterdam — Printed in The Netherlands

POLAROGRAPHY OF DISODIUM PENTACYANONITROSYLFERRATE(II)

Part 2. Determination at Therapeutic Levels in Serum, Plasma, and Whole Blood

O. R. LEEUWENKAMP,* E. J. VAN DER MARK, H. JOUSMA, W. P. VAN BENNEKOM and A. BULT

Department of Pharmaceutical Analysis and Analytical Chemistry, Subfaculty of Pharmacy, State University Leiden, Gorlaeus Laboratories, P.O. Box 9502, 2300 RA Leiden (The Netherlands)

(Received 15th March 1984)

SUMMARY

Disodium pentacyanonitrosylferrate(II) (sodium nitroprusside) is determined at therapeutic (ng ml^{-1}) levels in plasma, serum and blood with conventional and high-performance differential pulse polarography (d.p.p. and h.p.d.p.p.) at a dropping mercury electrode or a static mercury drop electrode. Serum or plasma (3 ml) is treated with perchloric acid containing 1 mg ml^{-1} potassium hexacyanoferrate(II), centrifuged for 10 min and subjected to polarography. For spiked serum, calibration graphs are linear over the range 30—1000 ng ml^{-1} sodium nitroprusside, regardless of the polarographic technique; the estimated detection limit is 15 ng ml^{-1} (5×10^{-8} M). Calculated therapeutic levels range from 100 to 1000 ng ml^{-1}. Similar results were obtained for spiked plasma. A similar procedure is suitable for whole blood and was used to study the in-vitro degradation of sodium nitroprusside (200 ng ml^{-1}) on incubation at 37°C. The in-vitro loss is rapid ($t_{1/2} \approx 6$ min) but meaningful in-vivo levels can be obtained when the blood is collected in a 0.9% sodium chloride solution at 0°C. Thiocyanate, the main metabolite of nitroprusside, and thiosulphate, which is a potential antidote for cyanide, do not interfere.

Sodium nitroprusside ($Na_2[Fe(CN)_5NO] \cdot 2H_2O$) is currently administered by infusion to reduce blood pressure in case of hypertensive emergencies, to induce controlled hypotension in anaesthesia and to improve heart function after an infarction [1]. Two important disadvantages of its clinical usage are the in-vivo release of toxic cyanide [1] and the wide variability in infusion rates required to attain therapeutic effect [2—4]. In view of these disadvantages, observation of blood-pressure lowering with concomitant monitoring of nitroprusside levels is desirable. For routine measurements of therapeutic nitroprusside concentrations in biological materials, a selective, sensitive and rapid method is required.

Quantitation of nitroprusside in various biological media has been described [5, 6]. Rodkey and Collison [5] developed an indirect spectrophotometric method, which is applicable to serum, plasma and whole blood. The method

0003-2670/84/$03.00

is, however, time-consuming and nitroprusside can be measured only when it is infused at substantially higher than therapeutic rates [7]. Alkayer et al. [6] described a phase-sensitive sine-wave polarographic determination of nitroprusside in serum; the detection limit was 2 μg ml^{-1}.

Because therapeutic concentrations of the drug in body fluids are rarely, if ever, determined, the steady-state levels, C_{SS}, are calculated for infusion rates of 80—800 μg min^{-1} from the equation [4],

$$C_{SS} = 1.43(D/T)(V_d/t_{1/2})$$

where D/T is the infusion rate (80—800 μg min^{-1}), D and T being the total infused dose and duration of the infusion, respectively; V_d is the distribution volume, and $t_{1/2}$ is the biological half-life of sodium nitroprusside (ca. 2 min) [8, 9]. For V_d, a value of 5 l was assumed in case of blood and a value of 2.5 l for plasma and serum, taking a hematocrit value of approximately 50% into account. The value of 2.5 l is justified by the finding of Rodkey and Collison [5], that over 90% of sodium nitroprusside is exclusively present in the plasma. Based on the calculation, plasma and serum levels will lie in the range 100—1000 ng ml^{-1}, whereas the whole blood concentrations will cover the range 50—500 ng ml^{-1}. Thus it can be concluded that the sensitivity of the earlier polarographic method [6] is also insufficient for determination of therapeutic nitroprusside levels.

Improvement of the detection limit was expected from conventional and high-performance differential pulse polarography (d.p.p. and h.p.d.p.p.) [10, 11]. The previous study of the pulse-polarographic behaviour of nitroprusside showed that maximum sensitivity for d.p.p. as well as for h.p.d.p.p. is obtained in 1 M perchloric acid [12]. The detection limit reported for both polarographic techniques at the DME and the static mercury drop electrode (SMDE) was 2 ng ml^{-1}, inferring that therapeutic levels in body fluids might be determined after treatment of the biological material with perchloric acid followed by centrifugation of the precipitated proteins.

In the present paper, a rapid and simple procedure is presented utilizing d.p.p. or h.p.d.p.p. for measurement of nitroprusside at therapeutic levels in plasma, serum and blood. It is also shown that the method is powerful for studies of the in-vitro degradation of sodium nitroprusside (200 ng ml^{-1}) on incubation in whole blood at 37°C. In-vivo studies are also possible. The primary aim of this study was the development of a rapid and reliable method for quantifying nitroprusside at in-vivo levels.

EXPERIMENTAL

Polarographic apparatus and procedure

A PAR 174A polarographic analyzer (EG. & G. Princeton Applied Research Corp., Princeton, NJ), modified for h.p.d.p.p. (schematic diagrams are available on request), was used with a matched drop timer (PAR 174/70) and x—y recorder (Omnigraphic model 2200-4-3).

For measurements, an aluminium foil-wrapped, wall-jacketed vessel (EA-876-5, 5 ml, Metrohm) was thermostatted at 25°C. A three-electrode configuration was used, consisting of a dropping mercury electrode (DME), a saturated sodium chloride calomel reference electrode (SCE) (EA-402, Metrohm) and a Pt-wire auxiliary electrode (EA 202, Metrohm). During the measurements, the height of the mercury column was kept constant at 700 mm. At open circuit the flow rate was 3.28 mg s^{-1} with a corresponding drop time of 2.35 s (1 M perchloric acid). During the experiments on blood, the mercury flow rate slowly decreased to a value of 2.82 mg s^{-1}. For the studies of in-vitro degradation in blood, a new capillary was used; it had a flow rate of 4.49 mg s^{-1} and corresponding drop time of 1.97 s.

Measurements were also done with a static mercury drop electrode (PAR 303) in the large drop-size mode (drop weight 5.17 mg) with a cycle time of 1.0 s. For these measurements, the vessel (10 ml) was not thermostatted but was wrapped in aluminium foil. A saturated sodium chloride reference Ag/AgCl electrode was used in combination with a Pt wire as auxiliary electrode.

Prior to polarography, solutions were purged for 10 min with oxygen-free and water-saturated nitrogen that was passed over the solution while the potential was scanned.

The potential was scanned from 0 to −1500 mV vs. SCE at a rate of −2 mV s^{-1}. For d.p.p., the delay time δ was 5 ms; for h.p.d.p.p., delay times δ_1 = 5 ms and δ_2 = 70 ms were used. The modulation amplitude ΔE was −100 mV, sampling windows were 20 ms and the memory time constant was 9.1 ms. These conditions were used unless stated otherwise. For measurements of nitroprusside in supernatant fluid obtained from biological materials (see below), the output current offset was used.

Reagents and materials

Sodium nitroprusside (Merck) and all the other chemicals were of analytical grade and were used as received. Water obtained from a Millipore Milli-Q water purification system was used for the preparation of all solutions. Aqueous stock solutions of sodium nitroprusside were prepared for spiking and standard additions; the containers were wrapped in aluminium foil to prevent light-induced degradation [13].

Serum and plasma were obtained from blood of apparently healthy volunteers and divided into portions of ca. 50 ml, which were stored at −20°C. Each day a new portion was used. Blood from a normal subject was collected in heparinized tubes (ca. 20 ml) and also stored at −20°C.

Procedures for plasma, serum and whole blood samples

Plasma and serum. Frozen plasma and serum was slowly thawed immediately before use. For spiking, 50 μl of an appropriate aqueous stock solution of sodium nitroprusside was added to 3.0 ml of plasma or serum. Subsequently, 12.0 ml of 1.25 M perchloric acid containing 1 mg ml^{-1} potassium

hexacyanoferrate(II) was slowly added, while shaken by hand, to 3.0 ml of spiked plasma or serum, and after centrifugation for 10 min (5000 rpm) the polarographic measurements were done in the clear colourless supernatant solution (procedure B). Initially, another procedure (A) was used, but this proved to be less suitable (see below); in procedure A, 12.0 ml of 1.25 M perchloric acid without potassium hexacyanoferrate(II) was added to spiked serum or plasma.

Whole blood. Blood was thawed and spiked as outlined above for plasma and serum. To 3.0 ml of spiked blood, 12.0 ml of 1.25 M perchloric acid containing a larger amount of potassium hexacyanoferrate(II) (4 mg ml^{-1}) was added with swirling. A dark brown material precipitated. After centrifugation (10 min, 5000 rpm), the resulting yellowish but clear supernatant liquid was used for polarography.

In-vitro degradation in blood

Blood obtained shortly before use from a normal subject was collected in a heparin-containing (200 μl of Heparin-Novo) 250-ml silanized bottle and then divided into 3.0 ml portions, which were immediately frozen (−20°C) until use. None of the portions used showed visible signs of hemolysis [14]. The blood samples were thawed slowly at room temperature and after a pre-incubation period (10 min) in a water bath at 37°C with exclusion of light, the samples were spiked with 50 μl of an aqueous nitroprusside solution to give an initial concentration of about 200 ng ml^{-1}. At selected times, the incubated tubes were promptly transferred to an ice bath and the method outlined above for whole blood was applied. For polarography, 10.0 ml of the supernatant liquid was pipetted into the vessel. After the initial scan(s), 25 μl of the spiking solution was added (equivalent to 150 ng ml^{-1} in blood) in order to calculate the nitroprusside concentration retained in the blood after incubation.

In an analogous way, the in-vitro stability of sodium nitroprusside in whole blood incubated at 21°C and 8°C, respectively, was examined, as well as the effect of direct addition of 5.0 ml of iso-osmotic sodium chloride solution (0°C) to very recently spiked blood at 37°C, followed by storage at 8°C. The samples diluted with normal saline were treated with 7.0 ml of 2.1 M perchloric acid containing 6.4 mg ml^{-1} potassium hexacyanoferrate(II).

RESULTS AND DISCUSSION

Serum and plasma

Maximum sensitivity was previously obtained in 1 M perchloric acid [12], thus it was thought that procedure A (see Experimental) would be appropriate. Before measurements on spiked serum, the validity of this procedure was tested by adding 50 μl of an aqueous nitroprusside solution to 10.0 ml of the obtained supernatant solution, to give a concentration of 25 ng ml^{-1}. This procedure involves five-fold dilution, thus a concentration of 24 ng ml^{-1}

corresponds to 120 ng ml^{-1} sodium nitroprusside in spiked serum. It was observed that the d.p.p. and h.p.d.p.p. peak currents were substantially lower than in 1 M perchloric acid and further the peaks were considerably distorted (Fig. 1). Purging of the supernatant liquid with nitrogen prior to polarography led to foaming, indicating that adsorbable constituents were present in the obtained blank supernatant. Moreover, the mercury drops did not coalesce at the bottom of the polarographic vessel, again suggesting the presence of substances adsorbed at the mercury/water interface. In an attempt to remove adsorbable species, 100 mg of active charcoal was added to serum simultaneously with the perchloric acid; there was then less foaming and less coalescence of the mercury drops, but no significant improvement in peak shape was observed, and it was concluded that some other phenomenon played a role.

According to the literature, the nitroprusside anion and some transition and post-transition metal ions form poorly soluble coordination polymers which are analogs of Prussian Blue [15]. Non-linear adsorption of these slightly (water) soluble polymers at the mercury surface might account for the distorted (doubly peaked) polarograms as described by Flanagan et al. [16]. Quantitatively, Cu(II), Fe(II) and Zn(II) [17] are the most important metal ions in plasma and serum that might form such polymers. During treatment of the biological materials with perchloric acid, these metal ions are released from metalloproteins and, considering the free concentrations in plasma and serum, concentrations of about 4×10^{-6} M, 5×10^{-6} M and 3×10^{-6} M were calculated for the supernatant liquid. The supposed effect of Cu(II) was verified by adding progressively 5×10^{-7} up to 2×10^{-6} M to a

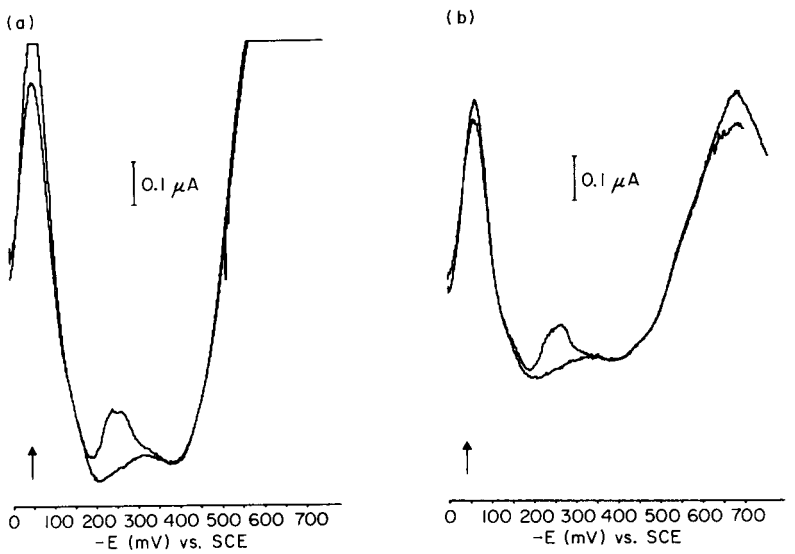

Fig. 1. Polarograms of sodium nitroprusside (24 ng ml^{-1}) added to blank supernatant liquid obtained by procedure A: (a) d.p.p., with 080 offset; (b) h.p.d.p.p. without offset.

solution of nitroprusside (5×10^{-7} M) in 1 M perchloric acid; further additions of Cu(II) caused no more changes. In Fig. 2 the effects of the added Cu(II) on peak current and peak shape are depicted. The possible effects of Fe(II) and Zn(II) were investigated similarly, but these metal ions did not affect the peak current and peak shape even in large excess. Obviously, Cu(II) is at least in part responsible for the decrease and distortion of the d.p.p. and h.p.d.p.p. peaks.

Because Fe(II) and Zn(II) did not affect the d.p.p. and h.p.d.p.p. peak currents, it is very unlikely that the effect of Cu(II) can be ascribed to formation of poorly soluble and adsorbable polymers. Consequently, the Cu(II)/nitroprusside system was studied in more detail. To 10^{-4} M nitroprusside in 0.04 M acetate buffer pH 5.0 was added stepwise Cu(II) (1×10^{-5}–1.3×10^{-4} M) and polarograms (s.d.c.p., n.p.p., d.p.p. and h.p.d.p.p.) were recorded. The acetate buffer pH 5.0 was chosen in order to examine the influence of Cu(II) on the first two reduction waves of nitroprusside which are separated at this pH value in contrast to pH 0 [12], and because it has low complexing properties for Cu(II). On progressive addition of Cu(II) to 10^{-4} M nitroprusside, the first reduction wave of nitroprusside decreased gradually and vanished when a stoichiometric amount of copper was present. Besides, a large adsorption maximum appeared on the second wave, especially in the n.p.p. mode. Thus it was concluded that nitroprusside (NP) is chemically reduced in a one-electron step, probably by Cu(Hg), with the formation of species which strongly adsorb onto the mercury electrode

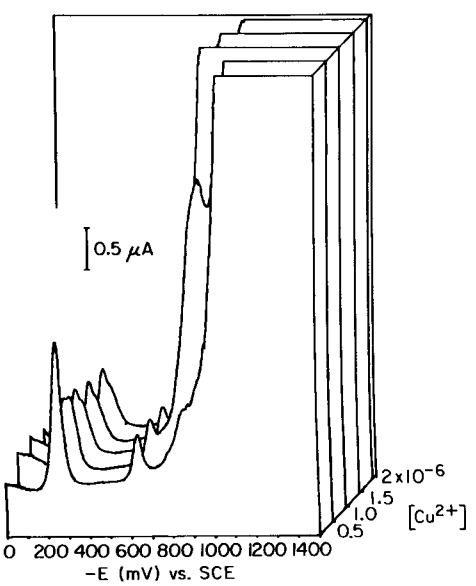

Fig. 2. Effect of Cu^{2+} (5×10^{-7}–2×10^{-6} M) on the nitroprusside peak (5×10^{-7} M) in 1 M perchloric acid (scan rate —5 mV s^{-1}).

$$Cu(Hg) + NP^{2-}_{ox} \rightarrow [Cu(I)]_3NP^{3-}_{red}$$
amalgam

The process is favoured by the strong adsorption of the resulting Cu(I) species.

Because the formation of Cu(Hg) proceeds via Cu(II), the above process might be suppressed by an anion which is strongly associated in solution with Cu(II). The solubility of copper(II) hexacyanoferrate(II) is low in water ($\log S = -15.89$) [18]. Thus, procedure A was modified by adding perchloric acid containing a relatively large amount of potassium hexacyanoferrate(II) (1 mg ml^{-1}) to serum or plasma. When this procedure (B) was applied, regular d.p.p. and h.p.d.p.p. peaks were observed after addition of 50 μl of aqueous nitroprusside solution to the supernatant liquid (24 ng ml^{-1}). Moreover, the large peak current just anodic to the nitroprusside peak (arrowed in Fig. 1) almost completely vanished. This modified procedure was used to prepare calibration graphs for spiked serum (20—1000 ng ml^{-1}) covering the calculated therapeutic concentration range (50—1000 ng ml^{-1}) for sodium nitroprusside. Typical d.p.p. and h.p.d.p.p. recordings are shown in Fig. 3 for spiked serum. The calibration graphs for d.p.p. and h.p.d.p.p. at both the DME and SMDE are linear (Table 1), while the estimated detection limit is 15 ng ml^{-1} sodium nitroprusside (5×10^{-8} M). Compared to 1 M perchloric acid medium, the slopes of the calibration graphs are 25% lower; this might be explained as incomplete recovery from the biological material and/or suppression of the peak current in the medium used. From a comparison of peak currents for spiked serum (120 ng ml^{-1}) sodium nitroprusside added to blank supernatant liquid (24 ng ml^{-1}) a recovery of 85% ($n = 4$, $s = 3.0\%$) was calculated. This recovery cannot fully explain the slopes which are 25% lower than in 1 M

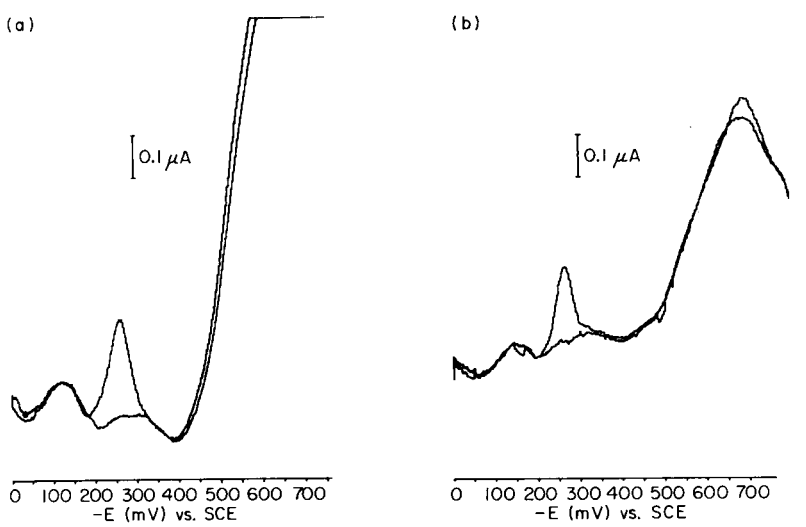

Fig. 3. Recordings for serum spiked with 120 ng ml^{-1} sodium nitroprusside and treated as in procedure B: (a) d.p.p.; (b) h.p.d.p.p.

TABLE 1

Calibration graphs for sodium nitroprusside in spiked serum in the concentration range 30—1000 ng ml^{-1} of serum (n = 7)

	DME		SMDE	
	D.p.p.	H.p.d.p.p.	D.p.p.	H.p.d.p.p.
Slope (nA ml ng^{-1})	1.67(0.033)[a]	1.26(0.014)	1.98(0.021)	1.68(0.017)
Intercept (nA)	16.97(10.65)[a]	8.75(4.48)	1.79(5.73)	6.78(4.77)
Correlation coefficient	0.9990	0.9997	0.9998	0.9998
Slope (in 1 M $HClO_4$) [12]	11.16	8.06	13.45	11.31
Corrected[b] slope (serum)	8.35	6.30	9.9	8.40
Slope ratio (%)[c]	74.8	78.2	73.6	74.3

[a]Standard deviations are given in parentheses. [b]Taking into account the five-fold dilution in procedure B. [c]Corrected slope for serum divided by the slope in 1 M perchloric acid.

perchloric acid. The deficit of 10% is most probably related to peak-current suppression by the medium (e.g., a lower diffusion coefficient caused by higher viscosity and/or the presence of adsorbable constituents). The linear calibration graphs show that the recovery is constant (85%) over the entire concentration range studied. The reproducibility of the method was examined for 120 ng ml^{-1} sodium nitroprusside; the relative standard deviation (n = 4) was always within 6% (DME with d.p.p. and h.p.d.p.p.; SMDE with d.p.p. and h.p.d.p.p.).

The advantage of the less steep polarographic background for h.p.d.p.p. is cancelled out by lower peak currents, while the advantage of higher peak currents with the SMDE is largely annulled by the steeper background.

For spiked plasma processed in an analogous way, comparable results were obtained.

Whole blood

Rodkey and Collison [5] determined nitroprusside in plasma obtained from blood after centrifugation at 4°C. In principle, nitroprusside in blood could be quantified after treatment of the resulting plasma or serum as in the above procedure B. However, because of the possible rapid decomposition of nitroprusside in blood [1], a rapid simple method is preferable. Therefore, direct application of procedure B to whole blood was examined. Addition of the perchloric acid solution caused the blood cells immediately to disintegrate. Serum proteins, high-molecular-weight constituents and fragments of the blood corpuscles were easily removed by centrifugation.

When procedure B was applied to blood spiked with 120 ng ml^{-1} sodium nitroprusside, a small h.p.d.p.p. peak on a steep polarographic background was observed, whereas no d.p.p. peak was discernible. Attempts to improve the polarographic background and to raise the peak height by increasing the amount of potassium hexacyanoferrate(II) in the perchloric acid solution were

successful. A representative h.p.d.p.p. recording for blood spiked with 150 ng ml^{-1} sodium nitroprusside and treated with a perchloric acid solution containing 4 mg ml^{-1} potassium hexacyanoferrate(II) is shown in Fig. 4.

For the evaluation of nitroprusside levels in blood samples from patients, standard addition is the method of choice provided that the recovery is (nearly) quantitative and calibration graphs are linear. These requirements were shown to be fulfilled. The standard addition method was used to examine reproducibility and precision for 120 ng ml^{-1} sodium nitroprusside. This concentration is equivalent to the value expected for blood when sodium nitroprusside is infused at the average adult infusion rate of 200 $\mu g\ min^{-1}$ [4]. For four determinations (n = 4), the relative standard deviation was 4.4%, while the average calculated concentration was 123 ng ml^{-1}, deviating about 2.5% from the theoretical value.

Surprisingly, the recovery appeared to be quantitative in contrast to plasma and serum; probably the nature of the material removed by centrifugation plays a role. The peak currents were, however, lower than for serum spiked with an identical concentration. This discrepancy was explained by the observed decrease of the mercury flow rate and thus drop area with respect to serum and plasma (see Experimental).

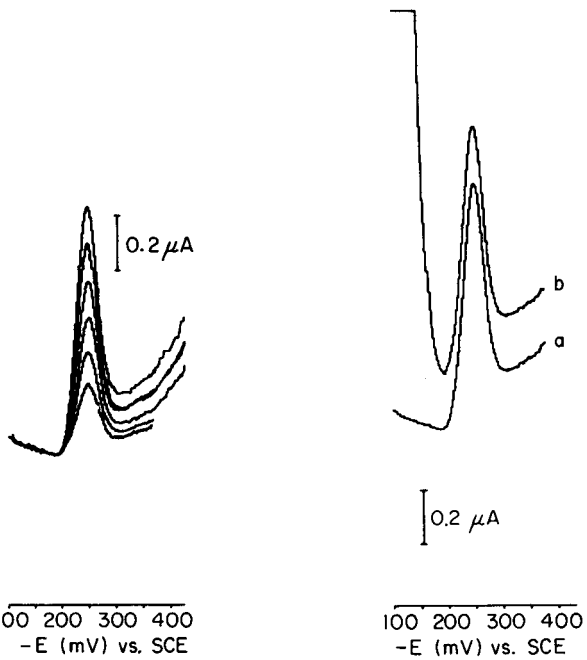

Fig. 4. The smallest peak current is for blood spiked with 150 ng ml^{-1} sodium nitroprusside. The other peak currents correspond to additions of 50 μl of an aqueous nitroprusside solution to 10.0 ml of supernatant liquid: +18.4, 36.6, 54.7, 72.6 and 90.3 ng ml^{-1} of supernatant, respectively.

Fig. 5. H.p.d.p.p. recordings for supernatant fluid containing 5.6×10^{-7} M nitroprusside: (a) $+5.6 \times 10^{-6}$ M thiocyanate; (b) $+5.0 \times 10^{-4}$ M thiosulphate.

Subsequently, the applicability of the method to blood samples from patients was investigated. These samples will also contain thiocyanate, the main metabolite of nitroprusside, and cyanide [19]. The latter metabolite was removed as hydrogen cyanide at the low pH used during purging with nitrogen. Consequently, only the effect of thiocyanate on the h.p.d.p.p. peak current was checked. Furthermore, the effect of thiosulphate, a possible antidote for cyanide intoxication [19], was also studied. Neither thiocyanate nor thiosulphate had any effect in concentrations of 5.6×10^{-6} M and 5×10^{-4} M, respectively (Fig. 5). These concentrations are reasonable for supernatant liquids according to calculations based on literature data [19]. With thiosulphate, there is a large peak just anodic of the nitroprusside peak; this can be attributed [20] to the reaction $Hg + S_2O_3^{2-} \rightarrow HgS_2O_3$ ($E_{1/2}$ = —0.18 V vs. SCE).

In-vitro degradation

The rate of in-vitro degradation is obviously of extreme importance in connection with the determination of in-vivo nitroprusside levels. Recently, Kreye and Reske [7] determined the in-vitro half-life ($t_{1/2}$) for sodium nitroprusside (20 μg ml^{-1}) on incubation in whole rat blood at 37°C, reporting a value of about 43 min. Because a concentration-dependent loss cannot be excluded, the rate of disappearance on incubation in human blood at 37°C was evaluated here at the relevant (i.e., therapeutic) level of 200 ng ml^{-1}. Figure 6 shows typical polarograms for incubation times of zero and 5 min. From the concentration/time course, an in-vitro half-life of approximately 6 min was found by interpolation (Fig. 7). For nitroglycerin, which probably degrades by interaction with thiol groups as is the case with sodium nitroprusside, $t_{1/2} \approx 6$ min has recently been reported [21]. The observed

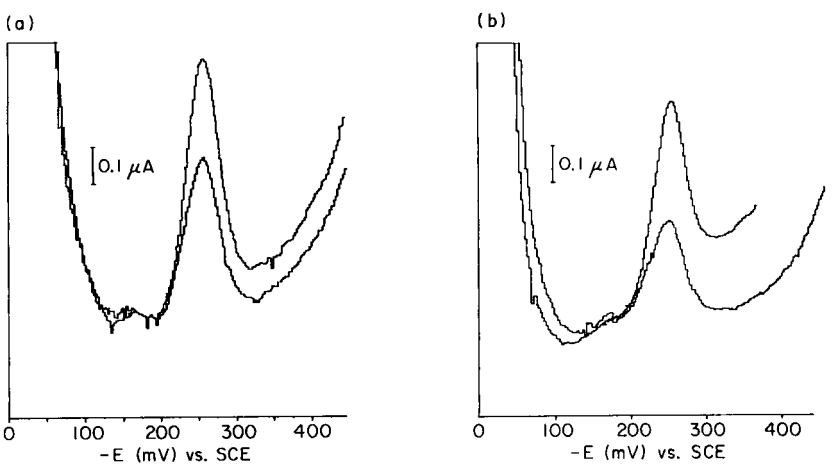

Fig. 6. Representative h.p.d.p.p. traces for incubated human blood (200 ng ml^{-1}) at 37°C: (a) t = 0 min; (b) t = 5 min. The upper polarograms correspond to standard additions equivalent to 150 ng ml^{-1} in blood.

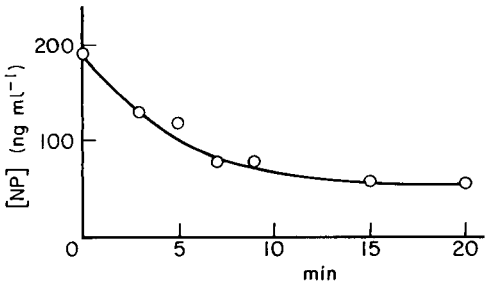

Fig. 7. Concentration/time relation for nitroprusside (200 ng ml^{-1}) on incubation in whole blood (37°C).

rapid in-vitro decomposition largely explains the in-vivo half-life of ca. 2 min [8, 9].

Because of the rapid loss of nitroprusside in blood at 37°C, immediate treatment of blood samples taken from patients is essential. At $t = 0$ min, a concentration of 193 ng ml^{-1} was calculated, compared to the theoretical value of 197 ng ml^{-1}, demonstrating only slight in-vitro loss upon rapid treatment. However, rapid treatment of blood samples with the hexacyanoferrate(II)-containing perchloric acid solution is not convenient. Therefore, the temperature dependence of the degradation was investigated. On incubation for 15 min at 21°C, 34% degradation was found, whereas storage at 8°C gave essentially no decomposition. When a cold iso-osmotic sodium chloride solution (5.0 ml, 0°C) was added to 3.0 ml of spiked blood at 37°C with cooling in an ice bath, no decrease in the nitroprusside concentration was observed even after subsequent storage at 4°C. This procedure is an elegant means of avoiding in-vitro loss and meaningful in-vivo concentrations are thus obtainable. Finally, it must be noted that in serum the decomposition of sodium nitroprusside proceeds very slowly compared to blood; after 1 h (37°C), ca. 70% was left. Obviously, erythrocytes play an important role in the degradation process, as already suggested in the literature.

Further work on the determination of in-vivo levels, and therapeutic and pharmacological aspects will be repeated elsewhere.

REFERENCES

1 J. H. Tinker and J. D. Michenfelder, Anaesthesia, 45 (1976) 340.
2 F. Conso, A. Marsac and I. Petit, Bull. Med. Leg. Toxicol., 21 (1978) 215.
3 H. Kruszyna, R. Kruszyna and R. P. Smith, Anaesthesia, 57 (1982) 303.
4 A. Goodman Gilman, L. S. Goodman and A. Gilman, The Pharmacological Basis of Therapeutics, 6th edn., MacMillan, New York, 1980, pp. 24, 806.
5 F. L. Rodkey and H. A. Collison, Clin. Chem., 23 (1977) 1969.
6 M. Alkayer, J. J. Vallon and Y. Pegon, Anal. Lett., 14 (B6) (1981) 399.
7 V. A. W. Kreye and S. N. Reske, Naunyn-Schmiedeberg's Arch. Pharmacol., 320 (1982) 260.
8 R. F. Palmer and K. C. Lasseter, N. Engl. J. Med., 292 (1975) 294.

9 V. A. W. Kreye, E. Marquard, Naunyn-Schmiedeberg's Arch. Pharmacol., 306 (1979) 203.
10 W. P. van Bennekom and J. B. Schute, Anal. Chim. Acta, 89 (1977) 71.
11 W. P. van Bennekom, Anal. Chim. Acta, 101 (1978) 283.
12 O. R. Leeuwenkamp, H. Jousma, E. J. van der Mark, W. P. van Bennekom and A. Bult, Anal. Chim. Acta, 156 (1984) 51 (Part 1).
13 M. J. Frank, J. B. Johuson and S. H. Rubin, J. Pharm. Sci., 65 (1976) 44.
14 Martindale, The Extra Pharmacopeia, 28th Edn., The Pharmaceutical Press, London, 1982, p. 322.
15 L. A. Gentil, E. J. Boron and P. J. Aymonino, Inorg. Chim. Acta, 20 (1976).
16 J. B. Flanagan, K. Takahashi and F. C. Anson, J. Electroanal. Chem., 81 (1977) 261.
17 K. Diem and C. Lentner, Wissenschaftliche Tabellen Documenta Geigy, 7. Ausgabe, Georg Thieme Verlag, Stuttgart, 1975, p. 562.
18 L. G. Sillén and A. E. Martell, Stability Constants, The Chemical Society, London, 1971.
19 J. R. Krapez, C. J. Vesey, L. Adams and P. V. Cole, Br. J. Anaesth., 53 (1981).
20 J. Heyrovský and P. Zuman, Practical Polarography, Academic Press, London, 1968, p. 188.
21 T. D. Sokoloski, C. C. Wu, L. S. Wu and A. M. Burkman, J. Pharm. Sci., 72 (1983) 335.

Analytica Chimica Acta, 166 (1984) 141—151
Elsevier Science Publishers B.V., Amsterdam — Printed in The Netherlands

STRIPPING VOLTAMMETRIC DETERMINATION OF TRACES OF PEPTIDES AND PROTEINS CONTAINING DISULPHIDE LINKAGES

ULF FORSMAN

Astra Läkemedel AB, Pharmaceutical Research and Development, S-151 85 Södertälje (Sweden)

(Received 25th May 1984)

SUMMARY

Stripping voltammetry has been investigated for the determination of traces of ribonuclease, somatostatin, oxytocin, felypressin, insulin and oxidized glutathione at concentrations down to 1.5×10^{-9} M. Repeated cyclic potential scans with an initial cathodic scan were used after accumulation at + 0.1 to —0.3 V vs. Ag/AgCl at a hanging mercury drop electrode. In presence of excess of copper(II) ion, the first two compounds yield a well-defined peak couple at —0.5 to —0.6 V, with cathodic and anodic peaks of equal height, the accumulated product being adsorbed in both its oxidized and reduced state. Oxytocin and felypressin first yield two unresolved cathodic peaks, one of which disappears in the second scan cycle. Oxidized glutathione yields a large cathodic peak but a small anodic peak because of desorption in the reduced state. Excess of copper(II) is reduced during the accumulation, so that the electrode is actually copper amalgam. The peaks obtained with copper(II) present are considered to be due to redox reactions of copper complexes formed with the cysteine parts of the molecules. These peaks are suitable for quantitative purposes; calibration equations are given. Without copper(II), the substances show stripping responses of different complexity and magnitude. Insulin gives usable stripping peaks only without copper ions.

Analysis for traces of peptides and proteins is of major importance in biochemistry and pharmacology and the development of new analytical techniques in this area is important. The highly selective and sensitive techniques of immunoassay can be used for proteins where antigen/antibody reactions are available. For certain peptides, such as felypressin, oxytocin and related substances, bioassay procedures are applicable [1] but these methods are tedious and costly. Recently [2], it was shown that the stripping voltammetry is applicable for trace determinations of felypressin; this peptide was investigated in concentrations down to 5×10^{-9} M (5 ng ml^{-1}). The stripping activity of felypressin seems to be connected with the sulphur bridge of the molecule [2]. Stripping voltammetry could therefore offer a selective and sensitive complement to existing trace determinations of proteins and peptides containing disulphide bridges. The high speed and low cost of stripping voltammetry are obvious factors of interest for application of the technique.

0003-2670/84/$03.00

Analogues to the peptide vasopressin which contains one disulphide bridge, have previously been investigated by direct current (d.c.) polarography [3]. The peptides gave a diffusion-controlled reduction wave in the pH range 1—13; results from solutions of about 5×10^{-5}—5×10^{-4} M were reported. Oxytocin has been studied at a dropping mercury electrode [4]; the formation of mercury—cysteine bridges with redox properties was suggested and additional voltammetric signals of both faradaic and capacitive origin were discussed. The analytical utility of the peaks obtained was not mentioned.

In the study described here, some well-known disulphide-containing proteins and peptides were investigated by stripping voltammetry. The effect of copper(II) ions in the solution for analysis is discussed. It was previously shown [5, 6], that copper(II) ion influences the stripping voltammetric behaviour of thiols such as cysteine and penicillamine, and that stripping voltammetry based on accumulation of a copper complex of these thiols yields significantly lower detection limits than those possible when accumulation of the mercury complex is utilized. The present study shows that for the investigated proteins and peptides, except insulin, stripping voltammetry in presence of excess of copper(II) ions results in well-defined voltammetric patterns and detection limits of about 2×10^{-9} M.

EXPERIMENTAL

Equipment, samples and reagents

A PAR-174 polarographic analyzer was used. The working electrode was a Metrohm EA-290 hanging mercury drop electrode (HMDE); a drop with a surface area of 0.9 mm^2 was used throughout. A platinum auxiliary electrode and a silver/silver chloride (3 M KCl) reference electrode were also used. All potentials given refer to this Ag/AgCl electrode.

Ribonuclease-A (91% w/w), insulin (26.5 I.U. mg^{-1}) from bovine pancrease, and oxytocin (lyophilized, 50 I.U. mg^{-1}) were obtained from Sigma. Somatostatin acetathydrat (80% w/w) was a personal gift from Kabi AB, Sweden. Other samples were oxidized glutathione (puriss; Fluka) and felypressin in solution (25 I.U. ml^{-1}; Sandoz). All samples were used as received. Stock solutions of the samples were made in acetate buffer immediately before use.

The acetate buffer, pH 4.6, was composed of 0.05 M acetic acid and 0.05 M sodium acetate in water purified with a Millipore water purification system. Stock solutions of copper(II) nitrate were 1×10^{-2}—1×10^{-4} M. All reagents were of analytical grade.

Procedure

An aliquot of the solution to be investigated was added to 5 ml of deaerated pH 4.6 buffer solution. When the voltammetric behaviour in presence of Cu(II) ion was examined, an appropriate amount of Cu(II) stock solution was added to produce the desired concentration. Stripping analysis in presence of Cu(II) was done, with magnetic stirring, by accumulation at

—0.30 V for 1 min, unless otherwise stated. A repetitive cyclic scan of 200 mV s^{-1} with an initial cathodic scan direction was then applied. Scan reversal was done manually at the desired potentials. Stripping voltammetry in the "absence" of Cu(II) ion was mostly done by accumulation at +0.10 V in order to avoid copper amalgam formation arising from residual Cu(II) ions. (Absence of Cu(II) means that the Cu(II) level was $<2 \times 10^{-8}$ M, measured by anodic stripping voltammetry.)

Cyclic voltammetry without accumulation was done from —0.80 V at 200 mV s^{-1} with an initial anodic scan direction.

RESULTS

Ribonuclease

Cyclic voltammetry of this enzyme at a bulk concentration of 5×10^{-5} M in absence of Cu(II) ions is shown in Fig. 1(a). The anodic and the cathodic peaks are well defined and of equal height; the peak potentials are —0.43 V and —0.47 V, respectively. To test the stripping activity, ribonuclease (5×10^{-8} M) was accumulated at +0.10 V for 1 min and stripped by cyclic voltammetry; the peaks (Fig. 1b) appeared at about the same potential as in Fig. 1(a). The anodic and cathodic peaks were of equal height, and were obtained on repeated cyclic scans, which shows that the accumulated product is adsorbed in both its oxidized and reduced states. The current response obtained after only 1-min accumulation, compared to the response of the 1000-fold stronger solution without accumulation (Fig. 1a) indicates strong adsorption of the electroactive product.

In the cyclic voltammogram (Fig. 1c) for ribonuclease after the addition of equimolar amounts of Cu(II), a second peak couple appeared about 150 mV more negative than the one discussed above. The stripping voltammogram obtained after addition of excess of Cu(II) ion (Fig. 1d) shows a well-defined peak couple at about —0.55 V, which is the same potential as the more negative peak couple in voltammogram (c). Copper(II) evidently results in the formation of an adsorbed species which is electroactive at more negative potentials than the product obtained in absence of copper(II). This behaviour is in line with the stripping pattern of cysteine and penicillamine previously investigated [5, 6]. It should be noted that during the accumulation time at —0.30 V, excess of Cu(II) ion is reduced, so that the stripping voltammogram is actually obtained at a copper amalgam electrode rather than at a pure mercury electrode.

When 5×10^{-5} M Cu(II) was added, with a 1-min accumulation time, the calibration graph of ribonuclease was linear between 1.5 and 8×10^{-8} M. The cathodic peak was evaluated, and i_p (nA) = $1.42 \times 10^9 \times C + 1.1$ (r^2 = 0.9999). Above this range, the slope rapidly decreased, presumably because of saturation of the electrode surface. Figure 1(e) shows the stripping voltammogram obtained from 1.5×10^{-9} M ribonuclease after a 5-min accumulation. The sensitivity that can be achieved by prolonging the accumulation time is clearly shown.

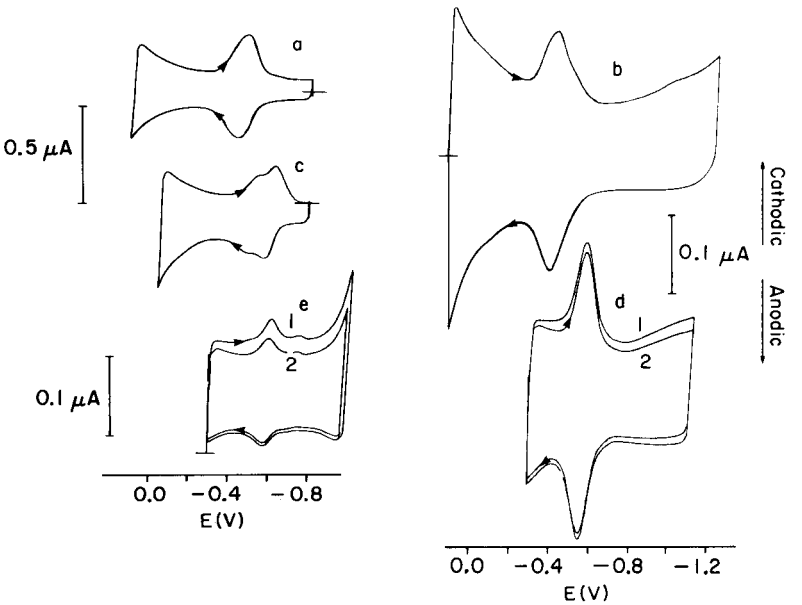

Fig. 1. (a) Cyclic voltammogram of 5×10^{-5} M ribonuclease; (b) stripping voltammogram of 5×10^{-8} M ribonuclease ($E_{acc} = +0.10$ V); (c) as for (a) with 5×10^{-5} M Cu(II) added; (d) as for (b) with 6×10^{-5} M Cu(II) added ($E_{acc} = -0.30$ V); (e) stripping voltammogram of 1.5×10^{-9} M ribonuclease (5-min accumulation). (1 and 2 refer to the first and second scan cycles, respectively.)

Somatostatin

Cyclic voltammetry of 1.5×10^{-5} M somatostatin in absence of copper(II) shows one well-defined peak couple at about −0.45 V (Fig. 2a). Addition of Cu(II) ions gave a second peak couple about 130 mV more negative, analogously to ribonuclease. This second couple was obtained alone at higher Cu(II) ion levels (Fig. 2b). The stripping voltammogram obtained from 1.4×10^{-7} M somatostatin in absence of Cu(II) ion shows a peak couple at −0.40 V (Fig. 2c), probably of the same origin as the one shown in Fig. 2(a). With excess of Cu(II) present, this peptide yielded an excellent stripping peak couple at −0.58 V (Fig. 2d). These peaks should correspond to the peak couple of Fig. 2(b). The peak separation between the anodic and cathodic stripping peaks in (d) is about 15 mV. A calibration graph for 3×10^{-8}–3×10^{-7} M somatostatin in presence of 5×10^{-5} M Cu(II) was linear, with the equation $i_p(\text{nA}) = 1.48 \times 10^9 \times C + 28$ ($r^2 = 0.9972$).

The accumulated product is adsorbed in both its oxidized and reduced state. This can be used to clean up a voltammogram obtained from a buffer solution containing impurities which yield interfering stripping peaks but which desorb at negative potentials. This situation is illustrated in Fig. 2(e), which shows the voltammogram obtained from 1.3×10^{-9} M somatostatin in presence of 5×10^{-5} M Cu(II). In the first cathodic scan, two peaks arise

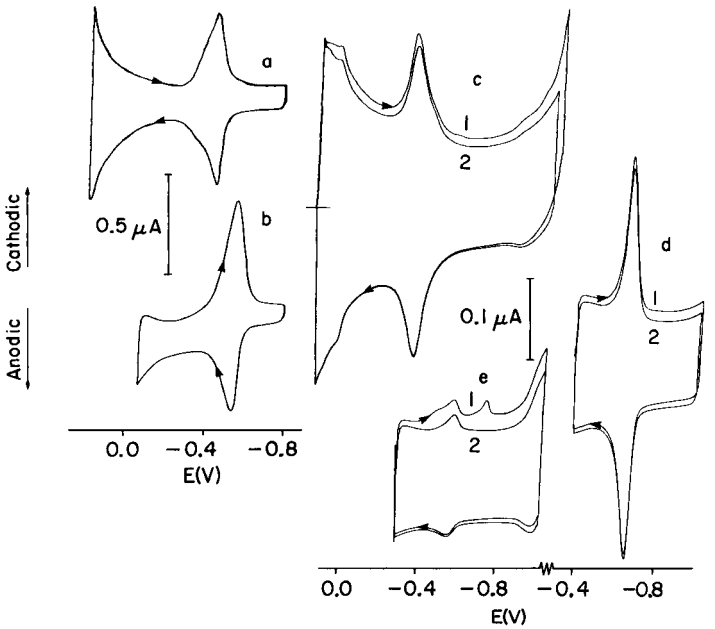

Fig. 2. (a) Cyclic voltammogram of 1.5×10^{-5} M somatostatin; (b) as for (a) with 5×10^{-5} M Cu(II) added; (c) stripping voltammogram of 1.4×10^{-7} M somatostatin (E_{acc} = +0.10 V); (d) as for (c) with 5×10^{-5} M Cu(II) added (E_{acc} = −0.30 V); (e) stripping voltammogram of 1.3×10^{-9} M somatostatin (5-min accumulation).

from impurities of the buffer, one of which interferes with the somatostatin peak. In the second cathodic scan, as well as in the anodic scans, these extra peaks are gone, leaving the somatostatin peak couple for evaluation. Such low levels of peptide concentration are only accessible in practice by using the stripping peak couple obtained in presence of Cu(II) ion. If the peak couple obtained in absence of Cu(II) ion (Fig. 2c) is to form the basis of the determination, the Cu(II) level of the buffer must be kept well below 1×10^{-9} M, which is very difficult in practice. This statement is valid for all the compounds investigated here.

Oxytocin and felypressin

These two peptides are similar in structure and show certain voltammetric characteristics which are different from the two substances discussed above. Both peptides yield rather complicated patterns in absence of Cu(II) ion. Cyclic voltammetry of 7×10^{-5} M oxytocin gave indistinct anodic peaks and three cathodic peaks, the peak at −0.42 V being very sharp (Fig. 3a). Addition of Cu(II) ion decreased this peak; instead, a cathodic peak appeared at −0.58 V (Fig. 3b). With increasing amounts of Cu(II) ion, this new peak predominated. Cyclic voltammetry of 8×10^{-5} M felypressin is shown in Fig. 3(c and d). Two anodic and cathodic peaks appeared in the absence of

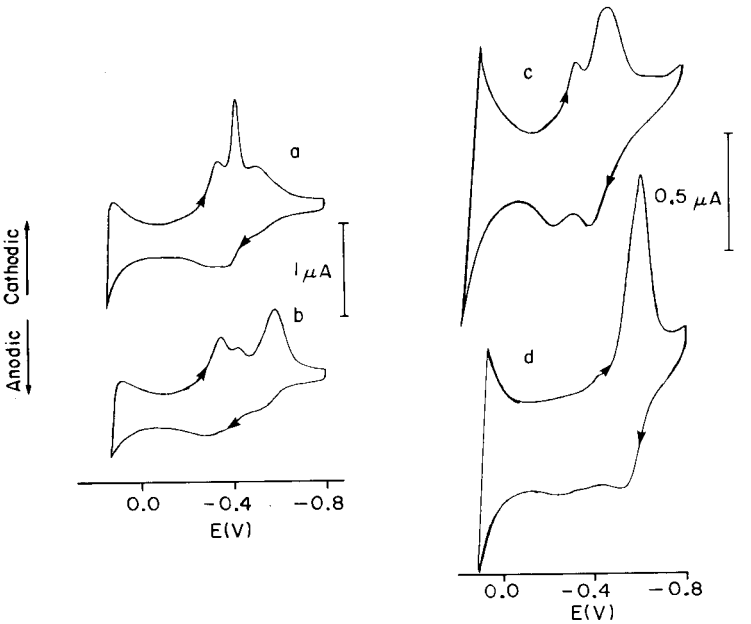

Fig. 3. Cyclic voltammograms: (a) 7×10^{-5} M oxytocin; (b) as for (a) with 2×10^{-5} M Cu(II) added; (c) 8×10^{-5} M felypressin; (d) as for (c) with 3×10^{-5} M Cu(II) added.

Cu(II) ion. Addition of Cu(II) ion again gave rise to a new cathodic peak at more negative potentials. The sharp cathodic peak at —0.42 V was not obtained from felypressin.

Stripping voltammograms for 2×10^{-7} M oxytocin are shown in Fig. 4. Without Cu(II) ion, there were a sharp cathodic peak at —0.50 V and an anodic peak at —0.37 V. With Cu(II) ion, these peaks disappeared and a peak couple arose at about —0.6 V (Fig. 4b). The cathodic peak in the first scan cycle with Cu(II) ion present seems to comprise two different signals. One of these is lost in the second scan cycle, leaving a peak couple which is very similar to that obtained from felypressin [2]. Felypressin gives only a small additional cathodic peak slightly positive to the main peak; this peak is lost in the second scan cycle, as for oxytocin [2]. Linearity between peak height of the cathodic peak of oxytocin and concentration was investigated for the 5×10^{-8}—2×10^{-7} M range with a 1-min accumulation and 5×10^{-5} M Cu(II) present. The equation was linear with $i_p(\text{nA}) = 1.57 \times 10^9 \times C - 0.5$ ($r^2 = 0.9995$).

Oxidized glutathione

Cyclic voltammetry of 3×10^{-5} M oxidized glutathione gave a small anodic peak in the initial anodic scan, and a large cathodic peak at —0.35 V on scan reversal (Fig. 5a). This peak couple should correspond to the formation and reduction of an adsorbed mercury complex of glutathione, in accordance

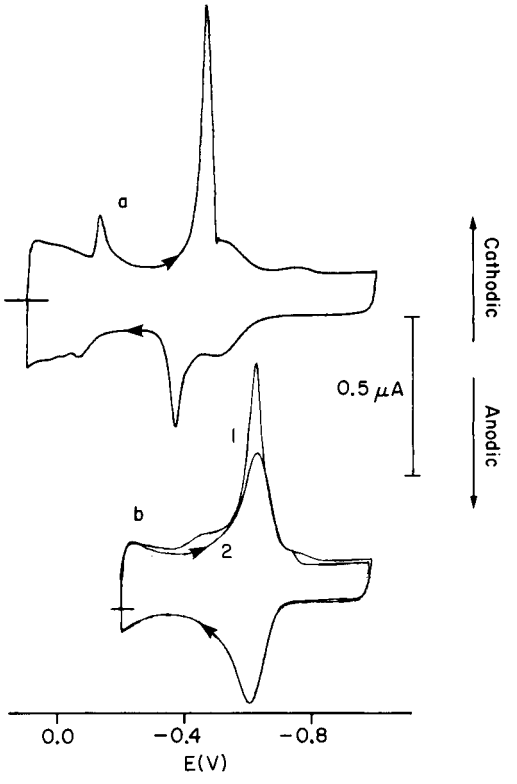

Fig. 4. Stripping voltammograms: (a) 2×10^{-7} M oxytocin ($E_{acc} = +0.10$ V); (b) as for (a) with 5×10^{-5} M Cu(II) added ($E_{acc} = -0.20$ V).

with the reported polarographic behaviour of oxidized and reduced glutathione [7, 8]. In presence of copper ions, this peak couple is replaced by a new couple about 130 mV more negative (Fig. 5b). This voltammetric pattern is very similar to that of cysteine [5]; it is therefore probable that much of the previous discussion on cysteine is also valid for oxidized glutathione.

Stripping voltammograms of 5×10^{-7} M oxidized glutathione are shown in Fig. 5(c and d). Without Cu(II) ion, the reduction peak of an adsorbed mercury complex is observed at −0.35 V, whereas with Cu(II) present this peak is replaced by a cathodic stripping peak at about −0.5 V. This is in accordance with the above results by cyclic voltammetry. (The solution used for curve c contained about 1×10^{-7} M Cu(II), which explains the small peak at −0.4 V.)

The major difference between the voltammetric patterns of oxidized glutathione and the larger peptides reported above, is that the electrode reaction product of oxidized glutathione is strongly adsorbed only in its oxidized state. This is obvious from the small anodic peak compared to the cathodic one. Further, the peak potential of the cathodic peak is about 0.1 V more positive than the peak potentials obtained from the other peptides.

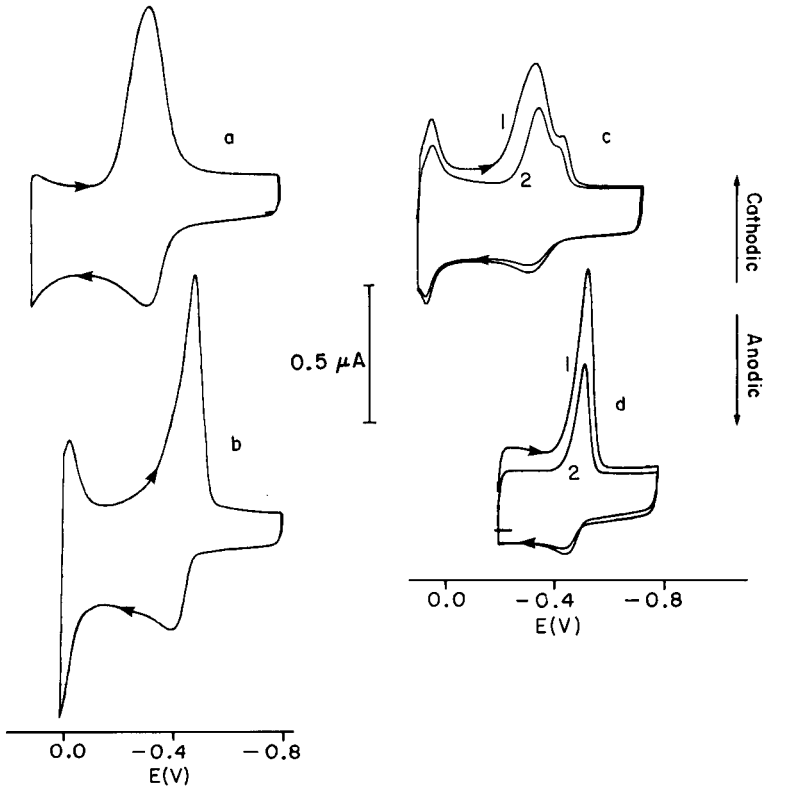

Fig. 5. (a) Cyclic voltammogram of 3×10^{-5} M oxidized glutathione; (b) as for (a) with 5×10^{-5} M Cu(II) added; (c) stripping voltammogram of 5×10^{-7} M oxidized glutathione (E_{acc} = +0.10 V); (d) as for (c) with 5×10^{-5} M Cu(II) added (E_{acc} = −0.20 V). (1 and 2 refer to the first and second scan cycles, respectively.)

Insulin

This protein gave a well-defined peak couple at about −0.4 V on cyclic voltammetry from 9×10^{-5} M solution (Fig. 6a). When Cu(II) ion was added, there was a new cathodic peak but no anodic counterpart (curve b). Stripping voltammetry of 1×10^{-7} M insulin gave a peak couple at −0.43 V. Addition of Cu(II) provided a second peak couple, but the first was not completely lost, as was the case for all compounds discussed above. Both peak couples decreased rapidly in height after the addition of Cu(II) ion. Clearly, there are interfering reactions (possibly precipitation) that form products not amenable to stripping analysis. Insulin can thus be determined by stripping voltammetry only in solutions as free from Cu(II) ion as possible.

Peptides not containing disulphide bridges

Substance P (m.w. 1348), adrenocorticotropic hormone (m.w. 4500), and neurotensin (m.w. 1673) are three polypeptides that do not contain cystine.

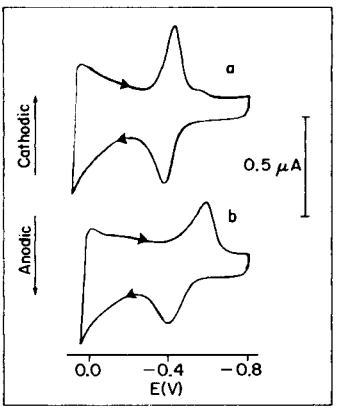

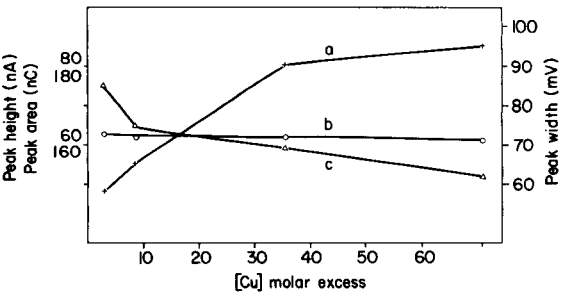

Fig. 6. (a) Cyclic voltammogram of 9×10^{-5} M insulin; (b) as for (a) with 1.6×10^{-5} M Cu(II) added.

Fig. 7. Cathodic stripping peak of 1.4×10^{-7} M somatostatin as a function of the molar excess of Cu(II): (a) peak height; (b) peak area; (c) peak width.

None of these peptides gave any voltammetric response when investigated with cyclic and stripping voltammetry between 0.0 and −1.2 V. The peptides were tested in concentrations up to 2×10^{-5} M in the absence and presence of Cu(II) ions.

DISCUSSION

Analytical utility of stripping peaks

Stripping voltammetry seems to have possibilities for quantifying traces of the compounds investigated. The reproducibility of the stripping peaks is good. For example, the relative standard deviation of the peak height obtained from five different solutions of 2×10^{-7} M felypressin in presence of 5×10^{-5} M Cu(II) was 2%. Linear relationships between peak height and concentration were obtained within useful concentration intervals. The limit of detection after a 5-min accumulation time was about 1×10^{-9} M. This corresponds to 0.6 ng ml^{-1} for oxidized glutathione but 12 ng ml^{-1} for ribonuclease. Increasing the accumulation time might decrease this limit further.

Electrode mechanisms

The electrode mechanisms were not investigated in detail. Some parallels to the behaviour of cysteine in absence and presence of Cu(II) ions [5, 9, 10] can be observed. Cysteine forms anodically an adsorbed mercury complex (HgRS) which can be reduced back to the free thiol thus yielding a cathodic stripping peak. When copper amalgam is formed, by reduction of excess of Cu(II) ions, a copper complex (CuRS) is adsorbed. This complex yields a cathodic stripping peak about 100 mV more negative than the mercury complex [5]. Only the complexes and not the free thiol are strongly adsorbed.

The voltammetric pattern of oxidized glutathione, as reported above, is almost identical to that of cysteine, suggesting that oxidized glutathione forms strongly adsorbed mercury and copper complexes, respectively, of reduced glutathione. The reduction of these complexes then produces the cathodic stripping peaks.

The formation of a complex between mercury and the cysteine part of oxytocin was previously suggested [4]. Such interaction may explain the major peak couples obtained for the other peptides studied here in the absence of Cu(II) ion. If so, the well-defined peak couples obtained with Cu(II) ion present might be explained as reduction and oxidation peaks from an adsorbed complex between copper and the cysteine parts of the molecules. The important difference in the voltammetric pattern of the investigated peptides and that of free cysteine and oxidized glutathione, is that the peptides are strongly adsorbed in both their oxidized and reduced states, whereas the latter two compounds desorb on reduction. This is evident from the relative heights of the anodic and cathodic peaks (see Results).

The cathodic stripping peak of cysteine becomes narrower and higher with increasing excesses of Cu(II) ion, though its area remains constant [5]. This effect was interpreted as a change in the kinetics of the reduction process as more copper amalgam is formed during the accumulation. A similar effect on the peak shapes was observed for all the compounds investigated here (except insulin); Fig. 7 illustrates this for 1.4×10^{-7} M somatostatin.

Correlation between structure and voltammetric response

Peptides and proteins with differences in molecular weight and content of cystine were chosen in order to investigate whether such parameters influence the voltammetric behaviour. The molecular size and the charge obtained from the stripping peak area at full coverage of the electrode are correlated (Table 1). This relation is as expected; the larger the molecule, the fewer can occupy the electrode surface.

Because the peak potentials of the stripping peaks obtained from ribonuclease, somatostatin, oxytocin and felypressin in presence of Cu(II) ions

TABLE 1

Correlation between molecular weight and charge at full coverage[a]

Substance	M.w.	Charge (μC cm^{-2})
Ribonuclease	12.640	8
Somatostatin	1.639	22
Felypressin	1.040	20
Oxytocin	1.007	26
Ox. glutathione	612	60

[a]The cathodic peak obtained in presence of excess of Cu(II) ions was evaluated. Concentrations were chosen so that peak areas were independent of concentration.

are very similar, it is difficult to distinguish between these peptides. Oxidized glutathione, however, yields its stripping peak about 100 mV more positive. The former four peptides are all adsorbed in both their oxidized and reduced states whereas oxidized glutathione desorbs on reduction. These differences make it possible to determine oxidized glutathione and one of the larger peptides in presence of each other. Stripping analysis for oxidized glutathione and felypressin in mixtures has been reported [2].

Ribonuclease contains four sulphur bridges, while somatostatin, oxytocin and felypressin contain only one, but ribonuclease shows no voltammetric response that can be clearly related to the extra three sulphur bridges, possibly because of its tertiary structure. Insulin is different from the other peptides tested in that it contains two polypeptide chains and three sulphur bridges, but its voltammetric response in presence of Cu(II) ions is poor. However, the stripping voltammetric features reported for these peptides with disulphide bridges (i.e., containing cystine) should be useful for detecting disulphide bridges in unknown peptide mixtures at low concentration levels.

REFERENCES

1 U.S. Pharmacopeia XIX, U.S. Pharmacopeial Convention, Inc., 1975, pp. 356, 534.
2 U. Forsman, Anal. Chim. Acta, 156 (1984) 43.
3 J. Krupica and M. Zaoral, Collect. Czech., Chem. Commun., 34 (1969) 678.
4 J. Rishpon and I. R. Miller, Bioelectrochem. Bioenerg., 2 (1975) 215.
5 U. Forsman, J. Electroanal. Chem., 152 (1983) 241.
6 U. Forsman, J. Electroanal. Chem., 111 (1980) 325; 122 (1981) 215.
7 W. Stricks and I. M. Kolthoff, J. Am. Chem. Soc., 74 (1952) 4646.
8 C. A. Mairesse-Ducarmois, G. I. Patriarche and J. L. Vandenbalck, Anal. Chim. Acta, 76 (1975) 299.
9 M. T. Stankovich and A. J. Bard, J. Electroanal. Chem., 75 (1977) 487.
10 W. Stricks and I. M. Kolthoff, J. Am. Chem. Soc., 73 (1951) 1723.

Analytica Chimica Acta, 166 (1984) 153—161
Elsevier Science Publishers B.V., Amsterdam — Printed in The Netherlands

DETERMINATION OF TOTAL PHTHALATE ESTERS IN WASTEWATERS BY DIFFERENTIAL PULSE POLAROGRAPHY

KAZUYOSHI TANAKA* and MASAHIRO TAKESHITA
College of Engineering, Kanto-Gakuin University, 4834 Mutsuura, Kanazawa-ku, Yokohama 236 (Japan)

(Received 2nd April 1984)

SUMMARY

A reliable procedure for the determination of total phthalate esters as phthalic acid in environmental samples is based on differential pulse polarography (d.p.p.). The phthalate esters are extracted from the sample water with hexane; concentrated sulphuric acid/hexane partitioning provides effective removal of organic interferences. The individual phthalate esters are hydrolyzed by refluxing with 10 M potassium hydroxide to phthalic acid, which is extracted with ethyl acetate followed by evaporation of the extract. This procedure gives recoveries of 83—90%. The residue is dissolved in 0.1 M acetic acid/0.1 M potassium chloride for d.p.p. The otpimal conditions for polarography are discussed. The calibration graphs are linear over the range 2×10^{-6}—1×10^{-4} M and the detection limit for phthalic acid is 5×10^{-7} M. The method was successfully applied to determine total phthalate esters over the range 0.3—30 $\mu g\ l^{-1}$ in crude and treated wastewaters.

The phthalate esters commonly used as plasticizers in the production of poly(vinyl chloride) plastics, have three main constituents, namely, di(2-ethylhexyl)phthalate (DEHP), dibutyl phthalate (DBP) and diheptyl phthalate (DHP). Because of the increasing use of plastics, these esters are widely distributed and are important organic pollutants. Phthalate esters and their metabolites, the monoesters, have inhibition characteristics and have been shown to exert a variety of subtle toxic effects [1—4]. The determination of traces of these esters in environmental samples is of diagnostic value, and simplified measurements and confirmation of total phthalate esters would be significant.

In general, the instrumental methods used for determining the esters in water, sediment, soil and biological samples are high-performance liquid chromatography (h.p.l.c.) [5], gas chromatography [6, 7] and gas chromatography/mass spectrometry (g.c./m.s.) [8]. Spectrophotometric h.p.l.c. detectors are rather insensitive for the esters and phthalic acid. Although the g.c. approach is useful for determining the individual esters in mixtures, it has the following disadvantages: (1) g.c. conditioning is complicated if good reproducibility is to be achieved; (2) the electron-capture detector is not specific to the esters, so that the presence of interfering compounds can cause difficulties in identifying and quantifying the esters; (3) the detector is not

0003-2670/84/$03.00

very sensitive to the esters and gives a narrow linear dynamic range; (4) sample preparation is time-consuming. An improved technique involving alkaline hydrolysis, esterification and g.c. has been developed to determine the esters as derivatized bis(2,2,2-trifluoroethyl)phthalate which is defined as total phthalate esters and gives a sensitive signal with the detector [9]. However, this procedure requires time-consuming clean-up by column chromatography and a long reaction time (20 min) for the esterification under anhydrous conditions. In a preliminary examination of this method, a recovery of only 60% was obtained. Thus a more reliable method is needed to determine the range of the residual esters in environmental samples.

Electrochemical techniques have become widely accepted for the determination of low concentrations of electroactive molecules and their metabolites [10, 11]. Polarography has been applied to the determination of maleic, fumaric and phthalic acids in synthetic polyesters [12—14]. The d.c. polarographic behaviour of individual esters has been studied systematically [15—18], but the small differences between their half-wave potentials causes difficulties in handling mixtures. Modern polarographic techniques, such as differential pulse polarography (d.p.p.), are extremely sensitive and levels of organic species down to 10^{-7} M, or lower, can be quantified. Therefore, the possibility of using d.p.p. for monitoring total phthalate esters as phthalic acid in environmental samples was considered worthy of investigation in order to provide a fundamental preliminary estimate of ester pollution. Direct detection of phthalic acid after alkaline hydrolysis of the esters would provide a simpler procedure than is needed for g.c. and would reduce the risk of contamination. The application of d.p.p. in routine analysis for total phthalate esters down to 0.7 $\mu g\ l^{-1}$ is discussed in this paper.

EXPERIMENTAL

Reagents and standard solutions

All solvents used were of g.c. grade or pesticide quality (Wako Chemicals, Tokyo). The phthalate esters used (DEHP and DBP) were of >99.55% purity (Wako Chemicals). All other chemicals were of analytical grade unless otherwise stated. Standard solutions of phthalate esters were made by dissolving appropriate amounts of the standard compounds in hexane. Standard solutions of phthalic acid for calibration were prepared by dissolving potassium hydrogenphthalate in distilled water. The distilled water was obtained from a conventional distillation system with potassium permanganate added. All the distilled water used in the procedure was extracted twice with hexane to remove possible interferences. The acetic acid and potassium chloride used as supporting electrolytes showed no contamination on polarographic examination. Anhydrous sodium sulphate used for dehydration was heated at 400°C overnight and stored in a glass jar to prevent contamination.

Instrumentation

A Fuso Model 312 polarographic analyzer was operated in the d.c., sampled-d.c., normal pulse and differential pulse modes. The three-electrode system comprised a dropping mercury electrode, a saturated calomel reference electrode and a platinum wire auxiliary electrode. About 5 ml of test solution in a 10-ml electrolysis cell was maintained at 25° C by water circulation, and the polarograms were recorded with a Rikendenshi Model D-52 X-Y recorder. Controlled drop times of 1 s for d.p.p. were obtained with a drop timer.

In order to identify and quantify the individual constituents of the esters by g.c., a Shimazu Model 4BM chromatograph equipped with an electron capture detector (^{63}Ni, 10 mCi) was used with a glass column (1.5 m × 3 mm i.d.) packed with OV-1(methyl silicone) on 80/100 mesh Chromosorb W. The injector and detector were isothermal at 230° C, and the oven temperature was kept at 210° C. The retention time of DEHP was about 10 min.

Procedure

About 800 ml of wastewater in a separating funnel was shaken for 10 min with 200 ml of hexane to extract the phthalate esters; the phases were allowed to separate, and the water layer was drawn off into another funnel. This extraction was repeated; the hexane extracts were combined, dried through anhydrous sodium sulphate, and evaporated to 5 ml under reduced pressure. The clean-up for the extract was done by concentrated sulphuric acid/hexane partitioning instead of time-consuming Florisil column chromatography as follows. The extract was transferred to a test tube, 2 ml of concentrated sulphuric acid was added, the mixture was shaken for 2 min, and then the hexane was withdrawn and discarded to remove organic interferences. Complete removal of organic interferences from the extract required another two or three extractions with 5 ml of hexane. The sulphuric acid layer was carefully diluted with 20 ml of water under cooling, and the esters were re-extracted into 50 ml of hexane. The hexane layer was washed twice with water and centrifuged to complete the separation.

Alkaline hydrolysis of the esters to phthalic acid was then done by adding 2 ml of 10 M potassium hydroxide solution to the hexane extract and refluxing for about 20 min. After the addition of sodium chloride (15 g) and 10% (v/v) hydrochloric acid to adjust the pH to 3, the phthalic acid obtained was extracted into 50 ml of ethyl acetate, and the extract was evaporated just to dryness at ca. 60° C. To the residue were added appropriate amounts of acetic acid and potassium chloride as supporting electrolytes, and finally the sample solution for polarographic measurements was made up to exactly 5 ml with distilled water.

For verification of the clean-up partitioning process, preliminary results obtained by g.c. are shown in Fig. 1; organic compounds such as chloroform, polychlorinated biphenyl (PCB) and *p,p'*-DDT are completely removed. Certain hydrolyzed products of these compounds are likely to be electroactive and interfere with polarographic determinations.

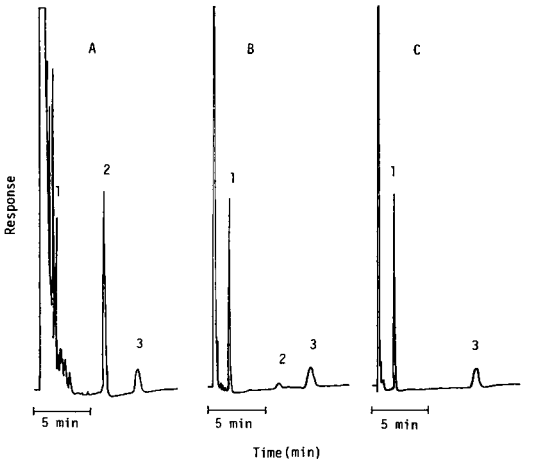

Fig. 1. Gas chromatograms of phthalate esters and organic substances after successive clean-up processes by sulphuric acid/hexane partitioning: (A) mixtures of chloroform, PCB, DBP (peak 1), *p,p'*-DDT (peak 2) and DEHP (peak 3); (B) after the first step of clean-up; (C) after the third repeated step of clean-up.

RESULTS AND DISCUSSION

Polarography

Although the polarographic behaviour of phthalic acid and the esters have been reported previously [15—18], the electrochemical characteristics of phthalic acid were re-examined to ensure the optimal conditions for the determination of the analytes. The d.c. polarographic results obtained at various hydrogen ion concentrations are shown in Fig. 2; the reduction current appears below pH 4.2 and constant current is obtained below pH 2.5, and the plot of half-wave potential vs. pH value has a slope of —60 mV. These results are in a good agreement with those reported by Ryvolová and Hanuš [17]. In further investigations, the electrode reaction mechanisms of phthalic acid were elucidated. The instantaneous current—time curve at pH 3.3 shown in Fig. 3 indicates that the component x in the current—time relationship $i = kt^x$ is 0.63, which corresponds to the theoretical value 0.67 [19] and indicates that the limiting current is kinetically controlled. The plot of log $[(i_l - i)/i_l]$ vs. potential under the same conditions had a slope of 27 mV, showing that two hydrogen ions participate in the rate-determining step of the electrode reactions. The correlation between the limiting current and the square root of the mercury column height also suggested kinetic current over the pH range 2.5—4.2, whereas the limiting current below pH 2.3 was diffusion-controlled. Cyclic voltammetry at a hanging mercury drop electrode was used to study the reversibility of the reaction; a single cathodic peak was observed without any trace of anodic peaks corresponding to re-oxidation of the reduction products. These results support the view that the reduction product of phthalic acid in acidic medium is phthalide which is reducible at more negative potential as suggested by Whitnack et al. [16].

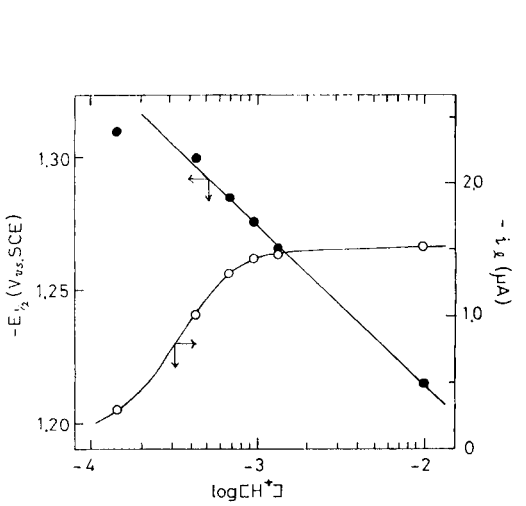

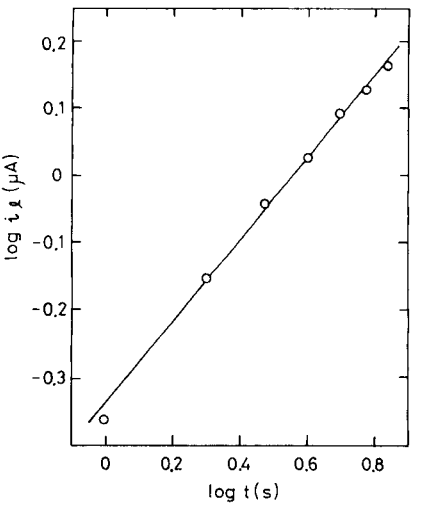

Fig. 2. Effect of hydrogen ion concentration on d.c. polarographic limiting current and half-wave potential of 1×10^{-4} M phthalic acid in 0.1 M potassium chloride solution.

Fig. 3. Instantaneous current—time curve plots of 1×10^{-4} M phthalic acid at $E = -1.372$ V vs. SCE in 0.1 M potassium chloride at pH (HCl) 3.3.

Various acidic solutions (sulphuric, hydrochloric and acetic acids) were examined to establish the most suitable conditions for the determination of phthalic acid. In the polarographic curves obtained below pH 2.3, the limiting current appeared just before the steep rise in background current corresponding to reduction of hydrogen ion; the best separated wave was observed in acetic acid solution. Because of its buffering action, 0.1 M acetic acid was used to adjust the hydrogen ion concentration, and 0.1 M potassium chloride was added as supporting electrolyte. The half-wave potential of phthalic acid was then −1.27 V vs. SCE.

For comparison, d.c. and differential-pulse polarograms are shown in Fig. 4; d.p.p. was superior to the other modes tested (d.c., sampled-d.c. and normal pulse), and was used exclusively for quantitative work. The peak current of phthalic acid was measured after subtraction of the current arising from any overlapping electrochemical responses of the blank. This subtraction method proved to be accurate for d.p.p. responses that were incompletely resolved from the background. The relationship between peak current and phthalic acid concentration was linear over the range 2×10^{-6}—1×10^{-4} M phthalic acid and the detection limit was 5×10^{-7} M, corresponding to about 0.7 μg l^{-1} phthalic acid when the preconcentration factor in procedure described above is considered.

Recovery tests

Recoveries of the cited standard phthalate esters were studied at the levels of 1.4—6.9 $\times 10^{-5}$ M; the results are summarized in Table 1. The overall

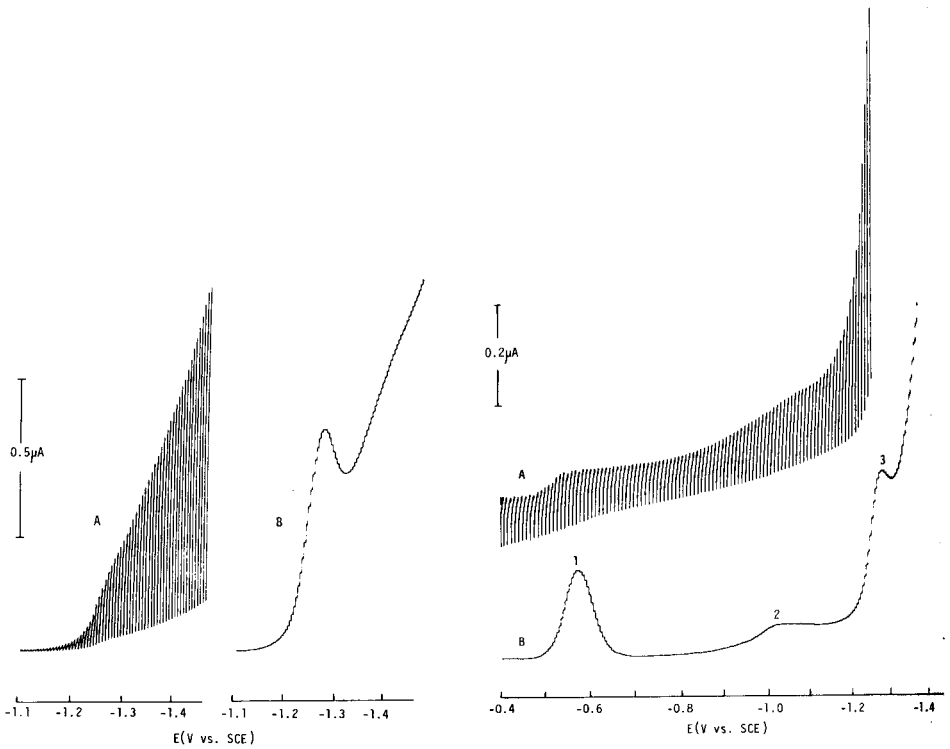

Fig. 4. Typical d.c. (A) and d.p. (B) polarograms of 5×10^{-5} M phthalic acid in 0.1 M acetic acid/0.1 M potassium chloride at 25° C. For d.p.p. the scan rate was 2 mV s^{-1} and the pulse modulation amplitude was —20 mV.

Fig. 5. Typical d.c. (A) and d.p. (B) polarograms of wastewater samples. Experimental conditions as for Fig. 4. Peaks 1 and 2 are unknown; peak 3 is ascribed to the reduction of phthalic acid.

TABLE 1

Recovery from samples spiked with standard phthalate esters

Ester	Added (M)[a]	Found (M)[b]	Recovery (%)
DBP	6.93×10^{-5}	$(5.75 \pm 0.60) \times 10^{-5}$	83.0
DEHP	6.93×10^{-5}	$(5.91 \pm 0.88) \times 10^{-5}$	85.3
DEHP + DBP[c]	1.39×10^{-5}	$(1.26 \pm 0.04) \times 10^{-5}$	90.6

[a]A hexane solution (5 ml) of the esters was added to water (800 ml) and used as test sample. [b]Standard deviation from duplicate runs. [c]Concentration of each ester was 6.93×10^{-6} M.

recoveries obtained exceeded 80% while the recovery of DEHP/DBP mixtures was about 90%, thus the proposed method is adequate for quantifying phthalic esters. Because the esters are miscellaneous and can be adsorbed onto glass, it is difficult to extract them completely from water samples with any organic solvent. The low recoveries obtained are probably due to cumulative losses in the various extraction and separation steps. Although diethyl ether has been reported to be effective for the extraction of phthalic acid after alkaline hydrolysis [9], ethyl acetate was found here to give a satisfactory recovery in the extraction.

Pretreatment procedures for g.c. are based on a combination of classical chromatographic separation and time-consuming esterification. In contrast, the proposed method based on direct determination of phthalic acid by d.p.p. provides a simple, relatively quick procedure with reduced risks of contamination.

Measurement of total phthalate esters in wastewaters

Two wastewater samples (crude and treated waters) were examined. The crude (untreated) wastewater was sampled at the outlet sewage pipe after the neutralization process. The treated sample had been subjected to neutralization, aeration, active charcoal filtration and coagulative precipitation. These treatments without activated sludge process are considered to be inadequate for the complete removal or decomposition of organic substances. Floating oil was frequently found in the crude water, and phthalate esters were probably dissolved and dispersed in the oil phase.

The proposed d.p.p. method was applied to determine the amounts of phthalic acid as total phthalate esters in these samples. Typical polarograms recorded from a starting potential of −0.4 V are shown in Fig. 5. Two well-defined peaks in both samples were observed at −0.57 V (peak 1 in Fig. 5) and −1.27 V (peak 3), the latter corresponding to the reduction of phthalic acid. An ill-defined peak appeared at −1.03 V. The substances corresponding to peaks 1 and 2 could not be identified, but from their peak potentials and polarographic behaviour, they may be ascribed to some nitro compound and/or organic acid in the waters.

These waters were collected over several months. The results listed in Table 2 showed reasonable agreement with g.c. findings. The concentration of total phthalate esters was higher in the crude waters. There is obviously considerable decomposition and removal of organic substances by the treatment processes. The most likely source of the esters in the sample waters seems to be a plasticizer in the poly(vinyl chloride) used as the sewage pipe material; organic solvents in the laboratory drains would extract the esters from the materials effectively.

Because of unavoidable contamination in the analytical procedure, a blank test is necessary for evaluation of the amount of phthalic acid from the measured d.p.p. peak. The presence of phthalic acid in sample 7 (blank) in Table 2 is mainly due to contamination. Thus, cleaning of flasks and other

TABLE 2

Results for total phthalate esters in wastewaters collected at different times

Sample no.	Phthalic acid found[a] (M)	Total phthalate esters calculated[b] ($\mu g\ l^{-1}$)
1 (crude)	3.05×10^{-5}	31.7
2 (crude)	2.05×10^{-5}	21.3
3 (treated)	6.99×10^{-6}	7.27
4 (treated)	9.6×10^{-7}	1.0
5 (treated)	1.55×10^{-5}	16.1
6 (treated)	3.0×10^{-7}	0.31
7 (blank)	2.29×10^{-6}	2.38

[a]These values were obtained from the d.p.p. peak by using the subtraction method described above. [b]In the case of $a \times 10^{-6}$ M phthalic acid (m.w. = 166) found in solution (5 ml), total phthalate esters in the wastewater (800 ml) were calculated from the equation: $166 \times a \times 5/800 = 1.04 \times a$ ($\mu g\ l^{-1}$).

glassware with concentrated sulphuric acid was used throughout the present work. When a d.p.p. peak in the blank was detected, the phthalic acid below detection limit in the sample could be quantified by the subtraction method described above.

Environmental research on phthalate esters in Japanese river water indicates that the mean concentration of DBP is 0.5 $\mu g\ l^{-1}$, that of DEHP is 0.19 $\mu g\ l^{-1}$ and that of total phthalate esters is 1.6 $\mu g\ l^{-1}$ [20]. Recent research on marine samples in Texas shows a similar order of DEHP concentrations in estuarine waters [21].

REFERENCES

1 F. P. Bell and E. V. Hubert, Bull. Environ. Contam. Toxicol., 25 (1980) 487.
2 F. L. Mayer, D. L. Stalling and J. L. Johnson, Nature, 238 (1972) 411.
3 B. G. Lake, P. G. Branton, S. D. Gangolli, K. R. Butterworth and P. Grasso, Toxicology, 6 (1976) 431.
4 Conference on Phthalates, June 9—11, 1981, Washington, DC, in Environ. Health Perspect., 45 (1982) 1.
5 S. C. Amundson, J. Chromatogr. Sci., 16 (1978) 170.
6 E. Weisenberg, Y Shoenberg and N. Ayalon, Analyst (London), 100 (1975) 857.
7 Planning and Co-ordination Bureau, Official Methods of Analysis (in Japanese), Japan Environment Agency, 1975, pp. 43, 82.
8 R. A. Hites, J. Chromatogr. Sci., 11 (1973) 570.
9 R. Takeshita, E. Takabatake, M. Minagawa and Y. Takigawa, J. Chromatogr., 133 (1977) 303.
10 W. Franklin Smyth (Ed.), Electroanalysis in Hygiene, Environmental, Clinical and Pharmaceutical Chemistry, Analytical Chemistry Symposia Series, Vol. 2, Elsevier, Amsterdam, 1980.
11 B. J. Birch and J. P. Hart, in W. Franklin Smyth (Ed.), Polarography of Molecules of Biological Significance, Academic Press, London, 1979.
12 M. E. Traxton, Chem. Ind. (London), 39 (1966) 1613.

13 V. Novak and V. Forst, Chem. Prum., 14 (1964) 541; Chem. Abstr., 62 (1965) 637.
14 E. G. Gintsberg, B. M. Kovarskaya and V. F. Pilyaeva, Plast. Massy (USSR), 12 (1968) 56; Chem. Abstr., 70 (1969) 84153h.
15 N. H. Furman and C. E. Bricker, J. Am. Chem. Soc., 64 (1942) 660.
16 G. C. Whitnack, J. Reinhart and E. S. C. Gantz, Anal. Chem., 27 (1955) 357.
17 A. Ryvolová and V. Hanuš, Collect. Czech. Chem. Commun., 21 (1956) 359.
18 P. Zuman and C. L. Perrin, Organic Polarography, Interscience, New York, 1969.
19 A. A. Vlček, Progress in Inorganic Chemistry, Vol. 5, Interscience, New York, 1963.
20 National Research Data on Chemical Compounds, reported by Planning and Coordination Bureau, Japan Environment Agency, 1977.
21 H. E. Murray, L. E. Ray and C. S. Giam, Bull. Environ. Contam. Toxicol., 26 (1981) 769.

Analytica Chimica Acta, 166 (1984) 163—170
Elsevier Science Publishers B.V., Amsterdam — Printed in The Netherlands

SPECTROELECTROCHEMICAL DETECTOR FOR FLOW-INJECTION SYSTEMS AND LIQUID CHROMATOGRAPHY

HOWARD D. DEWALD and JOSEPH WANG*

Department of Chemistry, New Mexico State University, Las Cruces, NM 88003 (U.S.A.)

(Received 9th May 1984)

SUMMARY

Flow-through spectroelectrochemical detectors for flow-injection systems and liquid chromatography are described. The detectors have a rectangular flow channel with a reticulated vitreous carbon working electrode followed by an open optical window.The dead volumes of the cells are 27 μl (liquid chromatography) and 80 μl (flow injection). In situ spectral monitoring of reaction products and intermediates for compounds that are both weakly and highly absorbing is demonstrated by using *o*-tolidine and *N,N,N',N'*-tetramethyl-*p*-phenylenediamine. As a detector for flow-injection systems, components in two-component mixtures can be quantified. As a detector for liquid chromatography, simultaneous absorbance and electrochemical chromatograms allow more eluting compounds to be identified and quantified. Mixtures of nitro- and chloro-phenols are used to illustrate the simultaneous profiling of spectral and redox properties.

The combination of electrochemistry and spectroscopy, known as spectroelectrochemistry (s.e.c.) has been used successfully for at least twenty years [1]. Several reports have been published describing the utility of s.e.c. for studies of a variety of chemical reactions [2—5]. Various designs of s.e.c. cells, made with different electrode materials have been described [6—11]. However, apart from indirect coulometric titrations [4, 5] and derivative cyclic voltammetry/spectrophotometry [12], s.e.c. has been used sparingly if at all for quantifying solution components.

Thus far, nearly all s.e.c. studies have relied on measurement in batch systems. If the redox properties of a single analyte are of importance, then these batch systems are satisfactory. However, with increasing interest in continuous flow sample processing [13] and the desire to quantify multiple analytes, new detectors are required that will permit rapid determinations in complex clinical, environmental, and industrial samples. The growth in flow injection [14], liquid chromatography [15], and other approaches [16] emphasizes the need for flow-through detectors.

In this paper, the fabrication and characterization of a flow-through spectroelectrochemical detector based on reticulated vitreous carbon (RVC) in a thin-layer rectangular channel for flow-injection systems and liquid chromatography are discussed. The detector offers the advantages of simultaneous (real-time) profiling of redox and spectral properties, resolution of

0003-2670/84/$03.00

co-eluting compounds from a chromatographic column in which only one species is electroactive and the other absorbs, both are electroactive but only one absorbs, or both absorb but only one is electroactive, and mechanistic studies on short-lived electrogenerated absorbing intermediates. Thus, the use of a second detection scheme provides additional information from a single sample injection. Application of the detector will be illustrated by data on a variety of test systems including *o*-tolidine, dopamine, chloro- and nitro-phenols, and *N,N,N',N'*-tetramethyl-*p*-phenylenediamine.

EXPERIMENTAL

Construction of detector

Two spectroelectrochemical flow cells having different dimensions were evaluated (Fig. 1). The construction of both detectors was similar. Reticulated vitreous carbon (RVC; 2 X 3-S, 100 pores per in., ERG, Oakland, CA) served as the working electrode. The flow channel (5 mm X 15 mm for flow injection, and 2 mm X 12 mm for chromatography) was cut from half a mounting square spacer (3M, St. Paul, MN; cat. no. 111). The mounting square defined the exact geometry of the window and the detector thickness (1.2 mm). After the mounting square had been glued to a clean 1 X 3-in glass slide, the inlet and outlet flow channels were made with a needle inserted and twisted in the mounting square material. Teflon tubing (0.5 mm i.d. X 1 mm o.d.) was pushed through the channels flush with the window walls. The RVC was cut to dimension (5 mm X 7.5 mm for flow injection, and 2 mm X 6 mm for chromatography) and positioned in the inlet side of

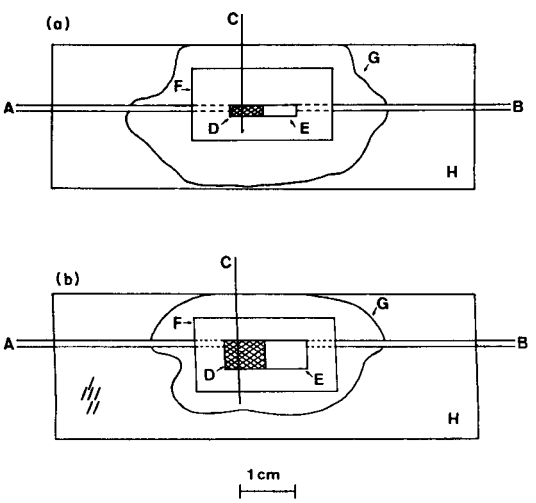

Fig. 1. Spectroelectrochemical detectors tested: (A) solution inlet; (B) solution outlet; (C) platinum wire contact; (D) RVC working electrode; (E) spectral window; (F) mounting square spacer; (G) epoxy seal; and (H) glass microscope slide. (a) For liquid chromatography; (b) for flow injection.

the flow channel. Either a 1-mm diameter glassy carbon rod (pushed through the mounting square and half way into the RVC) or a 24-gauge platinum wire (laid across the surface of the mounting square and RVC) served to make electrical contact. Nonconducting epoxy was applied around the edges of the mounting square and a second glass slide was pressed in place and sealed. Strips of PVC insulating tape covered the outer body, except the window, to avoid light scatter and also held the detector in position in the spectrophotometer. The total dead volumes of the cells were 27 μl (chromatography detector) and 80 μl (flow-injection detector). Air bubbles were dislodged from the RVC by pumping solution through the detector.

Apparatus

Absorption spectra were recorded with a Perkin-Elmer 320 spectrophotometer with 2-s response and 2-nm manual slit width. Electrochemical measurements were obtained with a EG&G PAR Model 364 Polarographic Analyzer. All potentials were measured against a Ag/AgCl (3 M NaCl) reference electrode housed in the RC-2A compartment (Bioanalytical Systems, W. Lafayette, IN) located downstream from the outlet. The stainless steel tube of the reference compartment was used as the auxiliary electrode. The combination of large-area working electrode and the downstream positioning of the reference and auxiliary electrodes results in ohmic drops of 150—300 mV for the flow-injection detector and 50—100 mV for the chromatographic detector (depending on the analyte concentration).

In the flow-injection system, samples were injected with a Rheodyne Model 7010 valve and carrier solution was pumped from a 400-ml Nalgene reservoir by a Cole-Palmer Model 7553-10 variable-speed masterflex pump with a 7013-20 pump head. Sample solution was contained in a 250-ml Nalgene reservoir and filled the sample loop by gravity.

Liquid chromatograms were obtained with the BAS LC-303 consisting of a dual piston pump (PM-30A), a Rheodyne Model 7125 sample injection valve (20-μl loop), and a Biophase ODS-5 μm reversed-phase column (25 cm $\times$ 4.6 mm i.d.).

Connecting tubing was teflon (1 mm i.d. $\times$ 2 mm o.d.) with polypropylene tube-end fittings. The lengths of teflon tubing were sealed in tygon tubing to minimize oxygen permeation. Oxygen-free samples were maintained by bubbling nitrogen through solutions. All experiments were done at ambient temperature.

Reagents and samples

The samples used were: dopamine hydrochloride, *N,N,N',N'*-tetramethyl-*p*-phenylenediamine dihydrochloride (TMPD) and *o*-tolidine (Sigma Chemical Company); acetonitrile, *o*-chlorophenol, *p*-chlorophenol, 2,4-dinitrophenol and *p*-nitroaniline (Aldrich Chemical Company); picric acid and potassium hexacyanoferrate(II) trihydrate (J. T. Baker); phenol (Fisher); and *o*-nitrophenol and *p*-nitrophenol (MCB). All other chemicals were ACS-certified reagent grade and were used as received.

The mobile phase was filtered through a fritted-glass Büchner funnel and degassed prior to use. All solutions were prepared with deionized/glass-distilled water.

RESULTS AND DISCUSSION

The greatest utility of reticulated vitreous carbon (RVC) has been for detection in flow systems [17—21]; its properties as an electrode material have been reviewed [22]. Norvell and Mamantov [23] and Owens et al. [24] have used RVC for batch spectroelectrochemical measurements. In the present design for an s.e.c. detector, initial interest lay in exploiting the relatively high conversion efficiency of the RVC for generating spectrally active species.

The detector designs are shown in Fig. 1. The rectangular flow channel is easy to design, has relatively low volume with rapid wash-out time, can be used in two positions for electrochemical-optical or optical-electrochemical measurements (depending on the solution flow direction), and allows maximum light transmission because no loss in intensity occurs through the "open" window as would happen through the RVC, although the RVC transmittance is still acceptable [23]. The dependence of the degree of conversion on the solution flow rate was evaluated under continuous flow conditions, using a 5 μM hexacyanoferrate(II) solution. The degree of conversion, R, is the fraction of electroactive species electrolyzed while the solution flows through the electrode and depends on the residence time of an element of solution in the electrode; decreasing the flow rate provides a larger conversion efficiency. For the flow rates used in this study, R increases from 0.07 at 1.9 ml min^{-1} to 0.22 at 0.5 ml min^{-1} (flow-injection cell) and from 0.05 to 0.14 (chromatographic detector). Hence, the detectors are only partial electrolysis cells.

Flow-injection system

Generation of absorbing species. Figure 2 shows spectra for the application of the s.e.c. flow cell for flow-injection measurements of *o*-tolidine. These spectra were obtained by applying different potentials to generate the absorbing product. The sample was injected and the wavelength was scanned while the sample zone of highest concentration was in the optical window. Similar spectra were reported for *o*-tolidine in batch s.e.c. systems [10]. Using fixed potential (1.5 V) and wavelength (437 nm), the absorbance peak response increased linearly with increasing concentration in the 0.05—0.25 mM range. Least-squares treatment of the data (n = 5 injections at each of five concentrations) gave the equation: Absorbance = $(185 \pm 5)C(\mathrm{M}) + 0.0016 \pm 0.00084$ with $S_{y/x} = 0.00080$ and $r = 0.999$.

With the s.e.c. flow cell, it was possible to monitor the oxidation of dopamine to its unstable *o*-quinone intermediate [25] and the electrochemical and atmospheric oxidation of *N,N,N',N'*-tetramethyl-*p*-phenylenediamine dihydrochloride (TMPD) to its blue cation radical [25].

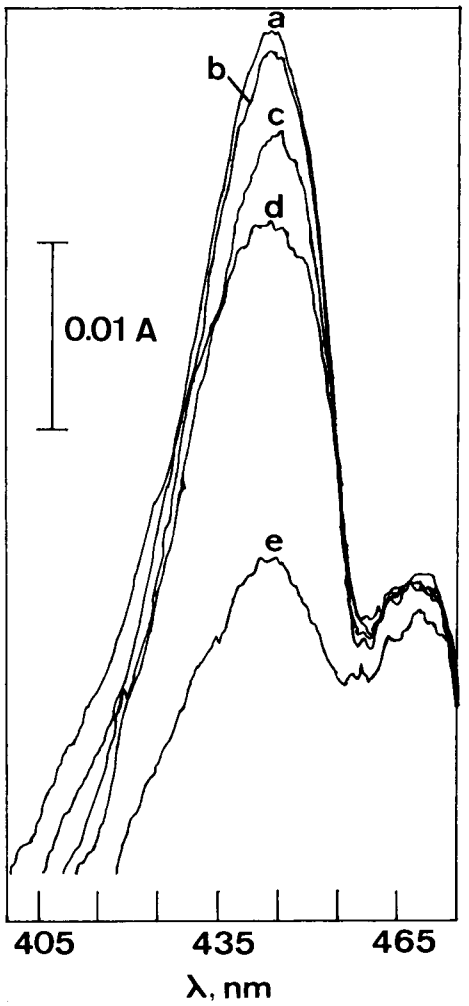

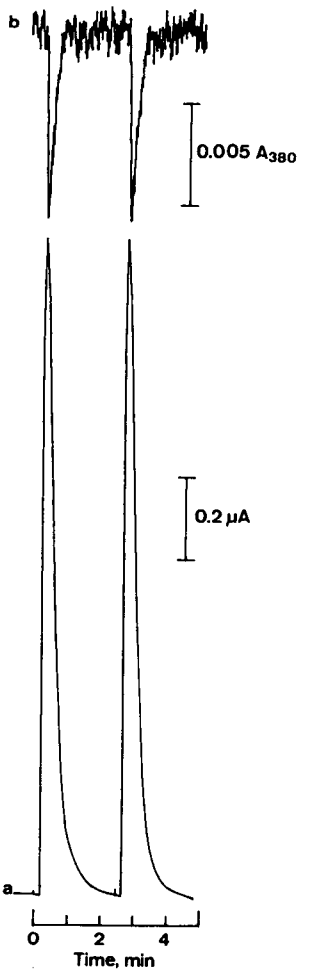

Fig. 2. Absorption spectra of 2.5×10^{-4} M *o*-tolidine in 0.1 M HCl for different values of applied potential: (a) 1.2; (b) 0.9; (c) 0.6; (d) 0.3; (e) 0.0 V vs. Ag/AgCl. Scan rate 120 nm min^{-1}; flow rate 2 ml min^{-1}; sample volume 20 μl.

Fig. 3. Flow-injection system: (a) electrochemical and (b) spectral responses for a mixture of 2.5×10^{-4} M $Fe(CN)_6^{4-}$ and 2.5×10^{-4} M *p*-nitroaniline. Potential +0.9 V vs. Ag/AgCl; 0.1 M phosphate buffer (pH 7.4); flow rate 2 ml min^{-1}; sample volume 20 μl.

Naturally absorbing species. Figure 3 illustrates the use of s.e.c. in a flow-injection system for a mixture of hexacyanoferrate(II) and *p*-nitroaniline. Both hexacyanoferrate(II) and *p*-nitroaniline have absorption maxima near 400 nm, but the nitro group is a much stronger chromophore than the metal—ligand complex, while the hexacyanoferrate is more easily oxidized than the aniline functionality. Thus, Fig. 3(a) presents the oxidation of hexa-

cyanoferrate(II) to hexacyanoferrate(III) and Fig. 3(b) shows the absorption of *p*-nitroaniline. Neither compound interferes with the other at its respective detector.

Figure 4 illustrates another example in which s.e.c. can be used to obtain information on a mixture. Chloro- and nitro-phenols are oxidized at similar potentials, but have different absorption maxima (280 nm and 350 nm, respectively). Figure 4(a, b) shows the flow injection/amperometric response for

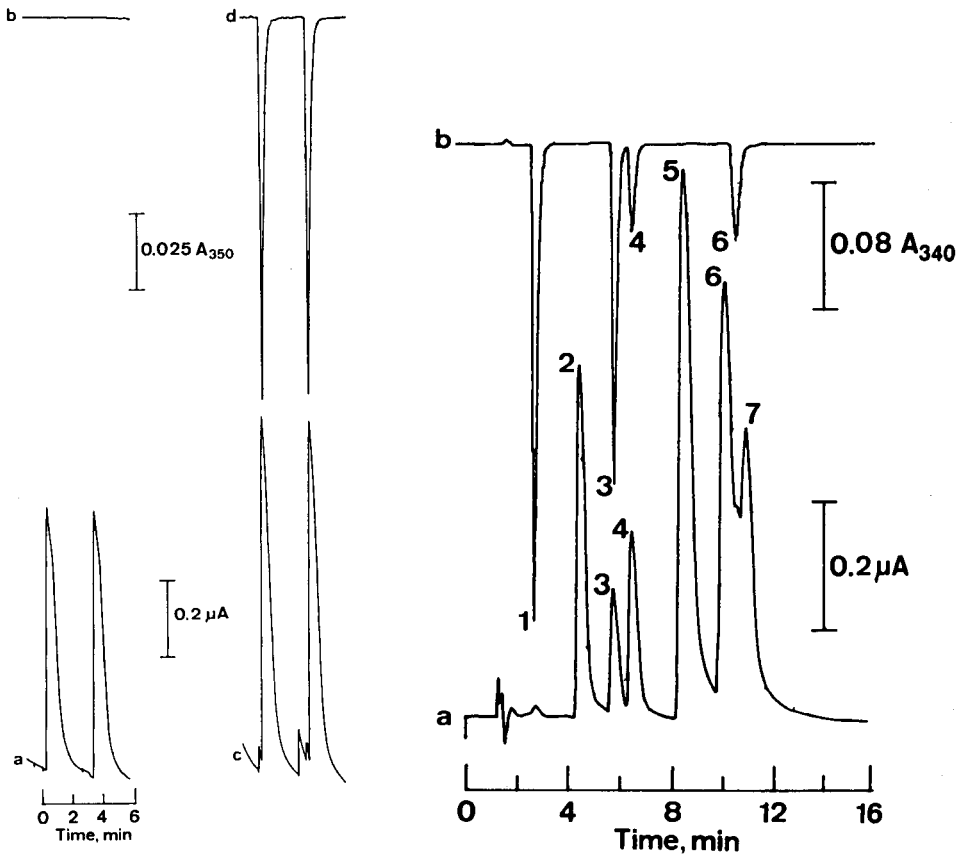

Fig. 4. Flow-injection system: response for oxidation of (a) 3.9×10^{-4} M *p*-chlorophenol at 1.6 V vs. Ag/AgCl; (b) no response obtained at fixed wavelength. 4.2×10^{-3} M *o*-nitrophenol mixed with *p*-chlorophenol solution: electrochemical response (c) is a combined peak while spectral response (d) is solely for *o*-nitrophenol. Supporting electrolyte was 0.2 M $NaClO_4$ and 0.005 M sodium citrate adjusted to pH 4.2 with glacial acetic acid and 25% acetonitrile (v/v). Flow rate 1.5 ml min^{-1}; sample volume 20 μl.

Fig. 5. Liquid chromatograms for mixture of phenols: (a) electrochemical oxidation; (b) visible absorption. Peaks: (1) 1.98 mM picric acid; (2) 0.44 mM phenol; (3) 2.2 mM 2,4-dinitrophenol; (4) 4.37 mM *p*-nitrophenol; (5) 2.05 mM *o*-chlorophenol; (6) 4.45 mM *o*-nitrophenol; (7) 0.79 mM *p*-chlorophenol. Flow rate 1.8 ml min^{-1}; applied potential 1.3 V vs. Ag/AgCl; mobile phase was 0.2 M $NaClO_4$/0.005 M sodium citrate acidified to pH 4.4 with glacial acetic acid and 30% acetonitrile (v/v).

the oxidation of *p*-chlorophenol and the corresponding lack of an absorption peak at 350 nm. When the solution also contained *o*-nitrophenol, a combined oxidation peak was recorded, as in Fig. 4(c), but the absorption peak would be assigned to the *o*-nitrophenol (Fig. 4d). The wavelength could then be changed to the maximum of the *p*-chlorophenol and its absorption measured, if desired, if the s.e.c. detector were made of quartz.

A series of ten successive injections of a 0.5 mM *o*-nitrophenol solution was used to evaluate the precision of the responses. A mean peak absorbance of 0.059 with a range of 0.056—0.064 and a relative standard deviation of 4.8% were obtained at 350 nm. A mean peak current of 0.40 μA with a range of 0.38—0.41 μA and a relative standard deviation of 2.6% were obtained at +1.3 V for 200 μl of sample flowing at 2.0 ml min^{-1}.

Liquid chromatography

Spectroelectrochemical detection is analogous to dual (parallel)-electrode [26] or dual-wavelength [27] detection schemes. The compounds chosen for this study were phenols because of their amenability to both absorbance and electrochemical measurements. The liquid chromatograms shown in Fig. 5 are for a mixture of chloro- and nitro-phenols, as well as phenol itself. An absorption wavelength of 340 nm was chosen for spectral observation of the nitro chromophore. In Fig. 5(a), six of the seven compounds in the sample solution were oxidizable at the potential applied (1.3 V vs. Ag/AgCl); only picric acid with its three strong electron-withdrawing nitro groups was not. However, in the absorbance chromatogram (Fig. 5b), the picric acid is observed as a large peak, because of its large absorptivity. The porous nature of the RVC electrode results in some extra-column peak broadening, but resolution is still good. Peaks 6 and 7, for *o*-nitrophenol and *p*-chlorophenol, have incomplete baseline resolution. If a slight increase in the organic modifier (from 30% to 40% acetonitrile) is made, the two compounds co-elute. For samples containing more highly substituted phenols, (e.g., 2,4-dichlorophenol, 2,4,5-trichlorophenol or pentachlorophenol) the organic modifier has to be increased significantly in order to achieve reasonable elution times. Thus, the s.e.c./l.c. approach would indicate where overlapping peaks of lower substituted phenols are occurring.

In addition to simultaneous detection, the RVC electrode can serve as a conditioning electrode for improving the selectivity via an additional redox or screen step (e.g., change of the oxidation state of an eluting compound that changes its optical properties). In this way, responsive analytes can be obtained by on-line, post-column electrochemical derivatization. Similarly, an opposite flow direction (optical followed by electrochemical) can be used to produce electrochemically active species in an on-line photolysis.

REFERENCES

1 T. Kuwana, R. K. Darlington and D. W. Leedy, Anal. Chem., 36 (1964) 2023.
2 T. Kuwana, Ber. Bunsenges. Phys. Chem., 77 (1973) 858.
3 N. Winograd and T. Kuwana, in A. J. Bard (Ed.), Spectroelectrochemistry at Optically Transparent Electrodes in Electroanalytical Chemistry, Vol. 7, M. Dekker, New York, 1974.
4 T. Kuwana and W. R. Heineman, Acc. Chem. Res., 9 (1976) 241.
5 W. R. Heineman, Anal. Chem., 50 (1978) 390A.
6 W. N. Hansen, R. A. Osteryoung and T. Kuwana, J. Am. Chem. Soc., 88 (1966) 1062.
7 W. N. Hansen, T. Kuwana and R. A. Osteryoung, Anal. Chem., 38 (1966) 1810.
8 R. W. Murray, W. R. Heineman and G. W. O'Dom, Anal. Chem., 39 (1967) 1666.
9 A. Yildiz, P. T. Kissinger and C. N. Reilley, Anal. Chem., 40 (1968) 1018.
10 T. P. DeAngelis and W. R. Heineman, J. Chem. Educ., 53 (1976) 594.
11 E. F. Bowden, D. J. Cohen and F. M. Hawkridge, Anal. Chem., 54 (1982) 1005.
12 E. C. Bancroft, J. S. Sidwell and H. N. Blount, Anal. Chem., 53 (1981) 1390.
13 H. A. Mottola, Anal. Chem., 53 (1981) 1312A.
14 J. Růžička and E. H. Hansen, Flow Injection Analysis, Wiley-Interscience, New York, 1981.
15 T. M. Vickrey (Ed.), Liquid Chromatography Detectors, M. Dekker, New York, 1983.
16 T. C. Pinkerton, K. Hajizadeh, E. Deutsch and W. R. Heineman, Anal. Chem., 52 (1980) 1542.
17 A. N. Strohl and D. J. Curran, Anal. Chem., 51 (1979) 353.
18 W. J. Blaedel and J. Wang, Anal. Chem., 51 (1979) 799.
19 J. Wang and H. D. Dewald, J. Chromatogr., 285 (1984) 281.
20 D. J. Curran and T. P. Tougas, Anal. Chem., 56 (1984) 672.
21 J. Wang and H. D. Dewald, Talanta, 29 (1982) 453.
22 J. Wang, Electrochim. Acta, 26 (1981) 1721.
23 V. E. Norvell and G. Mamantov, Anal. Chem., 49 (1977) 1470.
24 J. L. Owens, H. A. Marsh and G. Dryhurst, J. Electroanal. Chem., 91 (1978) 231.
25 J. S. Mayausky and R. L. McCreery, Anal. Chem., 55 (1983) 308.
26 D. A. Roston, R. E. Shoup and P. T. Kissinger, Anal. Chem., 54 (1982) 1417A.
27 K. Sartoh and N. Suzuki, Anal. Chem., 51 (1979) 1683.

Analytica Chimica Acta, 166 (1984) 171—177
Elsevier Science Publishers B.V., Amsterdam — Printed in The Netherlands

EVALUATION OF HIGH-PERFORMANCE LIQUID CHROMATOGRAPHY WITH A DUAL WORKING-ELECTRODE ELECTROCHEMICAL DETECTOR FOR THE DETERMINATION OF CATECHOLAMINES IN HUMAN CEREBROSPINAL FLUID

SAM A. McCLINTOCK and WILLIAM C. PURDY*

Department of Chemistry, McGill University, 801 Sherbrooke St. West, Montreal, Quebec H3A 2K6 (Canada)

SIMON N. YOUNG

Department of Psychiatry, McGill University, 1033 Pine Avenue West, Montreal, Quebec H3A 1A1 (Canada)

(Received 7th June 1984)

SUMMARY

A procedure is described for quantifying norepinephrine [1-(3,4-dihydroxyphenyl)-2-aminoethanol] and dopamine [4-(2-aminoethyl)-1,2-benzenediol] in cerebrospinal fluid by high-performance liquid chromatography (h.p.l.c.) with dual working-electrode electrochemical detection. An ion-pairing reversed-phase h.p.l.c. technique is used after clean-up and preconcentration of the fluid on alumina. The dual working-electrode electrochemical detector used provides amplification in the electrochemical response per unit concentration of material passing through the detector. This is achieved by locating two working electrodes on the opposite walls of a thin-layer cell, holding them close together and at potentials that will induce a sequence of oxidations/reductions. The greater the number of oxidation/reduction cycles, the greater the amplification of the electrochemical response. Peak height ratios are linear over the range expected and detection limits are 3 pg for norepinephrine and 5 pg for dopamine. The concentrations of norepinephrine and dopamine in human cerebrospinal fluid were found to be 141 pg ml^{-1} and 262 pg ml^{-1} with relative standard deviations of 6.8 and 5.8%, respectively.

One of the most popular methods for studying catecholamine metabolism in the central nervous system of living humans is to determine catecholamine metabolites in cerebrospinal fluid. There is good evidence that levels of homovanillic acid and 3-methoxy-4-hydroxyphenylethylene glycol (MHPEG) in cerebrospinal fluid reflect metabolism of the parent amines (dopamine and norepinephrine) in the central nervous system [1]. Amounts of homovanillic acid and MHPEG are determined because they are the main metabolites. The minor unmethylated metabolites, dihydroxyphenylacetic acid and dihydroxyphenylethylene glycol, are present in human cerebrospinal fluid at about 1.4% [2] and 20% [3], respectively, of the concentration of their *O*-methylated analogues. Recent evidence indicates that dopamine can also be metabolized to its conjugate, which is present in human cerebrospinal fluid [4].

0003-2670/84/$03.00

In studies of such fluids, amine metabolites have usually been determined. However, with suitable methodology it would be preferable to determine the amines, rather than their metabolites. In some circumstances, the levels of dopamine and homovanillic acid [5] and of norepinephrine and MHPEG [3] in cerebrospinal fluid show significant positive correlations, suggesting that the amine metabolites can reflect functionally significant amine levels in the central nervous system. However, this is not always necessarily so. For example, antidepressants, such as monoamine oxidase inhibitors and tricyclic uptake inhibitors, will decrease the levels of catecholamine metabolites, because of inhibition of metabolite formation by the monoamine oxidase inhibitors or because of a secondary decrease in amine metabolism caused by the uptake inhibitors. The decline in metabolite levels obviously does not reflect the increased amine function. The greater usefulness of catecholamine measurements in cerebrospinal fluid in such circumstances is illustrated by the finding that the increase in norepinephrine on treatment of depressed patients with a monamine oxidase inhibitor is highly correlated with clinical response [6].

Radio-enzymatic assays of sufficient sensitivity have been developed for norepinephrine and dopamine in cerebrospinal fluid; however, samples require extensive preparation and manipulation [7, 8]. Gas chromatography/mass spectrometry (g.c./m.s.) has also been used in the determination of norepinephrine and dopamine in such fluid; this has been done by the technique of mass fragmentometry (selective-ion monitoring). The main problems with this technique are not only the high cost and limited availability of equipment but that catecholamines do not possess suitable thermal properties; therefore, tedious derivatization is needed [7, 9, 10]. Liquid chromatography with electrochemical detection based on a single working electrode has become firmly established as a major technique for the separation and detection of trace amounts of electroactive species [11], but its use for cerebrospinal fluid is still limited to the determination of norepinephrine and dopamine metabolites [12—14] which appear in higher concentrations than the parent amine. Recently, attention has been focused on the inclusion of more than one working electrode in electrochemical detectors [15]. Such cells have become known as dual or multiple working-electrode detectors and have been used to improve either the selectivity or the sensitivity of a particular chromatographic measurement.

The detector used in this work is a parallel-opposed dual electrode detector, which means it has two working electrodes located on the opposite walls of a thin-layer cell. In the simplest case, for any compound that is electrochemically reversible or quasireversible, one electrode is held at a potential at which oxidation takes place and the second electrode is held at a potential at which this oxidized form is reduced back to the starting material. The current produced increases proportionally to the number of conversions that take place at each working electrode. This has the effect of producing a larger signal for a given amount of material. Weber and Purdy [16] have analyzed

the geometric requirements for a coulometric-type cell and McClintock and Purdy [17, 18] have designed a detector that improves the signal-to-noise ratio for a set of catecholamine standards by as much as a factor of six. This paper describes the use of this type of detector combined with h.p.l.c. to provide a routine method for the determination of norepinephrine and dopamine in cerebrospinal fluid.

EXPERIMENTAL

Apparatus and reagents

The h.p.l.c. system was constructed from an M6000-A pump (Waters Associates), an injection valve (Valco Instrument, Houston, TX) and Heath-Schlumberger recorders. The design and construction of the dual working-electrode detector and controlling electronics have been described previously [17, 18]. The potential of one electrode was set at +0.75 V vs. Ag/AgCl and the second electrode was set at −0.1 V vs. Ag/AgCl. The outputs from the two electrodes were added and the combined signal was filtered with an 8-pole low-pass Butterworth filter with a 1-Hz cut-off frequency.

Materials and their sources were as follows: norepinephrine(arterenol)-hydrogentartrate and dopamine(3-hydroxytyramine)hydrochloride (Sigma Chemical Co.), 3,4-dihydroxybenzylamine hydrobromide (Aldrich Chemical Co.), sodium octyl sulfate (Eastman Kodak) and acid-washed aluminum oxide (Bioanalytical Systems, West Lafayette, IN).

Chromatographic conditions

The chromatographic conditions chosen were a mobile phase consisting of 97% 0.07 M phosphate buffer, pH 3.0, containing 500 mg l^{-1} sodium octyl sulfate, and 50 mg l^{-1} EDTA and 3% methanol with a 15-cm column packed with 5-μm C_{18} Spherisorb, (C.S.C., Town of Mount Royal, Quebec). The mobile phase was pumped at a flow rate of 1 ml min^{-1}. It should be noted that these conditions may need to be adjusted slightly, depending on the type, age, and previous history of the packing material.

Sample preparation

The cerebrospinal fluid was a pooled sample from a general hospital population with a variety of neurological disorders. Fluid remaining after routine determinations was pooled and divided into 1-ml plastic vials and frozen at −70°C. These aliquots were thawed just before use. The separation and concentration of norepinephrine and dopamine from biological samples by adsorption onto alumina has been thoroughly documented in the classical study by Anton and Sayre [19]. In alkaline solution, pH 8.6, catecholamines selectively form a stable complex with alumina, which can be washed to remove undesired compounds from the sample. The catecholamines can then be stripped from the alumina with dilute acid. This technique has been used successfully for norepinephrine and dopamine in rat brain parts [19—21],

and was adapted for use in this study. An aliquot (1 ml) of standard solution containing a known amount of catecholamine or 1 ml of cerebrospinal fluid was transferred to a plastic screw-cap vial which contained 1 ml of pH 8.6 Tris buffer and 90 mg of alumina. The vial was immediately vortexed for 1 min and then shaken on a reciprocal shaker for 10 min. The alumina was allowed to settle and the supernatant liquid was removed by aspiration. The alumina was washed three times with 3 ml of distilled water, the excess of water being aspirated after each washing. After 50 μl of 0.1 M perchloric acid had been added, the vial was vortexed again for 1 min and centrifuged at 3000 rpm for 5 min. The supernatant liquid was then ready for injection into the h.p.l.c. system.

RESULTS AND DISCUSSION

Chromatography

The first step in establishing a separation for norepinephrine and dopamine in cerebrospinal fluid was to consider the various factors which influence the retention of these substances. Three extensive studies [22—24] which elucidate the empirical effects of pH, ionic strength of the buffer, "ion-pair" carbon chain length, "ion-pair" concentration, and mobile-phase organic modifier on the separation of catecholamines were used as a starting point for this study. As can be seen from Fig. 1, mobile-phase conditions were adjusted until adequate separation was achieved. Four peaks can be detected after the clean-up and preconcentration procedure, the two of interest, the internal standard and an interfering compound with a retention time close to norepinephrine.

System linearity

The linearity of the response for norepinephrine and dopamine was established in two ways. First, the system was tested with aqueous standards from 10 pg to 1000 pg (the expected range for catecholamines in cerebrospinal fluid). The detector response was linear for both substances with least-squares equations of current (nA) vs. mass (pg) of

$y = -0.015(\pm 0.003) + 0.026(\pm 0.0002)x$ (norepinephrine)

$y = 0.055(\pm 0.004) + 0.014(\pm 0.0002)x$ (dopamine)

with a standard estimate of error of 0.217 for norepinephrine and 0.164 for dopamine and $r = 0.999$ in each case.

Secondly, the system was tested by adding standard amounts of norepinephrine and dopamine (100—400 pg ml^{-1}) to a pooled sample of cerebrospinal fluid. The detector response was again linear for both compounds, with least-squares fits of current (nA) vs. mass (pg) giving

$y = 1.300(\pm 0.102) + 0.0095(\pm 0.0002)x$ (norepinephrine)

$y = 2.046(\pm 0.315) + 0.0081(\pm 0.0004)x$ (dopamine)

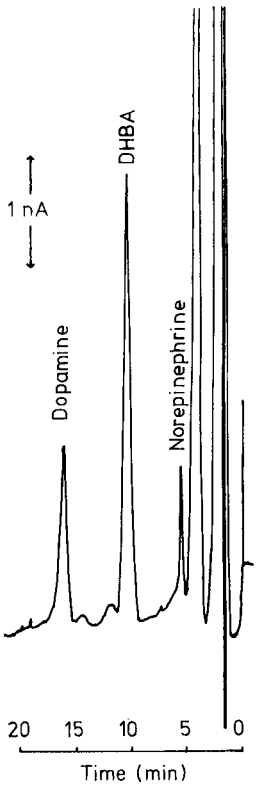

Fig. 1. Chromatogram for a 1-ml sample of human cerebrospinal fluid extracted on alumina and reconstituted in 50 μl of 0.1 M perchloric acid and injected into the h.p.l.c. For chromatographic conditions see text.

with a standard estimate of error of 0.056 for norepinephrine and 0.112 for dopamine and $r = 0.999$ in each case.

Recovery, precision and detection limits

Data in Table 1 summarize the recovery and precision for the norepinephrine and dopamine. The extraction efficiencies are somewhat lower than

TABLE 1

Typical values obtained with the proposed method

	Norepinephrine	Dopamine
Mean for cerebrospinal fluid sample ($n = 7$)	141 pg ml^{-1}	262 pg ml^{-1}
R.s.d. (%)	6.8	5.8
Extraction efficiency for stds. ($n = 10$)	51.4%	56.4%
R.s.d. (%)	5.1	3.8

the 60% reported in another study [20]; this may be accounted for by the smaller amounts of material being examined.

If the detection limit is defined as a signal that is twice the peak-to-peak background noise, then the detection limits are 3 pg for norepinephrine and 5 pg for dopamine.

The concentrations of norepinephrine and dopamine in the pooled cerebrospinal fluid sample were quantified by the technique of standard addition, in a similar manner to the linearity study. The values established (see Table 1) are in the expected range and compare well with the few other studies available for comparison [7, 8, 25].

Conclusion

To validate the procedure fully, samples from a wide range of patients with various clinical conditions will be required in order to establish that this technique, which has the capability of monitoring norepinephrine levels as low as 20 pg ml^{-1} and dopamine levels as low as 30 pg ml^{-1} routinely, can cover the range required. The use of h.p.l.c. with dual working-electrode detection has been shown to operate successfully, permitting for the first time, the quantitation of norepinephrine and dopamine in human cerebrospinal fluid by this technique.

The authors are indebted to the Natural Sciences and Engineering Research Council and the Medical Research Council of Canada for support of this work, which is taken (in part) from the Ph.D. dissertation (1983) of S. A. M.

REFERENCES

1 E. Garelis, S. N. Young, S. Lal and T. L. Sourkes, Brain Res., 79 (1974) 1.
2 F. Karoum, W. Bunney, J. C. Gillin, D. Jimerson, D. van Kammen and R. J. Wyatt, Biochem. Pharmacol., 26 (1977) 629.
3 J. C. Ballenger, R. M. Post and F. K. Goodwin, in J. H. Wood (Ed.), Neurobiology of Cerebrospinal Fluid, Vol. 2, Plenum Press, New York, 1983, p. 143.
4 N. S. Sharpless, G. T. Tyce, L. J. Rhal, J. M. Waltz, K. Tabaddor and L. I. Wolfson, Brain Res., 217 (1981) 107.
5 G. Bagdy, M. Arato, K. Baraczka and M. I. K. Fekete, Life Sci., 32 (1983) 2667.
6 L. F. Major, C. R. Lake, S. Lipper, P. Lerner and D. L. Murphy, Prog. Neuropsychopharmacol., 3 (1979) 5.
7 M. G. Zeigler, C. R. Lake, F. H. Foppen, I. Shoulson and I. J. Kopin, Brain Res., 108 (1976) 436.
8 J. Montplaisir, J. de Champlain, S. N. Young, K. Missala, T. L. Sourkes, J. Walsh and G. Remillard, Neurology, 32 (1982) 1299.
9 F. Cattabeni, S. H. Koslow and E. Costa, Science, 178 (1972) 166.
10 F. Artigas and E. Gelpi, Anal. Biochem., 92 (1979) 223.
11 R. E. Shoup (Ed.), Recent Reports on Liquid Chromatography/Electrochemistry, Bioanalytical Systems Press, West Lafayette, IN, 1982.
12 R. M. Whightman, P. M. Plotsky, E. Strope, J. R. Delecore and R. N. Adams, Brain Res., 131 (1977) 345.
13 G. M. Anderson, J. G. Young, D. J. Cohen, B. A. Shaywitz and D. K. Batter, J. Chromatogr., 222 (1981) 112.

14 P. J. Langlais, W. J. McEntee and E. D. Bird, Clin. Chem., 26 (1980) 786.
15 D. A. Roston, R. E. Shoup and P. T. Kissinger, Anal. Chem., 54 (1982) 1417A.
16 S. G. Weber and W. C. Purdy, Anal. Chem., 54 (1982) 1757.
17 S. A. McClintock and W. C. Purdy, Anal. Lett., 14(B10) (1981) 791.
18 S. A. McClintock and W. C. Purdy, Anal. Chim. Acta, 148 (1983) 127.
19 A. H. Anton and D. F. Sayre, J. Pharmacol. Exp. Ther., 138 (1962) 360.
20 L. J. Felice, J. D. Felice and P. T. Kissinger, J. Neurochem., 31 (1978) 1461.
21 S. K. Salzman and M. S. Sellers, J. Chromatogr., 232 (1982) 29.
22 J. H. Knox and J. Jurand, J. Chromatogr., 125 (1976) 89.
23 T. P. Moyer and N. S. Jiang, J. Chromatogr., 153 (1978) 365.
24 I. Molnar and C. Horvath, J. Chromatogr., 145 (1978) 371.
25 J. H. Wood (Ed.), Neurobiology of Cerebrospinal Fluid, Plenum Press, New York, 1980, p. 153.

Analytica Chimica Acta, 166 (1984) 179—188
Elsevier Science Publishers B.V., Amsterdam — Printed in The Netherlands

DETERMINATION OF FATTY ACID METHYL ESTERS
Elimination of Tissue-Derived Contamination and Artefacts and Preparation of a Support-Coated Acid-Modified Polyester Liquid Phase

EDWARD J. MATUSIK, Jr.*, VALERIE B. REEVES and VINCENT P. FLANAGAN

Lipid Nutrition Laboratory, Beltsville Human Nutrition Research Center, Agricultural Research Service, U.S. Department of Agriculture, Beltsville, MD 20705 (U.S.A.)

(Received 29th May 1984)

SUMMARY

Fatty acid methyl esters made by transesterification of extracted plasma lipids with methanolic hydrochloric acid were found to contain substances which interfered with quantitation by gas-liquid chromatography. A method to eliminate most interfering materials and a procedure that allows reproducible wetting of an inert support with acid-modified ethylene glycol succinate are reported. Hydrocarbon contamination and artefacts produced during transesterification from substances native to tissue matrices were identified by gas chromatography/mass spectrometry and removed by chromatography over 6% hydrated alumina. Ethylene glycol succinate was treated with orthophosphoric acid to improve wetting of silanized supports and extend the thermal stability of the polymer. Quantitation was achieved by using synthetic triheptadecanoin as an internal standard.

Routine determinations of fatty acids in human plasma still present challenging chemical problems. Generally, reagents are cited as causing sample contamination, but procedural artefacts originating from naturally occurring materials in the sample matrix can be even more troublesome. Straight- and branched-chain alkane and alkene contamination could occur from solvent sources, but it has been shown that these hydrocarbons are also native to tissues [1, 2]. Mixed phthalic acid esters and octadecanoic acid esterified with ethyl-, butyl-, and longer-chained alcohols are commonly used plasticizers which could be leached into extraction solvents from container caps. Because of the prevalence of plastic packaging, these synthetic additives are being detected in biological systems more frequently even when special precautions are taken to exclude external contamination during sample preparation [3, 4].

The procedure proposed here was developed to provide the operator with maximum control over the chemical purity of a mixture of methylated fatty acids derived from complex lipids. It has been found that by using these modifications, a laboratory dedicated to fatty acid analysis can achieve a high degree of precision with increased confidence in component identification.

EXPERIMENTAL

Materials

Organic solvents (AR brand; Mallinckrodt) were redistilled before use. Acetyl chloride (reagent grade), diethyl ether (for spectrophotometry), and neutral alumina (Brockman Activity I, 80/200 mesh) were used without further purification. Lipid and methyl ester standards and all other supplies for gas-liquid chromatography (g.l.c.) came from Supelco.

Preparation of modified ethylene glycol succinate (EGS). Ethylene glycol succinate polymer (25 g) was placed in a 2-l beaker. Approximately 200 ml of methanol was added and the beaker was heated on a steam bath. While heating, chloroform was added slowly until all solids were dissolved. The liquid was brought to a boil and the volume was reduced by 25%. The beaker was covered and allowed to cool to room temperature. After 12 h, the remaining liquid was decanted and the solid was dried in a vacuum oven at 100°C and 20 torr.

A ratio of 21 mg (0.22 mmole) of orthophosphoric acid per gram of polymer was used. For 25 g of polymer, 0.35 ml of 85% phosphoric acid was dissolved in a minimum volume of methanol. The methanol solution was added with stirring to a chloroform solution of EGS and the solvent was evaporated on a steam table. The white solid was pulverized and then stored in a glass jar. Modified EGS had a maximum shelf life of six months at room temperature.

Supelcoport (100/120 mesh) was coated at a 10% level (1 g liquid phase/9 g support) with modified EGS by a slurry technique. After air-drying, the coated support was resized to 100/120 mesh and two 1.8-m stainless steel columns (3.2 mm o.d. × 2.1 mm i.d.) were packed; one column was used as the reference and the other as the separation column. Columns must be conditioned for 48 h at 210°C with a helium flow of 30 ml min^{-1}. After curing, columns not in use are maintained at 200°C with reduced carrier gas flow. For prolonged storage, cured packed columns were found to be stable up to two years at room temperature.

Flow rates, temperatures and times used for quantitation are given in the legend of Fig. 1.

Instrumentation

Either a Hewlett-Packard 5700A gas chromatograph coupled to a model 3385A automation system or a Hewlett-Packard 5840A gas chromatograph was used. All instruments were equipped with dual flame-ionization detectors and model 7671A automatic samplers. Detection was in the dual differential mode.

Electron-impact mass spectra (70 eV ionizing energy) were obtained on a Hitachi, RMU-6E magnetic sector mass spectrometer under the control of a Finnigan INCOS 2300 data system. The mass spectrometer was interfaced to a Hewlett-Packard 5750 gas chromatograph by means of a single-stage glass

jet separator. A 1.8-m × 2-mm i.d. glass column packed with 5% SP 2340 on Chromosorb W/AW (100/120 mesh) was used for chromatography.

Procedures

Lipid extraction. Plasma lipids were extracted by a modification of a method by Sperry and Brand [5]. A 50-ml screw-cap test tube was substituted for the volumetric glassware used [5]. Chloroform (0.5 ml) containing 0.50 mg of triheptadecanoin was placed in the tube followed by 8.5 ml of methanol. A portion (1 ml) of plasma was introduced, the contents were swirled gently, and 8.5 ml of chloroform was added. The tube was capped and the contents were mixed on a vortex mixer. After heating for 8 min at 80° C in a water bath, the tube was cooled and the contents were supplemented with 7.0 ml of chloroform.

Further purification of the extract was an adaptation of Sperry and Brand's "Procedure 2" [5]. The organic phase was first washed with water as in the original procedure and then treated with a 1.8 mM calcium chloride "upper phase" wash solution equilibrated with 0.6 times its volume of a 2:1 chloroform/methanol (v/v) mixture. To expedite phase separations during washes, tubes were centrifuged at 1000 rpm for 10 min at 4° C.

After back-washing was complete, the organic phase was transferred to a 25-ml screw-cap test tube and the solvent was evaporated to dryness with a stream of clean, dry nitrogen. The residue was redissolved in fresh 2:1 chloroform/methanol and stored at −25° C until processed further.

Methylation. Fatty acid methyl esters (FAME) were prepared through transesterification with a methanolic hydrochloric acid reagent [6]. Solutions of lipid with 5 ml of reagent in tightly sealed 25-ml screw-capped test tubes were heated for 2 h at 80° C. When the samples were cool, 5 ml of water was added slowly, and the esters were extracted with three 3-ml portions of hexane. The hexane aliquots were pooled in a glass-stoppered 15-ml conical centrifuge tube and evaporated to dryness at room temperature with nitrogen. The waxy white solid was redissolved in 0.1 ml of hexane prior to alumina column chromatography.

Alumina chromatography. Brockman Activity I neutral alumina was hydrated to a 6% level by adding 30 ml of water to 500 g of the solid. Disposable glass pipets (Fisher Scientific, Catalog 13-678-8), 4-ml volume, were plugged loosely with silanized glass wool. Hydrated alumina (3 g) was dry-packed into the pipet and a small quantity of washed ignited sea sand was layered on top. The column was rinsed with 15 ml of hexane. The methylated sample was placed on the column with a 100-μl syringe, the syringe was rinsed once with hexane and this rinse also was placed on the column. Materials less polar than FAMEs were eluted with 5 ml of hexane. The solvent was changed to a 10% diethyl ether in hexane. The next 5 ml was saved as the FAME fraction.

Solvent was removed from the FAME fraction with nitrogen at room temperature. The resulting clear odorless oil was quantitatively transferred to

a 5-ml volumetric flask with several rinses of iso-octane, and diluted to volume with iso-octane. An appropriate aliquot of this solution was placed in an autoinjector vial for g.l.c. The extent of loss of individual FAME components caused by alumina chromatography was measured with aliquots of the FAME standard mix used for instrument calibration. The aliquots were evaporated and chromatographed on alumina as described for methylated samples. The recovered FAME fraction was reconstituted to the original aliquot volume and component concentrations quantified by g.l.c.

RESULTS

Overall method precision was tested with a single plasma sample (Table 1). Additional samples obtained by venipuncture from 24 male volunteers ranging from 41 to 67 years of age were examined. Each subject was sampled on three separate occasions spaced at 14-day intervals. These data are presented in Table 2.

Recovery of heptadecanoic acid (internal standard) added to all samples as a synthetic triacylglycerol was 94.00 ± 0.01% (SEM) for 686 plasma samples processed during a six-month period.

Alumina chromatography

Recovery of a standard FAME mixture is illustrated in Table 3. Esters were recovered at a 95% level or greater with a mean recovery of 97.8%. Fractions of FAME derived from plasma lipids after alumina treatment appeared, after solvent evaporation, as odorless clear oily droplets which dissolved readily in iso-octane.

TABLE 1

Replicate total fatty acid composition from a single plasma sample

Fatty acid[a]	Mean plasma concentration (mg dl^{-1})	Standard error (n = 12)	Percent of total	Fatty acid[a]	Mean plasma concentration (mg dl^{-1})	Standard error (n = 12)	Percent of total
12:0	0.35	0.01	0.1	20:0	4.64	0.04	1.2
14:0	6.07	0.05	1.6	20:3ω6	7.52	0.06	2.0
15:0	0.86	0.03	0.2	20:4ω6	29.85	0.21	7.9
16:0	94.93	0.69	25.3	20:5ω3	2.79	0.03	0.7
16:1ω7	13.73	0.11	3.7	22:5ω3	2.29	0.02	0.6
18:0	24.97	0.18	6.6	22:6ω3	4.30	0.04	1.1
18:1ω9	82.86	0.68	22.1	24:0	2.21	0.05	0.6
18:2ω6	92.01	0.82	24.5	24:1ω9	3.68	0.03	1.0
18:3ω3	2.81	0.02	0.8				

[a]Acid chain length:no. of double bonds.

TABLE 2

Total fatty acids in adult male plasma

Fatty acid[a]	Mean plasma concentration (mg dl^{-1})	Range (mg dl^{-1})	Percent of total	Fatty acid[a]	Mean plasma concentration (mg dl^{-1})	Range (mg dl^{-1})	Percent of total
16:0	73.52	47.9—110.2	21.8	20:0	1.74	1.1—2.5	0.5
16:1ω7	7.89	2.2—13.8	2.3	20:3ω6	6.65	4.3—9.2	2.0
18:0	22.84	15.3—34.3	6.8	20:4ω6	25.48	17.3—41.9	7.5
18:1ω9	79.86	51.1—130.9	23.6	22:6ω3	5.04	3.2—11.6	1.5
18:2ω6	107.92	73.9—139.6	31.9	24:0	1.45	0.8—2.0	0.4
18:3ω3	2.75	1.6—5.1	0.8	24:1ω9	2.74	1.5—3.4	0.8
				Total	337.88	242.9—493.4[b]	

[a]Acid chain length:no. of double bonds. [b]Normal range is 150—500 mg dl^{-1} [7].

TABLE 3

Recovery of FAME after alumina chromatography

FAME[a]	Initial concentration (ng μl^{-1})	Final concentration (ng μl^{-1} ± SE)[b]	Recovery (%)
14:0	47.26	43.48 ± 0.13	92
16:0	197.72	195.74 ± 0.03	99
17:0	150.64	150.64 ± 0.27	100
18:0	122.86	119.17 ± 0.41	97
18:2ω6	152.68	149.63 ± 0.14	98
20:4ω6	181.26	177.64 ± 1.60	98
22:6ω3	83.94	83.10 ± 0.44	99
24:0	41.00	40.59 ± 0.44	99

[a]Acid chain length:no. of double bonds. [b]$n = 4$.

Modified EGS and gas-liquid chromatography

The melting point range of EGS as purchased was found to be 75—97° C. After precipitation from a methanol/chloroform solution, the range narrowed to 93—97° C and remained unchanged after phosphoric acid addition. No discoloration was observed in the melt of polymer supplemented with mineral acid and heated to 200° C. Supelcoport remained a free flowing solid after coating with 10% (w/w) modified liquid phase. One 1.8-m column required approximately 2.3 g of coated support.

A chromatogram of a standard FAME mixture used for peak identification is shown in Fig. 1. Total run time was 95 min. Resolution (R) between methyl eicosanoate and methyl linolenate calculated by the equation $R = 2d/(w_1 + w_2)$ (where d is the separation between peak centers, and w_n the base peak width) was 1.6, indicating complete resolution.

Solutions of FAME's with concentrations ranging from 0.012 to 1.5 μg ml^{-1} were run to establish a linear range for instrumental response. By linear

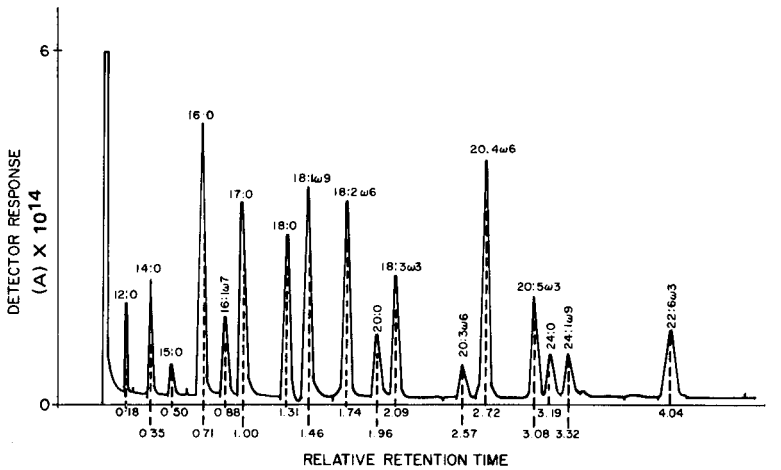

Fig. 1. Chromatogram of a standard FAME mixture. Peaks are identified as chain-length:number of double bonds and position of the first double bond from the methyl terminal end of the molecule. Instrument conditions were: injector temperature 200°C; detector temperature 250°C; carrier flow (He) 20 ml min^{-1}. Temperature program: initial temperature 140°C held for 16 min after injection; rate 1°C min^{-1}; upper temperature of 190°C held for 32 min.

regression, a squared correlation coefficient (r^2) of 0.9999 was obtained when the integrated area was plotted against concentration.

Figure 2A shows the total fatty acid profile of human plasma. Table 1 gives the sample composition. The reconstructed ion chromatogram generated by gas chromatography/mass spectrometry during component verification of the sample is shown in Fig. 2B. The mass spectrum associated with each peak was compared with that of authentic material for positive identification. Figure 2C, D are the g.l.c. and reconstructed ion chromatograms, respectively, of the same sample before alumina cleanup. The peak at a relative retention time (RRT) of 4.14 is attributable to cholest-3,5-diene.

DISCUSSION

Three problem areas can be defined in attempting precise analysis for fatty acids in lipids from biological matrices. They are incomplete extraction and conversion to the desired derivatized form for separation and measurement, difficulty in obtaining a solution of the derivatives which is chemically homogeneous, and instrumental problems associated with obtaining the necessary resolution and precision. The literature is rich in modifications of extraction procedures to isolate lipids. Original work by Folch et al. [7–9] and simultaneously but independently by Sperry and Brand [5], demonstrated two approaches differing slightly in the ratios of organic to aqueous phases for producing lipid extracts. Sperry and Brand's basic methodology

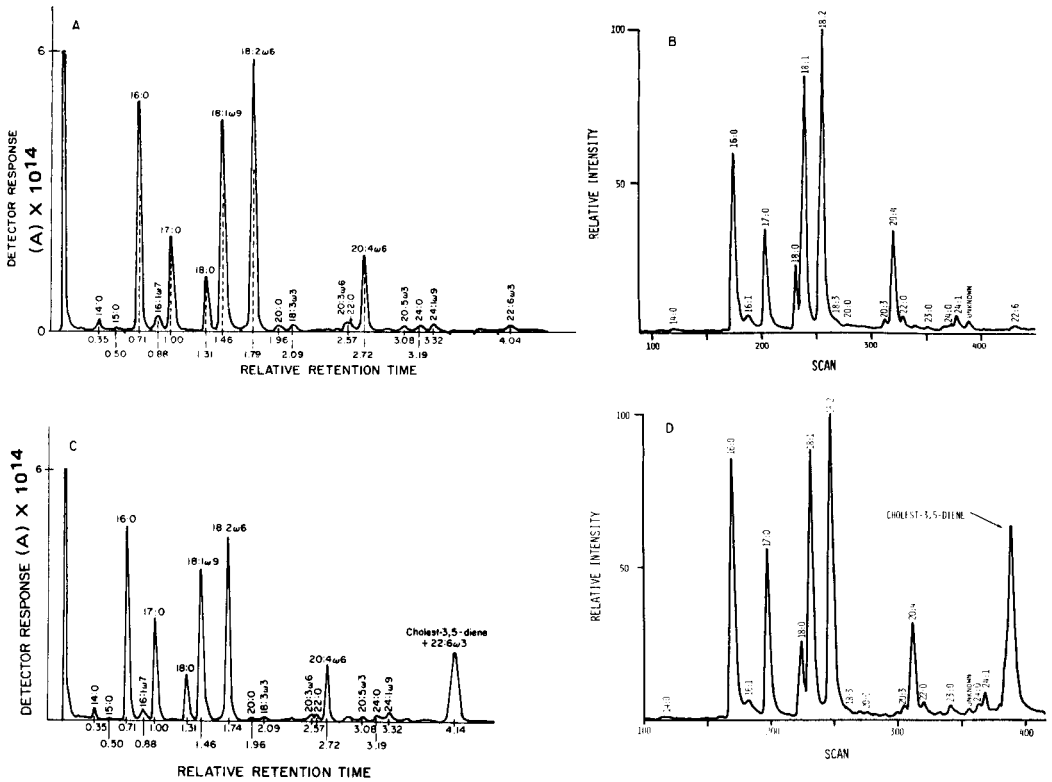

Fig. 2. (A) Chromatogram of the total fatty acid profile from 1 ml of plasma; peaks identified as in Fig. 1; sample was prepared as described in the text. (B) Reconstructed ion chromatogram of the plasma sample shown in A; component peaks were identified by comparing the relative mass spectra with those of authentic materials determined under identical conditions. (C) Chromatogram run on the modified EGS columns but without the alumina clean-up step. The sample source is identical with that shown in A. (D) Reconstructed ion chromatogram of material run in C; the identity of cholest-3,5-diene was confirmed by comparison with authentic materials.

was used as the starting point in this work because the application of heat to the mixture facilitates partitioning of lipid between the phases and because transfer manipulations required to produce a final extract are at a minimum. Heating the extract in sealed tubes does not appear to cause excessive oxidative damage to polyunsaturated fatty acids (PUFAs). No oxidation products were detected by mass spectrometry.

Another advantage of this technology over the procedures of Folch et al. is the smaller volume of water carried over in the final organic phase. Caution must be exercised in layering the calcium chloride solution to prevent mixing. With practice, the procedure as outlined will give consistently good recoveries of lipid.

In the work with plasma, it was found that cholesterol esters contributed the greatest quantity of artefact under the anhydrous conditions used for

acid-catalysed transesterification. Christie [10] reported the formation of methoxy cholesterol during methylation but this compound did not interfere with the present chromatography, as its relative retention time was 5.41 on the modified EGS column. Cholest-3,5-diene, the dehydration product of cholesterol, had a relative retention time (RRT) of 4.14 and greatly interfered with methyl docosahexaenoate (RRT = 4.04). Two additional byproducts, cholesteryl acetate and cholesteryl chloride, were formed from cholesterol. Figures 3 and 4 show the mass spectra of two of these products found in a plasma transesterification mixture. The spectra are identical with those of

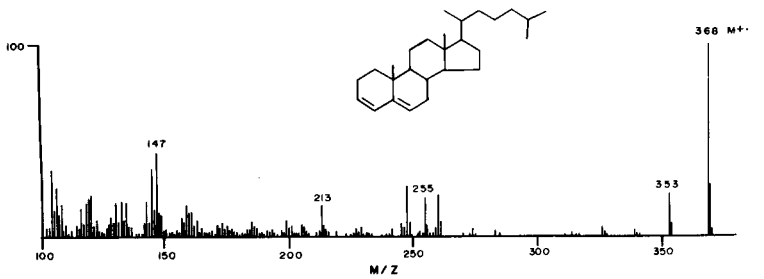

Fig. 3. Mass spectrum of cholest-3,5-diene as found in a plasma sample after methylation with mineral acid catalysis (scan no. 390 in Fig. 2D).

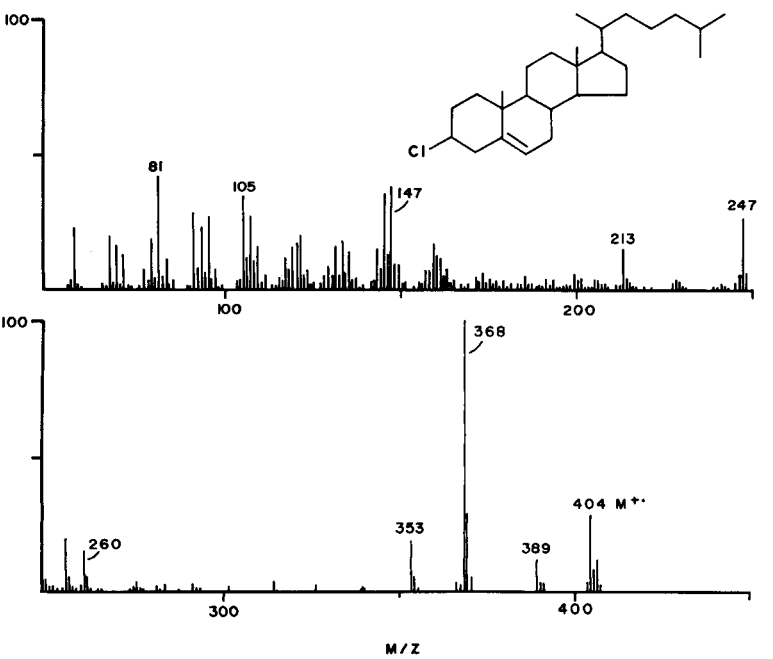

Fig. 4. Mass spectrum of cholesteryl chloride produced in small quantity during transesterification with methanolic hydrochloric acid.

authentic products synthesized from pure starting materials. One interesting observation was made during the synthesis. In an experiment designed to determine the extent of dehydration of cholesterol by the methanolic hydrochloric acid reagent, cholesterol, cholesteryl acetate, and cholesteryl palmitate were heated in separate tubes with the reagent under the reaction conditions used for methylation. The results showed that the ester derivatives produced much greater quantities of the dehydration product, cholest-3,5-diene, than did cholesterol. The level of the dehydrated species obtained from pure cholesterol was actually near the limit of detection of the mass spectrometer system. The cholesterol esters produced the chlorine-substituted derivative as well. It can be expected then that tissue sources rich in cholesterol esters will yield an artefact peak large enough to mask the 22:6ω3 region of a FAME chromatogram if no effort is made to purify the FAME mixture after methylation. However, cholest-3,5-diene also occurs when tissues with a low ratio of esterified to free cholesterol are processed. The dehydrated and chlorinated species are easily removed by chromatography with hydrated alumina.

The most troublesome hydrocarbon contamination encountered was squalene, introduced from adhesives used to secure cap liners in screw caps. If not removed, this contaminant can be erroneously identified as methyl tetracosanoate. Ester plasticizers coelute with FAMEs from the hydrated alumina. Only careful technique can minimize the levels of these substances in the extracts and solutions used.

Lastly, the ultimate success of any g.l.c. method depends on the reliability of the column. Methyl esters of PUFAs require a liquid phase of high polarity for adequate resolution. It is widely agreed that polyester-type phases provide the best conditions for packed column separation of FAME mixtures. These same phases, however, because of their polarity, do not effectively wet the more efficient inert solid supports. Additionally, high bleed rates and thermal decomposition properties limit column lifetime. To reduce thermal instability, Metcalfe [11, 12] used phosphoric acid with DEGS at a 25% liquid phase load on celite for the chromatographic separation of free fatty acids and FAMEs. Craig and Murty [13] first synthesized EGS and showed it to be suitable for the separation of FAME mixtures with a high PUFA content. Since its introduction, many investigators have used EGS and in a study done by Niewiadomski [14] it was shown that phosphoric acid was the best agent for extending the useful thermal limits of this liquid phase. Effective wetting of the support is attained if the preparative sequence outlined under Materials is faithfully executed. In this way, the usefulness of a modern high-efficiency support and the separating power of a polar liquid phase are fully realized. Chromatographic columns, when prepared and cured as described, afford excellent separation of the components of a standard mixture of FAMEs as shown in Fig. 1. Some phase bleeding still persists but it can be compensated by dual-column operation. The lifetime of these columns, when coupled with the other aspects of the outlined procedure, can be as high as one year although a period of eight months is more common with heavy usage.

REFERENCES

1 V. P. Flanagan and A. Ferretti, J. Lipid Res., 14 (1973) 306.
2 A. Ferretti and V. P. Flanagan, Lipids, 12 (1977) 198.
3 J. C. Pascal and R. G. Ackman, Comp. Biochem. Physiol., 53B (1976) 111.
4 M. Ishida, K. Suyama and S. Adachi, J. Chromatogr., 189 (1980) 421.
5 W. M. Sperry and F. C. Brand, J. Biol. Chem., 213 (1955) 69.
6 Gas-Chrom Newsl., Applied Science Laboratories, Vol. 11, No. 4, July/August 1970.
7 J. Folch, I. Ascoli, M. Lees, J. A. Meath and F. N. LeBaron, J. Biol. Chem., 191 (1951) 833.
8 J. Folch, M. Lees and G. H. Sloane-Stanley, Fed. Proc., 13 (1954) 209.
9 J. Folch, M. Lees and G. H. Sloane-Stanley, J. Biol. Chem., 226 (1957) 497.
10 W. W. Christie, in Lipid Analysis, Pergamon Press, New York, 1973, p. 117.
11 L. D. Metcalfe, Nature, 188 (1960) 142.
12 L. D. Metcalfe, J. Gas Chromatogr., 1 (1963) 7.
13 B. M. Craig and N. L. Murty, Can. J. Chem., 36 (1958) 1297.
14 H. Niewiadomski, (1970) Final Report, U.S. Dept. of Agric. Project No. U.R.-E21-/-60/29, Grant No. FG-Po-173.

Analytica Chimica Acta, 166 (1984) 189—197
Elsevier Science Publishers B.V., Amsterdam — Printed in The Netherlands

DETERMINATION OF SEVEN TRACE ELEMENTS IN NATURAL WATERS BY NEUTRON ACTIVATION ANALYSIS AFTER PRECONCENTRATION WITH 1-(2-PYRIDYLAZO)-2-NAPHTHOL

H. BEM[a], and D. E. RYAN*

Trace Analysis Research Centre, Department of Chemistry, Dalhousie University, Halifax, Nova Scotia, B3H 4J1 (Canada)

(Received 7th June 1984)

SUMMARY

A procedure is described for the preconcentration of Cd(II), Co(II), Cr(III), Cu(II), Mn(II), U(VI) and Zn(II) from 800 ml of water and sea-water samples by coprecipitation with 1-(2-pyridylazo)-2-naphthol (PAN) prior to neutron activation. Chromium is reduced to Cr(III) by hydroxylammonium chloride at pH 4 before the preconcentration step. Coprecipitation of 30 mg of PAN was most effective at pH 9 with final recoveries of 76—91% for six elements and 50% for uranium. The scheme is based on double irradiation of the same samples. Short (10 min) irradiation followed by γ-spectrometry counting for 10 min gives data for Cd (^{111m}Cd), Co, Cu, Mn and U (^{239}U). A second 16-h irradiation permits determination of zinc and uranium (^{239}Np) after a waiting time of 6 h, cadmium (^{115}Cd) after 24 h and chromium after a waiting period of 2 weeks followed by counting for 30 min. Detection limits are 0.04 ng g^{-1} for Co, 0.8 ng g^{-1} for Cd, 0.3 ng g^{-1} for Cu, 0.2 ng g^{-1} for Cr, 0.006 ng g^{-1} for Mn, 0.006 ng g^{-1} for U and 0.3 ng g^{-1} for Zn. A further decrease of the detection limit for chromium to 0.05 ng g^{-1} can be achieved by separation of interfering nuclides and scintillation counting of ^{51}Cr with a NaI(Tl) well-type detector.

The average levels of several important trace elements in natural waters are below the detection limits for direct determination by most quantitative methods, and a preconcentration step is usually necessary. Enrichment of trace components permits the use of a large amount of water sample and detection limits can be substantially lowered. Among different methods for preconcentration of trace elements prior to neutron activation, freeze drying suffers the lowest contamination risk but can be applied to surface waters only [1] because of the high concentration of the alkali metals in sea water. For all other methods, such as preconcentration on ion-exchange resins, reagent-loaded foams, chemically-modified solid supports, sorption of metal chelates on activated carbon, adsorbing colloid flotation, or coprecipitation with inorganic or organic collectors, the purity of the solid phase and the chemicals used during the procedure are limiting factors for quantification of ultra-trace amounts of elements [2, 3].

[a]On leave from the Technical University of Lodz, Poland.

0003-2670/84/$03.00

Coprecipitation of trace elements with organic chelating reagents seems to be the most attractive method for neutron activation in terms of relative purity of the collecting matrix, its lack of affinity for alkali metal ions and low induced activities in the matrix. A proper choice of precipitant and working conditions for real samples is a serious problem, as the mechanisms of coprecipitation are still not completely understood. Generally, a suitable reagent should have the ability to react with many metallic species forming compounds more insoluble than itself although its solubility should be also low to insure quantitative recovery.

Among different organic collectors, 1-(2-pyridylazo)-2-naphthol (PAN) seems to be the most promising for neutron activation; PAN reacts with many heavy metals [4, 5] and has been applied for preconcentration of metals from natural waters and artificial sea water in conjunction with x-ray fluorescence spectrometry [6—8] and for relative evaluation of neutron activation, x-ray fluorescence and spark-source mass spectrometry for multi-elemental analysis of geothermal waters [9]. Combination of different irradiation and counting cycles permitted quantification of seven trace elements after preconcentration with PAN but high values of the blank for other elements, particularly chromium, was a drawback of this method. Very recently, PAN was also successfully applied for the neutron-activation determination of uranium after selective preconcentration from sea water and biological materials [10].

The aim of the present study was to develop a method which would be applied to multi-element determinations in surface and sea waters with particular emphasis on chromium. It is known that trace amounts of chromium play a role in some metabolic processes but in larger concentrations the element in the Cr(VI) form is toxic. In natural waters, chromium is present at the $\mu g\ l^{-1}$ concentration and the accurate determination at this level still presents a considerable challenge.

EXPERIMENTAL

Reagents and samples

A 1% solution of PAN (Baker) in acetone (Aristar, BDH) was used. Standard solutions of Cd(II), Co(II), Cu(II), Mn(II), U(VI) and Zn(II) (Alfa-Ventron) were used to establish the optimum conditions for preconcentration. The ^{51}Cr tracer solutions used for the same purpose were obtained by irradiation of potassium dichromate or chromium nitrate (analytical-reagent grade; Fisher) in the SLOWPOKE reactor followed by their dissolution and dilution to the desired concentrations and activities. For pH adjustment, solutions of hydrochloric acid (Ultrex; Baker), potassium hydroxide (Suprapur; Merck) and potassium hydrogen phthalate (Fisher Certified ACS) were used. The thenoyltrifluoroacetone (TTA) used for extraction of neptunium was 99% (Aldrich). All other chemicals were analytical-reagent grade (Fisher).

The sea water was from the Northwest Arm, Halifax, Nova Scotia, and

was taken directly from a tap in the Oceanography Laboratory of the University; the water is filtered through sand before entering the building. It was further filtered through a Metricel filter (pore size 0.45 μm; Gelman Science).

Samples (ca. 25 g) of the National Bureau of Standards SRM 1643a (Trace Elements in Water) were processed to evaluate the accuracy of the method.

Apparatus

All samples were irradiated in an inner site of the SLOWPOKE reactor at a flux of 5×10^{11} n cm^{-2} s^{-1}. After a 10-min irradiation and 1-min decay time, the samples were counted for 10 min with a 60-cm^3 Canberra Ge(Li) detector, with 9.5% relative efficiency and 1.9-keV resolution at 1332 keV, in conjunction with the Jupiter Multichannel Analyser (Canberra). The samples were then re-irradiated for 16 h at the same flux and counted for 30 min after decay times of 6 h, 24 h and 2 weeks.

The activity of ^{51}Cr radionuclide for recovery studies and in the irradiated samples (after a decay time of 2 weeks) was measured with a 7.5 cm × 7.5 cm well type (NaI(Tl) detector in conjunction with a 4096-channel pulse-height analyzer (Canberra 8100). The irradiation and counting conditions, chosen on the basis of preliminary experiments, are shown in Table 1.

Preconcentration procedure

To 800 ml of sea water, 200 mg of hydroxylammonium chloride was added and the pH was adjusted to 4.0 with concentrated hydrochloric acid. The solution was stirred for 1 h and, after the pH had been readjusted to 9.0, 3 ml of the PAN solution was added slowly. The suspension was heated at 80°C for 1 h, allowed to cool and then filtered under suction through a Metricel filter (pore size 0.45 μm). The wet precipitate was transferred to a small (2/5 dram) polyethylene irradiation vial and then dried in an oven at 60°C.

The same procedure was applied for SRM 1643a, except that 25-g samples were diluted with doubly distilled water to a total volume of 500 ml and the pH was adjusted to 4 with potassium hydroxide before reduction with hydroxylammonium chloride.

TABLE 1

Irradiation conditions for multi-element quantitation after preconcentration with PAN

Irradiation time	Decay time	Counting time (min)	Elements quantified
10 min	1 min	10	Cd(^{111m}Cd), Co, Cu, Mn, U(^{239}U)
16 h	6 h	30	Mn, Zn, U(^{239}Np)
16 h	24 h	30	Cd(^{115}Cd — ^{115m}In)
16 h	≈2 weeks	30	Cr

Separation of interfering nuclides and measurement of chromium-51

The irradiated precipitate, after 2 weeks of waiting, was quantitatively transferred to a separatory funnel and dissolved in 5 ml of chloroform. The chloroform phase was washed with two 5-ml volumes of water. The chromium, together with some fission products from uranium (when present), was stripped from the chloroform to the water phase by shaking with 5 ml of 0.8 M nitric acid. The aqueous phase was separated and 0.25 g of iron(II) chloride and 0.35 g of hydroxylammonium chloride were added. After 1 h, Np(IV) and some fission products were extracted with 5 ml of 0.5 M TTA in xylene. The organic phase was discarded and 1 ml of concentrated hydrochloric acid was added to the aqueous phase followed by a second extraction with 5 ml of 0.5 M TTA in xylene. Finally, the water phase of total volume of 6 ml was transferred to a plastic vial for scintillation counting of ^{51}Cr.

RESULTS AND DISCUSSION

It is known that pH has a considerable effect on the formation of PAN chelates [5]. In order to choose the optimal pH for multi-element preconcentration, the recoveries of six elements from 500 ml of water spiked with 10 μg of Cd(II), Cr(III), Cu(II), Zn(II) and 1 μg of Co(II) and Mn(II) were determined at various pH values. It is evident from Fig. 1 that recoveries for all investigated elements increased with increased pH values.

However, for practical samples, particularly sea water at pH above 9.2,

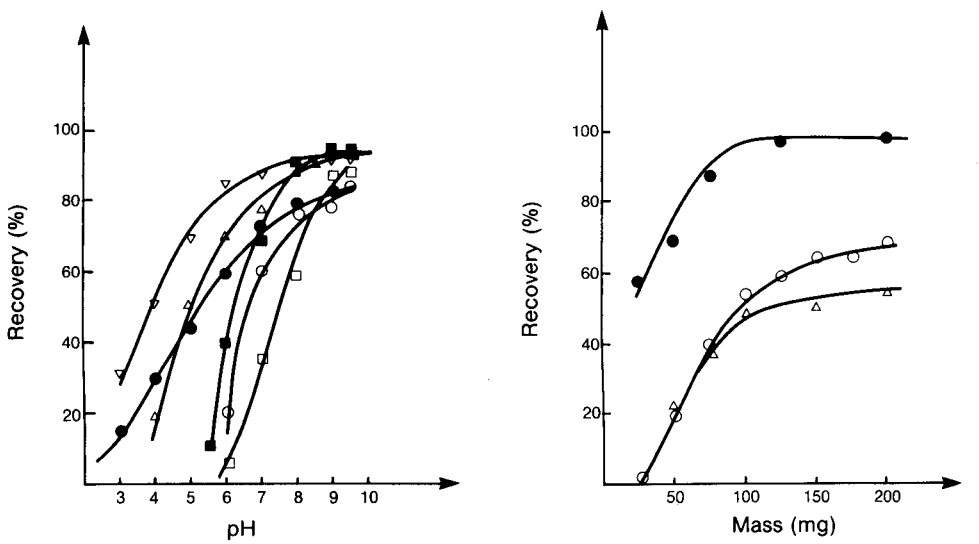

Fig. 1. Effect of pH on the collection metals: (○) Cd^{2+}; (●) Co^{2+}; (▪) Cr^{3+}; (△) Cu; (□) Mn^{2+}; (▽) Zn^{2+}.

Fig. 2. Influence of the amount of reducing agent on the recovery of chromium: (●) $NH_2OH \cdot HCl$, pH 4; (○) $NH_2OH \cdot HCl$, pH 5.6; (△) $NH_2NH_2 \cdot 2HCl$, pH 3.5.

considerable amounts of magnesium and some calcium coprecipitate with PAN, making the determination of manganese impossible after short irradiation because of the 844-keV γ-rays interference from ^{26}Mg. On the basis of these results, a pH of 9 was chosen for routine precipitation. At this pH, recoveries were relatively high (above 76%) and consistent not only for distilled water but also for 500 and 800 ml of sea water (see Table 2). In addition, uranium was also collected with a recovery of 51% under these conditions [10]. The recoveries for Cr, Cu, Mn and Zn are somewhat lower than those obtained by others [8], because of losses during transfer of the precipitate from the Metricel filter to an irradiation vial. Average losses were 7 ± 2% and were determined by experiments with chromium-51 tracer.

Choice of the reduction procedure for chromium

Because PAN reacts with Cr(III) but not with Cr(VI), the water samples must be chemically reduced before coprecipitation. Despite some controversy about the oxidation state of chromium in natural waters, it has been shown that in sea water the total amount of chromium exists as 15% inorganic Cr(III), 25% inorganic Cr(VI) and ca. 60% organically-bound chromium [11]. Sodium sulphite has been used to reduce Cr(VI) in waters adjusted to 1—2 M sulphuric acid [12, 13] or at pH $\geqslant$1.5 [14]. Here, because relatively large amounts of acid would have to be added to the 800-ml water samples for reduction, and would then require adjustment to pH 9 with potassium hydroxide for preconcentration, the risk of additional contamination of samples with trace elements is high. Other reducing agents (ascorbic acid, hydrazinium dichloride and hydroxylammonium chloride) were therefore tested as potential reductants for chromium(VI) in sea water. These experiments were done with 800 ml of sea water spiked with 10 μg of Cr(VI) with ^{51}Cr tracer. The solution was left for 1 h at natural pH to allow for equilibrium between added Cr(VI) and other constituents in sea water. After addition of reducing agent, the solution was again left for 1 h before the pH was adjusted to 9 and the normal preconcentration procedure was applied. The precipitate, however, was put into the plastic vial together with filter and was

TABLE 2

Recovery studies of trace metal ions added to water samples at pH 9.0

Element	Recovery (%)		
	Sea water (800 g)	Sea water (500 g)	Distilled water (500 g)
Cd	71 ± 4	76 ± 3	76 ± 3
Co	72 ± 3	78 ± 4	82 ± 4
Cr(III)	91 ± 3	93 ± 2	94 ± 2
Cu	83 ± 3	86.5 ± 3	93 ± 4
Mn(II)	85 ± 4	85 ± 3	87 ± 4
U	51 ± 2	49 ± 2	53 ± 2
Zn	85 ± 4	93 ± 4	93 ± 4

directly counted with a NaI(Tl) scintillation counter. Up to 200 mg of ascorbic acid was quite ineffective. The data for the other reagents are shown in Fig. 2. Hydroxylammonium chloride was superior to hydrazinium dichloride and at pH 4, 100 mg was sufficient to reduce the 10 μg of Cr(VI) added to 800 ml of sea water. Routinely, a two-fold excess (200 mg) of the reagent was used.

Almost quantitative recovery (>98%) of added Cr(VI) confirms the complete reduction of Cr(VI) to Cr(III) but this does not necessarily mean that naturally occurring chromium in sea water, especially organically bound, is collected with the same efficiency. In order to evaluate this problem, different amounts of Cr(III) with ^{51}Cr tracer (0.5—10 μg) were added to 800 ml of sea water and an entire preconcentration procedure was repeated for each sample. Although it is known that isotopic exchange of chromium in solution between $Cr(H_2O)_6^{3+}$ and some organic chromium complexes is very slow [15], one can expect that after 1-h equilibration at the natural pH of sea water (7.8) followed by 1-h reduction at pH 4 and finally during 1-h heating at 80°C after addition of PAN, some part of added ^{51}Cr(III) can be complexed by organic matter in sea water and isotopic exchange between ^{51}Cr(III) and organically bound chromium should partially occur. In effect, if PAN collects only the inorganic forms of chromium in sea water, the recovery of ^{51}Cr in the PAN precipitate would be incomplete, especially for lower amounts of ^{51}Cr(III) added to sea water (comparable to naturally occurring amounts). Recoveries of 0.5, 1.0, 3.0, 5.0, and 10.0 μg of Cr(III) added to 800 ml of sea water were 98.1, 104.0, 98.3, 99.8, and 98.6, respectively. These data show that recovery of ^{51}Cr(III) is quantitative over the whole range of added tracer, indirectly indicating that all forms of chromium present in sea water are collected by PAN in this procedure.

Choice of detection conditions

All investigated elements can be determined in SRM 1643a by instrumental neutron activation/γ-ray spectrometry with a Ge(Li) detector after preconcentration with PAN.

However, for sea water, which contains approximately 3 μg kg^{-1} uranium, cadmium cannot be detected via the ^{115}Cd nuclide (E_γ = 336 keV) because of strong 334-keV interference from ^{239}Np (daughter product from ^{239}U). In addition, both radionuclides have the same half-life (2.3 days). Therefore cadmium in sea water can be quantified only via short-lived ^{111m}Cd after a 10-min irradiation with a relatively poor detection limit of 0.8 μg l^{-1}. The high value of Compton background in the ^{60m}Co region (59 keV) also makes it impossible to quantify cobalt in sea water; the detection limit was 0.04 μg l^{-1}. Copper can be also determined only via short-lived ^{66}Cu ($t_{1/2}$ = 5.1 min); the more sensitive long-lived ^{64}Cu ($t_{1/2}$ = 12.8 h) could not be used because, even after a 6-h waiting period, there was still a considerable contribution from the other nuclides to the 511-keV annihilation peak. Both short and long irradiation are convenient for determinations of manganese and uranium but the latter gives lower detection limits.

Chromium can be quantified with a Ge(Li) detector via long-lived ($t_{1/2}$ = 27.8 d) chromium-51 after a decay period of at least two weeks, but the detection limit is rather high ($\approx 0.2\ \mu g\ l^{-1}$). The detection limit depends on the detection efficiency of nuclear radiation and the background in the region of interest. Application of the well-type NaI(Tl) scintillation counter should improve the detection limit. Unfortunately, these detectors have poor energy resolution and, as is evident from Fig. 3(a), even after 2 weeks one can observe the strong interference of ^{239}Np and partially ^{131}I in the 320-keV region. Both of these nuclides must be removed by a radiochemical procedure before scintillation counting of ^{51}Cr. Some ^{131}I activity is stripped to the water phase by washing the chloroform phase containing dissolved PAN complexes with two 5-ml volumes of water. Some fission products are also partially removed but ^{239}Np, ^{141}Ce and ^{95}Nb remain in the organic phase together with chromium chelate. All these elements, except for organically bound iodine, are transferred to the water phase by shaking with 0.8 M nitric acid. Neptunium, after reduction to the Np(IV) state by iron(II) chloride and hydroxylammonium chloride, is quantitatively extracted with 0.5 M TTA in xylene [16]. Chromium(III) is not extracted by TTA from this medium [17] and remains in the water phase. Figure 3(b) shows no interference from other nuclides in the ^{51}Cr region after this procedure. The only possible interference (but very unlikely) is from ^{233}Pa (a daughter product of ^{233}Th, if thorium is present in a large amount in irradiated samples). This nuclide has almost the same half-life (27.4 days) and 312-keV γ-rays, but

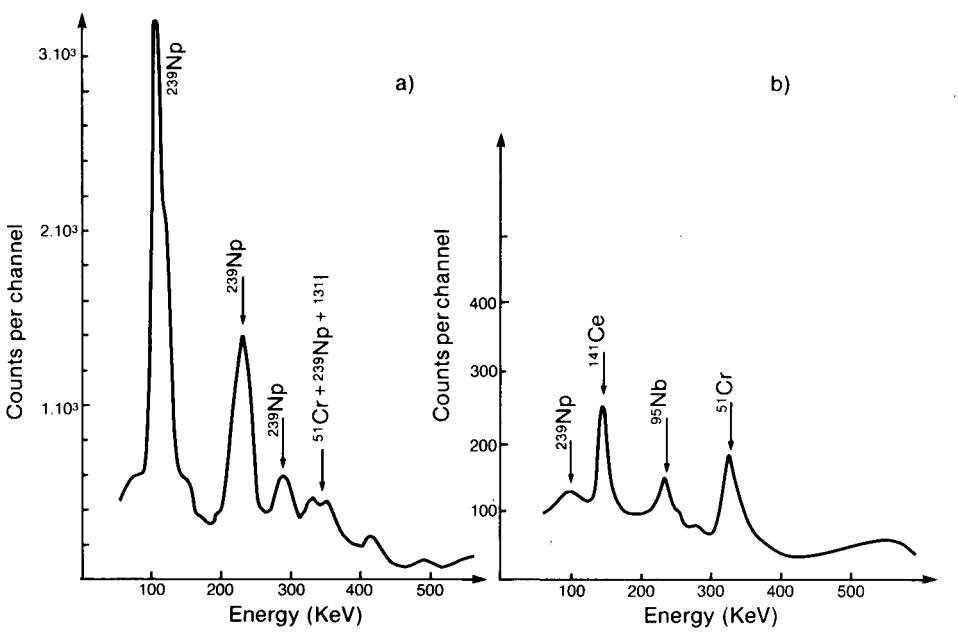

Fig. 3. γ-Spectra of the PAN precipitate: (a) after a decay time of 2 weeks; (b) after radiochemical removal of ^{239}Np and ^{131}I (same sample).

TABLE 3

Determination of selected elements in SRM 1643a and in sea water

Element	Nuclide measured	SRM 1643a			Sea water		
		Conc. ($\mu g\ l^{-1}$)	Detection limit (μg)	Certified value ($\mu g\ l^{-1}$)	Conc. ($\mu g\ l^{-1}$)	Detection limit (μg)	Literature value ($\mu g\ l^{-1}$)
Cd	^{115}Cd	9.4 ± 1	0.05	10 ± 1	<0.8	0.6[a]	<0.03 [19]
Co	^{60m}Co	19.5 ± 0.6	0.02	19 ± 2	<0.04	0.03	—
Cr	^{51}Cr	16.6 ± 0.7	0.04[b]	17 ± 2	0.55 ± 0.05	0.05[b]	0.44 [20]
Cu	^{66}Cu	19.2 ± 2	0.2	18 ± 2	0.7 ± 0.1	0.25	0.66; 0.72 [19]
Mn	^{56}Mn	31.5 ± 2	0.005	31 ± 2	0.4 ± 0.05	0.005	—
U	^{239}Np	<0.01	0.005	—	3.3 ± 0.1	0.005	3.2 [21] [10]
Zn	^{69m}Zn	72.5 ± 2	0.3[c]	68 ± 4	1.1 ± 0.2	0.3[c]	—

[a]Determined via ^{111m}Cd nuclide. [b]Determined after separation of ^{239}Np and ^{131}I and detection of ^{51}Cr in a scintillation counter. [c]The value of blank introduced during preconcentration.

should also be removed with ^{239}Np during extraction with TTA. The final purification from traces of ^{239}Np and ^{233}Pa (if present) can be done by addition of concentrated hydrochloric acid to the water phase to make its concentration about 2 M and making a second extraction with 0.5 M TTA in xylene [18]. The water phase can be transferred to the plastic vial and ^{51}Cr can be quantified in a scintillation counter with good efficiency. The detection limit for chromium after this procedure is four times lower (0.05 $\mu g\ l^{-1}$).

Precision and accuracy

The accuracy of the method was evaluated for SRM 1643a samples and sea water. The results are presented in Table 3. The absolute detection limits in μg were calculated on the basis of 3 times the square root of the background; their values are close to the blank introduced during preconcentration, except for zinc, the blank for which was remarkably higher. The literature values for sea water were taken from the data obtained in the same laboratory for different methods of preconcentrating trace elements from sea water. The good agreement between determined values and those certified (for SRM 1643a) or reported by others supports the suitability of the method.

This work was supported by a grant from the Natural Sciences and Engineering Research Council of Canada.

REFERENCES

1 K. H. Lieser, W. Calmano, E. Heuss and V. Neitzert, J. Radioanal. Chem., 37 (1977) 717.
2 R. S. S. Murthy, J. Holzbecher and D. E. Ryan, Rev. Anal. Chem., VI, 2 (1982) 113.
3 H. A. Das, Pure Appl. Chem., 54 (1982) 755.
4 K. L. Cheng and R. H. Bray, Anal. Chem., 27 (1955) 782.

5 S. Shibata, Anal. Chim. Acta, 23 (1960) 367.
6 R. Puschel, Talanta, 16 (1969) 351.
7 H. Watanabe, S. Berman and D. S. Russel, Talanta, 19 (1972) 1363.
8 M. G. Vanderstappen and R. E. Van Grieken, Talanta, 25 (1978) 653.
9 W. Blommaert, R. Vandelamoote, L. Van't Dack, R. Gijbels and R. Van Grieken, J. Radioanal. Chem., 57 (1980) 383.
10 H. Bem and D. E. Ryan, Anal. Chim. Acta, 158 (1984) 119.
11 E. Nakayama, T. Kuwamoto, H. Tokoro and T. Fujinaga, Anal. Chim. Acta, 131 (1981) 247.
12 D. P. Nikolelis and T. P. Hadjioannou, Mikrochim. Acta, (1978) 105.
13 K. Yashimura and S. Ohashi, Talanta, 25 (1978) 103.
14 H. A. Van Der Sloot, J. Radioanal. Chem., 37 (1977) 727.
15 W. R. King Jr. and C. S. Garner, J. Am. Chem. Soc., 74 (1952) 5534.
16 F. L. More, Anal. Chem., 29 (1957) 941.
17 S. K. Majumdar and A. K. De, Anal. Chem., 32 (1960) 1337.
18 A. M. Poskanzer and B. M. Foreman, J. Inorg. Nucl. Chem., 16 (1961) 323.
19 R. S. S. Murthy and D. E. Ryan, Anal. Chim. Acta, 140 (1982) 163.
20 H. F. Zhang, J. Holzbecher and D. E. Ryan, Anal. Chim. Acta, 149 (1983) 385.
21 J. Holzbecher and D. E. Ryan, J. Radioanal. Chem., 74 (1982) 25.

Analytica Chimica Acta, 166 (1984) 199—205
Elsevier Science Publishers B.V., Amsterdam — Printed in The Netherlands

ETUDE DE LA COMPLEXATION DES LANTHANIDES TRIVALENTS PAR LES SIX ISOMÈRES DE L'ACIDE DIAMINOCYCLOHEXANETÉTRAACÉTIQUE

Partie 2. Les Constantes d'Acidité et les Constantes de Formation des Complexes 1:1 avec l'Acide *trans*-1,4-Diaminocyclohexane-*N,N,N',N'*-Tétraacétique

E. MERCINY et J. FUGER*

Laboratoire de Chimie Analytique et Radiochimie, Université de Liège, B-4000 Sart Tilman-Liège (Belgium)

(Reçu le 25 Avril 1984)

SUMMARY

(*Study of the complexation of trivalent lanthanides by the six isomers of diaminocyclohexanetetraacetic acid. Part 2. Acidity constants and formation constants of the 1:1 complexes of* trans-*1,4-diaminocyclohexane*-N,N,N',N'-*tetraacetic acid*)

Potentiometric measurements of the acidity constants of *trans*-1,4-diaminocyclohexane-*N,N,N',N'*-tetraacetic acid (*trans*-1,4-DCTA) and of the stability constants of its 1:1 complexes with the trivalent lanthanides are reported for an ionic strength of 1 (KCl) at 25°C. The behaviour of this ligand is similar to that of monoaminodiacetic acids, suggesting that only one $-N-(CH_2COO^-)_2$ group participates in chelation. The selectivity of *trans*-1,4-DCTA for the lanthanides is better than that reported for the monoaminodiacetic acids.

RÉSUMÉ

Les auteurs déterminent, par titrage coulométrique suivi potentiométriquement dans un milieu de force ionique égale à 1 (KCl) à 25°C, les constantes d'acidité de l'acide *trans*-1,4-diaminocyclohexane-*N,N,N',N'*-tétraacétique (*trans*-1,4-DCTA) et les constantes de stabilité et les constantes d'acidité des complexes de stoechiométrie 1:1 qu'il forme avec les lanthanides trivalents. Le comportement de ce ligand est comparable à celui des acides monoaminodiacétiques, ce qui semble prouver qu'un seul des groupements $-N-(CH_2-COO^-)_2$ participe à la chélation. La sélectivité du *trans*-1,4-DCTA pour les lanthanides est, par contre, meilleure que celle que l'on observe avec les ligands monoaminodiacétiques.

Dans une publication précédente [1], nous avons décrit le protocole expérimental appliqué pour la réalisation des synthèses de cinq isomères de l'acide diaminocyclohexanetétraacétique. Nous rendions compte également des valeurs mesurées pour les constantes d'acidité de l'acide *trans*-1,2-diaminocyclohexane-*N,N,N',N'*-tétraacétique et les constantes de formation des complexes de stoechiométrie 1:1 de ce ligand avec les lanthanides trivalents, dans un milieu de force ionique égale à 1 (KCl) et à 25°C. Dans le présent travail, nous étudions les propriétés acido-basiques et les propriétés complexantes vis-à-vis des lanthanides trivalents de l'acide *trans*-1,4-di-

0003-2670/84/$03.00

aminocyclohexane-*N,N,N',N'*-tétraacétique (*trans*-1,4-DCTA) dont nous avons mesuré les mêmes constantes dans les mêmes conditions de milieu. Les méthodes de mesure et de calcul pour l'interprétation des courbes de titrage potentiométrique sont également identiques à celles utilisées dans le travail précédent.

CARACTÉRISATION DE L'AGENT COMPLEXANT ÉTUDIÉ

Le *trans*-1,4-DCTA se présente sous la forme d'un solide blanc cristallin dont le poids moléculaire se stabilise à 382,4 après séchage prolongé sous vide (0,5 mm Hg) à température ordinaire. Le poids moléculaire théorique étant de 346,36, il semble donc que ce composé cristallise avec deux molécules d'eau. Même sous sa forme neutre multiprotonée H_4L, sa solubilité dans l'eau est très élevée (environ 300 g l^{-1}) alors que celle de l'isomère *trans*-1,2 est inférieure à 0,5 g l^{-1}.

Rejetés aux deux extrémités de la molécule de cyclohexane, les deux groupements aminodiacétiques sont assez éloignés l'un de l'autre. On doit donc attendre que l'isomère *trans*-1,4 forme des complexes relativement peu stables avec les cations des lanthanides qui pourraient n'être que partiellement déshydratés au sein des complexes. Par contre, en considérant la distance assez grande et variable entre les deux azotes et la rigidité relative de la molécule, on peut imaginer une déshydratation du cation métallique variable en fonction du nombre atomique du lanthanide et obtenir ainsi une sélectivité intéressante.

PARTIE EXPÉRIMENTALE

Détermination des constantes d'acidité. On réalise, par pesée, des solutions 0,01 M en complexant amenées aux environs de pH 1,2 par ajout de volumes mesurés d'acide chlorhydrique de titre connu. On ajoute encore la quantité de KCl nécessaire pour fixer la force ionique à 1.

Détermination des constantes de formation des complexes. Les oxydes de lanthanides (pureté 99,95%; Labelcomat, Bruxelles) sont calcinés à 1200°C. On en pèse la quantité nécessaire à la réalisation de solutions 10^{-2} M en cation métallique que l'on introduit dans des ballons jaugés de 200 ml. La mise en solution est réalisée par de l'acide chlorhydrique 6 M et l'excès d'acide évacué par chauffage à 60°C sous courant d'azote. On ajoute alors 0,7648 g de DCTA et 14,91 g de KCl réalisant ainsi des solutions 0,01 M en Ln^{3+}, 0,01 M en complexant dont la force ionique est égale à 1. Dans le cas du cérium, une solution chlorhydrique, réalisée à partir de carbonate céreux, est étalonnée par gravimétrie de l'oxalate.

RÉSULTATS ET DISCUSSION

Les constantes d'acidité du trans*-1,4-DCTA.* La courbe de titrage de l'acide tétrabasique est représentée sur la Fig. 1. Les valeurs des p*K* auxquels

conduit son interprétation sont: $pK_{a0} = 1{,}66 \pm 0{,}01$; $pK_{a1} = 1{,}949 \pm 0{,}005$; $pK_{a2} = 2{,}466 \pm 0{,}003$; $pK_{a3} = 8{,}419 \pm 0{,}004$; $pK_{a4} = 11{,}15 \pm 0{,}01$; $\log K_{K^+} = 0{,}02 \pm 0{,}01$; avec $pK_{ai} = -\log [H_{4-i}][H^+]/[H_{4+1-i}L]$ et $\log K_{K^+} = \log[KL^{3-}]/[L^{4-}][K^+]$. La façon dont nous calculons l'erreur dont sont affectées ces constantes a été détaillée antérieurement [1]. La complexation des ions K^+ est négligeable et il n'en sera pas tenu compte dans le calcul des constantes de formation des complexes avec les lanthanides trivalents. Dans le Tableau 1, nous comparons ces valeurs à celles d'autres acides diaminotétraacétiques [2].

La protonation des ligands polyaminopolyacétiques procède par l'addition successive des protons sur tous les atomes d'azote tandis que les groupements carboxyliques n'ont que très peu d'affinité pour les ions H_3O^+ [3—8]. Le pK_{a4} du *trans*-1,4-DCTA, plus faible d'environ 1 unité que celui du *trans*-1,2-DCTA, est cependant nettement plus élevé que dans le cas des autres ligands qui lui sont comparés. Ainsi, il semble que ce soit la rigidité de la molécule qui soit particulièrement favorable à la fixation du premier proton, d'autant qu'à ce stade de la protonation les encombrements stériques n'interviennent que fort peu. Il en va tout autrement pour la fixation du deuxième proton caractérisée par la valeur de pK_{a3}; cette fois, elle est nettement plus élevée que pour l'EDTA ou le *trans*-1,2-DCTA. Sa valeur est intermédiaire entre celle de TMDTA et celle de TTMDTA et, ici, il semble que ce soit la longueur de la chaîne, autrement dit la distance entre les deux fonctions aminodiacétiques, qui soit déterminante. Quant aux valeurs de pK_{a2} et pK_{a1} du *trans*-1,4-DCTA, elles sont de nouveau très proches de celles de TMDTA et TTMDTA et plus faibles que pour l'EDTA et le *trans*-1,2-DCTA.

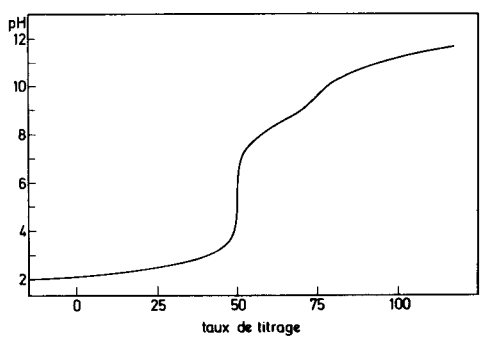

Fig. 1. Courbe de titrage coulométrique de l'acide *trans*-1,4-diaminocyclohexane-*N*,*N*,*N*',*N*'-tétraacétique. Conditions de titrage: voir Tableau 3 [1]. Solution à titrer: 76,777 ml de solution 0,01 M en ligand et de force ionique égale à 1 (KCl).

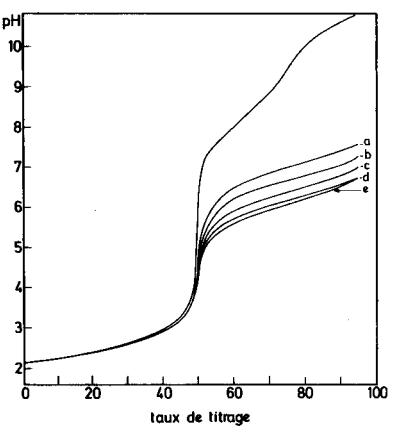

Fig. 2. Comparaison entre les courbes de titrage coulométrique du ligand seul et de ce même ligand en présence de quantité stoechiométrique d'ions lanthanides: (a) Nd^{3+}; (b) Gd^{3+}; (c) Ho^{3+}; (d) Tm^{3+}; (e) Lu. Les conditions de titrage sont les mêmes que pour la Fig. 1.

TABLEAU 1

Comparaison des pK_a du *trans*-1,4-DCTA avec ceux d'autres acides diaminotétraacétiques

Complexant	pK_{a0}	pK_{a1}	pK_{a2}	pK_{a3}	pK_{a4}
EDTA	1,5	2,0	2,66	6,16	10,24
Trans-1,2-DCTA	1,56	2,42	3,25	6,01	12,73
TMDTA[a]	—	1,88	2,57	8,02	10,46
TTMDTA[b]	—	1,90	2,45	9,05	10,66
Trans-1,4-DCTA	1,66	1,95	2,47	8,42	11,15

[a] L'acide triméthylènedinitrilotétraacétique. [b] Acide tétraméthylènedinitrilotétraacétique.

Ceci peut paraître logique si, comme on le suppose, les groupements carboxyliques sont plus fortement impliqués dans la fixation des deux premiers protons.

Les constantes de formation des complexes de stoechiométrie 1:1 avec les lanthanides trivalents. La figure 2 fournit une comparaison entre les courbes de titrage du ligand seul et de ce même ligand en présence de la quantité stoechiométrique de divers ions Ln^{3+}. L'interprétation mathématique de ces courbes de titrage conduit aux valeurs des constantes de formation des complexes 1:1 et des constantes d'acidité des espèces $LnLH_2^+$ et LnLH

TABLEAU 2

Constantes de formation des complexes de stoechiométrie 1:1 des lanthanides trivalents avec l'acide *trans*-1,4-diaminocyclohexanetétraacétique (25,00 ± 0,01)° C[a]

Lanthanides	log K[b]	pK_1[c]	pK_2[d]	$\alpha_{La^{3+}}^{Ln^{3+}}$[e]
Lanthane	7,3 ± 0,2[f]	5,8 ± 0,3	7,4 ± 0,3	1,0
Cérium	7,5 ± 0,1	5,84 ± 0,08	7,3 ± 0,1	1,58
Praséodyme	7,76 ± 0,02	5,89 ± 0,05	7,18 ± 0,06	2,88
Néodyme	7,96 ± 0,01	5,91 ± 0,03	7,03 ± 0,03	4,57
Samarium	8,56 ± 0,01	6,02 ± 0,01	6,45 ± 0,02	18,2
Gadolinium	8,56 ± 0,01	5,95 ± 0,01	6,41 ± 0,01	18,2
Terbium	8,79 ± 0,01	5,82 ± 0,01	6,28 ± 0,01	30,9
Dysprosium	9,03 ± 0,01	5,75 ± 0,01	6,14 ± 0,01	53,7
Holmium	9,27 ± 0,01	5,66 ± 0,01	6,03 ± 0,01	92,3
Erbium	9,46 ± 0,01	5,62 ± 0,01	5,86 ± 0,01	144
Thulium	9,69 ± 0,01	5,56 ± 0,01	5,70 ± 0,01	248
Ytterbium	9,83 ± 0,01	5,49 ± 0,01	5,67 ± 0,01	339
Lutétium	9,90 ± 0,01	5,44 ± 0,01	5,67 ± 0,01	399

[a] La précipitation des hydroxydes $Ln(OH)_3$ limite l'interprétation des courbes de titrage à pH ⩽ 7,5 au niveau du lanthane, à pH ⩽ 6,0 au niveau du lutétium. [b] $\log K = \log [LnL^-]/[Ln^{3+}][L^{4-}]$. [c] $pK_{LnLH_2^+} = -\log [LnLH][H^+]/[LnLH_2^+]$. [d] $pK_{LnLH} = -\log [LnL^-][H^+]/[LnLH]$. [e] $\alpha_{La^{3+}}^{Ln^{3+}} = K_{Ln^{3+}}/K_{La^{3+}}$. [f] La façon dont nous calculons les erreurs dont sont affectées ces constantes a été détaillée [1].

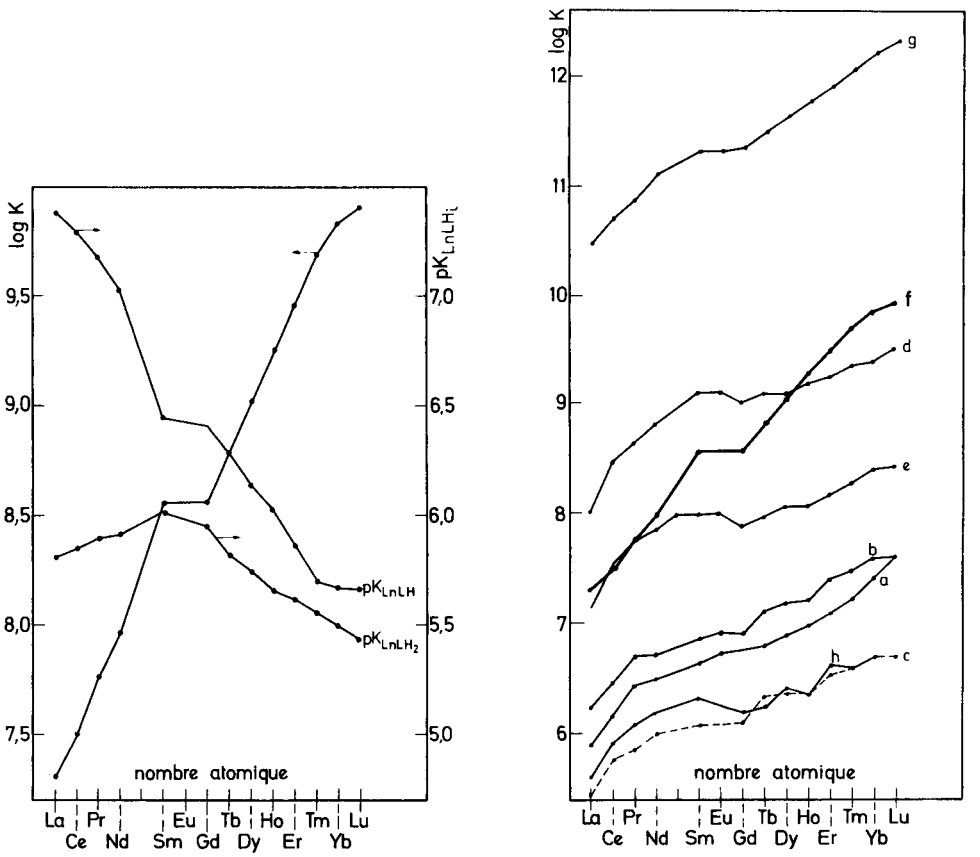

Fig. 3. Evolution des constantes de formation et des constantes d'acidité des complexes de stoetchiométrie 1:1 formés entre les lanthanides trivalents et l'acide *trans*-1,4-DCTA en fonction du nombre atomique des cations métalliques, à 25° C, dans un milieu de force ionique égale à 1 (KCl).

Fig. 4. Comparaison des valeurs des constantes de formation des complexes de stoechiométrie 1:1 avec les lanthanides trivalents, de l'acide *trans*-1,4-DCTA et divers acides aminopolyacétiques [2]: (a) iminodiacétique; (b) *N*-méthyliminodiacétique; (c) *N*-benzyliminodiacétique; (d) *N*-(2hydroxyéthyl)iminodiacétique; (e) *N*-(2-méthoxyéthyl)iminodiacétique; (f) *trans*-1,4-DCTA; (g) nitrilotriacétique; (h) *N*-2-(méthylthio)éthyliminodiacétique.

rassemblées au Tableau 2. L'évolution de ces constantes en fonction du nombre atomique des lanthanide est représentée à la Fig. 3. La figure 4 permet de comparer les valeurs obtenues avec celles que donnent certains acides aminodiacétiques. Comme dans le cas du *trans*-1,2-DCTA, l'allure de la courbe de log K en fonction du nombre atomique des lanthanides est monotone du lutetium au gadolinium et du samarium au lanthane avec une discontinuité très marquée au niveau du gadolinium.

Mais, ce qui est remarquable, c'est l'ordre de grandeur des constantes mesurées, qui sont très faibles si on les compare à celles que donnent habituellement les acides diaminotétraacétiques. Elles situent le *trans*-1,4-DCTA au niveau des acides iminodiacétiques comme il ressort de la comparaison réalisée à la Fig. 4. Au niveau des terres yttriques, les constantes sont comparables à celles obtenues avec l'acide hydroxyéthyliminodiacétique alors qu'au niveau des terres cériques, elles sont très proches de celles de l'acide méthoxyéthyliminodiacétique. Ainsi, il semble qu'un seul des groupements $-N(CH_2COO^-)_2$ participe à la chélation, l'action du second n'étant guère plus influente que celle d'un groupement —OH ou $-OCH_3$. Cette hypothèse semble par ailleurs confirmée par le fait que, même lié aux ions lanthanides, le *trans*-1,4-DCTA garde une grand affinité pour les protons puisque ses complexes protonés sont des acides relativement faibles: dans le cas du lanthane, la valeur de pK_{a2} n'est différente que d'une unité de la valeur du pK_{a3} du ligand libre.

Par contre, la sélectivité du *trans*-1,4-DCTA est nettement supérieure à celle qui caractérise habituellement les complexants monoazotés (Fig. 4). A ce point de vue, il semble intéressant d'étudier en détail l'allure des courbes de pK_{LnLH_2} et de pK_{LnLH} en fonction de Z (Fig. 3): alors que ces deux constantes d'acidité sont très proches l'une de l'autre du lutétium à l'erbium, leur valeur s'écarte de l'erbium au samarium; mieux même, au-delà de cet élément, si pK_{LnLH} continue d'augmenter très rapidement, on assiste par contre à une diminution de pK_{LnLH_2}. Si l'on admet qu'une augmentation de la constante d'acidité correspond à une participation plus forte de l'azote à la complexation du cation métallique et vice-versa, on peut supposer que pour les gros ions (partiellement déshydratés comme le laissent présumer les valeurs des constantes de formation), il n'y a pas place dans la cavité chélatante: ils se trouvent repoussés à l'une des extrémités de la molécule, ne subissant ainsi que l'influence d'un seul groupement complexant. Avec la diminution de la dimension des ions (ou leur plus forte déshydratation), la pénétration progressive de ceux-ci entre les deux azotes devient possible: ils subissent ainsi de façon plus intense l'influence du second groupement iminodiacétique.

Quoi qu'il en soit, ce phénomène confère au *trans*-1,4-DCTA une sélectivité intéressante qui pourrait être mise à profit pour une séparation des lanthanides: des milieux de pH neutre ou faiblement basique sont évidemment souhaitables en raison de la valeur des constantes de formation. Signalons enfin que la solubilité dans l'eau du *trans*-1,4-DCTA comme celle de ses complexes est très élevée.

Il nous est agréable d'exprimer notre gratitude à l'Institut Interuniversitaire des Sciences Nucléaires (Bruxelles) pour l'octroi de subsides à notre Laboratoire.

REFERENCES

1 E. Merciny et J. Fuger, Anal. Chim. Acta, 160 (1984) 87.
2 A. E. Martell, Critical Stability Constants, Vol. 1: Amino Acids (1974), Plenum Press, New York.
3 J. L. Sudmeier et C. N. Reilley, Anal. Chem., 36 (1964) 1699.
4 P. Letkeman et A. E. Martell, Inorg. Chem., 18 (1979) 1284.
5 P. Letkeman et J. B. Westmore, Can. J. Chem., 49 (1971) 2086.
6 J. E. Tackett et D. T. Sawyer, Inorg. Chem., 3 (1964) 304.
7 R. J. Kula et D. T. Sawyer, Anal. Chim. Acta, 3 (1964) 458.
8 E. Merciny et N. Zaman, Anal. Chim. Acta, 47 (1969) 91.
9 G. Schwarzenbach et G. Ackermann, Helv. Chim. Acta, 30 (1947) 1978.

Analytica Chimica Acta, 166 (1984) 207—219
Elsevier Science Publishers B.V., Amsterdam — Printed in The Netherlands

CHARACTERISTICS OF THE BINDING OF EUROPIUM(III) TO TETRACYCLINE

LINDA M. HIRSCHY[a], T. F. VAN GEEL[b] and J. D. WINEFORDNER*

Department of Chemistry, University of Florida, Gainesville, FL 32611 (U.S.A.)

R. N. KELLY and S. G. SCHULMAN

Department of Pharmaceutics, College of Pharmacy, University of Florida, Gainesville, FL 32611 (U.S.A.)

(Received 7th March 1983)

SUMMARY

Lanthanide-sensitized luminescence was described previously as a sensitive means of quantifying tetracycline in solution. The results of potentiometric, absorbance, fluorescence and lifetime measurements on the tetracycline/Eu^{3+} system are presented here. The tetracycline/Eu^{3+} complexes which exist in aqueous solution have 1:1 stoichiometry; their formation constants are a function of pH.

The use of lanthanide ions (Eu^{3+}) as luminescence probes for quantifying tetracyclines in solution was recently introduced [1]. The technique involves the formation of a Eu^{3+}/tetracycline complex which has a broad-band absorption spectrum characteristic of the tetracycline ligand. After irradiation with visible light, the excited complex transfers its energy to a 4f level within the ion. The luminescence of the complex consists of the narrow bands characteristic of the Eu^{3+} ion. Because the normally broad-banded radiation from tetracycline is channelled into a few narrow bands, the peak intensity of the luminescence of the complex is much greater than that of the free ligand, and therefore, offers a means of improving the sensitivity for luminescent detection. The 617-nm Eu^{3+} line is in a region of the spectrum that is relatively free of the pernicious fluorescence background of biological samples and the long luminescence lifetime (20 μs) offers an additional means of improving signal-to-noise ratios through time resolution.

Considerable research effort has been devoted to the study of the coordination chemistry of the tetracyclines [2—15] and binding constants for many different types of metals have been calculated [2, 3, 5, 8]. This aspect of tetracycline chemistry is quite complex because of the existence of three

---

[a]Present address: Tektronix, P.O. Box 500, Delivery Station 50-289, Beaverton, OR 97077, U.S.A.

[b]Present address: Hoofdweg 6-II, Amsterdam, The Netherlands.

0003-2670/84/$03.00

or more binding sites and four sites of prototropic dissociation on each molecule and because the affinity of these sites for metal ions as well as the charge on the complex may change markedly with pH.

Tetracyclines are derived from a system of four six-membered rings arranged linearly with characteristic double bonds (Fig. 1). The conjugated regions comprise two distinct chromophores separated by a small unconjugated region. The A-ring system represents one chromophore while the BCD system forms the other.

Four prototropic dissociations have been observed for the tetracyclines, with $pK_1 = 3.30, pK_2 = 7.68, pK_3 = 9.69$ and $pK_4 = 10.7$ [5, 6]. The first pK_a is associated with an enolic hydroxy group on the A ring. Most studies agree that at pH < 3 and before the first ionization (loss of the enolic H on the A ring) takes place, no complexation occurs. Complexation below pH 3 has been observed only with lanthanide species [10]. The second and fourth pK_a values have been associated with the BCD hydroxy groups [5]. Many studies have concluded that at pH > pK_2, metal binding by the BCD β-diketone system becomes important [10, 12, 13]. The third pK_a at 9.7 has been attributed to deprotonation of the A-ring dimethylammonium group [5].

As one would expect, the luminescence characteristics of tetracyclines and their metal complexes are highly pH-dependent [9]. This must be due directly or indirectly to the changes in spectroscopic properties of the ligands and complexes accompanying successive deprotonations. In the present work, the pH dependences of the absorption and luminescence spectra of solutions of varying concentrations and molar ratios of Eu^{3+} and tetracycline were studied in order to understand better the nature of the luminescing complexes.

EXPERIMENTAL

Reagents and apparatus

Europium nitrate (Alfa Products, Danvers, MA) and tetracycline hydrochloride (Sigma Chemical Co., St. Louis, MO) were used to prepare aqueous solutions with distilled water.

Absorbance studies were done with a Varian (Palo Alto, CA) 634S double-beam spectrophotometer. All fluorescence measurements were made with a laboratory-constructed fluorimeter as described previously [1]. This is a

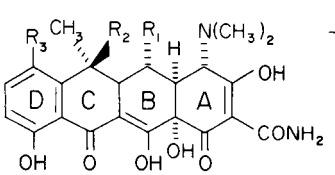

R_1	R_2	R_3	
H	OH	H	Tetracycline
H	OH	Cl	Chlortetracycline
OH	H	H	Doxycycline

Fig. 1. Structure of tetracycline and some of its derivatives.

moderate-resolution instrument with a continuum source. Lifetimes were measured by another laboratory-constructed fluorimeter. The lifetime system has a pulsed laser source and gated detection system.

Procedures

The pH titrations were done in unbuffered, distilled water. A solution containing ca. 10^{-5} M tetracycline hydrochloride and variable concentrations of Eu^{3+} was titrated with 1.2×10^{-2} M sodium hydroxide and aliquots were periodically monitored for absorbance, fluorescence and pH. After each spectroscopic measurement, the aliquot was returned to the titration vessel to minimize loss of reagents.

The luminescence decay times of the complexes were measured for several points during both complexiметric and pH titrations done as described above. The aliquots in quartz cuvettes were placed in the pulsed laser fluorimeter. While the samples were illuminated with the laser, the boxcar gate delay was scanned from 0 to 100 μs at a rate of 10 μs min^{-1}. The resulting chart recorder output showing the exponential decay of the signal was used to calculate the lifetimes.

RESULTS AND DISCUSSION

Complex formation between Eu^{3+} and tetracycline

Major confusion in the literature arises from the presence of several sites in tetracycline that might chelate metal ions (Fig. 1). Some of these binding sites become substantially more nucleophilic after deprotonation, so that the chelating capability might be expected to vary with pH.

In the earliest studies, Albert [2, 3] determined binding constants for a number of transition metal ions. He concluded that only the group having $pK_a \approx 7$ underwent ionization on chelation. Coibon and Laszlo [5] suggested that $pK_a = 7.7$ is due to the β-diketone system of the BC rings. Doluisio and Martin [15] thought that the group having $pK_a = 7.7$ was the dimethylamino group on the A ring, and so they concluded that A-ring binding occurs. Other workers [11, 12] concluded that for sodium ion in 1:1 water/dimethylsulfoxide, binding occurred only in the A ring. Circular dichroism studies by Mitscher et al. [13] showed that at very low pH, no binding occurs; at pH 3—7, A-ring binding occurs, and at pH above 7.5, binding is at the BC β-diketone region. Durckheimer [4] agreed with Mitscher et al. [13] that no binding occurs below pH 3, while Celotti and Fazakerley [10] have shown through n.m.r. studies that tetracycline complexed Gd^{3+} ions at pH 2 in the A-ring and at higher pH in the BCD ring system.

When tetracycline (TC) hydrochloride is titrated potentiometrically with sodium hydroxide (Fig. 2), a single equivalent of base is consumed by the ligand in bringing the solution to an equivalence point near pH 7. This corresponds to the neutralization of the fairly strongly acidic enolic proton in the A ring of the singly charged cation (H_4TC^+). When the molar ratio of

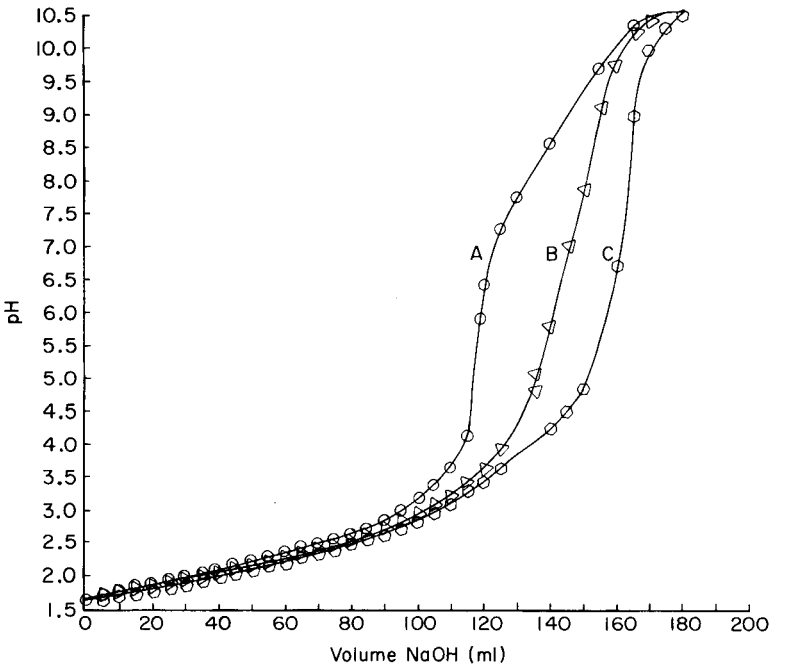

Fig. 2. Potentiometric titrations of 5.00 × 10^{-3} M tetracycline hydrochloride and 2.26 × 10^{-2} M HCl (50 ml of solution) with 1.153 × 10^{-2} M sodium hydroxide: (A) with no Eu^{3+} present; (B) with the test solution 2.50 × 10^{-3} M in Eu^{3+}; (C) with the test solution 5.00 × 10^{-3} M in Eu^{3+}.

tetracycline hydrochloride to Eu^{3+} is 2:1 (Fig. 2) and the formal concentration of the former is the same as above, two equivalents of sodium hydroxide are required to produce a sharp equivalence point near pH 7. This would suggest that Eu^{3+} forms a 1:2 complex with the singly negative anion of the tetracycline (H_2TC^-), a complex similar to those reported by earlier investigators employing a variety of transition and non-transition metal ions. However, when the molar ratio of tetracycline hydrochloride to Eu^{3+} is 1:1 (Fig. 2) and the formal concentration of tetracycline is the same as above, three equivalents of sodium hydroxide are required to produce a sharp equivalence point near pH 7. This indicates that three protons are displaced by Eu^{3+} from the singly charged tetracycline cation to form a 1:1 complex (near pH 7) with the doubly negative anion of tetracycline (HTC^{2-}). If the latter suggestion is true, the titration behavior of the system containing a 2:1 excess of tetracycline over Eu^{3+} could be explained by assuming that half of the tetracycline hydrochloride forms a 1:1 complex with Eu^{3+} yielding 3/2 equivalent of easily titratable protons while the remaining half equivalent of tetracycline yields 1/2 equivalent of easily titratable protons (the proton from the enolic group of the A ring). The sum of the two sources of protons

adds up to the two protons per tetracycline monocation titrated at neutrality. If, however, a 2:1 complex is formed, the solution which is equimolar in tetracycline hydrochloride and Eu^{3+} should have a titer equal to that of the system containing the two-fold excess of tetracycline hydrochloride (or perhaps slightly lower if some 1:1 complex with the same ligand species is present). Mole ratio and continuous variation plots of the long-wavelength absorption and luminescence spectra of the Eu^{3+}/tetracycline system, at pH 7, support the conclusion that the complex existing in the neutral pH region has 1:1 stoichiometry. This conclusion is in agreement with the work of Silva and Dias [16] who found that several transition metals form 1:1 complexes with H_2TC^- which dissociate to form 1:1 complexes with HTC^{2-}.

The absorptiometric and pH titrations of the Eu^{3+}/tetracycline systems in the presence of a 1000-fold molar excess of Eu^{3+}, are shown in Fig. 3. These titration curves show that there is complexation between Eu^{3+} and tetracycline over the pH region 1—10 and that the complexes formed are not the same throughout the pH region investigated. In the pH region 0.5—2.5, there is no change in the longest wavelength band of the tetracycline monocation (H_4TC^+) at 355 nm but the band at 265 nm is displaced to 268 nm with increasing pH. This is similar to the red shift of the 265-nm band of H_4TC^+ to 272 nm upon dissociation to form the zwitterion H_3TC in the pH region 1.3—5.3. The latter process also causes no shifting of the long wavelength band at 355 nm, an observation which suggests that the absorption in the

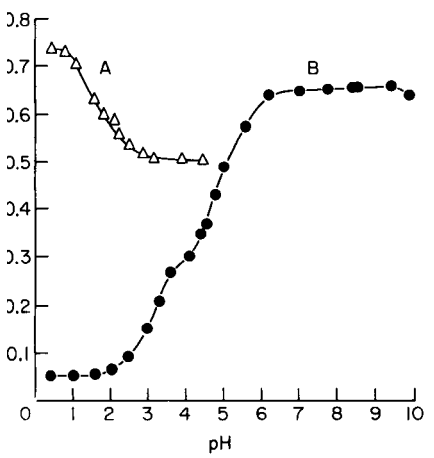

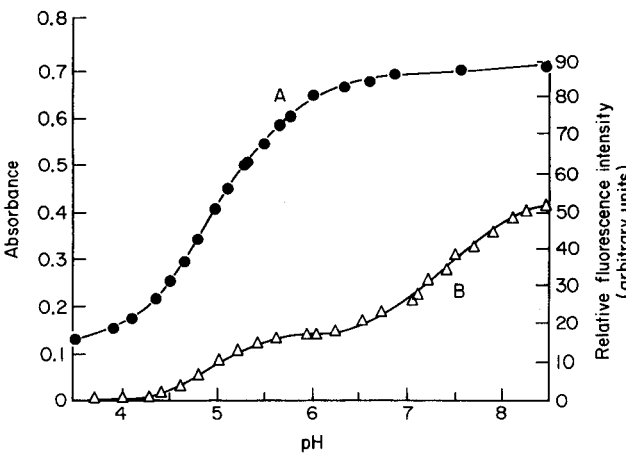

Fig. 3. Titrations of 1.00×10^{-5} M tetracycline hydrochloride and 1.00×10^{-2} M Eu^{3+} containing 0.100 M HCl with 1 M NaOH: (A) monitored spectrophotometrically at 260 nm; (B) monitored at 400 nm. Absorbances are corrected for volume changes from addition of the titrant.

Fig. 4. Titration of 2.50×10^{-5} M tetracycline hydrochloride and 2.50×10^{-5} M Eu^{3+} with 2.26×10^{-2} M NaOH: (A) monitored spectrophotometrically at 400 nm; (B) monitored fluorimetrically at 617 nm.

265—272-nm region is due primarily to the small, relatively isolated A-ring chromophore. Presumably, the metallochromic shift in that band is due to complexation in the A ring. By doing the pH titration of the Eu^{3+}/tetracycline system, using a 1000-fold molar excess of Eu^{3+} over tetracycline and monitoring the progress of the titration by following the changes in the spectrum at 265 nm, it was possible to estimate the equilibrium constant K for the reaction

$$Eu^{3+} + H_4TC^+ \rightleftharpoons Eu(H_3TC)^{3+} + H^+$$

where

$$K = [Eu(H_3TC)^{3+}][H^+]/[Eu^{3+}][H_4TC^+]$$

If the formation constant k_1 for $Eu(H_3TC)^{3+}$ is given by $k_1 = (Eu(H_3TC)^{3+})/(Eu^{3+})(H_3TC)$ and the first acidity constant of H_4TC^+ ($10^{-3.30}$) is $K_{a1} = (H^+)(H_3TC)/(H_4TC^+)$, then after a Debye—Hückel correction of K, k_1 can be calculated from $k_1 = K/K_{a1}$. In the present work, k_1 was found to be $(3.0 \pm 0.3) \times 10^3$ indicating that at pH < 3, there is complexation of H_3TC, but it is very weak.

In the pH region 3—4, the long-wavelength absorption maximum of the $Eu(H_3TC)^{3+}$ complex is red-shifted to 374 nm and is similar in appearance to the long-wavelength absorption band of H_2TC^- at 370 nm which is prevalent at pH 7—8. Presumably, the former spectral shift results from the dissociation of $Eu(H_3TC)^{3+}$ to form $Eu(H_2TC)^{2+}$. The shorter-wavelength absorption band, attributed to the A-ring chromophore, remains unchanged at 268 nm in the complex and is blue-shifted from 272 nm to 266 nm in the free ligand, with increasing pH during these transformations. The substantial red shifts of the long-wavelength absorption bands in both cases suggest that in both $Eu(H_3TC)^{3+}$ and H_3TC, the process occurring entails dissociation of the phenolic group of the D ring and in the complex may be represented by

$$Eu(H_3TC)^{3+} \rightleftharpoons Eu(H_2TC)^{2+} + H^+$$

The conditional acidity constant for this reaction is

$$K'_{a2} = [H^+][Eu(H_2TC)^{2+}]/[Eu(H_3TC)^{3+}]$$

If the formation constant for $Eu(H_2TC)^{2+}$ is given by $k_2 = (Eu(H_2TC)^{2+})/(Eu^{3+})(H_2TC)$, and the second acidity constant of H_3TC ($10^{-7.68}$) is $K_{a2} = (H^+)(H_2TC^-)/(H_3TC)$, then k_2 can be calculated from $k_2 = k_1K'_{a2}/K_{a2}$, if K'_2 is corrected to infinite dilution.

On changing the pH from 4 to 6, the long-wavelength absorption band of $Eu(H_2TC)^{2+}$ is red-shifted to 390—400 nm and the short-wavelength absorption band of the same complex is blue-shifted to 264 nm. Presumably this is due to dissociation of $Eu(H_2TC)^{2+}$ to form $Eu(HTC)^+$.

When the pH is changed from 8 to 10, the corresponding phenomenon can be observed in H_2TC^-, in which its dissociation to HTC^{2-} results in a small red-shift of the long-wavelength absorption band from 370 nm to 376 nm

and the short-wavelength band splits into two bands, one at 266 nm and one at 286 nm. Although this dissociation in the free ligand has been attributed to the dimethylamino group [5], the small spread between pK_{a2}, pK_{a3}, and pK_{a4} of tetracycline indicates that substantial tautomerism of the ligand must occur between pH 8 and pH 11, and it is probably incorrect to attribute pK_{a3} and pK_{a4} (possibly pK_{a2} as well) to dissociations from single groups on the ligand. This statement is supported by the fact that there is shifting of the long-wavelength band, which is probably indicative of dissociation of the hydroxy group in the B ring, and splitting of the short-wavelength band which is probably related to the dissociation of the dimethylammonium group of the A ring.

The large red-shift of the long-wavelength absorption band of $Eu(H_2TC)^{2+}$ accompanying dissociation to $Eu(HTC)^{+}$ is anomalous by comparison with the corresponding shift in the free ligand and may be indicative of more than simple dissociation. It has been suggested that the site of metal binding changes from the A ring to the BCD-ring system at higher pH [10, 13] and this may be what is occurring here. Especially if the Eu^{3+} ion were coordinated by the hydroxy group of the B ring and the carbonyl group of the C ring, in $Eu(HTC^{+})$, leaving the phenolic group dissociated, the positive polarization introduced into the carbonyl group by coordination would be adequate to account for the anomalously large red shift of the long-wavelength absorption band accompanying dissociation of $Eu(H_2T)^{2+}$. The latter dissociation

$$Eu(H_2TC)^{2+} \rightleftharpoons Eu(HTC)^{+} + H^{+}$$

has the conditional acidity constant

$$K'_{a3} = [H^{+}]\,[Eu(HTC)^{+}]/[Eu(H_2TC)^{2+}]$$

which is related to the formation constant of $Eu(HTC)^{+}$ by $k_3 = (Eu(HTC)^{+})/(Eu^{3+})(HTC^{2-})$, which is calculated from the ionic strength-corrected value of K'_{a3} and the acidity constant, K_{a3}, of H_2TC^{-} by the relationship $k_3 = K'_{a3}k_2/K_{a3}$.

The spectrophotometric pH titration curve of tetracycline in the presence of a 1000-fold molar excess of Eu^{3+}, monitored at 400 nm is shown in Fig. 3. This titration curve shows that the inflection regions for the dissociation equilibria described by K'_{a2} and K'_{a3} overlap considerably and are reasonably well separated from the dissociation equilibria occurring at lower and higher pH. At pH > 7, it is impossible to monitor the system containing ca. 10^{-2} M Eu^{3+} because of precipitation, probably of hydroxo- or oxo-complexes of Eu^{3+}. The data represented in the titration curve of Fig. 3 were solved for K'_{a2} and K'_{a3} by means of the Robinson—Biggs equation [17]:

$$(A - A_T)(H^{+})^2 + (A - A_D)K'_{a2}(H^{+}) + (A - A_M)K'_{a2}K'_{a3} = 0 \qquad (1)$$

where A is the absorbance at any given pH in the inflection region (corresponding to hydrogen ion activity (H^{+})), A_T is the absorbance of the isolated

trication $Eu(H_3TC)^{3+}$ at pH $\approx$ 2, A_M is the absorbance of the isolated monocation $Eu(HTC)^+$ at pH $\approx$ 6 and A_D is the absorbance of the isolated dication $Eu(H_2TC)^{2+}$. Because of the overlap of the two successive equilibria encompassed in the titration curve, A_D cannot be determined directly but rather can be eliminated or calculated along with K'_{a2} and K'_{a3}, as a third unknown parameter by simultaneous solutions of Eqn. 1. This treatment yielded corrected values of $1.7 \pm 0.3 \times 10^{-4}$ and $8.9 \pm 0.4 \times 10^{-6}$ for K'_{a2} and K'_{a3}, respectively. These in turn were used to calculate values of $2.5 \pm 0.5 \times 10^7$ and $1.1 \pm 0.3 \times 10^{12}$ for k_2 and k_3, respectively.

A solution 1.00×10^{-5} M in both tetracycline hydrochloride and Eu^{3+} was titrated with sodium hydroxide and the progress of the titration was monitored spectrophotometrically at 400 nm and fluorimetrically at 617 nm, over the pH range 4—7. The respective titration curves are shown in Fig. 4. In the pH region 4—6.5, both curves are essentially identical and represent predominantly the formation of $Eu(H_2TC)^{2+}$ from H_3TC and Eu^{3+} in the pH region 4—5 and the formation of $Eu(HTC)^+$ from $Eu(H_2TC)^{2+}$ in the pH region 5—6.5. From pH 6.5 to 8.5, the absorbance at 400 nm is essentially constant. However, in the same pH region, the luminescence again rises sharply, leveling off at pH 8.2—8.7 and then dropping at pH > 8.7. At pK > 8.7, the absorbance at 400 nm also decreases. The rise in fluorescence from pH 6.5 to 8.5 can be attributed to the release of the last dissociable proton on the coordinated tetracycline molecule, according to the reaction

$$Eu(HTC)^+ \rightleftharpoons EuTC + H^+.$$

Indeed, the data represented in the fluorimetric titration curve of Fig. 4 can be fitted well to the Henderson—Hasselbalch equation to yield $K'_{a4} = (4.7 \pm 0.5) \times 10^{-8}$ where $K'_{a4} = [H^+][EuTC]/[Eu(HTC)^+]$. The failure of the absorbance at 400 nm to show significant changes over the pH region where $Eu(HTC)^+$ dissociates suggests that the site of dissociation is the dimethylammonium group of the A ring. In the free ligand, this dissociation has an associated pK_{a4} of 10.7. It is possible using this value to estimate k_4 for the reaction

$$Eu^{3+} + TC^{3-} \rightleftharpoons EuTC$$

where $k_4 = (EuTC)/(Eu^{3+})(TC^{3-})$, from the relationship $k_4 = K'_{a4}k_3/K_{a4}$. The estimated value of k_4 is 3×10^{15}. Evidently, with each successive prototropic dissociation, the complex of Eu^{3+} with tetracycline becomes stronger. At pH 8.5 where EuTC is virtually the sole form of the complex, there is less than 1% dissociation of the complex when Eu^{3+} and tetracycline are present in equimolar amounts at 1×10^{-6} M. In the presence of excess of Eu^{3+}, the formation of EuTC can be easily made quantitative into the subnanomolar concentration region. The constants obtained are summarized in Table 1.

The increasing strength of the Eu^{3+}/tetracycline complex with increasing pH probably also accounts for the fact that anti-acids containing Al^{3+}, Ca^{2+} and Mg^{2+} interfere with the absorption of orally administered tetracycline

TABLE 1

Summary of prototropic dissociation constants (pK'_a) and formation constants ($\log k$) of the complexes derived from Eu^{3+} and tetracycline

Reaction	pK'_a
$Eu(H_3TC)^{3+} \rightleftharpoons Eu(H_2TC)^{2+} + H^+$	3.77 ± 0.07
$Eu(H_2TC)^{2+} \rightleftharpoons Eu(HTC)^+ + H^+$	5.05 ± 0.02
$Eu(HTC)^+ \rightleftharpoons EuTC + H^+$	7.33 ± 0.04
	$\log k$
$Eu^{3+} + H_3TC \rightleftharpoons Eu(H_3TC)^{3+}$	2.48 ± 0.04
$Eu^{3+} + H_2TC^- \rightleftharpoons Eu(H_2TC)^{2+}$	7.40 ± 0.09
$Eu^{3+} + HTC^{2-} \rightleftharpoons Eu(HTC)^+$	12.40 ± 0.12
$Eu^{3+} + TC^{3-} \rightleftharpoons EuTC$	15.4 (est.)

from the gut, notwithstanding that Ca^{2+} and Mg^{2+} form weak complexes with most ligands [18].

Although there have been reports of polynuclear complex formation of lanthanide ions with a number of ligands [19], the data obtained in these experiments showed no evidence for this process up to pH 9, as all pH-dependent transformations of the 1:1 complex could be fitted well to simple monoprotic equilibria and monomeric 1:1 complex formation.

Luminescence intensity and lifetime

The luminescence decay times of the various complexes derived from Eu^{3+} and tetracycline show a pH dependence (Fig. 5) which is similar to the luminescence intensity/pH profile. In the pH region below 3, where a small amount of $Eu(H_3TC)^{3+}$ may exist at the low concentrations of Eu^{3+} and tetracycline used in this study (10^{-5} M), the very weak observable luminescence has a decay time of about 1 μs. In the region where $Eu(H_2TC)^{2+}$ forms, the decay time abruptly increases to about 14 μs and remains approximately constant through the pH region 4—6 where both $Eu(H_2TC)^{2+}$ and $Eu(HTC)^+$ predominate. It would appear that both of these species have identical decay times. In the region where EuTC forms (pH 6—8), the decay time increases to 24 μs and remains relatively constant through the region where EuTC predominates. At pH > 9, the decay time drops, as does the luminescence intensity.

The observed luminescence decay time (τ) in each species is expressed by

$$\tau = \phi_{ET}/(k_l + k_d)$$

where ϕ_{ET} is the efficiency of excitation transfer from the ligand to the metal ion (similar to the intersystem crossing efficiency in phosphorimetry), k_l is the rate constant for radiative decay of the metal ion, and k_d is the sum of the pseudo-first-order rate constants for all radiationless deactivation processes of the luminescing state of the Eu^{3+} ion. The energy transfer efficiency, ϕ_{ET}, in turn is given by

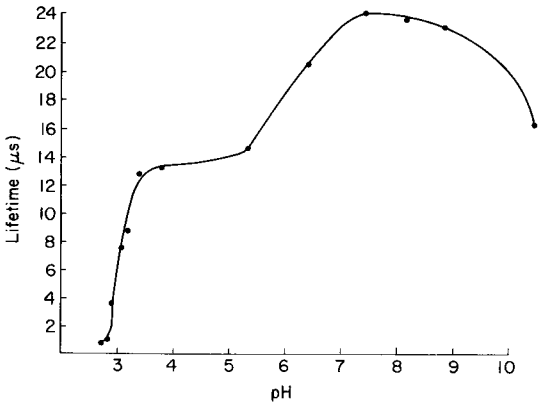

Fig. 5. Luminescence decay times of the Eu^{3+}/tetracycline complexes as a function of pH. The solution was 6.00×10^{-5} M in both tetracycline HCl and Eu^{3+}.

$$\phi_{ET} = k_{ET}/(k_f + k_{ET} + k'_d)$$

where k_f is the rate constant for fluorescence of the complexed ligand (the reciprocal of the natural lifetime of the lowest excited singlet state of the ligand), k_{ET} is the rate constant for energy transfer and k'_d is the sum of all pseudo-first-order radiationless processes, exclusive of energy transfer to Eu^{3+}, of the ligand.

The luminescence intensity in each complex species is related to the molar absorptivity of the complexed ligand at the wavelength of excitation and the quantum yield, ϕ_l, of luminescence of the complex. The latter is given by

$$\phi_l = \phi_{ET}\, k_l/(k_l + k_d)$$

The luminescence intensity of $Eu(H_3TC)^{3+}$ is too small to be measured accurately but the ratios of the ratios of the luminescence intensities (1:1:3.1) to the ratios of the estimated absorptivities at 400 nm (1:1:1.8) of $Eu(H_2TC)^{2+}$, $Eu(HTC)^{+}$, and EuTC indicate that ϕ_l for these species is in the ratio 1:1:1.7 and because τ for each of these species is also in the ratio 1:1:1.7, k_l for each species is in the ratio 1:1:1.

This result is easy to rationalize on theoretical grounds. The radiative rate constant k_l is the probability of spontaneous radiative transition between two *f*-orbitals of Eu^{3+}, both being antisymmetric with respect to inversion. These transitions are forbidden by the LaPorte selection rule which also accounts for their low molar absorptivities and long luminescence decay times. In *d*-block transition elements, coordinated ligands can perturb the *d*-orbitals and break down the symmetry of the various electronic states derived from the *d*-orbitals, resulting in relaxation of the LaPorte selection rule. This causes intensification of *d*—*d* absorption spectra. In Eu^{3+}, however, the *f*-orbitals are well shielded from the environment within the ionic kernel. Hence, perturbation by coordinated ligands, especially the hard bases that

tend to react with lanthanide ions, is extremely weak. This conclusion is supported by the fact that the emission for all of the Eu^{3+} complexes studied here occurs at the same place in the spectrum and with the same bandwidth regardless of the fact that the more highly dissociated forms of the ligand interact more strongly with the Eu^{3+} ion. Because of the shielding of the *f*-orbitals of Eu^{3+} from the environment, it is also doubtful that k_d is affected much by changes in the state of protonation of the ligand. This means that the variations in τ for various states of protonation of the complex must originate with ϕ_{ET}. Now ϕ_{ET} depends on k_f, k_{ET} and k'_d, but k_f, which can be estimated from the integrated long-wavelength absorption band [20] for each coordinated ligand species, is 1.5×10^8 s^{-1} for $Eu(H_2TC)^{2+}$ and 1.4×10^8 s^{-1} for both $Eu(HTC)^+$ and EuTC. Obviously, the discrepancies between ϕ_{ET} and hence, between τ for the various species, must arise with either k_{ET} or k'_d (or both). The rate constant for energy transfer, k_{ET}, is largely governed by spin-orbital coupling between the singlet state of the ligand and the septet state of the Eu^{3+} ion. This is dominated by the magnetic field generated by the paramagnetic Eu^{3+} ion and the separation in energy between the lowest excited singlet state of the ligand and the excited septet state of the metal ion responsible for luminescence [21]. Because the lowest excited singlet state of the ligand is in all cases derived from the BCD chromophore, the influence of the magnetic field arising from the Eu^{3+} ion ought to be about the same and maximal for all complexes in which the metal ion is coordinated by groups in the BCD region of tetracycline. However, because the BCD chromophore is farther from the metal ion when the latter is coordinated by groups in the A ring, the degree of spin-orbital coupling caused by magnetic induction of Eu^{3+} should be smaller when the latter circumstance occurs.

Spin-orbital coupling is also maximal when there is a very small energy gap between the lowest excited singlet state of the ligand and either the emitting septet state of the metal ion or a higher septet state which can be populated by intersystem crossing and then undergo internal conversion to the emitting state [21]. In Eu^{3+}, there is such a state giving rise to a weak, narrow absorption band at 392 nm. Overlap of this band with the long-wavelength absorption band of the ligand is very slight in $Eu(H_3TC)$, substantial in $Eu(H_2TC)^{2+}$, and great in $Eu(HTC)^+$ and EuTC. On this basis, one might expect $Eu(HTC)^+$ and EuTC to luminesce about equally intensely and with equal decay times, both of which would be greater than that of $Eu(H_2TC^{2+})$. This would also be expected if, as suggested earlier, Eu^{3+} is coordinated by A-ring groups in $Eu(H_2TC)^{2+}$ and by BCD-ring system groups in $Eu(HTC)^+$ and EuTC. However, it is the decay times and quantum yields of $Eu(H_2TC)^{2+}$ and $Eu(HTC)^+$ that are identical and less than those of EuTC. Consequently, it appears that differences between k_{ET} are inadequate to explain the differences between the luminescences of the various Eu^{3+}/tetracycline chelates.

Finally, k'_d, the collective rate constant for radiationless deactivation of the lowest excited singlet state of tetracycline, must be considered. This rate constant will be related primarily to deactivation by internal conversion (or

external conversion) by collision with solvent phonons. Although it is difficult to prove unambiguously, conjugate acid–base pairs often have different fluorescence quantum yields and decay times as a result of different degrees of interaction with solvents, especially hydrogen-bonding solvents such as water. For example, the fluorescence of 8-methoxyquinoline has a decay time of 1.6 ns while its conjugate acid has a decay time of 4.0 ns in water, although the values of k_f for each are almost identical, and no phosphorescence is observed from either [22]. Alternatively, intersystem crossing arising from factors intrinsic to the ligand and its interactions with the solvent also could have a dramatic effect on k'_d and hence, on k_{ET}. For example, it is well known that *N*-heterocyclic and aromatic carbonyl compounds fluoresce poorly or not at all in hydrocarbon solvents because efficient intersystem crossing results from the presence of sp^2-hybridized unbonded electron(s). In hydroxylic solvents, however, these compounds often fluoresce with moderate intensity and short decay time because of the inversion of the lowest $^1n,\pi^*$ and $^1\pi,\pi^*$ states as a result of electrostatic interaction with the solvent [20]. Protonated *N*-heterocyclic and carbonyl compounds, however, fluoresce well in all solvents because the $^1\pi,\pi^*$ state is always lowest.

In summary, then, it would appear to be the k'_d term which is influenced by solvation, that has the greatest effect on ϕ_{ET} and ultimately on τ in the various states of protonation of the Eu–TC chelates. Because the *f*-orbitals of Eu^{3+} are shielded from the environment, k_l and k_d should be relatively independent of the nature of the ligand and the solvent and therefore, attempts to optimize the luminescence of Eu^{3+} complex should be directed at driving ϕ_{ET} toward unity either by control of the state of ionization of the ligand or by judicious choice of the solvent.

This research was supported by grant NIH-GM-11373-19.

REFERENCES

1 L. M. Hirschy, E. G. Dose and J. D. Winefordner, Anal. Chim. Acta, 147 (1983) 311.
2 A. Albert, Nature, 172 (1953) 201.
3 A. Albert, Nature, 177 (1956) 433.
4 W. Durckheimer, Angew. Chem., 14 (1975) 721.
5 C. Coibon and P. Laszlo, Biochem. Pharmac., 28 (1979) 1367.
6 C. R. Stephens, K. Murai, K. J. Brunings and R. B. Woodward, J. Am. Chem. Soc., 78 (1956) 4155.
7 P. J. Neuvonin, G. Gothoni, R. Hackman and K. Bjorksten, Br. Med. J., 4 (1970) 532.
8 M. Saiki, M. Nastisi and F. Lima, J. Radioanal. Chem., 64 (1981) 83.
9 M. Mathew and P. Balaram, J. Inorg. Biochem., 13 (1980) 339.
10 M. Celotti and G. V. Fazakerley, J. Chem. Soc., Perkin Trans. 2, (1977) 1319.
11 J. Gulbis, G. Everett, Jr. and C. Frank, J. Am. Chem. Soc., 98 (1976) 1280.
12 J. Gulbis and G. Everett, Jr., J. Am. Chem. Soc., 97 (1975) 6248.
13 L. Mitscher, A. Bonacci, B. Slatereng, A. K. Hacker and T. D. Sokoloski, Antimicrob. Agents Chemother, (1969) 111.
14 L. Benet and J. Goyan, J. Pharm. Sci., 55 (1966) 1184.
15 J. Doluisio and A. Martin, J. Med. Chem., 6 (1963) 16; 6 (1963) 20.

16 J. J. R. F. Silva and M. H. M. Dias, Rev. Port. Quim., 14 (1972) 159, 170; 15 (1973) 1.
17 R. Robinson and A. I. Biggs, Aust. J. Chem., 10 (1957) 128.
18 L. S. Goodman and A. Gilman, The Pharmacological Basis of Therapeutics, 4th ed., Macmillan, New York (1970) p. 1258.
19 Z. Koneatis and H. G. Brittain, Inorg. Chim. Acta, 40 (1980) 51.
20 T. Förster, Fluoreszenz organischer Verbindungen, Vandenhoech and Ruprecht, Göttingen, 1951, p. 154.
21 R. S. Becker, Theory and Interpretation of Fluorescence and Phosphorescence, Wiley-Interscience, New York, 1969, Ch. 8.
22 S. G. Schulman and L. S. Rosenberg, Anal. Chim. Acta, 115 (1980) 211.

Analytica Chimica Acta, 166 (1984) 221—231
Elsevier Science Publishers B.V., Amsterdam — Printed in The Netherlands

INTERACTIONS ENTRE LES SERINGUES NON RÉUTILISABLES ET LES MÉDICAMENTS
Migration d'un Accélérateur de Vulcanisation Benzothiazolique et de Composés Apparentés

CH. B. AIRAUDO*, A. ASSAF et A. GAYTE-SORBIER

Laboratoire de Bromatologie, Diététique et Analyse appliquée à l'Expertise, Faculté de Pharmacie, 27 Bd. Jean Moulin, 13385 Marseille Cedex 5 (France)

G. SALMONA et E. J. VINCENT

Laboratoire de Chimie organique physique, Faculté des Sciences et Techniques, Rue Henri Poincaré, 13397 Marseille Cedex 13, (France)

(Reçu le 15 Mai 1984)

SUMMARY

(*Interactions between disposable syringes and drugs. Leaching of a benzothiazole vulcanization accelerator and related compounds*)

Disposable syringes (three brands) filled with water very quickly yielded one or more compounds with u.v. absorption peaks. The rubber plunger seals were identified as the source of contaminant. Their analysis by t.l.c. showed the presence of 2-mercaptobenzothiazole, used as vulcanization accelerator. The compounds extracted into water were identified by mass spectrometry (electron impact and methane chemical ionization) as 2-mercaptobenzothiazole, 2-methylthiobenzothiazole, 2-hydroxybenzothiazole, 2-(2-hydroxyethylthio)benzothiazole and 2-(2-hydroxyethoxy)benzothiazole. The last three compounds were formed during sterilization of the syringes with ethylene oxide. The role of the precise nature of the vulcanization accelerator in this reaction is briefly described (zinc ions seem to be necessary), as are the analytical interferences resulting from the observed phenomena.

RÉSUMÉ

Il a été constaté que des seringues non réutilisables de trois marques cédaient très rapidement à l'eau une ou plusieurs substances présentant un spectre d'absorption u.v. Les têtes de piston en élastomère ont été identifiées comme la source de la contamination. Leur analyse par c.c.m. a mis en évidence la présence de mercapto-2 benzothiazole, utilisé comme accélérateur de vulcanisation. Les substances extraites par l'eau ont été identifiées par spectrométrie de masse (impact électronique et ionisation chimique par le méthane). Il s'agit du mercapto-2 benzothiazole, du méthylthio-2 benzothiazole, de l'hydroxy-2 benzothiazole, de l'(hydroxy-2 éthylthio)-2 benzothiazole et de l'(hydroxy-2 éthoxy)-2 benzothiazole. Les trois derniers composés se forment au cours de la stérilisation des seringues par l'oxyde d'éthylène. L'influence de la nature exacte des accélérateurs de vulcanisation au cours de cette réaction est brièvement évoquée, la présence de zinc paraissant déterminante, ainsi que les interférences analytiques résultant des phénomènes constatés.

0003-2670/84/$03.00

Du fait de leurs avantages, les seringues non réutilisables ont été de plus en plus employées au cours des dernières années et ont même conquis la totalité du marché dans de nombreux pays [1]. Elles présentent cependant l'inconvénient d'être éventuellement incompatibles avec les médicaments injectables dont le solvant n'est pas exclusivement aqueux, les matériaux utilisés pour leur fabrication n'étant pas totalement inertes. Les rares travaux expérimentaux effectués à ce propos ont été analysés dans une étude préalable [2]. Nous y indiquions déjà avoir aussi observé des interactions avec les préparations injectables strictement aqueuses, alors qu'on pouvait penser que ce problème au moins était résolu depuis longtemps: de l'eau bidistillée mise au contact de seringues de plusieurs marques présentait en effet très rapidement un spectre d'absorption u.v. Dès 1965, Inchiosa [3] avait obtenu dans des circonstances analogues le même spectre et avait supposé qu'il était dû au méthylthio-2 benzothiazole. Dernièrement, Petersen et al. [4] ont rapporté que de l'(hydroxy-2 éthylthio)-2 benzothiazole était cédé à de l'eau par de telles seringues. Cette récente publication et notre observation rapportée plus haut montrent que les problèmes de relargage en milieu aqueux sont toujours actuels et soulignent l'intérêt de leur étude du point de vue analytique.

Nous rapportons ici les résultats que nous avons obtenus sur plusieurs marques de seringues munies d'une tête de piston rapportée en élastomère. La démarche analytique suivie a consisté à rechercher d'abord par spectrophotométrie d'absorption u.v. quelle était la partie des seringues responsable du relargage observé. Après qu'il eût été établi qu'il s'agissait des têtes de piston, les élastomères constituant ces têtes ont été partiellement analysés par chromatographie sur couche mince (c.c.m.), afin de restreindre le champ des recherches ultérieures. Les substances relarguées dans l'eau ont ensuite été identifiées par spectrométrie de masse (s.m.). Enfin, l'origine de plusieurs d'entre elles, dont la présence paraissait a priori inexplicable, a pu être précisée en recourant aux mêmes méthodes analytiques.

PARTIE EXPÉRIMENTALE

Les seringues testées appartenaient à trois marques couramment disponibles en France et à l'étranger. D'après une autre étude effectuée parallèlement [5], il s'agissait de seringues de bonne qualité, en ce sens qu'elles satisfaisaient à la plupart des normes de la Pharmacopée française et de l'Association française de Normalisation.

Parmi les produits utilisés comme substances de référence, seuls seront cités ici ceux de structure mercapto-2 benzothiazolique: benzothiazolethiol-2 (I, Tableau 1) ou mercapto-2 benzothiazole (Prolabo, qualité pour analyses), dithio-2,2′ bis-(benzothiazole) (II), ou disulfure de benzothiazyle (Vulnax, nom déposé: Vulcafor MBTS), bis-(benzothiazolethiolate-2) de zinc (III), ou mercapto-2 benzothiazolate de zinc (Vulnax, nom déposé: Vulcafor ZMBT), et méthylthio-2 benzothiazole (IV; Eastman Kodak). Les trois premiers produits sont des accélérateurs de vulcanisation couramment utilisés dans

TABLEAU 1

Composés de référence (I—IV) et produits identifiés (I, IV—VII)

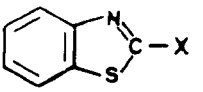

N°	Dénomination	X
I	Benzothiazolethiol-2	
II	Dithio-2,2' bis-(benzothiazole)	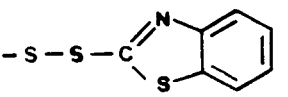
III	Bis-(benzothiazolethiolate-2) de zinc	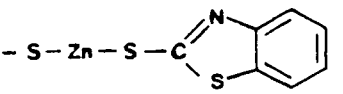
IV	Méthylthio-2 benzothiazole	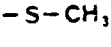
V	Hydroxy-2 benzothiazole	
VI	(Hydroxy-2 éthoxy)-2 benzothiazole	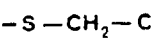
VII	(Hydroxy-2 éthylthio)-2 benzothiazole	

l'industrie des élastomères. Ce n'est pas le cas du quatrième qui a seulement été ajouté à cause de l'hypothèse d'Inchiosa [3] rapportée plus haut.

Méthodes d'analyse

Étude par spectrophotométrie u.v. L'appareil utilisé était un spectrophotomètre Perkin-Elmer type 554. Les solutions examinées ont été obtenues à partir de seringues de 5 ml, en les maintenant remplies d'eau bidistillée pendant 5 min et 1 h à la température ambiante, voisine de 20°C. En vue de déterminer la partie des seringues responsable du relargage, les têtes de piston en élastomère ont été séparées de leurs tiges et immergées individuellement pendant le même temps dans des tubes de verre borosilicaté contenant 5 ml d'eau bidistillée. Les produits de référence étaient en solution dans l'éthanol absolu à la concentration de 0,001% (p/v). L'éthanol a été choisi en raison de la médiocre solubilité des produits dans l'eau et il a été vérifié que les spectres étaient identiques dans les deux solvants.

Analyse des élastomères par chromatographie sur couche mince. Les têtes de piston prélevées sur les seringues ont été débarrassées de la plus grande partie de leur lubrifiant par essuyage à sec et réduites en morceaux de 1 à 2 mm de côté. Des prises d'essai de 20 g ont été traitées pendant 6 h dans un appareil de Soxhlet par 250 ml d'acétone, les extraits étant concentrés à 10 ml environ au cours du dernier cycle d'extraction. Les produits de référence étaient en solutions acétoniques à 0,5% (p/v) (composés I et IV) ou en solutions saturées (composés II et III). Des prises d'essai de 2 μl de chacun

des extraits acétoniques et de chacune des solutions de référence ont été déposées sur des plaques de gel de silice G sans indicateur fluorescent de 0,25 mm d'épaisseur (Merck). Les chromatogrammes ont été développés sur 15 cm dans deux mélanges proposés par Kreiner et Warner [6] pour l'identification des accélérateurs de vulcanisation: benzène/acétate d'éthyle/acétone (100:5:1) et benzène/acétate d'éthyle/n-butanol (100:2:2). Les taches ont été révélées en vaporisant successivement sur les plaques, après séchage à l'air, une solution aqueuse de tétraborate de sodium (23,4 g l^{-1}) et d'hydroxyde de sodium (3,3 g l^{-1}), puis une solution méthanolique fraîchement préparée de *N*-chloro dichloro-2,6 *p*-benzoquinone monoimine (1 g l^{-1}). Ce réactif, utilisé en réalité par ces mêmes auteurs pour la révélation des phénols, met aussi en évidence les composés mercaptobenzothiazoliques.

Étude par spectrométrie de masse. Cent têtes de piston de chaque marque, préalablement essuyées et séparées de leur tiges, ont été immergées pendant 24 h à la température ambiante dans 100 ml d'eau bidistillée. Les liquides ont été évaporés sous vide à température inférieure à 40°C et les résidus secs repris par 2 ml de méthanol, ou parfois d'éthanol absolu afin d'apprécier le rôle éventuel du solvant. Les analyses ont été effectuées sur ces solutions alcooliques, essentiellement par impact électronique, avec un spectromètre Kratos type MS-50. Les solutions alcooliques ont été évaporées à siccité dans le porte-échantillon de la sonde d'introduction directe. La température de la chambre d'ionisation était de 150°C, mais des analyses ont aussi été effectuées sans chauffage préalable de façon à vérifier l'absence de décomposition thermique. Pour la même raison, la sonde a été utilisée sans chauffage, puis à température programmée jusqu'à 150°C. Les spectres ont été obtenus à haute et basse énergie (70 eV et 10 eV), les ions résultant des transitions métastables étant enregistrés avec un détecteur de Daly. Les déterminations de masse exacte ont été réalisées à haute résolution (20 000, 10% de vallée). L'ionisation chimique par le méthane a également été utilisée afin de confirmer la présence des ions moléculaires déjà observés en impact électronique à basse énergie.

Stérilisation par l'oxyde d'éthylène

Afin de préciser l'origine de certains des produits relargués, nous avons stérilisé nous-mêmes des têtes de piston reçues en vrac. La stérilisation par un mélange de 15% d'oxyde d'éthylène et 85% d'anhydride carbonique (5 h à 50°C) et la désorption (7 jours à 50°C) ont été conduites dans des conditions couramment utilisées pour le matériel médico-chirurgical. Les résultats obtenus sur ces têtes avec les trois mêmes méthodes analytiques que ci-dessus ont été comparés à ceux donnés par des têtes du même lot de fabrication, mais non stérilisées. Des échantillons des substances de référence ont aussi été stérilisés, puis analysés de la même façon par rapport à des produits des mêmes lots non stérilisés.

RÉSULTATS ET DISCUSSION

La Figure 1 montre le spectre d'absorption que présente de l'eau bidistillée maintenue dans une seringue de 5 ml pendant 5 min (courbes a et a') et 1 h (courbe b). L'eau en contact avec les têtes de piston séparées a qualitativement les mêmes caractéristiques d'absorption. Ces spectres, identiques pour les trois marques, ont le même aspect que celui qu'Inchiosa [3] avait attribué au méthylthio-2 benzothiazole, mais seulement en le comparant avec les données d'un atlas et non avec un échantillon authentique. Cependant, ce produit n'est pas utilisé dans la formulation des mélanges à vulcaniser et sa formation ne paraît pas être due aux réactions qui se produisent au cours de la vulcanisation. Néanmoins, en raison des résultats obtenus au cours de l'analyse des élastomères par c.c.m., les spectres de composés apparentés couramment employés comme accélérateurs de vulcanisation ont été tracés. En fait, le spectre obtenu sur l'eau maintenue au contact des seringues diffère profondément de ceux des autres dérivés mercapto-2 benzothiazoliques, dont quelques-uns sont présentés dans la Fig. 1 (courbes d, e, f).

D'après ces résultats, les seringues des trois marques testées cèdent à l'eau la même ou les mêmes substances. La partie responsable de la migration est la tête des pistons en élastomère. Le principal produit cédé serait le méthylthio-2-benzothiazole, ou une molécule apparentée présentant le même spectre d'absorption. C'est pour tenter d'élucider la nature exacte du produit que l'analyse partielle des élastomères a été effectuée par c.c.m.

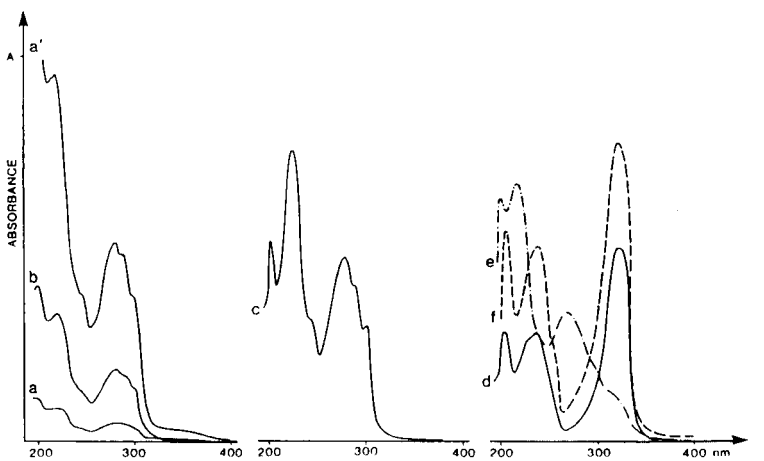

Fig. 1. Spectres d'absorption dans l'ultraviolet (trajet optique 10 mm). (a, a' et b) Eau bidistillée (5 ml) maintenue dans une seringue de 5 ml pendant 5 min (a et a') et 1 h (b) (a et b, A = 1; a', A = 0,1). (c, d, e et f) Solutions éthanoliques (0,001% p/v) de méthylthio-2 benzothiazole (IV, A = 1,5), mercapto-2 benzothiazole (I, A = 3), disulfure de benzothiazyle (II, A = 1,5) et mercapto-2 benzothiazolate de zinc (III, A = 0,1), respectivement.

Étude par chromatographie sur couche mince

Dans le solvant benzène/acétate d'éthyle/acétone (100:5:1), les composés **I, II** et **III** donnent des taches orangées de R_f respectifs 0,18; 0,40 et 0,17 cette dernière plus claire que les précédentes. Le méthylthio-2-benzothiazole (**IV**) ne donne qu'une tache jaune très pâle, de R_f = 0,44. Dans le solvant benzène/acétate d'éthyle/n-butanol (100:2:2), les composés **I, II, III** et **IV** présentent des R_f égaux respectivement à 0,15, 0,40, 0,14 et 0,43, les colorations étant identiques à celles observées dans le cas précédent. Les extraits acétoniques obtenus à partir des têtes de piston des trois marques ont montré plusieurs taches, dont l'une de même couleur et de même R_f que celle observée pour le mercapto-2 benzothiazole dans le solvant correspondant.

Un accélérateur mercaptobenzothiazolique a donc bien été utilisé dans la formulation des élastomères constituant les têtes de piston. Il peut s'agir soit du mercapto-2 benzothiazole proprement dit, soit d'un composé apparenté qui se transforme en mercapto-2 benzothiazole au cours de la vulcanisation [7].

Étude par spectrométrie de masse

La Figure 2 montre les spectres complets obtenus en impact électronique à 70 eV et à 10 eV. Cinq ions moléculaires sont observés dans ce dernier cas, respectivement à *m/z* 211, 195, 181, 167 et 151. Ces résultats ont été confirmés par les spectres obtenus en ionisation chimique avec le méthane, qui montrent les ions moléculaires protonés MH^+ et les ions d'addition caractéristiques ($M + C_2H_5^+$) et ($M + C_3H_5^+$).

Les intensités relatives des ions *m/z* 151, 167 et 181 en impact électronique à basse énergie sont respectivement de 18%, 100% (pic de base) et 19%. Les

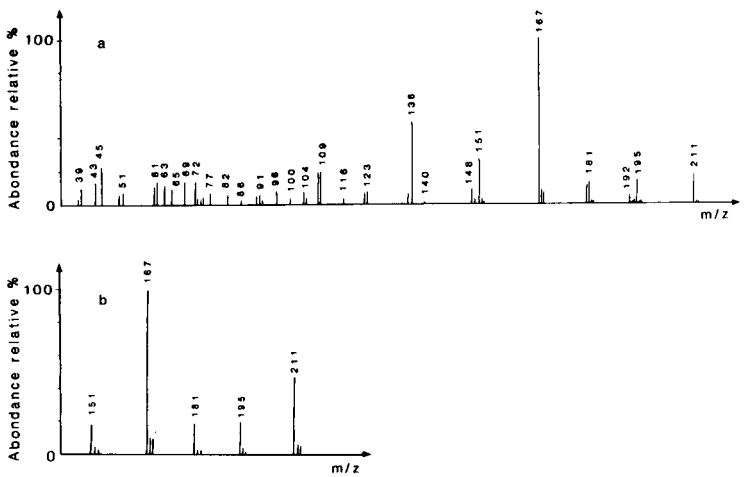

Fig. 2. Spectres de masse obtenus en impact électronique: (a) à haute énergie (70 eV); (b) à basse énergie (10 eV).

intensités des pics isotopiques (M + 2) dus à ^{34}S montrent que le premier de ces ions ne contient qu'un seul atome de soufre et que les deux autres en comportent deux. Ils sont été identifiés comme étant l'hydroxy-2 benzothiazole, le mercapto-2 benzothiazole et le méthylthio-2 benzothiazole. On retrouve en effet dans le spectre les mêmes ions-fragments que ceux rapportés à propos de ces trois composés dans un travail antérieur [8]. Plusieurs transitions métastables confirment en outre ces structures (Tableau 2).

L'ion *m/z* 211, dont l'intensité relative à basse énergie est de 48%, contient deux atomes de soufre. Il peut correspondre a priori aussi bien à l'(hydroxy-2 éthylthio)-2 benzothiazole (**VII**) qu'au (méthoxy méthylthio)-2 benzothiazole (**VIII**), tous deux pouvant perdre après réarrangement C_2H_4O et CH_2O en conduisant au mercapto-2 benzothiazole (*m/z* 167) et au méthylthio-2 benzothiazole (*m/z* 181), déjà cités précédemment en tant qu'ions moléculaires (Fig. 3). Cependant la présence de l'ion *m/z* 193, qui correspond à la perte de l'eau, signale l'existence d'une fonction alcool et permet de conclure en faveur du composé **VII**. Le dernier ion moléculaire *m/z* 195, dont l'intensité à basse énergie est de 20%, ne contient qu'un seul atome de soufre.

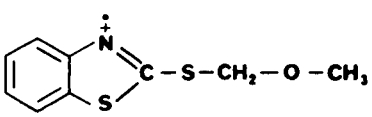

(VIII)

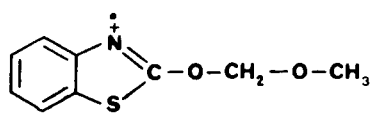

(IX)

Comme dans le cas précédent, deux structures sont possibles, soit l'(hydroxy-2 éthoxy)-2 benzothiazole (**VI**), soit le (méthoxy méthoxy)-2 benzothiazole (**IX**), toutes deux pouvant éliminer C_2H_4O et conduire à l'hydroxy-2 benzothiazole *m/z* 151. La perte de l'eau, conduisant à l'ion *m/z* 177, permet là encore de conclure en faveur de la structure alcool (**VI**). Les transitions métastables rapportées (Tableau 2) confirment l'identité des composés **VI** et **VII**.

L'étude par spectrométrie de masse permet donc de conclure que les produits migrant dans l'eau dans les conditions retenues sont l'hydroxy-2

TABLEAU 2

Transitions métastables observées

m_1	m_2	Fragment éliminé	m^*	m_1	m_2	Fragment éliminé	m^*
151	123	CO	100,2	181	149	S	122,6
151	108	HNCO	77,2	181	148	SH·	121,0
123 (151—CO)	96	HCN	74,8	181	136	CHS·	102,1
167	140	HCN	117,3	181	135	CH_2S	100,7
167	123	CS	90,5	195	151	C_2H_4O	116,9
167	91	CS_2	49,5	211	181	CH_2O	155,3
				211	167	C_2H_4O	132,2

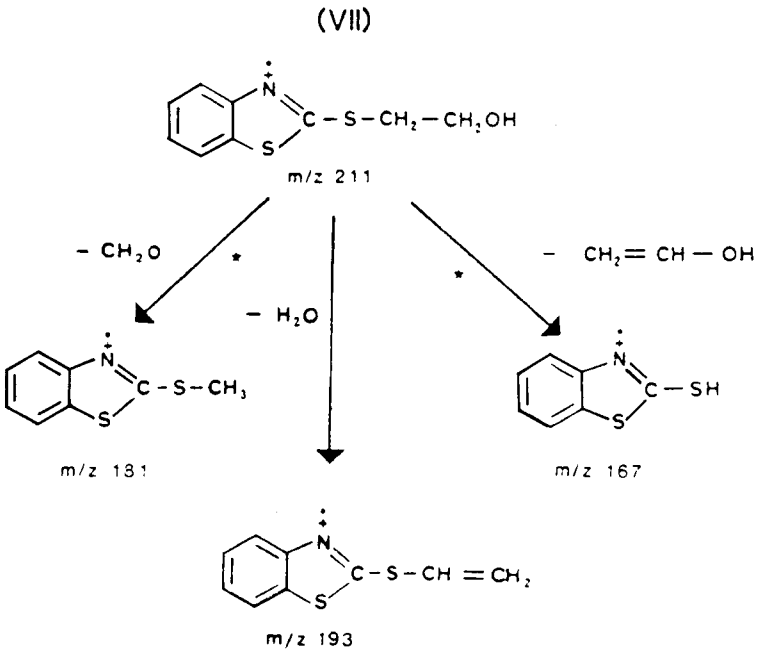

Fig. 3. Voies de fragmentation de l'(hydroxy-2 éthylthio)-2 benzothiazole (VII) (impact électronique, 70 eV).

benzothiazole, le mercapto-2 benzothiazole, le méthylthio-2 benzothiazole, l'(hydroxy-2 éthoxy)-2 benzothiazole et l'(hydroxy-2 éthylthio)-2 benzothiazole.

Origine des produits identifiés

Mercapto-2 benzothiazole. Le mercapto-2 benzothiazole a pu être introduit tel quel, en tant qu'accélérateur, dans les mélanges à vulcaniser, ou bien s'être formé au cours de la vulcanisation, par suite de la décomposition d'un produit de structure apparentée (composés II et III par exemple). Les quatre autres composés ne semblent pas être utilisés comme accélérateurs et leur présence ne paraît pas non plus pouvoir être expliquée par des réactions survenant au cours de la vulcanisation.

(Hydroxy-2 éthylthio)-2 benzothiazole et (hydroxy-2 éthoxy)-2 benzothiazole. Ayant remarqué que toutes les seringues testées avaient été stérilisées par l'oxyde d'éthylène, nous avons émis l'hypothèse que ces deux produits s'étaient formés sous l'action de ce gaz au sein même des élastomères, respectivement à partir du mercapto-2 benzothiazole et de l'hydroxy-2 benzothiazole. Afin de la confirmer, plusieurs vérifications ont été effectuées, fondées sur la comparaison des résultats concernant d'une part des têtes de piston non stérilisées et les produits de référence I et III, d'autre part les mêmes têtes et produits après stérilisation.

La c.c.m. a montré que la stérilisation par l'oxyde d'éthylène entraînait une diminution du taux résiduel de mercapto-2 benzothiazole présent dans les élastomères, les taches obtenues étant beaucoup moins intenses après stérilisation. La s.m. à basse énergie a d'autre part montré que les solutions alcooliques préparées à partir des têtes non stérilisées ne présentaient pas de pics à *m/z* 151, *m/z* 195 et *m/z* 211, alors que ceux-ci étaient par contre importants après stérilisation. Cela indiquait que non seulement les composés **VI** et **VII** prenaient naissance dans l'élastomère au cours de la stérilisation, mais aussi le composé **V**. Par ailleurs, le mercapto-2 benzothiazole (I) présentait le même spectre d'absorption u.v. qu'il ait été ou non stérilisé (Fig. 1, courbe d), alors qu'au contraire le mercapto-2 benzothiazolate de zinc (III) montrait après stérilisation un spectre identique à celui des substances relarguées à partir des seringues (Fig. 1, courbe b). Enfin, en s.m. à haute énergie, le mercapto-2 benzothiazole montrait de même des spectres identiques avant et après stérilisation, ce qui n'était pas le cas du mercapto-2 benzothiazolate de zinc. Après stérilisation, le spectre de ce dernier était identique à celui obtenu à partir de l'extrait des têtes prélevées sur les seringues, alors que le spectre du produit non stérilisé était celui présenté dans la Fig. 4: il est caractérisé par l'absence de pic moléculaire *m/z* 397 et implique deux voies de fragmentation (Fig. 5). Les seuls pic ayant une intensité importante sont ceux des ions *m/z* 167 (100%), *m/z* 135 (60%), *m/z* 109 (35%) et *m/z* 108 (46%). De même, à basse énergie, le spectre de masse du mercapto-2 benzothiazolate de zinc stérilisé était strictement superposable à celui des têtes prélevées sur les seringues, alors que celui du produit non stérilisé ne montrait que l'ion-fragment *m/z* 167.

Ces résultats montraient que les composés **V**, **VI** et **VII** ne se formaient sous l'action de l'oxyde d'éthylène qu'à partir du mercapto-2 benzothiazolate de zinc et non à partir du mercapto-2 benzothiazole. Comme preuve finale, il a été remarqué que dans les spectres de masse des produits relargués apparaissaient avec de faibles intensités le pics caractéristiques du mercapto-2 benzothiazolate de zinc non stérilisé (Fig. 4). Ceci signifiait que la vulcanisation avait été effectuée avec cet accélérateur, ou encore avec du mercapto-2 benzothiazole en présence d'oxyde de zinc [7].

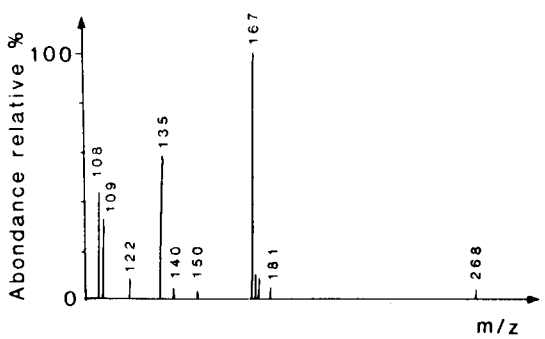

Fig. 4. Spectre de masse du mercapto-2 benzothiazolate de zinc (III) (impact électronique, 70 eV).

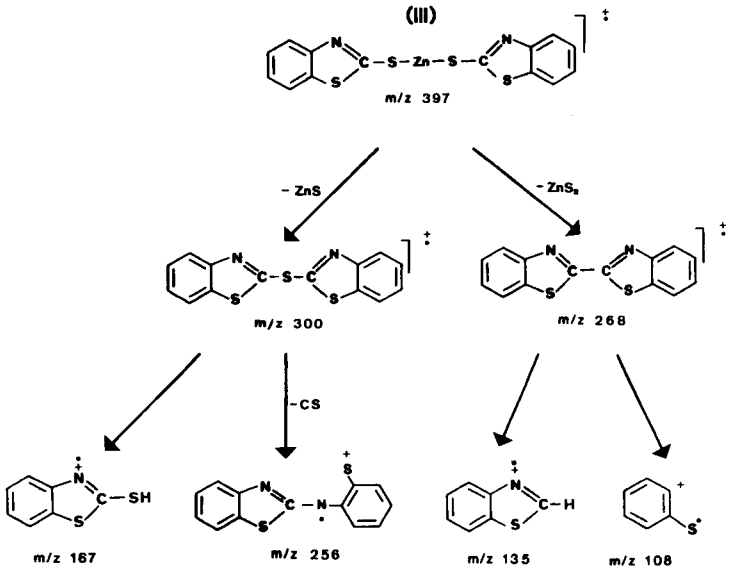

Fig. 5. Voies de fragmentation du mercapto-2 benzothiazolate de zinc (III) (impact électronique, 70 eV).

L'ensemble des résultats rapportés permet donc de conclure que trois des produits cédés par les têtes de piston des seringues (V, VI, VII) sont formés au sein de celles-ci au cours de la stérilisation par l'oxyde d'éthylène, par suite de réactions entre ce gaz et le mercapto-2 benzothiazolate de zinc. Guess et O'Leary [9] avaient signalé incidemment la formation du seul composé VII à partir du mercapto-2 benzothiazole. Il semble en fait d'après nos résultats que la présence d'un dérivé du zinc soit nécessaire.

Hydroxy-2 benzothiazole. L'hydroxy-2 benzothiazole (V) peut se former par chauffage du composé VII à 200°C [10] et il est légitime de se demander si une telle décomposition a pu commencer à se produire au cours de la préparation des échantillons. En fait, l'hydroxy-2 benzothiazole a aussi été retrouvé après stérilisation du mercapto-2 benzothiazolate de zinc, alors que ce produit a été analysé à l'état pulvérulent et n'avait donc même pas subi d'évaporation. Il est peut-être possible d'envisager sa formation comme un début de décomposition thermique du composé VII au cours même de la stérilisation ou de la désorption. Cette hypothèse permettrait d'expliquer la formation de l'(hydroxy-2 éthoxy)-2 benzothiazole (VI) par action de l'oxyde d'éthylène dégagé pendant la désorption sur l'hydroxy-2 benzothiazole formé au cours de la stérilisation ou au début de la désorption.

Méthylthio-2 benzothiazole. Lorsque les résidus secs sont repris par l'éthanol au lieu du méthanol, l'analyse par s.m. ne met en évidence aucune trace d'éthylthio-2 benzothiazole. L'existence du méthylthio-2 benzothiazole (IV) ne résulte donc pas d'une réaction entre le mercapto-2 benzothiazole et le méthanol utilisé comme solvant. Son origine n'a pas été clairement définie.

CONCLUSION

Cinq composés benzothiazoliques sont donc cédés par les seringues dans les conditions indiquées. L'(hydroxy-2 éthylthio)-2 benzothiazole avait seul été identifié précédemment [4] après isolement d'une fraction par c.l.h.p. Quant au méthylthio-2 benzothiazole initialement soupçonné [3], il n'est d'après la s.m. que l'un des produits les moins abondants. La stérilisation par l'oxyde d'éthylène est à l'origine de trois de ces composés.

Une telle migration dans les médicaments injectables pourrait éventuellement ne pas être sans conséquences toxicologiques si les effets observés chez l'animal se retrouvaient chez l'homme [9], d'autant plus que les dispositifs d'injection automatique actuels réalisent un contact prolongé. Elle peut de plus être cause d'interférences analytiques dans les dosages par c.l.h.p. sur des prélèvements sanguins effectués avec des seringues non réutilisables [11, 12].

Les auteurs remercient la firme Vulnax qui leur a gracieusement fourni certains des produits de référence nécessaires.

RÉFÉRENCES

1 Ch. B. Airaudo, A. Gayte-Sorbier et M. Audibert, Labo-Pharma Probl. Tech., 27 (1979) 411.
2 Ch. B. Airaudo et A. Gayte-Sorbier, Labo-Pharma Probl. Tech., 29 (1981), 673 et 779.
3 M. A. Inchiosa, Jr., J. Pharm. Sci., 64 (1965) 1379.
4 M. C. Petersen, J. Vine, J. J. Ashley et R. L. Nation, J. Pharm. Sci., 70 (1981) 1139.
5 Ch. B. Airaudo, A. Gayte-Sorbier, F. Amoyal et D. Rouire, Labo-Pharma Probl. Tech., 30 (1982) 719.
6 J. G. Kreiner et W. C. Warner, J. Chromatogr., 44 (1969) 315.
7 F. Scholl, Atlas of Polymer and Plastics Analysis, Vol. 3, 2ème édn., Additives and Processing Aids, Spectra and Methods of Identification, Weinheim, Verlag Chemie, 1981, p. 125.
8 B. J. Millard et A. F. Temple, Org. Mass Spectrom., 1 (1968) 285.
9 W. L. Guess et R. K. O'Leary, Toxicol. Appl. Pharmacol., 14 (1969) 221.
10 W. A. Sexton, J. Chem. Soc., (1939) 470.
11 N. K. Athanikar, G. W. Peng, E. L. Nation, S. Huang et W. L. Chiou, J. Chromatogr., 162 (1979) 367.
12 M. C. Petersen, R. L. Nation et J. J. Ashley, J. Chromatogr., 183 (1980) 131.

Analytica Chimica Acta, 166 (1984) 233—241
Elsevier Science Publishers B.V., Amsterdam — Printed in The Netherlands

INTERACTIONS OF HALOPHENOLS WITH AQUEOUS MICELLAR SYSTEMS

EDMONDO PRAMAURO, GUIDO SAINI and EZIO PELIZZETTI*
Istituto di Chimica Analitica, Università di Torino, 10125-Torino (Italy)
(Received 2nd April 1984)

SUMMARY

The interaction of a series of halophenols with sodium dodecyl sulphate and hexadecyltrimethylammonium bromide micelles was studied by different techniques (high-performance liquid chromatography, apparent acidity constant, spectral shift). The contributions of the halogens to the free energy of transfer from water to micelles are calculated. Correlations between the free energy of transfer for water/micellar solutions and for the classical octanol/water system are good. The application of micellar systems in chromatography and acid-base titrations is verified.

Continuing interest in the environmental behavior of halophenols [1] has prompted investigations of their physicochemical properties [1, 2] and the development of several methods for their determination [3—6].

For a long time, two-phase water/organic solvent systems (e.g., octanol/water) have found wide use for the correlation and prediction of the biological activities of solutes [7, 8]. This choice has been criticized [9]; micellar systems can provide a useful and simple alternative, particularly as they possess some properties in common with biological structures such as hydrophobic and hydrophilic character in different parts of their structure [10]. Moreover, the use of micellar systems in analytical techniques has received increasing attention [11—14]. The present work deals with the determination of the association constants of halophenols with anionic and cationic micelles, as well as with the effect of the micellar interaction on the apparent acidity constants. Analytical applications in high-performance liquid chromatography (h.p.l.c.) and acid—base titrations are described.

EXPERIMENTAL

Reagents and apparatus

The phenols (Aldrich or K & K) were recrystallized before use, as were sodium dodecyl sulphate (SDS; Fluka), hexadecyltrimethylammonium bromide (HTAB; Fluka) and hexadecylpyridinium chloride (HPC; Merck). All other reagents were of analytical grade.

A Cary 219 spectrophotometer and an Orion 801 potentiometer were

0003-2670/84/$03.00

used. The Perkin-Elmer S2 chromatograph used was equipped with a C_{18} reversed-phase column (Perkin-Elmer ODS-HC-SIL-X1; 25 cm long, 2.6 mm i.d.). The surface tension data were collected with a Krüss K 10 tensiometer equipped with a platinum blade.

Surface tension measurements

The critical micellar concentration (c.m.c.) showed the usual shifts caused by salts and solubilizates compared to the c.m.c.'s measured in distilled water [10]. For SDS, the c.m.c. lies in the range $3.0—3.3 \times 10^{-3}$ M, whereas the c.m.c. for HTAB was 8×10^{-5} M.

Association to micelles

If the surfactant is in large excess, the binding constant is given by

$$K_B = [S_m]/[S_w]C \quad (1)$$

where S represents the solute concentration, C the surfactant concentration exceeding the c.m.c. and the subscripts m and w denote the solute in the micellar and aqueous pseudophases, respectively. Calculation of K_B can be based on different techniques, such as the absorbance method, variation of the apparent acidity constant and chromatography. The binding constants are collected in Table 1. The errors in the quoted K_B values are in the range 8—15%, in agreement with literature data [13, 14, 16].

Absorbance method. This method is based on the spectral shift of phenols when incorporated in HTAB micelles. The spectra of solutions containing a fixed amount of phenols (concentrations in the range $1—2 \times 10^{-4}$ M) and increasing concentrations of HTAB were recorded, in the presence of 0.02 M hydrochloric acid (acidic form) or 0.02 M sodium hydroxide (phenoxide ion). The wavelengths chosen were those at which the changes in absorbances are greatest (260—320 nm). The ionic strength was 0.05 M (NaCl). The temperature was kept at 25.0 ± 0.2°C.

The extent of micellar binding can be estimated [15] from the expression

$$(A_d - A_w)^{-1} = (A_m - A_w)^{-1} + [(A_m - A_w)K_B C]^{-1} \quad (2)$$

where A_d, A_w and A_m are the absorbances in surfactant, in water and when the substrate is completely bound, respectively. Figure 1 shows the plots corresponding to Eqn. 2 for some halophenols in the presence of increasing amounts of HTAB.

Dissociation constant method. This method is based on the decrease of the apparent acidity constants of weak acids when incorporated in anionic micelles. The acidity constant was evaluated from spectrophotometric measurements (at the wavelength where the absorptivities of the protonated and deprotonated forms are sufficiently different) and pH measurements, at 25.0 ± 0.2°C; 0.02 M hydrochloric acid and 0.02 M sodium hydroxide were used for the measurements in acidic and basic media, respectively. Intermediate and known pH values were obtained by using suitable buffers

TABLE 1

Binding constants (K_B, l mol^{-1}) and free energies of transfer ($-\Delta\mu_t^\circ$, cal mol^{-1}) of the halophenols investigated in the presence of SDS and HTAB micelles

Compound	SDS			HTAB			
	K_B (HA)[a]	K_B (HA)[b]	$-\Delta\mu_t^\circ$ (HA)	K_B (HA)[c]	$-\Delta\mu_t^\circ$ (HA)	K_B (A^-)[c]	$-\Delta\mu_t^\circ$ (A^-)
Phenol	8[d]	10[d]	3610	120	5220	750	6300
4-Methylphenol	24[d]	24[d]	4260	220	5570		
4-Fluorophenol	17	16	4060	140	5310	1100	6530
4-Chlorophenol	30	39	4390	690	6250	3200	7160
4-Bromophenol	60	67	4800	910	6420	4500	7360
4-Iodophenol	140	123	5310	1280	6620	7000	7620
2,3,5,6-Tetrafluorophenol	86		5020	235	5610	2000	6880
Pentafluorophenol	145		5330				
3,5-Dichlorophenol	92	105	5060	3200	7160	17000	8150
2,4,5-Trichlorophenol	280		5720				
2,3,4,5-Tetrachlorophenol	830		6360				
Pentachlorophenol	2350		6980				
2,4,6-Tribromophenol	2050		6900				
2,4,6-Triiodophenol	22500		8320				
1-Naphthol	180		5460				
4-Chloronaphthol	550		6120				
6-Bromonaphthol	1100		6530				

[a]Variation of the apparent acidity constant. [b]H.p.l.c. [c]Absorbance method. [d]From [14]. The errors in the quoted K_B values are in the range 8—15%, in agreement with the literature data [13, 14, 16].

(acetic acid/acetate, Tris/HCl and glycine/NaOH). The ionic strength was adjusted to 0.05 M with sodium chloride.

A simplified equation [16] was adopted

$$K_a/K_{a(app)} = 1 + K_B C \tag{3}$$

where K_a and $K_{a(app)}$ represent the acidity constants in the absence and in the presence of surfactant. The measured K_a agreed with literature data. Plots corresponding to Eqn. 3 are shown in Fig. 2.

Chromatographic method. The basis and the general outline of this method have recently been reported [13, 14]. Mobile phases were prepared by dissolving the surfactant in water and filtering through a 0.45-μm cellulose membrane filter (Millipore). Each solute was dissolved in SDS before the runs; 5—10 μl of the sample solution at a concentration in the range 1×10^{-3}—1×10^{-2} M were injected. All the solutes were eluted at a flow rate of 1 ml min^{-1} and their absorbances were monitored at 290 nm. The temperature was 25 ± 2°C (room).

The equation [13] used was

$$V_s/(V_e - V_m) = (1/P_{sw}) + \bar{V}C(P_{mw} - 1)/P_{sw} \tag{4}$$

where V_s, V_e and V_m are the volumes of sample injected, the stationary

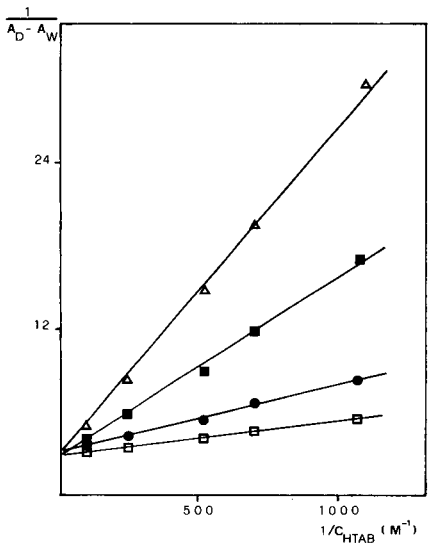

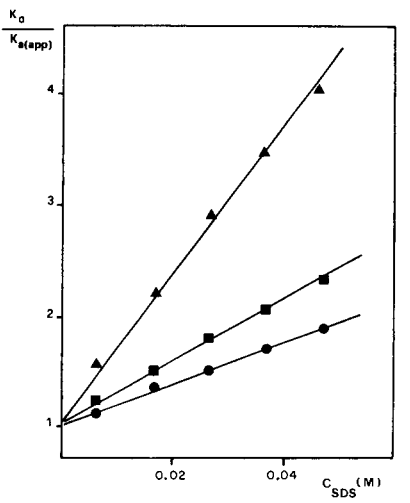

Fig. 1. Plots of Eqn. 2 for: (△) 4-fluorophenol (HA); (□) 4-fluorophenol (A^-); (■) 2,3,5,6-tetrafluorophenol (HA); (●) 4-chlorophenol (HA).

Fig. 2. Plots of Eqn. 3 for: (●) 4-fluorophenol; (■) 4-chlorophenol; (▲) 4-bromophenol.

phase and the mobile phase, respectively, $\bar{V}$ is the partial molar volume of SDS; P_{mw} and P_{sw} represent the partition coefficients of solutes between the micellar and aqueous pseudophases and between the stationary and aqueous phase, respectively.

Table 2 collects the variation of the capacity factors with surfactant concentration and Fig. 3 shows the plots corresponding to Eqn. 4 for some of the compounds investigated.

The calculated partition coefficients P_{mw} are related to the association constant K_B through the equation [18]

TABLE 2

Variation of the capacity factor $(V_e - V_m)/V_s V_m$ of the investigated compounds with the surfactant concentration in the mobile phase

Compound	Capacity factors for changing total SDS conc. (M)					
	0.04	0.05	0.06	0.07	0.08	0.10
4-Fluorophenol	4.3	3.8	3.5	3.4	3.0	2.6
4-Chlorophenol	9.4	7.5	6.5	6.0	5.2	4.3
4-Bromophenol	10.9	8.7	7.5	6.8	5.8	4.7
4-Iodophenol	13.5	10.4	8.7	7.9	6.6	5.4
3,5-Dichlorophenol	—	14.9	12.8	11.3	9.6	7.6

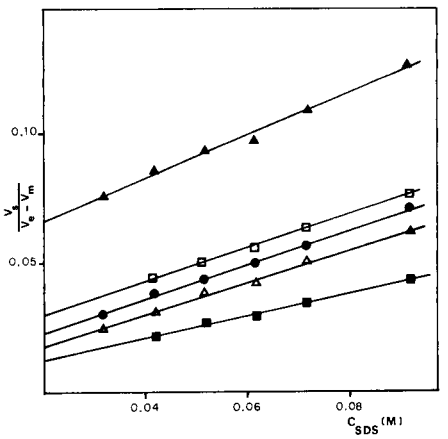

Fig. 3. Plots of the chromatographic parameter $V_s/(V_e - V_m)$ as a function of the micellized surfactant concentration in the mobile phase: (▲) 4-fluorophenol; (□) 4-chlorophenol; (●) 4-bromophenol; (△) 4-iodophenol; (■) 3,5-dichlorophenol.

$$K_B = (P_{mw} - 1)\bar{V} \quad (5)$$

For SDS, $\bar{V} = 0.26\ M^{-1}$ was assumed [19].

Potentiometric and visual titrations. Potentiometric titrations of halophenols (5×10^{-3}—2×10^{-2} M) in 0.1 M HPC were done with sodium hydroxide (0.1—1 M), at 25°C. Several minutes were necessary for equilibration of the glass electrode after each addition of titrant. Hexadecylpyridinium chloride was chosen because its good solubility in water makes it possible to prepare quite concentrated solutions, which can easily dissolve the hydrophobic compounds investigated.

For visual titrations, weighed amounts of each compound (100—250 mg) were dissolved in about 50 ml of 0.1 M HPC and titrated with 1 M sodium hydroxide in the presence of phenolphthalein or thymolphthalein indicator; end-points were sharp.

DISCUSSION

Free energy of transfer from water to micellar pseudophase

The free energy of transfer, $\Delta\mu_t^\circ$, per mole of solute from water to micelles is given [20] by

$$\Delta\mu_t^\circ = \mu_m^\circ - \mu_w^\circ = -RT \ln (55.5\ K_B) \quad (6)$$

If the phenol residue and each of the halogen atom is assumed to contribute independently to $\Delta\mu_t^\circ$, then

$$\Delta\mu_t^\circ = \Delta\mu_{Ph}^\circ + n\Delta\mu_{Hal}^\circ \quad (7)$$

This makes it possible to calculate the contribution of each moiety to the binding of the solute to the micelles.

Binding with SDS micelles. Table 1 lists the binding constants of the phenols with anionic SDS micelles. The agreement of the values obtained from the variation of the apparent acidity constant and from the chromatographic data is quite good.

The data plotted according to Eqn. 7 (see Fig. 4A) enable the hydrophobic contribution of the halogens to the transfer from water to anionic micellar pseudophase to be estimated: −330 cal mol^{-1} for fluorine, −640 cal mol^{-1} for chlorine; −1030 cal mol^{-1} for bromine; and −1500 cal mol^{-1} for iodine. Interestingly, very similar values can be derived from a comparison of 4-chloro-1-naphthol and 6-bromo-1-naphthol with 1-naphthol itself: −660 cal mol^{-1} for chlorine and −1070 cal mol^{-1} for bromine.

Binding with HTAB micelles. The data concerning the binding of phenols and phenoxide ions to HTAB aggregates are also collected in Table 1. It is evident that the contribution of the aromatic moiety is substantially greater in cationic than in anionic micelles, suggesting that the electron cloud of the benzene ring can interact with the positively charged head groups of the cationic aggregate. The negative charge of the phenoxide ion increases the transfer from aqueous to cationic pseudophase with an incremental free energy of ca. −1000 cal mol^{-1} (very close to the value reported for alkylphenol derivatives [20]). The effect of the negative charge may be due to the interaction between the anionic oxygen and the positively charged surface or to the above-mentioned increased interaction of the benzene ring with cationic head group. The effect is not related, as expected, to the surface potential of the micelles, probably because of increased solvation of the phenoxide compared to phenol compound.

The values of the incremental free energy of transfer caused by the halogens (both in phenol and phenoxide ion) are comparable with those in anionic micelles, and are also very close to the values found for substituted aniline association with HTAB [21]; −120 for fluorine; −950 for chlorine; −1100 for bromine; and −1400 cal mol^{-1} for iodine (averaged over phenol and phenoxide). The values for incremental free energy for halogens in anionic and cationic micelles are lower than the corresponding values in the octanol/water system [22].

Comparison between micelle/water and organic solvent/water systems

The incorporation of a solute in a micellar aggregate can occur in different parts of the organized structure, such as micellar surface, hydrophobic core or intermediate layers. Spectroscopic and kinetic studies have been used in order to obtain information on the solubilization process and preferential sites [23].

A comparison of the binding constants in micellar systems with those in the more classical two-phase system, such as octanol/water, can give insight into the phenomena that drive the transfer of the solute from water to a micellar aggregate [24]. It must be recalled that in order to compare the standard free energy of solubilization, it is necessary to consider the different

concentration scales that are often adopted for the partition coefficients, i.e., mole fraction scale and molarity scale. The relation between the two scales is

$$\log P_{(X)} = \log P_{(M)} + \log [(MW)_O d_w/(MW)_w d_O] \quad (8)$$

where $(MW)_O$, $(MW)_w$, d_O and d_w represent the molecular weight and the density of octanol and water, respectively.

Figure 4B shows the correlation between the free energy of transfer from water to micelle compared with that from water to octanol. The slopes for the two surfactants are quite similar with a value of 0.68 ± 0.05. These values of the slopes, coupled with the above consideration on the incremental free energy for halogens, suggest that the molecules are partitioned between the bulk aqueous phase and micelles in a partially hydrated media. However, when compared on the same concentration scale, the values referring to SDS and octanol/water are of the same order of magnitude, whereas the HTAB data are higher, suggesting other contributions to the overall interaction, as previously mentioned.

Analytical applications

The h.p.l.c. method for the determination of the partition coefficient of a solute with micelles has been proved to be particularly versatile; the method is not restricted to any particular type of compound, provided that a suitable detector is used. In addition, the potential of aqueous micellar solutions as mobile phases in liquid chromatography has received increasing attention because of the unusual selectivities offered [25].

Applications in acid-base titrations originated with the observation that

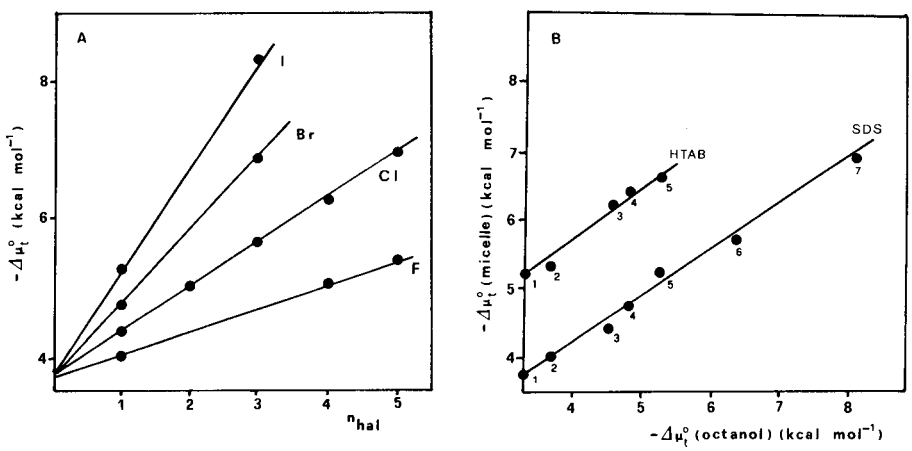

Fig. 4. (A) Free energies of transfer of halophenols from water to SDS as a function of the number of the halogen atoms (n_{hal}). (B) Correlation between the free energies of transfer from water to micelles (HTAB and SDS) and from water to octanol for the following compounds: (1) phenol; (2) 4-fluorophenol; (3) 4-chlorophenol; (4) 4-bromophenol; (5) 4-iodophenol; (6) 2,4,5-trichlorophenol; (7) pentachlorophenol.

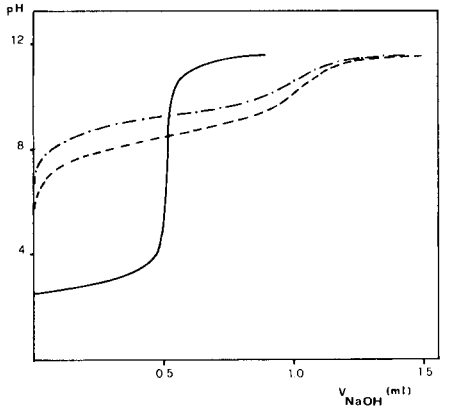

Fig. 5. Potentiometric titration curves for 4-chlorophenol (2×10^{-2} M) in 0.1 M HPC (---) and in water (- · -), and for pentachlorophenol (1×10^{-2} M) in 0.1 M HPC (—).

the incorporation of organic acids in charged micelles can induce large pK_a shifts [12]. Potentiometric as well as visual acid—base titrations were tested for the halophenols investigated. The utility of the micellar aggregates of HPC is in solubilizing the less water-soluble compounds and in lowering the apparent acidity constants of the phenols. For example, a very hydrophobic compound such as pentachlorophenol, which is scarcely soluble in water (less than 0.002% w/v), can be easily dissolved in micellar media. Working solutions containing 0.2—0.3% (w/v) of this compound were used for the experiments. For more soluble compounds exhibiting lower acidity constants (e.g., monohalophenols), the use of HPC improves the titration curves. Figure 5 and Table 3 show the satisfactory application of micellar cationic solutions in acid-base titrations of weak acids.

TABLE 3

Visual titrations of some halophenols with 1 M sodium hydroxide[a]

Compound	Present (mg)	Found[b] (mg)	S.d. (mg)	R.s.d. (%)
3,5-Dichlorophenol[c]	163.0	164.8	2.0	1.21
2,4,5-Trichlorophenol	220.2	223.0	3.1	1.39
2,3,4,5-Tetrachlorophenol	115.8	117.2	1.0	0.85
Pentachlorophenol	160.0	163.0	2.8	1.72
2,3,5,6-Tetrafluorophenol	226.5	228.4	2.5	1.09
Pentafluorophenol	209.0	206.0	2.7	1.31
2,4,6-Tribromophenol	190.0	192.3	2.0	1.04

[a]Solutions in 0.1 M HPC; phenolphthalein indicator. [b]Mean from 4 replicate titrations. [c]Thymolphthalein.

Conclusions

The binding of halophenols with anionic and cationic micellar aggregates was investigated by different techniques. The binding constants compared with octanol/water partition coefficients give information about the interaction of these compounds with organized structures having hydrophobic and hydrophilic regions, which resemble biological structures [26]. In addition, the solubilization properties, the shift in the apparent pK_a and the use of micellar solutions as mobile phase in liquid chromatography can be profitable in analytical applications for separation and determination of halophenols.

This work was supported by Regione Piemonte (Ricerca Sanitaria Finalizzata), C.N.R. (Rome), and Ministero Pubblica Istruzione (Rome).

REFERENCES

1 C. Rappe, in O. Hutzinger (Ed.), The Handbook of Environmental Chemistry, Springer Verlag, Vol. 3A, Berlin, 1980, p. 157.
2 K. Ranga Rao (Ed.), Pentachlorophenol; Chemistry, Pharmacology and Environmental Toxicology, Plenum Press, New York, 1978.
3 M. C. Rand, A. Greenberg and M. J. Taras (Eds.), Standard Methods for the Examination of Waste and Wastewater, American Public Health Association, 14th edn., Washington, DC, 1976.
4 T. R. Edgerton, P. F. Moseman, E. M. Lores and L. H. Wright, Anal. Chem., 52 (1980) 1774.
5 A. B. McKayne, J. Chromatogr., 208 (1981) 287.
6 R. E. Shoup and G. S. Mayer, Anal. Chem., 54 (1982) 1164.
7 A. Leo, C. Hansch and D. Elkins, Chem. Rev., 71 (1971) 525.
8 P. Y. Lu and R. L. Metcalfe, Environ. Health Persp., 10 (1975) 269.
9 K. W. Miller, L. Hammond and E. G. Porter, Chem. Phys. Lipids, 20 (1977) 229.
10 C. Tanford, The Hydrophobic Effect. Formation of Micelles and Biological Membranes, Wiley, 2nd edn., New York, 1980.
11 W. L. Hinze, in K. L. Mittal (Ed.), Use of Surfactant and Micellar Systems in Analytical Chemistry, Solution Chemistry of Surfactants, Plenum Press, Vol. 1, New York, 1979.
12 A. L. Underwood, Anal. Chim. Acta, 140 (1982) 89.
13 D. W. Armstrong and F. Nome, Anal. Chem., 53 (1981) 1662.
14 E. Pramauro and E. Pelizzetti, Anal. Chim. Acta, 154 (1983) 153.
15 L. Sepulveda, J. Colloid Interface Sci., 46 (1974) 372.
16 E. Pramauro and E. Pelizzetti, Anal. Chim. Acta, 126 (1981) 253.
17 Y. Yukawa, Handbook of Organic Structural Analysis, Benjamin, New York, 1965.
18 I. V. Berezin, K. Martinek and A. K. Yatsimirskii, Russ. Chem. Rev., Engl. Transl., 42 (1973) 787.
19 J. M. Corkill, J. F. Goodman and T. Walker, J. Chem. Soc., Faraday Trans. I, 63 (1967) 768.
20 C. A. Bunton and L. Sepulveda, J. Phys. Chem., 83 (1979) 680.
21 R. Graglia, E. Pramauro and E. Pelizzetti, Ann. Chim. (Rome), 74 (1984) 41.
22 A. Leo, C. Hansch and D. Elkins, Chem. Rev., 71 (1971) 525.
23 J. H. Fendler and E. J. Fendler, Catalysis in Micellar and Macromolecular Systems, Academic Press, New York, 1975.
24 C. Treiner, J. Colloid Interface Sci., 93 (1983) 33.
25 D. W. Armstrong and G. Y. Stine, Anal. Chem., 55 (1983) 2317; J. Am. Chem. Soc., 105 (1983) 6220.
26 J. H. Fendler, Membrane Mimetic Chemistry, Academic Press, New York, 1983.

Analytica Chimica Acta, 166 (1984) 243—251
Elsevier Science Publishers B.V., Amsterdam — Printed in The Netherlands

STABILITY AND EXTRACTION FEATURES IN THE DETERMINATION OF IRGANOX-1330 IN A POLYALKENE COPOLYMER

ULLA GASSLANDER and HANS JAEGFELDT*[a]

Astra Läkemedel AB, Research and Development Laboratories, S-151 85 Södertälje (Sweden)

(Received 21st May 1984)

SUMMARY

The determination of Irganox-1330 in a polypropene/polyethene copolymer is described. The unstable antioxidant can be extracted from the copolymer without degradation at refluxing temperature by using decalin, hexane, chloroform or tetrahydrofuran if adequate protection is provided. The time needed for quantitative extraction is 30 min if the particle size of the polymer is <1.0 mm for any of the solvents. The standard-addition procedure described provides accurate results even when the sample is extracted after being immersed directly in the extracting solvent. For practical purposes, hexane is the preferred extractant. A modified direct-phase high-performance liquid chromatographic system provided a fast, sensitive and stable means of completing the determination.

Polyolefins such as polypropene and polyethene are subject to thermal and oxidative degradation particularly during processing at elevated temperatures. To protect the polymer during this phase of handling and to give long-term stability, antioxidants are added. The antioxidants act as radical scavengers and interrupt the chain propagation steps of the auto-oxidation of the polymer [1].

The procedures used to determine antioxidants in polymers, and the problems associated with these methods, have been reviewed by Wheeler [2], Crompton [3] and Walter and Johnson [4]. The main problems arise from the more or less insoluble polymer matrix, the high reactivity and low stability of the antioxidant and its low concentration (0.1—1%). A successful analysis depends primarily on extracting the antioxidant without decomposition at the low concentrations encountered.

Several different solvents have been suggested as well as different extraction equipment and milling procedures [2—4]. Milling the polymer samples to smaller particles increases the surface/weight ratio and thus speeds up the rate of solid/liquid extraction. It is probable that a large amount of work has been done in this direction but not published because of the proprietory nature of many in-house methods. However, a few papers have appeared. Spell and Eddy [5] showed that the extraction rate was a function of the particle size and the permeability of the solvent. This was confirmed by

[a]Present address: Research and Development Laboratories, AB Draco, Box 34, 22100 Lund, Sweden.

0003-2670/84/$03.00

Wims and Swarin [6], who concluded that tetrahydrofuran (THF) was the most efficient extraction solvent. In a recent paper by Vadakkott et al. [7], carbon tetrachloride and THF were shown to be suitable solvents for low-density polyethene and propene, respectively; higher-boiling solvents led to the decomposition of the antioxidant during the extraction. However, Schabron and co-workers [8, 9] used hot (110°C) decalin (decahydronaphthalene) to dissolve polyethene granules completely for extraction of the antioxidants. Using this procedure, they avoided problems connected with solvent penetration into the polymer; they did not refer to antioxidant degradation.

Apart from a paper by Lichtentaler and Ranfelt [10], no systematic investigation of the problems of quantitative solid/liquid extraction has been reported. Also, no attempts to study and to minimize the decomposition and loss of antioxidant during extraction seem to have been made. In particular, knowledge about decomposition seems vital because most methods of analysis involve heating to increase the speed of extraction. This paper reports on the determination of Irganox-1330 in a commercial polypropene/polyethene (98/2 % w/w) copolymer. Different extraction solvents are compared. The importance of protecting the antioxidant from oxidation during extraction is discussed. A simple standard-addition procedure is used to prevent "matrix effects" from the polymer from affecting the accuracy of the determination.

A nitro-group modified direct-phase column was chosen for the high-performance liquid chromatographic (l.c.) separations. This column yielded reproducible retention times, fast separations and better selectivity [11—13] than some reverse-phase non-aqueous systems recently reported [7, 14]. The compatibility between the chromatographic system and the extractants used here is discussed.

In view of the fact that monitoring of polymer additives has become increasingly important because of stricter laws and regulations, the need for fast and reliable analytical methods has increased. This is especially true for the pharmaceutical industry, as particular interest is focused on additives in medical plastics and food packaging.

EXPERIMENTAL

Chemicals and chromatographic equipment

Commercial-grade Irganox-1330 {2,2′,2″,6,6′,6″-hexa-t-butyl-4,4′,4″-[(2,4-6-trimethyl-1,3,5-benzenetriyl)trismethylene] triphenol} was obtained from Ciba-Geigy. Reagent-grade 2,6-di-t-butyl-4-methylphenol (BHT) was obtained from Janssen Chimica (Belgium). A commercial polypropene containing only Irganox-1330 as antioxidant was used. The solvents were reagent-grade (Merck) for the extractions and spectroscopic grade (Fluka) for the chromatographic work.

For chromatography, a Waters 6000-A pump was used with a Rheodyne injector (20-μl loop). The steel column was 150 × 4 mm i.d. and the support

was Nucleosil-5 NO_2 (5 μm; Macherey-Nagel, Düren). The mobile phase was 99.0—99.5% hexane and 0.5—1.0% THF. The detector was a Pye-Unicam 4020 variable-wavelength model and the measurements were made at 230 nm. The integrator was a Pye-Unicam PU-4810 model.

Sample preparation and extraction procedure

The polymer granules were frozen either with liquid nitrogen or in a CO_2(s)/ethanol bath to temperatures well below the glass-point. The brittle granules were then pulverized in an ultracentrifuge mill (Retsch, Type ZM1). Pulverized samples (0.5—5.0 g) were immediately soaked in 25—100 ml of solvent and extracted with reflux for 40 min. The extraction solvents used were decalin, hexane, chloroform and THF. When the antioxidant was extracted with decalin, no pulverization was necessary as the granules dissolved at the reflux temperature (ca. 180° C).

After reflux and upon cooling in any of the solvents used, greater or smaller amounts of dissolved polymer always precipitated, leading to the necessity of filtration. The sample solutions were filtered through glass microfibre filters (Whatman GF/A) in order to avoid clogging of the inlet of the chromatographic column. After filtration, the polymer particles on the filter were carefully rinsed and the sample solution was made up to volume.

When chloroform or THF was used as the extracting solvent, the sample solutions were diluted with hexane 5- and 10-fold, respectively. This was done in order to achieve acceptable chromatographic behaviour (see below). For quantitative work (Table 1), a 100-fold molar excess of BHT (0.5—1.5 mg ml^{-1}) was added to the extracting solvent in order to protect the Irganox-1330 from oxidation during extraction. Soxhlet extraction was not used, because it would not have allowed the protection of the antioxidant in the polymer with another synergic antioxidant in solution. This kind of additional protection, besides nitrogen purging, was found to be particularly important for the extraction with decalin.

In the determination of the mass/particle size distribution of the pulverized polymer granules, four brass sieves were used (Retsch; 0.43-, 1.0-, 1.6- and 2.0-mm mesh, sieve diameter 10 cm). Pulverized samples (ca. 15 g) were

TABLE 1

Determination of Irganox-1330 in polypropylene by refluxing with solvents of widely different polarity and boiling temperatures. Samples were milled to < 1.0 mm particle size.

Sample	Irganox-1330 found ($\mu g\ g^{-1}$)			
	Decalin	Hexane	$CHCl_3$	THF
1	800	764	810	793
2	815	771	801	813
3	—	771	—	—
4	—	822	—	—
Mean ± SD	808 ± 10	782 ± 27	806 ± 7	803 ± 14

sifted for 20 min (Fritsch Analysette sieve shaker) after which the different fractions were collected and weighed.

Standard-addition procedure

For this method, four samples of polymer were weighed. To each sample was added the appropriate solvent containing known amounts of Irganox-1330. This procedure was used in order to reach equilibrium in the solid/liquid extraction for each sample. The peak areas resulting from the chromatographic recordings for each sample were then plotted against the known added concentration and the concentration in the polymer was calculated in the usual way. This procedure was used so that the data could be quantified even when the sample was steeped directly in the extractant solution. The requirement for success of the method is that distribution equilibrium of the antioxidant between polymer and solution is achieved (see below). Full mathematical justification of this standard-addition procedure is available from the authors on request.

RESULTS AND DISCUSSION

Stability

As antioxidants are designed to be sensitive to oxidation, they obviously have to be protected from this during extraction. Figure 1 summarizes the results of different treatments. As can be seen, when oxygen-saturated decalin solutions containing 10 μg ml^{-1} Irganox-1330 were refluxed at 180°C, the antioxidant concentration decreased dramatically within 30 min (curve A). Even when the solution was continuously purged with nitrogen, there was slow degradation of the antioxidant (curve B). However, when the nitrogen purging was combined with a 100-fold molar excess of BHT, the decomposition rate was virtually negligible (curve C). Thus, it is possible to protect a sensitive antioxidant even at high temperature if suitable precautions are taken.

Another way to retard or stop oxidation is to lower the temperature of the extraction [7]. Figure 2 shows the results when oxygen-saturated solutions of Irganox-1330 were refluxed at 60—70°C with hexane or THF with and without a 100-fold molar excess of BHT. No appreciable degradation was observed for the hexane solutions with or without BHT, but for THF protection against oxidation was necessary for prolonged extractions. This is not surprising, given the tendency for THF itself to react with oxygen to form peroxides which will, of course, oxidize the antioxidant. When chloroform was used, no detectable degradation with or without BHT was observed. It can be concluded, therefore, that low temperature during an extraction will lead to good stability if no other effects can cause degradation.

The rate of extraction from milled polymer was then studied at room temperature. The aim was not to elucidate stability problems, but to study the influence of particle size on extraction rate. As shown in Fig. 3, when the

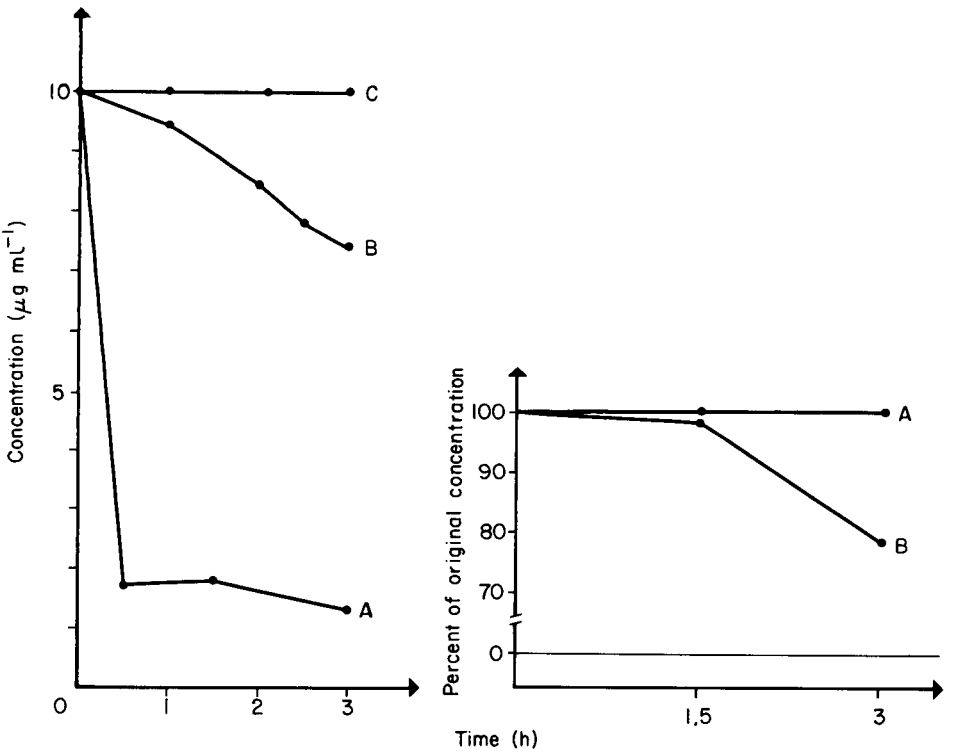

Fig. 1. Degradation of Irganox-1330 (10 μg ml^{-1}) during reflux in decalin at ca. 180° C: (A) oxygen-saturated solution; (B) continuous nitrogen purging; (C) continuous nitrogen purging and a 100-fold molar excess of BHT.

Fig. 2. Reflux of Irganox-1330 (50 μg ml^{-1}) in hexane or THF at 60—70° C: (A) hexane with or without BHT; (B) THF without BHT.

particle size was 0—1.0 mm, a plateau was reached after about 4 h (curve A) but, as expected, extraction was slower when particles smaller than 0.4 mm were removed (curve B). However, when the larger sifted polymer particles were extracted without excess of BHT, severe degradation of the antioxidant was observed (curve C). This effect was not observed for unsieved polymer. It is concluded that very small amounts of metal (from the brass sieve used) can severely increase the rate of degradation of the antioxidant. This is of course not new, but it emphasizes the importance of protection against oxidation even at low temperatures. In this context, it should be kept in mind that even trace catalyst residues in the polymer might exert a catalytic effect on degradation during extraction in the presence of oxygen, particularly at high temperatures. The degradative effect of minute amounts of trace metal from the brass sieve was observed also for chloroform and hexane extractions. It was smallest for hexane and greatest for THF.

Extraction

As discussed above, degradation of the antioxidant can be retarded by lowering the temperature during extraction. However, lowering of the

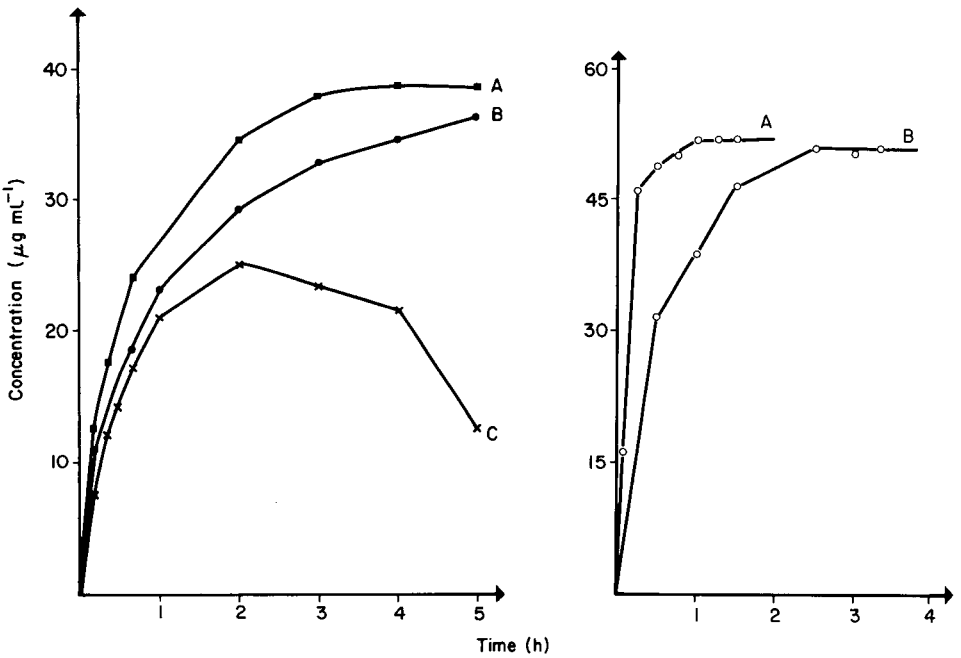

Fig. 3. Extraction of Irganox-1330 of different particle sizes with THF at ambient temperature. Particle size: (A) 0—1.0 mm, excess of BHT added; (B) 0.4—1.0 mm, excess of BHT added; (C) 0.4—1.0 mm, no BHT added.

Fig. 4. Extraction of the antioxidant from two 3-g samples by refluxing with THF. Particle size: (A) 0—1.6 mm; (B) 3—6 mm.

temperature by refluxing with, for example, THF, chloroform or hexane changes the system from a liquid/liquid (refluxing with decalin) to a solid/liquid extraction, because of the poor solubility of polypropene in low-boiling solvents. However, the slow rate of solid/liquid extractions is not necessarily a problem in quantifying an antioxidant in a polymer matrix. The surface/volume ratio of the solid sample (and so the speed of extraction) may be increased considerably by milling. Still, precise knowledge of the degree of extraction versus time is essential in order to define when the extraction process is complete. When two samples were extracted by refluxing with THF, the sample with the smaller particle size (<1.6 mm) gave a complete yield much more quickly than the other (3—6 mm), as shown in Fig. 4. Both extraction curves levelled off at the same concentration, indicating that the solvent completely penetrated both samples. The steady state also suggests that distribution equilibrium between the solid polymer and the liquid extractant is reached.

When the extraction is done by placing the sample directly into the extractant (as in this work), distribution equilibrium defines when the

extraction process is complete. Obviously, 100% extraction is never quite achieved because of the finite distribution between the two phases, but 100% extraction is not essential if a properly designed standard-addition procedure is applied. Yet, it could be argued that a steady-state extraction level does not necessarily mean that distribution equilibrium prevails throughout the sample, because crystallites, for example, may not be penetrated completely. Total penetration and extraction by a low-boiling solvent was indicated by the following experiments. It was shown (Fig. 1) that the antioxidant can be stabilized even in refluxing decalin (ca. 180°C) which completely dissolves the polypropene. When Irganox-1330 was determined in a commercial polypropene/polyethene (98/2 % w/w) granulate by the standard-addition procedure described under Experimental with different solvents, including some in which the polymer did not dissolve, the results obtained were very similar. Table 1 summarizes the data acquired with decalin, hexane, chloroform and THF as extractants. All these solvents yielded the same concentration of the antioxidant in the sample, within the precision of the method (±3%). It can therefore be concluded that any of these solvents can be used successfully to extract the antioxidant concentration in the polymer for quantitative work, provided that the sample is milled to particles <1.0 mm. Figure 5 shows the mass/particle-size distribution given by the milling procedure (see Experimental) for the determinations in Table 1.

Figure 6 shows that the difference in the rate of extraction at ambient temperature with hexane, chloroform or THF is surprisingly small, considering the wide range of polarity of these solvents. When the polymer particles are small enough, differences in polarity obviously play a minor role in the extraction rate. When extractions were done with hexane at refluxing temperature, the extraction "plateau" was reached after 30 min.

Choice of extraction method

The choice of extraction method depends on its simplicity, chemical efficiency and compatibility with the chromatographic system. Dissolution of the polypropene sample in decalin requires a minimum of work-up. The procedure is only slightly complicated by the necessity of nitrogen purging and addition of another antioxidant. However, if many samples are to be analyzed, practical considering of cleaning glassware tends to favour one of the other solvents, which do not dissolve the polymer. The risk of degradation is negligible for any of the "protected" solvents and the recovery time for a sample is about the same (<1 h).

The incompatibility of chloroform and THF with the liquid chromatographic system used here is illustrated in Fig. 7. When the Irganox-1330 is dissolved in hexane, the peak is narrow with minimal baseline disturbance. The second chromatogram (B) mimics the situation if chloroform is used as extractant; although the mock chloroform extract is diluted five times with hexane, the peak becomes lower and broader than for a pure hexane solution. The incompatibility is even more pronounced for THF (chromatogram C).

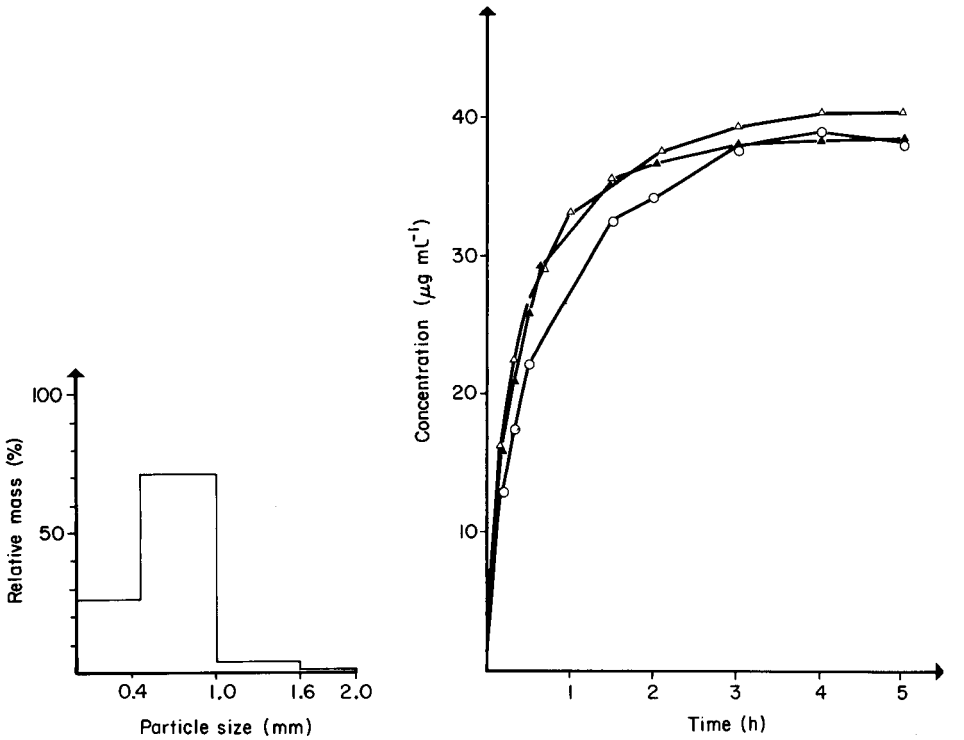

Fig. 5. Mass/particle-size distribution obtained by the milling procedure used for the determinations in Table 1.

Fig. 6. Rate of extraction of Irganox-1330 from polypropene (<1.0 mm particle size) at ambient temperature with different solvents: (△) hexane; (▲) $CHCl_3$; (○) THF.

If THF is chosen, the solution must be diluted 10 times in order to obtain acceptable peak shapes. Figure 8 shows the relative peak heights for sample solutions containing increasing volumes of chloroform or THF added to hexane. Clearly, these rather polar solvents block the adsorption sites to a large extent and cause the performance of the column to deteriorate. The combined effects of dilution and peak-broadening lower the sensitivity by a factor of 10 or 20 for chloroform or THF, respectively.

The final choice of hexane as the best extractant for routine work based on the system described is obvious from the point of view of the chromatography. Hexane has the further advantages of low toxicity, ease of disposal, and low absorption at the wavelength used. Sample filtration is easy, because of the low solubility of the polymer, and hexane is less dense than the polymer so that submerging the samples is no problem.

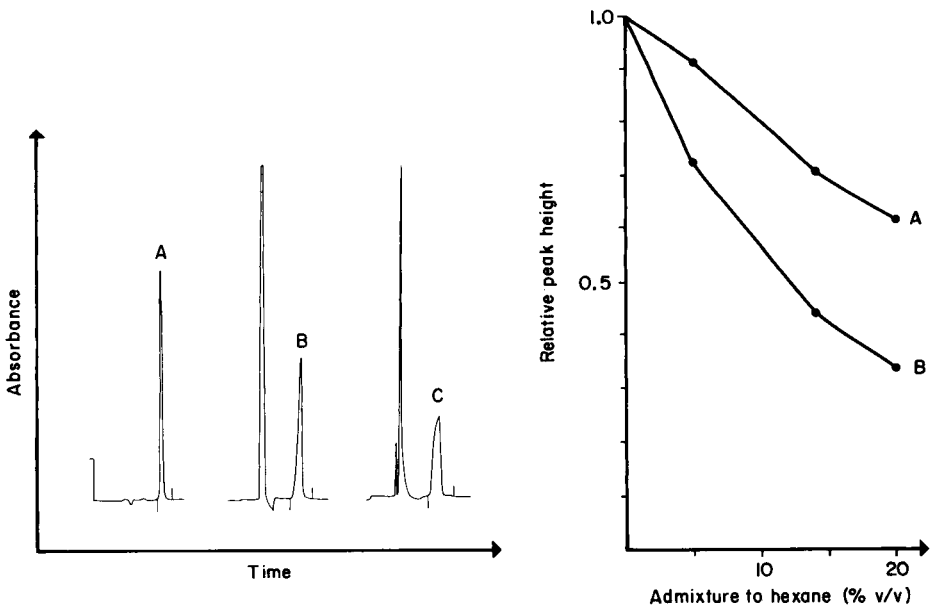

Fig. 7. Chromatograms from 20-μl samples containing 20 μg ml^{-1} Irganox-1330 with the same eluent, hexane/THF (99/1): (A) antioxidant dissolved in pure hexane; (B) antioxidant dissolved in 20/80 chloroform/hexane; (C) antioxidant dissolved in 20/80 THF/hexane.

Fig. 8. Effect on peak height of adding chloroform (A) or THF (B) to hexane solutions of Irganox-1330 (20 μg ml^{-1}). Other conditions as for Fig. 7.

REFERENCES

1 R. Gächter and H. Müller, Taschenbuch der Kunststoff-Additive, Carl Hanser Verlag, München, 1979, pp. 4—68.
2 D. A. Wheeler, Talanta, 15 (1968) 1315.
3 T. R. Crompton, Chemical analysis of additives in plastics, 2nd edn., Pergamon Press, 1977.
4 R. B. Walter and J. F. Johnson, J. Polym. Sci., Macromol. Rev., 15 (1980) 29.
5 H. L. Spell and R. D. Eddy, Anal. Chem., 32 (1960) 1811.
6 A. M. Wims and S. J. Swarin, J. Appl. Polym. Sci., 19 (1975) 1243.
7 C. F. Vadakkott, N. S. Yoginder and S. B. Ishwar, Angew. Makromol. Chem., 113 (1983) 219.
8 J. F. Schabron and L. E. Fenska; Anal. Chem., 52 (1980) 1411.
9 J. F. Schabron, V. J. Smith and J. L. Ware, J. Liquid Chromatogr., 5 (1982) 613.
10 R. G. Lichtentaler and F. Ranfelt, J. Chromatogr., 149 (1978) 553.
11 P. Roumeliotis, K. K. Unger, G. Tesarek and E. Mühlberg, Z. Anal. Chem., 298 (1979) 241.
12 J. Berg, C. Mohl, R. Deelder and J. Thijssen, Clin. Chim. Acta, 78 (1977) 165.
13 E. D. Lankmayer and K. Müller, J. Chromatogr., 170 (1979) 139.
14 M. A. Haney and W. A. Dark, J. Chromatogr. Sci., 18 (1980) 655.

Analytica Chimica Acta, 166 (1984) 253—260
Elsevier Science Publishers B.V., Amsterdam — Printed in The Netherlands

RESOLUTION OF STRONGLY OVERLAPPED RESPONSES IN SQUARE-WAVE VOLTAMMETRY BY USING THE KALMAN FILTER

CAROLINE A. SCOLARI and STEVEN D. BROWN*

Department of Chemistry-4630, Washington State University, Pullman, WA 99164 (U.S.A.)

(Received 9th May 1984)

SUMMARY

Various approaches have been proposed for resolving overlapped voltammograms. Such methods have become increasingly important since the advent of small computers and commercial electrochemical instrumentation capable of rapid-scan techniques. The combination of high-resolution, rapid-scan square-wave voltammetry and a linear, recursive estimator known as the Kalman filter is described. Results of the application of this combination to mixtures of thallium(I) and lead(II) in 0.9 M nitric acid are shown. Practical considerations for filter usage such as the choice of models, variances, and initial guesses are discussed, as are limits to the filter. With the Kalman filter, it was possible to quantify thallium in solutions containing as much as a 30-fold excess amount of lead, and it was possible to quantify lead in solutions containing a 60-fold excess amount of thallium. The filter is thus a useful tool for use with empirical models in multicomponent quantitation.

Microprocessor-based electrochemical instrumentation offers a number of significant advantages over more conventional equipment. One of these is the opportunity to use the peak resolution methods developed over the last fifteen years. Most approaches to peak resolution rely on curve-fitting of some model to the overlapped electrochemical response. The model can be an empirical description of the responses of individual components suspected in the mixture, in which case linear regression is used [1—5], or it can be a more complex expression, often based directly on electrochemical theory [6—9]. For the latter case, nonlinear least-squares fitting is usually necessary.

Although many of the methods proposed for peak resolution work well on closely overlapped systems when component ratios are near unity, surprisingly little has appeared on resolution of such systems when component ratios differ substantially from unity. Binkley and Dessy [3] estimated that Tl(I)/Pb(II) mixtures with concentration ratios of up to 1:15 should be resolvable, while Bondreau and Perone [7] observed that a 17.6:1 ratio of Tl(I)/Cd(II) was resolvable. In the In(III)/Cd(II) system, successful resolution of 5:1 ratios was possible [1, 2]. In view of the frequency with which unequal mixtures of closely overlapped components arise in practise [4], evaluation of an approach with unequal concentrations is a critical and realistic test.

0003-2670/84/$03.00

The Kalman filter has been used previously to resolve overlapped electrochemical responses [5, 10, 11]. The filter is ideal for use on a microprocessor because it has minimal memory requirements and it is rapid. Studies of synthetic data showed that successful resolution of arbitrarily closely overlapped responses could be achieved by using the filter, given suitably high point densities [5]. This paper reports the use of the filter in resolving a closely overlapped system in which peak height ratios are adjusted from values close to unity to values significantly different from unity.

GENERAL CONSIDERATIONS

The details of the use of the Kalman filter in multicomponent quantitation have been reported elsewhere [5]. To clarify the approach, however, some explanation is necessary. The Kalman filter is a recursive linear estimator which requires models for the system dynamics and the measurement process. Because the concentrations of the components do not change during the electrochemical scan, a simple system model can be used. The measurement process model

$$Z(k) = \mathbf{S}^{\mathrm{T}} \cdot \mathbf{X}(k) + \nu(k) \tag{1}$$

relates the measurement of current at potential k, $Z(k)$, to the component concentrations by a proportionality vector $\mathbf{S}^{\mathrm{T}}$. This vector is simply the slope of the current/concentration relation obtained for each of the N pure components included in the model. Here, $\mathbf{X}(k)$ is the vector of the N component concentrations ($1 \times N$) at potential k, and $\nu(k)$ is the measurement noise present at potential k. In essence, this method provides a point-by-point linear least-squares fit of the model component responses to the experimental data. The output is a statistically optimal estimate of the N component concentrations, provided that certain noise assumptions [5, 10] are met, although substantial deviations from the noise requirements appear to have little effect on the quality of the results [12].

The formulation of the Kalman filter described above allows rapid and efficient peak resolution because the usual matrix inversion needed for least-squares fits [13] is reduced to a mathematical division. Computer memory requirements are reduced because data are processed in a recursive, rather than a batch, mode. Only the pure component responses which describe the model need be kept in memory. These empirical models are limited (either the number of components or the point density used) only by the size of the memory; the model components can even be stored on disk for recall. Thus, a library of electrochemical responses can be generated for pure components under well-defined conditions, and this library can be used to provide empirical models containing all possible components suspected in an overlapped, multicomponent response. Fitting of such models to the overlapped response will return concentrations of zero for those components which are not present (subject to the limitations discussed below), while non-zero

concentrations will be assigned to components detected in the overlapped response. Omission of components in the model, or erroneous model components are easily detected [5, 10—12], and methods for compensating for these errors have been proposed [10, 11].

Two other aspects of the filter are appropriate for discussion here. If strongly overlapped components are to be separated, it must be established that the components are observable [5]. The criterion of observability insures that sufficient information exists in the measurement to allow estimation of the state vector, **X**. Here, the observability criterion demands that component (model) voltammograms all must differ by at least one point from each other. Thus, the point density of the digitized model and multicomponent data determine the theoretical limits in resolving overlapped systems with the filter.

A second factor is the accuracy of the initial guess made for the covariance matrix. This variance estimate determines whether it is possible to distinguish small perturbations on large, noisy signals, as might happen when a small amount of one component coexists with a large amount of a second component. Careful estimates of the within-run measurement variance, σ_z^2, are necessary to distinguish signal from noise in this case. Various methods have been used to estimate the diagonal elements of the covariance matrix [10]. Previously, the experimental reproducibility has been used; however, such a practice may lead to biased estimates if the initial guesses for the covariance matrix are low. Here, the initial estimate for the covariance matrix is based on the level of confidence in the initial guess of concentrations, a more reliable approach [10].

EXPERIMENTAL

Reagents, cells, electrodes and equipment

A stock solution of 1.877×10^{-2} M lead(II) was prepared by dissolving reagent-grade lead nitrate in reagent-grade nitric acid and then diluting with Super-Q water. A stock solution of 2.24×10^{-2} M thallium(I) was prepared by dissolving reagent-grade thallium(I) sulfate (99.5%) in dilute nitric acid. These solutions were standardized with EDTA using methods described by Schwarzenbach [14]. Lead(II) and thallium(I) stock solutions were added to a supporting electrolyte of 0.9 M nitric acid, prepared by diluting reagent-grade acid with Super-Q water.

A Bioanalytical Systems cell was used for all runs. This cell was thermostatted at 28.4°C. The counter electrode was a length of platinum wire, and the reference electrode was a Bioanalytical Systems Ag/AgCl (3 M NaCl) electrode. The working electrode was a Princeton Applied Research Model 9223 HMDE, which had a capillary siliconized just prior to the experiments reported here. All data were collected in triplicate. A new drop was used for each run. The reproducibility observed for repetitive measurements with new drops was 1.4%. Potentials were applied to the cell from an IBM Model 225 potentiostat which was interfaced to a Digital Equipment Corp. LSI-11/23

computer via an isolated 16-bit digital-to-analog converter and a 12-bit analog-to-digital converter. Details of the equipment used have been previously reported [9].

Computer programs

Data were obtained using SQWV, a FORTRAN and MACRO-11 assembly language program which runs on the LSI-11/23 under the RT-11 monitor. FORTRAN-based subroutines comprising SQWV allow input of square-wave parameters from either disk file or the keyboard, run checks on the parameters, generate the voltage sequence to be applied, and allow both plotting and storage of the experimental data. The MACRO-11 subroutines allow an external device to trigger the square-wave scan, to control the potential scan, and to collect the current responses. The point density for a square-wave scan is calculated by the program from the various parameters input to it. Typical square-wave scans include about 500 current difference measurements made in 2 s, within a potential scan of about 1 V. For faster scans, or for potential scans wider than 1 V, fewer current differences are taken. For the studies reported here, a voltage range of 0.600 V was used, with a scan time of 10.0 s, giving 491 current differences across the potential range. The point density was thus 1.22 mV per point in this study. The square-wave height was 50.0 mV.

In addition to starting potential, potential range, and scan time, parameters input to the program include square-wave height, forward and backward sampling delays, and square-wave symmetry parameter (the ratio of the forward pulse time to the sum of the times taken by both the forward and background pulses). A variable pre-scan delay, and point and scan averaging are also available. The voltammograms were Fourier-filtered and background-subtracted prior to application of the Kalman filter. Details of these methods have been reported previously [5, 8].

The Kalman filter was a modified version of the FORTRAN program previously reported [5]. This interactive version was not optimized for either speed or size. Processing of experimental voltammograms for a two-component model required about 3 s. The program size was about 14 kwords, including storage for a six-component model measured at 512 points, and allowing for space for the FORTRAN run-time monitor.

RESULTS AND DISCUSSION

The thallium(I)/lead(II) system has been studied extensively by a variety of methods [3, 4, 6]. In 0.9 M nitric acid supporting electrolyte, the observed peak-to-peak separation for the thallium(I)/lead(II) system is 68 mV, and the peak widths at half-height for thallium(I) and lead(II) in 0.9 M nitric acid are 94 mV and 58 mV, respectively; all measurements refer to data collected at 0.060 V s^{-1} scan rates and 50 mV square-wave height.

Model

Empirical models were used here. These models were obtained by measurement of the square-wave voltammetric response of single species in 0.9 M nitric acid, under the same conditions as those used in the measurement of the overlapped voltammetric responses. Measurements of lead(II) standards over the concentration range 6.25×10^{-6}—6.06×10^{-4} M gave peak current responses with a slope of $(1.108 \pm 0.006) \times 10^{5}$ μA M^{-1} and an intercept of $(-2 \pm 2) \times 10^{-2}$ μA. The correlation coefficient (n = 15) was 0.9996. For thallium(I), measurement of standards over the concentration range 7.46×10^{-6}—1.66×10^{-3} M gave peak current responses with a slope of $(5.455 \pm 0.009) \times 10^{3}$ μA M^{-1} and an intercept of $(-2.2 \pm 0.8) \times 10^{-1}$ μA. The correlation coefficient (n = 19) was 0.9999. Models were chosen from these standards by selecting the responses closest to the least-squares line, the slope of which is used in the S vector. The models used are reported in Table 1.

In all of the mixtures, the initial value for the covariance matrix, one part of the initial guess required to start the filter, was taken as 1×10^{-4} μA^2. This value was obtained by fitting thallium(I) standards to a $sech^2$ waveform by means of a non-linear least-squares routine [8]. The $sech^2$ model is an adequate descriptor of the square-wave peak shape for thallium(I) because the response is close to that expected for a reversible system, as evidenced by peak half-width. A reversible one-electron process should have a peak half-width of 91 mV [15]; the observed thallium peak half-width was 94 mV. The other part of the initial guess required to start the filter is an estimate of the component concentrations for all species included in the model. Various initial guesses were used. Initial guesses of zero for all components gave results identical to those obtained with initial guesses close to the true value. Initial guesses which were larger than the true values were not used, because these guesses are known to provide non-optimal results [10], and it is easy to avoid high guesses by guessing zero.

Fitting of overlapped responses

Two sets of data were processed with the Kalman filter, one with thallium(I) as the major component and the other with lead(II) as the major component.

TABLE 1

Models used in peak resolution

Mixture	Model[a]
1—4	5.96×10^{-5} M Tl, 1.861×10^{-4} M Pb
5—7	1.48×10^{-4} M Tl, 1.861×10^{-4} M Pb
8—13	1.53×10^{-3} M Tl, 4.986×10^{-5} M Pb
14—17	1.53×10^{-3} M Tl, 1.861×10^{-4} M Pb

[a]Concentrations of pure species in 0.9 M nitric acid for which model responses were collected. Model consists of voltammetric responses for both components.

All concentrations were corrected for the small volume changes. The experimental conditions above were chosen for convenience; other mixtures are equally amenable to processing by the filter.

Results obtained in fitting these data are shown in Tables 2 and 3. In all cases, the quality of fits is good, as is indicated by the coefficients of determination given in the Tables. A typical fit obtained by use of the filter is shown in Fig. 1, for which the thallium and lead are present at a ratio of 6:1; the difference between the observed (curve A) and the fitted (curve E) voltammograms is very small. The error in the estimated concentrations is

TABLE 2

Results for Pb/Tl mixtures with lead as major component

Mixture	Molarity ratio (Pb:Tl)	Peak height ratio (Pb:Tl)	Concentration				Error (%)		Coefficient of determination
			Prepared (10^{-5} M)		Computed[a] (10^{-5} M)				
			Pb	Tl	Pb	Tl	Pb	Tl	
1	50:1	113:1	36.8	0.732	36.6	0.656	−0.5	−10.0	0.9999
2	33:1	74:1	24.6	0.736	24.7	0.758	+0.4	+3.0	0.9999
3	25:1	55:1	36.8	1.46	37.7	1.40	+2.4	−4.1	0.9999
4	13:1	28:1	36.8	2.92	36.0	2.75	−2.2	−5.8	0.9999
5	3:1	6:1	36.6	13.1	36.0	13.3	−1.6	+1.5	0.9998
6	2:1	4:1	36.5	20.3	37.3	20.6	+2.2	+1.5	0.9998
7	1:1	3:1	36.4	27.5	37.9	28.4	+4.1	+3.3	0.9997

[a]In all mixtures, the uncertainty in the computed concentrations was 1×10^{-7} M.

TABLE 3

Results for Pb/Tl mixtures with thallium as major component

Mixture	Molarity ratio (Pb:Tl)	Peak height ratio (Pb:Tl)	Concentration				Error (%)		Coefficient of determination
			Prepared (10^{-5} M)		Computed[a] (10^{-5} M)				
			Pb	Tl	Pb	Tl	Pb	Tl	
8	1:60	1:29	2.34	140	2.20	140	−6.0	0.0	1.000
9	1:54	1:27	2.36	127	2.19	127	−7.2	0.0	1.000
10	1:48	1:24	2.37	113	2.42	113	+2.1	0.0	1.000
11	1:40	1:20	1.82	72.2	1.72	70.8	−5.5	−1.9	0.9999
12	1:30	1:14	4.68	140	4.75	140	+1.5	0.0	1.000
13	1:20	1:9	7.01	139	7.11	140	+1.4	+0.7	1.000
14	1:15	1:7	9.34	139	9.27	141	−0.7	+1.4	1.000
15	1:12	1:6	11.6	139	11.5	139	−0.9	0.0	1.000
16	1:8	1:4	17.4	139	17.4	138	0.0	−0.7	0.9999
17	1:6	1:3	23.2	138	23.1	138	−0.4	0.0	1.000

[a]In all mixtures, the uncertainty in the computed concentrations was 1×10^{-7} M.

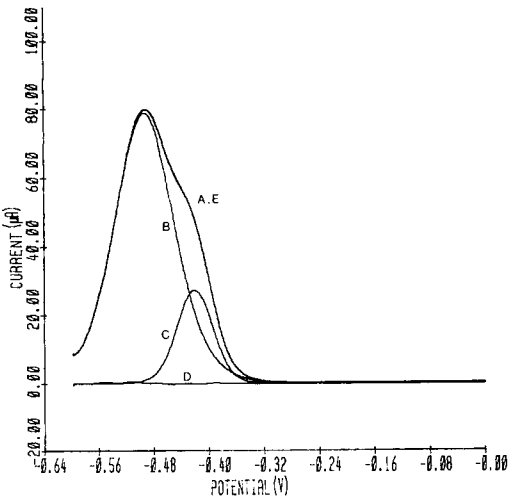

Fig. 1. Deconvolution of overlapped lead and thallium responses: (A) experimental data obtained for mixture 17 (see Table 3); (B) fitted thallium response; (C) fitted lead response; (D) residuals of the fitting; (E) sum of the fitted components.

generally below 5%, with the error in the estimated concentration for the minor component increasing as the concentration of the minor component decreases. The error in the concentration of the major component remains fairly constant. These errors reflect the degree to which the models chosen describe the individual components of the overlapped response. Models for thallium perform quite well. When thallium is the major component, fitting errors of about 1% are typical; when thallium is the minor component, the accuracy of peak resolution remains good up to a Pb:Tl peak height ratio of 113:1, where the lead is present in a fifty-fold excess amount. Models for lead are not as suitable. When lead is the major component, fitting errors of about 2% are observed, while errors of 2—5% are observed when lead is the minor component. However, even with a Tl:Pb molarity ratio of 60:1, the error in fitting increases only to about 7%, a remarkable result given the relative widths of the two peaks and the peak separation. In all cases, initial guesses of zero concentration input to the filter did not affect the accurate determination of either of the components. The filter remains useful for quantitative work down to concentration levels near the detection limit of the minor component.

The insensitivity of fits using the Kalman filter to components of the model which are not relevant to describing the experimental measurement was demonstrated by the inclusion of a cadmium(II) response in the model. In no case did the cadmium concentration found by using the filter differ significantly from zero; typical values found ranged near -1×10^{-8} M, with filter estimation uncertainty [5] of about 10^{-7} M. The observed results for lead and thallium were unchanged from those obtained without cadmium in the model.

The speed, small memory requirements, and accuracy of the Kalman filter make it attractive for use with empirical models in multicomponent quantitation. The lack of significant sensitivity of the method to additional components or to the initial guess makes it useful for qualitative as well as quantitative applications.

This work was supported, in part, by the Graduate School, Washington State University, through a Grant-in-Aid. Additional funding was provided by the Department of Energy (DE-FG06-84ER13202).

REFERENCES

1 W. F. Gutknecht and S. P. Perone, Anal. Chem., 42 (1970) 906.
2 L. B. Sybrandt and S. P. Perone, Anal. Chem., 43 (1971) 382.
3 D. P. Binkley and R. E. Dessy, Anal. Chem., 52 (1980) 1335.
4 A. M. Bond and B. S. Grabaric, Anal. Chem., 48 (1976) 1624.
5 T. F. Brown and S. D. Brown, Anal. Chem., 53 (1981) 1410.
6 L. Meites and L. Lampugnani, Anal. Chem., 45 (1973) 1317.
7 P. A. Boudreau and S. P. Perone, Anal. Chem., 51 (1979) 811.
8 J. J. Toman and S. D. Brown, Anal. Chem., 53 (1981) 1497.
9 D. M. Caster, J. J. Toman and S. D. Brown, Anal. Chem., 55 (1983) 2143.
10 S. C. Rutan and S. D. Brown, Anal. Chim. Acta, 160 (1984) 99.
11 T. F. Brown, D. M. Caster and S. D. Brown, Natl. Bur. Stand. (U.S.), Spec. Publ., No. 618 (1981) 163.
12 T. F. Brown, Ph.D. Dissertation, University of Washington, 1982.
13 J. V. Beck and K. J. Arnold, Parameter Estimation in Engineering and Science, Wiley, New York, 1977.
14 G. Schwarzenbach, Complexometric Titrations, Methuen, London, 1969.
15 L. Ramaley and M. S. Krause, Anal. Chem., 41 (1969) 1362.

Analytica Chimica Acta, 166 (1984) 261—270
Elsevier Science Publishers B.V., Amsterdam — Printed in The Netherlands

MULTIVARIATE DATA ANALYSIS FOR X-RAY FLUORESCENCE SPECTROMETRY

M. BOS

Technical University Twente, Department of Chemical Technology, P.O. Box 217, 7500 AE Enschede (The Netherlands)

(Received 9th May 1984)

SUMMARY

A multivariate data analysis procedure that uses singular value decomposition and the Ho-Kashyap algorithm is proposed to obtain calibration constants for x-ray fluorescence spectrometry. These calibration constants can be used to obtain results from experimental data by means of a simple dot product calculation. The method was tested on experimental data from the literature. Comparison of results showed that the method performs at least as well or better than the Rasberry—Heinrich method or its modifications. The method can be used to express calibration results obtained with a theoretically based program in such a way that they can be used conveniently in routine applications.

In multicomponent determinations, the problem is to extract information about the separate components of a mixture from a set of measurements on the sample. For most instrumental methods, this is possible only after calibration against a number of samples of known composition. Depending on the complexity of the sample and the selectivity of the measurements, the complete procedure of calibration and evaluation can vary from the straightforward to the very complicated.

Especially in the field of ultraviolet-visible spectrophotometry and fluorescence measurements, many methods that deal with this problem have been published, e.g., least squares [1, 2], generalized standard addition [3—5], multiple regression [6], Kalman filtering [7, 8], factor analysis followed by multiple regression [9], partial least-square models in latent variables [10, 11], and matrix rank annihilation [12]. The newer methods take care of the problems of highly correlated measurements which give rise to mathematical difficulties in the straightforward least-squares and multiple regression techniques.

Presumably because of the greater inherent selectivity of x-ray fluorescence (x.r.f.), the approach to data analysis in this field has been either of theoretical [13, 14] or empirical [15] nature, in which interactions between the components in the sample during spectrometry are taken into account by means of influence coefficients or correction constants.

0003-2670/84/$03.00

In this work, the experimental data given by Budesinsky [16] in a paper on the comparison of the various mathematical methods and the data of Rasberry and Heinrich [15] were treated by a general procedure for multivariate data analysis developed earlier [17], in order to assess the ability of the procedure to correct automatically for interelement effects. The advantage over the method of Rasberry and Heinrich is that the results of a calibration are expressed as a set of calibration constants that can be used in a simple non-iterative procedure (the calculation of a dot product) which allows very fast computation of the results.

The method was also applied to calibration data obtained with a fundamental method by means of the computer program NRLXRF [13, 18], to test its functioning as a fast and convenient method of data evaluation that can be done by hand on a small computer after the NRLXRF calculations have been completed on a mainframe computer.

THEORY

The general theory of multivariate quantitative data analysis with the use of singular value decomposition and the Ho—Kashyap algorithm (SVDHK method) was given earlier [17] but will be restated here in terms of x.r.f. parameters and equations.

Mathematically, the problem is to find from a set of n intensity measurements I_1—I_n on each of m standard samples with known concentrations of the component under study

$$\begin{array}{ll} I_{11}, I_{12}, \ldots, I_{1n} & C_1 \\ I_{21}, I_{22}, \ldots, I_{2n} & C_2 \\ \ldots\ldots\ldots\ldots & \cdot \\ \ldots\ldots\ldots\ldots & \cdot \\ I_{m1}, I_{m2}, \ldots, I_{mn} & C_m \end{array} \qquad (1)$$

the evaluation function that relates the measured intensities of an unknown sample to the concentration of the component under study. The models in use for this evaluation function have been surveyed [15]. A general model that includes most types of interactions can be written as [19]

$$\text{Conc.} = \sum_{j=1}^{n} b_j I_j + \sum_{j=1}^{n} \sum_{l=1}^{n} d_{jl} I_j I_l + a \qquad (2)$$

where conc. denotes the concentration of the component under study, I is the measured fluorescence intensity at the lines of the various components and b, d and a are the calibration constants.

To calculate the calibration constants, the data matrix has to be extended to include the quadratic and cross-intensity terms:

$$I_{11}, I_{12}, \ldots, I_{1n}, I_{11}^2, I_{11}I_{12}, \ldots, I_{11}I_{1n}, I_{12}^2, I_{12}I_{13}, \ldots, I_{12}I_{1n}, \ldots, I_{1n}^2, 1$$

$$I_{21}, I_{22}, \ldots, I_{2n}, I_{21}^2, I_{21}I_{23}, \ldots, I_{21}I_{2n}, I_{22}^2, I_{22}I_{23}, \ldots, I_{22}I_{2n}, \ldots, I_{2n}^2, 1$$

$$\ldots\ldots\ldots\ldots\ldots\ldots\ldots\ldots\ldots\ldots\ldots\ldots\ldots\ldots\ldots\ldots\ldots\ldots\ldots\ldots\ldots\ldots$$

$$I_{m1}, I_{m2}, \ldots, I_{mn}, I_{m1}^2, I_{m1}I_{m2}, \ldots, I_{m1}I_{mn}, I_{m2}^2, I_{m2}I_{m3}, \ldots,$$

$$I_{m2}I_{mn}, \ldots, I_{mn}^2, 1 \qquad (3)$$

If this data matrix is denoted by A, the calibration constants b, d and a by the vector **w** and the concentrations of the compound under study in the set of standard samples (the training set) by the vector **c**, the problem is to find the vector **w** from the matrix equation

$$\mathbf{Aw} = \mathbf{c} \qquad (4)$$

Generally the set of Eqns. 4 is overdetermined and has no exact solution. Moreover, it is very likely that the data matrix will contain a number of dependent or nearly dependent columns. By singular value decomposition and use of the Ho—Kashyap algorithm [20], Eqn. 4 can be solved under these conditions, as described in detail earlier [17].

Solving the set of Eqns. 4 in this way constitutes the training or calibration phase and produces the vector **w**. This vector can then be used in recognition (i.e., to check how well it reproduces the calibration results) or in prediction of analytical results for unknown samples with the following equation

$$\text{Conc.} = \mathbf{w}_1 I_1 + \mathbf{w}_2 I_2 + \ldots + \mathbf{w}_n I_n + \mathbf{w}_{n+1} I_1^2 + \mathbf{w}_{n+2} I_1 I_2$$

$$+ \ldots + \mathbf{w}_{n(n+1)/2} I_n^2 + \mathbf{w}_{[n(n+1)/2+1]} \qquad (5)$$

RESULTS AND DISCUSSION

The SVDHK procedure applied directly to experimental data

The Fe/Ni/Cr system. The data at 45 kV on the Fe/Ni/Cr system from the paper by Rasberry and Heinrich [15] were used to test the performance of the method applied directly to experimental data. The training set consisted only of the data concerning the ternary mixtures and included the samples treated as unknowns in Table 3 of the paper, except for specimen number 3987. The data on two-component mixtures could not be used, because no intensities were given at the line position of the absent element. For this ternary system the calibration results are expressed as

$$\text{Conc.} = \mathbf{w}_1 I_{\text{Fe}} + \mathbf{w}_2 I_{\text{Ni}} + \mathbf{w}_3 I_{\text{Cr}} + \mathbf{w}_4 I_{\text{Fe}}^2 + \mathbf{w}_5 I_{\text{Fe}} I_{\text{Ni}} + \mathbf{w}_6 I_{\text{Fe}} I_{\text{Cr}}$$

$$+ \mathbf{w}_7 I_{\text{Ni}}^2 + \mathbf{w}_8 I_{\text{Ni}} I_{\text{Cr}} + \mathbf{w}_9 I_{\text{Cr}}^2 + \mathbf{w}_{10} \qquad (6)$$

Table 1 shows the values of the vectors **w** for Fe, Ni and Cr calculated with seven non-zero singular values and the resulting root mean square (RMS) error in the recognition process. This RMS error is calculated from $\sqrt{\Sigma(\text{conc}_{\text{calc}} - \text{conc}_{\text{chem}})^2/10}$.

TABLE 1

SVDHK calibration results for Fe/Ni/Cr data set [15]

Intensity term	Values of $w_i - w_{10}$		
	Fe	Ni	Cr
I_{Fe}	1.27250	−0.67920	−0.54945
I_{Ni}	−0.58703	0.62360	−0.27812
I_{Cr}	0.17149	−0.59771	0.33422
$I_{Fe}I_{Fe}$	−0.80201	0.17902	0.38542
$I_{Fe}I_{Ni}$	−0.90793	0.70134	0.00483
$I_{Fe}I_{Cr}$	1.61510	−1.29050	−0.54450
$I_{Ni}I_{Ni}$	0.58780	−0.55446	−0.06831
$I_{Ni}I_{Cr}$	0.39872	0.09506	−0.38565
$I_{Cr}I_{Cr}$	−1.01780	0.05392	0.68526
1.0000	0.10682	0.67828	0.32797
RMS error in recognition (% absolute)	0.002	0.002	0.0005

To test the predictive power of the method, the leave-one-out technique was followed, i.e., 10 members of the data set were used as the training set and the concentrations of the eleventh member were calculated with Eqn. 6. The results are given in Table 2. As can be seen, the SVDHK method performs as well as the Rasberry—Heinrich method in all but the very low concentration ranges.

The Cu/Fe/S system. A second ternary test system was found in the data of Budesinsky [16] on copper smelter mattes. Table 3 shows the SVDHK calibration results together with the RMS errors in the recognition process in comparison with the standard deviations obtained by Budesinsky who used the expanded square-intensity method. The results were calculated with six non-zero singular values. Prediction performance for a number of samples taken from various parts of the concentration range, obtained with the leave-one-out technique, is summarized in Table 4. The RMS error is increased somewhat compared to the recognition, but is still very close to the errors obtained by the Rasberry—Heinrich method or its modifications, even though the latter are not given for the leave-one-out situation.

The $Cu/SiO_2/Fe/S$ system. To test the method on a more complicated system, the data of Budesinsky [16] on copper smelter converter slags were used. The calibration results then comprise four 15-element w vectors. With the use of six non-zero singular values, the recognition results listed in Table 5 were obtained. It is clear that when this way of representing the calibration results is used, the data are followed more closely by the six latent variables of the SVDHK method than by the six theoretical interactive constants plus two empirical constants used in the best performing method from the comparisons made by Budesinsky.

TABLE 2

Prediction of the composition of Fe/Ni/Cr samples with the leave-one-out method

Sample[a] no.	Fe (%) SVDHK	Fe (%)[a] Chem.	Absolute error (%)	Fe (%)[a] R + H	Ni (%) SVDHK	Ni (%)[a] Chem.	Absolute error (%)	Ni (%)[a] R + H	Cr (%) SVDHK	Cr (%)[a] Chem.	Absolute error (%)	Cr (%)[a] R + H
5074	68.65	68.38	0.27		4.87	4.98	−0.11		25.16	25.25	−0.09	
5181	68.86	69.45	−0.59		10.11	9.96	1.49		19.94	19.88	−0.06	
5324	53.19	52.80	0.39		18.52	19.27	−0.75		27.13	26.96	0.17	
5321	59.11	59.19	−0.08		20.57	20.02	0.55		19.86	19.88	−0.02	
7271	73.08	71.59	1.49		7.45	8.29	−0.84		18.75	18.79	−0.04	
161	15.09	15.01	0.08		62.58	64.29	−1.71		17.66	16.88	0.78	
1189	4.02	1.40	2.62		75.96	72.60	3.36		20.73	20.30	0.43	
5054	72.12	72.50	−0.38	72.29	0.54	0.15	0.39	0.15	25.86	25.77	0.09	25.22
5202	63.28	63.03	0.25	62.27	14.56	14.80	−0.24	15.07	21.23	21.30	−0.07	20.90
5364	46.62	47.21	−0.59	47.50	24.50	23.57	0.93	24.07	27.67	27.84	−0.17	26.75
1188	6.18	6.60	−0.42	6.55	74.21	72.65	1.56	72.36	14.34	15.40	−1.06	14.21
RMS absolute error (%)			1.0	0.5			1.4	0.4			0.4	1.0

[a]From Rasberry and Heinrich [15].

TABLE 3

SVDHK calibration results for the Cu/Fe/S system for experimental data from Budesinsky [16]

Intensity term	Values of $w_1 - w_{10}$		
	Cu	Fe	S
I_{Cu}	2.43060	−0.26105	1.71770
I_{Fe}	0.63527	0.41521	0.59317
I_S	1.59250	0.22511	1.42390
$I_{Cu}I_{Cu}$	0.11686	−0.01742	−0.06147
$I_{Cu}I_{Fe}$	1.26370	0.20399	−0.10877
$I_{Cu}I_S$	0.19492	0.18370	−0.01923
$I_{Fe}I_{Fe}$	−0.37549	1.78100	0.17309
$I_{Fe}I_S$	−0.36715	1.59710	−0.04623
I_SI_S	0.00324	−0.28706	0.33389
1.0000	0.67779	0.04782	0.56552
RMS error (% absolute)	0.088	0.107	0.092
Std. Dev.[a] (% absolute)	0.245	0.211	0.136

[a] From Budesinsky [16].

TABLE 4

Prediction of Cu/Fe/S samples in the leave-one-out procedure

Sample no.	Cu (%)		Fe (%)		S (%)	
	Found	Lit.[a]	Found	Lit.[a]	Found	Lit.[a]
1	32.12	31.81	33.72	33.97	24.95	24.81
2	34.33	33.36	34.17	34.62	26.69	26.98
3	35.44	35.46	32.34	32.07	25.29	25.28
4	36.97	37.06	31.50	31.63	25.35	25.44
10	45.08	45.10	25.75	25.63	25.03	25.10
15	52.05	51.94	20.20	19.97	24.51	24.38
19	58.81	59.34	14.61	14.46	23.45	23.54
RMS error (% absolute)	0.47		0.27		0.15	

[a] From Budesinsky [16].

Table 6 shows the prediction performance of the SVDHK method in the leave-one-out procedure for a number of samples chosen in different regions of the data set. The data on reverbatory slags with six components [16] could not be evaluated with the SVDHK method because the **w** vector then has 28 elements which cannot be calculated from a data set with 20 members.

TABLE 5

SVDHK calibration results for the $Cu/SiO_2/Fe/S$ system for experimental data from Budesinsky [16]

Intensity term	Values of $w_1 - w_{15}$			
	Cu	SiO_2	Fe	S
I_{Cu}	0.37521	0.83572	0.97300	0.03764
I_{Si}	0.09310	2.79550	2.10110	−0.07505
I_{Fe}	0.45545	11.07800	10.66700	−0.43682
I_S	0.00758	1.01480	0.78676	0.01660
$I_{Cu}I_{Cu}$	0.25059	−0.66370	−1.50160	−0.10125
$I_{Cu}I_{Si}$	0.37466	−3.12210	−2.62140	0.28917
$I_{Cu}I_{Fe}$	1.57400	−0.41092	0.92427	0.41387
$I_{Cu}I_S$	0.06218	0.49322	−0.09122	−0.02707
$I_{Si}I_{Si}$	−0.00098	3.49980	1.86640	−0.08174
$I_{Si}I_{Fe}$	−0.11268	0.49476	−1.94530	0.12763
$I_{Si}I_S$	−0.01531	−1.62030	−1.73430	0.16992
$I_{Fe}I_{Fe}$	−0.07578	−1.88390	0.00934	0.07295
$I_{Fe}I_S$	−0.14930	0.07106	−0.47556	0.28607
I_SI_S	−0.12587	0.99937	0.40766	−0.00982
1.0000	0.19634	4.76170	4.49810	−0.18865
RMS error (% absolute)	0.045	0.285	0.242	0.076
Std. dev.[a] (% absolute)	0.079	0.751	0.325	0.128

[a] From Budesinsky [16].

TABLE 6

Prediction of $Cu/SiO_2/Fe/S$ samples in the leave-one-out procedure

Sample no.[a]	Cu (%)		SiO_2 (%)		Fe (%)		S (%)	
	Found	Lit.[a]	Found	Lit.[a]	Found	Lit.[a]	Found	Lit.[a]
1	1.36	1.32	28.55	28.65	47.43	47.47	0.84	0.92
2	1.40	1.45	25.95	26.31	48.97	48.94	0.96	1.11
3	1.82	1.82	25.58	25.18	48.99	49.35	1.01	1.03
4	2.22	2.19	24.80	24.87	49.48	49.16	1.18	1.12
10	4.79	4.74	22.66	22.43	48.61	48.63	1.96	1.90
19	16.22	15.90	18.66	16.78	41.20	41.91	5.45	4.60
RMS error (% absolute)	0.15		0.88		0.43		0.39	

[a] From Budesinsky [16].

The SVDHK procedure applied to data from a theory-based computer program

The Cu/Fe/S system. The NRLXRF computer program of Criss [18] can generate relative intensity data for samples of known composition and can calculate results from measured intensity data. It is a large program running

on a mainframe computer and is therefore not well suited for routine application on large series of samples or for on-line use. The use of the SVDHK method to represent calibration data generated off-line by the NRLXRF program should make the results of the latter program applicable for routine analysis.

To test this suggestion, relative intensity data for copper, iron and sulphur were generated for samples containing the following elements in the concentration ranges 25—65% Cu, 10—40% Fe, 20—30% S and 10—50% O. Altogether, 300 samples covering these ranges evenly were simulated. Pseudo-random, normally distributed noise with zero mean and a standard deviation of 10^{-5} was added to the intensity data before the SVDHK procedure was entered. The calibration results of the SVDHK procedure with seven non-zero singular values are given in Table 7. It should be noted that these calibration vectors are valid only for the relative intensities generated by the NRLXRF program, which are relative to the pure elements, and for concentrations expressed as weight fractions not as percentages. To use the results on experimental data, the experimentally found intensities have to be converted to this type of relative intensity and the results will be found as weight fractions.

The experimental data of Budesinsky on the reverbatory mattes containing Cu, Fe and S, used above in the direct approach, were converted with the use of the NRLXRF prediction of relative intensities (RI) for the first sample: RI (Cu) = 0.224489, RI (Fe) = 0.413568, RI (S) = 0.107115. Table 8 shows the recalculated relative intensities and the results found with the calibration constants from the SVDHK procedure, compared with the concentrations given by Budesinsky. The RMS errors between the calculated results and the wet chemical results given by Budesinsky [16] are around 1% absolute and are probably mainly due to the deviation between the NRLXRF-generated and experimentally measured data. For instance, sample number 10 is predicted by the NRLXRF program to have relative intensities of 0.336949

TABLE 7

Calibration results for the Cu/Fe/S system for data generated by the NRLXRF program

Intensity term	Values of $w_i - w_{10}$		
	Cu	Fe	S
I_{Cu}	−1.4682	−0.33434	0.15855
I_{Fe}	−1.1980	−0.29151	0.10975
I_S	2.8775	1.39480	2.35970
$I_{Cu}I_{Cu}$	3.0724	0.49056	0.21352
$I_{Cu}I_{Fe}$	6.9195	2.16510	1.02760
$I_{Cu}I_S$	−2.1887	−0.33772	0.48990
$I_{Fe}I_{Fe}$	1.6765	1.89250	0.27390
$I_{Fe}I_S$	−1.9160	−0.79475	0.37874
I_SI_S	2.5858	1.00470	0.78684
1.0000	−0.1662	−0.16219	−0.30525

TABLE 8

Prediction results for the composition of Cu/Fe/S samples based on calibration data from the SVDHK/NRLXRF programs

Sample no.	Cu			Fe			S		
	RI	Found (%)	Lit.[a] (%)	RI	Found (%)	Lit.[a] (%)	RI	Found (%)	Lit.[a] (%)
1	0.224489	30.94	31.81	0.413568	32.17	33.97	0.114600	24.00	24.81
2	0.231637	34.31	33.36	0.411805	33.35	34.62	0.122975	26.78	26.98
3	0.252205	35.23	35.46	0.395410	31.02	32.07	0.115183	25.07	25.28
4	0.264721	37.03	37.06	0.387277	30.45	31.63	0.114934	25.39	25.44
5	0.275469	38.03	38.20	0.377784	29.54	30.45	0.114314	25.48	25.30
6	0.292490	40.14	40.19	0.366548	28.61	29.52	0.112864	25.48	25.21
7	0.310959	41.58	42.21	0.349074	26.96	27.73	0.112321	25.48	25.21
8	0.317179	42.14	42.99	0.343624	26.49	27.23	0.112246	25.54	25.16
9	0.327709	43.81	43.93	0.338154	26.24	26.67	0.112120	25.87	25.14
10	0.338649	44.57	45.10	0.329308	25.33	25.63	0.110409	25.55	25.10
11	0.345435	45.03	45.84	0.322008	24.73	24.99	0.111199	25.75	25.16
12	0.355299	45.39	46.70	0.313039	23.74	24.04	0.109354	25.29	25.15
13	0.368413	46.97	47.92	0.305163	23.18	23.42	0.108275	25.34	24.99
14	0.389709	48.18	49.99	0.286150	21.44	21.70	0.106953	25.07	24.74
15	0.413213	50.51	51.94	0.270591	20.25	19.97	0.104943	24.97	24.38
16	0.429041	51.85	53.32	0.259310	19.35	19.29	0.103641	24.83	24.31
17	0.449609	53.70	54.92	0.245896	18.27	17.96	0.101216	24.49	24.00
18	0.433937	50.25	52.78	0.253691	17.82	18.08	0.095651	22.49	22.67
19	0.503986	57.65	59.34	0.206564	15.21	14.46	0.096872	23.76	23.54
RMS error (% absolute)		1.1			0.9			0.4	

[a]From Budesinsky [16].

for copper, 0.322943 for iron and 0.107115 for sulphur, whereas the experimental data recalculated with the predictions for the first sample are 0.345435 for copper, 0.329308 for iron, and 0.110409 for sulphur. Another indication for this explanation can be found from a comparison between Tables 8 and 4; the RMS error of the results from the direct application of the SVDHK procedure is much lower. Nevertheless, it will be clear that the SVDHK way of summarizing data from NRLXRF simulations can be used successfully if the required accuracy is not below 1% absolute.

REFERENCES

1 I. M. Warner, E. R. Davidson and G. D. Christian, Anal. Chem., 49 (1977) 2155.
2 H. Gampp, M. Maeder and A. D. Zuberbuehler, Talanta, 27 (1980) 1037.
3 B. E. H. Saxberg and B. R. Kowalski, Anal. Chem., 51 (1979) 1031.
4 C. Jochum, P. Jochum and B. R. Kowalski, Anal. Chem., 53 (1981) 85.
5 J. H. Kalivas, B. R. Kowalski, Anal. Chem., 54 (1982) 560.
6 D. L. Massart, A. Dijkstra and L. Kaufman, Evaluation and Optimization of Laboratory Methods and Analytical Procedures, Elsevier, Amsterdam, 1978, p. 296.
7 H. N. J. Poulisse, Anal. Chim. Acta, 112 (1979) 361.
8 C. B. M. Didden and H. N. J. Poulisse, Anal. Lett., 13 (1980) 921.
9 H. Martens, Anal. Chim. Acta, 112 (1979) 423.
10 R. W. Gerlach, B. R. Kowalski and H. O. A. Wold, Anal. Chim. Acta, 112 (1979) 417.

11 M. Sjostrom, S. Wold, W. Lindberg and J. Persson, Anal. Chim. Acta, 150 (1983) 61.
12 C. N. Ho, G. D. Christian and E. R. Davidson, Anal. Chem., 53 (1981) 92.
13 J. W. Criss, L. S. Birks and J. V. Gilfrich, Anal. Chem., 50 (1978) 33.
14 N. Broll and R. Tertian, X-Ray Spectrom., 12 (1983) 30.
15 S. D. Rasberry and K. F. J. Heinrich, Anal. Chem., 46 (1974) 81.
16 B. W. Budesinsky, X-Ray Spectrom., 12 (1983) 121.
17 M. Bos and G. Jasink, Anal. Chim. Acta, 103 (1978) 151.
18 J. W. Criss, NRLXRF, A Fortran Program for X-Ray Fluorescence Analysis, Naval Research Laboratory, Washington, DC, 1977.
19 H. J. Lucas-Tooth and C. Pyne, Adv. X-Ray Anal., 7 (1964) 523.
20 Y. C. Ho and R. L. Kashyap, IEEE Trans. Electron. Comput., EC-14, No. 5, (1965) 683.

Analytica Chimica Acta, 166 (1984) 271—276
Elsevier Science Publishers B.V., Amsterdam — Printed in The Netherlands

Short Communication

SPECTROPHOTOMETRIC DETERMINATION OF COPPER AS A DITHIOCARBAMATE BY FLOW INJECTION ANALYSIS

ROGER M. SMITH* and TONY G. HURDLEY

Department of Chemistry, Loughborough University of Technology, Loughborough, Leics. LE11 3TU (Great Britain)

(Received 23rd May 1984)

Summary. Copper(II) ions (1—20 mg l^{-1}) are determined at 385 nm by injection into an aqueous carrier solution containing EDTA (0.05 M), carbon disulphide (0.03%) and diethanolamine (0.1%) in aqueous ammonia solution (0.5%) adjusted to pH 8.0. Chromium(VI) and, to a minor extent, iron(III) interfere. In the absence of EDTA, cobalt, iron(II), nickel, and manganese ions interfere but the sensitivity to copper is higher.

Flow-injection systems for the determination of copper(II) ions have been based on atomic absorption spectrometry [1, 2], inductively-coupled plasma emission spectrometry [3, 4], stripping voltammetry on a mercury drop [5—8], amperometric detection [9, 10] and ion-selective electrodes [11]. Other approaches have involved detection of copper ions at the nanogram level by their catalytic effect on the chemiluminescent reaction of flavin mononucleotides with hydrogen peroxide [12] and their catalysis of the oxidation of 2,2′-dipyridylketone hydrazone by oxygen with fluorimetric detection [13].

Chelates of copper ions often absorb at characteristic wavelengths and can be selectively determined spectrophotometrically. Flow-injection determinations of copper ions have been based on chelation with bathocuproine [14] or pyridylazoresorcinol [15—17]. It seemed worthwhile to examine other chelating reagents to establish if greater selectivity could be achieved. In earlier work, a dithiocarbamate was incorporated into the mobile phase for high-performance liquid chromatography [18]; injection of suitable metal ions gave the chelates, which were then separated and detected. Copper diethyldithiocarbamate absorbed at 430 nm and this reaction seemed feasible for direct flow-injection determinations of copper. This communication describes the selection of a suitable dithiocarbamate reagent and modification of the carrier solution to reduce interferences. Although dithiocarbamates are widely used in conventional determinations of copper and other metal ion [19], their application in flow injection analysis has been restricted to extraction prior to atomic absorption spectrometry [20].

0003-2670/84/$03.00

Experimental

Reagents and solutions. Metal salt solutions and buffers were prepared from analytical-grade reagents and distilled water. Diethanolamine and carbon disulphide were reagent-grade. The reagent carrier solution contained diethanolamine (0.1% w/v) and carbon disulphide (0.03% v/v), EDTA (0.05 M) and ammonia solution (0.5% v/v from ammonia liquor) to give a nominal concentration of ammonium diethanoldithiocarbamate of 0.1% (w/v). This solution was adjusted to pH 8.0 with dilute hydrochloric acid.

Apparatus. An Ismatec Mini-S 840 peristaltic pump, a Rheodyne Model 50 rotary valve and an MSE Spectroplus variable-wavelength spectrometer fitted with a 80-μl flow cell were used. Teflon tubing (i.d. 0.58 mm) was used for connecting tubing and mixing coils.

Recommended procedure. Samples (113 μl) were injected at a rate of 60 h^{-1} into a reagent carrier stream containing diethanoldithiocarbamate (0.1%) and EDTA (0.05 M) flowing at 5.0 ml min^{-1} through a 0.5-m mixing coil. Peaks were detected at 385 nm. Peak heights were measured.

If no interfering metal ions are present, copper ions can be determined by using a reagent carrier solution containing diethanolamine (0.1% w/v), carbon disulphide (0.03% v/v) and ammonia (0.5% v/v) without pH adjustment and detection at 430 nm. The sensitivity is higher than in the above procedure but there are many interferences.

Standard samples. Certified alloys (Bureau of Analysed Samples, Middlesbrough) were dissolved in a minimum of nitric acid, neutralized and diluted with distilled water before injection to give expected copper concentrations in the 10—20 mg l^{-1} range.

Results and discussion

Selection of the dithiocarbamate reagent. In the conventional spectrophotometric determination of copper with diethyl- or tetramethylene-dithiocarbamate, the insoluble chelate is extracted into chloroform or butyl acetate for measurement. The optimum wavelength for the complex can be used, as background interference from the reagent is negligible. Although on-line extraction is now frequently used in flow-injection systems, homogeneous reactions are easier to handle.

The initial concept here was to adapt the earlier method [18] to flow injection analysis by using a wholly aqueous carrier, to avoid methanol which can reduce the lifetime of pump tubing. However, tests showed that the copper chelates of readily available dithiocarbamates were insufficiently soluble even at trace levels for aqueous solutions to be used directly. Even 1—10 mg l^{-1} copper gave turbid solutions when mixed with aqueous diethyl-, tetramethylene- or dimethyl-dithiocarbamates. The more polar *N*-ethyl- and *N*-methyl-dithiocarbamates did not form coloured chelates.

A water-soluble copper chelate is formed with diethanoldithiocarbamate [21, 22] but the reagent is not commercially available. It was therefore prepared in situ by adding an excess of diethanolamine and sufficient carbon

disulphide to the carrier stream to give a 0.1% solution of the dithiocarbamate. When copper ions were injected, the water-soluble complex formed had maximum absorption at 430 nm, which was free from background absorption from the reagent. The sensitivity was similar to that reported for other copper dithiocarbamates. The responses to 113-μl injections of 0—20 mg l^{-1} solutions of copper ions were linear (Table 1). The repeatability (r.s.d.) was 1.5% at 1 mg l^{-1} and 4.3% at 0.1 mg l^{-1} copper. This direct reaction thus gives good results for simple solutions containing no other metal ions.

Interferences from other metal ions. The effects of some likely interfering ions were examined. The responses relative to copper are listed in Table 2. Some ions had little or no effect even at high levels but Co(II), Cr(VI), Ni(II) and Mn(VII) showed relative responses of 10% or more. Interferences of cadmium, lead, zinc and manganese(II) by formation of turbid solutions with the reagent were reported for the manual method [21], but in the present study lead had no effect even at 500 mg l^{-1}. Mercury was reported to inhibit development of the copper chelate [21] but under the present condi-

TABLE 1

Response to copper ions (1—20 mg l^{-1}) in the recommended flow-injection manifold

Carrier stream	0.1% reagent	0.1% reagent + 0.05 M EDTA
Wavelength (nm)	430	385
Correlation coefficient[a]	0.9990	0.9998
Slope	19.7	5.99
Intercept	2.9	18.7
Standard deviation	5.75	0.70
R.s.d. at 1 mg l^{-1} (%)[b]	1.5	4.3

[a]Based on the mean peak height of triplicate injections. [b]For 10 injections.

TABLE 2

Relative responses (peak height) to metal ions (100 mg l^{-1}) in the flow-injection procedures with dithiocarbamate

Metal ion	Relative response		Metal ion	Relative response	
	0.1% reagent	0.1% reagent/ 0.05 M EDTA[a]		0.1% reagent	0.1% reagent/ 0.05 M EDTA[a]
Cu^{2+}	100.0	100.0	Pb^{2+}	0.0	0.0
Cd^{2+}	0.0	0.0	Ni^{2+}	10.5	0.0
Cr(VI)	8.7	97.1	Mn(VII)	21.8	—0.2
Co^{2+}	10.5	—0.4	Mn^{2+}	2.0	—0.2
Fe^{2+}	5.1	0.7	Hg^{2+}	0.2	0.0
Fe^{3+}	4.8	7.3	Zn^{2+}	0.1	—

[a]In the presence of 1 mg l^{-1} Cu^{2+}.

tions the ultraviolet spectrum suggested that the solution was turbid. Cobalt, iron(II) and nickel give coloured chelates [21] whereas dichromate absorption overlaps the peak from the copper complex. The reaction of chromium with dithiocarbamates can be very slow [23] so that no reaction would be expected in a flow-injection procedure.

Similar interference problems are well known whether dithiocarbamates are used spectrophotometrically [19] or amperometrically [24]. EDTA is commonly used as masking agent in these procedures; Hulanicki [19] suggested that increased selectivity could be obtained for copper at pH 11.2. It was found here that when 0.02 M EDTA was added to the carrier stream, adjusted to pH 9.8, the absorption maximum of the copper chelate appeared at 385 nm and its intensity was reduced. The reagent also absorbed at 385 nm but this did not cause a serious problem. When the pH was increased to 11.2 (with ammonia), no absorbance was detected at 385 nm. Adjusting the pH to 7.5 caused the peak maximum to return to 430 nm but under these conditions the reagent solution was unstable; after 1—2 days, the sensitivity to copper was greatly reduced. However, at pH 7.5, interferences from cobalt and nickel were largely eliminated by EDTA. As a compromise between stability and selectivity, pH 8.0 was used in subsequent studies. The reagent showed no loss of sensitivity even after 4 days but the complex absorbed at 385 nm. From earlier work [22], this lower wavelength of maximum absorption reflects the formation of a 1:1 metal/dithiocarbamate complex rather than the usual 1:2 complex. Absorption spectra of the complexes at pH 8.0 suggested that chromium(VI) would still interfere because its absorption maximum is at 370 nm. In test-tube studies, this response was suppressed by increasing the EDTA concentration to 0.08 M but the reaction with the chromium was very slow. Within the timespan of a flow-injection run virtually no effect was observed. This level of EDTA also increased the background absorption.

When the relative responses of the metals were re-examined for diethanoldithiocarbamate in pH 8.0 carrier solution containing 0.05 M EDTA, most of the interferences were negligible but the chromium(VI) interference became much worse and iron(III) interfered somewhat (Table 2). Under these conditions, there was a significant peak for injection of the distilled water, but the calibration graphs for 0—20 mg l^{-1} copper based on the corrected absorbances at 385 nm were linear (Table 1). When the more selective wavelength of 430 nm was used, the response was non-linear. The repeatability at 385 nm was slightly worse than in the absence of EDTA probably because of the significant background signal (Table 1).

Instrumental parameters. The effects of changing the lengths of the injection and mixing coils were examined for a 20 mg l^{-1} copper solution (Table 3). With a 113-μl injection loop, increasing the coil length from 0.5 m to 8 m increased the dispersion; clearly, the reaction proceeded very rapidly. Even when the longest coil (8 m) was used, there was insufficient time for any reaction between chromium(VI) and EDTA to reduce its interference.

TABLE 3

Effects of injection volume and mixing coil length on the response to 20 mg l^{-1} copper under the recommended conditions with EDTA present

Injection volume (μl)	Peak heights (mm) obtained for different coil lengths (m)[a]					
	0.5	1.0	1.5	2.0	4.0	8.0
113	57.8	50.5	47.4	37.9	31.4	23.2
213	(52.9)	(51.7)	(50.5)	50.5	42.3	37.4
263	(52.1)	(53.0)	(54.5)	(54.3)	(47.3)	41.8
413	(57.1)	(58.4)		(58.9)		(51.2)

[a]Peaks given in parentheses were split into two parts.

Increasing the sample size gave a single peak with the longer mixing coils, but peak areas were then a better reflection of total sample size than peak heights. With medium and short coils and larger samples, the double peaks can be attributed to incomplete mixing. From Table 3, the most suitable conditions are a 113-μl injection loop with a 0.5-m mixing coil. The response was linear for 0—20 mg l^{-1} copper and the sample throughput was 60 h^{-1} without overlap.

Test samples. The recommended conditions were used to determine copper in solutions obtained conventionally from samples of alloys. For simple alloys such as cupro-nickel (found 67.1%, certified 67.36%), and Monel alloy (found 33.8%, certified 32.93%) results were satisfactory but the presence of chromium or iron in significant amounts (e.g., in a low-alloy steel) produced severe interference.

An Advanced Course Studentship to T.G.H. from the Science and Engineering Research Council is acknowledged.

REFERENCES

1 W. R. Wolf and K. K. Stewart, Anal. Chem., 51 (1979) 1201.
2 K. Fukamachi and N. Ishibashi, Anal. Chim. Acta, 119 (1980) 383.
3 A. O. Jacintho, E. A. G. Zagatto, H. Bergamin F°, F. J. Krug, B. F. Reis, R. E. Bruns and B. R. Kowalski, Anal. Chim. Acta, 130 (1981) 243.
4 E. A. G. Zagatto, A. O. Jacintho, F. J. Krug, B. F. Reis, R. E. Bruns and M. C. U. Araujo, Anal. Chim. Acta, 145 (1983) 169.
5 J. Růžička and E. H. Hansen, Anal. Chim. Acta, 99 (1978) 37.
6 A. Hu, R. E. Dessy and A. Graneli, Anal. Chem., 55 (1983) 320.
7 L. Anderson, D. Jagner and M. Josefson, Anal. Chem., 54 (1982) 1371.
8 J. Janata and J. Růžička, Anal. Chim. Acta, 139 (1982) 105.
9 S. J. Lyle and M. I. Saleh, Talanta, 28 (1981) 251.
10 P. W. Alexander, U. Akapongkul, Anal. Chim. Acta, 148 (1983) 103.
11 W. E. Van Der Linden and R. Oostervink, Anal. Chim. Acta, 101 (1978) 419.
12 M. Yamada and S. Suzuki, Chem. Lett., 11 (1982) 1748.
13 F. L. Boza, M. D. Luque de Castro and M. V. Cases, Analyst (London), 109 (1984) 333.

14 R. A. Leach, J. Růžička and J. M. Harris, Anal. Chem., 55 (1983) 1669.
15 A. Deratani and B. Sebille, Anal. Chem., 53 (1981) 1742.
16 D. Betteridge, E. L. Dagless, B. Fields and N. F. Graves, Analyst (London), 103 (1978) 897.
17 D. Betteridge and B. Fields, Anal. Chim. Acta, 132 (1981) 139.
18 R. M. Smith and L. E. Yankey, Analyst (London), 107 (1982) 744.
19 A. Hulanicki, Talanta, 14 (1967) 1371.
20 L. Nord and B. Karlberg, Anal. Chim. Acta, 145 (1983) 151.
21 W. C. Woelfel, Anal. Chem., 20 (1948) 722.
22 T. E. Cullen, Anal. Chem., 36 (1964) 221.
23 A. M. Bond and G. G. Wallace, Anal. Chem., 54 (1982) 1706.
24 V. I. Usatenko and F. M. Tulyupa, Izvest. Vysshykh Ucheb. Zavadenii, Khim. i Khim. Tekhnol., 3 (1958) 56; Chem. Abs. 53 (1959) 1991.

Analytica Chimica Acta, 166 (1984) 277—282
Elsevier Science Publishers B.V., Amsterdam — Printed in The Netherlands

Short Communication

DETERMINATION OF THE FUNGICIDE DICHLONE BY NORMAL AND FIRST-DERIVATIVE SPECTROFLUORIMETRY

C. CRUCES and F. GARCÍA SÁNCHEZ*

Department of Analytical Chemistry, Faculty of Sciences, The University, Málaga-4 (Spain)

(Received 18th January 1984)

Summary. The influence of solvents on the sensitivity of the spectrofluorimetric determination of dichlone (2,3-dichloro-1,4-naphthoquinone) is discussed. Linear normal and first-derivative calibration graphs are established for 10—50 $\mu g\ ml^{-1}$ dichlone; relative standard deviations are 3.8 and 2.2%, respectively. Application to synthetic mixtures is described.

Dichlone (2,3-dichloro-1,4-naphthoquinone) is a contact fungicide used on various fruit and vegetable crops and for the treatment of ponds to control blue-green algae. It is used in the form of a 50% wettable powder. In view of its uses, a reliable method for its determination is required. Methods which have been suggested include spectrophotometry [1] and gas—liquid chromatography [2].

Spectrofluorimetry has well-established high sensitivity and its selectivity is normally superior to that of absorption spectrophotometry. Derivative spectrometry is very useful for increasing resolution of overlapping bands and the enhancement of small spectral shoulders. Derivative spectrofluorimetry has found application in crude oil determinations [3], analysis of mixtures without separations [4] and clinical analysis [5].

Because of their structure and constitution (highly halogenated, unsaturated, phosphorus-containing etc) very few pesticides fluoresce sufficiently to enable them to be determined directly [6]. Therefore, spectrofluorimetry has only found limited use in direct pesticide residue determinations. This lack of fluorescence has been alleviated by preparing fluorescent derivatives of many of the common non-fluorescent pesticides by hydrolysis [7—9], oxidation, chelation [10] or derivatization [11]. Pesticides can show phosphorescence [12] but the impurities found in practical samples may cause quenching, which, with the additional precautions required for working at low temperatures, makes phosphorescence methods more complicated. Recently, phosphorescence in micellar media [13—16] has been shown to avoid this problem.

0003-2670/84/$03.00

In the present communication, two methods are proposed for the determination of microgram amounts of dichlone, by normal and first-derivative spectrofluorimetry.

Experimental

Reagents. The pesticides used were obtained as analytical standards from PolyScience Corp. (6366 Gross Point Road, Niles, IL 60648) and were used as received. A stock solution of dichlone was prepared by weighing 2.5 mg of the fungicide into a 50-ml volumetric flask followed by dissolution in dioxan. Solutions of lower concentrations were prepared by successive dilutions with dioxan. All solvents used were of spectroscopic grade.

Apparatus. All fluorescences were measured on a Perkin-Elmer fluorescence spectrophotometer, model MPF-43A, equipped with a Osram XBO 150-W lamp. All spectra were recorded on a Perkin-Elmer 023 chart recorder. A standard bar of rhodamine B (1×10^{-7} M) gave an emission of 64 units under the following conditions: λ_{ex} = 480 nm, λ_{em} = 570 nm slits 5 nm, sensitivity at 10 coarse and 7 fine, temperature 25° C; this was used to adjust the spectrofluorimeter daily. The fluorescence data are given without spectral correction. An ultrathermostated water-bath circulator (Frigiterm S-382) was used for temperature control. To obtain the derivative spectrum, a differential corrected spectrum unit, Perkin-Elmer model DCSU-2, was connected to the MPF-43A spectrofluorimeter. Absorbances were measured with a Shimadzu UV-240 Graphicord spectrophotometer.

Procedures. For normal spectrofluorimetry, to a 10-ml volumetric flask add the volume of stock solution needed to obtain a final concentration of dichlone between 10 and 50 μg ml^{-1}. Dilute with dioxan. Measure the fluorescence intensity at 423 nm, with excitation at 395 nm, against a reagent blank.

For first-derivative spectrofluorimetry, prepare the samples exactly as above, record the first-derivative spectrum at $\Delta\lambda$ = 10 nm, from 400 nm, on a chart recorder by using a time constant of 0.3 s and a scan speed of 120 nm min^{-1}, and measure the first-derivative peak height (vertical distance from peak to trough).

Results and discussion

The excitation and emission spectra of dichlone in dioxan are shown in Fig. 1. The proximity of the emission (423 nm) and excitation maxima (395 nm) gives the scatter peak near 400 nm.

Effect of experimental variables. In order to evaluate the effect of solvents on the absorbance and fluorescence intensity, the fluorescence and absorption spectra of dichlone in seven solvents were recorded. All solutions were left in daylight during the measurements, which were made at 25 ± 0.5° C, without any change occurring. Table 1 summarizes the principal spectral characteristics of dichlone in these solvents.

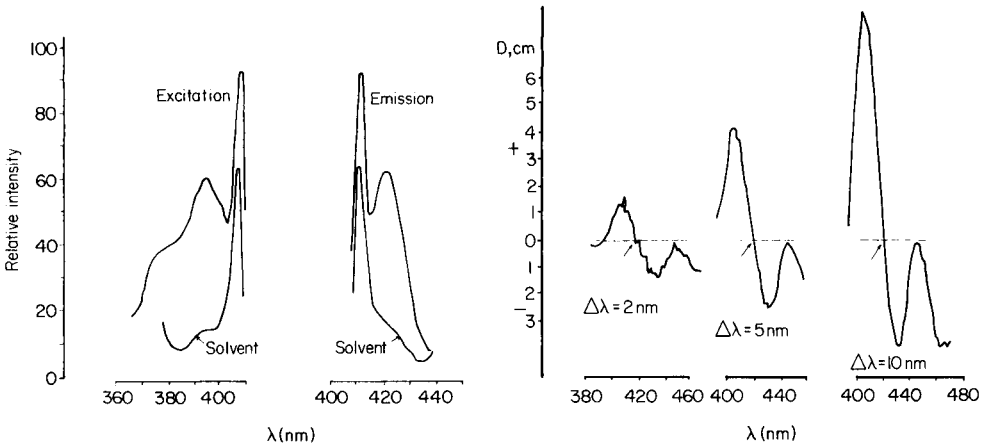

Fig. 1. Excitation and emission spectra of 2.2×10^{-4} M dichlone in dioxan, and solvent blank. (Sensitivity: coarse 3, fine 10; slits 10 and 10 nm).

Fig. 2. Influence of $\Delta\lambda$ (scan speed 120 nm min^{-1}, time constant 0.3 s) on the first-derivative spectrum of 57 $\mu g\ ml^{-1}$ dichlone in dioxan. Arrows denote 423 nm.

TABLE 1

Spectral characteristics of dichlone in different solvents

Solvent	Dielectric constant[a]	λ_a (nm)	λ_f (nm)	$\Delta\lambda$[b] (nm)	ϵ_{max} (l mol^{-1} cm^{-1})	RFI	Relative efficiency[c] (10^{-3} cm mol l^{-1})
Ethanol	24.55	336	400	64	2.86	38	13.3
Acetone	20.70	337	400	63	2.59	95	36.7
Dioxan	2.21	330	423	93	3.27	100	30.6
Acetonitrile	37.50	340	400	60	3.14	13	4.1
Hexane	1.88	332	408	76	3.82	102	26.7
Chloroform	4.81	342	410	68	3.14	41	13.1
Cyclohexane	2.02	332	412	80	4.36	20	4.6

[a]All values (N^{-1} m^{-2} cm^2) at 25° C, except for acetonitrile and cyclohexane (20° C). [b]Stokes shift, $\Delta\lambda = \lambda_f - \lambda_a$. [c]Relative fluorescence intensity/ϵ_{max}.

It can be seen that the Stokes shift increases when the solvent polarity (i.e., its dielectric constant) decreases, which indicates that the absorption and fluorescence bands involved come from $n \rightarrow \pi^*$ transitions. Also, in solvents of small dielectric constant, as in dioxan and hexane, the relative fluorescence intensity and the relative efficiency ratio are bigger, which increases the sensitivity of the determination. This is very important because, as can be deduced from the molar absorptivities, the fluorescence of dichlone is weak. The increase in fluorescence caused by using dioxan as solvent, as well as the greater Stokes shift than hexane, makes dioxan the most appropriate for enhancing the sensitivity of the determination.

When first-derivative spectrofluorimetry is used, the normal spectrum is differentiated with respect to wavelength. Selection of optimal instrumental parameters such as the time constant, scan speed and the differential wavelength interval, $\Delta\lambda$, are important. The effects of $\Delta\lambda$ and scan speed are shown in Figs. 2 and 3, respectively. In order to obtain good signal-to-noise ratios despite losing resolution, a small time constant (0.3 s), an intermediate scan speed (120 nm min^{-1}) and $\Delta\lambda$ = 10 nm were found to be optimal for the determination of dichlone.

Calibration, accuracy and precision. The normal and first-derivative calibration graphs were linear for 10—50 μg ml^{-1} dichlone in dioxan. The peaks and calibration graph for the first-derivative measurements are shown in Fig. 4.

The first-derivative value was defined as the vertical distance from a peak to a trough, measured under the recommended conditions at 423 nm. The equations for each graph were [dichlone] = 0.99 RFI — 1.48 for normal spectrofluorimetry, and [dichlone] = $4D$ + 6.32 for first-derivative spectrofluorimetry. Here RFI and D are the relative fluorescence intensity and the first-derivative value (cm), respectively, referred to the rhodamine B standard under the same conditions, and the dichlone concentration is given in μg ml^{-1}.

The limit of detection [17] is the minimum concentration of the substance that can be measured with 99% confidence that the concentration is

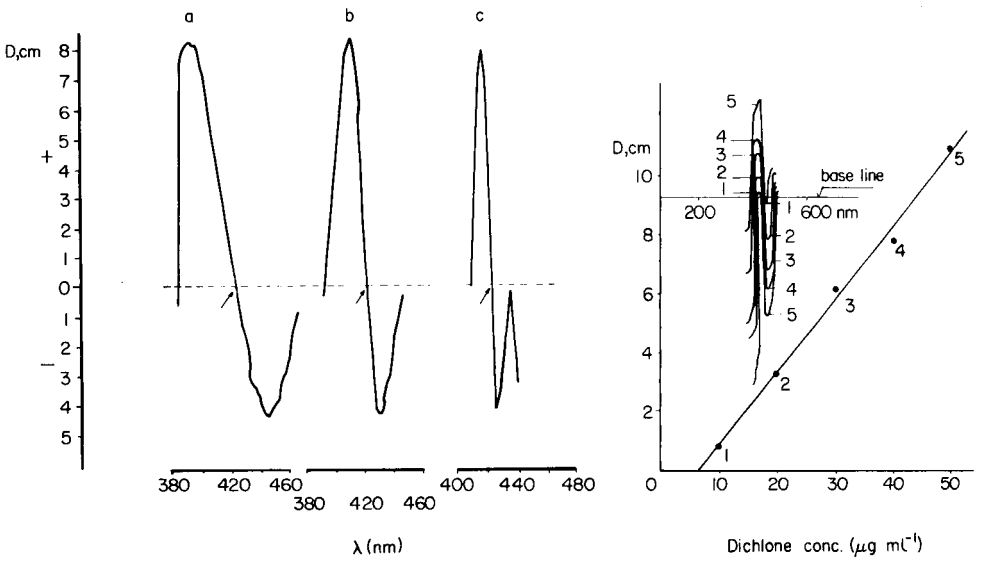

Fig. 3. Influence of scan speed ($\Delta\lambda$ = 10 nm, time constant 0.3 s) on the first-derivative spectrum of 57 μg ml^{-1} dichlone in dioxan. Scan rates: (a) 60; (b) 120; (c) 240 nm min^{-1}.

Fig. 4. Calibration graph for first-derivative spectrofluorimetry under the recommended conditions. (Sensitivity: coarse 3, fine 10.)

TABLE 2

Effect of insecticides on the determination of dichlone (10 μg ml^{-1}) by normal and first-derivative spectrofluorimetry

Insecticide[a]	Error (%)		Insecticide[a]	Recovery of dichlone (%)	
	Normal	First derivative		Normal	First derivative
Kepone (40)	−16.0	−0.8	Kepone (20)	95	99.5
Kepone (20)	−4.0	—	Kepone (20), Thiodan (20)	96	101
Thiodan (40)	−2.8	−0.4			
Monocrotophos (40)	−8.5	−0.6	Kepone (10), Thiodan (10), Monocrotophos (20)	94	101
Monocrotophos (20)	−4.0	—			

[a]In parentheses, concentration of insecticide (μg ml^{-1}).

greater than zero. The detection limits were found to be 14 μg ml^{-1} and 7.5 μg ml^{-1} for normal and first-derivative spectrofluorimetry, respectively. The relative standard deviation and relative error for 7 determinations of 30 μg ml^{-1} dichlone were 3.8% and 3.4% for normal spectrofluorimetry and 2.2% and 2.0% for first-derivative spectrofluorimetry.

Interference studies. The effects of other pesticides, particularly the insecticides kepone, thiodan and monocrotophos, on the determination of 10 μg ml^{-1} dichlone were examined. All conditions previously established for both methods were kept the same in each experiment. The results are shown in Table 2. The criterion for interference was a deviation of the fluorescence intensity, or of the first-derivative value, of $\geqslant$4%. It can be seen that the derivative method is less affected by the presence of other insecticides than the normal spectrofluorimetric procedure.

In order to apply the methods described to a commercial formulation containing dichlone and other pesticides, synthetic mixtures with one or two of the insecticides studied (kepone, thiodan, monocrotophos) were investigated. Table 2 also shows the results for some of these mixtures.

In conclusion, derivative spectrofluorimetry seems to offer some interesting possibilities for the determination of pesticides. This technique can convert a poorly defined normal spectrum to a well-shaped first-derivative spectrum which makes it easier to measure relative values and to avoid interferences. The accuracy and precision of the methods are good, with the added advantage of simplicity in routine application.

REFERENCES

1 J. R. Lane, J. Agric. Food Chem., 6 (1958) 746.
2 J. R. Lane, J. Agric. Food Chem., 17 (1969) 585.
3 G. L. Green and T. C. O'Haver, Anal. Chem., 46 (1974) 2191.

4 T. C. O'Haver and W. M. Parks, Anal. Chem., 46 (1974) 1886.
5 J. N. Miller, Proc. Anal. Div. Chem. Soc., 16 (1979) 56.
6 I. Hornstein, J. Agric. Food Chem., 6 (1958) 32.
7 R. Santi, G. Canale, M. Radice and G. Pizzingrilli, J. Agric. Food Chem., 20 (1972) 62.
8 J. M. Adams and C. A. Anderson, J. Agric. Food Chem., 14 (1966) 53.
9 J. J. Aaron and N. Some, Analusis, 10 (1982) 481.
10 F. Vernon, Anal. Chim. Acta, 71 (1974) 192.
11 D. W. Fink, Trends Anal. Chem., 1 (1982) 254.
12 N. L. Trautwein and J. C. Guyon, Mikrochim. Acta, (I) (1983) 413.
13 L. J. Cline Love, M. Skrilec and J. G. Habarta, Anal. Chem., 52 (1980) 754.
14 J. N. Miller, Trends Anal. Chem., 1 (1981) 31.
15 J. J. Donkerbroek, J. J. Elzas, C. Gooijer, R. W. Frei and N. H. Velthorst, Talanta, 28 (1981) 717.
16 L. J. Cline Love and M. Skrilec, Int. Lab., 11 (1981) 50.
17 Environmental Protection Agency (United States) E.P.A. 600/4-82-057, July, 1982.

Analytica Chimica Acta, 166 (1984) 283—288
Elsevier Science Publishers B.V., Amsterdam — Printed in The Netherlands

Short Communication

DETERMINATION OF SULFUR IN BIOLOGICAL SAMPLES BY VACUUM-ULTRAVIOLET INDUCTIVELY-COUPLED PLASMA ATOMIC EMISSION SPECTROMETRY

MASATOSHI MORITA*, TAKASHI UEHIRO and KEIICHIRO FUWA

National Institute for Environmental Studies, Onogawa 16-2, Yatabe, Tsukuba, Ibaraki 305 (Japan)

(Received 12th January 1984)

Summary. Sulfur is most sensitively determined at 180.7 nm, the detection limit being 10 $\mu g\ l^{-1}$. A comparison of digestion procedures shows that acid digestion in a teflon bomb gives least loss of analyte. Only calcium interferes spectrally at this wavelength. Results for various reference materials are presented.

Sulfur is found in proteins as sulfur-containing amino acids and contributes to redox changes and other metabolic functions; it is also present in some lipids. Classically, sulfur is determined by oxidation of organic sulfur to sulfate and weighing as barium sulfate. This method is still widely used [1]. More recent techniques for sulfur determinations include x-ray fluorescence spectrometry [2—4] and neutron-induced prompt γ-ray spectrometry for direct analysis [5, 6] and i.r. spectrometric, coulometric [7—9] or gas chromatographic measurement of sulfur dioxide after combustion of the sample. Inductively-coupled plasma atomic emission spectrometry (i.c.p./a.e.s.) can also be used.

Since the pioneering work of Greenfield et al. [10] and Wendt and Fassel [11], i.c.p./a.e.s. has been applied to the determination of many elements in various matrices. Such research has focussed on simultaneous multi-element determinations of metals and metalloids having emission lines above 190 nm, although some papers have referred to non-metallic elements having resonance lines in the vacuum-u.v. region. The resonance line of sulfur at 180.7 nm is sensitive [12—16] and thus sulfur can be determined simultaneously with other elements. This communication describes the application of i.c.p./a.e.s. to the determination of sulfur in biological samples.

Experimental

Materials. NBS standard reference materials (Bovine Liver SRM 1577, Orchard Leaves NBS 1571) were analyzed. Certified reference materials of chlorella (NIES No. 3), human serum (NIES No. 4), mussel (NIES No. 6) and hair (NIES No. 5) were prepared in this laboratory. Nitric and perchloric acids were of special grade for trace determinations (Wako PMA). Water was

0003-2670/84/$03.00

purified by distillation from quartz apparatus (Yamato WAU-12) after passing through a Milli-Q water purification system (Millipore).

Instrumentation. The plasma spectrometer was a Daini Seiko-Sha JY-38P, which contained an inductively-coupled plasma (Plasmatherm; HFP-5000D/APCS-3 r.f. generator, with ICP-5000/AMNPS plasma and matching system), a concentric glass pneumatic nebulizer, and a Jobin-Yvon monochromator (Czerny-Turner, f = 1 m, 3600 lines mm^{-1} holographic master grating). The optical interface between monochromator and plasma was one concave and one flat mirror fitted with a quartz nozzle to allow a purge of pure nitrogen. A demagnified image (1/2) of the plasma was focussed on the entrance slit. The entrance and exit slits were 20 μm × 5 mm and 40 μm × 10 mm, respectively.

The elemental analyzer used was a Model 1106 CHN analyzer (Carlo Erba) equipped with a Chromato-Pak R1A data processor (Shimadzu). Samples (1—4 mg) were weighed in tin capsules for insertion.

Sample decomposition. All samples were dried by heating at 80° C for 4 h, weighed and digested by bomb digestion, open digestion or alkali fusion. For high-pressure bomb digestion, ca. 200 mg of sample in a teflon container was weighed accurately, and 3 ml of nitric acid was added. The container was sealed in a stainless steel bomb and heated at 140° C for 2 h. After cooling, the digest was diluted with water, filtered, transferred to a pyrex glass volumetric flask and made up to 100 ml. For open digestion, an accurately weighed sample (ca. 200 mg) was placed in a 100-ml beaker (pyrex glass), 5 ml of concentrated nitric acid was added, and the beaker was covered with a watch-glass and placed on a hot plate. After vigorous emission of nitrous fumes had ceased, 5 ml of concentrated perchloric acid was added and the solution was heated for 24 h at ca. 120° C. The temperature of the hot plate was raised to ca. 200° C, and perchloric acid was evaporated as white fumes. Heating was continued until the final volume was ca. 1 ml. After cooling, the digest was diluted with water, filtered and made up to 100 ml in a volumetric flask. For alkaline fusion, samples were fused with sodium hydroxide and sodium nitrate (4:1) in a nickel crucible. After cooling, the contents were dissolved in water, neutralized with nitric acid, and made up to 100 ml.

Gravimetric determination of sulphate. The 100-ml solution obtained by acidic or alkaline treatment was placed in a 200-ml beaker and heated to boiling on a hot plate. Barium chloride solution (10 ml of 10%) was added to precipitate barium sulphate. After heating for 30 min, the suspension was cooled to room temperature and filtered through a previously weighed membrane filter (0.45 μm pore size). The filter was washed, dried in a desiccator for 2 days and weighed.

Measurement by i.c.p./a.e.s. The operational parameters for the plasma were as follows: r.f. power forward 1.3 kW, reflected power <5 W, nebulizer gas pressure 28 psi, sample uptake 2.1 ml min^{-1}, coolant gas flow 18 l min^{-1}, middle gas flow 0.1 ml min^{-1}, observation height 16 mm ± 5 mm above coil top.

Results and discussion

Selection of emission line. Emission lines of sulfur obtained from the i.c.p. are shown in Fig. 1. The most prominent lines are at 166.7 nm, 180.7 nm, 182.0 nm and 182.6 nm. Of these, the 180.7-nm line gave the greatest sensitivity. Figure 2 shows the relative intensities for the various lines for 3 mg l^{-1} sulfur. The signal-to-background values are also given. The detection limit (2 σ) at 180.7 nm was 6—10 μg l^{-1} sulfur. The practical detection limit, however, was affected by contamination which sometimes occurred in the water or the sample delivery system, including the nebulizer and torch. When carefully prepared water was used and the delivery system was completely washed, contamination was negligible. Otherwise the contamination could rise to 0.2 mg l^{-1} sulfur.

Spectral interference at the 180.7-nm line was not severe, except when calcium was present. Magnesium (1 g l^{-1}) gave a slight increase in baseline which corresponded to 0.05 mg l^{-1} sulfur, whereas 1 g l^{-1} carbon gave a positive error equivalent to 0.05 ppm mg l^{-1} sulfur. Sodium, potassium and phosphorus gave no significant spectral interference. Because sulfur is present at the 0.1—3% level in plant and animal tissues, spectral interference from these elements would be negligible for such samples. Spectral interferences from calcium was high because the 180.7-nm calcium line overlapped the sulfur line almost completely [14]. Thus, 1 g l^{-1} calcium gave an emission equivalent to 8 mg l^{-1} sulfur. The interference would therefore be negligible in the analysis of most biological samples that contain more sulfur than calcium. However, for the analysis of calcium-rich samples such as bone, teeth or shell, the use of the 182.0-nm sulfur line may be better, although it is less sensitive.

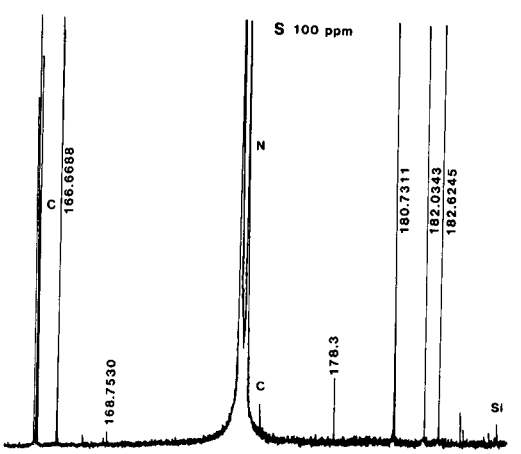

Fig. 1. Emission lines of sulfur in the plasma (165—185 nm) measured for 100 mg l^{-1} S.

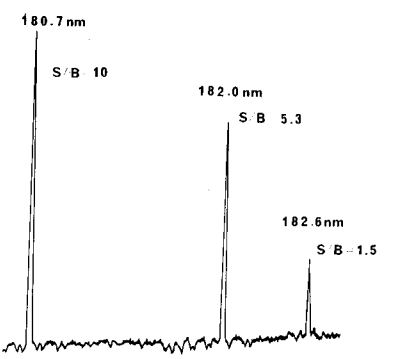

Fig. 2. Spectral intensities and signal-to-background ratios of the sulfur emission lines obtained by nebulizing 3 mg l^{-1} S.

Method of decomposition. The selection of digestion method was important. When the sample was digested in a covered glass beaker with nitric and perchloric acids as described under Experimental, significant loss of sulfur was observed (Table 1). The loss was also found for sodium sulfate treated in the same way. The precision of repeated analyses by open digestion was poor, suggesting irreproducible losses of sulfur. As with mercury and selenium, precautions against losses are necessary during digestion.

Digestion in a high-pressure teflon bomb gave good results. The loss of sulfur was prevented and the precision by repeated analysis was improved. Although this method was satisfactory with regard to least contamination and least loss, there remained the problem that the final acid concentration was rather high unless residual acid was removed by evaporation. Increasing the concentration of nitric acid above ca. 0.5 M decreased the efficiency of the nebulizer, so that it was necessary, at high nitric acid concentrations, to match the acid concentration of the standard solutions with that of the sample solutions.

Table 2 compares the results obtained for the same bomb digests by i.c.p./a.e.s. and gravimetry. Gravimetry gave 30—50% lower values, probably because of the solubility of the precipitate, nitrate interference and the problems of gravimetric techniques for low concentrations.

Two NBS standard reference materials were analyzed; the results are compared with previously reported values in Table 3. The relative standard deviations were 1.5% for Bovine Liver, for which there is no certified value, but 5% for the Orchard Leaves. The previously reported values were obtained by x-ray fluorescence spectrometry or neutron-induced prompt γ-ray spectrometry. These values are fairly close to the present values, especially for Bovine Liver.

Sulfur was also measured in NIES certified reference materials which are prepared and distributed by the National Institute for Environmental Studies. The relative standard deviation of the i.c.p. measurements was 1—2%. Accuracy was also good because the values obtained by i.c.p., gravimetry and elemental analysis were very similar, except for chlorella.

TABLE 1

Sulfur concentrations measured after different digestion methods by i.c.p./a.e.s.

Sample	Sulfur found ($\mu g\ g^{-1}$)[a]	
	Open digestion	Bomb digestion
Chlorella (NIES No. 3)	5860 ± 1100 (3)	6900 ± 100 (5)
Serum (NIES No. 4)	1010 ± 40 (3)	1068 ± 25 (5)
Hair (NIES No. 5)	34400 ± 800 (3)	45400 ± 900 (6)
Mussel (NIES No. 6)	9320 ± 90 (3)	11000 ± 100 (8)

[a]Mean ± s.d. (no. of results).

TABLE 2

Sulfur concentrations measured by i.c.p./a.e.s. and gravimetry

Sample	Sulfur found ($\mu g\ g^{-1}$)[a]	
	I.c.p./a.e.s.	Gravimetry
Chlorella	6900 ± 100 (5)	3230 ± 100 (3)
Serum	1068 ± 25 (5)	0.0764 ± 0.041 (3)
Hair	45400 ± 900 (6)	32200 ± 1100 (3)
Mussel	11000 ± 100 (8)	7720 ± 1200 (3)[b]
Bovine Liver	7410 ± 110(5)	3550 ± 2660 (3)

[a]Bomb digestion, mean ± s.d. (no. of results). [b]Alkaline fusion gave 10 300 ± 500 (3).

TABLE 3

Sulfur contents of NBS standard reference materials obtained by i.c.p. measurements

Sample	Sulfur content ($\mu g\ g^{-1}$)[a]		
	I.c.p.	Reference values	Ref.
Bovine Liver (SRM 1577)	7410 ± 110 (5)	7200 ± 400 (5)	3
		7020 ± 2620 (3)	2
		7200 ± 200 (2)	6
Orchard Leaves (SRM 1571)	1860 ± 90 (4)	1900	—[b]
		2300 ± 100 (4)	5
		2120	3
		2120 ± 50 (2)	2
		2150 ± 380 (7)	4
		1700 ± 200 (1)	6

[a]Mean ± s.d. (no. of results). [b]Non-certified.

TABLE 4

Sulfur determined in NIES certified reference material

Sample	Sulfur found ($\mu g\ g^{-1}$)[a]		
	I.c.p.	Gravimetry	Elemental analyzer
Chlorella	6900 ± 100 (5)	—	6180 ± 80 (4)
Serum	1068 ± 25 (5)	—	—
Hair	45400 ± 900 (6)	—	45300 ± 700 (4)
Mussel	11000 ± 100 (8)	10300 ± 500 (3)	10900 ± 110 (3)

[a]Mean ± s.d. (no. of results).

The monochromator and optical pathway were purged with nitrogen for most of the work, to allow measurements at 180.7 nm. However, there was no substantial difference between the use of this system and a vacuum polychromator (Jobin-Yvon 48 PVH), which gave a similar sensitivity and detection limit (10 $\mu g\ l^{-1}$).

REFERENCES

1 S. E. Allen (Ed.), Chemical Analysis of Ecological Materials, Blackwell, Oxford, 1974, p. 92.
2 K. K. Nielson, Anal. Chem., 49 (1977) 641.
3 J. A. Campbell, J. C. Laul, K. K. Nielson and R. D. Smith, Anal. Chem., 50 (1978) 1032.
4 F. W. Reuter, Anal. Chem., 47 (1975) 1763.
5 E. T. Jurney, D. B. Curtis and E. S. Gladney, Anal. Chem., 49 (1977) 1741.
6 M. P. Failey, D. L. Anderson, W. H. Zoller, G. E. Gordon and R. M. Lindstrom, Anal. Chem., 51 (1979) 2209.
7 W. Thurauf and Erdol Kohle, 27 (1974) 135.
8 M. C. van Grondelle, F. van de Craats and J. D. van der Laarse, Anal. Chim. Acta, 92 (1977) 267.
9 D. R. Beuerman and C. E. Meloan, Anal. Chem., 34 (1962) 319.
10 S. Greenfield, I. L. Jones and C. T. Berry, Analyst (London), 89 (1964) 713.
11 R. H. Wendt and V. A. Fassel, Anal. Chem., 37 (1965) 920.
12 T. Hayakawa, F. Kikui and S. Ikeda, Spectrochim. Acta, Part B, 37 (1982) 1069.
13 D. L. Miles and J. M. Cook, Anal. Chim. Acta, 141 (1982) 207.
14 J. Lee and M. W. Pritchard, Spectrochim. Acta, Part B, 36 (1981) 591.
15 G. F. Kirkbright, A. F. Ward and T. S. West, Anal. Chim. Acta, 62 (1972) 241.
16 D. R. Heine, J. S. Babis and M. B. Denton, Appl. Spectrosc., 34 (1980) 595.

Analytica Chimica Acta, 166 (1984) 289—292
Elsevier Science Publishers B.V., Amsterdam — Printed in The Netherlands

Short Communication

DETERMINATION OF SELENIUM IN A NICKEL ALLOY BY FLAME ATOMIC ABSORPTION SPECTROMETRY AFTER ELECTROCHEMICAL PRECONCENTRATION

RAGNAR BYE* and LIV ENGVIK
Department of Chemistry, University of Oslo, Box 1033, Blindern, Oslo 3 (Norway)
(Received 17th July 1984)

Summary. The nickel alloy is dissolved in nitric/hydrochloric/phosphoric acid mixture, and selenium is electrodeposited onto a platinum loop at —0.4 V (vs. Ag/AgCl). Selenium is atomized from the electrode in an argon/hydrogen flame with simultaneous electrothermal heating of the loop. For the NBS standard nickel-based high-temperature alloy (SRM 899), the mean value found was 9.7 $\mu g\ g^{-1}$ with a standard deviation of 0.4 $\mu g\ g^{-1}$ (certified value 9.5 ± 0.1).

Knowledge of the trace concentrations of selenium in nickel, nickel-based alloys and stainless steel is of metallurgical importance as selenium can affect the physical and mechanical properties of the alloy. Reliable methods for the determination of selenium in such materials are therefore needed.

Graphite-furnace atomic absorption spectrometry has been applied for this purpose. To avoid calibration with solutions of standard alloys or matrix-matched solutions, Kujirai et al. [1] separated the selenium from the matrix solution by coprecipitation with arsenic, and redissolved the precipitate in acid. Several authors have noted that the presence of iron in the sample solution results in erroneous background compensation when a deuterium source is used [2—4]. Recently, it was also observed that cobalt has the same effect as iron on the deuterium compensation [4], as do chromium and nickel when the signals are measured at the 204-nm line [4]. To ensure the elimination of these spectral interferences, very expensive and sophisticated instruments equipped with either the Zeeman [4] or Smith—Hieftje [5] background correcting systems are needed. Nickel is also one of the elements which seriously interfere in hydride-generation atomic absorption spectrometry. To determine selenium in nickel samples, Welz and Melcher [6] found it necessary to precipitate and filter off nickel as nickel hydroxide.

As an alternative it was decided to examine whether flame atomic absorption spectrometry (a.a.s.) with electrochemical preconcentration could be applied for the determination of selenium in nickel alloys. This technique has previously proved successful for other complicated matrices such as technical sulphuric acid [7]. The technique involves electrodeposition of the

0003-2670/84/$03.00

selenium from the sample solution onto a platinum electrode at an optimum cathodic potential for a fixed time (a few minutes). The deposited selenium is atomized in an argon-hydrogen flame; simultaneous electrical heating of the electrode loop ensures rapid atomization of the selenium. A detection limit of 0.5 $\mu g\ l^{-1}$ selenium has been obtained after 5 min electrolysis [8].

Experimental

Equipment and solutions. A Perkin-Elmer 300 atomic absorption spectrometer was used with a Radiometer Servograph REC-51 recorder. The instrument was equipped with an electrodeless discharge lamp for selenium and a three-slot burner head. The selenium signals were measured at the 196.0-nm resonance line. For atomization, an argon-hydrogen flame was used with flow rates of 11 and 2.5 l min^{-1}, respectively.

Special equipment included a quartz tube with a circular hole which was mounted above the burner head. The design of the platinum-loop electrode and electrolytic cell and the arrangement for electrothermal heating of the platinum loop were as described elsewhere [7, 8].

A standard selenium(IV) solution (5 mg l^{-1}) was prepared by diluting an aqueous 1.000 $g\,l^{-1}$ solution made from analytical-grade selenous acid. Nitric, hydrochloric and phosphoric acid and acetone were of p.a. quality (Merck).

Procedure. To 0.5 g of the nickel alloy, add 5 ml of water, 5 ml of concentrated nitric acid, 10 ml of concentrated hydrochloric acid and 25 ml of concentrated phosphoric acid in a 150-ml beaker. Cover the beaker with a watch glass, place on a boiling water bath and heat until the sample has dissolved. Add 25 ml of water, place the beaker on a hot plate at ca. 200° C and heat to boiling. Allow to boil for 5 min. Transfer the contents to a 500-ml volumetric flask (or one of suitable volume) and dilute to volume with water. Transfer 25 ml of the solution to the electrolytic cell. Electrolyze with efficient stirring at —0.4 V vs. sat. Ag/AgCl for 3 min (or some suitable time). Remove the electrode from the cell and rinse it with water and acetone without disconnecting the circuit. Allow the electrode to dry in air, place it in the holder in the atomic absorption spectrometer and connect it to the transformer. The electrical heating power of the platinum loop should be as high as possible, without risk of melting. Ignite the flame, move the electrode into its predetermined position just below the hole in the quartz tube, switch on the heating power, and record the signal. To further aliquots of sample solution, add $\leqslant 200\ \mu l$ of a standard selenium(IV) solution, and repeat the procedure. Finally, calculate the concentration of selenium from the results of these standard additions.

Results and discussion

Dissolution procedures. When an earlier method of dissolving the sample in a mixture of nitric and hydrofluoric acids [4] was used, no selenium deposited on the electrode. Addition of boric acid or aluminium-ions to the mixture after dissolution, in order to bind the fluoride was unsuccessful. A

precipitate of hydrated chromium(III) oxide, originating from the high chromium content of the sample, was formed when the sample was dissolved in perchloric acid with subsequent addition of hydrogen peroxide to reduce selenium(VI) to selenium(IV). This was also observed when the sample was dissolved in (3 + 1) nitric and hydrochloric acid (Lunge's mixture).

In the final procedure, an excess of hydrochloric acid over nitric acid and boiling with phosphoric acid ensured almost complete removal of the nitric acid. Moreover, phosphoric acid strongly complexes triply charged cations, thus decreasing the likelihood of chromium(III) precipitation.

Deposition potential. Nickel alloys often contain large concentrations of iron, chromium and cobalt. It is a disadvantage if these elements deposit on the electrode, because the atomization temperature used is not high enough to remove them completely from platinum. The elements will thus be built up on the surface and change the character of the electrode. For this reason, a deposition potential of −0.4 V was selected for selenium, although it can be seen from Fig. 1 that the degree of deposition is greater at more negative potentials. At potentials more negative than −0.45 V, however, both nickel and cobalt would deposit. At −0.40 V, lead, mercury, silver and copper will be deposited; of these metals, only copper will not be removed completely during atomization, and is thus the only metal of those mentioned that will interfere.

Analysis of standard alloy. Four 0.5-g portions of SRM 899 "Trace alloy" (Nickel-Base High-Temperature Alloy) from the National Bureau of Standards (NBS) were taken through the whole procedure. Four volumes of standards were added to each, and each addition was made in duplicate. The results obtained were 9.7, 9.1, 10.0 and 9.9 $\mu g\ g^{-1}$ giving a mean value of 9.7 and a standard deviation of 0.4 $\mu g\ g^{-1}$. The result is in good agreement with the certified value from NBS of 9.5 ± 0.1 $\mu g\ g^{-1}$.

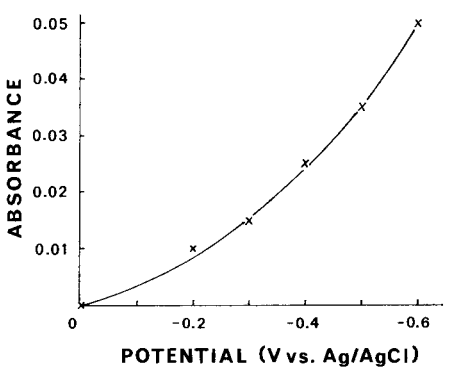

Fig. 1. Variation in peak height with deposition potential (0.5 g of SRM 899 dissolved as described; electrolysis time 3 min).

Conclusions

The proposed method has been shown to be useful for the determination of selenium in a nickel-based cobalt-chromium alloy. It should in principle also be applicable for other types of alloys such as stainless steel. Of the metals commonly found in alloys, copper is expected to interfere, as it is deposited simultaneously with selenium and is not completely removed from the electrode loop during atomization.

REFERENCES

1 O. Kujirai, T. Kobayashi, K. Ide and E. Sudo, Talanta, 30 (1983) 9.
2 D. C. Manning, At. Absorpt. Newsl., 17 (1978) 107.
3 K. Saeed, Y. Thomassen and F. J. Langmyhr, Anal. Chim. Acta, 110 (1979) 285.
4 F. J. Fernandez and M. M. Beaty, Spectrochim. Acta, Part B, 39 (1984) 519.
5 G. R. Dulude and J. J. Sotera, Spectrochim. Acta, Part B, 39 (1984) 511.
6 B. Welz and M. Melcher, Anal. Chim. Acta, 153 (1983) 297.
7 B. Holen, R. Bye and W. Lund, Anal. Chim. Acta, 131 (1981) 37.
8 B. Holen, R. Bye and W. Lund, Anal. Chim. Acta, 130 (1981) 257.

Analytica Chimica Acta, 166 (1984) 293—295
Elsevier Science Publishers B.V., Amsterdam — Printed in The Netherlands

Short Communication

DETERMINATION OF PENICILLIN V IN FERMENTATION SAMPLES BY FLOW INJECTION ANALYSIS

IB SCHNEIDER

Enzyme Microbiological Laboratory, Novo Industri A/S, Novo Alle, 2880 Bagsvaerd (Denmark)

(Received 9th April 1984)

Summary. Penicillin V in fermentation broths is determined, with linear response over the range 100—1000 U ml^{-1}, by enzymatic hydrolysis to penicilloic acid and subsequent formation of a molybdenum blue. The Auto-Analyzer and flow-injection procedures are compared.

Penicillin V in fermentation broth can be determined biologically or chemically. The biological method is accurate but very time-consuming. The chemical methods are various; the iodine method [1] has poor selectivity and the hydroxylamine method [2] has poor sensitivity. The method described by Pan [3], which has high selectivity and sensitivity is based on enzymatic hydrolysis of penicillin with penicillinase to give the corresponding penicilloic acid. In the presence of mercury(II) chloride, this acid reduces molybdoarsenic acid to form a "molybdenum blue", which is measured spectrophotometrically. This manual method was converted to an Auto-Analyzer method by Holm [4]. The use of a flow-injection system reduces the total time requirement significantly.

Experimental

Reagents. Demineralized water and Merck analytical-grade reagents were used, unless otherwise specified. Citrate-phosphate buffer pH 6.2 was prepared by dissolving 7.02 g of citric acid and 23.55 g of disodium hydrogen phosphate in 1 l of water; the pH was checked before sterilization. Mercury-(II) chloride (0.175 g) was dissolved in 1 l of water.

Molybdoarsenic acid reagent was prepared as follows: 30 g of ammonium heptamolybdate tetrahydrate was dissolved in 400 ml of water and 25.2 ml of concentrated sulphuric acid was added with cooling; then 3.6 g of disodium hydrogenarsenate heptahydrate dissolved in 25 ml of water was added, and the solution was diluted to 1 l with water. This solution was kept in a dark bottle and placed at 37°C for 24 h before use. Penicillinase solution was prepared by diluting an ampoule of Penase (500 000 units; Leo Pharmaceuticals) with 100 ml of citrate-phosphate buffer pH 6.2.

0003-2670/84/$03.00

Penicillin V standards were prepared by dissolving 165 mg of potassium penicillin V containing (1510 U mg^{-1}; Novo Industri) in 25 ml of the citrate-phosphate buffer. This solution (10 000 U ml^{-1}) was diluted as required with citrate-phosphate buffer so that the samples contained less than 1000 U ml^{-1} penicillin V.

Apparatus. The flow injection system comprised a peristaltic pump (Bifok, FIA-08) and a FIA-0.5 processing unit with a 30-μl injection valve. For detection, a filter photometer (Bifok, FIA-06) was used at 670 nm with an Omniscribe recorder (Houston Instruments). Pump tubings were of standard Tygon type; connecting tubing, mixing coils and reaction coils were of 0.5 mm i.d. teflon tubing. The temperature between the injection point and the detector was kept constant at 45°C and care was taken to degas the reagents. The recommended manifold is shown in Fig. 1.

Results and discussion

To verify that the enzyme caused complete hydrolysis of the penicillin under the given conditions in the reaction coils, a penicillin V standard (1000 U ml^{-1}) was prepared, mixed with a drop of the penase reagent and left for 15 min at room temperature. Thereafter it was injected as a blank value with citrate-phosphate as carrier stream. The signal recorded was the same as for the 1000 U ml^{-1} penicillin V standard injected into the buffered penase stream. This standard was chosen as the maximum concentration.

Increasing the length of the first coil from 20 to 50 or 100 cm had no effect; nor did increasing the second coil from 50 cm to 100 cm, apart from prolonging the residence time. The pumping speed and the tube diameter (0.5 mm i.d.) were chosen so that the total flow rate was 2.76 ml min^{-1}. Lowering the temperature from 45°C to 35°C had a dramatic negative effect on the highest standards.

A calibration graph prepared for the penicillin V range 100—1000 U ml^{-1} was a straight line; at higher concentrations, it levelled off.

In the analysis of fermentation broths, it must be noted that some of the

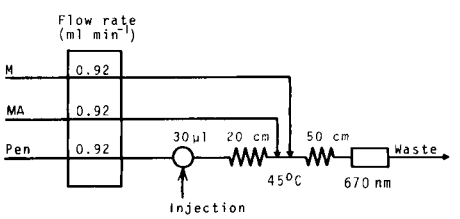

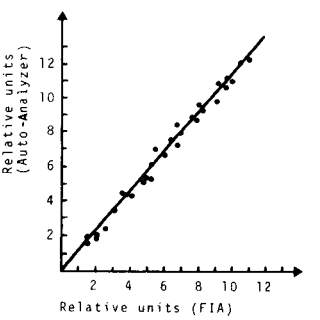

Fig. 1. Flow-injection system: M, mercury(II) chloride solution; MA, molybdoarsenate acid solution; Pen, pencillinase solution.

Fig. 2. Comparison between Auto-Analyzer method and f.i.a. method.

penicillin produced by the micro-organism is degraded to penicilloic acid and will contribute, in this assay, to the total amount of penicillin recorded. It is therefore necessary to run sample blank values, without the addition of penase to the carrier stream.

The absorption spectrum of a diluted fermentation broth showed a peak at 300 nm, with tailing to around 500 nm. However, the colour of the broth did not contribute to the total absorbance at 670 nm, and the results obtained by the recommended method can be interpreted on the basis that only penicilloic acid causes the blank value. Sensitivity would probably be improved at 800 nm.

Figure 2 shows a comparison between the results obtained by the Auto-Analyzer and flow-injection systems on filtered diluted fermentation samples. The differences are not systematic; the correlation coefficient was 0.954. With the flow-injection method, the limit of detection is 2.5 penicillin V units (1.7 μg of penicillin V). For 10 injections of one broth sample, the mean result was 623.8 U ml^{-1} with a standard deviation of 6.1 U ml^{-1}. The advantage in the flow-injection system lies in the short start-up and close-down times. The Auto-Analyzer system used routinely here has a sample capacity of around 60 h^{-1}. The flow-injection system described has a sample capacity around 90 h^{-1} without loss of precision or accuracy.

The author thanks P. W. Hansen, head of the Mycology Department, for his valuable help and criticism.

REFERENCES

1 R. R. Goodall and R. Davies, Analyst (London), 86 (1961) 326.
2 A. O. Niedermayer, F. M. Rüsso-Alesi, C. A. Lendzian and J. M. Kelly, Anal. Chem., 32 (1960) 664.
3 S. C. Pan, Anal. Chem., 26 (1954) 1438.
4 K. A. Holm, Anal. Chem., 44 (1972) 795.

Analytica Chimica Acta, 166 (1984) 297—299
Elsevier Science Publishers B.V., Amsterdam — Printed in The Netherlands

Short Communication

DIFFERENTIAL-PULSE ANODIC STRIPPING VOLTAMMETRY OF MERCURY WITH GOLD-FILM MICRO-ELECTRODES

GEORGE J. SVOBODA, JOHN P. SOTTERY and C. WILLIAM ANDERSON*
Paul M. Gross Chemical Laboratory, Duke University, Durham, NC 27706 (U.S.A.)
(Received 23rd January 1984)

Summary. Cylindrical gold film micro-electrodes are easily produced by plasma-sputtering of gold onto carbon fiber electrodes. The micro-electrodes produced were found to maintain their cylindrical geometry indefinitely, unlike gold wire electrodes of similar dimensions. Application of these electrodes in differential-pulse anodic stripping voltammetry provides a method for quantifying trace levels of mercury(II). Up to 100 $\mu g\ l^{-1}$ Hg(II) the area of the mercury stripping peak varied linearly with mercury concentration; the detection limit was 3.7 $\mu g\ l^{-1}$. With more than 100 $\mu g\ l^{-1}$ Hg(II) a new mercury stripping peak grows in at less positive potentials; its peak height is linear with Hg(II) concentration.

Recently, microvoltammetric electrodes (m.v.e.'s) have been attracting attention as novel electrochemical sensors. Applications of these sensors in a variety of electrochemical methods have demonstrated their utility [1]. To date, most work utilizing m.v.e.'s has been done with carbon, platinum, or gold electrodes. Recently, we have produced cylindrical gold-film m.v.e.'s by plasma-sputtering gold onto 7-μm diameter carbon fibers. These m.v.e.'s were found to maintain their cylindrical geometry indefinitely, unlike gold-wire m.v.e.'s of similar dimensions which tend to curl. Microvoltammetric electrodes exhibit enhanced mass transport over electrodes of conventional size. This feature is beneficially used in differential-pulse anodic stripping voltammetry (d.p.a.s.v.) [2]. Gold-film electrodes have been used advantageously for quantifying Hg(II) in solution [3, 4]. The merger of the above two applications has led to the present application of gold-film m.v.e.'s, the quantification of Hg(II) in solution by d.p.a.s.v.

Experimental

The gold-film m.v.e.'s were produced by plasma-sputtering gold onto low-modulus carbon fiber electrodes. The carbon fiber electrodes were prepared by connecting carbon fibers (7 μm diameter; Hercules Magnamite type AS4-12) to 16-gauge copper wire with conductive silver paint. An array of 20 such carbon fiber electrodes was placed in a Hummer VI sputtering system, fitted with a gold target ring (Technics). A 100 mTorr argon plasma with a plasma discharge current of 15 mA was used to sputter gold onto the carbon fibers electrodes. At magnifications up to 20 000×, gold EDAX maps and scanning

0003-2670/84/$03.00

electron micrographs of a gold-film m.v.e. both indicated that gold is deposited as a homogeneous film under these plasma-sputtering conditions. After removal of the electrodes from the plasma chamber, the silver-copper contact was covered with epoxy, and by sliding the insulation of the wire up, only the gold-coated fiber was exposed. The m.v.e.'s were then cut to a length of 1.0 cm. Details of the mechanics of constructing microvoltammetric electrodes in this manner have been given elsewhere [2].

Differential pulse voltammetry was done with a PAR model 174 polarographic analyzer and a Hewlett-Packard model 7015B X-Y recorder. For all differential pulse experiments, the supporting electrolyte was a 0.2 M (pH 7.0) ammonium acetate solution formed by appropriate dilution of isothermally distilled acetic acid and ammonia solution. Standard addition of mercury was conducted by adding the appropriate aliquots from a standard mercury solution prepared by dissolving triply distilled mercury in a small amount of nitric acid and diluting to volume with Milli-Q water (Millipore Corp.). All differential-pulse anodic stripping voltammograms were obtained after a 300-s deposition step at −0.090 V and were terminated at +1.410 V (vs. NHE). No conditioning step was used. Electrodes used in differential pulse voltammetry included a platinum disk auxiliary electrode (Orion) and a Ag/AgCl double-junction reference electrode (Sensorex). All voltammograms recorded were obtained with the same gold-film m.v.e.

Results and discussion

Bulk mercury stripping at gold-film m.v.e.'s can be observed after several monolayers of mercury have been deposited to form a gold-mercury amalgam. Bulk mercury stripping at these electrodes is observed as a broad peak for mercury concentrations less than 100 $\mu g\ l^{-1}$, with the peak potential shifting gradually from +0.540 V to +0.500 V with increasing mercury concentration. The variation of peak shape with mercury concentration for the stripping of mercury is shown in Fig. 1. The peak at +0.270 V was present in all d.p.a.s.v. work with the electrode but, while the magnitude of the peak changed with deposition time, it did not vary with mercury concentration, implying that it was not associated with the stripping of mercury.

At mercury concentrations less than 100 $\mu g\ l^{-1}$, the area of the broad stripping peak was found to vary linearly with mercury concentration. The linear response had a slope of 53.8 ± 1.0 $nC/\mu g\ l^{-1}$ (Hg(II), y-intercept of −5.2 ± 54.7 nC, $S_{y,x}$ = 97.7 nC, and correlation coefficient of 0.995. The detection limit was 3.7 $\mu g\ l^{-1}$, using twice the standard deviation of the least-squares plot as the minimum detectable signal.

As the mercury concentration is increased, a new mercury stripping peak grows in at +0.340 V. The symmetry of this peak allows the use of peak height as a measure of mercury concentration at concentrations greater than 100 $\mu g\ l^{-1}$. Over the range 120–250 $\mu g\ l^{-1}$, peak height varied linearly with mercury concentration. This peak yielded a linear response with a slope of 8.58 ± 0.10 $nA/\mu g\ l^{-1}$ Hg(II), y-intercept of −1036 ± 18 nA, $S_{y,x}$ = 10.5 nA,

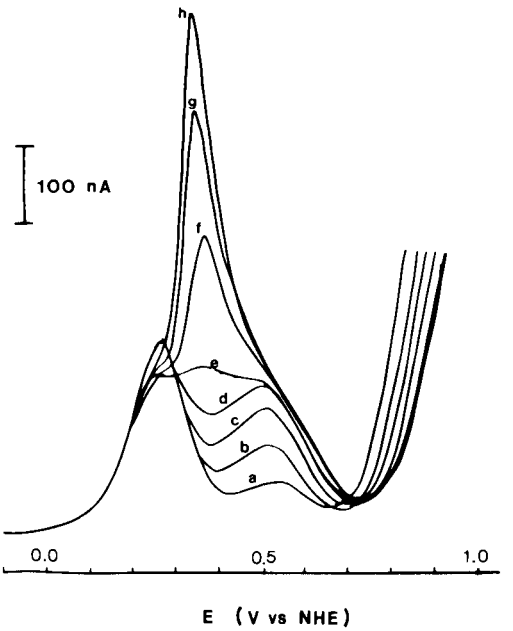

Fig. 1. Variation of the bulk mercury stripping peak at different Hg(II) concentrations: (a) 21.8, (b) 42.6, (c) 63.4, (d) 84.2, (e) 134, (f) 155, (g) 175, (h) 195 $\mu g\ l^{-1}$.

and correlation coefficient of 0.999. The shifting of peak potentials from +0.540 V to +0.340 V as the concentration of mercury is increased indicates that the first few layers of bulk mercury are stabilized by interacting with the gold-mercury amalgam. As the bulk mercury layer increases, less of the mercury interacts with the gold-mercury amalgam and less positive potentials are required to oxidize the mercury film. Similar behavior has been reported for the anodic stripping of mercury from gold film electrodes in thiocyanate media [5].

The gold-film m.v.e.'s described here were found to be electrochemically and mechanically durable; only minimal care is necessary to obtain satisfactory performance despite their small size. The plasma-sputtering of gold onto carbon fibers provides a method of producing a cylindrical gold m.v.e., a geometry unattainable with a gold-wire m.v.e. By an analogous process, it may be possible to prepare platinum film m.v.e.'s. Future work will address other applications of metal-film m.v.e.'s.

REFERENCES

1 R. M. Wightman, Anal. Chem., 53 (1981) 1125A.
2 M. R. Cushman, B. G. Bennett and C. W. Anderson, Anal. Chim. Acta, 130 (1981) 323.
3 R. W. Andrews, J. H. Larochelle and D. C. Johnson, Anal. Chem., 48 (1976) 212.
4 R. E. Allen and D. C. Johnson, Talanta, 20 (1973) 799.
5 R. Bilewicz and Z. Kublik, Anal. Chim. Acta, 152 (1983) 203.

Analytica Chimica Acta, 166 (1984) 301—304
Elsevier Science Publishers B.V., Amsterdam — Printed in The Netherlands

Short Communication

AMPEROMETRIC DETERMINATION OF ARACHIDONIC ACID WITH PROSTAGLANDIN ENDOPEROXIDE SYNTHETASE AS CATALYST

R. M. ACHMEDOV and A. T. MEVKH
Lomonosov State University, Moscow (U.S.S.R.)
J. J. KULYS*
Institute of Biochemistry, Lithuanian Academy of Sciences, Vilnius (U.S.S.R.)
(Received 27th April 1984)

Summary. Physiological concentrations of arachidonic acid in deproteinized serum can be determined amperometrically in the presence of prostaglandin endoperoxide synthetase and potassium hexacyanoferrate(II). A determination takes 1.5—2 min, by measuring the current at a glassy carbon electrode at 0.0 V vs. SCE.

The determination of polyunsaturated fatty acids, including arachidonic acid (5,8,11,14-eicosatetraenoic acid), is of considerable interest because these acids are the precursors of eicosanoids, and exhibit a very wide physiological spectrum [1, 2]. The concentration of free arachidonic acid in biological fluids can indicate the pathological state of an organism. Non-enzymatic determinations of arachidonic acid and its metabolites in living organisms have been described [1, 3, 4]. In the present communication, an amperometric determination of arachidonic acid in buffer solutions and deproteinized blood serum, with prostaglandin endoperoxide synthetase is described.

Experimental

Reagents. Prostaglandin and endoperoxide synthetase (PGH synthetase, E.C. 1.14.99.1) was isolated from sheep vesicular glands as described previously [5]. The enzymatic activity was measured by using a Clark-type oxygen electrode [6]. The protein concentration was 3.3—4.9 mg cm^{-3}. Arachidonic acid (Serva), hemin (Sigma), Tween-20 (Ferak, Berlin), L-adrenaline (Merck), $K_4Fe(CN)_6 \cdot 3H_2O$, $K_3Fe(CN)_6$ and Tris[tris(hydroxymethyl)-aminomethane] were of the highest purity available (Reachim, U.S.S.R.). The buffer solution used was 0.05 M Tris—HCl, pH 8.0.

Apparatus. Differential pulse voltammetric curves were recorded with a polarographic analyzer PA-2 (Laboratorni pristroje, Prague) in a glass cell (Radiometer) thermostatted at 25°C with a three-electrode circuit. A glassy carbon electrode (3 mm diameter) was used as the working electrode. Saturated calomel and platinum (surface area 120 mm^2) electrodes served as the reference and auxiliary electrodes, respectively. For amperometric

0003-2670/84/$03.00

measurements, a LP-7e polarograph (Laboratorni pristroje, Prague) was used with an OH-814/2 recorder (Radelkis, Budapest). The sensitivity of the measuring circuit was 0.2 nA mm^{-1} on the chart. For measurements, a three-electrode circuit based on the above working and reference electrodes was used at room temperature. The body of a titanium cell (3 cm^3 volume) served as the auxiliary electrode. Before measurements the working electrode was polished with fine emery paper and magnesium oxide and treated in hydrochloric acid. The electrode was covered with a dialysis membrane (55 μm thick). The solution was stirred by a disc magnetic stirrer (Radiometer).

Determination of arachidonic acid. A solution of arachidonic acid (20 mm^3) in ethanol or 0.2 cm^3 of deproteinized serum was introduced into the cell containing 2 cm^3 of buffer solution with 0.1% Tween-20, which was made 1.5—3.4 μM in hemin and 0.1 or 1.0 mM in potassium hexacyanoferrate(II), and the working and reference electrodes were immersed. The background response was recorded for 2 min, before 50 mm^3 of enzyme was introduced and the cathodic current was recorded at 0.0 V until the establishment of a steady-state current (1.5—2 min). The difference between the steady-state and background currents was used to plot the calibration graphs.

Deproteinized serum was prepared by protein precipitation from pig blood serum with 10% (w/v) trichloroacetic acid, with subsequent neutralization of the supernatant liquid with potassium hydroxide.

Arachidonic acid was also determined spectrophotometrically by using 1.5 mM adrenalin (enzyme concentration 0.12 mg cm^{-3}, 1.8 μM hemin) in place of potassium hexacyanoferrate(II). The molar absorptivity of the adrenaline oxidation products used was 4000 l mol^{-1} cm^{-1} at 480 nm [7].

Results and discussion

Electrochemical properties of hexacyanoferrate(III) in a 0.1% Tween-20 solution. Initially, the effect of 0.1% Tween-20 on the electrochemical properties of hexacyanoferrate(III) was studied because the arachidonic acid is determined in this solution. Hexacyanoferrate(III) reduction at the uncovered glassy carbon electrode in the buffer solution proceeds at 0.15 V (Fig. 1). When the electrode is covered with a dialysis membrane, the current is decreased 4.8 times, but the peak potential does not change. In the presence of detergent (0.1% Tween-20), there is a considerable increase in overpotential as well as a decrease in the current from mediator reduction in the absence of a membrane. The potentials of hexacyanoferrate(III) reduction at the membrane-covered electrode with or without detergent, however, are similar, and the difference in current is negligible. Further measurements were made with the electrode covered with the dialysis membrane.

Amperometric determination of arachidonic acid. The basis of the amperometric determination of arachidonic acid lies in substrate oxidation, catalyzed by PGH synthetase by the action of oxygen and potassium hexacyanoferrate(II) [2].

$$\underset{\text{acid}}{\text{Arachidonic}} + 2O_2 + 2Fe(CN)_6^{4-} + 2H^+ \rightarrow \text{prostaglandin-}H_2 + 2Fe(CN)_6^{3-} + H_2O$$

The hexacyanoferrate(III) formed can be determined amperometrically at 0.0 V [8].

On introduction of prostaglandin into the buffer solution containing 1 mM potassium hexacyanoferrate(II), 0.1% Tween-20, 3.4 μM hemin and 0.5 mM arachidonic acid, a cathodic current is produced. The rate of current increase vs. enzyme concentration is hyperbolic, eventually reaching a plateau. The Michaelis parameters of the hyperbolic dependence are: V_{max} = 21 nA min^{-1}, K_m = 0.088 mg cm^{-3}. At high enzyme concentration, the current is limited by the diffusion of the electrochemically active compound through the membrane. At constant enzyme concentration (0.08 mg cm^{-3}), and within the arachidonic acid concentration range 10—100 μM, 95% of the steady-state current is achieved in 1—1.5 min.

A calibration graph of the steady-state current dependence on the arachidonic acid concentration is linear up to 100 μM substrate (enzyme 0.08 mg cm^{-3}). At higher concentrations, the line curves, so that, for example, the sensitivity is approximately halved for 600 μM arachidonic acid.

The concentration of arachidonic acid in deproteinized serum was deter-

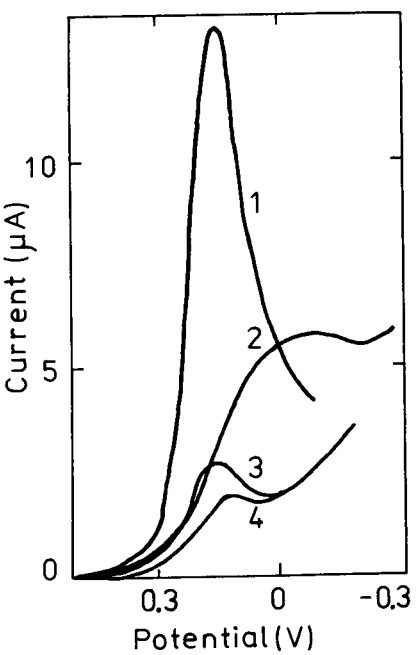

Fig. 1. Differential pulse voltammogram of potassium hexacyanoferrate(III): (1, 2) at the bare glassy carbon electrode; (3, 4) at the membrane-covered electrode. Tween-20 concentration: (1, 3) none; (2, 4) 0.1%. Other conditions: 0.59 mM $K_3Fe(CN)_6$, 0.05 M Tris—HCl, pH 8.0, scan rate 5 mV s^{-1}, modulation amplitude 50 mV, 25°C.

TABLE 1

Determination of arachidonic acid in deproteinized serum[a]

Arachidonic acid added ($\times 10^{-6}$ M)	Current (nA)	Corresponding arachidonic acid in undiluted serum ($\times 10^{-6}$ M)
0	2.7	71
25	13.1	346
50	23.7	621
75	33.7	896

[a]0.05 M Tris—HCl, pH 8.0, 0.1% Tween-20, 1.5 μM hemin, 0.1 mM $K_4Fe(CN)_6$, 0.12 mg cm^{-3} prostaglandin endoperoxide synthetase, 0.0 V vs. SCE.

mined by means of standard additions. For this purpose, the steady-state current for 11-fold diluted serum was determined first (Table 1). (As the current in the absence of enzyme or serum does not exceed 0.2 nA, the biocatalytic current of the electrode depends on the presence of arachidonic acid.) Measurements of arachidonic acid added to the serum were also made (Table 1). The acid concentration calculated from these measurements was 6.5 μM, so that the concentration in undiluted serum was 71 μM (S.E. 11%).

The concentration of arachidonic acid in deproteinized serum was also determined spectrophotometrically, and found to be 92 μM. The difference is probably due to the change in the molar absorptivities of the adrenalin conversion products (adrenochrome) in the medium in the presence of detergent.

The authors thank Dr. G. F. Sudjina for kindly supplying enzyme samples and Prof. S. D. Varfolomeev for useful discussion.

REFERENCES

1 K. Korte, P. C. MacDonald, J. M. Johnston, J. R. Okita and M. L. Casey, Biochim. Biophys. Acta, 752 (1983) 423.
2 A. T. Mevkh, P. V. Vrzetch, V. V. Basevich and S. D. Varfolomeev, in N. M. Emanuel, I. V. Berezin and S. D. Varfolomeev (Eds.), Chemical and Biochemical Kinetics, Moscow University, Moscow, 1983, p. 224.
3 A. Derksen and P. Cohen, J. Biol. Chem., 250 (1975) 9342.
4 J. M. Boeynaems, A. R. Brash, J. A. Oates and W. C. Hubbard, Anal. Biochem., 104 (1980) 259.
5 F. J. Van der Ouderaa, M. Buytenhek, D. H. Nugteren and D. A. Van Dorp, Biochim. Biophys. Acta, 487 (1977) 315.
6 A. T. Mevkh, P. V. Vrzetch, V. K. Shviadas, S. D. Varfolomeev, G. I. Miagkova and L. A. Jakusheva, Biorganicheskaya Khimija, 7 (1981) 695.
7 G. Takeguchi and C. J. Sih, Prostaglandins, 2 (1972) 169.
8 J. J. Kulys, V.-S. A. Laurinavicius, M. V. Pesliakiene and V. V. Gureviciene, Anal. Chim. Acta, 148 (1983) 13.

Analytica Chimica Acta, 166 (1984) 305—310
Elsevier Science Publishers B.V., Amsterdam — Printed in The Netherlands

Short Communication

A SIMPLE LABORATORY GENERATOR FOR LOW CONCENTRATIONS OF SULPHUR DIOXIDE

JAN LANGMAIER and FRANTIŠEK OPEKAR*

UNESCO Laboratory of Environmental Electrochemistry, J. Heyrovský Institute of Physical Chemistry and Electrochemistry, Czechoslovak Academy of Sciences, Jilská 16, 110 00 Prague 1 (Czechoslovakia)

(Received 12th March 1984)

Summary. The generator is based on permeation of sulphur dioxide through silicone rubber tubes immersed in a buffered, thermostatted solution of sodium hydrogensulphite. The generator contains three (or more) permeation tubes of different lengths immersed simultaneously in the generation solution. The tubes can be connected stepwise to the carrier gas source, so that three (or more) different concentrations of SO_2 in the carrier gas can be obtained from a single solution. The tested generator produced 1.25—25.4 ng s^{-1} SO_2, depending on the hydrogensulphite concentration in the solution. Long-term stability was tested for the production of 10.49 ng s^{-1} over 50 h; the relative standard deviation was 1.57%. The experimental conditions affecting the production of SO_2 are discussed. An equation is derived for estimating the SO_2 production for various solution compositions and surface areas of the permeation tubes.

In the laboratory testing and calibration of gas analyzers and sensors, it is useful to have a source of the test gas that permits changes in concentration of the tested components in the carrier gas with time in an experimentally simple way. Concentration changes of several orders of magnitude are often required, sometimes at a constant flow rate of the carrier gas. Classical permeation systems (permeation tubes and wafers) have various drawbacks: difficult laboratory preparation, the relatively long time required for such systems to produce a constant amount of gas, and the practical difficulties of changing this production. These have led to suggestions for a simple laboratory source for generating various gases: SO_2, NO + NO_2, NH_3, H_2S and HCN [1]. In such sources, the carrier gas is passed over a buffered dilute solution of a suitable salt ($NaHSO_3$, $NaNO_2$, NH_4Cl, Na_2S, KCN); after 30—40 min, the concentration of the required gas becomes constant. Simple changes of, for example, salt concentration, temperature or pH suffice to change the partial pressure of the generated gas above the solution and so its concentration in the carrier gas. Although this method of generation is simple and versatile, it can be used only for a few hours, because the salt in solution becomes depleted. Scarano et al. [2] produced low concentrations of hydrogen chloride by permeation into a carrier gas passed through a thin-walled teflon tube in a gas-tight vessel containing a strong hydrochloric acid solution.

0003-2670/84/$03.00

These principles for gas generation [1, 2] were combined in the construction of a laboratory source of low concentrations of hydrogen cyanide [3]. The same principle is used here to generate low concentrations of sulphur dioxide. The main advantage of the proposed generator is the possibility of obtaining several different concentrations of generated gas from a single solution at a constant flow rate of the carrier gas. Constant gas production can be maintained for several days.

Experimental

Apparatus. Figure 1 is a schematic diagram of the generator; the main components are made of plexiglas. The 100-ml generation vessel (V) has a lid with stationary and movable components. The stationary part (C1), which is screwed gas-tight into the vessel, has three pairs of openings, 1—3 and 1′—3′. Injection needles (I), onto which are fitted permeation tubes (P) of various lengths, are fitted into these openings in the lid as shown. Silicone rubber tubes (o.d. 2 mm, wall thickness 0.35 mm) were used. The tubes are fitted onto the needles to connect the corresponding openings, 1—1′, 2—2′, and 3—3′ (for simplicity, only a single tube is depicted in Fig. 1). The tubes are immersed in the generation solution in the vessel.

The movable part (C2) of the lid is fixed onto C1 with a screw so that it can be turned; C2 has two openings with tube fittings to connect up the tubing for inlet of the carrier gas and outlet of the enriched gas. The openings

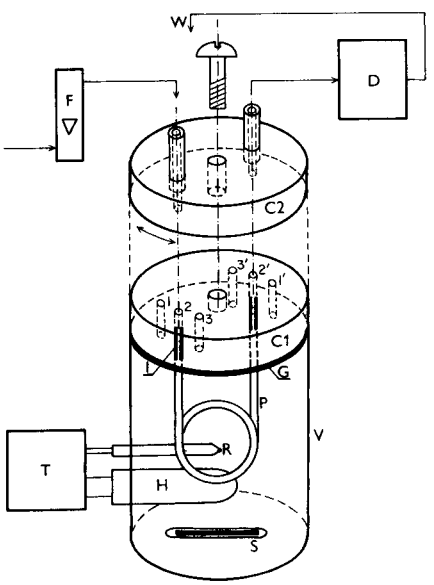

Fig. 1. Schematic diagram of the SO_2 generator: (V) generation vessel; (C1) stationary part of the lid; (C2) movable part of the lid; (G) seal; (I) injection needles; (P) permeation tube; (H) heater coil; (R) thermistor; (T) thermostat; (S) magnetic stirrer; (F) flow meter; (D) detector or calibration apparatus; (W) waste.

in C1 and C2 are located in such a way that the inlet and outlet tubes can be connected with a permeation tube of a particular length attached at 1—1′, 2—2′ or 3—3′. A simple turn of C2 thus provides generation of three different concentrations of gas from a single solution, as the gas production is a function of the length of the permeation tube (the generator could obviously be constructed with more permeation tubes). The contacting surfaces of C1 and C2 are polished and coated with a thin layer of silicone grease. Part C2 of the lid also has openings (not shown) for passing auxiliary gas to the permeation tubes not in use at a given lid position, to prevent accumulation of the generated gas in the disconnected tubes. Gas from outlet W was used as auxiliary gas.

Vessel V also contains a heater, a thermistor for recording and measuring the temperature of the solution and a magnetic stirrer.

Procedure. For generation of sulphur dioxide, vessel V was filled with 100 ml of a sodium hydrogensulphite solution with the required concentration in phthalate (Clark-Lubs) buffer, pH 5.00. At this pH, the solution contains a low concentration of free sulphur dioxide, which ensures the required low production; the solution thus acts as a reservoir of sulphur dioxide with a quite large capacity. Measurements were made at 30.0°C. Nitrogen served as carrier gas. After vessel V had been filled and the solution had been thermostatted, 30 min sufficed for the generator to produce a constant amount of sulphur dioxide.

To determine the sulphur dioxide produced, the carrier gas from the generator was passed for a defined time (minutes to hours) into 12 ml of 0.2 M sodium tetrachloromercurate in an absorber with a frit. Finally, 10 ml of this solution was used for the spectrophotometric measurement of sulphur dioxide after reaction with *p*-aminoazobenzene [4]. The sodium hydrogensulphite used to prepare the generation solution and for calibration of the spectrophotometric method was standardized iodimetrically.

Results and discussion

The concentration of sulphur dioxide in the generation solution is established by the dissociation equilibrium $SO_2 + H_2O \rightleftharpoons HSO_3^- + H^+$ ($K_a = 1.26 \times 10^{-2}$). The amount of sulphur dioxide in the carrier gas under defined experimental conditions (hydrogensulphite concentration, temperature, pH, geometry of the permeation tube) depends on the flow j (mol s^{-1}) of sulphur dioxide through the tube wall. If SO_2 permeates from the solution into a medium containing no SO_2, the stationary material flow can be described [5] by

$$j = D\,A\,c^{m}_{SO_2}/x \qquad (1)$$

where D ($cm^2\ s^{-1}$) is the diffusion coefficient of SO_2 in the material of the permeation tube, A (cm^2) is the permeation surface area, $c^{m}_{SO_2}$ (mol ml^{-1}) is the concentration of SO_2 at the tube wall in contact with the solution, and x (cm) is the wall thickness of the permeation tube. The assumption of perm-

eation into a medium with a negligible concentration of SO_2 is valid if the permeation tubes have a small internal volume and the carrier-gas flow rate is high. The production of SO_2 was shown to be independent of the nitrogen flow rate in the range 2.3—10.7 ml s^{-1} for permeation tubes with internal volumes of 0.04—0.3 cm^3.

The mass flow of SO_2 into the permeation tube can be expressed in terms of the generation constant K_g (ng s^{-1}), so that the concentration of SO_2 in the carrier gas can be evaluated in more frequently used units. Then $j = 10^{-9} K_g/M_{SO_2}$, where M_{SO_2} (64.06) is the molar mass of SO_2. Thus concentration $c^m_{SO_2} = k\, c^s_{SO_2}$, where k is the partition coefficient of SO_2 between the solution and the material of the permeation tube and $c^s_{SO_2}$ (mol ml^{-1}) is the concentration of SO_2 in the generating solution. Concentration $c^s_{SO_2}$ can be found for solutions at pH 4—6 from the above dissociation equation: $c^s_{SO_2} = (10^{-3}\, c^*_{NaHSO_3} c_{H^+})/(K_a M_{NaHSO_3})$, where $c^*_{NaHSO_3}$ is the concentration of sodium hydrogensulphite (mg ml^{-1}) in the generation solution with a hydrogen ion concentration $c_{H^+} = 10^{-pH}$ (mol l^{-1}), and M_{NaHSO_3} (104.06) is the molar mass of sodium hydrogensulphite. Equation 1 can then be rewritten in the form

$$K_g = (M_{SO_2}\, k\, D\, A\, c^*_{NaHSO_3} c_{H^+})/(M_{NaHSO_3} K_a x) \qquad (2)$$

Evaluation of K_g. For a certain concentration $c^*_{NaHSO_3}$, the generation constant was evaluated by measuring the amount of SO_2 absorbed in the tetrachloromercurate(II) solution during different times. The dependence of the amount of SO_2 on the absorption time is linear with a slope equal to K_g. The results of regression analysis of this dependence for various concentrations of sodium hydrogensulphite are given in Table 1.

The concentration of SO_2 in the carrier gas flowing with velocity v can be found from the relationship $c^g_{SO_2} = K_g/v$. When K_g is in ng s^{-1} and v is in ml s^{-1}, $c^g_{SO_2}$ is given in mg m^{-3}; or $c^g_{SO_2}$ (ppm) = 0.382 $c^g_{SO_2}$ (mg m^{-3}) (25° C, 101.3 kPa).

TABLE 1

The K_g values determined in the generation solution for various hydrogensulphite concentrations (permeation tube length 160 mm; pH 5.00; nitrogen flow rate 3.4 ml s^{-1}; 30.0° C)

$c^*_{NaHSO_3}$ (mg ml^{-1})	No. of points	K_g (ng s^{-1})	Intercept[a] (ng)
3.8	6	1.25 (0.05)[b]	436.46 (252.26)[b]
9.5	7	3.29 (0.17)	−134.00 (466.93)
19.0	7	6.68 (0.09)	−85.79 (188.48)
30.4	10	10.53 (0.09)	−31.85 (196.67)
36.1	9	12.30 (0.48)	308.47 (631.69)
72.2	7	25.40 (0.36)	440.50 (350.87)

[a]The zero value of the intercept of the regression straight line always lies within the confidence interval (for $\nu = n - 2$, $\alpha = 0.05$). [b]Standard deviations are given in parentheses.

In agreement with Eqn. 2, K_g was found to depend linearly on the permeation surface area in the range 3—25 cm^2, on the concentration of hydrogen ions in the range pH 4.6—5.2, and on the concentration of hydrogensulphite. The value of $D\,k$, characterizing the permeation properties of the permeation tube material, was found from the slope of the dependence of K_g on $c^*_{NaHSO_3}$. The value found, $D\,k = (2.45 \pm 0.07) \times 10^{-6}$ cm^2 s^{-1} is similar to the value 3.8×10^{-6} cm^2 s^{-1} for 25% dimethylsilicone rubber given by Ross et al. [6]. The composition of the silicone rubber used here was not known.

Equation 2 can be used to estimate the production of the generator for a given composition ($c^*_{NaHSO_3}$, pH) of the generation solution and geometric parameters of the silicone tubes used (A, x). After enumeration of the constants, and with the value $D\,k = 2.45 \times 10^{-6}$ cm^2 s^{-1}, Eqn. 2 yields the value K_g (ng s^{-1}) $\approx (1.2 \times 10^2\ A\ c^*_{NaHSO_3} c_{H^+})/x$. From this equation, values of A, x, c_{H^+} and $c^*_{NaHSO_3}$ can be selected so that the generator produces the required amount of SO_2.

Long-term stability. The stability of the production of SO_2 was tested over a period of 50 h with double interruption of output (i.e., stopping the carrier gas flow) for 17 and 16 h. The net output time was thus 17 h. For these tests, the generation solution contained 30.4 mg ml^{-1} sodium hydrogensulphite under the experimental conditions given in Table 1. The average K_g value found from 15 measurements was 10.49 ng s^{-1} SO_2 with a relative standard deviation of 1.57%. Theoretically, it would be possible to produce SO_2 for a period of 850 h from 100 ml of the generation solution under the given experimental conditions, with a decrease in the sulphite content of only 1%.

Temperature dependence. The dependence of K_g on the temperature was studied in the range 25—37°C. It was found that K_g increased linearly with temperature from 25 to 33°C with a temperature coefficient of 4.5%/°C. Thus the temperature of the generation solution must be maintained with a precision of ±0.1°C, to prevent variations in production from exceeding 1%. At higher temperatures, the K_g/temperature dependence was curved toward higher production values. The variations in the SO_2 production with temperature result from changes in the permeability of the tube material and from the temperature dependence of the ionic equilibria in solution [1].

Conclusions

In the simple generator described, the use of thin-walled tubing of a material with high permeability for sulphur dioxide results in constant production of the gas after 30 min, which is very much faster than is possible when classical permeation tubes are used. The construction permits production of three (or more) different SO_2 concentrations in the carrier gas at a constant gas flow rate from a single generation solution, by using different lengths of tubing. Low concentrations of sulphur dioxide can be produced from quite concentrated hydrogensulphite solutions, so that the lifetime of

the generator is long enough for laboratory applications. Obviously, the general principle used here can also be applied to the generation of other gases and vapours.

REFERENCES

1 Y. Hashimoto and S. Tanaka, Environ. Sci. Technol., 14 (1980) 413.
2 E. Scarano, C. Calcagno and L. Cignoli, Anal. Chim. Acta, 110 (1979) 95.
3 F. Opekar, Chem. Listy, 77 (1983) 884.
4 S. J. Kniseley and L. J. Throop, Anal. Chem., 38 (1966) 1270.
5 D. P. Lucero, Anal. Chem., 40 (1968) 707.
6 J. W. Ross, J. H. Riseman and J. A. Krueger, Pure Appl. Chem., 36 (1973) 473.

Analytica Chimica Acta, 166 (1984) 311—314
Elsevier Science Publishers B.V., Amsterdam — Printed in The Netherlands

Short Communication

AN IMPROVED METHOD FOR HIGH-PERFORMANCE LIQUID CHROMATOGRAPHY OF GOSSYPOL

CHARLES W. JEFFORD and HAMISH G. GRANT*[a]

Department of Organic Chemistry, University of Geneva, 1211 Geneva 4, (Switzerland)

(Received 28th May 1984)

Summary. Earlier liquid-chromatographic methods for the determination of gossypol, based on highly acidic methanolic solvents, provide broad tailing peaks. The use of acetonitrile with aqueous phosphoric acid/tri-n-butylammonium phosphate at pH 3.5 and a high-resolution radial-compression column gave greatly improved performance and excellent peak shape.

Gossypol (I), a toxic constituent of the pigment glands of cottonseed, has become of interest as a potential male fertility control agent. This compound is frequently isolated as a relatively stable crystalline complex containing one mole of acetic acid [1] and this form has been shown to be an active inhibitor of spermatogenesis in a number of mammalian species including man

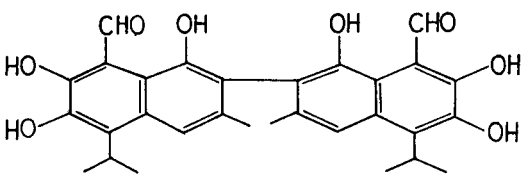

(I)

[2, 3]. Various chromatographic methods for the determination of gossypol have been described, including thin-layer [4], gas (of the per-TMS ether derivative) [5] and high-performance liquid [6, 7] chromatography (h.p.l.c.). Both h.p.l.c. methods required a μBondapak C-18 column and strongly acidic aqueous methanol as solvent, but the chromatograms obtained exhibited poor column efficiency and unsatisfactory peak symmetry. This less than optimum performance may be attributed to an essentially unsuitable solvent and column deterioration caused by operation at the lower pH limit tolerated by most bonded-phase columns.

It is shown here that greatly improved performance can be obtained with fully end-capped C-18 columns by using acetonitrile-based solvent systems

[a]Present address: Varian AG, Steinhauserstrasse, CH-6300 Zug (Switzerland).

0003-2670/84/$03.00

containing phosphoric acid and tri-n-butylammonium phosphate in the aqueous component.

Experimental

Gossypol-acetic acid (Sigma Chemical Co.) was used as received. Columns used were a μBondapak C-18 (10 μm, stainless steel) and a Nova-Pak C-18 (5 μm) radial compression cartridge mounted in a Z-module (all from Waters Associates). The principal solvent used was prepared by mixing 4 parts of acetonitrile (Fluka, puriss) with 1 part of aqueous 50 mM phosphoric acid (Fluka, puriss, in high-purity water) which had been adjusted to pH 3.5 by addition of tri-n-butylamine (Fluka, puriss). A Hewlett-Packard 3380S digital integrator was used for quantitation. A refractive index detector was used.

Results and discussion

The two previous h.p.l.c. methods for gossypol required 0.1% phosphoric acid in methanol/water (4 + 1) [6] and methanol/water/glacial acetic acid (77 + 20 + 3) [7] as eluent, respectively. The chromatograms showed relatively broad, tailing peaks with retention time/elution time ratios (t_R/t_0) of 2.0—2.5 (estimated). Given the potential for large solvent—solute interactions between methanol and gossypol with resultant peak broadening, the present investigations first involved a change to acetonitrile while the aqueous phosphoric acid component (0.1%) was retained. With a μBondapak C-18 steel column, these conditions immediately provided considerably enhanced performance, as shown in Fig. 1(a); t_R/t_0 was increased to ca. 4.5.

Because these rather aggressive conditions (aqueous phase at ca. pH 2) were considered as bad for the column packing, the effect on the separation of increasing the pH was examined. Addition of a few drops of triethylamine to the eluent mixture resulted in a distinct reduction in the width of the gossypol peak, despite a small increase in retention time. Optimum performance was obtained with an aqueous component at pH 3.5; the chromatogram (Fig. 1b) showed a much improved t_R/t_0 ratio of ca. 7.0 although some persistent low-level tailing was still seen.

To improve the method further, the performance of a Waters Nova-Pak C-18 (5 μm) radial compression cartridge (in a Z-module) was tested, as well as the effect of other bases added to the aqueous component of the eluent (tri-n-butylammonium phosphate and Waters PIC-A ion-pairing reagent tetra-n-butylammonium phosphate) adjusted to various pH values with phosphoric acid. Best results were obtained with aqueous phosphoric acid/tri-n-butylammonium phosphate at pH 3.5; this provided a peak for gossypol of excellent symmetry (Fig. 1c) and with a further improved t_R/t_0 ratio of about 8.2. Peaks with identical retention times were obtained from acetonitrile solutions of both commercial gossypol-acetic acid and free gossypol prepared from the complex by the method of Pons et al. [8].

A further reason for the avoidance of methanol in the eluent is the in-

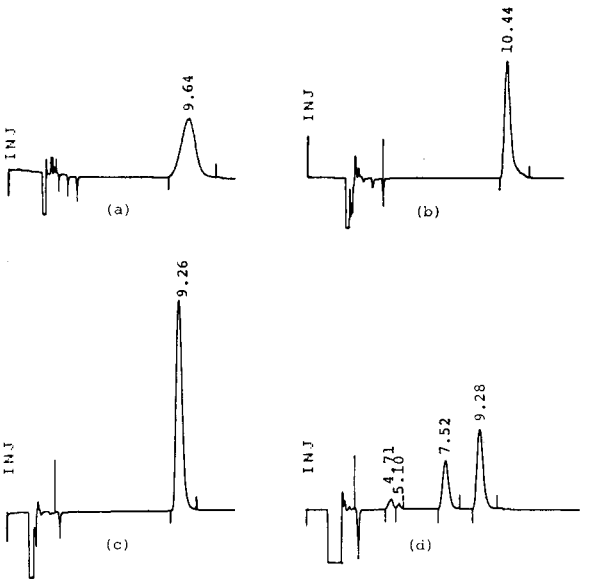

Fig. 1. Chromatograms for gossypol-acetic acid: (a) Waters μBondapak C-18 (steel) column with acetonitrile/aqueous 43 mM phosphoric acid (4 + 1) eluent at 1.0 ml min^{-1}; (b) as for (a) but the aqueous phosphoric acid component was first adjusted to pH 3.5 with triethylamine; (c) Waters Nova-Pak C-18 column in Z-module with (4 + 1) acetonitrile/aqueous 50 mM phosphoric acid adjusted to pH 3.5 with tri-n-butylamine as eluent at 1.5 ml min^{-1}; (d) column and eluent as for (c). (a—c) Sample in acetonitrile; (d) sample in methanol kept 35 h before injection. In all cases, 10-μl volumes containing 500 ng of compound were injected. Retention times are given in minutes.

stability of gossypol-acetic acid in this medium. Solutions of the compound in methanol were found to have a half-life of approximately 40 h at 22°C as determined by h.p.l.c., and decomposed to form one major and two minor products of decreased lipophilicity (Fig. 1d). In contrast, solutions in acetonitrile had a half-life exceeding two weeks at ambient temperature. Stability of gossypol in the recommended eluent was established quantitatively by injections of a solution in this medium containing an inert internal standard (1,2-diphenylethane). Comparison of the relative areas of the standard and gossypol peaks showed no significant variation over an 8-h period.

The conditions recommended provide a considerably improved method for the chromatography of gossypol and for studies of its stability and decomposition in various solvents. The excellent peak symmetry and very low tailing obtained with the Nova-Pak column would be particularly useful for quantitative purposes; 10—1000 ng of gossypol-acetic acid in the 10-μl injections would be a convenient range.

We are indebted to the Swiss National Science Foundation for financial support.

REFERENCES

1 C. L. Hoffpauir, J. A. Harris and J. P. Hughes, J. Assoc. Offic. Agric. Chem., 43 (1960) 329.
2 Qui-Xiau Shi, Yin-Gong Zhang and Yu-Yin Yuan, Tung Wu Hsueh Pao, 27(1) (1981) 22.
3 G. F. Weinbauer, E. Rovan and J. Frick, Andrologia, 14(3) (1982) 270.
4 Jiang Dehe, Xue Xiuhong, Shen Haibao and Zheng Jinfang, Yaoxue Tongbau, 16(8) (1981) 14.
5 M. A. McClure, J. Chromatogr., 54 (1971) 25.
6 S. A. Abou-Donia, J. M. Lasker and M. B. Abou-Donia, J. Chromatogr., 206 (1981) 606.
7 N. Sattayasai, J. Sattayasai and V. Hahnvajanawong, J. Chromatogr., 307 (1984) 235.
8 W. A. Pons Jr., J. Pominski, W. H. King, J. A. Harris and T. H. Hopper, J. Am. Oil Chem. Soc., 36 (1959) 328.

Analytica Chimica Acta, 166 (1984) 315—319
Elsevier Science Publishers B.V., Amsterdam — Printed in The Netherlands

Short Communication

SIMPLE APPROACH TO MICROCOMPUTER-CONTROLLED ELECTROCHEMISTRY

HENRY J. WIECK

Department of Chemistry and Physics, Kean College of New Jersey, Union, NJ 07083 (U.S.A.)

GEORGE H. HEIDER, JR. and ALEXANDER M. YACYNYCH*

Department of Chemistry, Rutgers, The State University of New Jersey, New Brunswick, NJ 08903 (U.S.A.)

(Received 1st May 1984)

Summary. A simple control and data-acquisition system for electrochemical experiments is described. The system is easily interfaced to most potentiostats; a voltage waveform is supplied and data are collected, processed and stored on disk for later use. This implementation is particularly useful for linear-scan and stepped-potential electrochemical experiments. The experimenter can program an experiment as well as apply specialized data treatments to collected information. Some examples of stepped-potential experiments on a chemically-modified electrode are presented.

Much interesting electrochemical work is currently being done on less than ideal electrodes. These electrodes may possess high surface areas, and may be slow in attaining a steady-state current in response to changes in applied potential. Obtaining useful data from these electrodes requires waveforms and data-collection techniques which are not currently available on commercially built instruments. For example, some stepped electrochemical experiments [1, 2], which are relatively simple, are labor-intensive, requiring operator intervention at intervals over long times. Other untraditional experiments, such as that done by Johnson et al. [3] on an enzyme-based electrode, could benefit from a more automated and flexible control system.

A microcomputer has been used to collect and store electrochemical data [4] but the system did not provide control of the experiment. A microcomputer-based electrochemical system has been described [5] and a similar system is commercially available (Bioanalytical Systems). This system is impressive in its repertoire of electrochemical experiments, but is quite expensive and no provision is presently made for permanent data storage (i.e., floppy disk). Other manufacturers of electrochemical instrumentation provide a module to allow for external computer control and data acquisition (E.G. & G., Princeton Applied Research, and ECO Instruments). Malloy and Soong [6] have recently reported the use of an IBM-PC fitted with a commercially available interface incorporating analog-to-digital converters and

0003-2670/84/$03.00

digital-to-analog converters for Riemann-Louiville transform polarography. The collected data can be stored on floppy disk, and is thus available for data-reduction techniques.

This communication describes the use of a commercial analog interface card in an Apple-II Plus microcomputer. The system is simple and relatively cheap. Available electrochemical equipment is easily updated. The computer can be programmed to collect data and to provide different waveforms for specific applications. Control of experiments, and data collection on less than ideal electrochemical systems, such as chemically-modified carbonaceous materials of high surface area, are discussed.

Experimental

Apparatus. An Apple-II Plus microcomputer equipped with 48 kbytes of random access memory (RAM) was used. The computer utilizes Applesoft BASIC which is a dialect of the popular Microsoft BASIC. The unit is equipped with dual 5¼-in. floppy disk drives and operated under DOS 3.3. The Adalab analog interface card used (Interactive Microware, State College, PA) encompasses several subsystems, including a single 12-bit dual-slope integrating ADC, having a conversion rate of 20 Hz and a single DAC operating at a maximum speed of 50 kHz. Both have jumper-selectable voltage ranges of ±4 V, ±2 V, ±1 V and ±0.5 V with precision of 0.025% and accuracy of 0.1%. Digital input and output are available using 16 bidirectional bits, which are individually selectable as inputs or outputs at TTL-compatible signal levels. The card also includes a timer subsystem which has available a 32-bit countdown timer, resolution of 10 μs, and two 16-bit timer/counters which can be configured in several different modes.

A Princeton Applied Research model 364 polarograph was used, although the system will work with most commercial and custom-built instruments. Serial communication to a Houston Instruments model DMP-4 digital plotter was accomplished with a serial (RS232C) communication card (SSM Microcomputer Products, San Jose, CA). A block diagram of the microcomputer system is shown in Fig. 1. The system was also interfaced to an Epson MX-80 dot matrix printer, using a Grappler parallel interface card (Orange Micro, Anaheim, CA) in order to provide hard copy of experimental parameters and screen graphics.

The response of electrodes made from reticulated vitreous carbon (RVC; ERG, Oakland, CA) was studied using the computer-controlled instrumentation. Some of the RVC electrodes were chemically modified with glucose oxidase (E.C. 1.1.3.4), as described previously [7]. These immobilized-enzyme, chemically-modified electrodes (IECME) catalyze the reaction of glucose with oxygen to form gluconic acid and hydrogen peroxide. The electrodes were held in a flow cell [8]. A saturated calomel reference electrode and a platinum auxiliary electrode were used. The stepped potential waveform aids in understanding this system.

Procedure. The DAC output of the microcomputer was used to supply a stepped waveform (Fig. 2) to the potentiostat. The current output of the

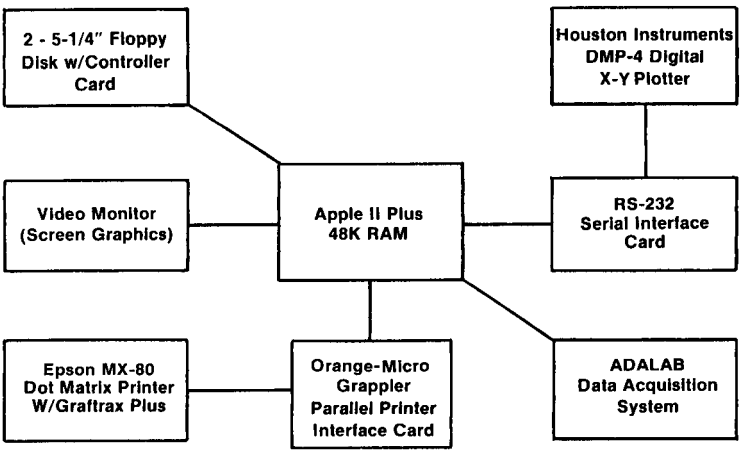

Fig. 1. Block diagram of the microcomputer system showing the various peripherals and interfaces.

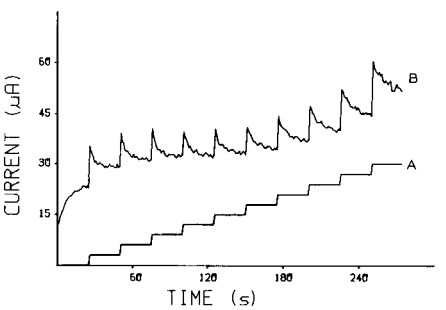

Fig. 2. (A) Microcomputer-generated waveform, 100 mV steps. (B) Flow-through RVC electrode, transient response.

potentiostat was fed into the ADC of the Adalab card, which allowed collection of the transient response of the electrode to the applied waveform. A simple BASIC program was written to monitor the transient current response; it collects 25 equally spaced data points during a specified time period, and then changes the potential to the next step value. A second program collected and averaged six data points at the end of each potential step. This program produced current/potential curves for the electrode under investigation. These programs were written entirely in BASIC. The actual analog input and output was achieved in only three or four statements, without need for programming in machine language.

Results and discussion

The transient response of a blank electrode in pH 10 Clark-Lubs buffer to the applied waveform is shown in Fig. 2. The charging current, observed as a

spike at the beginning of each potential step, decreases significantly by the end of the 25-s step used. The single averaged data point (collected after each 25-s step) was collected for the blank electrode in buffer and then again with buffer containing 10 mM hydrogen peroxide. The resulting curves are shown in Fig. 3. The IECME was characterized similarly; Fig. 4 shows the response of the IECME to phosphate pH 6.5 buffer (0.1 M) without and with 0.1 M glucose. The response shown is similar to that of the blank electrode to hydrogen peroxide; this indicates that the IECME responds to the hydrogen peroxide produced in the oxidation of glucose. Software (Interactive Microware) was used to do a 5-point smooth of the acquired data, to minimize the effect of noise. The smoothed data are presented in Fig. 4 as solid lines through each data set.

Because the waveform applied is the result of digital-to-analog conversion, it is incremental in nature, and so is easily utilized in potential-step voltammetry. A linear-ramp waveform is approached as the potential steps become very small. The smallest step available with the DAC described is 0.25 mV. With a moderately simple BASIC control program, it is possible to generate two steps per second and record the data. As presently configured, this system is not applicable to many transient electrochemical techniques, because of the use of the dual-slope ADC which has a sampling rate of 20 points per second. However, this limitation can be overcome by incorporating a faster ADC.

A versatile laboratory computer system, which is not dedicated, is both cost-effective and useful for other purposes, such as long-term, unattended experiments. The system described will also store the electrochemical data on floppy diskette for further use or data reduction.

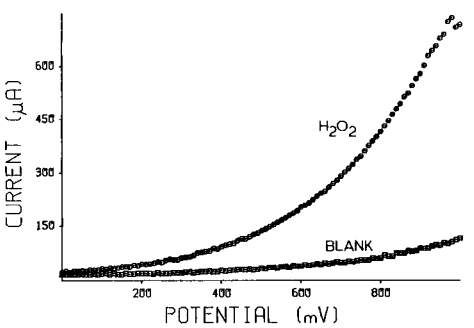

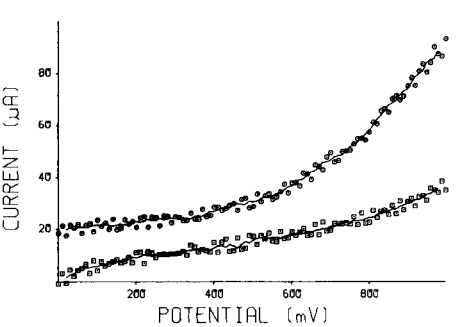

Fig. 3. Current vs. potential curves for unmodified RVC electrode: (□) Clark-Lubs pH 10 buffer; (○) buffer with 10 mM hydrogen peroxide.

Fig. 4. Current vs. potential curves for an immobilized-enzyme chemically-modified RVC electrode: (□) phosphate pH 6.5 buffer (0.1 M); (○) buffer with 0.1 M glucose.

REFERENCES

1 R. E. Icenhower, H. B. Urbach and J. H. Harrison, J. Electrochem. Soc., 12 (1970) 1500.
2 W. J. Blaedel and R. A. Jenkins, Anal. Chem., 13 (1974) 1952.
3 J. M. Johnson, H. B. Halsall and W. R. Heineman, Anal. Chem., 54 (1982) 1377.
4 J. F. Price, S. L. Cooke and R. P. Baldwin, Anal. Chem., 54 (1982) 1011.
5 P. He, J. P. Avery and L. R. Faulkner, Anal. Chem., 54 (1982) 1313A.
6 J. T. Malloy and F. C. Soong, 1983 Eastern Analytical Symposium, New York, paper 142.
7 H. J. Wieck, C. Shea and A. M. Yacynych, Anal. Chim. Acta, 142 (1982) 277.
8 H. J. Wieck, Ph.D. Thesis, Rutgers, The State University of New Jersey, 1983.

Analytica Chimica Acta, 166 (1984) 321—324
Elsevier Science Publishers B.V., Amsterdam — Printed in The Netherlands

Short Communication

IMPROVED ALGORITHM FOR ANALYSIS OF THE LEAST-SQUARES TREATMENT OF TITRATION DATA

EDWARD E. MERCER
Department of Chemistry, University of South Carolina, Columbia, SC 29208 (U.S.A.)
(Received 25th May 1984)

Summary. In least-squares data-processing, previous investigators have reported the evaluation of partial derivatives that show the effect on the parameters from errors in individual data points. By replacing the finite difference method used earlier, an increase in the speed of the computations by a factor of 40 or greater can be achieved.

Recently, Kateman et al. [1, 2] have reported the evaluation of nonlinear least-squares refinement of potentiometric acid—base titration curves. These papers are a part of a series by Meites and co-workers that originated in 1975 [3]. In these reports, the authors evaluated the changes produced in calculated values of parameters (acid concentration and K_a) when small changes are made in the variables (volume of base and pH). To accomplish this, they treated computed titration curves using the following steps: (1) the volume of titrant for data point 1 was incremented by a small amount, the least-squares refinement was repeated until convergence was obtained, and the change in each of the parameters that resulted was divided by the small change in volume that produced it; (2) the volume at point 1 was restored to its original value, a small increment was made to the pH for data point 1; the least-squares refinement was again repeated, and the $\Delta p/\Delta(\mathrm{pH})_1$ values were calculated for each of the parameters; (3) the pH of data point 1 was restored to its original value; (4) steps 1—3 were repeated for each of the points in the data set.

The authors used these quantities, calculated by finite difference, as approximations of the corresponding partial derivatives. In each of steps 1 and 2 at least two iterations through the least-squares procedure must be made; the first to alter the parameter values, and the second to be sure that convergence has been obtained. This means that at least $(2 \times n \times v)$ iterations must be made, where n is the number of data points and v is the number of variables that define a data point. For Meites' data sets, there were 2 variables and 25 points, requiring a minimum of 100 iterations. In this communication, an alternative means of obtaining more accurate values of the same quantities in a much more efficient manner is reported. In test runs with data sets equivalent to those in the earlier reports, less than 1/40 of the computing time was required by using the algorithm described here.

0003-2670/84/$03.00

Derivation

In a weighted nonlinear least-squares refinement, initial guesses of the parameters (p_i) are used to calculate correction terms (Δp_i). New estimates of the parameters are set equal to ($p_i - \Delta p_i$), and the least-squares treatment is repeated. This is continued until the changes in the parameters are less than some preset criterion. In each iteration, a set of simultaneous equations that are linear in the correction terms must be solved. These normal equations, with p equations for $k = 1 \ldots p$, are

$$\sum_{j=1}^{p} [\Delta p_j \sum_{i=1}^{n} w_i(\partial F_i/\partial p_k)\,(\partial F_i/\partial p_j)] = \sum_{i=1}^{n} w_i(\partial F_i/\partial p_k)F_i \qquad (1)$$

where F_i is a function of the parameters and variables, such that it is equal to zero for error-free values. The weights of each data point, w_i, are set equal to $(\sigma_{\mathrm{pH}}^2 + (\partial \mathrm{pH}/\partial v)^2\sigma_v^2)^{-1}$ in the report of Smit and Meites [2]. In general, the weights in least-squares regressions are chosen as functions of the variances of the variables and the partial derivatives of the function, F, with respect to the variables. Thus each iteration of the refinement consists of (1) evaluation of the function and the partial derivatives of the function with respect to all parameters and variables at each data point; (2) use of those quantities to find the weights and compute the sums needed in the normal equations; and (3) solving the normal equations for the corrections to the parameters. The third step is usually done by inverting the matrix of coefficients for the normal equations, which is then left multiplied into the vector that comprises the right-hand side of Eqns. 1.

After obtaining convergence with an ideal data set, the value of the function F_1 (the first data point) is incremented by a small amount ΔF_1. Equation 1 becomes

$$\sum_{j=1}^{p} [\Delta p_j \sum_{i=1}^{n} w_i(\partial F_i/\partial p_k)\,(\partial F_i/\partial p_j)] = \sum_{i=1}^{n} w_i(\partial F_i/\partial p_k) - w_i(\partial F_i/\partial p_k)\Delta F_1 \qquad (2)$$

Because convergence was obtained before changing the value of F_1, the summations on the right-hand sides of Eqns. 2 are essentially zero. Divided by ΔF_1, then in the limit as $\Delta F_1 \to 0$, these equations reduce to

$$\sum_{j=1}^{p} [\mathrm{d}p_i/\mathrm{d}F_1 \sum_{i=1}^{n} w_i(\partial F_i/\partial p_k)\,(\partial F_i/\partial p_j)] = -w_1(\partial F_1/\partial p_k) \qquad (3)$$

All of the partial derivatives in this equation were evaluated in the least-squares refinement, and their values were not changed significantly by the infinitessimal change $\mathrm{d}F_1$. Therefore, the values of $(\mathrm{d}p_j/\mathrm{d}F_1)$ are obtained by simultaneous solution of Eqns. 3. Repetition of this procedure for each data point results in the $(n \times p)$ different values of $(\mathrm{d}p_j/\mathrm{d}F_i)$; $j = 1 \ldots p$, $i = 1 \ldots n$.

The partial derivatives found by Kateman et al. are directly related to the total derivatives given above

$$\partial p_j/\partial z_{ik} = -(\mathrm{d}p_j/\mathrm{d}F_i)\,(\partial F_i/\partial z_{ik}) \quad (4)$$

where z_{ik} is used to denote the kth variable (volume of titrant or pH in the present case) at the ith data point. The indices used assume the following values: $j = 1 \ldots p$, $i = 1 \ldots n$, $k = 1 \ldots v$.

Outline of the algorithm

A conventional weighted nonlinear least-squares program is used. Required input is the standard deviation of each variable, the number of data points, values of all variables at each of the data points, and initial guesses for each of the parameters. Convergence is assumed when $|\Delta p_i/p_i| < 10^{-6}$. In each iteration, the function is evaluated for each data point. The partial derivatives of the function and the weights are found and stored in arrays. The matrix of coefficients (Eqn. 1) is accumulated in an array which is inverted after all data points have been treated. The corrections to the parameters are then found by matrix multiplication.

Once convergence has been obtained, the following matrices are present in memory: $\mathbf{N}^{-1}$, a $p \times p$ matrix, the inverted matrix of coefficients; **P**, a $p \times n$ matrix, the elements of which are $p_{ij} = \partial F_j/\partial p_i$; **D**, a $v \times n$ matrix with elements $\mathrm{d}_{ij} = \partial F_j/\partial z_{ji}$; and **W**, a $1 \times n$ matrix of the weights for each data point. The matrix **F**, a $p \times n$ matrix of $(\mathrm{d}p_i/\mathrm{d}F_j)/w_j$ is computed by using the equation $\mathbf{F} = \mathbf{N}^{-1}\mathbf{P}$. When the elements of each column in matrix **F** are multiplied by the weight of that data point, the solutions to equations like Eqn. 3 are obtained for each of the n data points. The values of $(\partial p_j/\partial z_{ik})$ are calculated in a straightforward manner as a part of the output routine, by finding the product of the appropriate elements in the **W**, **F** and **D** matrices.

All calculations were performed on a Radio Shack TRS-80 Model 4 microcomputer using programs written in interpreted BASIC.

Results and discussion

Cubic equations in hydrogen ion concentration were used to calculate the pH as a function of the volume of base added, when a solution of a weak acid of concentration C_A and ionization constant K_a is titrated with a strong base. In each data set, 25 points were computed, covering the entire buffer region and up to a 25% excess of added base. These data were then used as the input for the least-squares refinement of the same equation, C_A and K_a being treated as the parameters. Small rounding errors in the data and the computer routines resulted in small changes in the parameter values. The concentration of the weak acid and its equilibrium constant that were calculated agreed with the assumed values to better than 2 parts in 10^5.

Each data set was treated by using the algorithm described above, and also by the finite difference method [1]. For these data sets, the latter requires 50 runs of the least-squares refinement routine. For all data sets, the 50 partial derivatives obtained by each of the methods agreed to better than 0.2%. In most regions of the titration curve, the agreement was much closer

than this, approaching the rounding error of the computer. The discrepancies between the two methods, when large, were reduced considerably by using smaller increments of the variables. Thus it would appear that both methods are producing the same quantities.

The times for the computer to evaluate these numbers were 40—50 times longer using the method of the earlier investigators, when compared to the algorithm presented here. This computation-time factor should increase approximately linearly with the number of data points used for the regression. Thus it would be practical to evaluate these derivatives for much larger data sets by use of the algorithm given here.

REFERENCES

1 G. Kateman, H. C. Smit and L. Meites, Anal. Chim. Acta, 152 (1983) 61.
2 H. C. Smit and L. Meites, Anal. Chim. Acta, 153 (1983) 121.
3 L. Meites, Anal. Chim. Acta, 74 (1975) 177.

Analytica Chimica Acta, 166 (1984) 325–327
Elsevier Science Publishers B.V., Amsterdam — Printed in The Netherlands

Short Communication

DETERMINATION OF WATER CONTENT OF HYGROSCOPIC LITHIUM SALTS

ROBERT WEINTRAUB, ALEXANDER APELBLAT* and ABRAHAM TAMIR

Department of Chemical Engineering, Ben Gurion University of the Negev, Beer Sheva (Israel)

(Received 20th February 1984)

Summary. Determination of the water content in hygroscopic lithium chloride, lithium bromide, lithium nitrate and lithium sulfate by Karl Fischer reagent (KFR), Hydranal (Eugen Scholz reagent) and by thermal-vacuum drying is discussed. Agreement between the results of the KFR titrations and drying methods is satisfactory whereas the Hydranal titrations gave high values. Only the drying method was suitable for lithium sulfate.

During a study of precise measurements of the enthalpies of dissolution of unhydrated and hydrated lithium salts in water, the problem of the preservation and determination of the salt-to-water ratio was encountered. Because of the strongly hygroscopic behaviour of these salts, each handling operation (weighing, transference, storage, etc.) results in an increase in the water content of the samples, which in turn affects the measured enthalpy of dissolution. No published studies on the determination of the water content in lithium salts seem to be available.

Presented here is a summary of the experience gained in working with hygroscopic lithium salts and the results of water determinations based on thermal vacuum drying, titrations with conventional Karl Fischer reagent, and titrations with the recent Hydranal reagent, which is a pyridine-free Karl Fischer-type reagent.

Experimental

Titrations were done with the Metrohm E547 automatic Karl Fischer titrator. Weight losses were measured after vacuum drying in a Büchi TO-50 all-glass oven, connected to an Alcatel 2012A vacuum pump (specifications for base pressure $>10^{-4}$ mbar). The Karl Fischer reagent used was the Merck single solution. Hydranal titrant and solvent (Eugen Scholz reagent) were supplied by Riedel de Haën. Details of procedure depended on the sample and are therefore reported together with the results and discussion.

Results and discussion

Preliminary tests showed that in the systems considered, several factors can significantly affect the results. For example, the salts dissolve with

0003-2670/84/$03.00

difficulty, if at all, in spent titration reagents and this can prolong the time of titration. In spite of all precautions, this leads to absorption of moisture from the surroundings. Additional difficulty arises from insufficient mixing of the heterogeneous system (partially dissolved salts) during the titration. It became clear that manipulations (transfer from sample bottles, storage of materials, weighing, etc.) must be done with proper isolation from the atmosphere.

Lithium chloride. Lithium chloride samples were taken from different sources. Samples A, B and C were all Merck (cat. no. 5679, pro analysi, labelled LiCl). Sample A was from an old reagent container of unknown history. Sample B was from a freshly opened container. Sample C was a sample stored previously in an open glass beaker at 110°C, without vacuum. The results of determinations done with the Merck Karl Fischer reagent (KFR), Hydranal reagent, and thermal-vacuum drying, are shown in Table 1. Samples placed back into the vacuum oven for additional periods at the same temperatures showed no further weight losses. As can be seen, there is satisfactory agreement between the results obtained by the KFR and drying procedures, whereas titrations with the Hydranal reagent gave higher results. There is no clear explanation for the discrepancy observed. In all cases, the samples were only partially dissolved in the reagents; thus, it took some time to leach all the water from the solids. It was found that continuous mixing and titration for 5 min was sufficient before the automatic titration time of 30 s was applied. With longer periods (1—4 h), the amount of reagent needed increased significantly because of moisture absorbed from the surroundings.

TABLE 1

Determination of water in lithium chloride, bromide and nitrate

Sample	Water found (% w/w)		
	Titration		Thermal-vacuum drying
	Hydranal	KFR	
Lithium chloride			
A	31.3, 30.6	—	30.0[a]
B	3.1	—	2.1[b]
C	1.2	0.60, 0.42, 0.39	0.38[c] (0.45)[d]
Lithium bromide			
A	0.85	—	0.24[b]
B	—	0.36, 0.29	0.32[b]
C	—	24.3	24.8[e]
Lithium nitrate			
A	—	2.0	1.6[f]
B	—	2.5, 3.6, 3.1	3.0[f]
C	—	4.0, 3.9	3.8[f]

[a]20 h at 110°C. [b]22 h at 110°C. [c]4 h at 110°C. [d]Total weight loss after an additional 16 h at 200°C. [e]20 h at 200°C. [f]22—24 h at 200°C.

This was true in experiments with lithium chloride and also in standardization of the reagent. The calibration factors were determined by introducing weighed amounts of water from microlitre syringes into the titration cell. The results were found to be independent of the presence of spent lithium chloride solutions in the cell. As a rule, with all of the substances studied here, the calibration factor was determined in a clean cell and again in a cell containing a spent solution of the relevant lithium salt.

Lithium bromide. The titration procedure used for the determination of water in lithium bromide was the same as that for LiCl, except that the initial titration time was 10 min instead of 5 min as described above. The sources of lithium bromide samples were as follows: samples A and B were LiBr (Merck, cat. no. 5669); sample C was $LiBr \cdot H_2O$ (Alfa, cat. no. 87613, ultrapure) from a previously opened bottle. The results are shown in Table 1. As for lithium chloride, there is satisfactory agreement between the results of the KFR titrations and the thermal-vacuum drying. The Hydranal titrations again give higher results. The higher than theoretical value for water in $LiBr \cdot H_2O$ (theoretical 17.2%) is not unexpected, considering the history of the sample bottle.

Lithium nitrate. Lithium nitrate samples (Riedel-de Haen, cat. no. 13023) were from an old container of unknown history. The initial titration time was 15 min. The Hydranal reagent was not used for these samples. The results are listed in Table 1. The lithium nitrate in the sample container was in the form of clumps of crystals. The container was opened three times to remove samples A, B and C over a period of time, resulting in increased water content in the samples. The portion of sample B that was placed into the oven was first quickly ground with an agate mortar and pestle to obtain a small particle size. All of sample C was ground to ensure sample homogeneity and was then left overnight in an open weighing bottle. Sample inhomogeneity can explain the scatter of the results for samples A and B, which is absent in sample C.

Lithium sulfate. Lithium sulfate was found to be practically insoluble in spent Karl Fischer reagent. Further, titrations never reached the end-point, even after being left to run overnight. Unsuccessful attempts were made to measure the water content by converting lithium sulfate monohydrate to lithium chloride with a methanolic solution of calcium chloride followed by a KFR titration in the presence of the precipitated calcium sulfate. The results were too scattered to be useful. During this study, the results obtained by the titration and thermal-vacuum drying methods for calcium sulfate agreed well. Thermal-vacuum drying of $Li_2SO_4 \cdot H_2O$ from a freshly opened container (Merck, Suprapur, cat. no. 5697) yielded 13.35 and 13.07% (w/w) water (theoretical 14.08%).

The authors are indebted to Luna Wajsbrot for her fine technical assistance, and thank Chemitrade (Koppel and Co.) for a free sample of the Hydranal reagent.

Analytica Chimica Acta, 166 (1984) 329—333
Elsevier Science Publishers B.V., Amsterdam — Printed in The Netherlands

Short Communication

THE ACIDITY AND SOLUBILITY CONSTANTS OF TETRACYCLINES IN AQUEOUS SOLUTIONS

B. M. AHMED and R. D. JEE*

The School of Pharmacy, University of London, 29—39 Brunswick Square, London, WC1N 1AX (Great Britain)

(Received 10th May 1984)

Summary. Solubility measurements over the pH range 2.6—7.6 for tetracycline, chlortetracycline, dimethylchlortetracycline and oxytetracycline are used to determine thermodynamic values for the solubility constant and the first and second acidity constants of these compounds.

The low aqueous solubility of the tetracyclines in the mid-pH range makes it difficult to use potentiometric titrations for determining the first acidity constant. Solubility measurements provide an alternative but little used method for compounds of low solubility [1]. In this communication, the pH/solubility relationships for tetracycline, chlortetracycline, demethylchlortetracycline and oxytetracycline are described and used to evaluate the solubility constant and first and second acidity constants.

Relatively few solubility measurements have been reported for tetracyclines [2—6] and in most cases are restricted to the low pH region. The pH/solubility relationships for various tetracycline hydrochlorides [3, 4] in the low pH region have shown the importance of common ion effects, with dimerization in the case of doxycycline [4]. Little quantitative information on the solubility in the mid-pH region has been published. Higuchi et al. [2] presented experimental data for oxytetracycline and a theoretical equation explaining the variation of solubility with pH, but the solubility constant and acidity constants were not evaluated.

The tetracycline hydrochlorides ($H_3T^+Cl^-$) show three macroscopic pK_a values (ca. 3, 7 and 9) and the observed solubility (S_o) may be expressed by the mass-balance equation

$$S_o = [H_3T^+] + [H_2T] + [HT^-] + [T^{2-}] \quad (1)$$

In the pH range where the solubility is limited by the intrinsic solubility of the species H_2T, Eqn. 1 may be written as

$$S_o = K_{So}(1 + [H^+]/K_{a1} + K_{a2}/[H^+] + K_{a2}K_{a3}/[H^+]^2) \quad (2)$$

where K_{a1}, K_{a2} and K_{a3} are the macroscopic acidity constants and K_{So} is the solubility constant for H_2T. The use of macroscopic acidity constants

0003-2670/84/$03.00

represents an over-simplification of the true equilibria in solution, but the form of the solubility/pH relationship given by Eqn. 2 is indistinguishable experimentally from those derived from the micro-ionization schemes proposed by Asleson and Frank [7] and Rigler et al. [8]. By measuring the solubility, S_o, at different pH values and fitting the data to Eqn. 2, it is possible to evaluate the various constants. Measurements at different ionic strengths enable values for the constants at infinite dilution to be obtained.

Experimental

The hydrochloride salts of tetracycline, chlortetracycline and demethylchlortetracycline (Lederle Laboratories, Cyanamid of Great Britain) were used. Oxytetracycline hydrochloride was obtained from Pfizer. The free bases were prepared from these hydrochlorides as described by Higuchi et al. [2]. Oxytetracycline and chlortetracycline were isolated as dihydrates and tetracycline as the trihydrate. Demethylchlortetracycline contained about 10% water.

Solubilities were measured over the pH range 2.6—7.6; an acetic acid (0.01 M)/phosphoric acid (0.01 M) universal buffer was adjusted to the required ionic strength with potassium chloride. Saturated solutions were prepared by taking ca. 25 mg of the finely ground free base plus 10 cm^3 of the appropriate buffer and shaking for about 2.5 h in a water bath at 25.0° C. The solutions were protected from light throughout this period. The solid phase was removed by filtration through a glass wool plug.

The concentrations of the saturated solutions were determined spectrophotometrically. Aliquots of these solutions were suitably diluted with 0.1 M hydrochloric acid and the absorbances were measured at 355, 353, 364 and 366 nm for tetracycline, oxytetracycline, chlortetracycline and demethylchlortetracycline, respectively; a Cecil CE595 double-beam spectrophotometer was used. Calibration graphs in 0.1 M hydrochloric acid for each tetracycline in the range 5—40 $\mu g\ cm^{-3}$ were prepared by using the hydrochloride salts.

All pH measurements were made with a Beckman 4500 digital pH meter and Russell CMAWL combination electrode.

Results

Solubility/pH measurements for the four tetracycline free bases at 25.0° C were made in acetate/phosphate buffers at ionic strengths of 0.05, 0.1, 0.15 and 0.2 mol dm^{-3} in the pH range 2.6—7.6. Figure 1 shows the solubility curves for tetracycline at the various ionic strengths; it is typical of all the tetracyclines studied.

The possible presence of soluble impurities absorbing at the same wavelengths as those used for the tetracyclines was checked by varying the mass of compound taken to prepare the saturated solutions; doubling the mass changed the absorbance by less than 1%. Loss of material from solution during filtration by adsorption onto the filter was checked by varying the

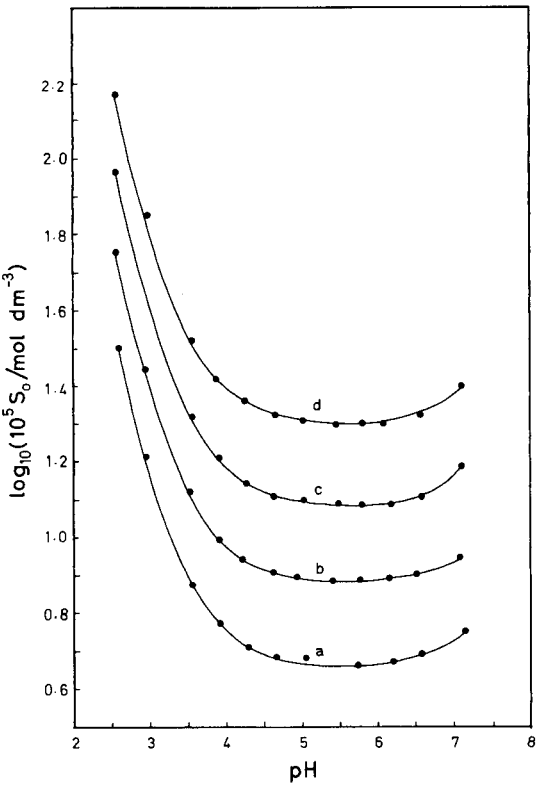

Fig. 1. Effect of pH on the solubility of tetracycline at various ionic strengths. Ionic strength (mol dm^{-3}): (a) 0.05; (b) 0.1; (c) 0.15; (d) 0.2. Curves b, c and d have been shifted upwards by 0.2, 0.4 and 0.6, respectively, for clarity.

size of the glass wool filter used; no significant adsorption effects were observed. The equilibration time required for preparation of saturated solutions was investigated for tetracycline and oxytetracycline by observing the change in absorption with time; the solutions came to equilibrium in about 2.5 h. In the case of oxytetracycline, complete pH/solubility curves were measured for 0.1 mol dm^{-3} ionic strength with equilibration times of 2.5 and 18 h. Fitting the data to Eqn. 2 gave identical values for the constants within experimental error. Equilibration times of 2.5 h were used for all subsequent measurements. A possible problem with long equilibration times is epimerization, but when the rate constants given by Remmers et al. [9] were used, epimerization was shown to be negligible (<1%) under the conditions used here.

The pH/solubility data were fitted to Eqn. 2 by using a least-squares program. The hydrogen ion concentration was calculated from the pH, using activity coefficients obtained from an approximate form of the Debye—Hückel equation ($\log_{10}\gamma_{H^+} = -0.5115\, I^{1/2}/(1 + 1.5\, I^{1/2})$. The final term of

Eqn. 2 was shown not to contribute significantly to the total solubility in the pH range examined and was not included in the data-fitting. Table 1 shows the results of the fitting process; the solubility of the tetracyclines may be calculated at any pH in the range 2.6—7.6 by using these constants and Eqn. 2. Differences between experimental and calculated solubilities are <5%. Values for the constants at infinite dilution (Table 2) were obtained by extrapolation to zero ionic strength. As would be expected, pK_{So} and pK_{a1} were little affected by ionic strength and the pK°_{So} and pK°_{1} values were obtained from simple pK vs. I plots. The second acidity constant depends on the values of three activity coefficients according to $K_{a2} = K_{a2}\gamma_{H_2T}/(\gamma_{H^+}\gamma_{HT^-})$. If a value of 1 is assumed for the neutral (or zwitterion) species H_2T, pK_{a2} should vary with ionic strength according to a function such as $-1.02\, I^{1/2}/(1 + BI^{1/2})$. The pK°_{a2} values in Table 2 were obtained by plotting pK_{a2} vs. this function and adjusting B to give the best fit. From the statistics of the fitting procedures, the standard errors on the pK°_{So} and pK°_{a1} values are about 0.01, and on the pK°_{a2} values is about 0.08; the latter is larger because of the more difficult extrapolation to zero ionic strength and the limited data in the high pH region. The few thermodynamic acidity constants of tetracyclines available in the literature were obtained by making activity coefficient corrections rather than extrapolations to zero ionic strength. The literature values included in Table 2 show good agreement with the present values; the present values for pK°_{a2} tend to be higher but are consistent with potentiometrically determined values [10]. No values for the solubility constants have previously been reported.

The solubility in the mid-pH range for the tetracyclines examined increases a little with increase in ionic strength, which is consistent with the H_2T species being zwitterionic in nature. A similar effect was observed by Bogardus and Blackwood [4] for doxycycline. The solubility order observed, DMCTC > CTC > OTC > TC, agrees with that expected from structural considerations. In oxytetracycline (OTC) the hydroxyl group increases the polarity

TABLE 1

Conditional solubility and dissociation constants for tetracyclines at various ionic strengths (temperature 25.0° C)

Compound	Ionic strength (mol dm^{-3})[a]											
	0.05 (0.824)			0.10 (0.777)			0.15 (0.760)			0.20 (0.732)		
	pK_{So}	pK_{a1}	pK_{a2}	pK_{So}	pK_{a1}	pK_{a2}	pK_{So}	pK_{a1}	pK_{a2}	pK_{So}	pK_{a1}	pK_{a2}
Tetracycline	3.33	3.29	7.65	3.31	3.26	7.78	3.31	3.25	7.59	3.30	3.25	7.53
Oxytetracycline	3.30	3.17	7.37	3.27	3.16	7.37	3.28	3.14	7.40	3.26	3.14	7.31
Chlortetracycline	2.90	3.25	7.29	2.90	3.24	7.25	2.88	3.24	7.23	2.89	3.24	7.14
Demethylchlortetracycline	2.59	3.39	6.96	2.58	3.38	6.93	2.57	3.39	6.85	2.57	3.38	6.81

[a] γ_{H^+} values are given in parentheses.

TABLE 2

Values of pK_a and pK_{So} extrapolated to zero ionic strength

	$pK^{\circ}_{S_o}$	pK°_{a1}	pK°_{a2}	Literature values		
				pK_{a1}	pK_{a2}	Ref.
Tetracycline	3.34	3.32	7.84	3.30	7.68	11
				3.33	7.70	12
Oxytetracycline	3.30	3.18	7.53	3.27	7.32	11
Chlortetracycline	2.90	3.26	7.49	3.30	7.44	11
				3.27	7.43	12
Demethylchlor-tetracycline	2.61	3.39	7.18	3.30	7.16	11

relative to that of tetracycline; the chloro group increases the polarity through inductive effects. The removal of the methyl group in demethylchlortetracycline, combined with the chloro group, contributes to the increased polarity and solubility.

B. M. A. thanks the University of Khartoum for financial support. The authors thank Lederle Laboratories, Cyanamid of Great Britain, Ltd., for providing samples.

REFERENCES

1 A. Albert and E. P. Serjeant, The Determination of Ionization Constants, 3rd ed., Chapman and Hall, London, 1984.
2 T. Higuchi, M. Gupta and L. W. Busse, J. Am. Pharm. Assoc. Sci. Ed., 42 (1953) 157.
3 S. Miyazaki, M. Nakano and T. Arita, Chem. Pharm. Bull. (Tokyo), 23 (1975) 1197.
4 J. B. Bogardus and R. K. Blackwood Jr., J. Pharm. Sci., 68 (1979) 188.
5 W. H. Barr, J. Adir and L. Garrettson, Clin. Pharmacol. Ther., 12 (1971) 779.
6 N. M. Ermakova, B. P. Bruns and V. B. Korchagin, Med. Prom. S.S.S.R., 14 (1960) 51; Chem. Abstr., 55 (1961) 3006a.
7 G. L. Asleson and C. W. Frank, J. Am. Chem. Soc., 98 (1976) 4745.
8 N. E. Rigler, S. P. Bag, D. E. Leyden, J. L. Sudmeier and C. N. Reilley, Anal. Chem., 37 (1965) 872.
9 E. G. Remmers, G. M. Sieger and A. P. Doerschuk, J. Pharm. Sci., 52 (1963) 754.
10 B. M. Ahmed, Ph.D. Thesis, University of London, 1982.
11 C. R. Stephens, K. Murai, K. J. Brunings and R. B. Woodward, J. Am. Chem. Soc., 78 (1956) 4155.
12 L. Z. Benet and J. E. Goyan, J. Pharm. Sci., 54 (1965) 983.

Analytica Chimica Acta, 166 (1984) 335—340
Elsevier Science Publishers B.V., Amsterdam — Printed in The Netherlands

Short Communication

EFFETS DE LA NATURE DE SUBSTITUANTS SUR LES CONSTANTES D'ACIDITÉ ET LES CONSTANTES DE STABILITÉ DES COMPLEXES DE QUELQUES ACIDES NITROSO-5-BARBITURIQUES

GÉRARD HUYGE-TIPREZ et JACQUES NICOLE*

Laboratoire de Chimie Analytique, E.N.S.C. Lille, B.P. 108, 59652 Villeneuve d'Ascq Cedex (France)

YVES VANDEWALLE

Laboratoire de Génie Chimique, I.D.N., B.P. 48, 59651 Villeneuve d'Ascq Cedex (France)

(Reçu le 1 Juin 1984)

Summary. (*The effects of substituents on the acidity constants and stability constants of complexes of some 5-nitrosobarbituric acids*). The acidity constants of some 5-nitroso-barbituric acids (violuric acids) vary according to the degree of substitution and the nature of the substituent at the 1- and 3-positions of the pyrimidine ring. The values obtained at ionic strength 0.5 mol l^{-1} made it possible to calculate the stability constants of simple complexes of divalent cations (Cu^{2+}, Ni^{2+}, Co^{2+}, Zn^{2+}, Fe^{2+}). Potentiometric titrations were applied.

Résumé. Nous avons déterminé par potentiométrie les variations des constantes d'acidité de quelques acides nitroso-5-barbituriques selon le degré de substitution et la nature du substituant en position 1 et 3 du cycle pyrimidinique. Leur connaissance, à force ionique 0,5 mol l^{-1}, a permis la détermination des constantes de stabilité des complexes simples des métaux divalents (Cu^{2+}, Ni^{2+}, Co^{2+}, Zn^{2+}, Fe^{2+}).

Les composés dérivant de l'acide barbiturique nitrosés en position 5 ont fait l'objet de nombreux travaux concernant leur préparation ou leurs propriétés chimiques. La variochromie de leurs sels n'a pas reçu d'explication satisfaisante. Elle est attribuée à l'existence de formes tautomères ou de complexes internes [1, 2], à des phénomènes de condensation [3], et à l'influence du degré d'hydration [4]. Elle est pourtant utilisée pour les dosages spectrophotométriques [5—8]. Les propriétés fongicides et algicides [9] et anticancéreuses [10] sont très étudiées.

Partie expérimentale

Réactifs. Les acides violuriques sont préparés par trois méthodes. La voie la plus directe est la nitrosation ($NaNO_2$ + HCl) des acides barbituriques. C'est le cas de l'acide violurique (VA) et de l'acide thio-2-violurique (thio VA). Dans les autres cas, deux voies se présentent: la première consiste, à

0003-2670/84/$03.00

partir des urées mono- et di-substituées, à faire une synthèse malonique conduisant aux acides barbituriques suivie de la nitrosation; la seconde est la dégradation des xanthines qui nécessite des conditions rigoureuses mais évite les dérivés secondaires. Elle s'effectue en 3 étapes: oxydation des xanthines en alloxantinnes tétrasubstituées, oxydation de ces dernières en alloxannes disubstituées, puis oximation donnant les acides violuriques substitués: acide monométhylviolurique (MMVA), acide monoéthylviolurique (MEVA), et acide diméthyl-1,3-violurique (DMVA).

Toutes les solutions sont préparées avec de l'eau distillée, déionisée et bouillie avant emploi. Elles sont conservées sous atmosphère inerte (hélium).

Techniques. Les titrages s'effectuent dans un vase muni de 5 rodages permettant l'introduction des électrodes, l'arrivée d'hélium et d'un thermomètre. Une circulation d'eau pulsée à partir d'un bain thermostaté régulé électroniquement maintient la température de la solution à 25°C ± 0,01. Un courant d'hélium saturé d'eau et maintenu à la température de travail est véhiculé constamment dans le vase. Un système automatique de titrage est utilisé à partir d'une autoburette ABU-80 (Radiometer) équipée d'une pointe anti-diffusion (Metrohm) et d'un pHmètre PHM 64 (Radiometer) avec sortie BCD. Un microordinateur HP-85 pilote l'autoburette par impulsions et remplit celle-ci (capacité 2,5 ml) par l'intermédiaire d'un interface GPIO. Il recueille, grâce à l'interface BCD, les indications du pHmètre. Ainsi, à tout ajout de réactif fixe ou variable, le volume délivré, le pH ou le potentiel et le temps d'équilibre sont consignés sur cassette HP puis réexploités à l'aide de programmes mathématiques élaborés pour l'étalonnage des électrodes et la détermination des constantes d'équilibre. Après étalonnage de la chaîne de mesure (tampons hydrogénophtalate de potassium et tétraborate de sodium), nous établissons la correspondance entre le pH indiqué et la concentration réelle en ions H^+. Pour ceci, dans un milieu de force ionique constante (0,5 mol l^{-1}), nous ajoutons de l'acide nitrique de concentration connue, maintenu à la même force ionique et établissons les relations $pH/f(-\log[H^+])$ dans le domaine 1—5. De 1 à 3, la relation est une droite, et de 3 à 5, une portion de parabole à grand rayon de courbure. La concentration de H^+ est alors représentée par l'équation

$$[H^+] = 10^{-(A_2 pH^2 + A_1 pH + A_0)}$$

La vérification de cette relation empirique pour un ensemble de valeurs conduit à une erreur absolue inférieure à 5.10^{-4} unité de pH.

Détermination des constantes d'acidité

Les acides violuriques étudiés présentent de 1 à 3 acidités selon le degré de substitution et leur stabilité en fonction du pH est un rapport direct avec le nombre de H^+ libérables. Quel que soit le nombre d'acidités, séparées en l'occurrence, nous avons employé la méthode d'Ivaska [11] pour obtenir les constantes d'acidité et les points équivalents.

La neutralisation d'un volume V_0 d'acide HA de concentration C_0 par un

volume V de soude de concentration C impose un point équivalent tel que $V_{eq}C = C_oV_o$. La conservation de masse en HA, compte tenu du facteur de dilution est: $[HA] + [A^-] = C_oV_o/(V_o + V)$. A partir de la constante mixte d'acidité K_M, nous obtenons $[HA] = [H^+][A^-]K_M^{-1}$, d'où $V_{eq} = \{V_o + V)/C\}\{[HA] + [A^-]\}$ et finalement

$$V_{eq}\{(V_o + V)/C\}\{[A^-] + [H^+][A^-]K_M^{-1}\}$$

La concentration de A^- est fournie par la neutralité électrique. En posant $Y = \{(V_o + V)/C\}[A^-]$ et $X = Y[H^+]$, nous obtenons l'équation d'une droite $Y = -K_M^{-1}X + V_{eq}$. Une régression linéaire fournit K_M à partir de la pente et V_{eq} comme ordonnée à l'origine. La méthode d'Ivaska ne nécessite pas la connaissance de la concentration en acide mais nécessite la corrélation très précise entre la concentration de H^+ qui intervient dans le calcul de A^- et le pH.

Les valeurs des constantes mixtes sont données dans le Tableau 1. Les troisièmes constantes de l'acide violurique et de l'acide thio-2-violurique n'ont pu être déterminées que par spectrophotométrie u.v.-visible en changeant, à chaque mesure, les solutions compte tenu de la dégradation du cycle pyrimidinique en milieu basique.

De ces résultats, il découle que: (1) la substitution d'un hydrogène par un groupe $-CH_3$ entraîne une variation ΔpK_a de l'ordre de 0,15 conforme aux données de la littérature [12]; (2) la substitution de $-CH_3$ par $-C_2H_5$ donne une variation ΔpK_a de 0,07, l'écart n'apparaissant plus au niveau des secondes acidités; (3) la substitution de l'oxygène en position 2 par le soufre apporte une augmentation de l'acidité ($\Delta pK_a = 0,5$). La stabilité des acides en fonction du pH est thio-VA $\simeq$ VA > MMVA $\simeq$ MEVA > DMVA.

Complexes simples des métaux divalents

Nous avons étudié la formation de complexes entre les acides précédents et les ions divalents suivants: Cu^{2+}, Ni^{2+}, Co^{2+}, Zn^{2+}, Fe^{2+}. L'addition de l'un quelconque de ces ions à une solution d'acide violurique conduit à une diminution relativement importante du pH ainsi qu'un changement de teinte. Dans certains cas (Fe^{2+}), nous avons pu mettre en évidence le complexe et

TABLEAU 1

Constantes d'acidité à 25°C et à force ionique 0,5 mol l^{-1} ($NaNO_3$)

Acide	pK_{a1}	pK_{a2}	pK_{a3}
VA	4,234	9,62	13,1[a]
MMVA	4,384	10,00	—
MEVA	4,456	10,00	—
DMVA	4,572	—	—
Thio-VA	3,792	8,75	13,3[a]

[a] Spectrophotométrie (I = 1).

TABLEAU 2

Signification des symboles utilisés

Symbol	Signification
β_j^H	Constante mixte de stabilité des acides, inverse de la constante mixte d'acidité: $\beta_j^H = [H_jA][H^+]^{-j}[A^{-j}]^{-1}$.
a	Concentration du ligand libre $[A^{-j}]$.
h	Activité de l'ion H^+; $h = [H^+]$.
A	Concentration totale en ligand sous toutes ses formes.
M	Concentration totale en métal sous toutes ses formes complexées ou non.
z_I	Valence de l'espèce I.
I	Caractérise le concentration de toute espèce qui ne contient ni A, ni M soit H^+, OH^-, Na^+, NO_3^-...
β_n	Constante globale de stabilité des complexes.
$\Sigma_I z_I\{I\}$	Charge totale de toutes les espèces I rassemblées dans le milieu.
$\bar{n}$	Nombre moyen de ligands par atome de métal.

déterminer sa constante de stabilité par spectrophotométrie u.v.-visible. Dans le cas général, deux complexes de type MA et MA_2 se forment.

La conservation de masse en métal, $M = \Sigma_0^n[MA_n]$, et en ligand, $A = \Sigma_0^j[H_jA] + \Sigma_0^n n[MA_n]$, et la neutralité électrique de la solution, $\Sigma_I z_I[I] + \Sigma_0^j(j-1)[H_jA] + \Sigma_0^{n=2}(2-n)[MA_n] = 0$, permettent de déterminer les constantes de stabilité, $\beta_c = [MA_c]/[M][A]^c$. (La signification des symboles utilisés est donnée dans le Tableau 2.) En utilisant les constantes de formation β_j^H des acides, nous pouvons exprimer a en fonction des espèces acides et des constantes β_j^H sous la forme

$$a = \sum_0^j j[H_jA] / \sum_0^j j\beta_j^H h^j$$

h désignant l'activité de l'ion H^+ puisque β_j^H est exprimée en constante mixte. Cette concentration a peut encore s'exprimer à partir de A, M, I

$$a = (A - 2M - \sum_I z_I[I]) / \sum_0^j j\beta_j^H h^j$$

La fonction de formation de Bjerrum, $\bar{n}$, se détermine à partir de la relation précédente

$$\bar{n} = (A - a\sum_0^j \beta_j^H h^j)/M$$

$\bar{n}$ peut aussi s'écrire en fonction des constantes de complexation β_n

$$\bar{n} = (\beta_1 a + 2\beta_2 a^2)/(1 + \beta_1 a + \beta_2 a^2)$$

pour les 2 complexes envisagés MA, MA_2, ce qui peut se mettre sous une autre forme directement applicable pour l'obtention de β_1 et β_2

TABLEAU 3

Constantes de stabilité à 25°C et à force ionique 0,5 mol l^{-1} ($NaNO_3$)

Acide	Ions			
	Cu^{2+}	Ni^{2+}	Co^{2+}	Fe^{2+}
VA	β_1 $1{,}78 \cdot 10^4$	$3{,}60 \cdot 10^3$	10^2	β_3 $4{,}45 \cdot 10^8$
	β_2 $1{,}96 \cdot 10^7$	$2{,}24 \cdot 10^6$	$1{,}01 \cdot 10^5$	
MMVA	β_1 $2.53 \cdot 10^4$	$3{,}10 \cdot 10^3$	10^2	β_3 $2{,}40 \cdot 10^9$
	β_2 $3{,}03 \cdot 10^7$	$3{,}75 \cdot 10^6$	$1{,}07 \cdot 10^5$	
MEVA	β_1 $2{,}63 \cdot 10^4$	—	—	—
	β_2 $3{,}45 \cdot 10^7$			
DMVA	β_1 $4{,}64 \cdot 10^4$	$5{,}70 \cdot 10^3$	$2{,}20 \cdot 10^2$	β_3 $1{,}77 \cdot 10^{10}$
	β_2 $8{,}82 \cdot 10^7$	$1{,}33 \cdot 10^7$	$3{,}28 \cdot 10^5$	
Thio-VA	β_1 $8{,}0 \cdot 10^3$	$3{,}20 \cdot 10^3$	$3{,}83 \cdot 10^2$	β_3 $4{,}0 \cdot 10^8$
	β_2 $1{,}0 \cdot 10^7$	$7{,}70 \cdot 10^5$	$5{,}90 \cdot 10^4$	

$$[\bar{n}/(1-\bar{n})a] + [(\bar{n}-2)a/(1-\bar{n})]\beta_2 = \beta_1$$

Nous avons neutralisé, à force ionique 0,5 mol l^{-1}, différents mélanges acide/ion divalent en conservant la concentration en acide constante. Pour la détermination des constantes, il a été tenu compte des complexes hydroxydes du type $CuOH^+$, $Cu_2(OH)_2^{2+}$ ou $Fe(OH)^{2+}$ dont les constantes ont été redéterminées dans le même milieu. Leur importance s'avère négligeable du fait de l'excès de ligande par rapport à l'ion métallique et du pH relativement acide. Le Tableau 3 donne les résultats obtenus.

Les complexes du type MA ont une stabilité supérieure aux complexes MA_2 dans le cas des ions Cu^{2+} et Ni^{2+}, mais nous constatons l'inverse pour Co^{2+}. Les ions fer(II) ne donnent qu'un seul complexe MA_3^- très coloré, absorbant dans la zone 605—615 nm et signalé par Leermakers et Hoffman [13].

Les ions Zn^{2+} se distinguent par le fait qu'ils ne forment qu'un seul complexe ZnA^+ assez peu stable ($\beta_1 \simeq 10^2$). Au vu de ces résultats, il apparaît que les acides violuriques sont des ligandes bidentés, que les complexes sont d'autant plus stables que les acides sont faibles. L'abaissement de pH, lors de l'addition d'ions métalliques, par rapport à la solution initiale en acide, donne un classement des stabilités des complexes. Pour la triade Cu^{2+}, Ni^{2+}, Co^{2+}, les complexes suivent la règle d'Irving-Williams (Cu > Ni > Co). Enfin, il faut noter la tendance spontanée de l'ion Co^{2+} à passer au degré III en présence d'air.

BIBLIOGRAPHIE

1 Hantzch, Berichte, 48 (1915) 7.
2 Dutt, Proc. Ind. Acad. Sci., 8(29) (1938) 145.
3 S. Valladas-Dubois et J. Lemerle, C. R. Acad. Sci., 268 (1969) 2137.
4 Drozdov et Krylov, Doklady Akad. Nauk., 135 (1965) 1135.

5 Tsuchiya Masaomi et Iwanami, Nippon Kagaku Kaishi, 8 (1980) 1256.
6 Matsusaki Koji, Yamaguchi Daigaku Kogakubu Keukyn Hokubu, 28(2) (1978) 249.
7 J. Moratal, J. Faus et M. Beltran, Rev. Acad. Cienc. Exactas, 31 (1976) 235.
8 J. C. Prado, An. Acad. Bras. Cienc., 50(3) (1978) 326.
9 J. D. Douros et F. Al Kerst, Brevet US 3728 461, 17 Apr. 1973; Brevet US 3928 017, 23 Déc. 1975.
10 A. Bloch, New Leads Cançer Ther., (1981) 65.
11 A. Ivaska, Talanta, 21 (1974) 377.
12 D. D. Perrin, B. Dempsey et E. P. Serjeant, pK_a Prediction for Organic Acids and Bases, Chapman and Hall, London, 1981.
13 P. A. Leermakers et W. A. Hoffman, J. Am. Chem. Soc., 80 (1958) 5663.

Analytica Chimica Acta, 166 (1984) 341
Elsevier Science Publishers B.V., Amsterdam — Printed in The Netherlands

Erratum

J. Růžička and E. H. Hansen, Integrated Microconduits for Flow Injection Analysis.

Anal. Chim. Acta, 161 (1984) 1—25.

The name of one of the authors in reference 8 has inadvertently been omitted. The reference should read: H. Engelhardt and U. D. Neue, Chromatographia, 15 (1982) 403.

ANALYTICA CHIMICA ACTA, VOL. 166 (1984)

AUTHOR INDEX

(Continued from inside back cover)

Continued from outside back cover)

(Continued on p. 346)

CONTENTS

(Abstracted, Indexed in: Anal. Abstr.; Biol. Abstr.; Chem. Abstr.; Curr. Contents Phys. Chem. Earth Sci.; Life Sci.; Index Med.; Mass Spectrom. Bull.; Sci. Citation Index; Excerpta Med.)

(Continued on inside back cover)